JOURNAL OF THE MECHANICS AND PHYSICS OF SOLIDS

EDITORIAL ADVISORY BOARD

J. F. BAKER—Cambridge W. M. BALDWIN– Cleveland
E. BRANDENBERGER– Zürich G. BUSCH—Zürich
A. H. COTTRELL—Harwell C. CRUSSARD– Paris M. J. DRUYVESTEYN—Delft
A. KOCHENDÖRFER—Düsseldorf N. F. MOTT—Cambridge
A. NADAI—Pittsburgh, Pa. G. SACHS—Syracuse, N.Y. E. SIEBEL—Stuttgart
V. V. SOKOLOVSKY—Moscow

EDITOR-IN-CHIEF

R. HILL
University of Nottingham

Volume 7
1958—59

PERGAMON PRESS · NEW YORK · LONDON · PARIS · LOS ANGLES

Contents of Volume 7

NUMBER 1 *Page*

G. LIANIS and H. FORD : Plastic yielding of single notched bars due to bending 1

R. SANKARANARAYANAN and P. G. HODGE, JR. : On the use of linearized yield conditions for combined stresses in beams 22

W. JOHNSON : Experiments in the cold extrusion of rods of non-circular section 37

E. T. ONAT : Analysis of shells of revolution composed of workhardening material 45

B. D. COLEMAN : On the strength of classical fibres and fibre bundles .. 60

F. J. LOCKETT : Effect of thermal properties of a solid on the velocity of Rayleigh waves 71

Book reviews :

"Experimental Crystal Physics," by W. A. WOOSTER (reviewed by B. Gale) .. 76

"Solid State Physics. Advances in Research and Applications." Vol. 5 edited by F. SEITZ and D. TURNBULL (reviewed by A. H. Cottrell) 76

NUMBER 2

M. LESSEN : Thermoelastic waves and thermal shock 77

T. O. MULHEARN : The deformation of metals by Vickers-type pyramidal indenters 85

N. BROWN and H. S. ROSENBAUM : The torsional yield stress of zinc single crystals 97

C. J. MAIDEN : The strain-rate sensitivity of α – uranium 106

W. E. BOYCE : A note on strain hardening circular plates 114

H. PAYNE : The slip theory of plasticity for crystalline aggregates 126

D. S. DUGDALE : Stress–strain cycles of large amplitude 135

Book Reviews :

"Dislocations and Mechanical Properties of Crystals," edited by J. C. Fisher, W. G. Johnstone, R. Thomson and T. Vreeland JR. (reviewed by T. Broom) .. 143

"The Calculation of Load and Torque in Hot Flat Rolling," (B.I.S.R.A.) (reviewed by A. P. Green) 144

"Proceedings of the Third Midwestern Conference on Solid Mechanics," (reviewed by R. Hill) 144

NUMBER 3

W. A. BASSALI : The transverse flexure of uniformly loaded and fully restrained thin isotropic plates with curvilinear edges 145

E. REISSNER : On torsion of thin cylindrical shells 157

G. T. VAN ROOYEN and W. A. BACKOFEN : Distribution of interface stress in plane strain and axial symmetric compression.. 163

G. EASON : The load carrying capacities of cylindrical shells subjected to a ring of force 169

R. J. KNOPS : A method for solving linear thermoelastic problems 182

F. LASZLO and H. NOLLE : On some physical properties of cementite .. 193

NUMBER 3 (*continued*) *Page*

R. HILL : Some basic principles in the mechanics of solids without a natural time 209

Papers to be published in future issues 226

Book Received 226

Notice 227

Erratum 228

NUMBER 4

A. D. COX and L. W. MORLAND : Dynamic plastic deformations of simply-supported square plates 229

E. REISSNER : On the solution of a class of problems in membrane theory of thin shells 242

J. B. WALSH and A. C. MACKENZIE : Elastic-plastic torsion of a circumferentially notched bar 247

P. G. HODGE, JR. : The effect of end conditions on the dynamic loading of plastic shells 258

J. DE FOUQUET : Modifications de structure cristalline produites par fatigue entre 20 et 750 °C sur un acier extra doux au carbone et sur un acier austenitique 18/8 264

W. A. BASSALI : Torsion of beams whose sections are bounded by certain quartic curves 272

D. S. DUGDALE : An experimental study of the V-notch fatigue test 282

Book Review :

" Conduction of Heat in Solids," by H. S. CARSLAW and J. C. JAEGER (reviewed by C. J. TRANTER) 288

Books Received 288

Author Index

(B) denotes book review

BACKOFEN, W. A. p. 163.
BASSALI, W. A. pp. 145, 272.
BOYCE, W. E. p. 114.
BROOM, T. p. 143 (B).
BROWN, N. p. 97.
COLEMAN, B. D. p. 60.
COTTRELL, A. H. p. 76 (B).
COX, A. D. p. 229.
DUGDALE, D. S. pp. 135, 282.
EASON, G. p. 169.
FORD, H. p. 1.
FOUQUET, J. DE p. 264.
GALE, B. p. 76 (B).
GREEN, A. P. p. 144 (B).
HILL, R. pp. 144 (B), 202.
HODGE, P. G. JR. pp. 22, 258.
JOHNSON, W. p. 37.
KNOPS, R. J. p. 182.
LASZLO, F. p. 193.
LESSEN, M. p. 77.
LIANIS, G. p. 1.
LOCKETT, F. J. p. 71.
MACKENZIE, A. C. p. 247.
MAIDEN, C. J. p. 106.
MORLAND, L. W. p. 229.
MULHEARN, T. O. p. 85.
NOLLE, H. p. 193.
ONAT, E. T. p. 45.
PAYNE, H. p. 126.
REISSNER, E. pp. 157, 242.
ROOYEN, G. T. VAN p. 163.
ROSENBAUM, H. S. p. 97.
SANKARANARAYANAN, R. p. 22.
TRANTER, C. J. p. 288 (B).
WALSH, J. B. p. 247.

Journal of the Mechanics and Physics of Solids, 1958, Vol. 7, pp. 1 to 21. Pergamon Press Ltd., London

PLASTIC YIELDING OF SINGLE NOTCHED BARS DUE TO BENDING

By G. Lianis and H. Ford
City and Guilds College, University of London

(*Received 3rd May*, 1958)

Summary

A General method is developed to evaluate the constraint factor of single notched bars subjected to pure bending under conditions of plane strain. Upper and lower bounds for the yield moment are obtained. Bounds for the constraint factor are calculated for (a) rectangularly, (b) trapezoidally, and (c) V-notched bars with circular fillets.

The theory is checked experimentally for both the overall yield loads and the actual stress distribution, for the above shapes and for circular and V-notches for which Green has worked out an upper bound solution. A new technique to obtain slip-line fields experimentally is also developed.

1. Introduction

When a bar, notched in the middle, is subjected to pure bending gradually increasing from zero, it is initially stressed elastically throughout. With increasing loading the bar first becomes locally plastic around the notch due to the stress concentration. The corresponding load is known as the *Elastic limit* and it could be calculated for instance by relaxation methods.

With increasing loading the elastic–plastic interface spreads into the elastic material. For a single notched bar, at some stage of the loading another plastic region starts from the flat side and with further loading the two plastic regions eventually join together. At this stage, large strains are free to develop with little or no further change of load and plastic flow is no longer contained. This load is defined as the *limit* or *collapse load*.

The bar is subjected to pure bending and is supposed to be of sufficient length for the collapse moment to be independent of the precise distribution of the surface tractions at the ends. The bar is wide compared with the thickness under the notch so that plane strain conditions can be assumed.

According to the theory of Limit Analysis an incomplete plastic solution based on the slip-line and velocity fields provides an upper bound for the yield moment, while a statically admissible stress field provides a corresponding lower bound. In the following, upper and lower bound solutions are obtained for a bar having a single notch of any shape, symmetrical about an axis normal to the top face of the bar, and applications to particular shapes of notches are illustrated.

2. General Solution

A. *Slip-line field (upper bound)*

Green (1953) has shown that his method of obtaining solutions is applicable to any shape of notch, but he does not give the general solution. Depending on the geometry of the notch there are two possible solutions.

Solution I (Fig. 1). We have the so-called second boundary-value problem since the hydrostatic pressure is known along the surface of the notch $(-k)$ and

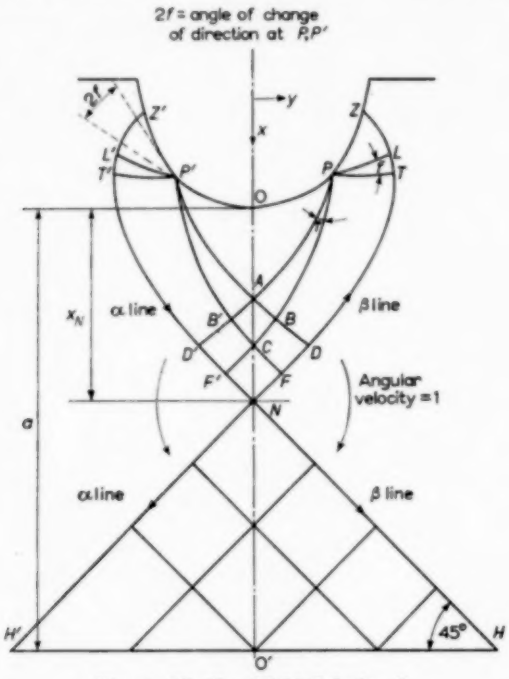

Fig. 1. Slip-line Field Solution I.

the surface of the flat side $(+k)$. Using the step-by-step method (Hill 1950, pp. 144-145) the slip-line field can be extended as far as the other conditions of the problem allow. It consists of two parts: (a) the lower part NHH' where the slip-lines are straight and there is a uniform compression $-2k$ parallel to the surface; (b) the upper part $Z\,L\,T\,D\,F\,N\,F'\,D'\,T'\,L'\,Z'$, the shape of which depends on the geometry of the notch. If the tangents are discontinuous at P and P' these points are singular points. The field is extended around P and P', starting from PA and $P'A'$, through an angular span f equal to half the jump of tangent direction on both sides of the singularities. The position of Z and therefore of N is defined by the equilibrium condition, i.e. the stresses across the minimum cross-section must be equivalent to a pure couple.

If σ_y is the tensile stress normal to ON the equilibrium condition is

$$\int_0^{x_N} \sigma_y \, dx = 2k\,(a - x_N), \tag{1}$$

from which x_N can be found. Then the yield moment per unit thickness of bar is

$$M_y = \int_0^{x_N} \sigma_y x dx + 2k \cdot \frac{(a - x_N)^2}{2}. \tag{2}$$

The *constraint factor* L is defined in the following as the ratio of the yield moment of the notched bar to the yield moment of a bar without notch having a cross-section equal to the minimum cross-section under the notch root. Therefore:

$$L = \frac{2M_y}{ka^2} = 2\left[\int_0^{x_N} \frac{\sigma_y}{k} \cdot \frac{x}{a} \cdot d\left(\frac{x}{a}\right) + \left(1 - \frac{x_N}{a}\right)^2\right]. \tag{3}$$

N is a point of stress discontinuity. The jump Δp of the hydrostatic pressure in N must not exceed the value $2k$ times the value of the angle of rotation of a discontinuous slip-line around N (HILL, 1954). In our case the angle of rotation is $\frac{1}{2}\pi$ and therefore, for the present solution to be valid,

$$\frac{\sigma_y}{k} \leqslant \pi. \tag{4}$$

Assuming the notch surface has an increasing angle of direction, with possible discontinuities, (Fig. 1) HENCKY's equations lead to

$$p_N = -k(1 + 2\theta_z), \qquad \sigma_y/k = 2(1 + \theta_z) \leqslant \pi,$$
$$\text{or } \theta_z \leqslant 32^\circ\, 40' \tag{5}$$

by equation (4). The limiting value of a is

$$a_{\text{lim}} = \int_0^{x_N} \frac{\sigma_y}{2k}\, dx + x_N \tag{6}$$

where x_N is such that $\theta_z = 32^\circ\, 40'$. For values of $\theta_z \geqslant 32^\circ\, 40'$ the yield criterion is violated in some part of the rigid zone around N.

Solution II (Fig. 2). The upper slip-line domain is completed in N and extended on either side as before. The extended domains bounded by the slip-lines NC and NC' join with the straight line field of the flat side by two circular arcs CF and $C'F'$. Thus, the central hinge being considered as a fixed rigid pivot, the rigid ends of the bar rotate by sliding over CF and $C'F'$ as rigid bodies. N is the point where the slip-lines from Z and Z', having $\theta = 32^\circ\, 40'$, meet the central axis. The unknowns of the problem are (a) the position of T on the notch surface, (b) the radius R of the arc of the central hinge. These can be found from the two equilibrium conditions, i.e. the resultant of the x and y stresses across any cross-section, such as $ONCFG'$, must be zero. Analytical expression of these two conditions in terms of the two unknowns, θ_T and R, is not possible for an arbitrary shape of notch and a trial and error procedure must be adopted. In the special cases investigated below such analytical expressions are achieved and the evaluation of the unknown is obtained in terms of the geometrical data of the bar. Once T and R have been found the sizes of the field are fixed and the constraint factor can be found.

Velocity field. The hodograph for Fig. 2, for points of the regions (I) and (II) across CF and $C'F'$ respectively, is a circular arc around the pole. Assuming a unit angular velocity, the radius of this arc is equal to the radius R of the slip-lines CF and $C'F'$, and its angular span equal to λ (Fig. 3). Across NC $v = 0$, hence $u = \text{const.}$, and NC in the hodograph is a circular arc $C_{iv}N_{iv}$ of angular span $(\lambda - \frac{1}{2}\pi)$. It can easily be proved that for a unit angular velocity the images

of CLT and $C'L'T'$ in the hodograph are similar curves rotated through 90°.

Having the distribution of the normal components across ZL and LT, the hodograph in ZLT can be extended to the boundary ZT. On either side of NZ and NZ' there is a tangential discontinuity of amount R, since, in N_{iv}, $u = 0$ and

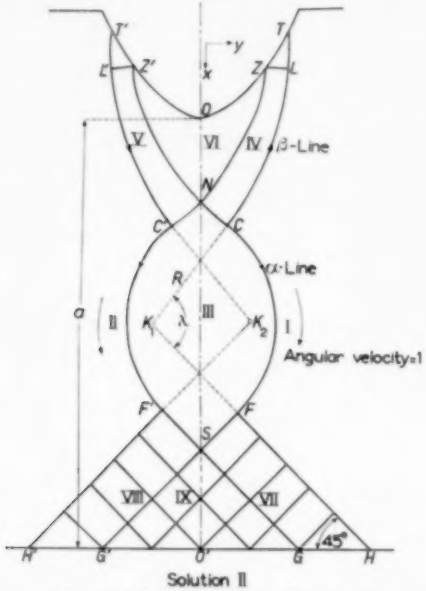

Fig. 2. Slip-line Field Solution II.

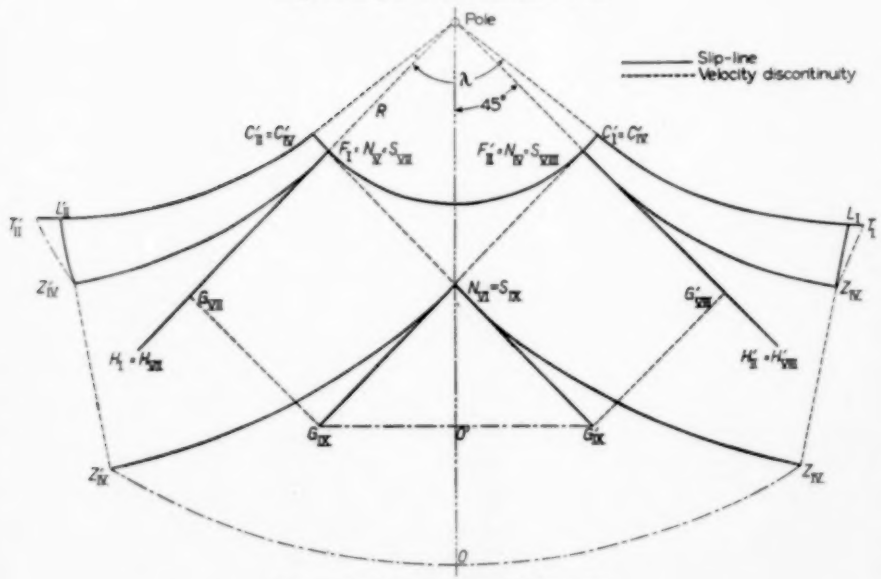

Fig. 3. Hodograph for Solution II.

in N_{iv}, $u = R$. $(NZ)_{vi}$ and $(NZ')_{vi}$ being known in the hodograph, the velocity field in the region $(NZZ')_{vi}$ can be constructed and extended until the boundary

ZOZ' is reached. The domains *VII* and *VIII* have their images coinciding in two straight lines having lengths equal to the relevant lengths of the physical plane since $d\phi = 0$ across them.

Another velocity discontinuity on both sides of $SG\,(v)$ and $SG'\,(u)$, equal to R, is demanded from the continuity of the normal velocities in S. The domain $SG'G$ has an exactly similar criss-cross image, the positions of the points G, G' being interchanged in the hodograph.

We shall give now a general proof of the following statement: *For a concave upwards symmetrical notch having monotonically increasing tangent direction (with possible discontinuities) the stress and velocity system of Figs.* 2 *and* 3 *cause nowhere in the plastic region negative rate of plastic work.*

Proof: The rate of plastic work is given (GREEN 1953) by

$$\dot{w} = k\dot{\gamma} = \frac{\partial u}{\partial s_\beta} + \frac{\partial v}{\partial s_\alpha} + \frac{u}{R} + \frac{v}{S} \tag{7}$$

or in terms of the radii of curvature R, S, of the slip-lines (physical plane) and R', S', (hodograph plane) by

$$\dot{w} = k\dot{\gamma} = k\left(\frac{S'}{S} - \frac{R'}{R}\right). \tag{8}$$

(i) *Upper region* (Fig. 2). It can be shown that, because the notch surface is a principal direction trajectory, the angle ϕ increases in the positive α and β directions. Therefore:

$$\frac{1}{R} = \frac{\partial \phi}{\partial s_\alpha} \geqslant 0, \qquad \frac{1}{S} = -\frac{\partial \phi}{\partial s_\beta} \leqslant 0. \tag{a}$$

Since on both lines ϕ increases they are both concave upwards. Their velocity images are therefore concave to the right and left respectively, and so are all the other lines of the two domains. Therefore, the curvatures of the hodograph are

$$\frac{1}{R'} = \frac{\partial \phi'}{\partial s_\alpha'} \leqslant 0, \qquad \frac{1}{S'} = -\frac{\partial \phi'}{\partial s_\beta'} \leqslant 0. \tag{b}$$

From (a) and (b) it follows that

$$S'/S \geqslant 0 \quad \text{and} \quad -R'/R \geqslant 0.$$

Therefore, everywhere in the upper region, $\gamma = 0$.

(ii) *Lower region*. Since $1/R$, $1/R'$, $1/S$, $1/S'$, are all zero (7) becomes

$$\dot{\gamma} = \frac{\partial u}{\partial s_\beta} + \frac{\partial v}{\partial s_\alpha}.$$

From the hodograph it follows that anywhere in the region, $\partial u/\partial s_\beta \geqslant 0$, $\partial v/\partial s_\alpha \geqslant 0$. Consequently $\gamma \geqslant 0$ in the lower region.

(iii) *Discontinuities NZ, NZ'*. Since, as we cross NZ moving in the positive α — direction, the jump of v is positive $\Delta v = +R$, $\partial v/\partial s_\alpha = +\infty$, $\dot{\gamma} = +\infty$. At the discontinuities FG' and $F'G$, as we cross FG' in the positive β-direction, u changes from $-R$ to 0, $\Delta u = +R$, $\partial u/\partial s_\beta = +\infty$, $\dot{\gamma} + \infty$.

The above analysis also holds for Solution I where N, C, F, S, F', C', coincide in the hodograph. The field remains the same in the regions $NZ'Z$ and $NH'H$ and the discontinuity R disappears.

B. *Stress field (lower bound)*

It can be shown that the discontinuous stress system shown in Fig. 4 is a statically admissible field if $\beta \leqslant 30°$. With this restriction, β is defined in each case so as to yield a maximum value to the constraint factor. Once the value of β has been chosen, ρ (Fig. 4) can be evaluated in terms of β and the dimensions of the bar, since AC is tangential to the notch surface.

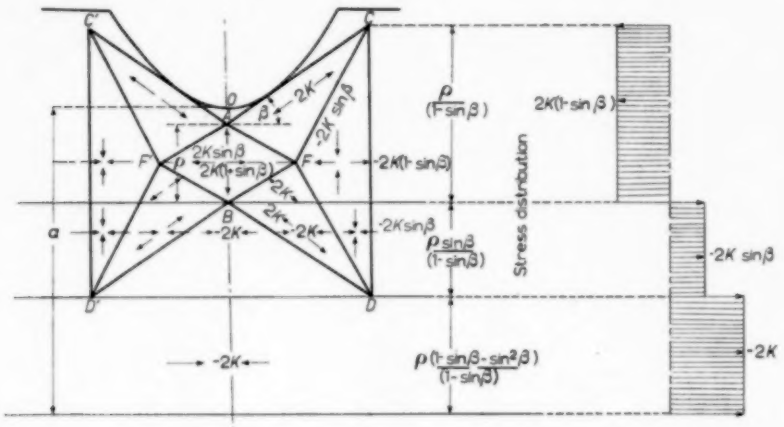

Fig. 4. Lower bound solution.

The constraint factor is

$$L = \frac{2M_y}{ka^2} = 2\frac{\rho^2}{a^2}(2 + 3\sin\beta + \sin^2\beta), \tag{10}$$

β being defined so as to maximize (10), i.e.

$$2(2 + 3\sin\beta + \sin^2\beta)\frac{d\rho}{d\beta} + \rho\cos\beta(3 + 2\sin\beta) = 0. \tag{11}$$

3. PARTICULAR CASES

(a) *Rectangularly notched bars*

The slip-line field for rectangular notches constructed according to the method given in Section 2B has already been described (LIANIS and FORD, 1957). There are two solutions depending upon whether the ratio $2b/a$ is greater or less than 0·575.

Lower bound. From Fig. 4

$$\frac{\rho}{a} = \frac{(1 - b/a\tan\beta)}{(2 + \sin\beta)}, \tag{12}$$

the stress trapezoid being tangential to the corner of the notch. The lower bound for the constraint factor is therefore

$$L = \frac{2(1 - b/a\tan\beta)(2 + 3\sin\beta + \sin^2\beta)}{(2 + \sin\beta)^2} \tag{13}$$

where β is determined in terms of $2b/a$ so as to maximize L in (13). Fig. 5 shows that the mean value does not differ from the bounds by more than $\pm 2{\cdot}5$ per cent; the maximum total stress under the notch in the plastic region, according to the upper bound solution, is also plotted.

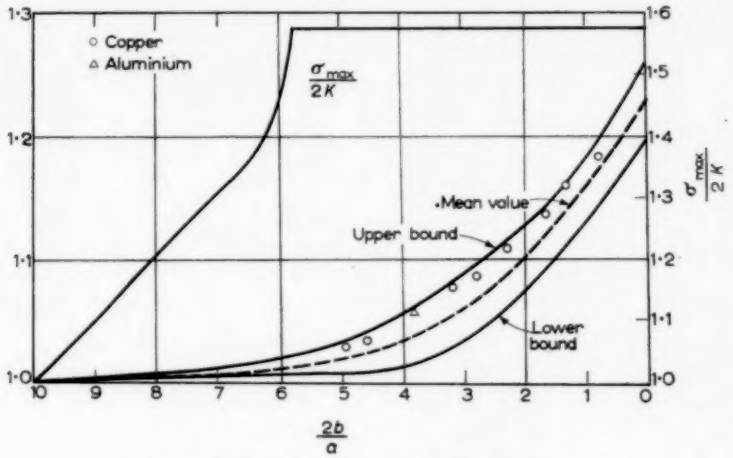

Fig. 5. Constraint factors. Rectangular notch.

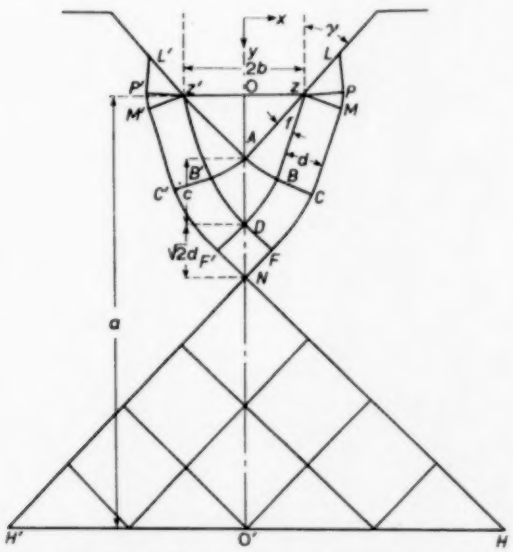

Fig. 6. Slip-line field, Solution I for trapezoidal notch.

(b) *Trapezoidally notched bars*

(i) *Solution I.* The field in Fig. 6 satisfies stress and velocity boundary conditions. The angle f is determined from the condition that the hydrostatic pressure is equal to $-k$ on the stress free surface ZL. Therefore,

$$f = \tfrac{1}{4}(\pi - 2\gamma). \tag{14}$$

The restrictions for the present solution to hold are that $f \geqslant 0$, and that the yield criterion must not be violated in N. These conditions are satisfied for

$$0 \leqslant f \leqslant \tfrac{1}{4}(\pi - 2) = \phi_1, \qquad \text{or} \qquad 57{\cdot}3^\circ = 1 \leqslant \gamma \leqslant \tfrac{1}{2}\pi. \tag{15}$$

Construction of the slip-line field for different values of f gives $AD = C(f)$. The only unknown in finding the shape of the field is d, the condition being that the stresses along $OADNO'$ constitute a pure couple:

$$2k\left[b + \int_A^D \frac{\sigma_y}{2k}\,dx + \frac{\sigma_y(f)}{2k}\sqrt{2}d - (a - b - c - \sqrt{2}d)\right] = 0,$$

$$\frac{d}{a} = \frac{1}{2\left(1 + \dfrac{\sigma_y(f)}{2k}\right)}\left[1 - \frac{2b}{a} - \frac{c}{a} - \frac{1}{a}\int_A^D \frac{\sigma_y}{2k}\,dx\right]. \tag{16}$$

We can evaluate $\int_A^D \frac{\sigma_y}{2K}\,dx$ and $\frac{\sigma_y(f)}{2K}$ numerically in terms of f or γ. For values of $2b/a$ which would make d negative the solution for the rectangular notch holds, i.e. the field is not extended on the sides of the notch.

Taking the moments of the stresses across $OADNO'$ about N we find the bending moment and the constraint factor:

$$L = \frac{2M_y}{ka^2} = \frac{4b}{a}\left(\frac{b}{2a} + \frac{c}{a} + \frac{\sqrt{2}d}{a}\right) + 4\int_A^D \frac{\sigma_y}{2k}\left(\frac{c}{a} + \frac{d}{a}\sqrt{2} - \frac{x}{a}\right)d\left(\frac{x}{a}\right) +$$

$$+ 4\,\frac{\sigma_y(D)}{2k}\cdot\frac{d^2}{a^2} + \tfrac{1}{2}\left(1 - \frac{b}{a} - \frac{c}{a} - \sqrt{2}\,\frac{d}{a}\right). \tag{17}$$

Values of L in terms of $2b/a$ for various angles γ can be calculated numerically from (17) (see Fig. 7).

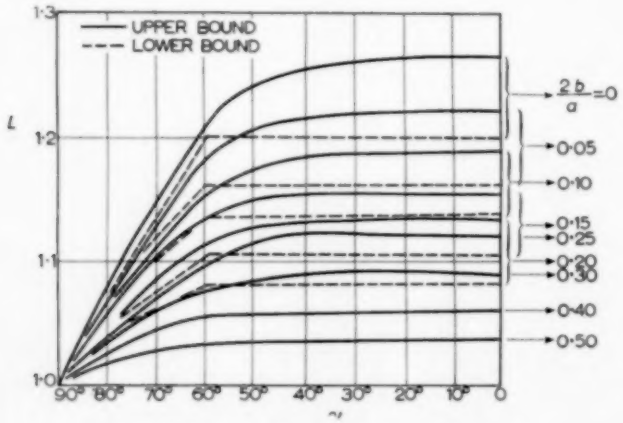

Fig. 7. Constraint factors, trapezoidal notch.

(ii) *Solution II.* The slip-line field for this solution is shown in Fig. 8. Following the argument p. 6 we can prove that $\phi_1 = \frac{1}{4}(\pi - 2)$. For the hydrostatic pressure to be $-k$ on the stress-free surface ZL, ϕ_2 must have the value determined by HENCKY's equation, which gives $\phi_2 = \frac{1}{2}(1 - \gamma)$. For $\phi_2 \geqslant 0$,

$$3{\cdot}2^\circ \leqslant \gamma \leqslant 57{\cdot}3^\circ. \tag{18}$$

From the two equilibrium equations along $OADEE^\circ FG'$ we find R/a and c/a in terms of $2b/a$ for each value of γ. Since c/a must be positive, Solution II for rectangular notches holds (i.e. the field does not extend to the oblique faces) for $2b/a$ smaller than that for which $c/a = 0$. By taking the moments of the stresses acting along $OADEE^\circ FG$ about K_1 the constraint factor is calculated and plotted in Fig. 7.

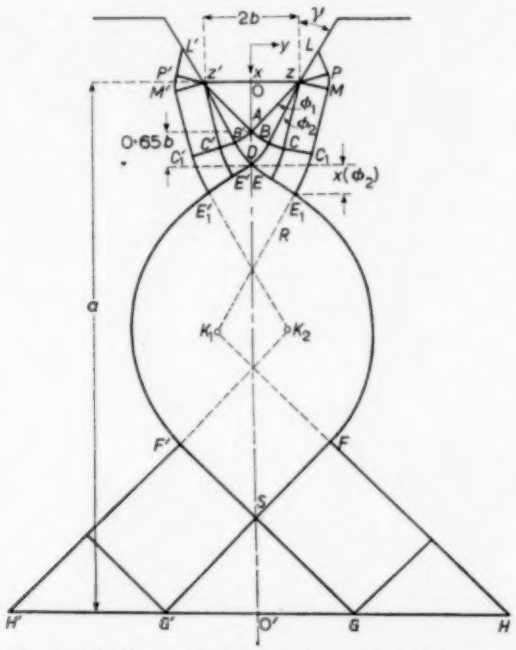

Fig. 8. Slip-line field, Solution II, trapezoidal notch.

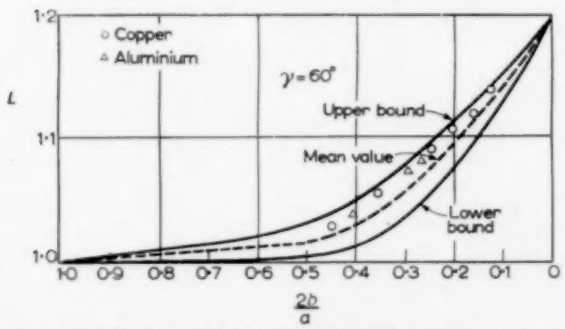

Fig. 9. Constraint factors, 60° trapezoidal notch, various ratios of $2b/a$.

Lower bound. The stress trapezoid is tangential to the corner of the notch and β is independent of γ provided that $\beta \leqslant 30^\circ$ and $\leqslant \frac{1}{2}\pi - \gamma$. Therefore, for values of β smaller than $\frac{1}{2}\pi - \gamma$, L is calculated by means of (13). It remains constant and independent of γ for $\gamma \leqslant \frac{1}{2}\pi - \beta_{max}$, where β_{max} is calculated by maximizing

(13). For $\gamma \geqslant \frac{1}{2}\pi - \beta_{max}$ the trapezoid is taken with its side coinciding to the oblique face of the notch and therefore $\beta = \frac{1}{2}\pi - \gamma$. In this case

$$L = \frac{2\,(1 - b/2\cot\gamma)\,(2 + 3\cos\gamma + \cos^2\gamma)}{(2 + \cos\gamma)^2}. \tag{19}$$

In Fig. 7 both bounds are plotted, the difference of the mean value from the bounds being smaller than $\pm$ 2·5 per cent. In Fig. 9 the bounds are plotted for constant $\gamma = 60°$ together with experimental points.

(c) *Circular notches*

GREEN (1953, 1956) has given the upper bound, and a lower bound can be calculated by taking the trapezoid tangential to the circular arc of the notch. It can be shown that

$$\frac{\rho}{a} = \left[1 - \frac{r}{a}\frac{(1 - \cos\beta)}{\cos\beta}\right] \Big/ (2 + \sin\beta) \tag{20}$$

where r = radius of notch and ρ is the dimension AB, Fig. 4. Putting this value into (11),

$$L = 2\left[1 - \frac{r}{a}\frac{(1 - \cos\beta)}{(\cos\beta)}\right]^2 (2 + 3\sin\beta + \sin^2\beta)/(2 + \sin\beta)^2, \tag{21}$$

where β is found from $\partial L/\partial\beta = 0$.

Upper and lower bounds for the constraint factor are plotted in Fig. 10.

(d) *V-notched bars*

An upper bound solution has been found by GREEN (1953, 1956) and the lower bound has been given by LIANIS and FORD (1957), who also showed that experimental values of the constraint factor agree closely with the upper bound.

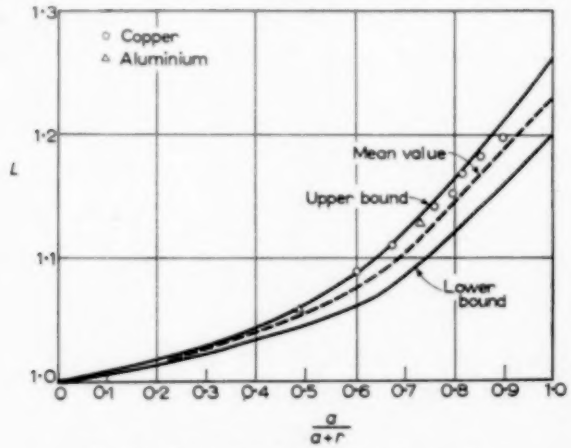

Fig. 10. Constraint factors, circular notch.

(e) *V-notched bars with circular fillets*

(1) *Solution I.* The slip-line field starting from P (the end of the circular fillet) consists of a family of logarithmic spirals, meeting the stress-free circular surface

in 45°, and it is completed as shown in Fig. 11. It can be shown that such a family fulfils all the properties of slip-lines. This solution is valid if the yield criterion is not violated in N. The jump in the hydrostatic pressure is

$$\Delta p = |P - P'_N| = k(2 + \pi - 2\gamma) \leqslant k\pi, \qquad \text{for} \qquad \tfrac{1}{2}\pi \geqslant \gamma \geqslant 1 = 57{\cdot}3°.$$

This solution is restricted more by the condition $d \geqslant 0$. It can be shown (see Fig. 11) that

$$\frac{d}{a} = \left[1 - \frac{r}{a}(\psi e^{\psi} + e^{\psi} - 1)\right] \Big/ (2 + \psi). \tag{22}$$

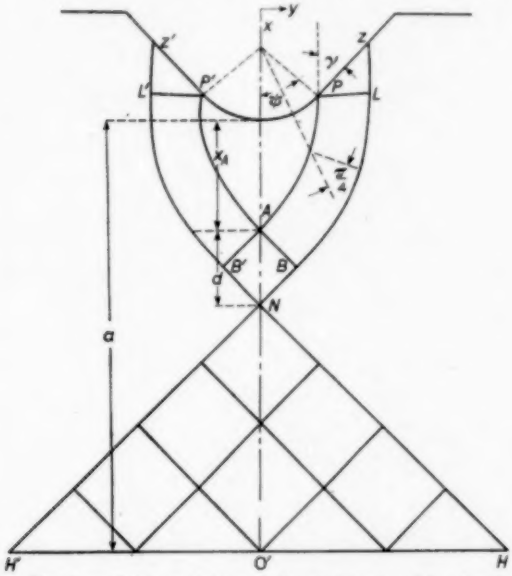

Fig. 11. Slip-line field, Solution I for V-notch with circular fillet.

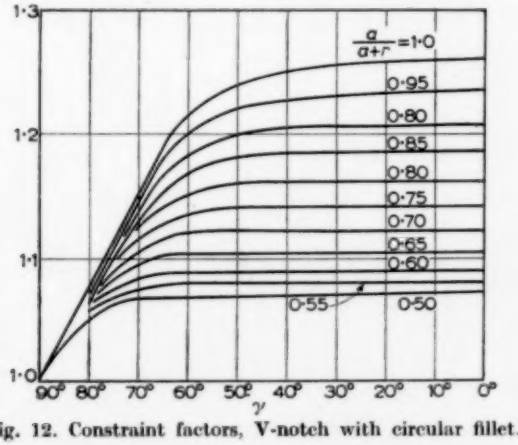

Fig. 12. Constraint factors, V-notch with circular fillet.

The equation for the constraint factor is too complicated to express analytically, but it is plotted in Fig. 12. For values of $a/(a + r)$ smaller than those for which $d/a = 0$, Solution I for circular notches holds.

Solution II in the upper part the field (logarithmic spirals) is extended inside the region $BCB'O$ (Fig. 13) where $\psi_2 = \frac{1}{2}\pi - 1 = 32{\cdot}1°$. The rest of the field is completed, as shown, to form a central pivot. The angle ψ_2 is given by $\psi_2 = \frac{1}{2}\pi - \gamma$. From the equilibrium conditions in the x- and y- directions along $OCDEFSO'$ the two unknowns c and R are determined. By calculating the moment

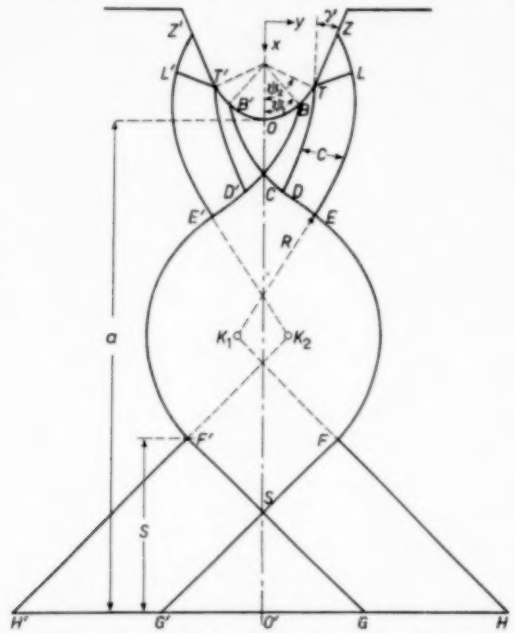

Fig. 13. Slip-line field, Solution II for V-notch with circular fillet.

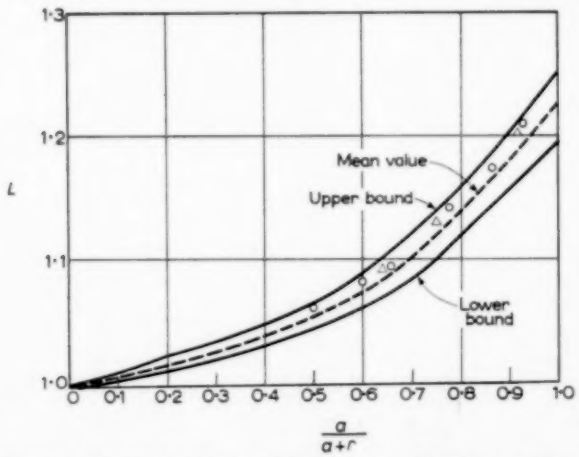

Fig. 14. Constraint factors, 30° V-notch with circular fillet.

of the stresses along the same path the constraint factor is calculated (Fig. 12) for various values of $a/(a + r)$. For values of γ smaller than those for which $c = 0$, Solution II of circular notches holds.

(ii) *Lower bound.* The stress trapezoid remains tangential to the circular root of the notch when $\gamma \leqslant \frac{1}{2}\pi - \beta$. For such angles the lower bound is calculated from (21) and remains constant for $\gamma \leqslant \frac{1}{2}\pi - \beta_{\max}$ where $\beta_{\max}$ is given by maximizing (21).

For $\gamma \geqslant \frac{1}{2}\pi - \beta_{\max}$ the sides of the trapezoid coincide with the oblique face of the notch and $\beta = \frac{1}{2}\pi - \gamma$. Whence

$$L = 2\left[1 - \frac{r}{a}\frac{(1-\sin\gamma)^2}{\cos\gamma}\right](2 + 3\cos\gamma + \cos^2\gamma)/(2+\cos\gamma)^2. \qquad (23)$$

In Fig. 14 both bounds and the experimental results for constant $\gamma = 30°$ are plotted.

4. Experimental Procedure

Two groups of tests have been carried out to confirm the theory experimentally. The first group was to measure the constraint factor, the second to check the slip-line field. Test pieces of high conductivity copper and commercially pure aluminium cold rolled to 30 per cent reduction, were used. Fig. 15 shows the type of stress–strain curve obtained. The metal showed a rapid change from elastic to plastic condition with a low workhardening rate. The yield stress in simple tension was taken as (a) copper, $Y = 22{\cdot}8$ tons/in^2 (b) aluminium, $Y = 8{\cdot}9$ tons/in^2. The Mises criterion, which is an approximation for copper and aluminium, was assumed. Both values of Y agree with the yield stress found by plane strain tests (Watts and Ford 1952-53) for 30 per cent reduction.

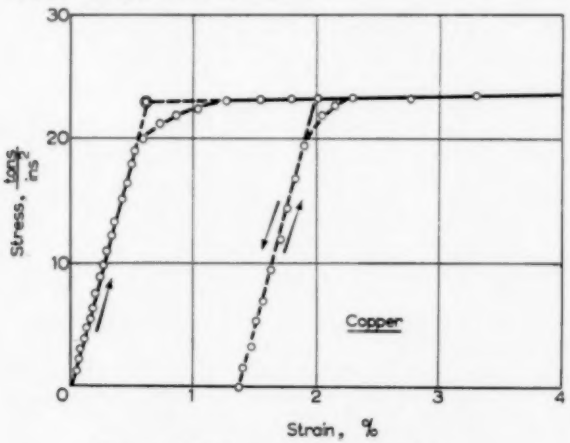

Fig. 15. Yield stress curve, aluminium.

The dimensions of the bars used were 3 in. × 1 in. for copper and 3 in. × 1¼ in. for aluminium. The notches were sufficiently deep so that plane strain conditions were ensured and the plastic zone did not spread to the un-notched part of the upper surface of the bar.

(a) *Constraint factor tests*

The specimens were subjected to four-point loading to give pure bending. The rig consisted of two pairs of steel rollers between which the test piece was placed, the deflexions being measured by dial gauges (Lianis and Ford 1957). The moment

Table 1. *Experimental results for single rectangularly notched bars*

Symbol	*Material*	*Dimensions* (in.)				M_y (tons. in.)		*L*		*Error* (%)
		$2b$	a	$2b/a$	W	*Theor.*	*Exp.*	*Theor.*	*Exp.*	
IR 1	*Copper*	0·064	0·793	0·087	3·1	16·00	15·9	1·194	1·185	− 0·9
IR 2		0·067	0·536	0·1275	2·875	6·36	6·35	1·165	1·163	− 0·2
IR 3		0·130	0·793	0·164	3·08	15·20	14·65	1·140	1·138	− 0·5
IR 4		0·140	0·610	0·223	2·89	8·00	7·87	1·113	1·111	− 0·2
IR 5		0·164	0·590	0·278	2·875	7·24	7·20	1·094	1·00	− 0·3
IR 6		0·189	0·606	0·312	2·880	7·57	7·55	1·083	1·080	− 0·3
IR 7	*Alum.*	0·250	0·725	0·345	2·95	4·22	4·20	1·070	1·065	− 0·5
IR 8		0·295	0·720	0·410	3·08	4·33	4·30	1·056	1·050	− 0·6
IR 9		0·3125	0·675	0·462	2·94	3·55	3·53	1·040	1·036	− 0·4
IR 10		0·3125	0·635	0·492	2·96	3·14	3·12	1·033	1·029	− 0·4

Table 2. *Experimental results for single trapezoidal notches (semiangle* $\gamma = 60°$)

Symbol	*Material*	*Dimensions* (in.)				M_y (tons. in.)		*L*		*Error* (%)
		$2b$	a	$2b/a$	W	*Theor.*	*Exp.*	*Theor.*	*Exp.*	
IT 1	*Copper*	0·125	0·833	0·130	2·930	15·32	15·25	1·145	1·140	− 0·4
IT 2		0·125	0·782	0·155	3·04	13·85	13·65	1·134	1·12	− 1·0
IT 3		0·125	0·625	0·200	2·930	8·60	8·35	1·114	1·109	− 0·5
IT 4		0·156	0·646	0·242	3·07	9·36	9·20	1·100	1·092	− 0·7
IT 5	*Alum.*	0·3125	0·996	0·295	2·98	8·15	8·10	1·080	1·075	− 0·45
IT 6		0·250	0·755	0·321	2·925	4·00	4·57	1·070	1·066	− 0·55
IT 7	*Copper*	0·250	0·705	0·355	2·930	10·13	10·1	1·060	1·057	− 0·30
IT 8	*Alum.*	0·3125	0·769	0·4065	2·790	4·37	4·4	1·047	1·04	− 0·7
IT 9	*Copper*	0·250	0·503	0·450	2·925	5·00	5·0	1·036	1·036	0

and deflexion could be accurately derived from the measurements. As soon as the limit moment was reached large deflexions occurred. The load remained constant, but the spring of the testing machine caused instability. To overcome this difficulty the load was increased a little above the desired value to cause rapid rotation of the indicator of the dial gauges and then left to decrease slowly until the rotation stopped. For deflexions well in the plastic region, however, continuous readings from the dial gauges under constant load were taken. By plotting the moment deflexion curve and extrapolating back to meet the elastic line the limit moment M_y was found. The constraint factor is given by

$$L = \frac{2\sqrt{3}\, M_y}{Ya^2 w}. \tag{24}$$

(b) *Preparation of test pieces*

Test pieces of length 1 ft were cut from 3 in. wide bars of copper and aluminium. Care was taken to ensure the accuracy of the dimension of the notches.

A series of V-cutters having semiangles 30°, 45°, 50°, 55°, 60°, 65°, 70° and 75° was used for the V, trapezoidal and V-notches with circular fillets together with radius cutters $R = \frac{1}{8}, \frac{1}{4}, \frac{3}{8}, \frac{1}{2}$, 1 in. For each case of single notched bars examined in the theory 9 – 10 specimens were prepared from both copper and aluminium. The exact notch dimensions were measured by a travelling microscope.

The bending direction was reversed in the single notched bars so that the notch was first opened and then closed to check the Bauschinger effect. No Bauschinger effect was found.

For tests on trapezoidal and fillet notches the angle of the notch was held constant and the ratios $2b/a$ and $a/(a + r)$ were varied since specimens with constant ratios and varying angles would be difficult to prepare to close tolerances.

The experimental results for the constraint factor are given in Tables 1 – 4 and Figs. 5, 9, 10 and 14, and generally lie within $1\frac{1}{2}$ per cent of the slip-line field results. These results confirm that the upper bound solution is the correct solution ; that the points lie slightly below the upper bound could easily be explained by the yield stress being a little overestimated.

As far as the deformation pattern is concerned another qualitative agreement with the theory has been found in single notched specimens. It has been shown in velocity field analyses that on the middle part GG' (Fig. 2) of the flat side of the bar the vertical component of the velocity is constant (Fig. 3). For a small initial deformation therefore the plane GG' must remain plane with two kinks at the points G', G, H' and H. Such a deformation picture has been detected in almost all the specimens, being particularly clear in Solution I where $H'H$ remained plane after a pronounced deformation with two distinct kinks on either side. The flat part of the rectangular and trapezoidal notches also remained plane in accordance with the hodograph. A more critical confirmation of the theory is found by examining experimentally the slip-line field as described below.

(c) *Slip-line field tests*

Preparation of the specimens ; grid measurements. If the bar is wide compared with the notch size, plane stress conditions are closely realized in the middle plane of the bar. It is necessary therefore to cut the test bar on its middle plane and scribe a reference on the cut face, afterwards joining the two pieces together to restore the continuity. The joint must be sufficiently strong to sustain the stresses

TABLE 3. *Experimental results for circularly notched bars*

Symbol	*Material*	*Dimensions* (in.)				M_y (tons. in.)		*L*		*Error* (%)
		r	*a*	$\frac{a}{a+r}$	*W*	*Theor.*	*Exp.*	*Theor.*	*Exp.*	
IC 1	*Copper*	0·0935	0·820	0·898	2·930	15·80	15·6	1·206	1·196	− 0·8
IC 2		0·0935	0·551	0·855	2·925	7·00	6·94	1·187	1·180	− 0·7
IC 3		0·0935	0·410	0·812	2·950	3·80	3·80	1·168	1·168	0
IC 4		0·1485	0·795	0·795	2·930	7·32	7·25	1·160	1·150	− 0·7
IC 5	*Alum.*	0·250	0·845	0·771	2·773	5·85	5·80	1·15	1·143	− 0·6
IC 6	*Copper*	0·250	0·753	0·750	2·485	4·21	4·21	1·17	1·17	0
IC 7	*Copper*	0·180	0·500	0·735	3·06	5·73	5·70	1·132	1·126	− 0·5
IC 8	*Alum.*	0·3125	0·828	0·727	2·156	5·63	5·57	1·133	1·127	− 0·5
IC 9	*Copper*	0·180	0·360	0·6735	2·95	2·81	2·76	1·112	1·095	− 1·5
IC 10		0·2345	0·350	0·600	2·92	2·60	2·60	1·088	1·088	0
IC 11	*Alum.*	0·500	0·490	0·495	2·785	1·83	1·82	1·080	1·057	− 0·2

TABLE 4. *Experimental results for single V-notches with circular fillets (semiangle* $\gamma = 30°$)

Symbol	*Material*	*Dimensions* (in.)				M_y (tons. in.)		*L*		*Error* (%)
		r	*a*	$\frac{a}{a+r}$	*W*	*Theor.*	*Exp.*	*Theor.*	*Exp.*	
1*CV*1	*Copper*	0·0625	0·830	0·930	2·880	15·90	15·8	1·219	1·210	− 0·75
1*CV*2	*Alum.*	0·0625	0·669	0·915	2·800	3·88	3·85	1·211	1·205	− 0·5
1*CV*3	*Copper*	0·125	0·8445	0·871	2·980	16·63	16·4	1·192	1·175	− 1·4
1*CV*4	*Copper*	0·125	0·443	0·780	2·880	4·30	4·25	1·153	1·143	− 0·9
1*CV*5	*Alum.*	0·3125	0·9315	0·750	2·890	7·32	7·25	1·140	1·13	− 0·9
1*CV*6	*Copper*	0·250	0·480	0·657	2·980	5·01	4·95	1·107	1·092	− 1·0
1*CV*7	*Alum.*	0·250	0·458	0·647	2·96	1·765	1·75	1·104	1·095	− 0·9
1*CV*8	*Copper*	0·500	0·750	0·600	2·880	11·61	11·56	1·090	1·084	− 0·55
1*CV*9	*Copper*	0·500	0·500	0·500	2·880	5·07	5·05	1·070	1·063	− 0·65

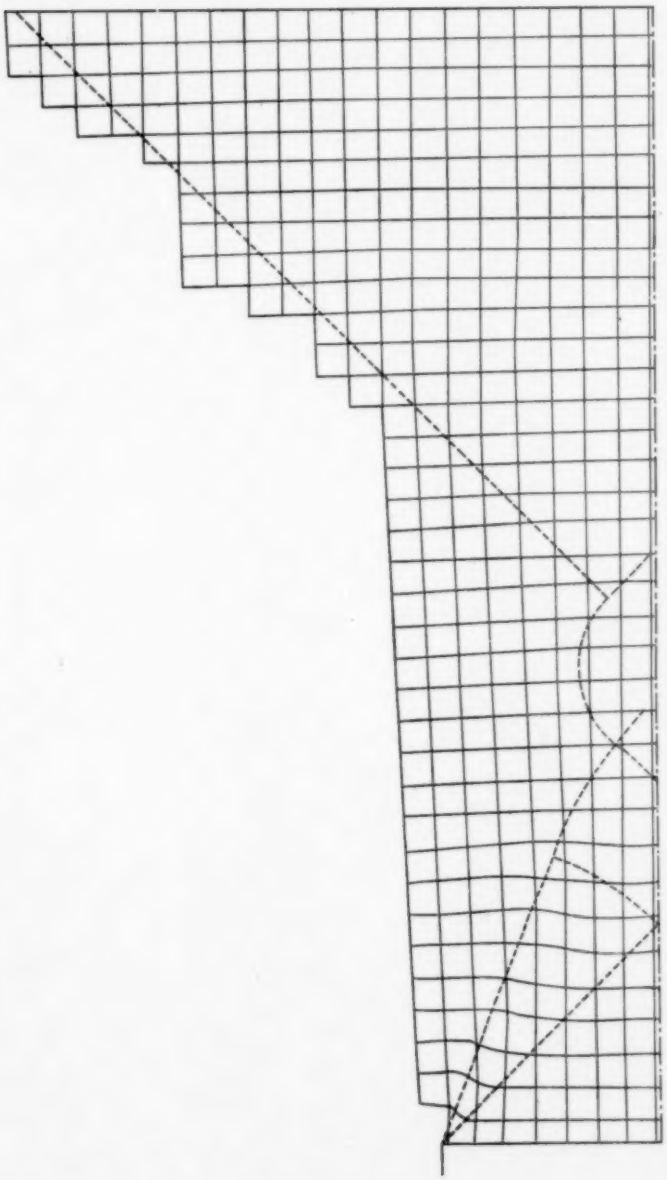

Fig. 16. Deformed grid, rectangular notch, $2b = 0{\cdot}295$in., $a = 0{\cdot}720$in.

developed during the loading. A new method of achieving these conditions was developed, using the cold rolled aluminium.

The specimens were cut in the middle plane and both surfaces were mirror polished after grinding. A square grid 0·020 in. × 0·20 in. was scribed on one surface and its accuracy checked by measuring nodal points with a micrometer microscope, having an accuracy of 0·00005 in. A thin layer of "Redux" was spread on both surfaces, the two pieces pressed together, and afterwards placed in an oven and heated to 150°C for 15 min. After cooling, the notch was cut and the specimen was bent through $4-5°$. The joint proved strong enough to withstand the stresses. The unscribed half of the specimen was removed by careful machining and the grid surface was cleaned from the glue layer by grinding. Finally the co-ordinates at the nodal points were again measured.

The method of calculation used is due to Ellis (to be published).

Results of the tests

During bending the notch shape changes, the slip-line following the deformation pattern. For a $4-5°$ angle of bending, however, the initial and final fields do not differ appreciably. The slip-line field for the following cases were constructed.

(i) *Rectangular notch. Solution II.* The dimensions of the specimen are $2b = 0{\cdot}295$ in., $a = 0{\cdot}720$ in. In Fig. 16 the deformed grid is shown. The intense shear near the corners of the notch is apparent from the locally broken grid lines, which also indicate the circular fan, while inside the hinge the grid remains unaltered. It is apparent also that the grid outside the plastic domain has undergone a simple rotation around the hinge and the deformation does not extend appreciably beyond the elastic–plastic interface. The measured maximum shear directions agree closely (within $2-3°$) with the theoretical slip-line directions.

(ii) *Trapezoidal notch. Solution I.* The dimensions of the bar were $2b = 0{\cdot}3125$ in., $a = 0{\cdot}769$ in., $\gamma = 60°$. Fig. 17 shows the maximum shear directions. They agree within $2-3°$ with the theoretical slip-line field. From the deformed grid (not reproduced) the broken grid lines near the corner of the notch show the intense shear due to the centred fan. The grid near the theoretical neutral point remained undeformed, having undergone a rigid body motion. Measurements taken along the flat side of the bar show that the part inside the plastic region remains plane with two kinks at the points of the elastic–plastic boundary.

(iii) *Circular notch. Solution II.* The dimensions of the bar were $r = 0{\cdot}250$ in., $a = 0{\cdot}750$ in. In Fig. 18 the slip-line field is shown. The maximum shear directions agree very well with the directions of the logarithmic spirals of the slip-lines and with the directions of the hinge boundary. The agreement in the lower part of the field is less satisfactory. This is due to inaccurate measurements, because in that part it was difficult to remove the Redux layer neatly.

(iv) *V-notch with circular fillet. Solution II.* The slip-line dimensions of the specimen are $r = 0{\cdot}0625$ in., $a = 0{\cdot}669$ in., $\gamma = 30°$. The field direction (Fig. 19) along the hinge boundary and in the lower compressive zone is in excellent agreement with the theory since the deformation does not affect appreciably its size.

(v) *V-notch.* The results for a 25° V-notch were given by Lianis and Ford (1957). Fig. 20 here shows the actual grid and illustrates the intense shear around the hinge surface and the undistorted region within the hinge.

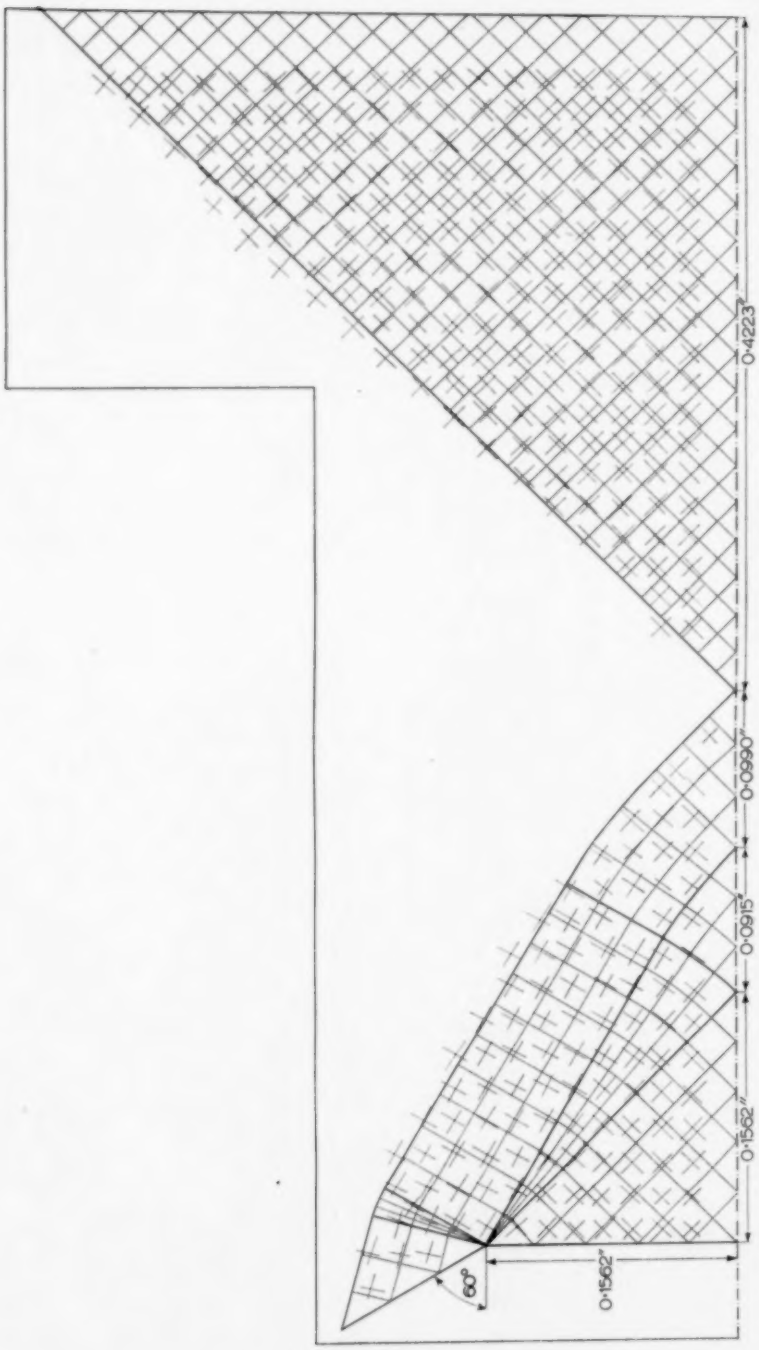

Fig. 17. Directions of maximum shear, trapezoidal notch, $2b = 0{\cdot}312$in., $a = 0{\cdot}709$in., $\gamma = 60°$.

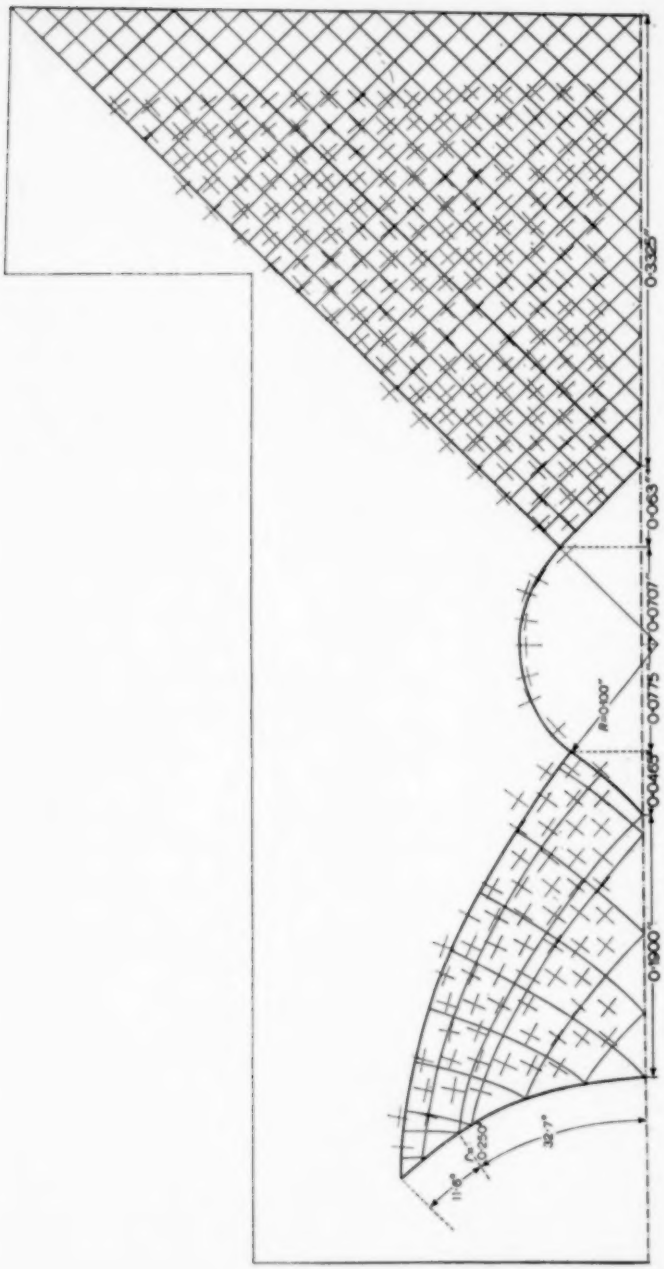

Fig. 18. Directions of maximum shear, circular notch, $r = 0{\cdot}250$in., $a = 0{\cdot}750$in.

Although upper and lower bound solutions have been found for the constraint factor, the experimental results both for the constraint factor and the point-by-point deformation pattern support the view that the slip-line fields (upper bounds) are the complete solution for the cases examined.

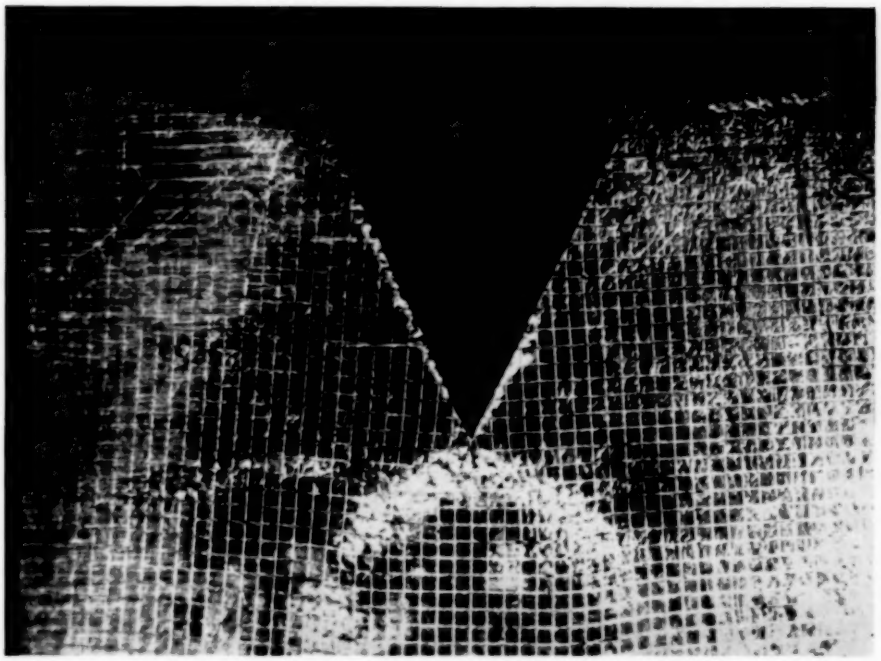

Fig. 20. Photograph of exposed grid, 25° V-notch.

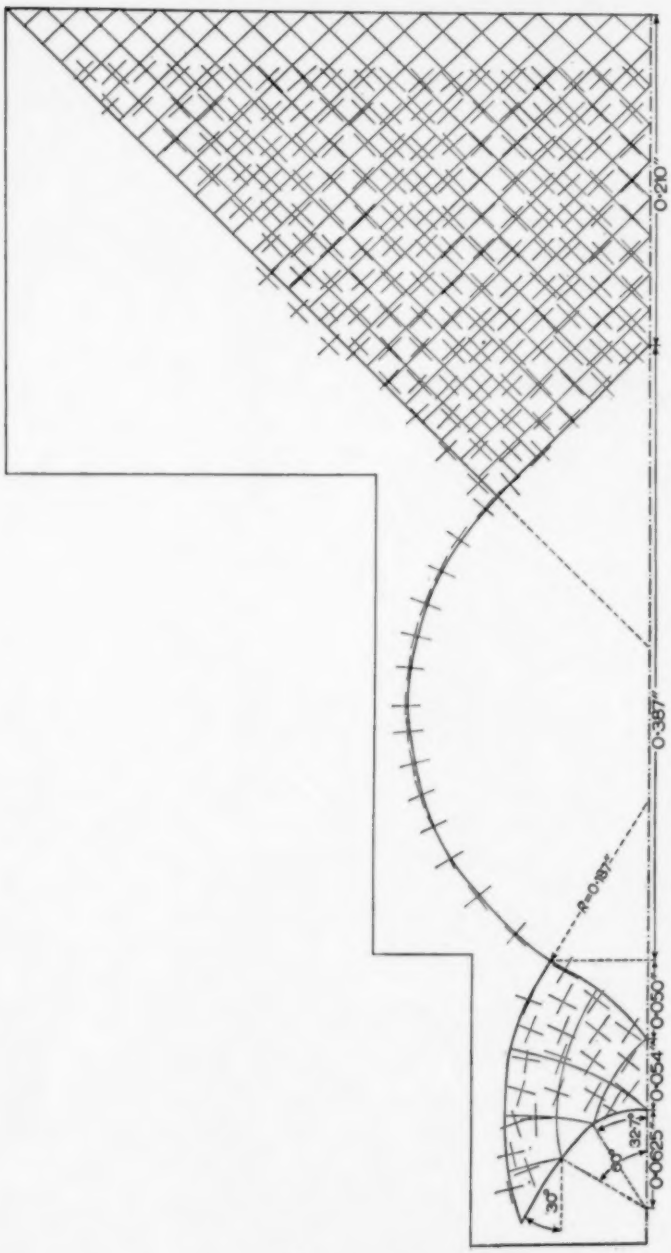

Fig. 19. Directions of maximum shear, 30° V-notch with circular fillet, $r = 0{\cdot}062$in., $a = 0{\cdot}669$in.

References

Bishop, J. F. W.	1953	*J. Mech. Phys. Solids* **2**, 43.
Bishop, J. F. W., Green, A. P. and Hill, R.	1956	*J. Mech. Phys. Solids* **4**, 156.
Ford, H.	1952-53	*Proc. Instn. Mech. Engrs.* **1 B**, 448.
Green, A. P.	1953	*Quart. J. Mech. Appl. Maths.* **6**, 223.
	1956	*J. Mech. Phys. Solids* **2**, 128.
Hill, R.	1950	*The Mathematical Theory of Plasticity* (Clarendon Press, Oxford).
	1954	*J. Mech. Phys. Solids* **2**, 278.
Lianis, G. and Ford, H.	1957	*Proc. 9th Int. Congr. Appl. Mech.* **8**, 235.
Watts, A. B. and Ford, H.	1952	*Proc. Inst. Mech. Eng.* **1 B**, 448.

Journal of the Mechanics and Physics of Solids, 1958, Vol. 7, pp. 22 to 30. Pergamon Press Ltd., London

ON THE USE OF LINEARIZED YIELD CONDITIONS FOR COMBINED STRESSES IN BEAMS*

By R. Sankaranarayanan and P. G. Hodge, Jr.
Illinois Institute of Technology

(*Received 22nd April, 1958*)

Summary

Yield criteria expressed in terms of stress resultants are obtained for typical engineering structures, using the first fundamental theorem of limit analysis. These yield criteria, which are often non-linear, are then replaced by inscribed piecewise linear approximations. The complete solutions based on these approximate yield criteria provide lower bounds ; the corresponding values for the upper bound can be obtained by multiplying the lower bound values by a suitable factor. A few examples are worked out to illustrate the simplicity achieved in determining the collapse load.

1. Introduction

The limit analysis of plane frames has been carried to a high degree of perfection, and the theory is being increasingly accepted by structural engineers as a means of determining the load carrying capacities for this class of structures. The relative simplicity of plane frame analysis is due to the fact that only one stress resultant, the bending moment, is considered. Although a general theory is available for more complex structures which must be described by two or more stress resultants, relatively few applications have been made as yet. One difficulty arising in these problems is that the yield criterion expressed in terms of generalized stresses is, in general, non-linear. Therefore, exact determination of the limit load involves considerable effort. However, reasonably close upper and lower bounds can be found if the yield condition is replaced by one that is piecewise linear. This linearized yield surface has the obvious advantage of simplifying both the yield function and the flow rule for the various plastic regimes. Thus the solution of important problems is made much simpler, with little resulting loss in accuracy. The errors introduced by this approximation may always be reduced through refinements in the yield polyhedron, and may, in some cases, be estimated.

2. Limit Analysis

The general concepts of limit analysis of statically indeterminate beams

*The investigation leading to the results in this paper was begun under the sponsorship of the Office of Naval Research while the authors were at the Polytechnic Institute of Brooklyn; it was concluded at the Illinois Institute of Technology under the sponsorship of the National Science Foundation. The paper is part of a thesis submitted by one of the authors (RS) in partial fulfillment of the requirements for the degree of Doctor of Philosophy in Mechanics at the Illinois Institute of Technology.

and frames were first formulated by GREENBERG and PRAGER (1951). The analysis was extended to perfectly plastic bodies of arbitrary shape under general conditions of loading and support by DRUCKER *et al.* (1952), who assumed that, up to the critical load intensity, the influence of the deformation on the equilibrium conditions could be neglected. An alternative approach was pointed out by HILL (1951) who considered a rigid, perfectly plastic body and defined as critical the load intensity at which the first deformation occurred. A general theory of limit analysis, using the concept of the generalized plastic potential and applying to perfectly plastic continua, was given by PRAGER (1955).

A rigid, perfectly plastic material can be defined as follows. If the generalized stresses Q_i are such that a certain function $f(Q_1, Q_2, \ldots, Q_n)$ is less than one, the material is rigid. If f is equal to one, the material may flow with associated generalized strain rates q_i of indefinite magnitude, but subject to the plastic potential flow law (MISES 1928)

$$q_i = \lambda \partial f / \partial Q_i, \qquad i = 1, 2, \ldots, n \tag{1}$$

where λ is a positive scalar factor. Finally, the material will not support stress combinations such that $f > 1$.

The yield condition and flow law can be given a convenient geometrical interpretation in a space with simultaneous stress and strain-rate co-ordinates Q_i and q_i. The yield surface is defined by $f(Q_1, Q_2, \ldots, Q_n) = 1$; it is assumed to be convex (DRUCKER 1951). If the stress point with co-ordinates Q_i is on the yield surface, the flow law states that the generalized strain-rate vector with components q_i is in the direction of the normal to the yield surface at the stress point. For a non-linear yield surface this implies that the plastic strain-rates depend explicitly upon the stresses. Thus, in general, the stress and velocity equations for any particular problem must be considered simultaneously. However, the normal to a linear surface has the same direction at all points, so that once a choice has been made of which linear surface is appropriate, the stress relations and velocity relations can be considered independently. Thus, for example, in a problem which has three stress and three strain-rate components, we may deal with one set of three equations and three unknowns and another set of two equations in two unknowns (the magnitude of the strain rates is undetermined), rather than a combined set of five equations in five unknowns. At an intersection of two linear surfaces, an additional restriction is placed upon the stress point, whereas the velocity vector has an additional degree of freedom. Thus stress and velocity equations are still independent, and the total number of equations is still the same. Similar results hold at the intersection of more than two linear surfaces. Therefore, a piecewise linear yield condition possesses some of the advantages of a linear theory. Also, the errors introduced by such an approximation may always be reduced through refinements in the yield polyhedron.

The relation between a solution based on an approximate yield surface and the solution based on the exact yield surface can be clarified by means of the theorems of limit analysis. These theorems may be stated in the following form :

Theorem I : If a stress-field can be found which is in equilibrium with the given load and satisfies the yield restriction, the load is at or below the collapse load. Such a stress-field is called statically admissible.

Theorem II: If, for any considered deformation pattern, the rate at which work is done by the external forces exceeds the rate of internal dissipation, then the load is at or above the collapse load. The considered deformation field is called kinematically admissible.

It follows immediately from the limit analysis theorems that a yield surface which circumscribes the exact one gives a value of the collapse load equal to or greater than the actual one, whereas an inscribed yield surface gives a collapse load equal to or less than the correct value. A lower bound on the collapse load is obtained by using the theorem I with an inscribed yield surface, whereas use of the theorem II with a circumscribed yield surface provides an upper bound. On the other hand, merely satisfying equilibrium with a circumscribed figure or computing dissipation rates from an inscribed figure gives an approximate result which cannot be identified as either an upper or a lower bound. However, a value which is exact for an inscribed surface provides a lower bound while that for a circumscribed one provides an upper bound on the collapse load. Thus, to obtain upper and lower bounds on the collapse load of a given structure, it would be necessary to solve the problem once according to the lower bound yield curve and once according to the upper. If the exterior approximation is geometrically similar to the inscribed one, both upper and lower bounds can be obtained from a single solution. Indeed, if the ratio of the magnitudes of the two surfaces is $1/\alpha$, it is obvious that the corresponding values of the collapse load will also be in the ratio $1/\alpha$.

In the examples to follow, exact solutions for inscribed yield functions will be found for various problems. These problems have all been considered elsewhere (HEYMAN 1951, 1952); our purpose in considering them at present is to show the relative simplicity achieved by using the piecewise linear approach. Since inscribed polygons are used, the collapse loads so determined represent lower bounds on the true carrying capacities; if upper bounds are desired, they are easily found by the above method.

3. Combined Bending and Torsion of Beams

If a beam is subjected to combined bending and torsion, appropriate generalized stresses are the dimensionless bending and twisting moments $m = M/M_0$ and $t = T/T_0$, respectively. Here M_0 and T_0 are the fully plastic moments under pure bending and pure torsion, respectively. The associated generalized strain-rates are the bending rate θ about the neutral axis and $\psi = \beta x$ where x is the physical angle of twist and $\beta = T_0/M_0$.

The exact determination of the yield curve in terms of m and t involves the solution of a non-linear differential equation. However, HILL and SIEBEL (1951) and GAYDON and NUTTALL (1957) have given techniques for finding inscribed and circumscribed curves. Results for a circular and square section are shown in Fig. 1. Details of the latter are due to STEELE (1954).

The present treatment is based on a conservative octagonal approximation to the inscribed curve, as shown by curves (3) in Fig. 1. Evidently any solutions so obtained will be lower bounds on the actual solution for any cross-section. If upper bounds are desired, they may be obtained by using a similar octagon exterior to the circumscribed curve as shown by curves (4) in Fig. 1.

The equations of the sides of the octagonal yield curve and the flow rule for each side are given in Table 1. Also shown is the internal energy dissipation rate

$$D = M_0 (m\theta + t\psi).$$

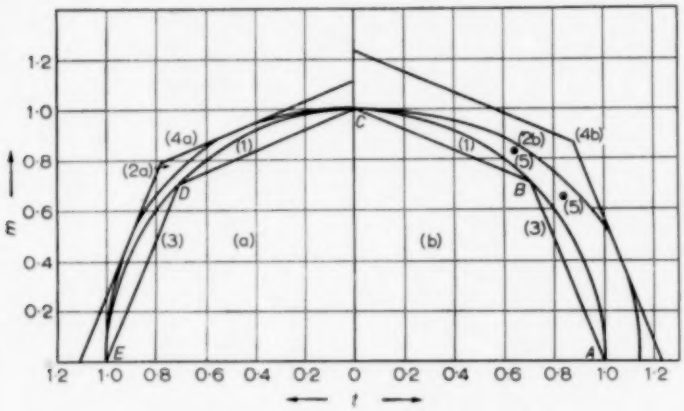

Fig. 1. Interaction curves for bending and torsion.

Curves:

(a) Circular bar
(b) Square bar
(1) Lower bound (HILL and SIEBEL 1951)
(2) Upper bound (STEELE 1954)
(3) Piecewise linear lower bound
(4) Piecewise linear upper bound
(5) Numerically computed points

TABLE 1. *Flow rule and energy dissipation for combined bending and torsion according to piecewise linear interaction curve*

Side	*Equation*	θ/ψ	D/M_0
AB	$(\sqrt{2}-1)\,m + t = 1$	$(\sqrt{2}-1)$	ψ
BC	$m + (\sqrt{2}-1)\,t = 1$	$(\sqrt{2}+1)$	θ
CD	$m - (\sqrt{2}-1)\,t = 1$	$-(\sqrt{2}+1)$	θ
DE	$(\sqrt{2}-1)\,m - t = 1$	$-(\sqrt{2}-1)$	$-\psi$
EF	$-(\sqrt{2}-1)\,m - t = 1$	$(\sqrt{2}-1)$	$-\psi$
FG	$-m - (\sqrt{2}-1)\,t = 1$	$(\sqrt{2}+1)$	$-\theta$
GH	$-m + (\sqrt{2}-1)\,t = 1$	$-(\sqrt{2}+1)$	$-\theta$
HA	$-(\sqrt{2}-1)\,m + t = 1$	$-(\sqrt{2}-1)$	ψ

In Sections 4 and 5 a few illustrative examples are worked out using the piecewise linear yield condition. These examples reveal the simplicity achieved in the solution of practical problems by using the piecewise linear approach. In these examples we make the usual assumption that the deformations are small compared with the over-all dimensions of the structure, so that it is permissible to satisfy the equilibrium equations in the undeformed rather than in the deformed configuration.

4. BENDING OF AN ANGLE BENT LOADED PERPENDICULAR TO ITS PLANE

As a first example, let us consider a right-angle bent carrying the load P at the midpoint of one leg from a built in end of the beam of arbitrary cross-section as shown in Fig. 2 (a). HEYMAN

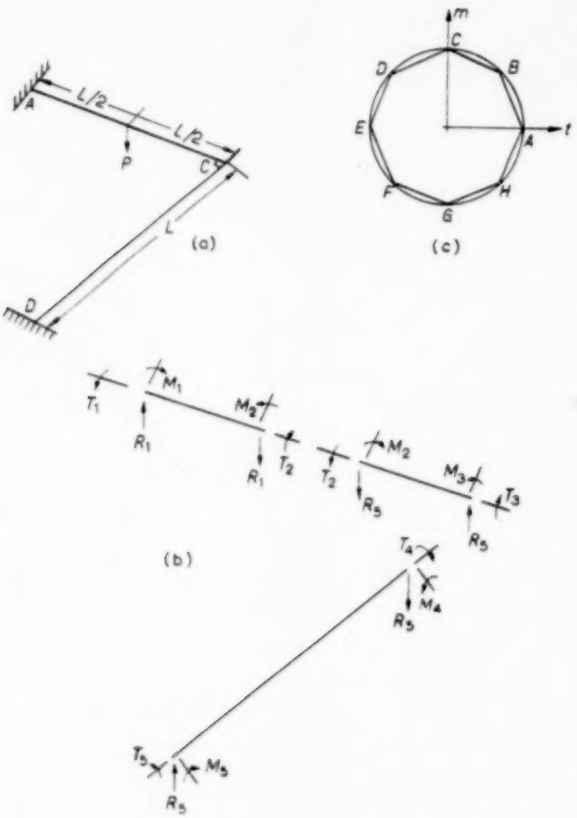

Fig. 2. (a) Loaded bend (b) Free body diagram
(c) Circular interaction curve and the corresponding piecewise linear approximation.

(1951) has considered this problem for a uniform cross-section of box form, using the circular interaction curve. There it was found that the solution of even such a simple problem leads to two non-linear algebraic equations ; more complicated problems would involve prohibitive work. We will show that by using the piecewise linear approximation, the solution is obtained relatively easily for a variety of cross-sections.

With reference to Fig. 2 (a), overall equilibrium considerations show that the torque is constant along either leg of the bent, but may have different values on the two legs. On the other hand, the moment will vary linearly from A to B, from C to B, and from D to C. It follows that the only possible locations for the yield hinges are the points A, B, C and D. The hinge at C may be on either leg. Therefore, we draw a free body diagram as indicated in Fig. 2 (b).

Using dimensionless quantities defined by

$$m_i = M_i/M_0, \qquad t_i = T_i/T_0, \qquad \beta = T_0/M_0$$
$$r_i = LR_i/M_0, \qquad \rho = LP/M_0, \tag{2}$$

we may write the following equilibrium equations

$$t_1 = t_2 = t_3 = m_4/\beta, \qquad t_4 = t_5 = m_3/\beta \tag{3a, b}$$

$$v_1 = 2\,(m_2 - m_1), \qquad v_5 = 2\,(m_2 - m_3) = m_4 - m_5 \tag{3c, d, e}$$

$$p = v_1 + v_5 \tag{3f}$$

The strain-rate variables at each of the five possible hinges must satisfy certain compatibility relations. If v_i denotes the upward vertical displacement, then it must have the same value computed from either end of the bent. Therefore

$$v_1/L = \theta_5 + \varkappa_5 + \varkappa_4 + \theta_3 + (\tfrac{1}{2}\,\theta_2) = 0,$$

$$v_2/L = \tfrac{1}{2}\,\theta_1 = \theta_5 + (\tfrac{1}{2})\,(\varkappa_5 + \varkappa_4 + \theta_3),$$

$$v_3/L = \theta_1 + \tfrac{1}{2}\,\theta_2 = \theta_5,$$

$$v_5/L = \theta_1 + \varkappa_1 + (\tfrac{1}{2})\,\theta_2 + \varkappa_2 + \varkappa_3 + \theta_4 = 0.$$

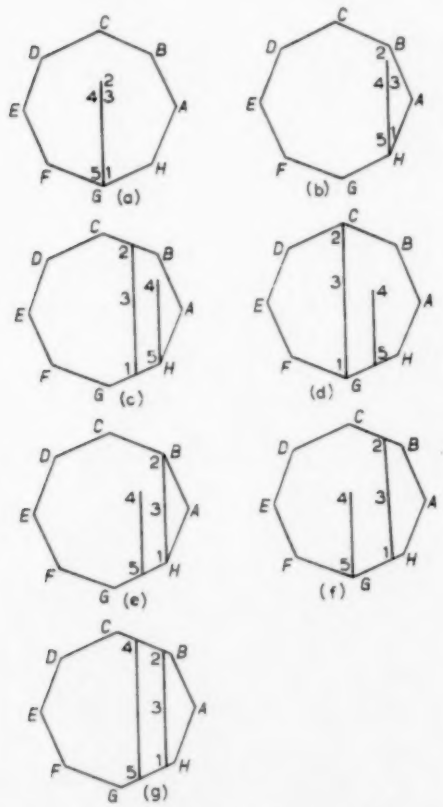

Fig. 3. Stress profiles for right-angle bent.

It is readily verified that only three of the above four equations are independent. On introducing the strain-rate variable $\psi = \beta\,\varkappa$, the independent relations can be written in the form

$$\beta\,(\theta_5 + \theta_3 + \tfrac{1}{2}\,\theta_2) + (\psi_4 + \psi_5) = 0, \tag{4a}$$

$$\theta_1 + \tfrac{1}{2}\,\theta_2 - \theta_5 = 0, \tag{4b}$$

$$\beta\,(\theta_1 + \tfrac{1}{2}\,\theta_2 + \theta_4) + (\psi_1 + \psi_2 + \psi_3) = 0. \tag{4c}$$

The strain-rate variables being known, the collapse load is determined from the principle of virtual work. The external rate of energy dissipation is

$$D_l/M_0 = (PL/M_0)(-v_1) = -\tfrac{1}{2}\rho\theta_1 \tag{5}$$

The actual mode of collapse depends on the value of the parameter β. For very small values of β, we would expect practically no resistance to torsion. Let us first investigate the extreme case when there is no twisting moment in either leg. It then follows from (3) that

$$t_1 = t_2 = t_3 = t_4 = t_5 = m_3 = m_4 = 0. \tag{6a}$$

Therefore the stress profile lies entirely on the m axis in Fig. 3(a). Evidently hinges must form at points A and D in order for there to be any motion. Therefore,

$$m_1 = m_5 = -1 \tag{6b}$$

The remaining moment, the reactions and the loads can now be computed to be

$$m_2 = \tfrac{1}{2}, \qquad v_1 = 3, \qquad v_5 = 1, \qquad \rho = 4. \tag{6c, d, e, f}$$

Evidently the stress distribution defined by equations (6) is statically admissible for all values of β. Therefore, (6f) furnishes a lower bound on the collapse load for all cases.

In order to determine the conditions under which (6) represents the desired solution, we must investigate the velocity pattern. Since there are hinges only at the built in ends of the beam, all strain-rates vanish except at points 1 and 5. It then follows from (4) that

$$\psi_1 = \psi_5 = -\beta\theta_1 = -\beta\theta_5. \tag{6g}$$

The internal rate of dissipation of energy is given by

$$D_i/M_0 = -\theta_1 - \theta_5 = -2\theta_1. \tag{6h}$$

Equating this value to the external energy (5) we regain (6f) for the collapse load. However, the velocity distribution is kinematically admissible only if the strain-rate vectors at the hinges are normal to the yield curve. Since the stress points are at a corner, the strain-rate vectors must lie between the limiting normals corresponding to sides FG and GH. Reference to Table 1 shows that this condition will be satisfied as long as

$$-\psi_1/\theta_1 = \beta \leqslant (\sqrt{2} - 1) = 0{\cdot}414 \tag{7}$$

Therefore, the solution (6) is valid provided β satisfies (7).

For β slightly larger than $(\sqrt{2} - 1)$, the strain-rate vectors at points 1 and 5 both exceed the limits set by side GH. This suggests various possibilities for the stress profile in such cases. We shall first assume that both vectors do, in fact, point in the direction predicted by (6). This implies that the stress points 1 and 5 are now at point H in the yield octagon. The corresponding stress profile is shown in Fig. 3(b). It may readily be verified that the solution for this case is

$$m_1 = m_5 = -1/\sqrt{2}, \quad m_3 = m_4 = \beta/\sqrt{2}, \quad m_2 = (1 + 3\beta)/2\sqrt{2},$$

$$t_1 = t_2 = t_3 = t_4 = t_5 = 1/\sqrt{2}, \tag{8a}$$

$$\psi_1 = \psi_5 = -\beta\theta_1 = -\beta\theta_5,$$

$$\psi_2 = \psi_3 = \psi_4 = \theta_2 = \theta_3 = \theta_4 = 0, \tag{8b}$$

$$\rho = 2\sqrt{2}(\beta + 1). \tag{8c}$$

The strain-rate vector at points 1 and 5 must satisfy

$$-(\sqrt{2} + 1) \leqslant \psi_1/\theta_1 \leqslant -(\sqrt{2} - 1),$$

and hence

$$(\sqrt{2} - 1) \leqslant \beta \leqslant (\sqrt{2} + 1). \tag{9a}$$

Equation (9a) is the condition that the solution be kinematically admissible. It will also be statically admissible if m_2, m_3 and m_4 are each less than $1/\sqrt{2}$ in magnitude. It is easily seen that the condition $m_2 \leqslant 1/\sqrt{2}$ is the most stringent of these ; it leads to

$$\beta \leqslant 1/3. \tag{9b}$$

Comparison of inequalities (9a) and (9b) shows that the above solution is never valid. However, the inequality (9b) shows that for β larger than $(\sqrt{2}-1)$, $m_2 > 1/\sqrt{2}$, suggesting that the stress profile 1-2 extends from the side GH to side BC, with hinges at both points 1 and 2, in addition to the hinge at point 5. Thus we are led to a three hinge mechanism with hinges at 1, 2 and 5; the corresponding stress profile is shown in Fig. 3(c). Under these conditions, the solution of equations (3) is

$$m_2 = -m_1 = \frac{5 - 3\sqrt{2} - \beta}{2(\sqrt{2}-1) + \beta},$$

$$t_1 = t_2 = t_3 = m_4/\beta = \frac{1}{\sqrt{2}} \frac{\sqrt{2} - 1 - 2\beta}{2(\sqrt{2}-1) + \beta}, \tag{10a}$$

$$t_4 = t_5 = m_3/\beta = 1/\sqrt{2}, \quad m_5 = -1/\sqrt{2},$$

$$p = \frac{\sqrt{2}\left[-\beta^2(\sqrt{2}+1) + \beta(3\sqrt{2}+10) + 3\right]}{\beta(\sqrt{2}+1) + 2}. \tag{10b}$$

Next, it follows from the assumed stress profile and Table 1 that

$$\theta_1 = -(\sqrt{2}+1)\psi_1, \qquad \theta_2 = (\sqrt{2}+1)\psi_2,$$
$$\theta_3 = \theta_4 = \psi_3 = \psi_4 = 0.$$

Substituting these values in the compatibility equations, we can solve for all the strain-rate quantities in terms of ψ_2, the results being

$$\psi_1 = \frac{\beta(\sqrt{2}+1) + 2}{2\left[\beta(\sqrt{2}+1) - 1\right]}, \qquad \psi_3 = \psi_4 = 0,$$

$$\psi_5 = \frac{(\sqrt{2}+1)\beta\left[4 - \beta(\sqrt{2}+1)\right]}{2\left[\beta(\sqrt{2}+1) - 1\right]}\psi_2, \tag{10c}$$

$$\theta_1 = -(\sqrt{2}+1)\frac{2 + \beta(\sqrt{2}+1)}{2\left[\beta(\sqrt{2}+1) - 1\right]}\psi_2, \qquad \theta_2 = (\sqrt{2}+1)\psi_2,$$

$$\theta_3 = \theta_4 = 0, \qquad \theta_5 = -\frac{3(\sqrt{2}+1)}{2\left[\beta(\sqrt{2}+1) - 1\right]}\psi_2.$$

It may be verified that the substitution of these values into (5) and (6h) again yields (10b) for the collapse load.

If equations (10) are to be the solution, they must be both statically and kinematically admissible. This requires that the stresses be such that point 2 is on the finite side BC (note that this also guarantees that point 1 is on side GH), m_3 lies between m_1 and m_2, and point 4 is in the interior of the hexagon. In view of equations (10a) these requirements may be written

$$\frac{1}{\sqrt{2}} \leqslant \frac{\beta(3\sqrt{2}-2) + (\sqrt{2}-1)}{\sqrt{2}\,\beta + (4 - 2\sqrt{2})} \leqslant 1, \tag{11a}$$

$$-\frac{\beta(3\sqrt{2}-2) + (\sqrt{2}-1)}{\sqrt{2}\,\beta + (4-2\sqrt{2})} \leqslant \frac{\beta}{\sqrt{2}} \leqslant \frac{\beta(3\sqrt{2}-2) + (\sqrt{2}-1)}{\sqrt{2}\,\beta + (4-2\sqrt{2})}, \tag{11b}$$

$$-\frac{1}{\sqrt{2}} \leqslant \frac{\beta}{\sqrt{2}} \frac{2\sqrt{2} - 1 - 2\beta}{2(\sqrt{2}-1) + \beta} \leqslant \frac{1}{\sqrt{2}}. \tag{11c}$$

In addition, the strain-rate vectors must be such that ψ_1, ψ_2 and ψ_5 are all positive, and the vector at point 5 lies between the normals to GH and HA. Taking ψ_2 as positive by definition we see that ψ_1 is positive if

$$\beta \geqslant (\sqrt{2}-1). \tag{11d}$$

With this restriction, θ_5 is negative ; hence the condition $\psi_5 > 0$ is included in the restriction that the vector at point 5 should have the proper direction, i.e.

$$-(\sqrt{2}+1) \leqslant (\beta/3)\left[\beta(\sqrt{2}+1)-4\right] > -(\sqrt{2}-1). \tag{11e}$$

It can be easily verified that of all the inequalities (11a, b, c, e) the most restrictive one is given by the right-hand side of (11a) which requires point 1 not to extend beyond G, and this reduces to

$$\beta \leqslant 0{\cdot}914. \tag{12}$$

Inequalities (11d) and (12) give the range of values of β for which the above solution is valid.

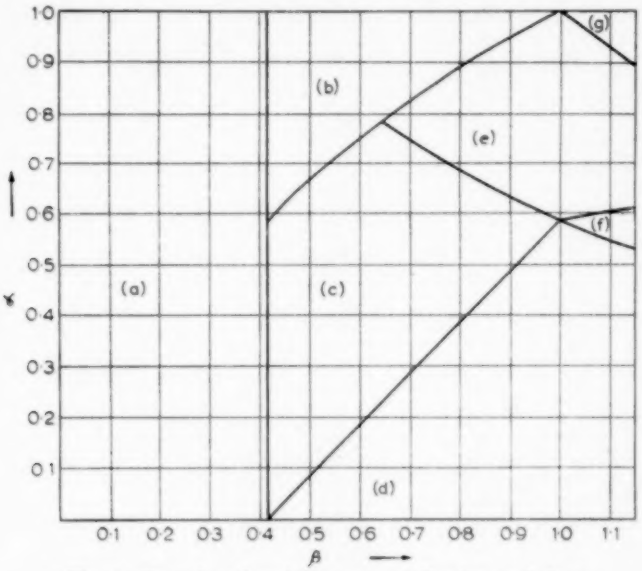

Fig. 4. Domains of various stress profiles for angle bent.

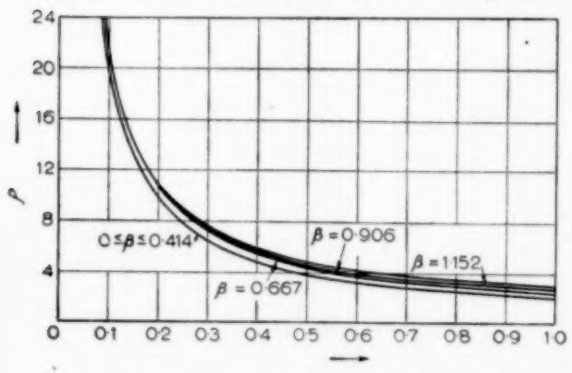

Fig. 5. Collapse load for angle bent.
Three square-grid.

For values of $\beta > 0{\cdot}914$ inequality (11a) suggests that the hinges at the points 1 and 2 are at the corners G and C respectively. With this configuration, the equilibrium equations will not be satisfied if we retain the hinge at 5 at the corner H. Accordingly we move the point 5 to side GH, and we are led to the stress profile shown in Fig. 3(d). The collapse load for this case turns out to be

$$\rho = 2\left[\frac{5(\sqrt{2}+1)\beta - 3}{2(\sqrt{2}+1)\beta - 1}\right]. \tag{13}$$

It can be easily verified that with this value of the collapse load, all the requirements on the stresses and the strain-rate vectors are satisfied for all $\beta \geqslant 0{\cdot}914$.

A similar analysis may be made for the more general case in which the load is applied at an arbitrary distance αL from the end of the beam. For certain values of α, other stress profiles are encountered as shown in Fig. 3. Fig. 4 shows the domain of validity of the different profiles in an $\alpha - \beta$ plane. The parenthetical letters in Fig. 4 refer to the correspondingly labelled stress profiles in Fig. 3. Fig. 5 shows the collapse load as a function of the load position α for various shape factors β. Evidently, the shape factor β has relatively little effect on the collapse load. Values of β for typical sections are shown in Table 2. Details of the general solution are reported elsewhere (HODGE 1958).

TABLE 2. *Values of the shape factor β for typical sections*

Section	β	
	TRESCA *material*	VON MISES *material*
square	0·67	0·77
circle	0·79	0·91
ideal box-beam	1·00	1·15

5. BENDING AND TORSION IN SQUARE GRIDS

As a second example we consider the bending and torsion of grids. This problem was first treated by HEYMAN (1952) who used the circular yield condition.

As before, we shall use the piecewise linear yield condition to analyse a three by three grid carrying a concentrated load P on each of its nine joints. In general, hinges can form at either end of each member of the grid. Due to symmetry only eight of these hinges are independent as shown in Fig. 6 (a). The most general symmetric deformation pattern is shown in Fig. 6 (b). The geometry is evidently defined by the vertical displacements of C, D and O; alternatively, it may be specified by the angles ϕ_1, ϕ_2 and ϕ_3. However, in addition, the bars AD and DC may undergo independent twists, ϕ_4 and ϕ_5, respectively. Due to symmetry there can be no twist in bars BC and BO. Finally, it is convenient to denote the rotations of the joints D and C about the line AA by ϕ_6 and ϕ_7, respectively.

The bending angle θ and the twisting angle x may now be given in terms of $\phi_1, \ldots, \phi_7$. Each angle ϕ_i, including the joint rotation, is measured from the undeformed position. Thus

$$\begin{aligned}
\theta_1 &= -\phi_1, & x_1 &= -\phi_4 \\
\theta_2 &= -(\phi_1 + \phi_2), & x_2 &= 0 \\
\theta_3 &= -\phi_7 + \phi_1 + \phi_2, & x_3 &= 0 \\
\theta_4 &= \phi_7 - \phi_3, & x_4 &= 0 \\
\theta_5 &= \phi_2, & x_5 &= \phi_5 - \phi_7 \\
\theta_6 &= -\phi_8 + \phi_1, & x_6 &= \phi_4 - \phi_6 \\
\theta_7 &= \phi_6 - \phi_2, & x_7 &= \phi_6 - \phi_5 \\
\theta_8 &= \phi_3, & x_8 &= 0
\end{aligned} \tag{14}$$

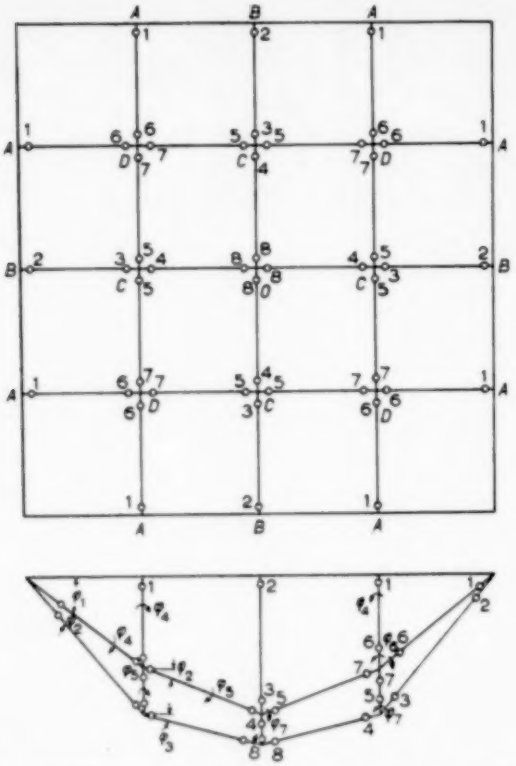

Fig. 6 (a). Location of yield hinges. (b) General collapse mechanism.

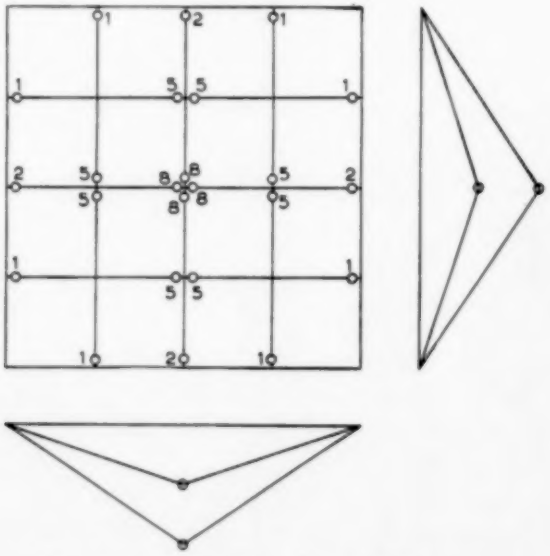

Fig. 6 (c). Deformation pattern without twist.

Subscripts on θ and x refer to the corresponding hinges in Fig. 6. All hinge angles, both bending and twisting, are taken as positive when their application to the out board end of a beam span tends to lower the grid centre.

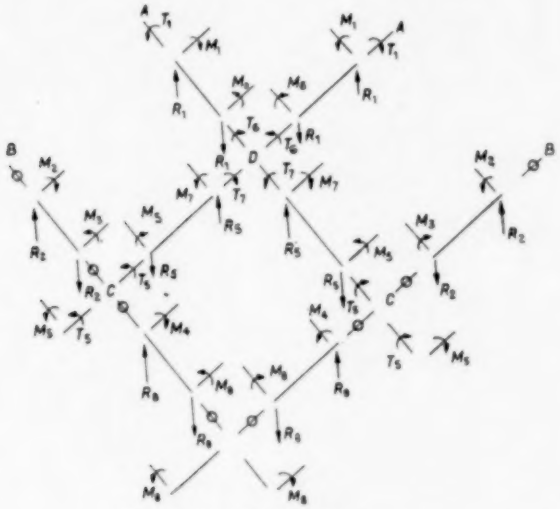

Fig. 6 (d). Free body diagram.

A general approach to the solution of this problem is to choose a one parameter deformation pattern and equate the internal and external work. The external work is given by

$$D_e = 4Pv_D + 4Pv_C + Pv_O = P(9\phi_1 + 5\phi_2 + \phi_3) \tag{15}$$

The internal work must be computed for each assumed stress profile according to Table 1.

The deformation pattern, in the absence of twist is shown in Fig. 6 (c). If there is little torsional rigidity, i.e. if β is small, we might expect the deformation pattern of Fig. 6 (c) to be still valid. This implies that there are hinges only at points 1, 2, 5 and 8. Therefore, θ and x must both vanish at the other four hinges. It follows from (14) that

$$\phi_1 = \phi_2 = \phi_4 = \phi_5 = \phi_6 = \phi$$

$$\phi_3 = \phi_7 = 2\phi \tag{16a}$$

so that the entire deformation is given in terms of the single parameter ϕ by

$$\begin{aligned} \theta_1 &= -\phi, & \psi_1 &= -\beta\phi \\ \theta_2 &= -2\phi, & \psi_2 &= 0 \\ \theta_5 &= \phi, & \psi_5 &= -\beta\phi \\ \theta_8 &= 2\phi, & \psi_8 &= 0 \end{aligned} \tag{16b}$$

all other angles vanishing.

The corresponding stress profile is shown in Fig. 7 (a). Evidently strain-rate vectors for hinges 2 and 8 are vertical, but those at hinges 1 and 5 are inclined towards the negative t axis. Therefore, this solution is valid only so long as

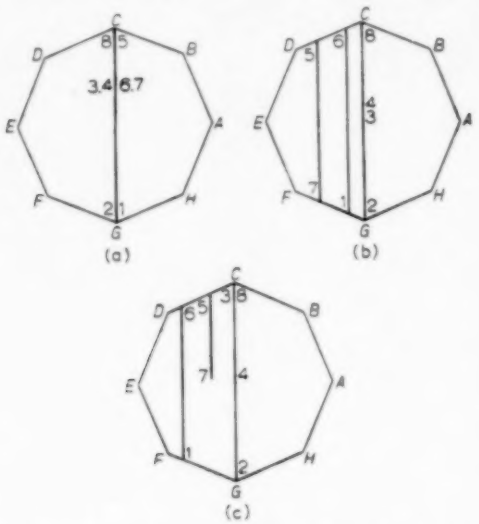

Fig. 7. Assumed stress profiles for three bar grid.

these vectors do not pass the normals to FG and CD, respectively. In view of Table 1,

$$\psi_1/\theta_1 = \beta \leqslant \sqrt{2} - 1 = 0{\cdot}414$$

Thus the solution provides an upper bound for all

$$0 \leqslant \beta' \leqslant 1 \tag{17}$$

where we have defined

$$\beta' = (\sqrt{2} + 1)\,\beta = 2{\cdot}414\,\beta. \tag{18}$$

The collapse load is obtained by the principle of virtual work. From Table 1 and (16), we see that

$$D_i = M_0(-8\theta_1 - 4\theta_2 + 8\theta_5 + 4\theta_2) = 32M_0\,\phi$$
$$D_e = 16\,Pl\,\phi$$

hence

$$\rho \equiv Pl/M_0 = 2 \tag{19}$$

is a kinematically admissible value for all β' satisfying (17).

In order to ensure that (19) is the exact solution we must construct a statically admissible stress field. It follows from equilibrium of the free body diagram in Fig. 6 (d) that the following relations must hold between the bending moments, twisting moments, and reactions:

$$\left.\begin{aligned} &T_1 = T_6, \qquad lR_1 = M_6 - M_1, \qquad lR_2 = M_3 - M_2 \\ &T_5 = T_7, \qquad lR_5 = M_5 - M_7, \qquad lR_8 = M_8 - M_4 \\ &2R_2 - 2R_5 = R_2 + 2R_5 - R_8 = 4R_8 = P \\ &T_6 + M_6 = T_7 + M_7, \qquad M_3 + 2\,T_5 = M_4 \end{aligned}\right\} \tag{20}$$

We may eliminate all of the reactions except

$$\nu = R_5\, l/M_0$$

from (20) and write the results in the form

$$\left.\begin{aligned} &t_1 = t_6, \qquad m_6 - m_1 = \rho/2 + \nu, \qquad m_3 - m_2 = 5\rho/4 - 2\nu \\ &t_7 = t_5, \qquad m_5 - m_7 = \nu, \qquad m_8 - m_4 = \rho/4 \\ &\beta\,(t_6 - t_7) + m_6 - m_7 = 0, \qquad m_3 - m_4 + 2\,\beta\, t_5 = 0 \end{aligned}\right\} \tag{21}$$

Equations (21) must hold for any stress profile. For the particular profile shown in Fig. 7 (a)

$$-m_1 = -m_2 = m_5 = m_8 = 1, \quad t_1 = t_3 = 0 \tag{22a}$$

Therefore, it follows from (21) that

$$m_3 = m_4 = m_6 = m_7 = \tfrac{1}{2}, \quad \rho = 2 \tag{22b}$$

The value of ρ is, of course, the same as that given by (19). Since all the moments are equal or less than one in magnitude, the stress profile is within or on the yield curve. Thus the stress distribution is statically admissible for all values of β; therefore, $\rho = 2$ is the correct value of the collapse load for all values of $\beta' > 1$.

To find a solution for $\beta' > 1$, we observe that the present solution breaks down because the strain-rate vectors at hinges 1 and 5 are no longer in an admissible direction for the corners G and C, respectively, and suggests that these hinges should be on sides GF and CD, respectively. However, it follows from Table 1 and equations (16a) that such a change will impose two additional relations upon the parameters ϕ_i. Therefore, we must introduce new hinges so as to eliminate two of (16a), thus leaving us with a single degree of freedom. Two possible stress profiles which do this are shown in Figs. 7 (b) and 7 (c). It turns out that the stress profile Fig. 7 (c) provides the desired solution for all $\beta' > 1$. The final results are

$$\begin{aligned}
&\phi_1 = (1 + \beta')\,\phi, \qquad \phi_2 = \phi_5 = \phi_6 = 2\phi \\
&\phi_3 = \phi_7 = 2\,(\beta' + 1)\,\phi/\beta', \qquad \phi_4 = -(\beta' + 1)\,\phi/\beta' \\
&\theta_1 = -(\beta' + 1)\,\phi, \qquad \psi_1 = -(\sqrt{2} - 1)\,(\beta' + 1)\,\phi \\
&\theta_2 = -(\beta' + 3)\,\phi, \qquad \psi_2 = 0 \\
&\theta_3 = (\beta'^2 + \beta' - 2)\,\phi/\beta', \quad \psi_3 = 0 \\
&\theta_5 = 2\,\phi, \qquad \psi_5 = -2\,(\sqrt{2} - 1)\,\phi \\
&\theta_6 = (\beta' - 1)\,\phi, \qquad \psi_6 = -(\sqrt{2} - 1)\,(\beta' - 1)\,\phi \\
&\theta_8 = 2\,(\beta' + 1)\,\phi/\beta', \qquad \psi_8 = 0 \\
&\theta_4 = \theta_7 = \psi_4 = \psi_7 = 0 \\
&-m_1 = m_6 = (\tfrac{9}{16})\,\rho - (\tfrac{1}{2}), \quad t_1 = t_6 = (\sqrt{2} + 1)\left[(\tfrac{9}{16})\,\rho - \tfrac{3}{2}\right] \\
&-m_2 = m_3 = m_8 = 1, \qquad m_4 = 1 - \rho/4, \qquad t_2 = t_3 = t_4 = t_8 = 0 \\
&m_5 = 1 - \rho/(8\,\beta'), \qquad t_5 = t_7 = -(\sqrt{2} + 1)\,(\tfrac{1}{8})\,\rho \\
&m_7 = 2 - \rho\,(1 + 5\,\beta')/(8\,\beta') \\
&\rho = \frac{8\,\beta'\,(3\,\beta' + 5)}{9\beta'^2 + 21\beta' + 2}
\end{aligned} \tag{23}$$

This solution may be shown to be both statically and kinematically admissible for all $\beta' > 1$. Fig. 8 shows the resulting collapse load of a three-square grid as a function of β'.

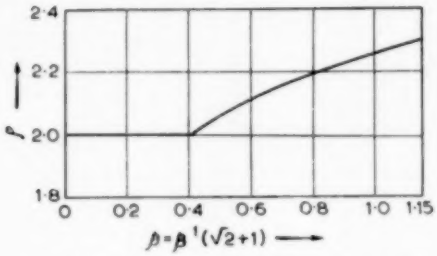

Fig. 8. Collapse load for three bar grid.

6. CONCLUSIONS

In order to keep the discussion simple, we have considered only relatively simple applications of the application of piecewise linear yield conditions to beam problems. Obviously, the savings in labour will become greater when more complex problems are considered. For example, HODGE and SANKARANARAYANAN (1958) have considered the angle bent of Fig. 2 when the load is applied at an arbitrary angle to the plane of the frame. In this case, two bending moments must be considered, since the moment is not applied in a plane of symmetry. To the authors' knowledge, the solution to the problem according to the non-linear yield curve is not known.

Other beam problems which have been solved by piecewise linear theory include the case of combined bending and tension in curved arches (ONAT and PRAGER 1953a) and plane frames (ONAT and PRAGER 1953b). It is planned to consider the most general case of combined bending in two planes, torsion, and axial force.

REFERENCES

DRUCKER, D. C.	1951	*Proc. 1st U.S. Nat. Congr. Appl. Mech.* 487.
DRUCKER, D. C., PRAGER, W. and GREENBERG, H. J.	1952	*Quart. Appl. Math.* **9**, 381.
GAYDON, F. A. and NUTTALL, H.	1957	*J. Mech. Phys. Solids* **6**, 17.
GREENBERG, H. J. and PRAGER, W.	1951	*Proc. A. S. C. E.* **77**, Sep. No. 59.
HEYMAN, J.	1951	*J. Appl. Mech.* **18**, 157.
	1952	*J. Appl. Mech.* **19**, 153.
HILL, R.	1951	*Phil. Mag.* **42**, 868.
HILL, R. and SIEBEL, M. P. L.	1951	*Phil. Mag.* **42**, 722.
HODGE, P. G.	1958	*Plastic Analysis of Structures* (McGraw Hill).
HODGE, P. G. and SANKARANARAYANAN, R.	1958	*The Determination of Safe Loads of Beams Subjected to Combined Bending, Bending, and Twisting Moments*, Technical Report DOMIIT 1–2, Department of Mechanics, Illinois Institute of Technology.
VON MISES, R.	1928	*Z. ang Math. Mech.* **8**, 161.
ONAT, E. T. and PRAGER, W.	1953a	*J. Mech. Phys. Solids* **1**, 77.
	1953b	*Proc. 1st Midw. Conf. Solid Mech.* 40.
PRAGER, W.	1955	*Proc. 8th Int. Congr. Theo. Appl. Mech.* **2**, 65.
STEELE, M.C.	1954	*J. Mech. Phys. Solids* **3**, 156.

Journal of the Mechanics and Physics of Solids, 1958, Vol. 7, pp. 37 to 44. Pergamon Press Ltd., London

EXPERIMENTS IN THE COLD EXTRUSION OF RODS OF NON-CIRCULAR SECTION

By W. Johnson
Department of Mechanical Engineering, University of Manchester

(*Received 29th January*, 1958)

Summary

Experiments in the extrusion of pure lead and tellurium lead rods of circular, square, rectangular triangular and I section form are described. These investigate the effects of section shape and punch speed on the necessary extrusion load, and on the nature of the flow of metal within the extruded rod. It is shown that, for a given reduction in area, the load is independent of section shape for all but re-entrant shapes and increases with increase in extrusion speed.

1. Introduction

In earlier papers (Johnson 1957; Dodeja and Johnson 1957), it was shown that the pressure to cause the extrusion of one or more cylindrical rods from a single solid cylindrical slug could be closely predicted. It was demonstrated that the pressure was primarily dependent on the total reduction in area achieved, and a functional relationship between these two was established such that, if a stress–strain curve of the extruded material was available, the necessary load could easily be calculated. This paper presents results of experiments in the extrusion of pure lead, tellurium lead and super-pure aluminium rods of non-cylindrical section in order to attempt to extend the general understanding of the extrusion process. The principal aim of the investigation was to ascertain the effect of the shape of an extrusion as a variable, and this was done by comparing the extrusion loads required to form variously shaped sections when the total reduction remained constant.

Secondary aims of the investigation were to examine flow patterns and coring patterns for the various shapes, and to observe the effect of speed on the loads attained when all other variables were constant.

Previous work on the effect of orifice shape on extrusion pressure when the reduction in area is constant is implied in work on multi-hole extrusions, but, excepting this, the only other explicit statement seems to be that contained in a British Patent, Number 779603 (1955). An empirical formula and method of estimating extrusion pressure is patented, the patentees recommending that this be increased by about 10 – 20 per cent for I sections and the like.

There appears to be little useful reference to flow and flow patterns for non-circular sections, apart from that of Sukolski (1956) on the extrusion of equal angle-sections and that of Smith and Swindell (1954) who described some of

the elements in die design aimed at securing 'even . . . rates of flow in different parts of a (non-uniform) section.'

Work on the effect of punch speed on extrusion load for the same range of speed as here has been given by THOMSEN (1957) for plane-strain and circular extrusions. The results presented in this paper corroborate THOMSEN's in their general form and, as far as load is concerned, show that section shape and speed of operation are independent variables.

2. EXPERIMENTAL

The form and details of the apparatus have been fully described in a previous paper (DODEJA and JOHNSON 1957). The dies used in this work were of heat-treated B.K.V. steel of the same overall dimensions as the previous ones and were again square and sharp-edged. The die shapes investigated were round, square,

TABLE 1.

Shape of section	*Reduction, r*	*Dimensions* (in.)			*Perimeter* (in.)
Circular	0·75		*d* 0·50		1·57
Triangular		*a*	*r*		
	0·75	0·673	0·388		2·02
	0·938	0·335	0·193		1·00
Rectangular		*b*	*d*		
	0·5	0·900	0·436	$b/d \simeq 2$	2·67
		0·762	0·513	$b/d \simeq 1{\cdot}5$	2·55
	0·75	0·636	0·318	$b/d \simeq 2$	1·89
		0·542	0·361	$b/d \simeq 1{\cdot}5$	1·81
Square	0·5		*d* 0·626		2·50
	0·75		0·443		1·77
	0·938		0·220		0·88
I section		*l*	*t*	*h*	
	0·75	0·500	0·125	0·535	2·41
	0·84	0·435	0·106	0·355	2·50
	0·86	0·375	0·094	0·390	2·50

rectangular, triangular and I section, all the orifices being symmetrically located with respect to the cylinder container. Details of the orifice proportions, reduction and shape are given in Table 1 and Fig. 1.

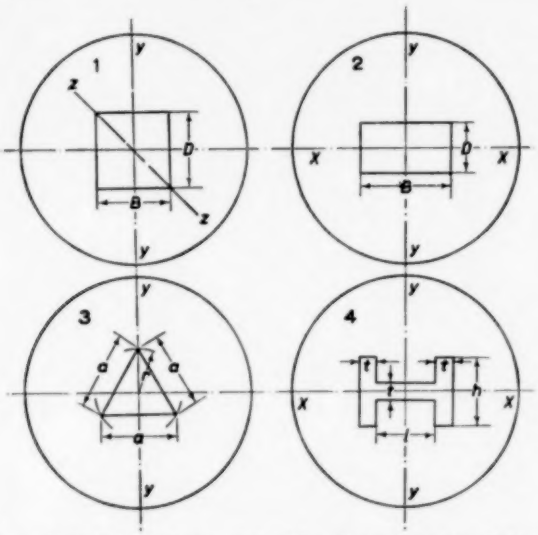

Fig. 1. Showing die shapes and orifice dimensions (see Table 1).

The materials extruded were pure lead, 0·065 per cent tellurium lead and super-pure aluminium. The pure lead was divided into two batches : one batch was annealed for 30 min in boiling water, and the other batch, which was not heat-treated, was used for the speed tests. The test specimens used for load measuring experiments were cylindrical blocks, 1 in. diameter and 1·3 in. long, supplied in the form of extruded rod 1 in. diameter. The load throughout the tests was recorded at intervals of 0·05 in. of punch travel, for distances of about 1·1 in. The hydraulic testing machine used was controlled to advance at the requisite speed of 0·1 in/min using a dial gauge and a stop watch. This means of controlling the punch speed was successful after passing the maximum load, which with lead occurs earlier in the operation, and it was not difficult with care and practice to control the operation manually up to punch speeds of 0·42 in/min.

3. Results

Most of the experiments performed were well lubricated forward extrusions and typical punch load/punch travel diagrams are shown in Figs. 2 (a) to (d). The true extrusion load is that load which is applied (over the whole of the punch) at the onset of coring ; it is clearly marked in the various Figures. Repeat tests usually agreed to within about 3 per cent.

(i) *Pressure and die shape*

In Table 2 the extrusion load for a punch speed of 0·1 in/min for some of the five reductions and the various shapes investigated, is given ; the load is stated to the nearest 0·05 tons, for loads greater than 2 tons.

TABLE 2.

Reduction r	*Shape*	*Extrusion load* (tons) *Pure lead*	*Tellurium lead*	*S.P. aluminium*
0·5	*Square*	1·69	2·60	8·0
	Rectangle $b/d = 1·5$	1·72	2·65	7·8
	Rectangle $b/d = 2·0$	1·72	2·65	8·0
0·75	*Circle*	2·70	4·35	
	Square	2·70	4·35	
	Rectangle $b/d = 1·5$	2·75	4·40	
	Rectangle $b/d = 2·0$	2·70	4·40	
	Triangle	2·75	4·35	
	I section	2·90	4·60	
0·84	*I section*	3·60	5·70	
0·860	*I section*	3·85	6·00	
0·938	*Square*	4·80	7·75	
	Triangle	4·75	7·95	

There are three immediate observations :—

(a) With the two kinds of lead, the true extrusion load is fairly clearly definable, i.e. the coring point is easily identifiable, and it is true to say that for all the shapes with the exception of the I section, which are convex and comparatively squat sections, the load is independent of the shape and wholly dependent on the reduction in area within the limits of experimental repeatability.

(b) The I section or re-entrant shape requires, in these experiments, a 5 – 10 per cent higher load than does the squat section of the same reduction.

A small number of tests with unlubricated specimens on the 0·75 reduction shapes increased the load in all cases by 6 – 8 per cent.

(c) Aluminium true extrusion pressures are not so easy to derive from an autographic diagram, especially for the smaller reductions, since the coring point is not clearly in evidence. In Fig. 2 the autographic diagrams for super-pure aluminium are shown for $r = 0·5$ for the square and rectangular sections. It will be observed that not only is the coring point indistinct so that it is difficult to define precisely what the extrusion pressure is, but also that the diagram shape changes slightly with the form being extruded. The point remains, however, that the load does not significantly alter with changes in squat section shape.

(ii) *Variation of load with punch speed*

Lubricated tests were performed with the second batch of pure lead and tellurium lead, to determine how the extrusion load altered with the speed of the punch

and the shape of the extruded section. As was to be expected from the earlier experiments at each particular punch speed, only the I section shapes produced definite increases in load when the reduction was constant. Thus, in Fig. 3 (a),

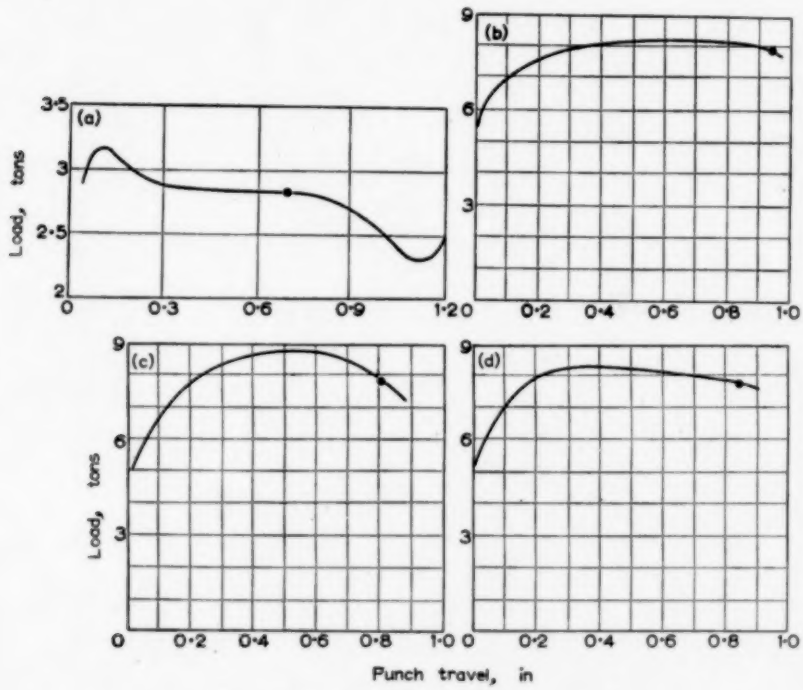

Fig. 2. Typical load/punch travel diagrams.
● Coring point.
(a) lubricated pure lead ; $r = 0{\cdot}75$.
(b) lubricated super-pure aluminium ; $r = 0{\cdot}5$, $b/d \simeq 2$.
(c) lubricated super-pure aluminium ; $r = 0{\cdot}5$, $b/d \simeq 1$.
(d) lubricated super-pure aluminium ; $r = 0{\cdot}5$, $b/d \simeq 1{\cdot}5$.

results of load versus punch speed for lead, with $r = 0{\cdot}75$ for I section shapes, plot as one distinct curve while the square and circular shapes give a different, lower, common curve ; Fig. 3 (a) includes results for $r = 0{\cdot}938$ and a triangular section extrusion. Fig. 4 shows similar results for square tellurium lead extrusions with $r = 0{\cdot}938$ and $0{\cdot}5$.

Both Figs. 3 (a) and 4 show quite clearly that, when extruding with both kinds of lead, for a given increment in speed, the effect on the load is more pronounced the slower the operation ; also the smaller the speed, the lower the load. These results corroborate those of Thomsen (1957) who performed experiments with pure lead to obtain reverse circular extrusions ; for comparison, his results are reproduced graphically as Fig. 3 (b).

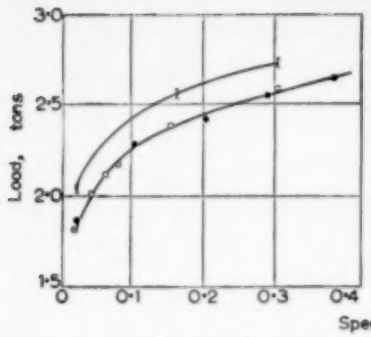

Fig. 3 (a) i

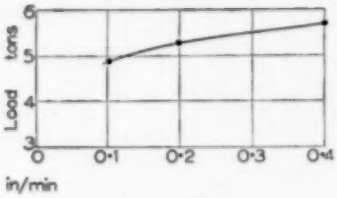

Fig. 3 (a) ii

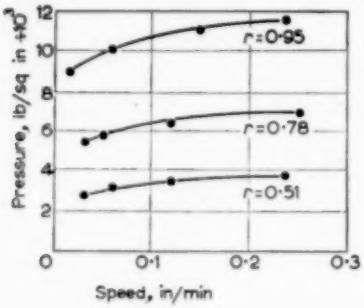

Fig. 3 (b)

Fig. 3. Showing the effect of punch speed on load :

(a) pure lead

(i) $r = 0{\cdot}75$; upper curve obtained with I section die ; lower curve obtained with square (□) and circular (●) dies.

(ii) $r = 0{\cdot}938$, results obtained with triangular die.

(b) THOMSEN's results for pure lead ; reverse circular extrusions.

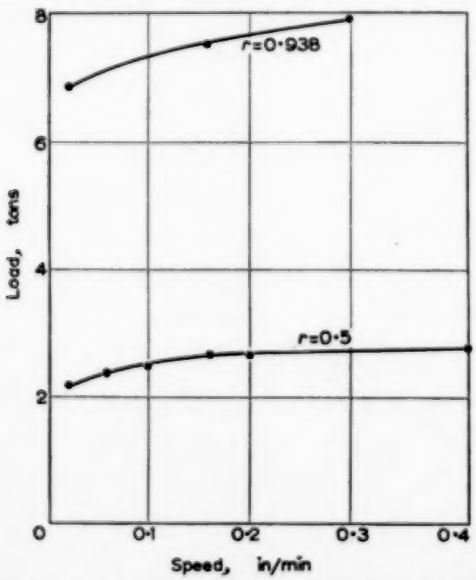

Fig. 4. Showing the effect of punch speeds on load for tellurium lead extruded through square dies ; $r = 0{\cdot}938$.

(i)

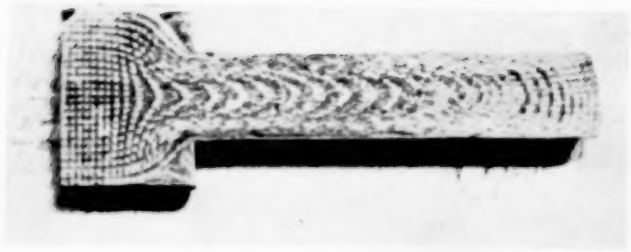

(ii)

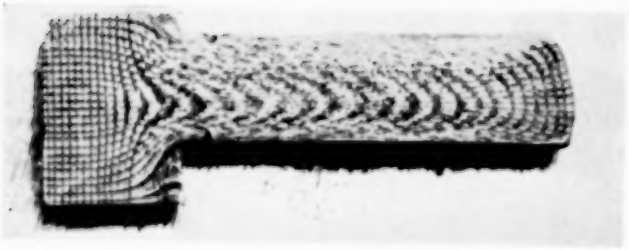

(iii)

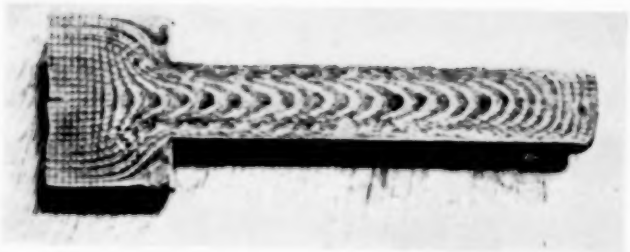

(iv)

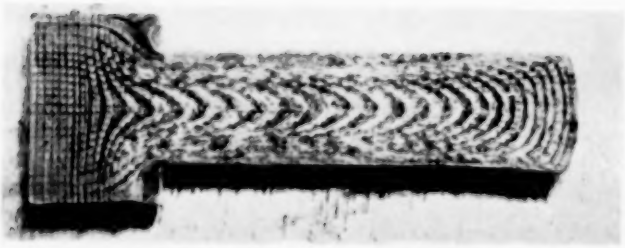

Fig. 5 (a). Showing the flow patterns on the following axial planes of symmetry ; refer also to Fig. 1.

(i) A diametral plane of a circular orifice.

(ii) *YY*, triangular. (iii) *YY*, square.

(iv) *ZZ*, square.

[See over]

(v)

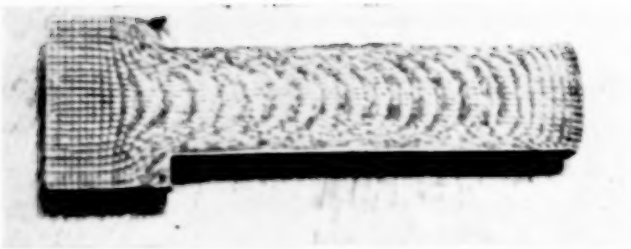

(vi)

(vii)

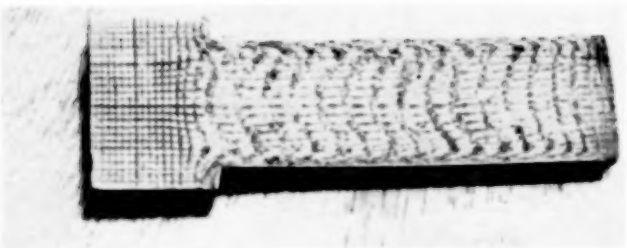

(viii)

Fig. 5 (a) contd.

(v) *XX*, rectangle, $b/d \simeq 2$. (vi) *YY*, rectangle, $b/d \simeq 2$.
(vii) *XX*, I section. (viii) *YY*, I section.

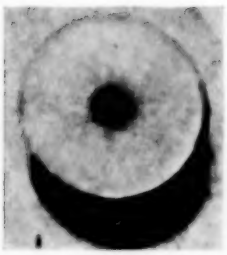

(i)

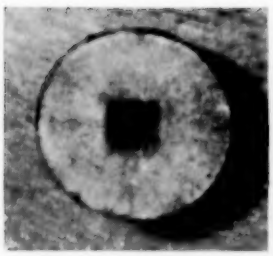

(ii)

(iii)

(iv)

(v)

(vi)

Fig. 5 (b). Coring patterns ; orifice shapes :—

(i) Circle. (ii) Square.
(iii) Triangle. (iv) Rectangle, $b/d \simeq 1{\cdot}5$.
(v) Rectangle, $b/d \simeq 2$. (vi) I section.

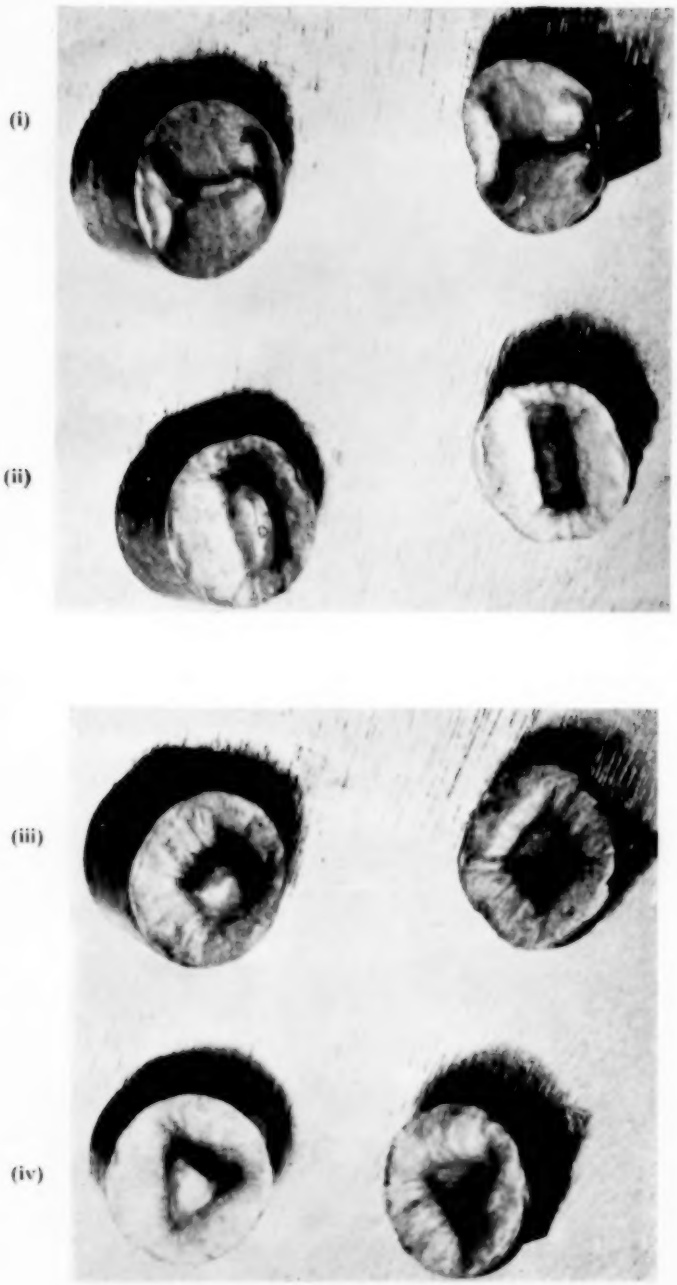

Fig. 3 (c). Internal coring patterns :—

(i) I-section **(ii) Rectangle $b/d \simeq 2$.**

(iii) Square. **(iv) Triangle.**

Fig. 5 (c). (v) to (viii) Effect of increasing amounts of extrusion from leading slug.

4. Flow Patterns

These were made up of three kinds :—

(a) The pattern of flow on axial planes of symmetry.

(b) Coring patterns revealed on the base of the slug adjacent to the compression disk and punch.

(c) Internal coring patterns obtained by examining the original transverse plane of contact between two slugs placed one behind the other in the container.

The photographs in Fig. 5 were obtained using lubricated tellurium lead with the 0·75 reduction dies. The techniques employed were the same as those previously used and described by Dodeja and Johnson (1957).

Three principal observations may be noted :

(i) For the regular shaped squat sections, originally transverse planes are so deformed that after emergence through the die orifice the most advanced points of the plane appear to be those which have passed through the orifice centroid. This asymmetrical position of the peak is seen most clearly by reference to the triangular extrusion, Fig. 5 (a) ii.

(ii) The general shape of the deformed patterns on planes of symmetry, e.g. for the rectangles in Fig. 5 (a) (v) and (vi), could well be anticipated by reference to plane-strain or axi-symmetric extrusions, the orifice width in the flow plane considered seeming to determine the overall pattern in that plane, regardless of other transverse dimensions.

(iii) The I section grid distortion, Fig. 5 (a) vii, presents what appears to be a novel pattern, with two peaks on the deformed transverse line rather than the usual single one. Each peak appears to have emerged just above the junction of the web and a flange. If one imagines the flange widths to remain constant, the portion of the line between the peaks will be the more retarded relative to the peaks the thinner the web. Ultimately when there is no connexion between the flanges the situation is then similar to that of the extrusion of two separate, equal diameter rods from one parent cylindrical slug, or the extrusion of two sheets from one block under conditions of plane strain ; photographs of these latter two cases are available in an earlier paper (Dodeja and Johnson 1957).

(b) The coring patterns on the base of each slug, which have been reduced to a final thickness of about 0·1 in., clearly imitate the shape of the die orifice ; see Fig. 5 (b).

(c) Internal coring patterns obtained with two slugs each 0·75 in. long (one behind the other) again closely follow the orifice shape ; see Fig. 5 (i) to (iv). Particular attention is drawn to Fig. 5 (v) to (viii), showing how the coring develops in a 0·75 reduction circular extrusion as the length of the extruded rod from the leading slug increases from 0·5 in. to 0·9 in.

Associated with the internal coring pattern is an autographic diagram of the

form shown in Fig. 6. Point *A* marks the onset of coring on the base of the leading slug and point *B* coring on the base of the trailing slug ; in most cases the residual slug length at which coring starts is about 0·50 in.

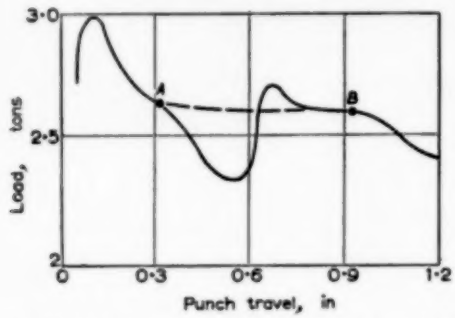

Fig. 6. Load/punch travel diagram from two pure lead slugs of equal length placed one behind the other in the extrusion container.
● A and B, coring points.

ACKNOWLEDGMENT

The author wishes to thank Mr. G. P. FODEN and Mr. H. HUNTSBACH for their assistance at various points in the work.

REFERENCES

DODEJA, L. C. and JOHNSON, W.	1957	*J. Mech. Phys. Solids* **5**, 281.
JOHNSON, W.	1957	*J. Inst. Metals* **85**, 403.
SMITH, C. and SWINDELL, N.	1954	*J. Inst. Metals Monographs, Reports Series* No. 16.
SUKOLSKI, P. J.	1956	*B.I.S.R.A. Report MW/G/83/56.*
THOMSEN, E. G.	1957	*Proc. Inst. Mech. Engrs, Conference on Properties of Materials at High Rates of Strain* (Advance Copy).

Journal of the Mechanics and Physics of Solids, 1958, Vol. 7, pp. 45 to 59. Pergamon Press Ltd., London

ANALYSIS OF SHELLS OF REVOLUTION COMPOSED OF WORKHARDENING MATERIAL*

By E. T. Onat
Division of Engineering, Brown University

(*Received* 10*th March*, 1958)

Summary

This paper is concerned with the mechanical behaviour of shells of revolution made of a rigid, workhardening material. The yield criterion and its dependence on the strain-history are determined in terms of stress resultants of the shell and the rates of extension and curvature of the middle surface. The nature of the mathematical problem that arises in the analysis of workhardening shells is discussed. Incipient plastic deformation of a cylindrical shell is treated as an example. The uniqueness of the incipient velocity field is discussed and the dependence of the velocity rates on the rate of surface tractions is established for a simple case.

1. Introduction

The plastic theory of thin-walled structures has been the subject of numerous publications in recent years. Circular plates under various rotationally symmetric conditions of loading and support were first considered by Pell and Prager (1951) and by Hopkins and Prager (1953). Drucker (1953), Onat (1955) and Hodge (1954) extended the concepts of plastic analysis to cylindrical shells subjected to various types of axially symmetric loading. The theory was later extended by Onat and Prager (1954) to shells of revolution made of a plastic-rigid material that obeys Tresca's yield condition and the associated flow rule. The work referred to above is concerned with shells made of a perfectly plastic material. More recently Prager (1956) and Boyce (1956) have considered the bending of circular plates composed of a workhardening material and Hodge and Romano (1956) and Hodge (1956) have included workhardening in the analysis of cylindrical shells by assuming a strain-history dependence for the relevant approximate yield rectangle.

In the present paper the plastic behaviour of shells of revolution is established from the usual assumptions of thin shell theory concerning the displacements and stresses and from the stress–strain relation of the shell material. For definiteness the discussion is restricted to two types of workhardening material, but the method employed in the derivation of stress–strain relations for generalized stresses and generalized strains is applicable to any inviscid plastic material.

* The results presented in this paper were obtained in the course of research sponsored by the Office of Ordnance Research, U.S. Army.

2. WORKHARDENING RIGID—PLASTIC MATERIALS

The state of stress at a generic point of a thin shell is essentially two-dimensional. For such states of plane stress the workhardening behaviour of a material is conveniently discussed in a rectangular Cartesian system (Figs. 1a, 2a) where

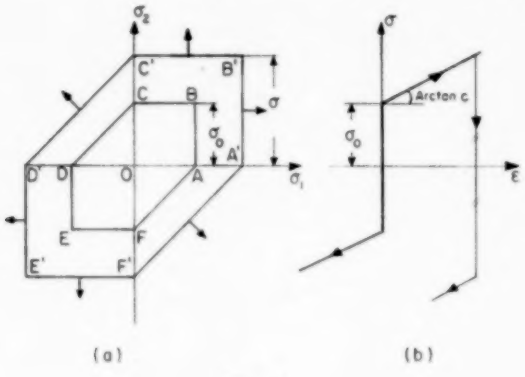

Fig. 1.

the principal stresses σ_1 and σ_2 are used as rectangular co-ordinates. If time effects are absent the reasonable and commonly accepted assumption regarding the behaviour of the rigid-plastic material is that there is a closed convex yield curve which specifies the plastic states of stress for a given state of hardening. If the point P representing the stress-state moves on this curve or towards the interior region then no plastic deformation takes place. If, on the other hand, the motion of the stress point is directed towards the exterior of the yield curve then plastic flow occurs.

For the isotropically workhardening material to be considered in this paper, plastic states of stress are represented by points on Tresca's yield hexagon shown in Fig. 1(a). The size of the yield hexagon is characterized by the current value of the yield stress σ, which is related to the previously suffered strains in the following manner:

$$\sigma = \sigma_0 + c \int_0^t \max |\epsilon| \, dt \tag{1}$$

where σ_0 is the yield stress at the annealed state, t is the time and ϵ stands for the principal strain-rates ϵ_1, ϵ_2 or $-(\epsilon_1 + \epsilon_2)$. For simplicity c is taken to be a positive constant, so that the uniaxial stress–strain diagram is composed of straight portions as shown in Fig. 1 (b).

The flow rule associated with the yield curve in Fig. 1 (a) specifies that only pure shear flows can be produced at a plastic state of stress which is represented by an interior point of a side of the yield hexagon. Such a shear flow may be represented by the vector plotted at the centre of the considered side of the yield hexagon, the components of this vector with respect to the co-ordinate axes being proportional to the strain-rates ϵ_1 and ϵ_2 with a positive factor of proportionality. On the other hand, if the plastic state of stress is represented by a corner of the yield hexagon, the plastic flow can be any linear combination, with positive coefficients,

of the shear flows corresponding to the adjacent sides. The strain-history dependence of the yield curve (1) and the flow rule described above completely describe the workhardening behaviour of the material. The rate d at which mechanical energy is dissipated in plastic flow per unit volume of the material plays a central role in the derivation of yield surfaces for shells. For the workhardening material considered it is easily evaluated using the flow law, and is

$$d = \sigma \max |\epsilon| \tag{2}$$

where ϵ again stands for ϵ_1, ϵ_2 or $\epsilon_3 = -(\epsilon_1 + \epsilon_2)$.

The stress–strain relations discussed above represent a simple incremental law which avoids the unsound features of total stress–strain laws: but even this simple law involves a rather complicated dependence on strain-history and therefore is not as tractable as the total laws. PRAGER (1956) has recently suggested a compromise which provides, to a large extent at least, the mathematical advantages of total stress–strain laws, while retaining the fundamental character of incremental laws.

A stress–strain law of the type suggested by PRAGER will now be described for the case of plane stress. For a given state of hardening the yield curve is Tresca's

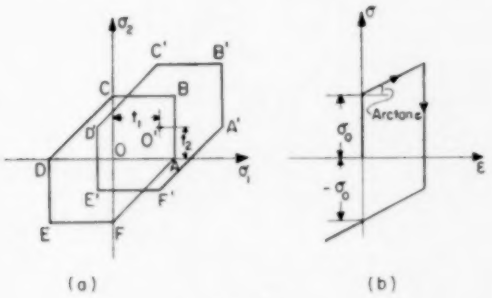

Fig. 2.

hexagon $A'\,B'\,C'\,D'\,E'\,F'$ shown in Fig. 2 (a). The size of the hexagon is assumed to be independent of the state of hardening, but the co-ordinates of the centre of the hexagon, t_1 and t_2, are linear functions of the strains suffered by the element:

$$\left.\begin{aligned} t_1 &= \tfrac{2}{3}\, c\,(2\bar{\epsilon}_1 + \bar{\epsilon}_2) \\ t_2 &= \tfrac{2}{3}\, c\,(2\bar{\epsilon}_2 + \bar{\epsilon}_1) \end{aligned}\right\} \tag{3}$$

where c is a positive constant, and $\bar{\epsilon}_1$ and $\bar{\epsilon}_2$ are principal strains.

The flow rule associated with this yield curve is similar to the one described for the isotropically workhardening material. The rate of energy dissipation d is found from the yield curve and the flow rule; per unit volume it has the value

$$d = \sigma_0 \max |\epsilon| + t_1\,\epsilon_1 + t_2\,\epsilon_2. \tag{4}$$

The uniaxial stress–strain curve for this material is shown in Fig. 2 (b). It is seen that for a loading programme starting from zero load, both type of materials considered here behave identically; however, if unloading occurs, the yielding in

the reverse direction takes place at a much lower stress intensity for the second type of material. This lowering of the yield stress by a prior plastic straining simulates the Bauschinger effect.

3. Generalized Stresses—Equations of Equilibrium

A three-dimensional theory for important structural elements such as plates and shells is bound to be too unwieldy to be useful. It is desirable, therefore, to develop a simplified theory which takes account of the fact that these structural elements are thin-walled and the state of stress at a generic point is essentially two-dimensional. Fig. 3 shows an element of a shell of revolution with the stress resultants transmitted across its boundary meridians and parallels. M_ϕ and M_θ are the bending moments, N_ϕ and N_θ the membrane forces and Q the shear force. The load per unit area of the middle surface of the shell has the components Y in the direction of the meridian and Z in the direction of the normal. The arrows in Fig. 3 indicate the usual conventions for positive forces and couples. The element has the distance r_0 from the axis of revolution and its principal radii of curvature are r_1 and r_2. Note that

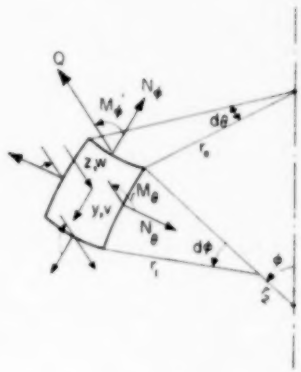

Fig. 3.

$$r_0 = r_2 \sin \phi.$$

The three-dimensional conditions of equilibrium for local stresses are then replaced by simpler equations for the stress resultants

$$\left.\begin{aligned} &(r_0 N_\phi)' - r_1 N_\theta \cos\phi - r_0 Q + r_0 r_1 Y = 0 \\ &r_0 N_\phi + r_1 N_\theta \sin\phi + (r_0 Q)' + r_0 r_1 Z = 0 \\ &(r_0 M_\phi)' - r_1 M_\theta \cos\phi - r_0 r_1 Q = 0 \end{aligned}\right\} \tag{5}$$

where the prime denotes differention with respect to ϕ (see, for instance, FLÜGGE 1934, p. 148).

During deformation of the shell due to plastic flow the usual assumption will be made that the particles originally on a normal to the undeformed middle surface continue to remain on that normal to the middle surface as the middle surface deforms. If the meridional and normal components of displacements of the middle surface are denoted by v and w respectively, the positive direction being those indicated by Y and Z in Fig. 1, the principal rates of extension in the middle surface are

$$e_\phi = \frac{1}{r_1}\left(\frac{dv}{d\phi} - w\right), \qquad e_\theta = \frac{1}{r_2}(v \cot\phi - w). \tag{6}$$

The principal rates of curvature of the middle surface are

$$\kappa_\phi = -\frac{1}{r_1}\frac{d}{d\phi}\left[\frac{1}{r_1}\left(v + \frac{dw}{d\phi}\right)\right], \qquad \kappa_\theta = -\frac{\cot\phi}{r_1 r_2}\left(v + \frac{dw}{d\phi}\right). \tag{7}$$

4. Yield Surface and Stress–Strain Law for the Generalized Stresses

From the point of view of limit design the stress resultants M_ϕ, M_θ, N_ϕ and N_θ are the generalized stresses of the present problem and κ_ϕ, κ_θ, e_θ and e_ϕ are the corresponding generalized strain-rates. For the discussion of flow rules and yield conditions it is convenient to treat the stress resultants as rectangular Cartesian co-ordinates in a four-dimensional stress space. The generalized strain-rates may be thought as components of a vector in this space.

Consider a rigid, workhardening shell element that is in a given state of hardening. The states of stress that the element can sustain are classified as plastic or rigid according to whether plastic deformation can or cannot be produced by infinitesimal changes of stress. In analogy with the two dimensional stress–strain relations

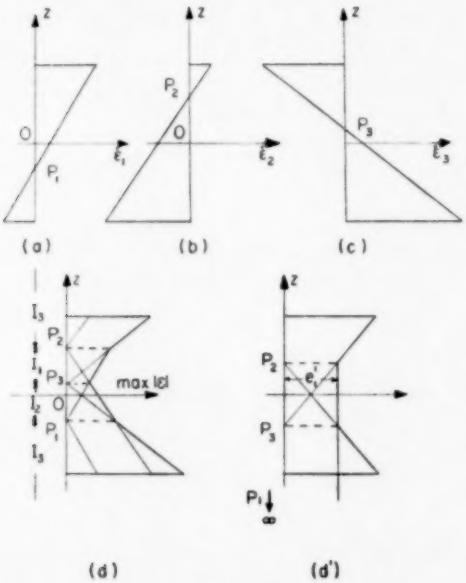

Fig. 4.

considered in the previous section, it is natural to expect that for a given state of hardening the points representing rigid states of stress will fill a convex domain in the four-dimensional stress space. The bounding surface of the rigid range will again be called the yield surface. The present discussion is mainly concerned with the derivation of the yield surface for an element of shell that is in a given state of hardening.

In the following it will be convenient to denote stress-resultants by N_α and M_α ($\alpha = 1, 2$) where α will not be prematurely identified with meridional or the circumferential stress. Let e_α be the principal rates of extension of the middle surface and κ_α the corresponding rates of curvature. The distribution of the principal

strain-rates over the thickness of the shell is then given by

$$\epsilon_\alpha = e_\alpha + \kappa_\alpha z \qquad \text{and} \qquad \epsilon_3 = -(\epsilon_1 + \epsilon_2) \ (\alpha = 1, 2). \tag{8}$$

Here z measures distance from the middle surface. Figs. 4 (a, b and c) show typical distributions of ϵ_α and ϵ_3. The zeros of these distributions (the points P_1, P_2 and P_3) have the ordinates

$$hp_i = -\frac{e_i}{\kappa_i}, \qquad (i = 1, 2, 3) \tag{9}$$

where e_3 and κ_3 are introduced to denote the following quantities

$$e_3 = -(e_1 + e_2); \qquad \kappa_3 = -(\kappa_1 + \kappa_2). \tag{10}$$

The derivation of the yield surface will be based (as in ONAT and PRAGER 1954) on the following remark concerning the rate of energy dissipation D per unit area of the middle surface. The workhardening materials considered in the previous section are inviscid. Therefore D must be homogeneous of the order one in e_α and κ_α. By Euler's theorem on homogeneous functions we have therefore

$$D = \frac{\partial D}{\partial e_1} e_1 + \frac{\partial D}{\partial e_2} e_2 + \frac{\partial D}{\partial \kappa_1} \kappa_1 + \frac{\partial D}{\partial \kappa_2} \kappa_2. \tag{11}$$

On the other hand the definition of generalized stresses and strain-rates implies that

$$D = N_1 e_1 + N_2 e_2 + M_1 \kappa_1 + M_2 \kappa_2. \tag{12}$$

Comparison of (11) and (12) furnishes the following expressions for the stress-resultants:

$$N_\alpha = \frac{\partial D}{\partial e_\alpha}, \qquad M_\alpha = \frac{\partial D}{\partial \kappa_\alpha}. \tag{13}$$

Now consider a shell element made of isotropically workhardening material. For such an element the state of hardening is characterized by the distribution of the current yield stress $\sigma(z, t)$ over the thickness of the shell, where $\sigma = \sigma(z, t)$ is related to the strain-history by (1).

The rate of energy dissipation D is obtained by integrating (2) over the thickness of the shell

$$D = \int_{-h/2}^{h/2} \sigma(z, t) \max |\epsilon| \, dz. \tag{14}$$

Equations (13) and (11) will then furnish the following expressions for the stress-resultants

$$\left.\begin{aligned} N_\alpha &= \int_{-h/2}^{h/2} \sigma(z, t) \frac{\partial \max |\epsilon|}{\partial e_\alpha} \, dz, \\ M_\alpha &= \int_{-h/2}^{h/2} \sigma(z, t) \frac{\partial \max |\epsilon|}{\partial \kappa_\alpha} \, dz. \end{aligned}\right\} \tag{15}$$

The evaluation of the partial derivatives in (15) constitutes the next step in the analysis.

Fig. 4 (d) shows a typical distribution of $\max |\epsilon|$. It is seen from the Figs. 4 (a, b, c) that

$$\max |\epsilon| = \epsilon_i \operatorname{sgn} \kappa_i \operatorname{sgn} (z - hp_i) \qquad \text{when} \qquad z \text{ is in } I_i \tag{16}$$

where I_1, I_2 denote the intervals (P_2, P_3), (P_3, P_1) and I_3 denotes the remainder of the range $-\infty < z < \infty$.* This observation concerning the distribution of $\max|\epsilon|$ and (8) enable one to evaluate the partial derivatives of $\max|\epsilon|$. For instance,

$$\frac{1}{z}\frac{\partial \max|\epsilon|}{\partial \kappa_1} = \frac{\partial \max|\epsilon|}{\partial e_1} = \begin{cases} 1 & \text{for} \quad z \geqslant hp_3 \\ 0 & \text{for} \quad hp_3 \geqslant z \geqslant hp_1 \\ -1 & \text{for} \quad hp_1 \geqslant z \end{cases} \tag{17}$$

Comparison of (15) and (17) furnishes the following expressions for N_1 and M_1:

$$\left.\begin{aligned} N_1 &= \int_{p_3 h}^{h/2} \sigma(z, t)\, dz - \int_{-h/2}^{p_1 h} \sigma(z, t)\, dz, \\ M_1 &= \int_{p_3 h}^{h/2} z\sigma(z, t)\, dz - \int_{-h/2}^{p_1 h} z\sigma(z, t)\, dz. \end{aligned}\right\} \tag{18}$$

The remaining stress-resultants are obtained in a similar manner :

$$\left.\begin{aligned} N_2 &= \int_{p_2 h}^{h/2} \sigma(z, t)\, dz - \int_{-h/2}^{p_3 h} \sigma(z, t)\, dz, \\ M_2 &= \int_{p_2 h}^{h/2} z\sigma(z, t)\, dz - \int_{-h/2}^{p_3 h} z\sigma(z, t)\, dz. \end{aligned}\right\} \tag{19}$$

Equations (18) and (19) constitute a parametric representation of a part of the yield surface. They do not represent the entire yield surface because they are derived from a Figure that incorporates a definite arrangement of the points P_i. The range of validity of (18) and (19) must therefore be explored.

In Fig. 4, $\kappa_1 > 0$, $\kappa_2 > 0$ and the points P_i fall within the interval $-h/2 \leqslant z \leqslant +h/2$ and arranged in the order P_1, P_3, P_2 in the direction of increasing values of z. If Figs. 4 (a and b) are redrawn so as to correspond to the opposite signs of the quantities e_α and κ_α, the values of the parameters p_i defined by (9) remain unchanged and the only modification needed in (18) and (19) is a change of signs of N_α and M_α.

The possibility that one or more of the points P_i fall outside the interval $-h/2 \leqslant z \leqslant h/2$ will now be investigated. If for example $p_1 < -\frac{1}{2} \leqslant p_3 \leqslant p_2 < \frac{1}{2}$, examination of (17) shows that (18) and (19) remain valid provided that p_1 is replaced by $-\frac{1}{2}$. By setting $p_1 = -\frac{1}{2}$ in (18) and (19), we express the four resultants in terms of two parameters, p_2 and p_3. The modified equations (18) and (19) therefore represent a three-dimensional edge of the four-dimensional yield surface. Here the term edge is used to indicate the fact that an infinite number of strain-rates may be associated with a given stress point defined by these modified equations. Similar remarks apply when more than one of the points P, Q and R fall outside of the thickness of the shell.

The above remarks are concerned with the part of the yield surface that is defined by (18) and (19). Further parts of the yield surface can be obtained in a similar manner by considering the remaining five possible arrangements of points P_i. It will be seen by inspection that equations (16), defining the distribution of $\max|\epsilon|$, are valid for any distribution of P_i, provided that the intervals I_i are

* The notation 'sgn' means "sign of."

defined in the obvious manner indicated in Fig. 4 (d). The partial derivatives of $\max |\epsilon|$ are therefore given by

$$\left[\frac{1}{z}\frac{\partial \max |\epsilon|}{\partial \kappa_\alpha} = \frac{\partial \max |\epsilon|}{\partial e_\alpha} = \delta_{i\alpha} \operatorname{sgn} \kappa_i \operatorname{sgn} (z - hp_i)\right] \quad \text{when} \quad z \text{ is in } I_i, \tag{20}$$

where $\delta_{11} = \delta_{22} = 1$, $\delta_{12} = \delta_{21} = 0$, $\delta_{31} = \delta_{32} = -1$. The stress resultants are then obtained from (15) and (20). The final parametric forms of N_α and M_α will not be given here.

It will be noticed that the discussion is so far limited to the case of distinct points P_i for which the partial derivatives of D are continuous with respect to e_α and κ_α and Euler's theorem is valid. However, if one of the following cases occur

$$e_i = \kappa_i = 0, \qquad (i = 1, 2, 3) \tag{21}$$

the partial derivatives of D are no longer continuous and the applicability of (15) to these cases must be critically examined. To discuss a typical case let us assume that $e_1 = \kappa_1 = 0$. Then $p_3 = p_2$, while p_1 is indeterminate. For a generic value of z we have $\epsilon_1 = 0$ from the first equations (8). It follows that the state of stress is represented by a point on the sides $C'B'$ or $E'F'$ of the yield hexagon of Fig. 2 (a). Accordingly, $\sigma_2 = \sigma(z, t)$ where $\epsilon_2 > 0$ and $\sigma_2 = -\sigma(z, t)$ where $\epsilon_2 < 0$. The stress-resultants M_2 and N_2 therefore depend on the single parameter $p_3 = p_2$, while the remaining stress-resultants are not uniquely determined. On the other hand for the values of the indeterminate parameter p_j satisfying the inequality $p_1 < p_3 = p_2$, (18) and (19) furnish precisely the same results regarding the stress-resultants. Therefore it can be seen that the parametric equations of the type (18) also represent the singular cases introduced by (21). In the preceding discussion (18 and 19) are considered as a parametric representation of a part of the yield surface. They may equally well be regarded as stress–strain relations, since they establish relations between the generalized stresses, the strain-rates and the strain-history.

In the theory of workhardening solids the relations between stress-rate and strain-rate play a central role. Similar relations for the generalized rates of strain and stress of the present problem will now be obtained by taking time derivatives of (18) and (19). From the first equation of (18) we obtain

$$\dot{N}_1 = \int_{p_2 h}^{h/2} \frac{\partial \sigma(z, t)}{\partial t}\, dz - \int_{-h/2}^{p_1 h} \frac{\partial \sigma(z, t)}{\partial t}\, dz + \dot{N}_1' \tag{22}$$

where

$$\dot{N}_1' = -h\left[\sigma(p_3 h, t)\, \dot{p}_3 + \sigma(p_1 h, t)\, \dot{p}_1\right]. \tag{23}$$

The rates of the remaining resultants may be written in a similar manner by introducing $\dot{N}_2'$, $\dot{M}_1'$ and $\dot{M}_2'$. A direct physical meaning may be given to the quantities $\dot{N}_\alpha'$ and $\dot{M}_\alpha'$ by considering neutral changes of stress. Such changes of stress leave the state of hardening unchanged:

$$\frac{\partial \sigma(z, t)}{\partial t} = 0, \tag{24}$$

and lead from one plastic state to another plastic state. It is seen from (22) and (24) that

$$\dot{N}_\alpha = \dot{N}_\alpha', \qquad \dot{M}_\alpha = \dot{M}_\alpha'$$

for such changes of stress.

It can also be shown using equations defining $\dot{N}_\alpha'$, $\dot{M}_\alpha'$ and (8) that

$$\sum_{1,2}(\dot{N}_\alpha' \epsilon_\alpha + \dot{M}_\alpha' \kappa_\alpha) = 0, \tag{25}$$

which expresses the fact that the strain vector **e** is in the direction of the normal to the yield surface at the considered plastic state of stress. Equation (25) will be used to eliminate the unknown quantities $\dot{p}_i$ from the equation (22) and the corresponding equations for remaining stress-rates. Before proceeding with the elimination of $\dot{p}_i$, we write (22) in the following form by making use of (1) and (17):

$$\dot{N}_1 = c \int_{-h/2}^{h/2} \max |\epsilon| \frac{\partial \max |\epsilon|}{\partial \epsilon_1} dz + \dot{N}_1'. \tag{26}$$

By multiplying $\dot{N}_\alpha$ and $\dot{M}_\alpha$ with ϵ_α and κ_α respectively we obtain, from (26) and the corresponding equations for the remaining stress-rates and from (25),

$$\sum_{1,2}(\dot{N}_\alpha \epsilon_\alpha + \dot{M}_\alpha \kappa_\alpha) = c \int_{-h/2}^{h/2} \left(\sum_{1,2} \epsilon_\alpha \max |\epsilon| \frac{\partial \max |\epsilon|}{\partial \epsilon_\alpha} \right) dz, \tag{27}$$

which constitutes the stress–strain law for the rates of stress and strain.

Equation (27) is derived for points P_i which fall within the interval $-h/2 \leqslant z \leqslant h/2$. If one or more of the points P_i fall outside of this interval, the unknown parameters $\dot{p}_i$ corresponding to the points that fall outside of the interval do not occur in the equations (23). The elimination of the remaining unknown quantities $\dot{p}_i$ will, therefore, produce more than one equation for the rates of stress and strain. As an example let us consider the case of $p_1 < p_3 < -\frac{1}{2}$ and $p_2 > \frac{1}{2}$. The stress resultants are obtained from (18) and (19) by replacing p_1, p_2 and p_3 by $-\frac{1}{2}$, $\frac{1}{2}$ and $-\frac{1}{2}$, respectively:

$$N_1 = \int_{-h/2}^{h/2} \sigma(z, t)\, dz, \qquad M_1 = \int_{-h/2}^{h/2} z\sigma(z, t)\, dz, \qquad N_2 = 0, \qquad M_2 = 0. \tag{28}$$

The stress point corresponding to (28) is a corner of the yield surface. Equation (16) indicates that for the generalized rates of strain satisfying the inequalities $p_1 < p_3 < -\frac{1}{2}$ and $p_2 > \frac{1}{2}$,

$$\max |\epsilon| = \epsilon_1 \qquad \text{for} \qquad -h/2 \leqslant z \leqslant h/2.$$

Thus, using time derivatives of (1) and (28), we obtain

$$\dot{N}_1 = c \int_{-h/2}^{h/2} \epsilon_1\, dz, \qquad \dot{M}_1 = c \int_{-h/2}^{h/2} z\epsilon_1\, dz; \qquad \dot{N}_2 = 0, \qquad \dot{M}_2 = 0. \tag{29}$$

It is interesting to note that (29) satisfy (27).

The yield condition for a shell element made of a material exhibiting a Bauschinger effect will now be briefly discussed. Equations (13) are again the basis of the analysis so that the evaluation of the rate of energy dissipation D per unit area of the middle surface will constitute the first step. By integrating (4) over the thickness of the shell we obtain

$$D = \int_{-h/2}^{h/2} \sigma_0 \max |\epsilon|\, dz + \int_{-h/2}^{h/2} \left[\sum_{1,2} t_\alpha \epsilon_\alpha \right] dz,$$

or, using (3) and (8),

$$D = \int_{-h/2}^{h/2} \sigma_0 \max |\epsilon|\, dz + \tfrac{1}{3} c \int_{-h/2}^{h/2} [(2\epsilon_1 + \epsilon_2)\epsilon_1 + (2\epsilon_2 + \epsilon_1)\epsilon_2]\, dz. \tag{30}$$

Equations (30), (8) and (13) furnish the following expressions for the stress-resultants:

$$\left.\begin{aligned} N_\alpha &= N_\alpha' + \tfrac{2}{3}\,\mathrm{ch}\,(2\,\bar{e}_\alpha + \bar{e}_\beta) && \alpha = 1,2 \\ M_\alpha &= M_\alpha' + \frac{\mathrm{ch}^3}{18}\,(2\bar{\kappa}_\alpha + \bar{\kappa}_\beta) && \beta = 1,2 \\ & && \alpha \neq \beta \end{aligned}\right\} \tag{31}$$

where $\bar{e}_\alpha$ and $\bar{\kappa}_\alpha$ are total extensions and curvatures and

$$N_\alpha' = \int_{-h/2}^{+h/2} \sigma_0 \frac{\partial \max|\epsilon|}{\partial e_\alpha}\,dz, \qquad M_\alpha' = \int_{-h/2}^{+h/2} \sigma_0 \frac{\partial \max|\epsilon|}{\partial \kappa_\alpha}\,dz. \tag{32}$$

Comparison of (32) and (20) shows that N_α' and M_α' constitute the strain-rate dependent components of the stress-resultants N_α and M_α. Equation (32) may be interpreted as a parametrical representation of a four-dimensional surface S_0. For an element of shell which is at the annealed state, $\bar{e}_\alpha = \bar{\kappa}_\alpha = 0$, and the corresponding yield surface is identical with S_0. The yield surface for an ideally plastic shell of revolution with the yield stress σ_0 is also the yield surface S_0 and investigated in detail by ONAT and PRAGER (1954).

The obvious geometrical interpretation of (31) is that the yield surface corresponding to a hardened state may be obtained by the translation of the surface S_0, the components of the translatory displacements being equal to the second terms on the right-hand side of (31). It is interesting to note that the strain-history dependence of the yield surface (32) is markedly similar to that of the yield hexagon of Fig. 2 (a).

Time derivatives of (31) again provide the relations between stress-rate and strain-rate at a plastic state of stress. It can easily be shown that $\dot{N}_\alpha'$ and $\dot{M}_\alpha'$ may be interpreted as rates corresponding to neutral changes of stress and such rates of stress satisfy the normality condition (25). From (25) and (31) we obtain

$$\sum_{1,2} (\dot{N}_\alpha e_\alpha + \dot{M}_\alpha \kappa_\alpha) = 2\,\mathrm{ch}\,(e_1^2 + e_1 e_2 + e_2^2) + \frac{\mathrm{ch}^3}{6}\,(\kappa_1^2 + \kappa_1 \kappa_2 + \kappa_2^2). \tag{33}$$

Comparison of this equation with (27) indicates once more the simplification effected by the adoption of the stress–strain law summarized in Fig. 2 (a). For $|p_i| \leqslant \frac{1}{2}$, (33) is the only relation which exists between the rates of stress and strains. For edge or corner states of stress some or all of the parameters satisfy $|p_i| > \frac{1}{2}$, and additional equations are obtained for the stress and strain-rates. The detailed discussion of such states of stress will not be given here.

The dependence of the yield surface on the strain-history is discussed above for shells made of two types of material which behave identically in a tension test. However, because of the marked difference in their behaviour in reversed loading, the stress–strain relations describing the plastic deformations of shells composed of these materials take different forms as seen from (18), (19) and (31). The following discussion will be concerned with a comparison of the predictions of both stress–strain laws for cylindrical shells with no axial force. If the circumferential and axial directions of the cylindrical shell are associated with the subscripts 1 and 2 of the present section, the geometry of the shell and the absence of the axial force require that

$$\kappa_1 = 0, \qquad 2e_2 + e_1 = 0, \tag{34}$$

where the second equation is assumed to be equivalent to $N_2 = 0$. This assumption will later be confirmed by the analysis.

The following problem will now be considered. Constant strain-rates $e_1^0 > 0$, $e_2^0 = -e_1^0/2$, $\kappa_1 = 0$ and $\kappa_2 > 0$ are applied to an element of shell which is originally at the annealed state. To find the yield curve at a given time for shells made of both types of materials. For shells composed of workhardening material, the parametric representation (15) of the yield curve at time t requires the evaluation of the yield stress $\sigma(z, t)$. For constant strain-rate loading considered here (1) becomes

$$\sigma(z, t) = \sigma_0 + ct \max|\epsilon^0|, \tag{35}$$

where the distribution of $\max|\epsilon^0|$ is similar to that shown in Fig. 4 (d′) and the corresponding points P_i have the ordinates

$$|\bar{p}_1| = \infty, \qquad \bar{p}_2 = \frac{e_1^0}{2\kappa_2^0\,h} \qquad \text{and} \qquad \bar{p}_3 = -\frac{e_1^0}{2\kappa_2^0\,h}.$$

The partial derivatives in (15) are evaluated from strain-rates which satisfy (34). When $e_1^0 > 0$, $\kappa_2 > 0$, equations (34) require that $p_2 > 0$, $p_2 + p_3 = 0$ and p_1 is infinite. For the above values of parameters p_i, (15) reduce to (18) and (19) where p_1 must be replaced by $-\frac{1}{2}$. Thus, the relevant stress-resultants are obtained from (35), (18) and (19)

$$n = \frac{N_1}{N_0} = \begin{cases} (1+\tau)\left(\frac{1}{2}+p_2\right) + \dfrac{\tau}{4\bar{p}_2}\left(\frac{1}{2}-\bar{p}_2\right)^2 & \text{for} \quad p_2 < \bar{p}_2 \\ (1+\tau)\left(\frac{1}{2}+p_2\right) + \dfrac{\tau}{4\bar{p}_2}\left[\left(\frac{1}{2}-\bar{p}_2\right)^2 + (p_2-\bar{p}_2)^2\right] & \text{for} \quad p_2 > \bar{p}_2 \end{cases} \tag{36}$$

where τ indicates the dimensionless time defined by

$$\tau = \frac{c}{\sigma_0} e_1^0 t, \qquad \text{and} \qquad N_0 = \sigma_0 h.$$

Similarly

$$m = \frac{M_2}{M_0} = \begin{cases} (1+\tau)(1-4p_2^2) + \dfrac{\tau}{2}\left[\dfrac{1}{3\bar{p}_2}(1-8\bar{p}_2^3) - (1-4\bar{p}_2^2)\right] & \text{for} \quad p_2 < \bar{p}_2 \\ (1+\tau)(1-4p_2^2) + \dfrac{\tau}{2}\left[\dfrac{1}{3\bar{p}_2}(1-8p_2^3) - (1-4p_2^2)\right] & \text{for} \quad p_2 > \bar{p}_2 \end{cases} \tag{37}$$

where

$$M_0 = \tfrac{1}{4}\sigma_0 h^2.$$

It will be seen from (19) that the symmetry in the distribution of $\sigma(z, t)$ and the condition $p_2 + p_3 = 0$ result in $N_2 = 0$ for all times.

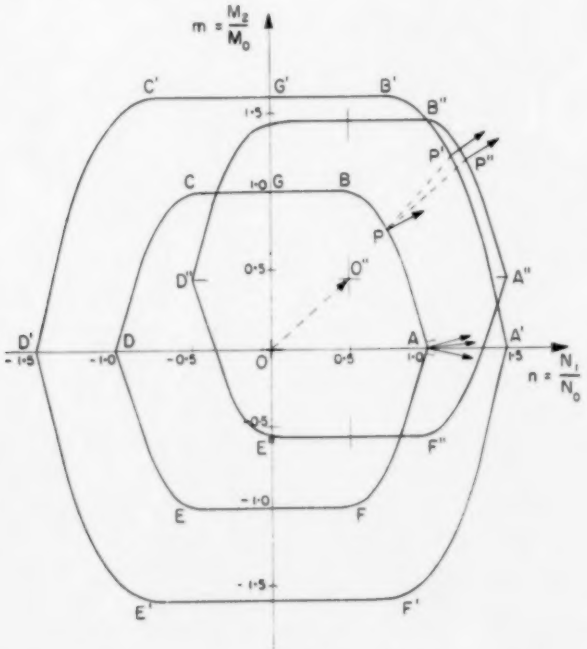

Fig. 5.

For $\tau = 0$, (36) and (37) reduce to $N_1/N_0 = \frac{1}{2} + p_2$, $M_2/M_0 = 1 - 4p_2^2$ which define the parabolic arc APB in Fig. 5. For a given positive value of τ, (36) and (37) constitute parametric

representations of the curves $B'P'$ and $P'A'$. The stress-resultants which must be applied to achieve the constant rates of strain ${e_1}^0$ and ${\kappa_2}^0$ are obtained from (36) and (37) by setting $p_2 = \bar{p}_2$. The corresponding stress path PP' is shown in Fig. 5.

The horizontal portions of the yield curve which fall in the first quadrant are obtained by considering the following rates of strain: $e_1 = e_2 = 0$, $\kappa_1 = 0$, $\kappa_2 < 0$ for which $p_2 = p_3 = 0$ and p_1 is indeterminate. For $p_1 < 0$, (18) and (19) are applicable and they give the horizontal portions BG and $B'G'$ for times 0 and τ respectively. The portions of the yield curves in the remaining quadrants of Fig. 5 are obtained by observing that the yield curve is symmetrical with respect to the origin. It will be noticed from Fig. 5 that the completed yield curves $ABCDEF$ and $A'B'C'D'E'F'$ are not geometrically similar.

For a shell element composed of material exhibiting a Bauschinger effect, the parametric representation of the yield curve is obtained immediately from (31) by setting $\bar{\epsilon}_1 = {e_1}^0 t$, $\bar{\epsilon}_2 = {e_2}^0 t = -\bar{\epsilon}_1/2$, $\bar{\kappa}_1 = 0$, $\bar{\kappa}_2{}^0 t = e_1/2\bar{p}_2{}^h t$:

$$\frac{N_1}{N_0} = \frac{N_1'}{N_0} + \tau \qquad \text{and} \qquad \frac{M_2}{M_0} = \frac{M_2'}{M_0} + \frac{2}{9}\frac{\tau}{\bar{p}_2} \tag{38}$$

where

$$\tau = \frac{c}{\sigma_0}\,{e_1}^0 t.$$

The previous remarks concerning the yield curve indicate that the strain-rate dependent components N_1'/N_0 and M_2'/M_0 can be interpreted as co-ordinates of the points of the virgin yield curve $ABCDEF$ in Fig. 5. The yield curve $A''B''C''D''E''F''$ at the time τ is therefore formed by the successive transplations of this curve by the amounts τ and $2\tau/9\bar{p}_2$ in the n and m directions respectively. The stress path corresponding to the constant strain-rate loading considered is PP''. It is seen from the comparison of the stress paths PP' and PP'' that the generalized stresses to be applied to both shells to obtain given strains are not too different for the case under consideration.

5. The Mathematical Problem — Example

Consider a shell of revolution made of a workhardening material and subjected to an axially symmetric type of loading. As the intensity of this loading is raised gradually, starting from zero, the shell at first remains rigid. Only when the load intensity reaches a critical value can the plastic-rigid shell begin to deform. If the changes in geometry are negligible, the further deformation of a shell composed of a workhardening material can proceed only with increasing load.

The mathematical problem is concerned with the determination of the generalized stresses, displacements, and generalized strains as functions of the load intensity. For slow deformations of the shell inertia effects can be neglected, so that the stress-resultants satisfy the equations of equilibrium (5). On the other hand, for the shells under consideration, stress-resultants are related to the generalized strains and to their rates by (15) or (31) and (32). Since the generalized strains are expressed in terms of displacements, $v(\phi, t)$ and $w(\phi, t)$, through (6) and (7), the equations of equilibrium (5) provide three equations for v, w and Q.

It is easily seen from (31), (32) and (20) that, for a shell made of material exhibiting a Bauschinger effect, this procedure results in non-linear partial differential equations. However, for an isotropically workhardening shell, the strain-history dependence is complicated and the resulting equations may be described as integro-differential equations. The solutions to these equations are not easily obtainable in general, although the mathematical problem for a shell obeying (31) and (32) is comparatively tractable. In many cases it is advantageous to divide the above

described problems into the sub-problems of the following type: given the strain history and the instantaneous generalized stresses throughout the shell together with the rates of the surface tractions, to find the stress-rates and the displacement-rates. Recently HILL (1956) and BOYCE and PRAGER (1957) considered this problem for workhardening rigid-plastic solids and established important results concerning the uniqueness of the displacement- and stress-rates. A similar study could be made for the shells obeying the generalized stress–strain relations (15) or (31) and (32). In the present paper, however, the discussion is restricted to a simple example. The incipient deformation of a simply supported cylindrical shell is considered. It is assumed that the shell is composed of isotropically workhardening material and is subjected to uniform internal pressure p (Fig. 6).

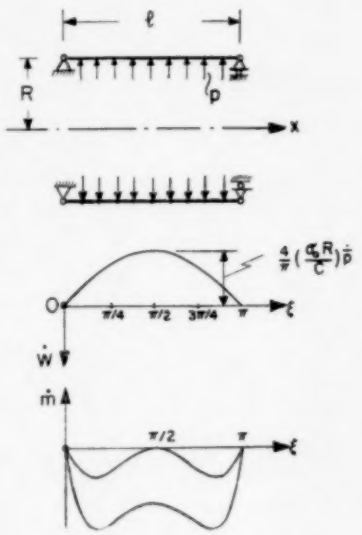

Fig. 6.

The sign convention introduced in Fig. 3 will be retained in the following analysis, but the axial co-ordinate x will be used and dx will replace $r_1\, d\phi$ in (5), (6) and (7). The relevant variable of the present problem are then M_x, N_θ, κ_x, e_θ and p, and they will be made dimensionless by dividing them by M_0, N_0, $N_0/M_0 = 4/h$, 1 and $\sigma_0\, h/R$ respectively. The letters m, n, κ, e and $\bar{p}$ will be used to denote the resulting dimensionless quantities.

In the absence of the axial force, the dimensionless equilibrium equations are reduced to a single equation by eliminating Q from (34):

$$\tfrac{1}{4}\frac{d^2 m}{d\xi^2} + n = \bar{p}, \qquad \text{where} \qquad \xi = \frac{x}{\sqrt{(Rh)}}. \tag{39}$$

The dimensionless generalized strain-rates e and κ are related to the radial velocity w by

$$e = -\frac{w}{R}, \qquad \kappa = -\frac{1}{4R}\frac{d^2 w}{d\xi^2}. \tag{40}$$

The plastic states of stress associated with the incipient deformations of the shell are represented by the points of the yield curve $ABCDEF$ in Fig. 5. The flow rule associated with this curve is that the strain-rate vector $\mathbf{e}$ (e, κ) is in the direction of the normal to the yield curve at the stress state considered. For a corner state of stress, such as A, the strain-rate vector $\mathbf{e}$ is not uniquely determined and can be anywhere between the normals drawn to the adjacent sides of the yield curve (Fig. 5). The shell is subjected to slowly increasing internal pressure $p\,(t)$ It remains rigid when the dimensionless pressure intensity $\bar{p}$ is less than unity. At $\bar{p} = 1$ the uniform equilibrium state of stress $n = 1$, $m = 0$, satisfies the stress boundary conditions and it is represented by the corner A of the yield surface $ABCDEF$. It is easily seen that a deformation mode satisfying boundary condition can be associated. The flow rule demands that

$$e \geqslant 0 \qquad \text{and} \qquad |e/4\,\kappa| \geqslant 1$$

or, by using (40),

$$w < 0 \qquad \text{and} \qquad |w/w_{\xi\xi}| \geqslant 1. \tag{41}$$

It is obvious that an infinite set of rates of displacement can generally be found satisfying (41) and the condition of zero displacement at both ends of the shell. If the shell were made of ideally material, there would be no additional equations by which one could select an actual mode of

deformation from the set of displacement rates satisfying (41). For a workhardening shell, however, the stress-rates and the displacement-rate w must in addition satisfy the equations of equilibrium (39), the stress and velocity boundary conditions

$$w = \dot{m} = 0 \qquad \text{at} \qquad \xi = 0 \qquad \text{and} \qquad \xi = l/\sqrt{(Rh)} \tag{42}$$

and the stress-rate and strain-rate relations which are associated with the state of stress A.

The last relations are easily obtained from the results of the previous section. The circumferential and axial directions are associated with the subscripts 1 and 2, the parameters p_1 have the values

$$p_1 = \pm\,\infty, \qquad p_2 = e/8\kappa, \qquad p_3 = -\,e/8\kappa.$$

For the strain-rates satisfying $|e/4\,\kappa| > 1$ and $e > 0$ the points P_1 fall outside of the interval $-\,h/2 \leqslant z \leqslant h/2$. Equations (23) can then be used to obtain

$$\left.\begin{aligned} \dot{n} &= \frac{c}{\sigma_0}\,e \\ \dot{m} &= 0 \end{aligned}\right\} \qquad \text{for} \qquad |e/4_\kappa| > 1, \qquad e > 0. \tag{43}$$

For $|e/4\,\kappa| = 1$ and $e > 0$, the points P_2 and P_3 are at $z = h/2$ and $z = -\,h/2$ respectively, and (27) must be employed to obtain the stress–strain-rate relations. For the case under consideration, $\kappa_1 = 0$, $\dot{N}_1 = 0$ and $\max|\epsilon| = e_1 = e$ for $-\,h/2 \leqslant z \leqslant h/2$ and (27) reduces to

$$\dot{M}_2\,\kappa_2 + \dot{N}_1\,e_1 = c e_1 \int_{-h/2}^{-h/2} e_1\,dz$$

or, in dimensionless variables,

$$\dot{m}\kappa + \dot{n}e = \frac{c}{\sigma_0}\,e^2,$$

from which we obtain

$$\dot{m} + 4\dot{n} = 4\,\frac{c}{\sigma_0}\,e \qquad \text{for} \qquad \frac{e}{4_\kappa} = 1, \qquad \dot{m} \geqslant 0\,; \tag{44}$$

$$-\,\dot{m} + 4\dot{n} = 4\,\frac{c}{\sigma_0}\,e \qquad \text{for} \qquad \frac{e}{4_\kappa} = -\,1, \qquad \dot{m} \leqslant 0. \tag{45}$$

Additional restrictions concerning the sign of $\dot{m}$ are physically obvious. The description of stress–strain-rate relations at the plastic state of stress A is complete by adding the following inequalities

$$\dot{n} \leqslant 0, \qquad \dot{m} \leqslant 4\dot{n} \qquad \text{for} \qquad e = \kappa = 0 \tag{46}$$

which describe the rigid behaviour. The problem is therefore to find w and $\dot{m}$ satisfying (39) and (43), (44) or (46) and the boundary conditions (42). The question of uniqueness of w and $\dot{m}$ will be discussed first.

According to Hill (1956) the investigation of uniqueness starts as usual from the remark that the boundary conditions and the principle of virtual work show that

$$0 = \int (\dot{\bar{p}}' - \dot{\bar{p}}'')\,(w' - w'')\,d\xi = N_0 \int \left[(\dot{n}' - \dot{n}'')\,(e' - e'') + (\dot{m}' - \dot{m}'')\,(\kappa' - \kappa'')\right] d\xi \tag{47}$$

where primes and double primes are used to distinguish between two solutions. In discussing the sign of the last integrand in (47), we must keep in mind that both solutions correspond to the same instantaneous stress represented by the point A in Fig. (5). At a generic section of the shell for each solution the rates satisfy one of equations (43) to (46). The sign of the integrand must be investigated for the ten cases corresponding to the combinations of four different types of behaviour which both solutions may exhibit. It is easily seen by considering these combinations that the last integrand in (47) is positive unless $e' = e''$ or, according to (90), $w' = w''$. This fact establishes the uniqueness of the velocity field, even though the rates $\dot{m}$ are not necessarily unique.

As an example for the determination of the unique displacement-rates w we consider a ' short ' shell of non-dimensional length $\xi l = l/\sqrt{(Rh)} = \pi$. We shall assume that (45) is satisfied throughout the shell. In terms of displacement-rate w, the condition $c/4\,\kappa = -1$ is equivalent to

$$w_{\xi\xi} + w = 0,$$

so that w must be of the following form

$$w = -V_0 \sin \xi, \tag{48}$$

where V_0 will be related to the rate of pressure intensity $\dot{\bar{p}}$.

From (39), (45) and (48) we obtain the following equation for $\dot{m}$:

$$\dot{m}_{\xi\xi} + \dot{m} = 4\left(\dot{\bar{p}} - \frac{c}{\sigma_0}\frac{V_0}{R}\sin\xi\right). \tag{49}$$

The general solution of (49) is

$$\dot{m} = a \sin \xi + b \cos \xi - 2\,\frac{c}{\sigma_0}\frac{V_0}{R}\,\xi \cos \xi,$$

where a and b are arbitrary constants. The stress boundary-conditions $\dot{m} = 0$ at $\xi = 0$ and $\xi = \pi$ require that

$$b = -4\dot{\bar{p}} \qquad \text{and} \qquad V_0 = \frac{4}{\pi}\left(\frac{\sigma_0}{c}R\right)\dot{\bar{p}}$$

where the last equation determines the ' magnitude ' of the displacement-rate as a function of the rate of pressure intensity for the incipient deformations of the shell.

The distribution of $\dot{m}$ contains the arbitrary constant a,

$$\dot{m} = a \sin \xi + 4\dot{\bar{p}}\left[(1 - \cos \xi) + \frac{2}{\pi}\,\xi \cos \xi\right].$$

The condition $\dot{m} \leqslant 0$ requires that

$$a < -\frac{c}{\sigma_0}\frac{V_0}{R}\,\pi$$

otherwise $\dot{m}$ is not uniquely determined as shown in Fig. 6. The uniqueness of w, on the other hand, justifies the assumption that $c/4\,\kappa = -1$ throughout the shell.

References

Boyce, W. E.	1956	*Quart. Appl. Math.* **14**, 277.
Boyce, W. E. and Prager, W.	1957	*J. Mech. Phys. Solids* **6**, 9.
Drucker, D. C.	1953	*1st Midw. Conf. Solid Mech.* (Urbana), 158.
Flügge, W.	1934	*Statik und Dynamik der Schalen* (Springer, Berlin).
Hill, R.	1956	*J. Mech. Phys. Solids* **4**, 247.
	1956	*J. Mech. Phys. Solids* **5**, 1.
Hodge, P. G., Jr.	1954	*J. Appl. Mech.* **21**, 336.
	1956	*J. Franklin Inst.* **263**, 13.
Hodge, P. G., Jr. and Romano, F.	1956	*J. Mech. Phys. Solids* **4**, 145.
Hopkins, H. G. and Prager, W.	1953	*J. Mech. Phys. Solids* **2**, 1.
Onat, E. T.	1955	*Quart. Appl. Math.* **13**, 63.
Onat, E. T. and Prager, W.	1954	*Proc. Koninkl. Ned. Akad. Wet.* Amst. B **57**, 534.
Pell, W. H. and Prager, W.	1951	*Proc. 1st Nat. Congr. Appl. Mech.* (Chicago) 547.
Prager, W.	1956	*J. Appl. Mech.* **23**, 493.

Journal of the Mechanics and Physics of Solids, 1958, Vol. 7, pp. 60 to 70. Pergamon Press Ltd., London

ON THE STRENGTH OF CLASSICAL FIBRES AND FIBRE BUNDLES

By B. D. Coleman
Mellon Institute, Pittsburgh

(*Received 20th February*, 1958)

Summary

This paper discusses tensile strength distributions for fibres (called 'classical fibres') whose strength is independent of the rate of loading. Reasons are presented for expecting, in the absence of all other information, that the tensile strength of long classical fibres from a common stationary source should obey the Weibull distribution. The statistical theory of the strength of bundles of classical fibres, as developed by Daniels, is applied to infinite bundles composed of fibres which obey the Weibull distribution. It is found that the ratio of the tensile strength (units of force at break per initial unit area) of a bundle to the mean tensile strength of the constituent filaments decreases montonically with increasing dispersion in the strength of the constituent filaments. In general, the tensile strength of a large bundle has the same order of magnitude, but is *less* than the mean strength of the component filaments. Previous calculations have yielded this conclusion for fibres with a special time-dependence to their tensile strength; here it is shown that the conclusion also applies to classical fibres.

1. Introduction

The words 'classical fibres' are used here to refer to fibres whose tensile strength is independent of the rate of loading. Several articles have appeared attempting to calculate tensile strength distributions for such fibres from static statistical models (e.g. Peirce 1926; Weibull 1939; Frenkel and Kontorova 1943). The relationship of these theories to the general statistical theory of extreme values (Fisher and Tippett 1928; Cramér 1946; Gumbel 1954) has been explained by Epstein (1948). We shall refer to these static-model theories as the 'classical theories' of strength distributions.

A statistical theory of mechanical breakdown in *time-dependent systems* was recently presented (Coleman, 1956; 1958b). This theory, called "the theory of breaking kinetics," was designed to permit calculations of the distribution of tensile strength in fibres for which the tensile strength does depend on the speed of measurement. It has been shown that the results of the different classical theories can be obtained from the theory of breaking kinetics as special cases. Of the various classical theories, however, that of Weibull (1939) follows most naturally from the theory of breaking kinetics.

It is common practice to assume that the strength (in units of force per initial unit area) of a simple parallel array of filaments† is equal to the average strength

†The words *fibre* and *filament* are used here as though they were synonomous. They refer to a cylindrical entity for which the stress can be represented by a monotonic-increasing, continuous, scalar function of strain up to the breaking point.

exhibited by the component filaments when tested separately. It has been pointed out by PEIRCE (1926) that this is not so. A rigorous statistical theory of the relationships between tensile strength distributions for bundles and strength distributions for the constituent filaments has been developed by DANIELS (1945). This theory is restricted to classical fibres.

Recently, methods have been developed for calculating relationships between the strength of bundles and the strength of their constituent filaments when the strength depends on the speed of testing (COLEMAN 1947, 1958a ; COLEMAN and MARQUARDT 1957). These methods are based on the theory of breaking kinetics. Numerical results reported for the special case in which the fibres have been sampled from a first-order ensemble‡ indicate that the strength (units of force at break per initial unit area) of a large bundle (with no twist and no interfibre friction) may be expected to be of the same order of magnitude, but in general, *less* than the average strength of the constituent filaments. In a future publication we shall present similar numerical results for fibres obeying time-dependent breakdown rules of greater generality. It is the main purpose of the present article to see whether *classical* fibres should be expected to lose strength when tested in bundles.

We shall here investigate the implications of the work of PEIRCE and DANIELS as regards the relative magnitudes of the mean strength of a large bundle and the mean strength of the component filaments. To get numerical results we must assume that we are dealing with fibres which, when tested separately, obey a specific tensile strength distribution function. We choose a function which was first proposed by WEIBULL. The discussion will consist of two parts. First, reasons will be given for believing that, in the absence of all other information, the tensile strength of separate long classical fibres from a common source should be expected to follow WEIBULL's distribution. Then, an expression will be obtained for the ratio, ϵ, of the mean strength, $E_\infty\{f^*\}$, of a large bundle to the mean strength, $E_1\{f^*\}$, of its component filaments, as a function of the coefficient of variation, $\sigma_1/E_1\{f^*\}$, in the strength of the component filaments.

If a classical fibre of length l is loaded with a dead weight, it either breaks immediately or lasts forever. Let $B_l(s^*)$ be the probability that the fibre breaks when the applied load is s^*, (in dynes). The function $B_l(s^*)$, which can depend on l, is called the cumulative distribution function of breaking loads. If the cross-sectional area of the fibre before loading is known to be A, then we can consider the variable $f^* = s^*/A$, which is called the tensile strength, and we write $G_l(f^*)$ for the cumulative distribution function of tensile strengths. If instead of suddenly applying static loads we gradually stretch the fibre, then $G_l(f^*)$ gives the probability that the fibre breaks before the stress reaches the value f^*.

In addition to assuming that $G_l(f^*)$ and $B_l(s^*)$ are independent of the rate of stretching, we shall also assume here that the entire load-elongation curves for our fibres are independent of the rate of stretching. When this is so, the load s corresponding to an elongation e can be written

$$s = s(e, \alpha_1 \ldots \alpha_n), \tag{1}$$

‡This is an ensemble of fibres whose strength depends on the speed of measurement in a manner such that the probability that a given fibre breaks in a small time interval is a function of the force on the fibre during that interval and is independent of the previous loading history. Such fibres are markedly different from classical fibres.

where $\alpha_1 \ldots \alpha_n$ represent n parameters defining the load-elongation curve specific to a particular fibre. The function $s(e, \alpha_1 \ldots \alpha_n)$ is monotonic-increasing in e. The load at break s^* is related to the elongation at break e^* as follows:

$$s^* = s(e^*, \alpha_1 \ldots \alpha_n). \tag{2}$$

The practical applications of our discussion of bundles will be further limited by the assumption that there is no interfibre friction or twist in the bundles. For treatments of the effects of twist on the distribution of stress among the component filaments, the reader is referred to the works of SULLIVAN (1942), PLATT (1950) and PLATT *et al.* (1952a, 1952b, 1954). These last three papers also contain discussions of the effect of fibre non-uniformity on the tensile strength of a bundle. The statistical treatments presented, however, cannot be considered adequate because they are based on the assumption that the tensile strength distribution for the component fibres is normal (Gaussian). This assumption is in contradiction with the notion that a fibre always breaks at its weakest cross-section. The first numerical calculations of the strength of bundles whose constituent filaments obey the normal distribution were presented by PEIRCE (1926). WILLIAMS and KLOOT (1952) have given calculations of bundle properties using another special distribution which differs from the one to be studied here.

2. SEPARATE FIBRES

If one is given a set of fibres and is told only the following information — that the fibre lengths l are great; that the fibre cross-sectional areas A are all equal; that the fibres are classical; that the fibres come from a common source which is stationary with respect to distance along the yard (say, from the same spool†); and that $G_l(f^*)$ is a continuous function of l and f^*; — one can (surprisingly) make a good guess about the functional form of $G_l(f^*)$. This is so because the following self-evident statements furnish further useful information about $G_l(f^*)$: (a) When a fibre is tested it breaks at its weakest cross-section. (b) The strength of a fibre must be positive regardless of the fibre length. (c) $G_l(f^*)$ must be a monotonic-increasing function of f^*.

To obtain a form for $G_l(f^*)$ from these postulates, we consider that each fibre in the collection may be regarded as a set of l non-interacting unit lengths. Let $x_1 \ldots x_i \ldots x_l$ be the tensile strength of each of the l unit segments in a given fibre. It is assumed that the positive random variables x_i have the *same* cumulative distribution function ‡ $Pr\{x_i < f^*\} = G_1(f^*)$. (That G_1 is the same for all the unit lengths is a consequence of the statement that the fibres come from a common stationary source.) According to item (a), the tensile strength of a fibre is the minimum of a sampling $(x_1 \ldots x_i \ldots x_l)$:

$$1 - G_l(f^*) = Pr\{\min(x_1 \ldots x_i \ldots x_l) > f^*\}. \tag{3a}$$

Or, in other words, the probability, $1 - G_l(f^*)$, that a given fibre has a tensile

† The word 'stationary' is borrowed from the theory of stochastic processes. As used here it implies (roughly) that all the statistical properties (mean, variance, skewness, etc.) of the strength distribution should be independent of distance along the yarn and thus free from long-range trends.

‡ The symbol $Pr\{\ \}$ is to be read *the probability of* $\{\ \}$. The subscript 1 on G_1 indicates that this distribution function refers to *unit* segments.

strength greater than f^* is equal to the probability that all of its l independent segments have a tensile strength greater than f^* :

$$1 - G_l(f^*) = [1 - G_1(f^*)]^l. \tag{3b}$$

For large l, the right side of (3b) vanishes whenever $G_1(f^*)$ differs appreciably from zero ; but, according to items (b) and (c), small $G_1(f^*)$ corresponds to small f^*. Thus the form of $G_l(f^*)$ for large l is determined by the behaviour of $G_1(f^*)$ as f^* approaches its lower bound of zero.

(a) *The expected case*

In the absence of any other information, one would expect $G_1(f^*)$ to be well-behaved near the origin in the sense that $G_1(f^*)$ goes to zero as some positive power of f^* :

$$\lim_{f^* \to 0} G_1(f^*) = cf^{*w} + o(f^{*w}) ; \tag{4a}$$

c and w are positive constants ; w is not necessarily an integer.

Here, we shall derive the WEIBULL distribution from an assumption which is a bit more general than (4a). We assume merely that for all $X > 0$

$$\lim_{t \to 0} \frac{G_1(tX)}{G_1(t)} = X^w, \tag{4b}$$

where t is any positive variable. Direct substitution shows that (4b) not only includes (4a) but also such cases as

$$\lim_{f^* \to 0} G_1(f^*) = cf^{*w} [\log(bf^*)]^a + O(f^{*w+1}). \tag{4c}$$

Determine the quantity t_l such that

$$G_1(t_l) = 1/l \tag{5a}$$

and consider a new random variable z_l defined by

$$z_l = t_l \min(x_1 \ldots x_i \ldots x_l). \tag{5b}$$

Note that as $l \to \infty$, $t_l \to 0$. The probability that z_l is greater than some fixed quantity X is

$$Pr\{z_l > X\} = [1 - G_l(t_l X)]^l. \tag{6a}$$

To evaluate the right side of (6a) for large l, we use (4b), putting $t = t_l$:

$$\lim_{l \to \infty} Pr\{z_l > X\} = \lim_{l \to \infty} [1 - G_1(t_l) X^w]^l, \tag{6b}$$

and from (5a) :

$$\lim_{l \to \infty} Pr\{z_l > X\} = \lim_{l \to \infty} \left[1 - \frac{1}{l} X^w\right]^l = \exp\{-X^w\}. \tag{6c}$$

To get (6c) into recognizable form we must reverse the change of scale introduced in (5a) and (5b). For this purpose we put $f^* = t_l^{-1} X$ and note that then

$$\begin{aligned} Pr\{z_l > X\} &= Pr\{\min(x_1 \ldots x_i \ldots x_l) > f^*\} \\ &= 1 - G_l(f^*). \end{aligned}$$

It is now clear that (6c) is equivalent to the statement that for long fibres

$$G_l(f^*) = 1 - \exp\{-(f^*/l_l)^w\}. \tag{7}$$

When (4a) is applicable, $t_l \sim (cl)^{-1/w}$, and (7) becomes

$$G_l(f^*) = 1 - \exp\{-lcf^{*w}\}. \tag{8a}$$

Actually, whenever (7) is a valid limiting form derived from (4b), (7) must be well approximated, for very large l, by (8a). This can be seen from the following argument. We note that, after having obtained a value of l large enough so that (7) is obeyed with arbitrary precision, we can use a new unit of length such that $l = 1$. We then ask the question : What is the functional form of $G_L(f^*)$, with $L \gg 1$ in the new units? To answer this, we note that in the new units (7) reads

$$G_1(f^*) = 1 - \exp\{-(f^*/t_1)^w\}$$
$$= (f^*/t_1)^w + O(f^{*w+1}).$$

Thus, $G_1(f^*)$ obeys (4a) with $c = t_1^{-w}$. If we now repeat the steps used to derive (7), we find that for fibres of length L,

$$t_L \sim (cL)^{-1/w}$$

and

$$\lim_{L\to\infty} G_L(f^*) = 1 - \exp\{-Lcf^{*w}\}.$$

Thus, (7) approaches (8a), in form, when L gets large, or when l gets very large.

Equation (8a) is the WEIBULL distribution. WEIBULL also studied a slightly more general distribution function which has the form

$$G_l(f^*) = 1 - \exp\{-lc(f^* - f_c)^w\}. \tag{8b}$$

Here, when $f^* < f_c$, $G_l(f^*) = 0$. GUMBEL (1954) has called this distribution function the 'third asymptotic probability of smallest values'; it may be derived by replacing our restriction that $G_l(f^*)$ vanish for all $f^* \leqslant 0$, by the restriction that $G_l(f^*) = 0$ for all f^* less than some critical stress f_c. WEIBULL found that many materials obey (8a) nicely, but for some materials (8b) gives a significantly better fit. For simplicity, the present discussion shall be limited to materials which obey (7).

The following facts about the distribution function (7) are well known. Its mth moment† $E_1\{f^{*m}\}$ is

$$E_1\{f^{*m}\} = \int_0^\infty f^{*m}\frac{dG_l}{df^*}df^* = t_l^m\,\Gamma(1 + m/w); \tag{9}$$

from which one can calculate the average strength, $E_1\{f^*\}$:

$$E_1\{f^*\} = t_l\,\Gamma(1 + 1/w); \tag{10}$$

the coefficient of variation :

$$\sigma_1/E_1\{f^*\} \equiv \frac{[E_1\{f^{*2}\} - E_1^2\{f^*\}]^{\frac{1}{2}}}{E_1\{f^*\}}$$
$$= \left[\frac{\Gamma(1 + 2/w)}{\Gamma^2(1 + 1/w)} - 1\right]^{\frac{1}{2}}; \tag{11}$$

and the coefficient of skewness :

$$\mu_1^3/\sigma_1^3 = \frac{E_1\{f^{*3}\} - 3E_1\{f^*\}E_1\{f^{*2}\} + 2E_1^3\{f^*\}}{[E_1\{f^{*2}\} - E_1^2\{f^*\}]^{3/2}}$$
$$= \frac{\Gamma(1 + 3/w) - 3\Gamma(1 + 1/w)\,\Gamma(1 + 2/w) + 2\Gamma^3(1 + 1/w)}{[\Gamma(1 + 2/w) - \Gamma^2(1 + 1/w)]^{3/2}}. \tag{12}$$

In (11) and (12), σ_1 is the standard deviation and μ_1 is the third central moment. The following limiting forms are occasionally useful :

$$\lim_{w\to\infty} \sigma_1/E_1\{f^*\} = \pi 6^{-\frac{1}{2}} w^{-1}, \tag{13}$$

†The subscript 1 on the expectation operator, E_1, indicates that we are talking about separate fibres, or bundles of one fibre each. The symbol E_∞ represents expectation operator for a bundle containing an infinite number of filaments.

$$\lim_{w \to \infty} \mu_1^3/\sigma_1^3 = -2\pi^{-3}\, 6^{3/2} \sum_{r=1}^{\infty} r^{-3}$$

$$= -1{\cdot}1395 \ldots\ldots \tag{14}$$

FREUDENTHAL and GUMBEL (1953) have shown that distributions of the same form as (7) play an important role in the statistical interpretation of fatigue tests. These authors have described in detail a reliable method for evaluating the parameters t_l and w from observed distributions. A rapid, though less sophisticated and perhaps less efficient, method of estimating these parameters can be developed from (10), (11) and (12). Estimates of the quantities, $E_1\{f^*\}$, $\sigma_1/E_1\{f^*\}$, and μ_1^3/σ_1^3, can be calculated from repeated measurements of f^* at fixed l. The parameter w may then be estimated from (11) and (12). Agreement between these two estimates for w, within the errors of random sampling, furnishes a check on (7). Once w is known, (10) may be used to obtain an estimate for t_l. The first three columns in Table 1 give a numerical evaluation of (11) and (12).

TABLE 1. *The quantities* $\sigma_1/E_1\{f^*\}$, μ_1^3/σ_1^3 *and* ϵ *as functions of* w, *based on* (11), (12) *and* (30)

w	$\sigma_1/E_1\{f^*\}$	μ_1^3/σ_1^3	ϵ
0·00	∞	∞	0·0000
0·25	40·9756	60·092	0·1954
0·50	2·2361	6·619	0·2707
0·75	1·3528	3·121	0·3250
1·00	1·0000	2·000	0·3679
1·25	0·8050	1·430	0·4036
1·50	0·6790	1·072	0·4340
1·75	0·5898	0·821	0·4605
2·00	0·5227	0·631	0·4839
2·25	0·4703	0·481	0·5048
2·50	0·4279	0·359	0·5237
2·75	0·3929	0·256	0·5408
3·00	0·3634	0·168	0·5564
3·50	0·3165	0·025	0·5839
4·00	0·2805	−0·087	0·6076
5·00	0·2291	−0·254	0·6463
6·00	0·1938	−0·373	0·6769
7·00	0·1680	−0·463	0·7017
8·00	0·1484	−0·534	0·7226
9·00	0·1329	−0·591	0·7403
10·00	0·1203	−0·638	0·7555
20·00	0·0620	−0·868	0·8412
50·00	0·0253	−1·025	0·9167
100·00	0·0127	−1·081	0·9509
∞	0·0000	−1·140	1·0000

The papers of WEIBULL (1939), and of FREUDENTHAL and GUMBEL (1953, 1954) contain tables of related functions†.

†The reader is cautioned that FREUDENTHAL and GRUMBEL use the expression 'coefficient of variation' with a different definition from that used here. They use it to denote a quantity which, in our notation, would be $w^{-1}\sigma_1$. Here it denotes $\sigma_1/E_1\{f^*\}$.

If measurements of f^* at different values of l are available, the validity of (7) may be checked through use of the fact that it predicts that $\sigma_1/E_1\{f^*\}$ and μ_1^3/σ_1^3 should be independent of l.

WEIBULL originally obtained his distribution function by semi-empirical methods which were not intended to constitute a rigorous derivation. Here we have shown that his distribution function is consistent with the self-evident postulates (a), (b) and (c), and can be derived as an asymptotic limit if (4b) is assumed. In the next Section we shall see that there are other limiting distribution functions compatible with postulates (a), (b) and (c), but these will appear to be mathematical anomalies with little physical interest.

It should be pointed out that those classical theories of strength distributions (see PEIRCE 1926; FRENKEL and KONTOROVA 1943; GUMBEL 1954, pp. 40-42) which lead, in the limit of large l, to the 'first asymptotic probability of smallest values' (i.e. the doubly exponential distribution) for f^* are consistent with postulates (a) and (c) but contradict postulate (b). These theories all yield a non-vanishing probability for negative tensile strengths; as l increases, the probability of a negative strength increases†. This does not mean that such theories should be dismissed as nonsense — they may be of value in certain limited ranges of l.

In his paper on statistical aspects of fracture problems, EPSTEIN (1948) uses techniques described by CRAMÉR (1946) to obtain an analysis of the consequences of five possible assumptions about the form of the *a priori* distribution function, $G_1(f^*)$. Two of the assumptions considered by EPSTEIN [his numbers (1) and (5)] yield results which obey postulate (b) for all l. In these cases $G_1(f^*)$ is (1) a rectangular distribution and (5) a WEIBULL distribution. For the three remaining cases $G_1(f^*)$ represents (2) a Cauchy distribution, (3) a Laplace distribution (with density function $g_1(f^*) = (2\lambda)^{-1}\exp\{-\lambda^{-1}|f^* - \mu|\}$), and (4) a normal (Gaussian) distribution. Although the point is not emphasized, it is clear from the results listed in his Table 1 that there exists for each of the asymptotic strength distributions resulting from (3), (4) and (5) a fixed *finite* value of l, say l_c, such that for all $l > l_c$ the mode of the strength distribution is negative; this cannot occur in real fibres.

(b) *An exceptional case*‡

According to postulate (b) we must have $G_1(0) = 0$. In (4b) it was assumed (roughly) that $G_1(f^*)$ goes to zero about as fast as some positive finite power of f^*. This assumption was essential to the derivation of (7). The use of (4b) is most reasonable and certainly represents a best first guess; but it is of interest to study the consequences of other assumptions.

Here, we shall explore the assumption that $G_1(f^*)$ approaches zero much faster than equations (4) indicate. We assume that for small f^*

$$G_1(f^*) \sim \exp\{-\phi(f^*)\} \tag{15a}$$

where

$$\lim_{f^* \to 0} \phi(f^*) = \infty. \tag{15b}$$

For a concrete example, we take

$$\phi(f^*) \sim \left(\frac{a}{f^*}\right)^b \tag{16}$$

where a and b are positive constants.

†This point is made by CHECHULIN (1954) in criticism of the theory of FRENKEL and KONTOROVA (1943).

‡The existence of the strange case discussed here was pointed out to the author by PROF. W. FELLER.

We once again let $x_1 \ldots x_i \ldots x_l$ be the tensile strengths of each of the l unit segments in a given fibre. This time we consider the random variable y_l defined by

$$y_l = (\log l)^{-1/b} \min (x_1 \ldots x_i \ldots x_l). \tag{17}$$

The probability that y_l is greater than a fixed quantity X is

$$Pr\{y_l > X\} = [1 - G_l\{(\log l)^{-1/b} X\}]^l. \tag{18}$$

From (15) and (16),

$$\lim_{\to \infty} Pr\{y_l > X\} = \lim_{l \to \infty} \left[1 - \exp\left\{-\left(\frac{a}{X}\right)^b \log l\right\}\right]^l \tag{19a}$$

$$= \lim_{l \to \infty} [1 - (1/l)^{(a/X)^b}]^l, \tag{19b}$$

which tends to 1 if $X < a$ and to 0 if $X > a$.

We thus have the strange result that, in the limit of large l, y_l is, with certainty, equal to a. In other words, the distribution of f^* is such that in the limit $l \to \infty$,

$$f^* \to a (\log l)^{-1/b}, \tag{20}$$

with no dispersion. All experience indicates that the variation in tensile strength is not negligible for long fibres ; it is therefore doubtful that real systems obey (15) and (16).

Results of this sort can be obtained more generally from (15a) and (15b) if instead of (16) we assume only that

$$\lim_{t \to 0} \frac{\phi(tX)}{\phi(t)} = \begin{cases} \omega(X) < 1, & X > 1 \\ \omega(X) > 1, & X < 1. \end{cases} \tag{21}$$

Equations (4), (15) and (21) appear to exhaust all imaginable distribution functions, $G_1(f^*)$, which satisfy postulates (b) and (c) and have a simple behaviour near the origin.

The treatment of asymptotic distributions of extreme values given here draws on the papers of Fisher and Tippett (1928), Gumbel (1954) and Gnedenko (1943), and particularly on a discussion with Prof. Feller. The purpose of the present treatment has not been to construct a rigorous derivation of (7), but rather to illustrate for physicists that the literature on probability theory suggests that the sufficient conditions for the application of this equation to strength distributions are far more general than is usually supposed. More complete discussions of the asymptotic forms of distributions of largest and smallest values are to be found in the works of von Mises (1936) and Gnedenko (1943). By using methods which differ from those used here, Gnedenko has proved that (4b) is not only sufficient, but also necessary, for the validity of (7) as a stable limiting form.

3. Bundles

Consider a bundle composed of a very large number, N, of classical filaments of equal length l. The bundle is imagined to have been placed in an apparatus which controls its total elongation, e, in such a manner that e increases monotonically with time. The constituent filaments are so clamped that at each moment all unbroken filaments have the same elongation, e. Let $x_l(e^*, \alpha_1 \ldots \alpha_n)\, de^*\, d\alpha_1 \ldots d\alpha_n$ be the probability that the breaking elongation, e^*, and the parameters, $\alpha_1 \ldots \alpha_n$, for a given fibre are in specified small intervals. Let $S(e)$ be the total load on the bundle. In the limit of large N, the dispersion in S is negligible, and S is given by the following equation :

$$S(e) = N \int_{-\infty}^{\infty} \cdots \int_{-\infty}^{\infty} \int_{e}^{\infty} s(e, \alpha_1 \ldots \alpha_n)\, x_l(e^*, \alpha_1 \ldots \alpha_n)\, de^*\, d\alpha_1 \ldots d\alpha_n. \tag{22}$$

Let e_τ be that value of e at which $S(e)$ reaches its maximum value, S^* :

$$\left.\frac{dS(e)}{de}\right|_{e=e_\tau} = 0 \tag{23}$$

$$S^* = S(e_\tau). \tag{24}$$

Clearly, the bundle can sustain any load less than S^*, but no load greater than S^*; thus, S^* is called the 'breaking load' for the bundle, and e_τ is the 'breaking elongation' for the bundle.

Our numerical results are restricted to the special case in which all the filaments have the same cross-sectional area A and stress–strain curves of the same shape, but differ in their values of the elongation at break. In other words, the dispersion in the quantities $\alpha_1 \ldots \alpha_n$ is assumed to be insignificant when compared with that in e^*. This represents the simplest type of bundle. In this case it can be shown that the distribution of the tensile strength, $f^* = S^*/NA$, of the bundle tends for large N toward a normal distribution, with an expectation

$$E_\infty \{f^*\} = f_\tau [1 - G_l(f_\tau)] \tag{25}$$

and a standard deviation

$$\sigma_\infty = f_\tau \{G_l(f_\tau)[1 - G_l(f_\tau)]\}^{\frac{1}{2}} N^{-\frac{1}{2}}, \tag{26}$$

where f_τ is that value of f which gives $f[1 - G_l(f)]$ its maximum value :

$$\left.\frac{d f[1 - G_l(f)]}{df}\right|_{f=f_\tau} = 0. \tag{27}$$

Here, $E_\infty \{f^*\}$, f_τ and σ_∞ all are in the units of force per unit area. Equation (25) can be obtained directly from (22). The proof of the theorem that the distribution of f^* for a large bundle is normal with the standard deviation shown in (26) is a much deeper and more difficult matter ; this theorem is due to DANIELS.

We are interested in obtaining the quantity $\epsilon = E_\infty \{f^*\}/E_1 \{f^*\}$ as a function of $\sigma_1/E_1 \{f^*\}$. For this calculation we need an explicit expression for $G_l(f^*)$. We use (7). When (7) is substituted into (27) the following expression is obtained for f_τ :

$$f_\tau = (lcw)^{-1/w}; \tag{28}$$

f_τ is actually the stress in each unbroken filament when the elongation of the bundle is equal to e_τ. Equation (28) is substituted into (25) to obtain the following expression for expected value of the tensile strength of the bundle :

$$E_\infty \{f^*\} = (lcw)^{-1/w} \exp\{-w^{-1}\}. \tag{29}$$

Comparing this with (10) we find that the ratio of the tensile strength of a bundle to the average tensile strength of its filaments is

$$\epsilon = [w^{1/w} \exp\{w^{-1}\}\, \Gamma(1 + 1/w)]^{-1}. \tag{30}$$

It is interesting to note that ϵ is independent of t_l and thus independent of l.

The fourth column in Table 1 lists values ϵ at selected values of w. Since $\sigma_1/E_1\{f^*\}$ and ϵ are both known functions of w, ϵ is now a known function of $\sigma_1/E_1\{f^*\}$. A graph of this function is shown in Fig. 1. It will be noticed that,

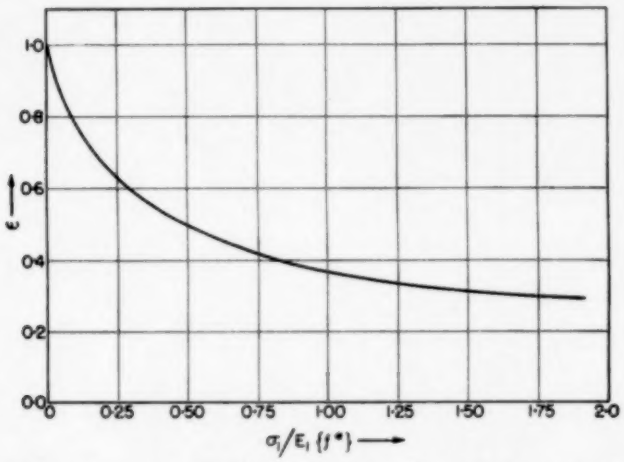

Fig. 1. The strength efficiency, ϵ, for an infinite bundle vs. the coefficient of variation, $\sigma_1/E_1\{f^*\}$, in the strength of the component filaments. Based on (11) and (30).

as expected, when there is no dispersion in the strength of the component filaments ($\sigma_1/E_1\{f^*\} = 0$, $w = \infty$), the strength of a bundle is exactly equal to that of its component filaments ($\epsilon = 1$). As $\sigma_1/E_1\{f^*\}$ increases above zero, however, ϵ decreases montonically and approaches zero in the limit of infinite dispersion. As a typical practical example, we note that when $\sigma_1/E\{f^*\}$ is about 10 or 20 per cent, ϵ is about 70 per cent. Thus, we expect to find for real fibres, even in the absence of twist and time-dependence effects, that the tensile strength of very large bundles has the same order of magnitude but is *less* than the average tensile strength of the constituent filaments.

Acknowledgments

The author is indebted to Prof. W. Feller of Princeton University for a very valuable discussion of extreme value statistics.

Thanks are due to Miss M. Burdick for her patient help with the numerical calculations.

References

Chechulin, B. B. 1954 *J. Tech. Phys. (U.S.S.R.)* **24**, 292.
Coleman, B. D. 1956 *J. Appl. Phys.* **27**, 862 (*Errata ibid.* **28**, 1514).
1957 *J. Appl. Phys.* **28**, 1058.
1958a *Trans. Soc. Rheology* **2**. In press.
1958b *J. Appl. Phys.* **29**. In press.
Coleman, B. D. and Marquardt, D. W. 1957 *J. Appl. Phys.* **28**, 1065.

CRAMÉR, H.	1946	*Mathematical Methods of Statistics*, Chap. 28 (Princeton University Press, Princeton).
DANIELS, H. E.	1945	*Proc. Roy. Soc.* A **183**, 405.
EPSTEIN, B.	1948	*J. Appl. Phys.* **19**, 140.
FISHER, R. A. and TIPPETT, L. H. C.	1928	*Proc. Camb. Phil. Soc.* **24**, 180.
FRENKEL, J. I. and KONTOROVA, T. A.	1943	*J. Phys.* (*U.S.S.R.*) **7**, 108.
FREUDENTHAL, A. M. and GUMBEL, E. J.	1953	*Proc. Roy. Soc.* A **116**, 309.
GNEDENKO, B.	1943	*Ann. Math.* **44**, 423.
GUMBEL, E. J.	1954	*Statistical Theory of Extreme Values and Some Practical Applications* (National Bureau of Standards, Washington, D.C., Appl. Math. Series No. 33).
VON MISES, R.	1936	*Rev. Math. l'Union Interbalkanique* **1**, 141.
PEIRCE, F. T.	1926	*J. Text. Inst.* **17**, T 355.
PLATT, M. M.	1950	*Text. Res. J.* **20**, 1.
PLATT, M. M., KLEIN, W. G. and HAMBURGER, W. J.	1952a	*Text. Res. J.* **22**, 641.
	1952b	*Ibid.* **22**, 827.
	1954	*Ibid.* **24**, 907.
SULLIVAN, R. R.	1942	*J. Appl. Phys.* **13**, 157.
WEIBULL, W.	1939	*Ing. Vetenskaps Akad. Handl.* **151**, **153**.
WILLIAMS, E. J. and KLOOT, N. H.	1952	*Austr. J. Appl. Sci.* **3**, 1.

Journal of the Mechanics and Physics of Solids, 1958, Vol. 7, pp. 71 to 75. Pergamon Press Ltd., London

EFFECT OF THERMAL PROPERTIES OF A SOLID ON THE VELOCITY OF RAYLEIGH WAVES

F. J. LOCKETT
Department of Mathematics, The University of Glasgow

(*Received 15th May*, 1958)

SUMMARY

THIS note is concerned with the propagation of Rayleigh waves in an isotropic thermoelastic solid. It is found that, within the frequency range normally attainable, the velocity of propagation of these waves can be determined from the classical equation merely by replacing the parameter $\beta^2 = (\lambda + 2\mu)/\mu$ occurring in that equation by $(1 + \epsilon)\beta^2$, where $\epsilon = \gamma^2 v_P^2 T(1 + \nu)^2/c(1 - \nu)^2$ where γ is the coefficient of linear expansion, v_P is the velocity of purely elastic longitudinal waves in the solid, T is the absolute temperature of the solid in its reference state of uniformly zero stress and strain, c is the specific heat at constant strain and ν is Poisson's ratio. A typical case is examined numerically and it is found that taking into account the thermal properties of the solid produces a difference of less than one per cent in the velocity and amplitude of the Rayleigh waves.

1. INTRODUCTION

IN a recent paper CHADWICK and SNEDDON (1958), using the formulation of the thermoelastic equations due to BIOT (1956), discussed the effect that the thermal properties have upon the form of plane waves travelling in an infinite elastic solid. This paper is concerned with the effect of these thermal properties on the velocity and form of the Rayleigh waves propagated in a semi-infinite medium. We use the system of units introduced by CHADWICK and SNEDDON, in which the unit of time is the reciprocal of a frequency ω^* characteristic of the solid and the unit of length is v_P/ω^* where v_P is the velocity of longitudinal elastic waves (P-waves) in the solid. The units of temperature and stress are taken to be the reference temperature T (at which the solid is initially in a state of zero stress and strain) and the rigidity modulus μ respectively. With this choice of units we obtain the equations in a form suitable for numerical work.

In Section 2 a general form for waves of the Rayleigh type in the solid is derived and in Sections 3 and 4 the solutions appropriate to specific boundary conditions are derived. The results are compared with those of the classical theory in Section 5.

2. GENERAL SOLUTION OF THE FIELD EQUATIONS

We consider a semi-infinite elastic solid $z \geqslant 0$ whose boundary $z = 0$ is free from stress. The classical theory of Rayleigh waves producing a displacement field of the type

$$\mathbf{u} = \mathbf{a}e^{-\alpha z + iq(x - ct)} \tag{1}$$

can be found in SNEDDON and BERRY (1958, p. 109). In this paper we consider how the form of these waves is affected when we take thermal properties into account. It is convenient to use the dimensionless forms of the thermoelastic field equations in which the reference state temperature T is taken to be the unit of temperature and the rigidity modulus μ is taken to be unit of stress, and the units of length l and time τ are given by the equations

$$\tau = \frac{1}{\omega^*} = \frac{k}{\rho c\, v_P{}^2}, \qquad l = v_P\, \tau, \tag{2}$$

where k is the conductivity, ρ the density, c the specific heat at constant volume and $v_P = [(\lambda + 2\mu)/\rho]^{\frac{1}{2}}$ is the velocity of P-waves in the elastic solid. In terms of these units the field equations become

$$\left.\begin{aligned} \nabla^2 \mathbf{u} + (\beta^2 - 1)\,\text{grad div}\,\mathbf{u} - b\,\text{grad}\,\theta &= \beta^2 \frac{\partial^2 \mathbf{u}}{\partial t^2} \\ \nabla^2 \theta &= \frac{\partial \theta}{\partial t} + g\,\frac{\partial}{\partial t}\,\text{div}\,\mathbf{u} \end{aligned}\right\} \tag{3}$$

(CHADWICK and SNEDDON, 1958, p. 225) where $\mathbf{u}$ is the displacement vector and $T(1 + \theta)$ is the temperature at a typical point in the solid,

$$\beta^2 = (\lambda + 2\mu)/\mu, \qquad b = \gamma(3\lambda + 2\mu)\,T/\mu, \qquad g = \gamma(3\lambda + 2\mu)/\rho c$$

and γ is the coefficient of linear expansion.

We now assume a solution of these equations of the form

$$\mathbf{u} = (a_1, 0, a_3)\, e^{i\phi}, \qquad \theta = \theta_1\, e^{i\phi}, \qquad \phi = q(x - ct) + i\alpha z. \tag{4}$$

We could, of course, have taken the more general displacement (1) but we should soon have discovered that $a_2 = 0$. If we substitute from equations (4) into equations (3) we find that

$$\left.\begin{aligned} \left[\alpha^2 - q^2\beta^2(1 - c^2)\right] a_1 - iq\alpha(\beta^2 - 1)\, a_3 - ibq\,\theta_1 &= 0, \\ -iq\alpha(\beta^2 - 1)\, a_1 + \left[\beta^2\alpha^2 - (1 - \beta^2 c^2)\, q^2\right] a_3 + b\,\alpha\,\theta_1 &= 0, \\ gcq^2\, a_1 + igcq\,\alpha a_3 - (\alpha^2 - q^2 + iqc)\,\theta_1 &= 0. \end{aligned}\right\} \tag{5}$$

Eliminating the ratios a_1/θ_1, a_3/θ_1 from these equations we find that

$$\begin{aligned} \left[\alpha^2 - (1 - \beta^2 c^2)\, q^2\right] \left[\beta^2\alpha^4 - (2\beta^2 q^2 - iqc\,\beta^2 - \beta^2 c^2 q^2 - ibqgc)\,\alpha^2 \right. \\ \left. + \left\{(1 - c^2)\,\beta^2 q^2 (q^2 - iqc) - ibq^3 gc\right\}\right] = 0. \end{aligned}$$

The roots $\alpha_1{}^2$, $\alpha_2{}^2$, $\alpha_3{}^2$ of this equation are given by the formulae

$$\begin{aligned} \alpha_1{}^2 = (1 - \beta^2 c^2)\, q^2, \qquad \alpha_2{}^2 + \alpha_3{}^2 = (2q^2 - iqc - c^2 q^2 - iqc\epsilon), \\ \alpha_2{}^2\,\alpha_3{}^2 = q^2(1 - c^2)(q^2 - iqc) - iq^3 c\epsilon, \end{aligned} \tag{6}$$

where we have written $\epsilon = bg/\beta^2$. The required square roots α_1, α_2, α_3 are those with positive real parts. To each of these roots α_i there corresponds a set of values of a_1, a_3, θ_1; we shall denote these values by a_{1i}, a_{3i}, θ_{1i}.

Case (*i*) $\alpha_i \neq \alpha_1$

From the first two equations of the set (5) we find that, if $\alpha_i \neq \alpha_1$,

$$\alpha_i a_{1i} + iqa_{3i} = 0 \tag{7}$$

and

$$ibq\,\theta_{1i} = \beta^2\left[\alpha_i^2 - (1 - c^2)\,q^2\right] a_{1i}. \tag{8}$$

Case (ii) $\alpha_i = \alpha_1$

From the second and third equations of the set (5) we find that $\theta_{11} = 0$ and that

$$a_{31}\,q\,(1 - \beta^2 c^2) = i\,\alpha_1\,a_{11}. \tag{9}$$

The general solution of the field equations is then of the form $\mathbf{u} = (u, 0, w)$ and θ where

$$\left.\begin{aligned} u &= (a_{11}\,e^{-\alpha_1 z} + a_{12}\,e^{-\alpha_2 z} + a_{13}\,e^{-\alpha_3 z})\,e^{iq(x\ ct)},\\ w &= (a_{31}\,e^{-\alpha_1 z} + a_{32}\,e^{-\alpha_2 z} + a_{33}\,e^{-\alpha_3 z})\,e^{iq(x-ct)},\\ \theta &= (\theta_{11}\,e^{-\alpha_1 z} + \theta_{12}\,e^{-\alpha_2 z} + \theta_{13}\,e^{-\alpha_3 z})\,e^{iq(x-ct)}. \end{aligned}\right\} \tag{10}$$

3. Radiation Condition on the Boundary

The boundary conditions are that the surface $z = 0$ is free from stress and that the radiation condition

$$\frac{\partial\theta}{\partial z} + h\theta = 0$$

holds over the boundary. With the forms (10) the shearing stress τ_{yz} is identically zero, and the three conditions $\tau_{xz} = \sigma_z = 0$, $\partial\theta/\partial z + h\theta = 0$ on $z = 0$ are satisfied if

$$(\alpha_1 a_{11} + \alpha_2 a_{12} + \alpha_3 a_{13}) = iq\,(a_{31} + a_{32} + a_{33}),$$

$$(\beta^2 - 2)\,iq\,(a_{11} + a_{12} + a_{13}) + \beta^2(\alpha_1 a_{31} + \alpha_2 a_{32} + \alpha_3 a_{33}) - b\,(\theta_{11} + \theta_{12} + \theta_{13}) = 0,$$

$$\alpha_1\theta_{11} + \alpha_2\theta_{12} + \alpha_3\theta_{13} = h\,(\theta_{11} + \theta_{12} + \theta_{13}).$$

With the aid of (6), (7), (8) and (9) we can write these equations in the form

$$-(\beta^2 c^2 - 2)\,\alpha_1 a_{11} + 2\,(1 - \beta^2 c^2)\,\alpha_2 a_{12} + 2\,(1 - \beta^2 c^2)\,\alpha_3 a_{13} = 0,$$

$$-2\,a_{11} + (\beta^2 c^2 - 2)\,a_{12} + (\beta^2 c^2 - 2)\,a_{13} = 0,$$

$$(h - \alpha_2)\left[\alpha_2^2 - (1 - c^2)\,q^2\right] a_{12} + (h - \alpha_3)\left[\alpha_3^2 - (1 - c^2)\,q^2\right] a_{13} = 0,$$

If we eliminate the ratios a_{12}/a_{11}, a_{13}/a_{11} and assume that $\alpha_2 \neq \alpha_3$ we find that

$$\left[(\beta^2 c^2 - 2)^2\,\alpha_1 h + 4\,(1 - \beta^2 c^2)\,\alpha_2\alpha_3\right]\left[\alpha_2^2 + \alpha_3^2 + 2\,\alpha_2\alpha_3\right]^{\frac{1}{2}}$$

$$= 4\,(1 - \beta^2 c^2)\,h\left[\alpha_2\alpha_3 + (1 - c^2)\,q^2\right] + (\beta^2 c^2 - 2)^2\,\alpha_1\left[\alpha_2^2 + \alpha_3^2 + \alpha_2\alpha_3 -\right.$$

$$\left. - (1 - c^2)\,q^2\right] \tag{11}$$

where α_1, α_2, α_3 are given by (6). Equation (11), with the substitutions made from (6), is in equation giving c in terms of q. We therefore find that dispersion occurs in the complete thermoelastic theory.

4. Insulated Boundary

The results corresponding to zero flux of heat across the boundary may be

obtained by putting $h = 0$ in the equations of the last Section. If we put $h = 0$ in (11), square both sides of the equation and substitute the appropriate expressions for α_1^2 and $\alpha_2^2 + \alpha_3^2$ from (6), we obtain

$$16\,(1 - \beta^2 c^2)\left[(1 - c^2)\,(\omega^2/c^2 - i\omega) - i\omega\epsilon\right](2\,\omega^2/c^2 - i\omega - \omega^2 - i\omega\epsilon + 2\,\alpha_2\,\alpha_3)$$
$$= (\beta^2 c^2 - 2)^4\,(\omega^2/c^2 - i\omega - i\omega\epsilon + \alpha_2\,\alpha_3)^2 \tag{12}$$

where $\omega = qc$, and

$$\alpha_2\,\alpha_3 = \left(\frac{\omega^4}{c^4} - \frac{\omega^4}{c^2} - \frac{i\omega^3}{c^2} + i\omega^3 - \frac{i\omega^3}{c^2}\,\epsilon\right)^{\frac{1}{2}}. \tag{13}$$

Now ω is $2\,\pi$ times the frequency of the wave and in the present system of units $\omega \ll 1$, so that a reasonable approximation can be expected by retaining only the lowest power of ω occurring in (12). In this way we obtain

$$16\,(1 - \beta^2 c^2)\,(1 - c^2 + \epsilon) = (\beta^2 c^2 - 2)^4\,(1 + \epsilon). \tag{14}$$

This approximate equation holds not only for the special case but also for the general case considered in the last Section. The proof is straightforward and is omitted here.

5. Comparison with the Classical Theory

To compare (14) with the classical theory we first write it in the form

$$(1 + \epsilon)\,\beta^2\,(\beta c)^6 - 8\,(1 + \epsilon)\,\beta^2\,(\beta c)^4 + 8\left[3\,(1 + \epsilon)\,\beta^2 - 2\right](\beta c)^2$$
$$- 16\left[(1 + \epsilon)\,\beta^2 - 1\right] = 0 \tag{15}$$

and then return to conventional units. If the velocity of S-waves in the solid is donated by v_S this becomes

$$(1 + \epsilon)\,\beta^2\left(\frac{c}{v_S}\right)^6 - 8\,(1 + \epsilon)\,\beta^2\left(\frac{c}{v_S}\right)^4 + 8\left[3\,(1 + \epsilon)\,\beta^2 - 2\right]\left(\frac{c}{v_S}\right)^2$$
$$- 16\left[(1 + \epsilon)\,\beta^2 - 1\right] = 0. \tag{16}$$

On comparing this with the equation for the determination of the velocity of the Rayleigh waves in the classical theory (Sneddon and Berry, 1958 eq. 71.16) we see that (16) is merely the classical equation with β^2 replaced by $(1 + \epsilon)\,\beta^2$.

We now consider a typical case. For the values $\beta^2 = 3$, $\epsilon = 0{\cdot}05$ (cf. Chadwick and Sneddon 1958) equation (16) becomes

$$3{\cdot}15\,x^6 - 25{\cdot}20\,x^4 + 59{\cdot}60\,x^2 - 34{\cdot}40 = 0 \tag{17}$$

whereas the corresponding classical equation is

$$3\,x^6 - 24\,x^4 + 56\,x^2 - 32 = 0. \tag{18}$$

where $x = c/v_S$. The root of (18) lying between 0 and 1 is 0·9194 and this gives $\alpha_1 = 0{\cdot}3933\,q$, $\alpha_2 = 0{\cdot}8475\,q$. The corresponding expressions for the components of the displacement vector are

$$\left.\begin{aligned} u &= A\,(0{\cdot}5774\,e^{-0{\cdot}3933qz} - e^{-0{\cdot}8475qz})\,e^{iq(x-ct)}, \\ w &= iA\,(1{\cdot}4679\,e^{-0{\cdot}3933qz} - 0{\cdot}8475\,e^{-0{\cdot}8475qz})\,e^{iq(x-ct)}. \end{aligned}\right\} \tag{19}$$

The other roots make α_1 and α_2 purely imaginary and do not lead to Rayleigh waves. The corresponding root of (17) is 0·9224 so that the percentage difference in the value of the velocity of propagation of Rayleigh waves is less than 1 per cent. (it is in fact about $\frac{1}{3}$ per cent). This root leads to the values $\alpha_1 = 0\,3863\,q$, $\alpha_2 = 0{\cdot}8422\,q$ and, if q is small, to the value $\alpha_3 = 0{\cdot}5288\,(1-i)\,q^{\frac{1}{2}}$, where we have neglected terms of order $q^{3/2}$ and above.

In the limiting case of q extremely small, these roots lead to the expressions

$$\left.\begin{aligned} u &= A\,(0{\cdot}5745\,e^{-0{\cdot}3863qz} - e^{-0{\cdot}8422qz})\,e^{iq(x-ct)}, \\ w &= iA\,(1{\cdot}4875\,e^{-0{\cdot}3863qz} - 0{\cdot}8422\,e^{-0{\cdot}8422qz})\,e^{iq(x-ct)}, \\ \theta &= -\,0{\cdot}0213\,\frac{iq}{b}\,Ae^{-0{\cdot}8422qz+iq(x-ct)}. \end{aligned}\right\} \qquad (20)$$

A comparison of the sets of equations (19) and (20) shows that the coefficients calculated on the thermoelastic theory differ from those calculated on the classical theory by amounts of the order of one per cent.

Acknowledgments

I am indebted to Professor I. N. Sneddon for suggesting this problem and to the Department of Scientific and Industrial Research for the award of a Research Studentship during the period in which the work was done.

References

Biot, M. A. 1956 *J. Appl. Phys.* **27**, 240.
Chadwick, P. and Sneddon, I. N. 1958 *J. Mech. Phys. Solids*, **6**, 3, 223.
Sneddon, I. N. and Berry, D. S. 1958 *Handbuch der Physik* Vol. 6, pp. 1-126 (Berlin, Springer-Verlag).

BOOK REVIEWS

W. A. Wooster: **Experimental Crystal Physics.** Clarendon Press, Oxford, 1957. 115 pp., 18s.

This book is based on courses given by the author and his colleagues in the Petrological and Mineralogical Department at Cambridge University. A number of experiments designed to illustrate the measurement of some of the more important crystal properties are described in detail. Most of the apparatus described could be easily assembled from equipment normally available in the laboratory and wherever special construction is required lucid instruction is given. Each experiment is prefaced by a short description of its theoretical basis and followed, in many cases, by an analysis of results actually obtained and the nature and magnitude of the errors encountered.

The first third of the book is devoted to the optical properties such as the measurement of refractive indices, specific rotations and reflectivities. There are three chapters describing measurements of the components of the second order tensors for dia- and para-magnetism, thermoelectricity, thermal conductivity and expansion and plastic deformation. Third order tensors are represented by the piezo- and pyro-electric properties with due caution emphasized in dealing with the latter. Finally there is a short chapter on the measurement of the elastic tensors with special reference to determining two of the quartz components.

There is one small criticism which might be made, especially as the author is so well known for his work in X-ray diffraction. The use of this technique is only mentioned in connexion with measuring thermal expansion. A brief description of a way of determining crystal orientation would have been a useful addition to the first chapter.

It is evident that this book has been carefully prepared and it is most pleasant to read. It is to be hoped that it will stimulate other teaching laboratories to devise courses in this most important subject.

B. Gale

Solid State Physics. Advances in Research and Applications. Vol. 5. Edited by F. Seitz and D. Turnbull. Academic Press, New York, 1957. xv. + 455 pp.

Volume 5 of this series fully maintains the high standard of its predecessors and follows the pattern established by them in offering its readers a small number of review articles in each of which some branch of the physics of solids is discussed very thoroughly. Only one of the articles in this volume, that by G. F. Koster on 'Space Groups and Their Representations,' deals with a 'classical' subject, and even in this article the relation of the theory of point groups to quantum mechanics is brought out. The other four articles deal with the electronic and nuclear properties of solids, mainly from a quantum-mechanical standpoint. They are 'Galvanomagnetic and Thermomagnetic Effects in Metals' by J.-P. Jan, 'Luminescence in Solids' by C. W. Klick and J. H. Schulman, 'Shallow Impurity States in Silicon and Germanium By W. Kohn, and 'Quadrupole Effects in Nuclear Magnetic Resonance Studies of Solids' by M. H. Cohen and F. Reif. It is a striking illustration of the development of the quantum mechanics of solids in recent years that although these articles, particularly those on luminescence, impurity states, and nuclear resonance, make so much use of quantum mechanics they are undoubtedly written for the experimental physicist. The subject is at the stage where quantum-mechanical ideas being used to explain more detailed and individualistic effects in solids, and to enable these effects to be exploited to the fullest extent to determine the impurity and imperfection structures of crystals. The series of which this book is a member has helped and is helping substantially in this rapid development of the subject.

A. H. Cottrell

J. Mech. Phys. Solids, 1959, Vol. 7, pp. 77 to 84. Pergamon Press Ltd., London. Printed in Great Britain

THERMOELASTIC WAVES AND THERMAL SHOCK

By M. Lessen
School of Civil Engineering, University of Pennsylvania

(*Received* 16*th June*, 1958)

Summary

The field equations governing the small displacements of a thermoelastic solid are derived and the properties of plane thermoelastic waves are investigated. Thermal shock solutions are developed using the thermoelastic wave solutions. In addition, the problem of thermal shock in an infinite cylinder is investigated.

1. Introduction

The study of thermoelasticity dates back many years to the work of Duhamel (1837) and Neumann (1885). The first formulation of the equations based on thermodynamics was done by Voigt (1910) and later by Jeffreys (1930). More recently, formulations of the theory and some applications to the problems of thermoelastic waves have appeared due to the efforts of Zener (1938), Päsler (1944), Lessen (1953, 1956), Biot (1956), Deresiewicz (1957) and others. It was only quite recently that the presence of two families of longitudinal thermoelastic waves was discovered by Lessen (1957) and Deresiewicz (1957).

The problem of thermal shock in the infinite half-space has received considerable attention of late by Danilovskaya (1950, 1952), Mura (1952), Sadowsky (1955), Sternberg and McDowell (1957) and others; the latter two authors having considered the quasi-static thermal stress problem in their investigations. With reasonably small and gradual temperature excitation at the free surface, the assumption of quasi-static strains that is tacit in the Fourier heat conduction equation and the lack of dynamical considerations in the analysis yield reliable answers but with large and sudden temperature excitation, the foregoing assumptions are no longer valid. For this reason, the formalization of the entire problem of thermal shock in the infinite half-space within the limitations of linearized theory is gone into at this point.

It will be shown that the existence of two classes of longitudinal waves in a thermoelastic solid simplifies the treatment of the complete thermal shock problem and gives some insight into phenomena which have not heretofore been explained.

2. Analysis

For the case of small displacements and displacement derivatives, the momentum

and energy (First Law) equations for a continuous homogeneous medium may be written as

Momentum : $$\rho \frac{\partial^2 u_i}{\partial t^2} = \tau_{ki,k} \tag{1}$$

Energy : $$\rho \frac{\partial U}{\partial t} = K_{mn} T_{,mn} + \tau_{mn} \frac{\partial u_{n,m}}{\partial t} \tag{2}$$

where ρ is density, u_i is displacement vector, t is time co-ordinate, τ_{ki} is stress tensor, U is specific internal energy, K_{mn} is thermal conductivity tensor, and T is the temperature. The subscript notation is that of Cartesian tensorial form and subscripts following a comma indicate partial differentiation with respect to the appropriate independent spatial variables.

The momentum and energy equations constitute four equations connecting the eleven dependent variables

$$u_i\,;\ \tau_{ij}\,;\ U\,;\ T.$$

Therefore, seven additional relations must be obtained in order to reduce the number of dependent variables to four. This reduction can be accomplished thermodynamically. The details of this reduction are repeated here to show that the postulation of the Duhamel–Neumann stress–strain–temperature equation is unnecessary with this reasoning.

For an elastic solid, where τ_{ij} ; ϵ_{ij} ; U and T are thermodynamic properties of a state, the Gibbs total differential equation may be written as

$$TdS = dU - \frac{1}{\rho} \tau_{ij}\, d\epsilon_{ij} \tag{3}$$

where S is the specific entropy, and $\epsilon_{ij} = \frac{1}{2}(u_{i,j} + u_{j,i})$ is equal to the pure strain. Therefore, from an assumed equation of state of the (normal) form

$$U = U(S, \epsilon_{ij}), \tag{4}$$

T and τ_{ij} can be obtained at once by

$$T = \frac{\partial U}{\partial S}, \qquad \tau_{ij} = \rho \frac{\partial U}{\partial \epsilon_{ij}}. \tag{5}$$

Expanding (4) about the reference state $S = S^{(0)}$, $\epsilon_{ij} = 0$, including second order terms, we obtain

$$U = U^{(0)} + sU^{(1)} + A_{ij}\,\epsilon_{ij} + \tfrac{1}{2} s^2\, U^{(2)} + sB_{ij}\,\epsilon_{ij} + \frac{1}{2\rho} C_{ijmn}\,\epsilon_{ij}\,\epsilon_{mn} \tag{6}$$

where $s = S - S^{(0)}$; $U^{(1)}$, $U^{(2)}$, A_{ij}, B_{ij}, C_{ijmn}, are the known properties $\partial U/\partial s$, $\partial^2 U/\partial s^2$, $\partial U/\partial \epsilon_{ij}$, $\partial^2 U/\partial \epsilon_{ij}\,\partial s$, $\rho\,\partial^2 U/\partial \epsilon_{ij}\,\partial \epsilon_{mn}$, respectively at the reference state. Therefore

$$T = U^{(1)} + sU^{(2)} + B_{ij}\,\epsilon_{ij}, \tag{7}$$

$$\tau_{ij} = \rho A_{ij} + \rho s B_{ij} + C_{ijmn}\,\epsilon_{mn}\,; \tag{8}$$

$U^{(1)}$ is seen in (7) to be the reference temperature $T^{(0)}$.

Substituting (7) and (8) in (1) and (2) yields (to the first order)

$$\rho \frac{\partial^2 u_i}{\partial t^2} = \rho B_{ij}\, s_{,j} + C_{ijmn}\, u_{m,nj} \tag{9}$$

and

$$\rho T^{(0)} \frac{\partial s}{\partial t} = K_{mn}\,(sU^{(2)} + B_{ij}\, u_{i,j})_{,mn} \tag{10}$$

Thus the reduction to four variables, s and u_i has been accomplished.

The reduction to the variables T and u_i may be accomplished by solving for s in (7) :

$$s = \frac{1}{U^{(2)}}\,(T - T^{(0)} - B_{mn}\, u_{m,n}), \tag{11}$$

and substitution in (9) and (10) :

$$\frac{\partial^2 u_i}{\partial t^2} = \frac{1}{U^{(2)}}\, B_{ij}\, T_{,j} + \left(\frac{1}{\rho}\, C_{ijmn} - \frac{1}{U^{(2)}}\, B_{ij}\, B_{mn}\right) u_{m,nj}, \tag{12}$$

$$\frac{\partial T}{\partial t} - B_{ij}\, \frac{\partial u_{i,j}}{\partial t} = D_{mn}\, T_{,mn}, \tag{13}$$

where

$$D_{mn} = \frac{U^{(2)}}{\rho T^{(0)}}\, K_{mn}. \tag{14}$$

For the case of isotropy,

$$B_{ij} = B\delta_{ij}\,; \qquad D_{mn} = D\delta_{mn}$$

$$C_{ijmn} = \lambda\delta_{ij}\,\delta_{mn} + \mu\,(\delta_{im}\,\delta_{jn} + \delta_{in}\,\delta_{jm})$$

and (12) and (13) become

$$\frac{\partial^2 u_i}{\partial t^2} = \frac{B}{U^{(2)}}\, B\, T_{,i} + \left(\frac{\lambda + \mu}{\rho} - \frac{B^2}{U^{(2)}}\right) u_{m,mi} + \frac{\mu}{\rho}\, u_{i,mm}, \tag{15}$$

$$\frac{\partial T}{\partial t} - B\, \frac{\partial u_{m,m}}{\partial t} = DT_{,mn}. \tag{16}$$

3. Thermoelastic Waves

If we consider solutions of (15) and (16) of the form

$$u_i = u_i^*\, \exp\,(a_k\, x_k + bt), \qquad T - T^{(0)} = T^*\, \exp\,(a_k\, x_k + bt),$$

and let

$$\frac{\mu}{\rho} = V^2, \qquad \frac{\lambda + 2\mu}{\rho} - \frac{B^2}{U^2} = V_T^{\,2},$$

$$\frac{\lambda + 2\mu}{\rho} = V_S^{\,2}, \qquad a_k\, a_k = A^2,$$

where V, V_S, V_T are the velocities of propagation of transverse, isentropic-longitudinal, and isothermal-longitudinal waves respectively, the determinantal equation of the system (15) and (16) may be written

$$(b^2 - V^2 A^2)\,[(b^2 - V_S^{\,2} A^2)\, b - (b^2 - V_T^{\,2} A^2)\, DA^2] = 0. \tag{17}$$

It should be noted that $(b^2 - V^2 A^2)$ is a factor of the determinantal equation (17) and therefore represents a normal mode of motion of the field. It should also be noted that no thermoelastic interactions are represented in this factor and that it describes the propagation of a shear (transverse) wave. The remainder of equation (17) represents two families of advancing and receding longitudinal waves. Although discussed elsewhere and most recently by CHADWICK and SNEDDON (1958), the characteristics of this equation will be briefly included here to form a basis for further discussion in this paper.

TABLE 1. *Characteristics of plane thermoelastic waves*

	Mechanical mode		*Thermal mode*	
m	Rl v	Im v	Rl v	Im v
0·00	1·02469	0·00000	0·00000	0·00000
0·01	1·02469	0·00020	0·06900	0·06897
0·02	1·02468	0·00045	0·09763	0·09754
0·03	1·02467	0·00068	0·11960	0·11944
0·04	1·02466	0·00091	0·13814	0·13789
0·05	1·02464	0·00114	0·15448	0·15413
0·06	1·02462	0·00138	0·16927	0·16881
0·07	1·02459	0·00161	0·18287	0·18230
0·08	1·02456	0·00184	0·19555	0·19485
0·09	1·02452	0·00207	0·20747	0·20663
0·10	1·02448	0·00230	0·21875	0·21776
0·20	1·02388	0·00450	0·31020	0·30748
0·30	1·02293	0·00651	0·38101	0·37618
0·40	1·02169	0·00826	0·44122	0·43414
0·50	1·02027	0·00970	0·49468	0·48535
0·60	1·01873	0·01082	0·54330	0·53187
0·70	1·01717	0·01165	0·58820	0·57488
0·80	1·01563	0·01219	0·63010	0·61514
0·90	1·01418	0·01251	0·66950	0·65317
1·00	1·01282	0·01264	0·70676	0·68932
2·00	1·00499	0·01017	1·00499	0·98485
3·00	1·00245	0·00757	1·23091	1·21243
4·00	1·00143	0·00591	1·42049	1·40378
5·00	1·00093	0·00482	1·58724	1·57200
6·00	1·00065	0·00405	1·73792	1·72385
7·00	1·00048	0·00350	1·87645	1·86334

If in equation (17), with the term $(b^2 - V^2 A^2)$ cancelled, we substitute

$$v^2 = \left(\frac{b}{V_T A}\right)^2; \qquad im = \frac{Db}{V_T^2}; \qquad k = \frac{V_S^2}{V_T^2}$$

we obtain

$$v^2 = (k + im)\, v^2 + im = 0, \tag{18}$$

where the real part of v is the dimensionless velocity of propagation in terms of the isothermal velocity of propagation, while the imaginary part of v represents the damping. The dimensionless disturbance frequency is given by m. Computations were carried out on equation (18) for $K = 1{\cdot}05$. The results are given in Table 1 and Fig. 1.

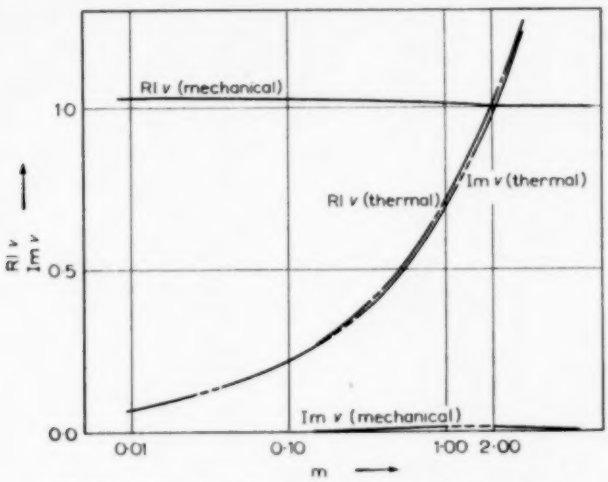

Fig. 1. Characteristisc of plane thermoelastic waves.

As noted previously, since equation (18) is biquadratic, it represents two different types of longitudinal waves, each type representing a different coupling between stress and temperature. One of the waves (due to the weak thermoelastic coupling) is predominantly mechanical whereas the other is predominantly thermal. The mechanical wave has the asymptotic properties of

$$\text{Rl}\, v \to (K)^{\frac{1}{2}} \quad \text{when} \quad m \to 0,$$

$$\text{Rl}\, v \to 1 \quad \text{when} \quad m \to \infty.$$

For the thermal wave, the corresponding behaviour is

$$\text{Rl}\, v \to 0 \quad \text{when} \quad m \to 0,$$

$$\text{Rl}\, v \to \infty \quad \text{when} \quad m \to \infty.$$

The cross-over point at which both families of waves have the same velocity occurs at $m = 2$. The damping associated with the thermal mode is seen to be very much greater than that associated with the mechanical mode of disturbance.

4. One-Dimensional Thermal Shock in the Half-Space

In the foregoing Section elementary disturbance solutions to the thermoelastic field equations were discussed. Since the thermoelastic field equations are a linear ensemble of partial differential equations, it is permissible to construct new solutions by taking linear combinations of known solutions.

Consider a half-space $x_1 > 0$ excited at $x_1 = 0$ by a temperature pulse in time, $T(t)$. The response of the half-space to a general temperature pulse may be synthesized from the response of the half-space to an exponential temperature pulse $\exp(bt)$. However, this response is given by a linear combination of the advancing waves of the two families discussed in the previous Section. The linear combination of the two waves is fixed by the stipulation that τ_{11} (normal stress) on $x_1 = 0$ is zero for the case of stress-free boundary, or that $u_1(0) = 0$ for the case where the displacement is constrained at the boundary. In any case, the response all over the half-space to a unit temperature exponential disturbance at the boundary is available from the foregoing. If the response of the displacement is denoted by $R^{(u)}(b; x_1, t)$ and the response of the temperature is denoted by $R^{(T)}(b; x_1, t)$, the response to a step function in temperature at the boundary is such that

$$T(t) = \begin{cases} T^{(S)}, & t > 0 \\ T^{(0)}, & t < 0 \end{cases}$$

is given by

$$u_1(x_1, t) = \frac{T^{(S)} - T^{(0)}}{2\pi i} \int_{-i\infty}^{i\infty} \frac{R^{(u)}(b; x_1, t)}{b}\, db,$$

$$T(x_1, t) = T^{(0)} + \frac{T^{(S)} - T^{(0)}}{2\pi i} \int_{-i\infty}^{i\infty} \frac{R^{(T)}(b; x_1, t)}{b}\, db,$$

and so the complete thermal shock problem for the half-space $x_1 > 0$ subjected to a step function excitation in temperature at $x_1 = 0$ is formally solved.

5. Generalized Thermal Shock in the Half-Space

Let us now consider a half-space $x_3 > 0$ with a thermal excitation at $x_3 = 0$ of $T - T^{(0)} = T^{(E)}(x_1, x_2, t)$. The boundary conditions on the stresses are $\tau_{31} = \tau_{32} = \tau_{33} = 0$ at $x_3 = 0$. The response to the thermal excitation may now be synthesized of Fourier components that correspond to the elementary disturbances considered in (17).

At fixed values of a_1, a_2, b we solve for a_3 in the determinantal equation (17). Because the determinantal equation is bi-cubic in a_3 there exist three sets of positive and negative values for a_3 corresponding to three families of advancing and receding waves. A linear combination of the three advancing waves from these families will satisfy the condition of a traction free surface ($x_3 = 0$) and will yield the response to a unit thermal excitation $T - T^{(0)} = \exp(a_1 x_1 + a_2 x_2 + bt)$ at that surface. If the temperature and displacement responses to this excitation are denoted respectively by $R^{(T)}(a_1, a_2, b; x_1, x_2, x_3, t)$ and $R^{(u_i)}(a_1, a_2, b; x_1, x_2, x_3, t)$, the responses to a unit step function in temperature at the surface $x_3 = 0$ of $T - T^{(0)} = 0$ when $x_1, x_2, t < \eta_1, \eta_2, \xi$ and $T - T^{(0)} = 1$ when $x_1, x_2, t \geqslant \eta_1, \eta_2, \xi$ are given by the Fourier integrals

$$T^{(S)} - T^{(0)} = G(x_1 - \eta_1, x_2 - \eta_2, x_3, t - \xi) =$$

$$- \frac{1}{8\pi^3 i} \int_{-i\infty}^{i\infty} \int\int R^{(T)}(a_1, a_2, b; x_1 - \eta_1, x_2 - \eta_2, x_3, t - \xi)\, da_1\, da_2\, db,$$

$$u_i^{(S)} = H_i(x_1 - \eta_1, x_2 - \eta_2, x_3, t - \xi) =$$

$$-\frac{1}{8\pi^3 i}\int_{-i\infty}^{i\infty}\int\int R^{(ui)}(a_1, a_2, b; x_1 - \eta_1, x_2 - \eta_2, x_3, t - \xi)\, da_1\, da_2\, db.$$

The response to a general temperature excitation at the surface $x_3 = 0$ of $T - T^{(0)} = T^{(E)}(x_1, x_2, t)$ may therefore be easily obtained from a Duhamel integral

$$T(x_1, x_2, x_3, t) = T^{(0)} + \int\int\int \frac{\partial^3 T^{(E)}}{\partial\eta_1\, \partial\eta_2\, d\xi} G(x_1 - \eta_1, x_2 - \eta_2, x_3, t - \xi)\, d\eta_1\, d\eta_2\, d\xi,$$

$$u_i(x_1, x_2, x_3, t) = \int\int\int \frac{\partial^3 T^{(E)}}{\partial\eta_1\, \partial\eta_2\, d\xi} H_i(x_1 - \eta_1, x_2 - \eta_2, x_3, t - \xi)\, d\eta_1\, d\eta_2\, d\xi,$$

where the surface in the x_1, x_2, t space that bounds the temperature excitation, $T^{(E)}$, is given by

$$P(x_1, x_2, t) = 0.$$

The problem is thus formally solved. The detailed solution for an actual problem would entail the solution of the determinantal equation which could be carried out in closed form, the synthesis of the elemental response over the half-space to a timewise and spacewise exponential temperature excitation at the free surface from the three elementary wave types, and the synthesis of the response to a three-dimensional step function in temperature excitation from the elemental response.

6. Generalized Thermal Shock of an Infinite Cylinder

If the general thermoelastic equations (15) and (16) are transformed to cylindrical polar co-ordinates r, ϕ, z, where the corresponding displacement coefficients are u, v, w, one might look for elemental solutions of the form

$$u, v, w = u^*, v^*, w^*(r) \exp\left(\frac{n}{2\pi}\theta + az + bt\right)$$

where u^*, v^*, w^* are eigenfunctions of r pertaining to discrete integer eigenvalues of n and continuous eigenvalues a and b. The formal solutions of a generalized thermal shock problem for an infinite cylinder may again be synthesized in a manner analogous to the previous Section from a double Fourier integral of a Fourier series.

7. Discussion

It is important to note from the computed properties of the thermoelastic waves that the thermal waves are much more highly damped than the mechanical waves. Hence, in thermal shock, thermal effects (gross temperatures changes) are limited to a narrow boundary layer next to the thermally excited surface whereas mechanical effects penetrate essentially undamped into the interior of the half-space. The mechanical effects propagate as a dispersing wave-packet in the complete theory. In the classical theory which excludes thermoelastic interactions in the energy equation, there would be no such dispersion ; hence sharp mechanical wave fronts would propagate unchanged, whereas according to the more complete theory presented here they would tend to smooth out.

In the case of strong thermal shock at a free surface, where the mechanical properties of the medium begin to degenerate at the excited surface, the fact that the thermal and mechanical waves are so phased as to give a traction-free surface may cause failure to occur (if at all) some distance within the solid where the properties of the medium are intact but the phasing of the two families of waves is such as to give high stresses (in which case the material spalls).

Since the thermo-viscoelastic theory developed by LESSEN (1957) yields a determinantal equation for elementary disturbances of the same form as the pure thermoelastic theory, all of the foregoing development may be applied to a thermo-viscoelastic solid as well.

A few examples of interest are now being investigated and calculated in detail.

ACKNOWLEDGMENT

The author would like to acknowledge the computation of the thermoelastic wave characteristics presented herewith by Mr. HERBERT SOMERSON of the Piasecki Aircraft Corporation.

REFERENCES

BIOT, M. A.	1956	*J. Appl. Phys.* **27**, 240.
CHADWICK, P. and SNEDDON, I. N.	1958	*J. Mech. Phys. Solids* **6**, 223.
DANILOVSKAYA, V. I.	1950	*Prikl. Mat. Mech.* **14**, 316.
	1952	*Prikl. Mat. Mech.* **16**, 341.
DERESIEWICZ, H.	1957	*J. Acoust. Soc. Amer.* **29**, 204.
DUHAMEL, J. M. C.	1837	*J. de l'Ecole Polytechn.* **15**, 1.
JEFFREYS, H.	1930	*Proc. Camb. Phil. Soc.* **26**, 101.
LESSEN, M.	1953	*Proc. 1st Midwest Conference on Solid Mechanics* (Hunter & Wroughton, Urbana).
	1956	*J. Mech. Phys. Solids* **5**, 37.
	1957	*Quart. Appl. Math.* **15**, 105.
	1957	*Proc. 3rd Midwest Conference on Solid Mechanics*, 20.
MURA, T.	1952	*Proc. 2nd Japan Congr. Appl. Mech.* 9.
NEUMANN, F. E.	1885	*Vorlesungen über die Theorie der Elasticität der festen Körper* (Leipzig).
PÄSLER, M.	1944	*Z. Phys.* **122**, 357.
SADOWSKY, M. A.	1955	*J. Appl. Mech.* **22**, 177.
STERNBERG, E. and McDOWELL, E. L.	1957	*Quart. Appl. Math.* **14**, 381.
VOIGT, W.	1910	*Lehrbuch der Kristallphysik* (Teubner-Verlag, Berlin).
ZENER, C.	1938	*Phys. Rev.* **53**, 90.

J. Mech. Phys. Solids, 1959, Vol. 7, pp. 85 to 96. Pergamon Press Ltd. London. Printed in Great Britain

THE DEFORMATION OF METALS BY VICKERS-TYPE PYRAMIDAL INDENTERS

By T. O. Mulhearn
Australian Defence Scientific Service, Defence Standards Laboratories, Sydney

(*Received 9th June*, 1958)

Summary

It has been confirmed that the mechanism of identation proposed by Hill *et al.* (1947), for the indentation of a plane surface by a wedge, operates when the wedge semi-angle is less than about 30°. If the wedge angle is greater than 30° a different mechanism appears and becomes progressively more important with increasing wedge angle. This mechanism approximates to a radial compression centred close to the line of first contact of the wedge.

Indentation by conical and pyramidal indenters having an apex semi-angle of 68° also approxmates to a radial compression which produces hemispherical surfaces of constant strain centred close to the first point of contact between the indenter and the specimen. With blunt indenters, variations in the indenter shape cause very little difference in the deformation mechanism except, perhaps, in a highly deformed region close to the indenter.

1. Introduction

It has been suggested previously (Samuels and Mulhearn 1957) that the mechanism of deformation of a plane specimen of 70 : 30 brass by a Vickers diamond pyramidal indenter may be regarded as occurring by the compression of a set of concentric hemispherical shells, except in a region very close to the indenter, and that the surface of the indentation is chiefly formed by folding down of the original surface about the edge of the impression as axis. This may be referred to as a compression-type mechanism and requires that:

(a) The deformed zone should extend beneath the indenter for approximately the same distance that it extends in a direction normal to the indenter axis.

(b) The displacement of any point should have only a small component in the plane of the surface.

(c) The height of the raised lip adjacent to the indentation should be of the order of one hundredth of the indentation diagonal.

Hill *et al.* (1947) have investigated the deformation of a plane surface by a wedge and, using the results of experiments on lead blocks with wedges of apex semi-angles between approximately 7° and 30°, have derived a theoretical model for the wedge indentation of an ideal rigid–plastic material. Hill (1950) and Tabor (1951) have suggested that the same mechanism may be applicable to

the deformation produced by a Vickers indenter. A cutting mechanism of indentation fundamentally different from that described above is postulated which requires that:

(a) The deformation should not extend to any considerable extent beneath the indenter.

(b) The displacement of points on the original surface should have a relatively large component parallel to that surface.

(c) The height of the raised lip adjacent to the indentation should be approximately one third the depth of the indentation and the profile of the lip should be a straight line.

The reason why the compression-type rather than the cutting mechanism operated under the conditions of the SAMUELS-MULHEARN experiment could have been any one of the following:

(a) Differences between the deformation characteristics of annealed 70:30 brass and the ideal rigid–plastic material.

(b) Differences between the mechanism of deformation for wedge and pyramid indenters.

(c) A change in the mechanism with change in wedge angle, the cutting mechanism being that which operates at small wedge angles and the compression mechanism being that which operates at large wedge angles.

The purpose of the present work was to establish the relative importance of these three factors.

2. EXTENT OF THE DEFORMED ZONE

(a) *Experimental methods*

Two experimental methods were used for determining the deformation of the metal during indentation, namely, (i) a composite block technique, and (ii) a metallographic etching technique.

In the composite block method, a number of blocks 1½ in. × ½ in. × ½ in. were accurately surface ground with flat sides and square corners, placed together in pairs and drilled and tapped for ¼ in. diameter machine bolts. The mating faces were polished to a good metallographic finish and one of these faces was ruled with a square grid of 0·5 mm spacing such that all intersections could be located within $\pm 3\mu$. The halves were then bolted together tightly and an indentation made at the parting line. The halves were split and the distortion of the ruled grid determined. The extent of the surface rumpling due to the indenting process could also be observed readily on the unruled face, maximum sensitivity being ensured by examining the face microscopically under phase contrast illumination.

Two metallographic techniques were used to detect the extent of the deformation in the interior of semi-infinite specimens of materials which more closely approach the ideal rigid–plastic material than 70 : 30 brass. The first was to polish a transverse section through the centre and parallel to a side of an indentation in a mild steel specimen and to etch the section in Fry's reagent, which preferentially darkens plastically deformed zones. Only certain batches of steel respond satisfactorily to this treatment; a highly sensitive steel (containing 0·20 per cent carbon, 0·52 per cent manganese and other elements less than 0·05 per cent) was selected by trial and error. The second metallographic technique was based on the carbide precipitation phenomenon described by WILSON (1954). The material used was a 0·7 per cent carbon steel which was water quenched from 800°C, indented by means of a diamond pyramid indenter and tempered after indentation

for 15 min. at 200°C. The sample was sectioned, polished, and etched in nital which shows the plastically strained material as a light-etching zone.

The composite block technique has the advantage that it can be applied to almost any type of material and that the displacements can be measured. It has the disadvantage that the division plane may relieve a large part of the elastic restraint which would have been present in a semi-infinite block and may thus introduce changes in the indentation mechanism. The metallographic methods have the advantage that they allow examination of the strain in a semi-infinite block. They have the disadvantage that it is only possible to determine one contour of uniform strain and that it is difficult to ascribe a definite magnitude to this strain.

(b) *Effect of the deformation characteristics of the material*

As a first step, the deformation pattern obtained with 70 : 30 brass was compared with a material which more closely approached the ideal rigid–plastic material. That chosen was a low-carbon steel containing 0·07 per cent carbon which was normalized from 950°C and cold rolled to 30 per cent reduction in five stages, each successive reduction being rolled at right angles to the previous one. Composite-block specimens were assembled from this material and an indentation made at the parting plane using a tungsten carbide indenter of the same form as a Vickers indenter, both indenter and specimen being lubricated with extreme pressure lubricant. The impression size was in every case less than the critical size for the specimen, as determined by DUGDALE (1955). The resulting deformation pattern is shown in Fig. 1.

The deformed area on the grid surface was approximately semi-circular with the centre near the bottom of the indentation, and in this respect was similar to that determined previously for 70 : 30 brass. As noted above, it is possible that this deformation pattern may have been affected by the release of constraint at the parting face of the composite specimen. The pattern was therefore compared with those determined by the metallographic methods for impressions in semi-infinite blocks of an annealed mild steel (Fig. 7a) and a hardened steel* (Fig. 7b). The general form of both of these deformation boundaries was similar to that shown in Fig. 1. It is therefore concluded that there is no major change in the deformation mechanism due to the presence of the parting plane.

None of the above techniques has a high sensitivity for detecting deformation, and it is possible that a larger zone of smaller deformation may exist which is not visible in these photographs. The unruled side of the composite block specimen was examined microscopically under phase contrast illumination for evidence of a zone of this type, but no such evidence was found.

As a further check on the effect of the parting plane, a composite block specimen of annealed 70 : 30 brass was indented in the same manner as the cold-worked steel specimen. The resulting deformation pattern, which is shown in Fig. 2, is more extensive than for the cold-worked steel but has the same general form. Examination of the unruled side of the block under phase contrast illumination showed that deformation was detectable for a distance of approximately 1·5

*The small crack below the indentation shown in Fig. 7b is of interest. Cracks of this type were found beneath every indentation and were found to occur only at positions immediately below the indenter tip. It is difficult to see how they could have formed during indentation ; it is much more likely that they formed due to the relief of residual elastic stress during the preparation of the section. They seem quite similar to the cracks often found to extend from the corners of pyramidal indentations in hard materials. These form after the indenter has been unloaded and may even form after an appreciable time delay. In the latter case, at least, the cracking certainly results from the relief of residual tensile stress.

impression diagonals from the centre of the indentation. This is in satisfactory agreement with the previous results of SAMUELS and MULHEARN (1957).

Since the same general shape of deformation zone is obtained for all the materials examined, it is concluded that differences in the deformation characteristics of the materials may affect the extent of the deformed zone and the slope of the strain gradient but have no significant effect on the shape of the contours of equal strain.

(c) *Difference between wedge and pyramid indenters*

Composite block specimens of a cold-rolled steel were indented with a wedge and a cone, respectively, each having an apex semi-angle of 68°; hardened steel (hardness DPN 800) was used for the indenters, which were lubricated with extreme pressure lubricant. The distortion of the grid on the parting face of each specimen was similar for both indenters and similar to that for the pyramidal indenter (cf. Figs. 3 and 6). A wedge indenter may therefore be considered as the two-dimensional analogue of both cone and pyramid indenters of the same apex semi-angle.

(d) *Effect of wedge angle*

Hardened steel wedge indenters were prepared with apex semi-angles of 20° and 40°, respectively. Indentations were made in composite blocks of the cold-rolled steel and the resulting deformation patterns compared with that for the wedge of 68° semi-angle. The deformed grid formed by the wedge of 20° semi-angle (Fig. 4) was very similar to that for the wedge of intermediate angle shown for the lead block experiment of HILL *et al.* (1947), and was in good agreement with their calculated grid. The shape of the elastic–plastic boundary was determined by examining the ruled face under oblique illumination; it is shown by the line drawn on the photograph. The deformation did not extend far beneath the tip of the indentation. The form of the surface rumpling strongly suggests that the lines of maximum shear stress agree with the slip lines calculated by the above authors.

In the case of the indentation produced by the wedge of 40° semi-angle a marked change has occurred (cf. Figs. 4 and 5). While there are still some similarities to the deformed grid pattern calculated by HILL *et al.* (1947), it is clear that the elastic–plastic boundary is now approximately semi-circular and that a new mechanism is beginning to modify the distortion. With increasing wedge angle this new mechanism becomes more important until the low angle mechanism has practically disappeared at a wedge angle of 68° (cf. Figs. 4 and 6).

(e) *Magnitude and direction of displacement*

Since the intersections on the ruled grids could be located with considerable accuracy before and after deformation, it was possible to estimate the amount and direction of the displacement of each intersection. This was calculated for the indentation of the cold-worked low-carbon steel by a wedge of 68° semi-angle; the results are shown in the left-hand side of Fig. 9. Each of the full lines is a line through points in the deformed material which have been displaced equal distances, the displacements being shown as percentages of the indentation half width (Δ). The broken lines are the directions along which these displacements have occurred. An estimate was also made of the lines of equal strain and these results are plotted in the right-hand side of Fig. 9. The strain was calculated as

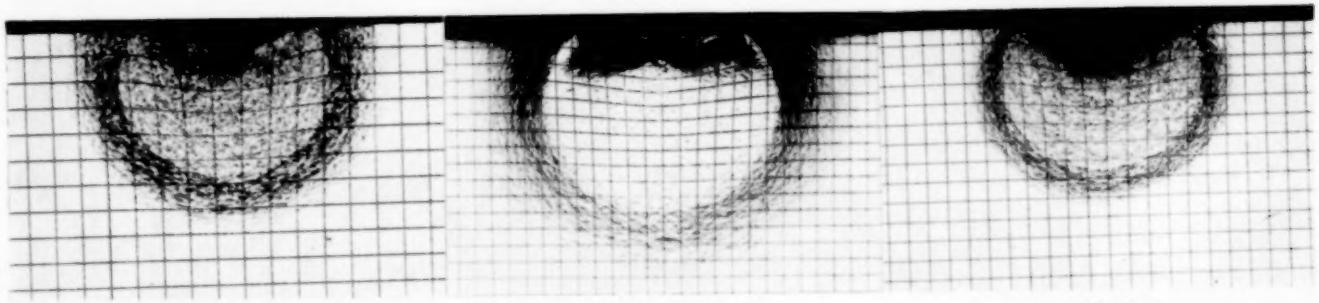

Fig. 1.

Fig. 1. Cold-rolled steel.
68° pyramidal indenter.

Fig. 2.

Fig. 2. Annealed 70 : 30 brass.
68° pyramidal indenter.

Fig. 3.

Fig. 3. Cold-rolled steel.
68° conical indenter.

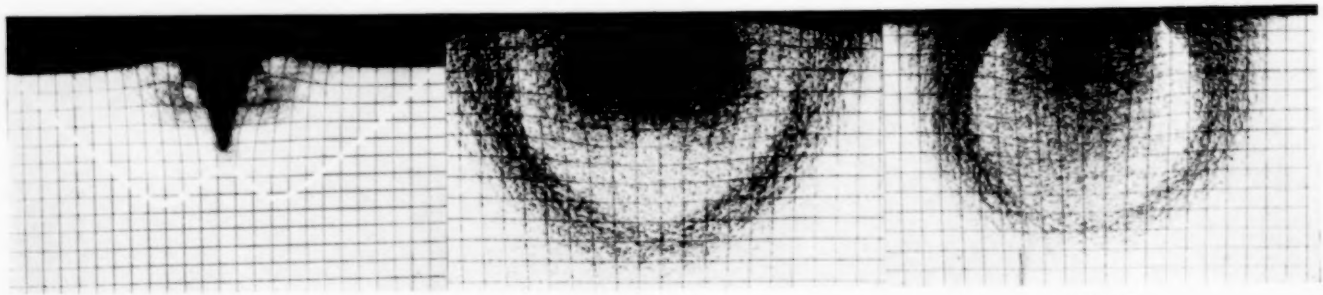

Fig. 4.

Fig. 5.

Fig. 6.

Fig. 4. Cold-rolled steel. 20° wedge indenter. Fig. 5. Cold-rolled steel. 40° wedge indenter. Fig. 6. Cold-rolled steel. 68° wedge indenter.
Appearance of the ruled face of composite-block specimens after indentation.

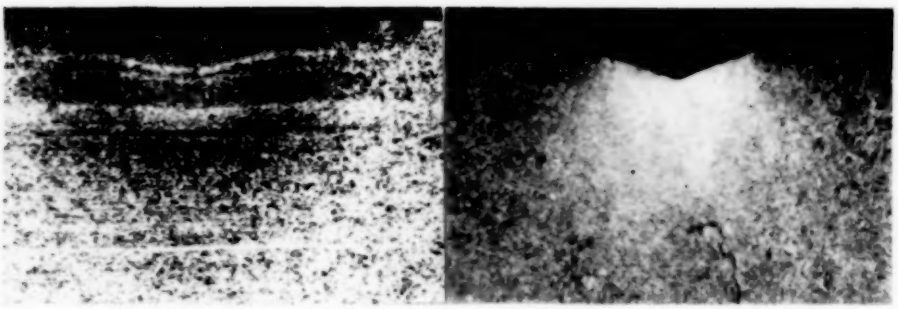

Fig. 7 (a) Fig. 7 (b).

Fig. 7. Sections through indentations made by Vickers diamond pyramid indenters in semi-infinite specimens.
(a) Annealed low-carbon steel.
(b) Hardened 0·7 per cent carbon steel.

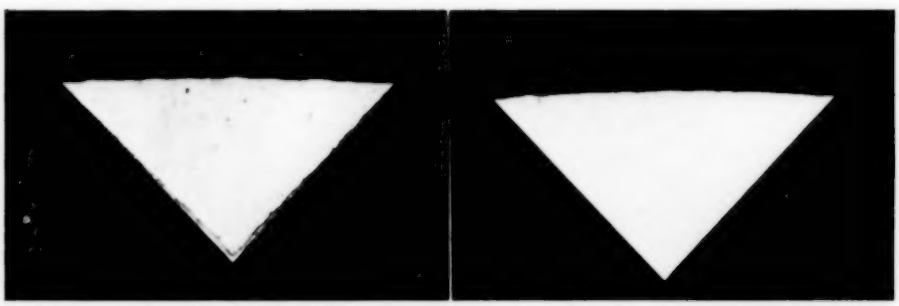

Fig. 8 (a). Fig. 8 (b).

Fig. 8. Faces of diamond pyramid indentations made in a steel specimen of which the surface had been copper plated.
(a) Indenter and specimen lubricated.
(b) Unlubricated.

the percentage reduction of length between two points in the direction of the corresponding displacement. The shape and position of the elastic–plastic boundary was judged from the rumple markings on the parting face ; some account was also taken of these markings in estimating the shape of some of the other boundaries.

The lines of equal strain are approximately arcs of circles centred close to the lowest point of the indentation. It is concluded that the deformation pattern may be approximately represented as a radial compression centred at or just below the bottom of the indentation.

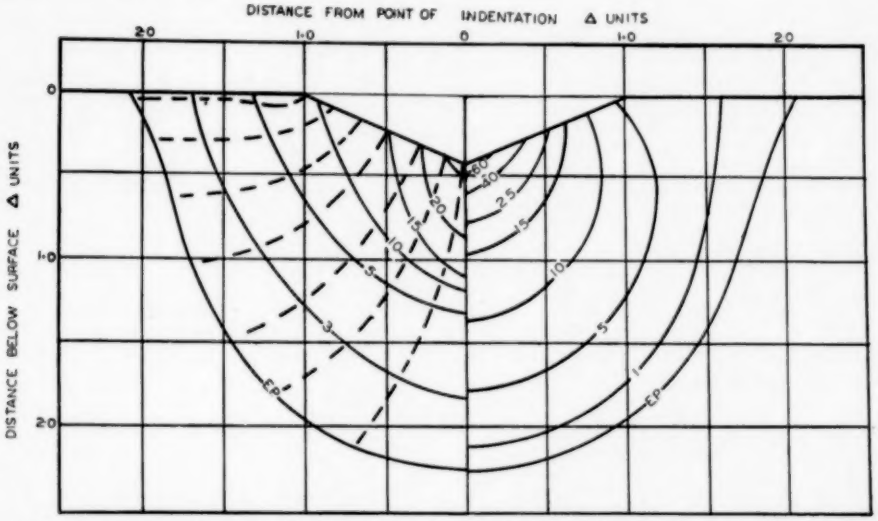

Fig. 9. Deformation of cold-rolled low-carbon steel by a wedge of 68° apex semi-angle.
Left-hand side : The full lines are profiles of equal displacement while the broken lines show the direction in which the displacement has occurred.
Right-hand side : The lines are profiles of equal percentage strain.
E.P. indicates the elastic-plastic boundary.
The units shown on the profiles are described in the text.

3. Displacements Parallel to Specimen Surface

If the mechanism of Hill *et al.* is applicable to indentation by a Vickers indenter it is to be expected that the point O in the sketch of Fig. 10, at which the apex of the indenter first contacts the surface, would move in a direction making an angle of 113″ with the axis and come to rest at the point K. Simple calculation shows that $BK = 0{\cdot}185\,d$ where d is the indentation diagonal.

This simple treatment ignores any effect of friction. Grunzweig *et al.* (1953) have calculated the angles at which slip lines meet the wedge surface for various coefficients of friction, the result for a wedge of semi-angle 70° and a coefficient of friction of 0·05* being 31° and 59°. If friction is considered, the point O would move in a direction making an angle of approximately 127° with the axis, so that $BK = 0{\cdot}13\,d$.

If, however, the original surface folds down about the line DE as axis, as proposed in the compression mechanism, and there is no stretching of the surface,

*Chosen as being a reasonable value for the coefficient.

the point O moves in an arc of a circle of radius CO to reach the point K'; then $BK' = CB - CO = 0{\cdot}03\,d$. The difference between the two estimates of the length BK is so great that it should be possible to distinguished between the two mechanisms on this basis. The following experiments were carried out with this purpose in mind.

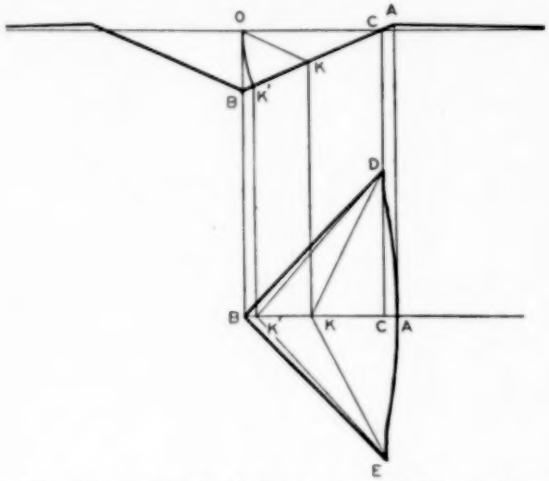

Fig. 10. Diagram to illustrate displacements parallel to specimen surface.

(a) *Examination of the pyramidal surfaces of the indentation*

Samples of selected materials were polished to a good metallographic finish and flash plated with a metal of a contrasting colour, namely, nickel plating for 70 : 30 brass and copper plating for steel. The specimen was indented with a standard diamond pyramid indenter and the pyramidal surfaces of the indentation were examined. Most of the experiments of this type were carried out on a steel of the type covered by *B.S.*970 : En 23 which had been hardened and tempered to a hardness of DPN 320. It was possible with this material to increase the contrast between the plating (representing the original surface) and the new surface formed during indentation by etching in nital.

In the first set of experiments, indentations were made in the steel specimen with a Vickers diamond pyramid which was lubricated with a heavy oil. A face of the indentation viewed normally is shown in Fig. 8 (a). The BK distance is small and could not be measured with a high degree accuracy, but it was clearly less than $0{\cdot}03\,d$. This is far smaller than required by the cutting mechanism, but is consistent with the compression mechanism.

The effect of friction must, however, be considered further before this evidence can be regarded as conclusive. In the previous experiment, the increment of area required to make up the difference between the pyramidal and projected areas of the impression has been formed by cutting at the edges of the indenter. The experiment was repeated after thoroughly degreasing both the specimen and the indenter; the appearance of a face of this indentation is shown in Fig. 8 (b). No detectable new surface has formed in this case. Moreover, new surface was not

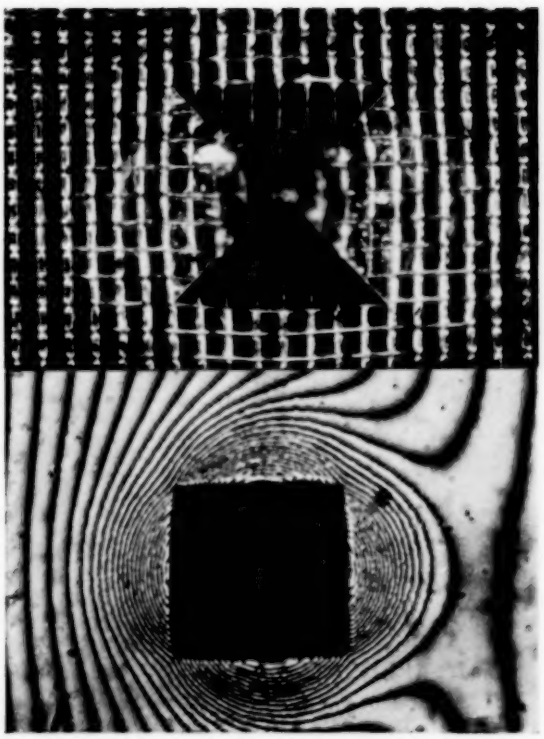

Fig. 11. Diamond pyramid indentation in a ruled surface of a specimen of cold-rolled low-carbon steel.

Fig. 12. Contours of surface elevation close to diamond pyramid indentation in cold-rolled low-carbon steel.

formed in specimens of either annealed or cold-worked brass and this was so whether they were lubricated or not.

There are two possible ways by which the triangular portion of the original surface can increase in area to form the pyramidal face of the indentation if indentation occurs by the compression mechanism. Firstly, additional surface may be formed by cutting at the pyramidal edges of the indenter. Secondly, the original surface may stretch. Combinations of the two are possible and the proportion of each depends on the relationship between the yield point of the specimen material and the coefficient of friction between the indenter and the specimen surface. It seems that with the types of material so far considered, relative movement between the indenter and the specimen surface is prevented by friction when the specimen is softer than approximately DPN 100 ; the increase of surface area then occurs by stretching. When the material is harder than approximately DPN 200, relative movement can occur more easily than stretching of the surface so that the extra surface is formed by cutting. The particular mechanism which operates between these hardness levels depends on the coefficient of friction between the indenter and the specimen surface.

Since the effect of friction is to reduce the apparent length of BK, the following experiment was carried out to determine whether this effect could have accounted for the low value of BK (i.e. 0·03 d) observed in the original experiment. A number of indentations were made in a plated specimen of hardened-and-tempered high-speed steel (hardness DPN 850). Both indenter and specimen were flooded with heavy oil and the indentation was carried out in ten stages at gradually increasing loads. Dugdale (1953) suggests that the latter practice results in an effective reduction in friction. The yield point of the specimen material is very high, so that the distance BK in this experiment should be close to a maximum. Nevertheless, it was found that BK never exceeded 0·03 d.

(c) *Examination of the indented surface*

Indentations were made on surfaces on which square grids had been ruled at a spacing of 0·5 mm. A typical indentation in the cold-rolled low-carbon steel used as an approximation to the ideal material is shown in Fig. 11. The lateral displacement undergone by the grid lines was always small and was approximately radial, at least outside a circle passing through the corners of the indentation. Within the circumscribing circle, four similar areas of distortion based on the sides of the indentation could be recognized. Each area may be considered as a zone of radial displacement centred at the middle of the side.

The cutting mechanism of indentation would require a much larger lateral displacement of points close to the indentation than that observed. The extent of the displacement is again more in accordance with a compression mechanism of indentation.

4. Vertical Displacements of the Indented Surface

The extent and shape of the lip around indentations produced in various materials by a Vickers indenter was determined by an interferometric method (Tolansky and Nickols 1949). The interference lines, which are effectively contour lines, around an indentation in cold-rolled low-carbon steel are shown in Fig. 12. The

contours are approximately circles centred at the indentation axis for the zone outside the circumscribing circle, while inside this boundary they are approximately arcs of circles centred at the midpoints of the sides. The surface topography may be considered as a concentric cone from the circumscribing circle to the intersection of the surface with the elastic–plastic boundary, while the four zones between the indentation and the circumscribing circles are each a half cone with the axis at the mid points of the side of the indentation. A typical profile along a radius through the mid-point of a side is shown in Fig. 13.

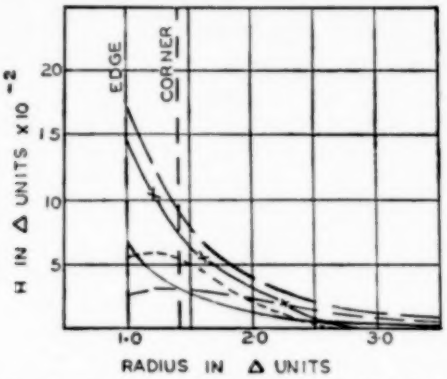

Fig. 13. Profiles of piled-up surfaces around diamond pyramid indentations.
— — Annealed 70 : 30 brass.
– – – – Cold-rolled 70 : 30 brass.
— × — Cold-rolled low-carbon steel.
— — — Calculated curve.

The general contour was similar for annealed 70 : 30 brass except that the height of the concentric cone was smaller and the radius of the cone was larger. The axes of the central cones were displaced slightly outwards and the surface near the edge of the indentation was drawn downwards, causing a rounding off of the sharp edge (Fig. 13). The profile for cold-rolled 70 : 30 brass was intermediate between those for the annealed brass and the cold-worked steel (Fig. 13).

The lip volume was estimated in each of these three cases ; the ratios of the lip volume to volume of the indentation were :

70 : 30 Brass, annealed	0·45
70 : 30 Brass, cold-rolled	0·65
Low-carbon steel, cold-rolled	0·85

5. A Model for the Compression Mechanism of Indentation

All the experimental evidence obtained in this and the earlier investigation supports the conclusion that the deformation mechanism which operates during indentation of a metal by a Vickers pyramid indenter approximates to a uniform radial displacement. The centre of the deformation is located at or close to the tip of the indentation.

For regions at distances from the centre which are large compared with the depth of the indentation, there will be little error in considering the deformation as being centred on the surface at the point of first contact of the indenter, and that the surfaces of equal displacement and

equal strain are hemispheres. In the ideal case it is also assumed that the material is incompressible. Then the volume displaced by an indentation of side $2\,\Delta$ is given by*

$$V = 4/3\ \Delta^2 \cot 68°. \tag{1}$$

If this material flows uniformly in a radial direction across a hemisphere of radius r the radial displacement is given by

$$U = \frac{V}{2\pi r^2}. \tag{2}$$

But the compressive strain is equal to the fractional change in the area of the hemisphere, so that the strain is

$$e = 2\,\frac{U}{r} \tag{3}$$

provided the displacement is small compared with the radius.

It has been shown above that the displacements in the plane of the surface are always small compared with the diagonal of the indentation and that the maximum vertical displacement is at the centre of the indentation and is equal to approximately one-seventh of a diagonal. In the zone outside the circumscribing hemisphere, equation (3) will not be seriously in error, so that

$$e = \frac{4}{3}\,\frac{\cot 68°}{\pi}\left(\frac{\Delta}{r}\right)^3. \tag{4}$$

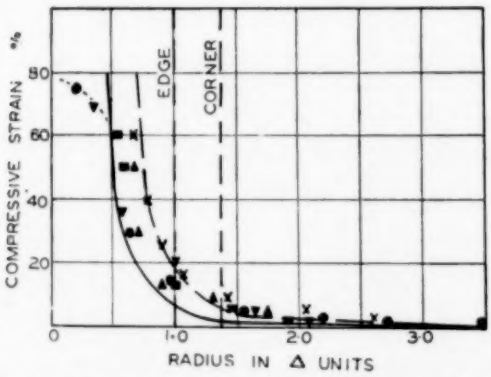

Fig. 14. Variation of strain with distance from the centre of the indentation.
The upper broken curve is that calculated for a 68° pyramidal indenter while the lower full curve is that calculated for a 68° conical indenter. The experimental values obtained with the various indenters and materials are identified as follows:

68° wedge in cold-rolled, low-carbon steel.
68° pyramid in cold-rolled, low-carbon steel.
68° pyramid in annealed 70 : 30 brass.
68° cone in cold-rolled, low-carbon steel.
60° cone in copper – from the results of Williams and O'Neill (1956).
The dotted curve indicates the probable trend of the experimental values.

It is convenient to measure the radius in units of length equal to Δ, so that

$$e = \frac{4}{3}\,\frac{\cot 68°}{\pi}\left(\frac{1}{R}\right)^3 \tag{5}$$

where

$$R = r/\Delta. \tag{6}$$

*The author is indebted to Dr. D. S. Dugdale for suggesting the mathematical treatment from this point to equation (4).

Inserting the appropriate values in (5),

$$e = 0{\cdot}17/R^3. \tag{7}$$

Following the same line of reasoning, analogous equations may be devised for a cone or a wedge :—

$$e\,(\text{cone}) = 0{\cdot}067/R^3 \tag{8}$$

where R is in units of length equal to the radius of the conical indentation and

$$e\,(\text{wedge}) = 0{\cdot}13/R^2 \tag{9}$$

where R is in units of length equal to half the width of the indentation. The curves calculated from (7) and (8) have been drawn in Fig. 14. The curve for the wedge has not been included since it lies close to that for the cone.

The displacement and strain pattern for the indentation of low-carbon steel by 68° conical and pyramidal indenters, and for the indentation of annealed 70 : 30 brass by a pyramidal indenter, have been estimated from the composite block specimens in the same manner as was done for the 68° wedge. From these patterns, an average radius from the first point of contact was estimated for each surface of constant strain. The strain for each of these indenters is plotted against radius in Fig. 14, the radius being shown in relative units (Δ) which are defined as follows:

Pyramidal Indentation: Half the length of the side

Conical Indentation: Radius

Wedge Indentation: Half the width.

WILLIAMS and O'NEILL (1956) have plotted the lines of equal workhardening in copper indented by a cone of 60° semi-angle and, for the same material, have measured the increase of hardness with reduction by rolling. The pattern of workhardening found by them is very similar to the above strain pattern. From their data, the workhardening has been converted to equivalent strain and plotted against radius in Fig. 14. It will be seen that all the results lie between the calculated curves for the pyramidal and conical indenters, even for zones inside the circumscribing sphere.

The above treatment assumes that the whole of the displaced volume sinks below the surface of the specimen. If part of the material were extruded above the surface, the strain would diminish more rapidly with distance from the centre than required by equations (7) and (8). In fact, the strain appears to be at least as great as that required for these equations except close to the centre of the indentation (Fig. 14). On the other hand, after removal of the indenting load, the volume of the raised lip adjacent to the indentation accounts for 70–90 per cent of the volume of the displaced material in the case of cold-worked materials, although it accounts for only about 45 per cent in the case of annealed 70 : 30 brass. Therefore, if the raised lip projects to any appreciable extent above the mean surface level while the indentation is under load, the agreement between the experimental results and the calculated curves is fortuitous. The above treatment is applicable if it does not. Unfortunately there is no experimental evidence available to indicate at which stage of indentation the lip does form, and this evidence would be difficult to obtain.

The most plausible assumption to fit in with the above treatment seems to be that extrusion above the original surface does occur under load but that there is a corresponding downward deflexion of the surface which is accommodated by elastic deformation of the specimen as a whole and which results in an approximately flat surface while under load. Elastic recovery occurs after release of the indenting load, so that the extruded lip now projects above the surface. On these assumptions, the deformation pattern would be the same for all materials while under load. The elastic recovery after unloading should also be the same for all materials if there is no residual stress.

Consider a hemispherical surface of radius r centred at the first point of contact. Plastic strain indentation will cause an increase in the area of this surface which will appear as a cylinder of area A and height h added to the hemisphere

$$A = 2\pi r h. \tag{10}$$

If the surface is to remain flat, the hemisphere must sink as a whole into the specimen by the distance h. From equations (3) and (10),

$$h = re \tag{11}$$

or expressed in characteristic units

$$H = Re = 0{\cdot}17/R^2 \tag{12}$$

where $H = h/\Delta$. The curve calculated from (12) is plotted in Fig. 13. This will be the height of the lip if complete recovery occurs. If residual stresses are present, the lip height will be less by an amount determined by these stresses.

The actual lip profiles for three representative materials are also shown in Fig. 13. The heights of the lips are of the right order of magnitude and in all cases are less than the calculated curve. The lip for the indentation in cold-rolled steel is the highest while that for the annealed 70 : 30 brass is the lowest, the cold-rolled brass being intermediate, i.e. the discrepancies increase as the rate of workhardening of the material increases. The residual stresses should then also increase with the rate of workhardening. It is not unreasonable to expect this because the radius of the elastic–plastic boundary has been found to increase with rate of workhardening of the material. Increase in the radius of the elastic–plastic boundary means a large increase in the volume of material in which deformation has occurred and consequently a larger misfit after recovery. It has also been shown that frictional effects cause pulling down of the lip in the case of the softer materials. This would also be expected to cause greater misfit in these materials and consequently greater residual stresses.

While the above model of deformation is probably oversimplified, it seems that equations (7) and (8) provide a reasonably close estimate of the strain pattern in the neighbourhood of an indentation. However, it was necessary, before certain secondary effects of indentation could be explained, to make a number of assumptions which cannot yet be supported by experimental evidence. It is proposed to examine this question further.

6. Discussion

It has been confirmed that the mechanism of indentation proposed by Hill *et al.* operates at small wedge angles but it has been shown that a second type of indentation mechanism becomes increasingly important with wedges of apex semi-angles greater than about 30°. This is a compression type of mechanism. A gradual change-over occurs from one type to another until, with a semi-angle of 68°, the cutting type of mechanism is relatively unimportant and the deformation approximates to a radial compression centred near the point of first contact. The deformation patterns for blunt indenters are all very similar irrespective of indenter shape. The deformation patterns for ball indenters investigated by Samuels and Mulhearn (1957) and by Dugdale (1956) are also very similar to those found here for pyramidal and conical indenters. The differences in deformation pattern which do occur are restricted to regions very close to the indenter. It is probable that, in these regions, large deformations occur in restricted areas to form a cap of dead metal which approximates to a hemisphere centred near the point of first contact. Outside this cap, the irregularities of strain are rapidly smoothed out and an approximately uniform radial strain is produced.

The observation made by Bishop *et al.* (1945) and by Dugdale (1954) that large variations in indentation wedge angle cause only small variations in mean pressure can be explained once it is realized that the stress pattern of blunt indenters is not greatly affected by the form of indenter. A partial explanation is also provided for the good agreement between the values of mean pressure for Brinell and Vickers hardness tests. Rockwell hardness results, on the other hand, are markedly affected by small variations in the form of the indenter. It is likely that this

variation is related to the fact that Rockwell hardness numbers are derived from depth measurements rather than to any marked difference in deformation mechanism, and is probably related to the large elastic strains occurring in the heavily deformed regions very close to the indenter. These results also indicate that a functional relationship between the different hardness scales derived from the area of the indentation is likely, and that a logical basis exists for conversions between these scales. The relationship between these scales and the Rockwell hardness scales is much more indirect and can therefore be justified on an empirical basis only.

ACKNOWLEDGMENTS

This paper is published with the permission of the Chief Scientist, Department of Supply, Melbourne, Australia. Helpful suggestions and criticisms received from Mr. L. E. SAMUELS and Dr. D. S. DUGDALE are gratefully acknowledged.

REFERENCES

BISHOP, R. F., HILL, R. and MOTT, N. F.	1945	*Proc. Phys. Soc.* **A57**, 147.
DUGDALE, D. S.	1953	*J. Mech. Phys. Solids* **2**, 14.
	1955	*J. Mech. Phys. Solids* **3**, 197.
	1956	*J. Iron Steel Inst.* **184**, 22.
GRUNZWEIG, J., LONGMAN, I. M. and PETCH, N. J.	1953	*J. Mech. Phys. Solids* **2**, 81.
HILL, R.	1950	*Phil. Mag.* **41**, 745.
HILL, R., LEE, E. H. and TUPPER, S. J.	1947	*Proc. Roy. Soc.* A **188**, 273.
SAMUELS, L. E. and MULHEARN, T. O.	1957	*J. Mech. Phys. Solids* **5**, 125.
TABOR, D.	1951	*The Hardness of Metals* (Clarendon Press, Oxford).
TOLANSKY, S. and NICKOLS, D. G.	1949	*Nature, Lond.* **164**, 103.
WILLIAMS, G. H. and O'NEILL, H.	1956	*J. Iron Steel Inst.* **182**, 266.
WILSON, D. V.	1954	*J. Iron Steel Inst.* **176**, 28.

J. Mech. Phys. Solids, 1959, Vol. 7, pp. 97 to 105. Pergamon Press Ltd., London. Printed in Great Britain

THE TORSIONAL YIELD STRESS OF ZINC SINGLE CRYSALS*

By N. Brown† and H. S. Rosenbaum‡

(*Received 27th June*, 1958)

Summary

The yield stress of circular cylindrical zinc crystals was measured both in torsion and in either shear or tension. Both type of tests were made on the same specimen. The yield stress in torsion varied with the angle between the basal plane and the axis of torsion. When the normal to the basal plane coincides with the axis of torsion, the maximum shear stress in torsion as calculated by the theory of elasticity was found to be 1·6 ± 0·1 times the critical resolved shear stress as measured by tension or shear. This value is greater than that found by previous investigators.

If it is assumed that the specimen has slipped almost entirely over its cross-section at the macroscopic yield point, then the average stress sustained by the crystal is 1·24 times the critical resolved shear stress.

1. Introduction

This work was undertaken for the purpose of determining the stress at which a single crystal yields when the stress distribution is non-homogeneous. In particular, we have chosen to study the yield stress of cylindrical crystals stressed in torsion about the cylinder axis. The elastic stress distribution in this case is given by

$$\tau = \frac{2Tr}{\pi a^4} \tag{1}$$

where τ is the shear stress on a plane perpendicular to the axis of torsion at a distance r from the cylinder axis; T is the applied torque; and a is the outer radius of the cylindrical specimen. The maximum shear stress which occurs at the surface is

$$\tau_{\text{tor}} = \frac{2T}{\pi a^3}. \tag{2}$$

There are several criteria which might be used to predict a yield stress in such a stress field. Schmid and Boas (1935) have stated the empirical law that single crystals undergo slip when the resolved shear stress reaches a critical value over a substantial part of the slip plane. Karnop and Sachs (1929) have suggested that the applied shear stress should be resolved on the slip direction and then averaged around the periphery of the slip plane. Implicit in Karnop and Sachs' analysis is the assumption that the stress required to activate slip on any particular slip

*This paper is partially based on a thesis submitted by H. S. Rosenbaum for the Master of Science Degree at the University of Pennsylvania, Philadelphia, Pennsylvania.

†University of Pennsylvania, Guggenheim Fellow at Cavendish Laboratory.

‡General Electric Research Laboratories, Schenectady.

system is just the critical resolved shear stress, τ_{ten} as measured in a tension or shear test; it is that critical stress to which Schmid and Boas (1935) referred. τ_{ten} is considered to be a physical property of the crystal and independent of the stress distribution.

If we consider a crystal oriented with a slip plane perpendicular to the cylinder axis, then all slip directions in that plane are equally stressed by the applied torque. We will henceforth refer to this orientation as ideal. For that case the criterion of Karnop and Sachs (1929) would predict a value of $\tau_{tor}/\tau_{ten} = 1{\cdot}05$ where τ_{tor} is the maximum shear stress given by (2) at the observed yield stress. Applying this criterion to an isotropic material (as might be done for the case of a h.c.p. metal crystal in the ideal orientation, since it is elastically isotropic in the basal plane) one expects $\tau_{tor}/\tau_{ten} = 1$. A different criterion was suggested by Brown (1955). Using an energy principle, he predicted that for both f.c.c. and h.c.p. crystals in the ideal orientation, $\tau_{tor}/\tau_{ten} = 1{\cdot}10$ at yielding.

Kochendörfer (1941) has applied the Schmid-Boas law to both bending and torsion. He concluded that to estimate the macroscopic (i.e. practically observable) yield stress one should average the stress over the entire slip plane. This leads to an estimate of $\tau_{tor}/\tau_{ten} = 1{\cdot}5$ for an ideally oriented crystal in torsion. He also concluded that at the observable macroscopic yield stress, slip must have already occurred on much of the slip plane. This means that τ_{tor}, as defined in (2), is not really the maximum stress borne by the outer fibres of the specimen at the time of macroscopic yielding. Thus, if the entire cross-section is plastic and there is no workhardening, $\tau_{tor}/\tau_{ten} = 1{\cdot}33$. The point of view and various methods of averaging the stress over the slip plane will be discussed in a later section of this paper. For the purpose of comparison we shall continue to refer to τ_{tor} as that defined by (2) regardless of whether or not it is actually the maximum stress on the crystal.

It must be emphasized that the estimates cited above are for the particular orientation where the slip plane is perpendicular to the axis of torsion. The way in which τ_{tor}/τ_{ten} may be expected to vary with orientation depends on the yield criterion adopted and has been discussed in the works of Karnop and Sachs (1929) and Kochendörfer (1941).

The experimental data available for comparison are meagre. In the work already cited Karnop and Sachs have measured the torsional yield stress for crystals of an Al : 5 per cent Cu alloy where the crystals had a variety of orientations. Extrapolating to the ideal orientation of a (111) plane perpendicular to the axis of torsion, their data show $\tau_{tor}/\tau_{ten} = 1{\cdot}1 \pm 0{\cdot}1$. A similar experiment on magnesium crystals was done by Hsu and Cullity (1954). Extrapolation of their data to the ideal orientation shows $\tau_{tor}/\tau_{ten} = 0{\cdot}5$ or $0{\cdot}6$, which is most surprising in the light of this discussion. We see that the available data are in marked disagreement.

In both of the experiments cited τ_{tor} and τ_{ten} were measured on different samples. Since τ_{ten} has been shown to be highly structure sensitive (Li *et al.* 1953), τ_{tor} and τ_{ten} can be compared only when they are both measured on the same specimen. This is done in the present investigation.

2. Experimental Procedure

The experimental investigation has two parts. Part I deals with crystals of

random orientation whose gauge lengths are long compared to their diameters; Part II deals with crystals of the ideal orientation whose gauge lengths are less than their diameters.

Part I

The zinc crystals of 99·999 per cent purity were made by the Bridgman method. The initial polycrystalline material was machined into the form of tensile specimens about 3 in. long, with $\frac{3}{8}$ in. diameter shoulders, and a 1 in. gauge length of $\frac{1}{4}$ in. diameter. One end of the specimen was machined to a point to provide a single nucleation site. To preserve the shape during the growing of the single crystal, the specimens were carefully packed in fine graphite powder. The resulting crystals were electropolished to produce a smooth surface on the gauge length, and the orientation was determined by X-rays. Before each test the crystals were sealed in an evacuated Pyrex glass tube, heated to 400°C for 3 hr and furnace cooled. Li *et al.* (1953) have pointed out the necessity for controlling the annealing procedure if reproducible yield points are to be obtained.

The crystals were pulled in tension using an Instron Tensile Machine. Care was taken to prevent bending by using universal joints at each end of the specimen. The resolved shear strain rate was maintained at 0·01 min^{-1}. The crystals were extended about 1 per cent in order to measure the yield stress. The crystals were annealed as before and the yield stress in tension was measured again. The yield stress was reproducible in that average resolved shear stress for all 9 crystals was 39·0 psi for the first tension test and 38·2 for the second.

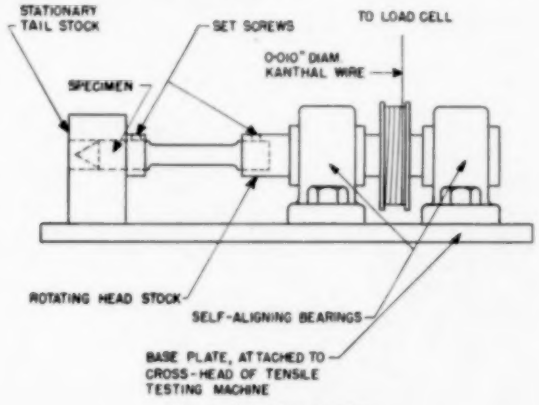

Fig. 1. Torsion device.

The crystals were brought back to their initial state again by annealing and then twisted. The sketch of the torsion device is shown in Fig. 1. The load to produce yielding varied from $\frac{1}{4}$ to 1 lb. The Instron Machine reads one pound full scale to an accuracy of $\pm \frac{1}{2}$ per cent. Friction was compensated by measuring the load to run the torsion device without a specimen and at the same speed as the actual test. The peripheral shear strain rate was 0·01 min^{-1} to match the resolved shear strain rate in the tension tests. The load–deformation curves were smooth and the yield stress load was taken as the first deviation from linearity*. τ_{tor} was calculated as in (2). In Fig. 2 τ_{tor}/τ_{ten} is plotted against ϕ, the angle between the basal plane normal and the cylinder axis. Extrapolation to the ideal orientation, is uncertain. τ_{tor}/τ_{ten} might have values of 1·5 to 3·5. In Figs. 2 the data of the previous investigators are also plotted. Fig. 3 shows the results on a stereographic projection indicating the complete orientations of the crystals.

An attempt was made to gather more information from these specimens which had been twisted a few degrees per inch. The specimens were electropolished to remove about 0·002 in. from their radii. After annealing, the yield stress in torsion was remarkably reproducible and in no

*This definition of the yield stress was chosen arbitrarily. It was found that other definitions of yield stress, i.e., point of maximum curvature of the load–deformation curve, or the stress at 0·1 per cent strain, do not significantly change the results of this investigation.

case was the yield stress from the second torsion greater than for the first torsion test. The crystals were electropolished and annealed again. Another tension test was performed. The average critical resolved shear stress was 61·7 psi as compared to an average of 38·6 psi before twisting. After torsion the zinc crystals are not straight in that both bending and twisting occur when the basal plane is not perpendicular to the axis of torsion.

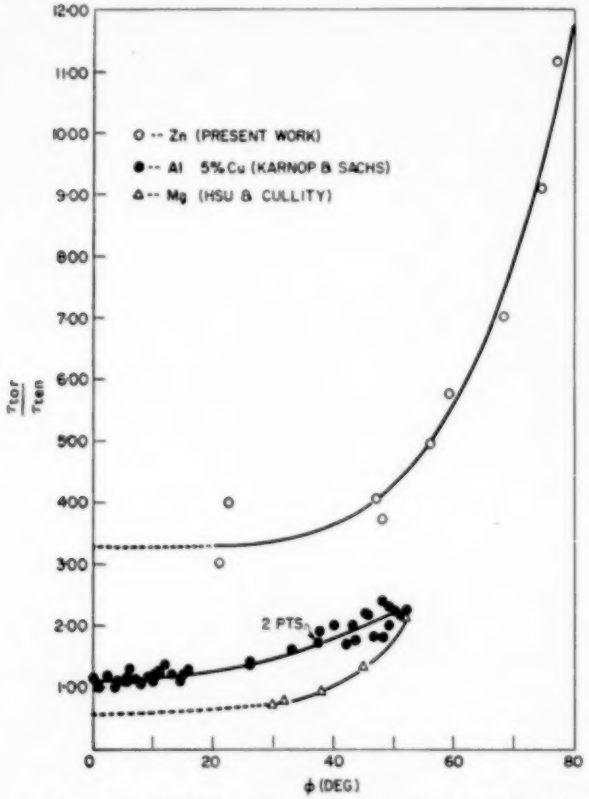

Fig. 2. τ_{tor}/τ_{ten} vs. angle between normal to basal plane and specimen axis.

Part II

All the specimens in Part II have the ideal orientation, and they were in the form of dumbbells which were machined from spherical single crystals. Specimens 21 and 23 were made at the General Electric Research Laboratory from 2 in. diameter spherical crystals of 99·999 per cent Zn grown in air. The dumbbell shape was obtained by turning on a lathe and then chemically polishing in a mixture of equal volumes of ethyl alcohol, conc. HNO_3, and H_2O_2 (GILMAN and DECARLO 1956) so as to maintain a very smooth surface. Chemical polishing was continued until no asterism was observed by X-rays (Laue back-reflexion technique). The final gauge length was about $\frac{3}{8}$ in. with about a 1 in. diameter. Specimen 26 was made at the University of Pennsylvania, and the dumbbell shape was acid machined from a spherical crystal of 99·99 per cent purity, also grown in air. The specimens were glued with Epon VI to grips which permitted the specimens to be twisted about an axis perpendicular to the basal plane or to be sheared parallel to the basal plane in the slip direction. The arrangement of the crystal in the testing apparatus is shown schematically in Fig. 4. After determining the yield stress by shear or torsion, the specimen was annealed. In turn out that not only were shear yield stresses reproducible after a previous shear test, but they were also reproducible after a previous torsion test if the crystal was untwisted prior to annealing. It was stated in Part I that for crystals of the non-ideal orientation that a shear after a torsion showed a very large increase in yield point when compared to a shear after a shear.

The stress-strain curves for the 99·999 per cent purity specimens were smooth both in shear and torsion. The stress–strain curve for the 99·99 per cent purity specimen showed a discontinuous yield point both in shear and torsion. The yield stresses were calculated from the loads which represented (1) the first deviation from linearity, (2) intersection of elastic and plastic parts of stress–strain curves, and (3) the upper yield point at the discontinuity. As was the case in Part I the final value of τ_{tor}/τ_{shear} was essentially independent of the yield definition. Thus the yield points for all crystals as reported in Table I are based on the first deviation from linearity. After each test, all specimens were heated to 165°C for 2 hr and then furnace cooled.

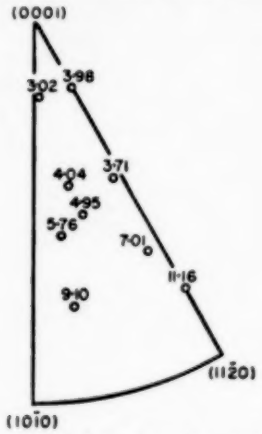

Fig. 3. Orientation of crystals.

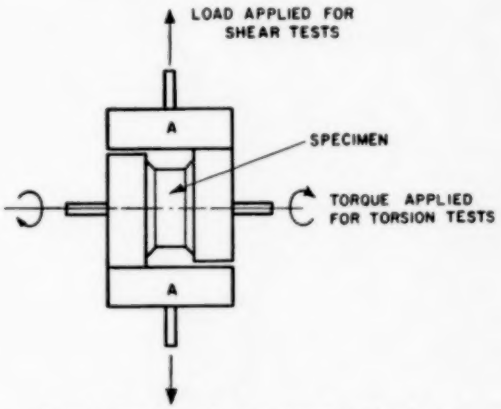

Fig. 4. Specimen for shear and torsion tests.

3. Discussion

The value of $\tau_{tor}/\tau_{shear} = 1{\cdot}65$ for the dumbbell specimens of ideal orientation is less than the value obtained in Part I by extrapolation. It is noted that the average critical resolved shear stress for all tests in Part I was 38·6 p.s.i. Specimens 21 and 23 had the same purity as the specimens in Part I, but their average yield stress in shear was 28·9 p.s.i. The discrepancy is not explained by the difference between a shear test and a tension test but rather by the difference in annealing treatment. Li *et al.* (1953) have shown such differences in annealing could shift the yield point by the magnitude observed in this investigation. It has been shown by Parker and Washburn (1953) that for a given purity and annealing condition $\tau_{shear} = \tau_{ten}$ for hexagonal close-packed crystals. We shall henceforth use these terms interchangeably.

The observed value of $\tau_{tor}/\tau_{ten} = 1{\cdot}65 \pm 0{\cdot}1$ for ideally oriented crystals is much higher than the values predicted. As mentioned before, the critical resolved shear stress criterion applied to an isotropic material predicts $\tau_{tor}/\tau_{ten} = 1{\cdot}00$; the resolved shear stress averaged circumferentially predicts $\tau_{tor}/\tau_{ten} = 1{\cdot}05$; and Brown's solution, based on the energy required to move dislocations predicts $\tau_{tor}/\tau_{ten} = 1{\cdot}10$. We shall now consider a criterion based on the average stress on the slip plane as suggested by Kochendörfer.

Let the average shear stress on a slip plane be

$$\bar{\tau} = \frac{\int_0^a \frac{r}{a}\,\tau_{tor}\,2\pi r\,dr}{\int_0^a 2\pi r\,dr}. \qquad (3)$$

If we now assume that the macroscopic yielding occurs when the average stress $\bar{\tau} = \tau_{ten}$, the critical resolved shear stress, we see that $\tau_{tor}/\bar{\tau} = \tau_{tor}/\tau_{ten} = 1{\cdot}50$. $\bar{\tau}$ is equal to the stress at $r = \frac{2}{3}a$.

We can extend this point of view in a method analogous to that of Karnop and Sachs (1929) by resolving this average stress along the slip direction:

$$\bar{\tau}_r = \frac{\int_{-\pi/6}^{\pi/6}\int_0^a 2\pi r . \frac{r}{a}\tau_{tor} . \cos\psi \, dr d\psi}{\int_{-\pi/6}^{\pi/6}\int_0^a 2\pi r \, dr d\psi}.$$

If we now assume that $\tau_{ten} = \bar{\tau}_r$, we get

$$\frac{\tau_{tor}}{\tau_{ten}} = 1{\cdot}05\,\frac{\tau_{tor}}{\bar{\tau}} = 1{\cdot}57.$$

Still another possible way of averaging is to average radially to obtain $\bar{\tau}$ as above, and then apply Brown's analysis (1955) for rotational slip where the stress to move a dislocation is taken as $\bar{\tau}$. Then

$$\frac{\tau_{tor}}{\tau_{ten}} = 1{\cdot}10\,\frac{\tau_{tor}}{\bar{\tau}} = 1{\cdot}65.$$

We now investigate the possibility that the initial yielding at the surface cannot be detected by the methods of the present investigation. After yielding has occurred at the surface, we can express the applied torque T as

$$T = \int_0^c \tau_0 \frac{r}{c} . 2\pi r . r dr + \int_c^a \tau_0 . 2\pi r . r dr$$

where r is the radial co-ordinate, c is the radius of the elastic-plastic interface, a is the outer radius of the specimen, τ_0 is the critical stress to produce yielding. It is assumed here that there is no work hardening and that τ_0 is a physical constant of the material and is equal to τ_{ten}. It now follows that

$$T = \frac{\pi\tau_0}{6}(4a^3 - c^3), \tag{4}$$

and, since $\tau = \dfrac{G\theta r}{l}$ for $r \leqslant c$,

$$c = \frac{\tau_0 l}{G\theta}. \tag{5}$$

Here, θ is the measured angle of twist, G is the shear modulus, and l is the gauge length. Thus

$$T = \frac{\pi\tau_0}{6}\left[4a^3 - \left(\frac{\tau_0 l}{G\theta}\right)^3\right]. \tag{6}$$

It is estimated that in this investigation the minimum detectable $\Delta\theta$ is 10^{-4} rad. Using the values $\tau_0 = 40$ psi, $G = 12 \times 10^6$ psi, $l = 1$ in., $\theta = 10^{-4}$ rad,

$$c^3 = \left(\frac{\tau_0 l}{G\theta}\right)^3 = 4 \times 10^{-5}\ \text{in.}^3$$

Since $4a^3 \approx 0{\cdot}5$ in^3, the contribution to the torque of the stress in the elastic region

is very small, and, under the assumed condition of no workhardening, slip has occurred over almost all of the slip plane before yielding was detected. This is the same conclusion reached by KOCHENDÖRFER (1941). Thus we can assert that

$$\tau_0 = \frac{3T}{2\pi a^3} = \tau'_{\text{tor}} \tag{7}$$

may be a more realistic value for the maximum shear stress sustained by the outer elements of the specimen at the point of macroscopic yielding. Comparing this with equation (2), we see that we can get a lower limit for the measured value

$$\frac{\tau'_{\text{tor}}}{\tau_{\text{ten}}} = \frac{3}{4}\frac{\tau_{\text{tor}}}{\tau_{\text{ten}}} = \left(\frac{3}{4}\right)(1{\cdot}65) = 1{\cdot}24.$$

That is, if we assume that micro-slip (slip prior to the observed macroscopic yielding) occurs and is accompanied by no workhardening, then the maximum stress supported by the material is $\frac{3}{4}$ of that value calculated for the case of no micro-slip.

The data of this investigation agree with the idea of averaging the stress over the entire slip plane, but are not sufficiently precise to distinguish between these suggested methods of averaging.

It is interesting to note that in a shear test the shear stress is non-homogeneous over the slip plane, as is the case for torsion. Yet, the macroscopic yield stress in a shear test is the same as the critical resolved shear stress in a tensile test (PARKER and WASHBURN 1953)*. This means that in pure shear the stress must be raised to such a level that the stress averaged over the entire slip plane equals τ_{ten}. There is, of course, the possibility that one could perform an experiment that measures the local strain in the middle of a shear specimen and find that yielding occurs locally at $\tau_{\max} = \tau_{\text{ten}}$. However, the macroscopic yield stress is really the condition at which the ratio of the strain increment to stress increment increases rapidly. This can occur only when the unslipped portion of the slip plane is small enough to offer little resistance to the advancing elastic–plastic interface, and then slip occurs over the entire slip plane.

The evidence of this investigation suggests that a similar situation exists in the case of torsion. The macroscopic yield stress is that stress at which the ratio of the strain to stress increment $d\gamma/d\tau$ increases rapidly. This is not possible as long as the unslipped portion of the slip plane is large enough to constrain the flow of material.

We shall now consider the workhardening in a torsion test. For a material that workhardens the shear stress at the outer element is given by HOFFMAN and SACHS (1953) :

$$\tau_{(0)} = \frac{3}{2\pi a^3}\left(\frac{\theta'}{3}\frac{dT}{d\theta'} + T\right) \tag{8}$$

where θ' is the angle of twist per unit of gauge length $\theta' = \theta/l$. The rate of work hardening in the region where $dT/d\theta'$ is approximately constant is

$$\frac{d\tau}{d\gamma} = \frac{2}{\pi a^4}\frac{dT}{d\theta'}. \tag{9}$$

*In a shear test the shear stress at the specimen surface is zero, and the maximum stress is at the centre of the cross-section. For a shear specimen with a circular cross-section the maximum shear is about 1·3 times the average shear stress (TIMOSHENKO 1940).

From the data of Fig. 5 we can calculate the coefficient of workhardening. We take $dT/d\theta' = 30$ lb in^2 at $\approx 0{\cdot}2$ in^{-1}, and we find that $d\tau/d\gamma$ is 300 psi. In a shear test at a corresponding strain of about 10 per cent the rate of workhardening is 160 psi. We see that workhardening as determined in a torsion test

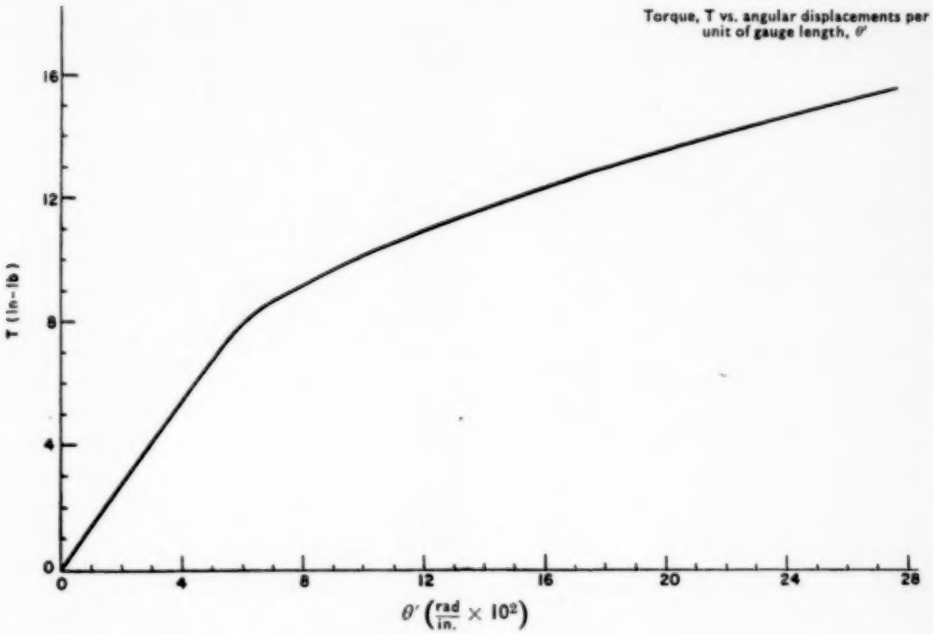

Fig. 5. Experimental curve of torque vs. displacement.

is about twice that in a shear test. Also, from equation (8) we can see that the workhardening alone cannot explain the experimental value of $\tau'_{\text{tor}}/\tau_{\text{ten}} = 1{\cdot}24$. To give such a value the coefficient of workhardening in torsion would have to be about 1000 times that observed. It seems likely that the greater workhardening observed in torsion is due to the pile-up of dislocations near the centre of the specimen.

It was previously mentioned that, after a torsional strain, crystals of the ideal orientation could be untwisted and annealed to return the crystal to its original condition, as manifested by its yield stress in a shear test. This was found to be true for torsional shear strains of ~ 1 per cent at the specimen surface. The fact that simply annealing is not sufficient to restore the crystal's condition indicates that the dislocation network that causes the work hardening in torsion cannot be relieved by a simple diffusion process such as climb of dislocations. However, it is not clear why simply annealing after a torsional strain can restore the torsional yield stress, but cannot restore the yield stress in shear without first untwisting. Untwisting after torsional strains of greater than 1 per cent was not attempted, nor was any attempt made to restore the critical resolved shear stress of crystals of non-ideal orientation (Part I) by untwisting.

4. Conclusions

1. At the macroscopic torsional yield stress the maximum applied shear stress based on an elasticity calculation was found to be $1{\cdot}6 \pm 0{\cdot}1$ times the critical resolved shear stress of the same crystal when the applied torque is about an axis normal to the slip plane. This value disagrees with the previous investigators (Karnop and Sachs 1929; Hsu and Cullity 1954) whose data were obtained on different materials and whose torsional yield stress and critical resolved shear stress were each determined on different specimens.

2. The actual maximum shear stress sustained by the specimen material at the observed torsional macroscopic yield stress is between 1·24 and 1·6 times the critical resolved shear stress.

3. The workhardening in torsion is about twice that observed in simple shear.

4. One can reproduce the original critical resolved shear stress of a crystal after a torsional strain (up to 1 per cent at the specimen surface) about the normal of the basal plane by untwisting the crystal prior to annealing.

Acknowledgments

The authors wish to thank J. J. Gilman and V. J. DeCarlo of the General Electric Research Laboratory for providing some of the spherical zinc crystals used in this investigation. Some of the experimental work was done on facilities at the Franklin Institute Laboratories for Research and Development that were made available to the authors through the courtesy of R. L. Smith. This work was partially supported by the United States Atomic Energy Commission.

References

Brown, N.	1955	*Trans. Amer. Inst. Min. (Metall.) Engrs.* **203**, 134.
Gilman, J. J. and DeCarlo, V. J.	1956	*Trans. Amer. Inst. Min. (Metall.) Engrs.* **206**, 511.
Hoffman, D. and Sachs, G.	1953	*Introduction to the Theory of Plasticity for Engineers* 137-139 (McGraw-Hill, New York).
Hsu, S. S. and Cullity, B. D.	1954	*Trans. Amer. Inst. Min. (Metall.) Engrs.* **200**, 305.
Karnop, R. and Sachs, G.	1929	*Z. Phys.* **53**, 605.
Kochendörfer, A.	1941	*Plastische Eigenschaften von Kristallen und metallischen Werkstoffen* (J. Springer, Berlin).
Li, C. H., Washburn, J. and Parker, E. R.	1953	*Trans. Amer. Inst. Min. (Metall.) Engrs.* **197**, 1223.
Parker, E. R. and Washburn, J.	1953	*Modern Research Techniques*, 186 (Amer. Soc. Met., Cleveland, Ohio).
Schmid, E. and Boas, W.	1935	*Kristalplastizität* (J. Springer, Berlin).
Timoshenko, S.	1940	*Strength of Materials*, Part I (Van Nostrand, New York).

J. Mech. Phys. Solids, 1959, Vol. 7, pp. 106 to 113. Pergamon Press Ltd., London. Printed in Great Britain

THE STRAIN–RATE SENSITIVITY OF α-URANIUM

By C. J. Maiden
Engineering Laboratory, University of Oxford*

(*Received* 12*th August*, 1958)

Summary

Experiments are described in which specimens from two different batches of uranium were subjected to both static and dynamic compression tests. From such tests static and dynamic stress–strain curves were obtained. These stress–strain curves indicate that α-uranium is slightly strain–rate sensitive; for instance, the effect of increasing the strain rate from $2{\cdot}5 \times 10^{-3}$/sec to several hundred per sec was to raise the stress, at any strain less than about 4 per cent, by approximately 10 per cent. After about 4 per cent strain the strain–rate sensitivity was found to decrease with increased deformation.

In order to determine the variation in dynamic strength of α-uranium with test temperature, as-cast specimens from the first batch of uranium were tested dynamically at − 41°C and − 84°C. The results obtained indicate that the rate of increase of strength with decreasing temperature is small, the effect of lowering the test temperature to − 84°C being to raise the dynamic stress–strain curve corresponding to given test conditions by only about 5 per cent. Also, to determine the effect of grain size on the dynamic strength of uranium, tests were made on the first batch of uranium in the β-quenched state. It was found that, for identical test conditions, the derived dynamic stress–strain curve for the β-quenched material was approximately 10 per cent higher than for the as-cast material.

The second batch of uranium was also tested dynamically in the 300°C rolled condition. The results of such tests indicate that the dynamic compressive strength of 300°C rolled uranium, in the direction of rolling, is slightly greater than the dynamic compressive strength of α-uranium in the as-cast state.

1. Introduction

The tests described in the present paper were made in order to help understand the phenomenon of radiation growth in uranium.

Growth is the term used to describe the change of shape that occurs in α-uranium under irradiation. The main characteristics of such growth have been summarized by Pugh (1956) and are as follows:

(a) In a crystal of α-uranium (ortho-rhombic structure) subjected to irradiation there is an increase in length along the [010] direction, a decrease along [100] and little change along [001]. The rate of increase in length along [010] is approximately the same as the rate of decrease in length along [100].

(b) The rate of growth is temperature sensitive in that it appears to be zero in the high α-range 500–660°C, a maximum at about 200°C and greatly reduced at − 196°C.

*Present address: D.S.S.O., Aerophysics Section, C.A.R.D.E., Quebec, Canada.

Two types of theory have been proposed to explain this growth. The first type are point-defect theories that depend on the anisotropic diffusion of interstitials and vacancies produced in fission spikes; whereas the second type are spike theories in which growth is a result of thermal strains caused by fission spikes. These spikes are produced by fission fragments and are very intense. For instance COTTRELL (1956) has estimated that a 100 MeV fission fragment will raise the temperature of a cylinder 10^4 atoms long and 50 atoms radius to 4,000°C. Also heat conduction considerations have shown that the lifetime of such a spike would only be about 10^{-11} sec. Hence, assuming a yield stress of 10,000 lb/in², a Young's modulus of 30×10^6 lb/in² (PUGH 1956), and that yield does occur due to thermal strains, strain rates of at least 10^7/sec must be attained in the uranium. Thus the behaviour of uranium when subjected to high rates of loading is of interest.

The present paper describes results of static and dynamic compression tests on two different batches of uranium. Unfortunately, the highest average strain rate obtainable in the dynamic apparatus was only several hundred per sec, a value small compared with 10^7/sec. However, it is thought that a comparison of the results obtained in the dynamic tests with those of the static tests will give an indication of the strain-rate sensitivity of uranium, and so will give an approximate idea as to its behaviour when subjected to loading rates likely to be reached in a fission spike.

The first batch of uranium was tested at room temperature in the as-cast and β-quenched states. When uranium is β-quenched a very fine grain structure is produced; hence, upon irradiation, the absolute growth of each grain is small and the surface phenomenon of wrinkling is relatively unimportant compared to that which occurs in coarse grained α-uranium. Dynamic tests were also performed on this as-cast uranium at temperatures of − 41°C and − 84°C. PUGH has suggested that below 200°C growth diminishes with decreasing temperature due to a corresponding increase in yield strength. The present low-temperature tests were made in order to find the variation in dynamic strength with test temperature.

The second batch of uranium was tested dynamically in the as-cast and cold-rolled (300°C) condition. Uranium rolled at 300°C has a texture that consists mainly of grains with the [010] direction along the rolling axis. As [010] is the direction along which single crystals elongate on irradiation, rods rolled at 300°C exhibit a marked increase in length when irradiated. The tested specimens were machined from a rolled bar with their longitudinal axes parallel to the rolling axis.

2. APPARATUS

(i) *Static*

Static testing was done on a 50-ton hydraulic compression machine on which rates of loading up to $2{\cdot}5 \times 10^{-3}$/sec could be obtained. The device used to eliminate eccentricity of loading has been described by MAIDEN and CAMPBELL (1958).

(ii) *Dynamic*

The impact machine used in the present investigation has been described in an earlier paper (CAMPBELL and MAIDEN 1957). The stress caused by a falling weight

was transmitted to the specimen through a high-tensile steel weighbar. Immediately below the specimen was an anvil bar, the length of which determined the time for which a specimen was loaded.

3. SPECIMENS

All the specimens were cylindrical in form, $\frac{3}{8}$ in. in diameter and $\frac{1}{2}$ in. in length. Specimens were obtained from two batches of uranium. The amounts of the most important impurities in each batch were as follows:

	Ni	Fe	Cr	C	O_2	N_2	Si
First batch	200p.p.m.	400p.p.m.	40p.p.m.	0·130%	0·028%	120p.p.m.	126p.p.m.
Second batch	7p.p.m.	30p.p.m.	15p.p.m.	0·075%	0·010%	40p.p.m.	70p.p.m.

Both batches of uranium were first cast in the form of $\frac{3}{4}$ in. diameter bars. From the first batch specimens were machined from the as-cast bars and also from a bar that had been β-quenched from 750°C. From the second batch specimens were machined from the as-cast bars and from a bar that had been reduced in area 56 per cent by rolling at 300°C.

4. EXPERIMENTAL RESULTS

First Batch

(i) *Mechanical properties*

(a) *As-cast uranium.* Two types of static tests were made in order to find the stress–strain curves corresponding to two slow loading rates. The first type of test was at a constant strain rate of $2{\cdot}5 \times 10^{-3}$/sec, and the second was made by adding successive small increments of load to a specimen and maintaining the load constant, after the application of each increment, until the strain reading became sensibly constant. This latter type of test was considered to represent an infinite loading time and henceforth will be referred to as a zero strain-rate test. Several specimens were tested in each manner and the results obtained showed that both stress–strain curves were repeatable to within $\pm$ 3 per cent. The average stress–strain curves, corresponding to the two types of loading, are shown in Fig. 1 (curves *C* and *D*), and it is seen that they are quite widely separated. This is due to the large amount of creep that occurred during a test at zero strain rate.

Room-temperature dynamic stress–strain curves were derived corresponding to impact velocities of 430 in/sec, 470 in/sec and 503 in/sec. To obtain such dynamic stress–strain curves elastic, weighbar and anvil bar records, corresponding to each impact velocity, were analysed by the method of CAMPBELL and DUBY (1956). The weighbar and elastic records were obtained from weighbar resistance strain gauges which were centred $\frac{3}{8}$ in. above the specimen upper face, the elastic record being obtained with a high-tensile steel dummy in place of the specimen. The anvil bar records were obtained from strain gauges on the anvil bar, centred $\frac{3}{8}$ in. below the specimen lower face. Typical stress-time oscillograms with calibration lines superimposed are shown in Figs. 2 (a)–(c); all the traces are interrupted every 2 μsec. It was found that records obtained at each gauge position under

identical impact conditions were consistent to within ± 2 per cent, i.e. there was a slightly greater reproducibility at the high rates of loading than there was in the static tests. In the derivation of each dynamic stress–strain curve the average of several records obtained at each gauge position was used.

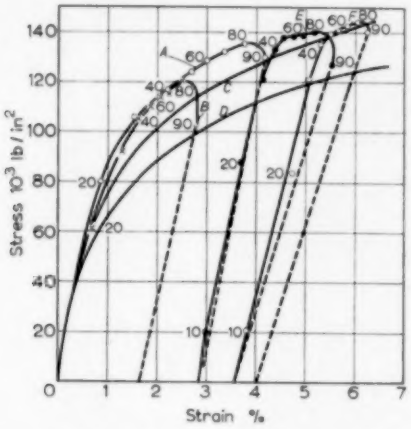

Fig. 1. Stress–strain curves for uranium in the as-cast condition (first batch).

Curve *A*: Impact velocity 503 in/sec. Average strain rate 460/sec. Maximum strain rate 800/sec.

Curve *B*: Impact velocity 430 in/sec. Average strain rate 300/sec. Maximum strain rate 600/sec.

Curve *C*: Static test at strain rate of $2{\cdot}5 \times 10^{-3}$/sec.

Curve *D*: Static test at zero strain rate.

Curve *E*: Second impact at 503 in/sec. Average strain rate 300/sec. Maximum strain rate 550/sec.

Curve *F*: Third impact at 503 in/sec. Average strain rate 300/sec. Maximum strain rate 590/sec.

The derived dynamic stress–strain curves corresponding to velocities of 503 in/sec and 430 in/sec are plotted in Fig. 1 (curves *A* and *B*), the time being indicated every 10 μsec. For clarity in Fig. 1 the curve corresponding to 470 in/sec has not been shown, as it is very close to curves *A* and *B*. To obtain an extension to curve *A*, the specimens impacted at 503 in/sec were impacted twice more at the same velocity and the records obtained were analysed to give curves *E* and *F* in Fig. 1. It is of interest to observe the loops formed on loading and unloading, i.e. between curves *E* and *F*. This effect has previously been observed by Jones and Munro (1953) when a rolled bar of uranium was subjected to repeated static loading and unloading.

In order to find the effect of test temperature on the dynamic properties of α-uranium, specimens were impacted at 503 in/sec at -41°C and -84°C. The derived stress–strain curve at -84°C is shown in Fig. 3 (curve *G*). For clarity the curve found at -41°C has been omitted; as would be expected it lay between the curves corresponding to room temperature and -84°C.

It is to be noted that in each dynamic stress–strain curve the stress plotted is the mean of the values derived for the upper and lower specimen faces ; and the strain plotted is the average strain in the specimen at the time concerned. Also, throughout each dynamic test the strain rate is by no means constant. The values of the average and maximum strain rates, corresponding to each dynamic stress–strain curve, are given in the caption to the figure in which the curve is shown.

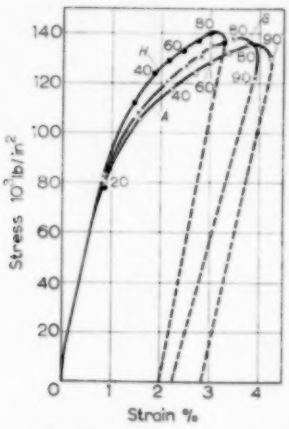

Fig. 3. The effect of temperature and grain size on the stress–strain curve corresponding to an impact velocity of 503 in/sec. (first batch).

Curve *A*: As-cast uranium tested at + 15°C.

Curve *G*: As-cast uranium tested at − 84°C. Average strain rate 430/sec. Maximum strain rate 740/sec.

Curve *H*: β-quenched uranium tested at + 15°C. Average strain rate 370/sec. Maximum strain rate 700/sec.

(b) *β-quenched uranium.* Specimens machined from a bar that had been β-quenched from 750°C were impacted at 430 in/sec and 503 in/sec. A typical anvil bar stress–time oscillogram is shown in Fig. 2 (d). It was found that records obtained at each gauge position under the same impact conditions were only repeatable to within ± 4 per cent. This relative lack of reproducibility was attributed to a grain size variation from specimen to specimen due to the severe nature of the heat treatment to which they had been subjected.

The derived dynamic stress–strain curve corresponding to an impact velocity of 503 in/sec is shown in Fig. 3 (curve *H*). As for the as-cast uranium it was found that the stress–strain curves at 430 in/sec and 503 in/sec were very close together; for this reason only the latter is presented in Fig. 3.

(ii) *Micrographic examination*

Several specimens were sectioned and examined micrographically after both static and dynamic tests. Fig. 4 (a) shows the microstructure of an as-cast specimen

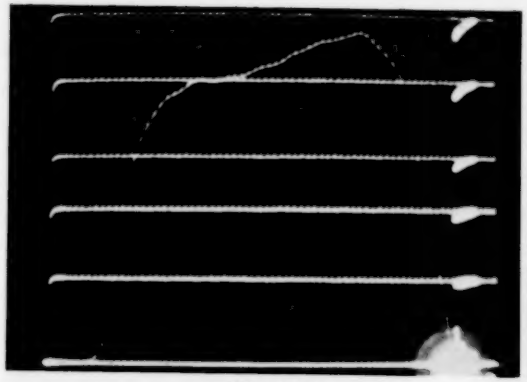

Fig. 2 (a).

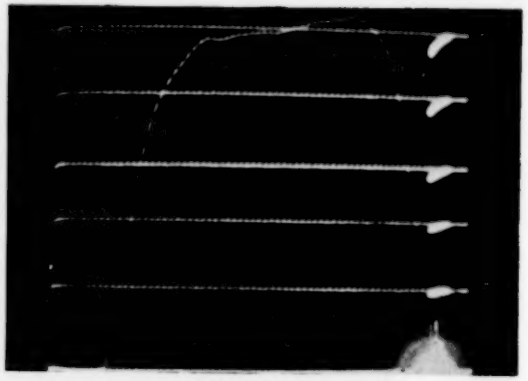

Fig. 2 (b).

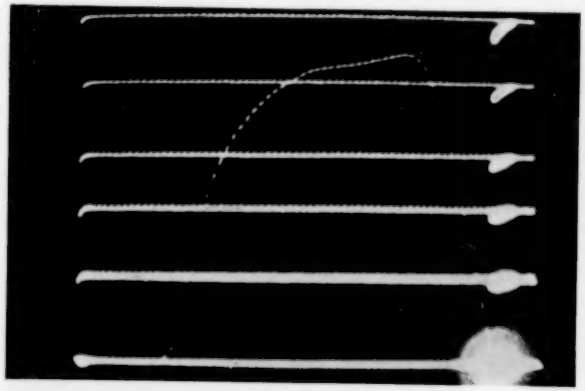

Fig. 2 (c).

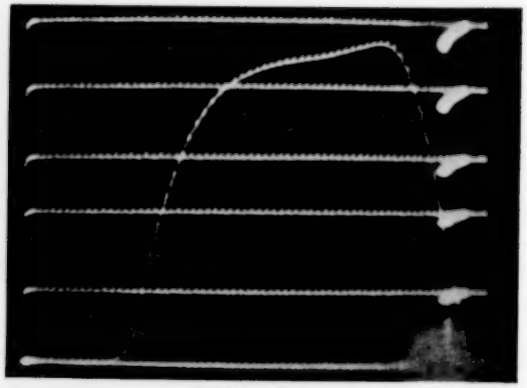

Fig. 2 (d).

Fig. 2. Stress–time oscillograms (first batch). Calibration lines correspond to stresses of 0, 30, 59, 84, 117 and 146 $\times$ 10^3 lb/in^2.

(a) Weighbar record for an as-cast specimen impacted at 470 in/sec.

(b) Weighbar record for an as-cast specimen impacted for the third time at 503 in/sec.

(c) Anvil bar record for an as-cast specimen impacted at 503 in/sec.

(d) Anvil bar record for a β-quenched specimen impacted at 503 in/sec.

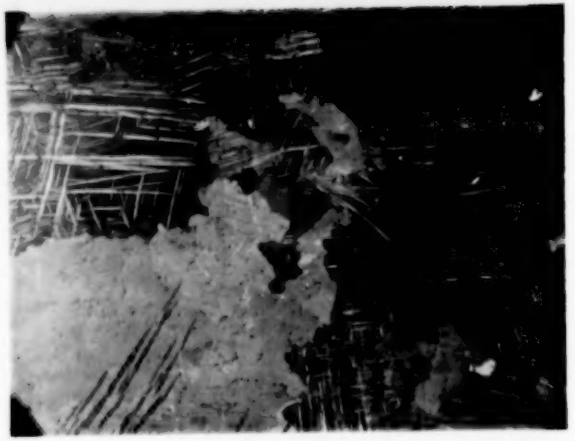

Fig. 4 (a).

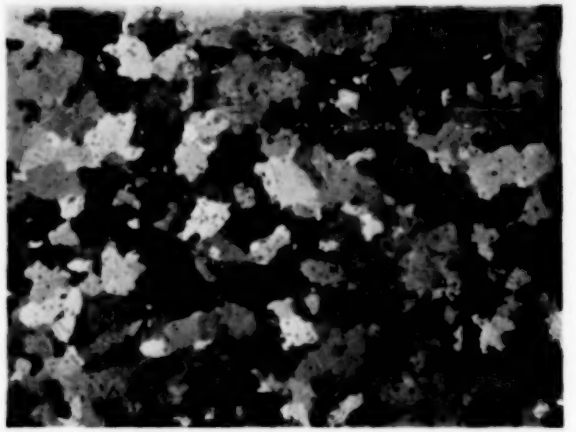

Fig. 4 (b).

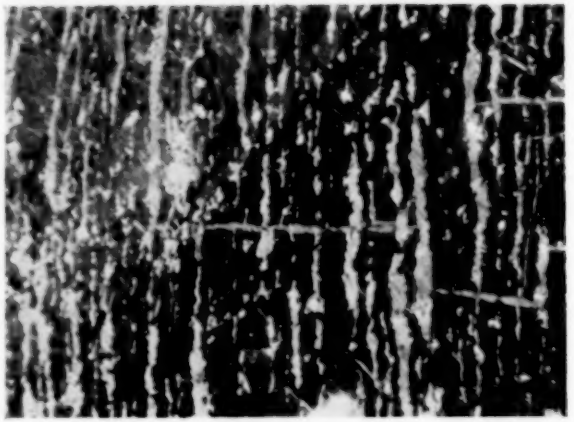

Fig. 4 (c).

Fig. 4. Microstructure of impacted specimens.

(a) As-cast specimen (first batch) strained 4 per cent by three successive impacts at 503 in/sec ($\times$ 140).

(b) β-quenched specimen strained 2 per cent by an impact at 503 in/sec ($\times$ 140).

(c) Cold-rolled specimen strained 2·4 per cent by an impact at 430 in/sec ($\times$ 350).

after 4 per cent dynamic strain, and Fig. 4 (b) the microstructure of a β-quenched specimen after 2 per cent dynamic strain. It is seen that twinning is a very important mechanism of dynamic deformation. This is rather to be expected as CAHN (1953) has found that the most frequently observed static deformation mechanism is slip on the (010) plane, and that the next most important mechanisms are twinning on the (130) composition plane and on planes having indices of approximately {172} and {176} respectively.

It also appeared that a specimen strained dynamically by a given amount contained slightly more twins, more uniformly distributed, than a specimen strained statically by the same amount. This is by no means a definite conclusion as in both statically and dynamically tested specimens a great number of twins were formed.

Second Batch

(a) *As-cast uranium.* Dynamic stress–strain curves were derived corresponding to impact velocities of 430 in/sec and 503 in/sec. The dynamic stress–strain curve for an impact at 503 in/sec and the two static stress–strain curves, obtained in the same manner as for the first batch, are shown in Fig. 5 as curves *I*, *J* and *K* respectively. The dynamic curve for a velocity of 430 in/sec once again differed only slightly from that for a velocity of 503 in/sec and for clarity is not shown in the Figure.

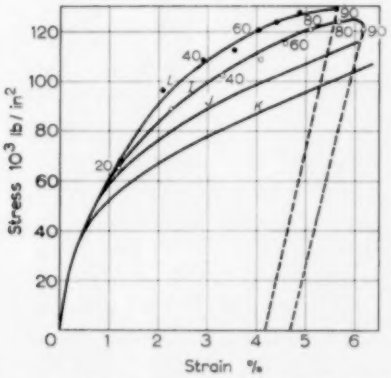

Fig. 5. Stress–strain curves for as-cast and cold-rolled uranium (second batch).
Curve *I*: As-cast uranium impacted at 503 in/sec. Average strain rate 880/sec. Maximum strain rate 1020/sec.
Curve *J*: As-cast uranium tested statically at strain rate of $2{\cdot}5 \times 10^{-3}$/sec.
Curve *K*: As-cast uranium tested statically at zero strain rate.
Curve *L*: Cold-rolled uranium impacted at 503 in/sec. Average strain rate 700/sec. Maximum strain rate 1080/sec.

(b) *Uranium rolled at* 300°C. Specimens were impacted at 503 in/sec in order to derive a dynamic stress–strain curve. It was found that the records obtained at each gauge position were only repeatable to within ± 16 per cent. Because of

this extremely large scatter it was decided to examine micrographically all the impacted specimens. This was done and it was found that the scatter was due to various degrees of recrystallization during rolling. PAINE and KITTEL (1955) have found that recrystallization can only begin at temperatures greater than 400°C. As the rolling was on a commercial roll with very little temperature control, temperatures greater than 400°C could easily have been reached in local hotspots. Several of the specimens did, however, exhibit a typical cold-rolled structure; a micrograph of such a specimen is shown in Fig. 4 (c).

Hence, in deriving the dynamic stress–strain curve, it was decided to use only those records obtained from specimens which did not exhibit any marked recrystallization. In this way it was found that the scatter in records obtained at a particular gauge was greatly reduced. The derived dynamic stress–strain curve is shown as curve *L* in Fig. 5.

5. Discussion and Conclusions

Figs. 1 and 5 show that α-uranium is slightly strain-rate sensitive. The results indicate that the effect on the stress–strain curve of increasing the strain rate from $2{\cdot}5 \times 10^{-3}$/sec to several hundred per sec, is about the same as the effect of an increase in strain rate from zero to $2{\cdot}5 \times 10^{-3}$/sec. This substantial raising of the stress–strain curve due to an increase in strain rate from zero to $2{\cdot}5 \times 10^{-3}$/sec is due to the large transient creep shown by α-uranium at low temperatures. As curves *A* and *B* in Fig. 1 almost coincided it was thought possible, although unlikely, that the stress–strain curve could be raised by increasing the strain rate from zero to about 10^{-1}/sec, whereas the application of a greater strain rate than 10^{-1}/sec might not raise the stress–strain curve any further. This possibility has been ruled out by the fact that the stress–strain curve corresponding to a given impact velocity was raised by lowering the test temperature (this is considered equivalent to a further increase in strain rate).

The dynamic stress–strain curves plotted in Fig. 3 indicate that lowering the test temperature from + 15°C to − 84°C raises the stress–strain curve by about 5 per cent. This seems to imply that the rate of increase in strength with decreasing test temperature is small; however, it is probably great enough to account for the decrease in growth that occurs below 200°C with diminishing temperature.

The dynamic tests on β-quenched uranium have indicated that in this condition uranium is appreciably stronger than in the as-cast state. As there is no preferential grain orientation in either as-cast or β-quenched uranium, it must be concluded that the increase in strength of β-quenched uranium is due to the small grain size alone. It is of interest to note that lowering the test temperature to − 84°C raised the stress–strain curve corresponding to an impact velocity of 503 in/sec by approximately 5 per cent, whereas β-quenching the uranium raised the curve by nearly 10 per cent.

Any changes in the dynamic strength properties of α-uranium due to cold-rolling must be predominantly caused by the combined effect of preferential grain orientation, the elongated grain shape and the change in average grain size. It appears impossible to separate these three effects from the results obtained in the present tests on 300°C rolled uranium. The only conclusion that can be drawn from a comparison of curves *I* and *L* in Fig. 5 is that the compressive impact

strength of a polycrystalline specimen of cold-rolled uranium in the direction of rolling is slightly greater than the compressive impact strength of the as-cast material.

Acknowledgments

This research was sponsored by the Atomic Energy Research Establishment, Harwell. The author is particularly grateful to Mr. S. F. Pugh and Dr. D. R. Harries of A.E.R.E., and to Dr. J. D. Campbell of the Oxford University Engineering Laboratory for valuable assistance during the course of this investigation.

References

Cahn, R. W. 1953 *Acta Met.* **1**, 49.
Campbell, J. D. and Duby, J. 1956 *Proc. Roy. Soc.* A**236**, 24.
Campbell, J. D. and Maiden, C. J. 1957 *J. Mech. Phys. Solids* **6**, 53.
Cottrell, A. H. 1956 *Met. Rev.* **1**, 479.
Jones, E. R. W. and Munro, W. 1953 *J. Mech. Phys. Solids* **1**, 182.
Maiden, C. J. and Campbell, J. D. 1958 *Phil. Mag.* **3**, 872.
Paine, S. H. and Kittel, J. H. 1955 *Geneva Conference Paper*, No. P/745.
Pugh, S. F. 1956 *Prog. Nucl. Energy* **1**, 652.

J. Mech. Phys. Solids, 1959, Vol. 7, pp. 114 to 125. Pergamon Press Ltd., London. Printed in Great Britain

A NOTE ON STRAIN HARDENING CIRCULAR PLATES

By W. E. Boyce
Rensselaer Polytechnic Institute, New York

(*Received* 22*nd October*, 1958)

Summary

Previous solutions for uniformly loaded simply supported circular plates are extended to plates which are partially clamped. A piecewise linear theory using Prager's hardening law is employed. The effect of perturbations in the initial yield stress on the post-yield stresses and displacements is also examined.

1. Introduction

Since the origin of piecewise linear strain-hardening plasticity by Prager (1955, 1956) and Hodge (1955), this type of theory has been used in the solution of a variety of problems involving structural elements. One of the first elements analysed was a simply supported uniformly loaded circular plate; it proved impossible, at least with similar methods, to solve the corresponding problem for a clamped plate. One purpose of this paper is to examine this situation in some detail by considering a plate with an intermediate support condition, a plate which is imperfectly clamped, so to speak.

Once a solution to such a problem is reached, expressions for the stresses and displacements depend on such parameters as the yield stress and hardening coefficient, as well as the dimensions of the body and the independent variables of space and load. The second purpose of the paper is to examine the nature of this dependence for the problem under investigation.

The solution obtained below is based on a theory of piecewise linear plasticity, utilizing Tresca's yield condition and a hardening law suggested by Prager (1955). The relevant equations have been discussed in considerable detail by Hodge (1957) and Shield and Ziegler (1958). A brief review of the more important features of this theory is included in order to make this paper reasonably self-contained.

2. Basic Equations

In developing a piecewise linear theory of plasticity it is natural to employ Tresca's yield criterion and the associated flow rule. In terms of principal stresses σ_1, σ_2, and σ_3, this criterion is represented by the familiar hexagonal cylinder in stress space (Fig. 1). As long as displacements are moderately small, the bending of a thin plate is essentially a plane stress problem, and Tresca's yield condition becomes the non-regular hexagon in the σ_1, σ_2 plane shown in Fig. 2. The flow rules will be derived from the three dimensional viewpoint, and then specialized to plane stress.

If the body is originally stress-free, the stress point for any material element will start at the origin, moving away as loading proceeds. The material element is assumed to remain rigid as long as its stress point is within the yield cylinder,

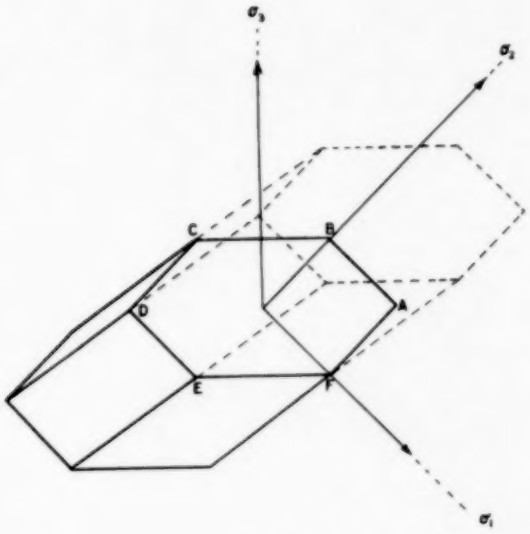

Fig. 1.

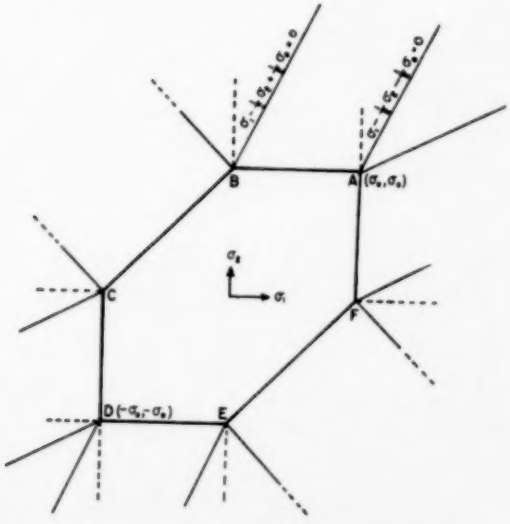

Fig. 2.

and becomes plastic when the stress point touches the yield cylinder. Thereafter several alternative assumptions are available regarding the nature of the hardening which takes place with strain. Here we assume PRAGER type hardening, which

means that as the stress point moves beyond the boundaries of the original yield cylinder, the yield cylinder undergoes translation in the normal direction just sufficient to keep the stress point on its surface.

The theory of the plastic potential states that whenever the stress point is on a face the strain-rate vector is normal to that face, and whenever the stress point is on an edge the strain-rate vector lies in the plane normal to that edge. If a constant hardening coefficient is properly defined it is then possible to identify the rate of translation of the yield cylinder in stress space with the strain-rate vector.

It is further assumed that the stress point moves in regular progression: that is, once it has made contact with a given face of the yield cylinder, it never thereafter relinquishes this contact, although it may slide into an adjacent edge. This restricts the nature of the path which a stress point may follow and, among other things, rules out the possibility that any element may unload after becoming plastic. The incremental flow rules can then be integrated in a simple manner (Hodge 1957, Boyce 1956), so that some of the advantages of a total strain law are enjoyed. The main difference between the simply supported and clamped plates mentioned earlier is that the former has only regularly progressing stress points, while the latter does not.

The flow rules can be determined from a consideration of the yield cylinder in Fig. 1. The face passing through the line AB in the σ_1, σ_2 plane is given originally by the equation

$$\sigma_2 - \sigma_3 - \sigma_0 = 0,$$

where σ_0 is the tensile yield stress; the unit outer normal vector to this face is

$$\mathbf{n} = \frac{1}{\sqrt{2}}(\mathbf{j} - \mathbf{k}), \tag{1}$$

$\mathbf{i}$, $\mathbf{j}$ and $\mathbf{k}$ representing unit vectors in the positive σ_1, σ_2 and σ_3 directions respectively. Since no rotation of the yield cylinder takes place, $\mathbf{n}$ does not vary during the loading process. Prager's hardening law states that the rate of displacement of the yield cylinder, given by the projection of the stress-rate vector $\dot{\boldsymbol{\sigma}}$ on to $\mathbf{n}$, is proportional to the associated plastic strain-rate $\dot{\boldsymbol{\epsilon}}$, the proportionality factor C being a constant. Hence

$$(\dot{\boldsymbol{\sigma}} \cdot \mathbf{n})\,\mathbf{n} = C\,\dot{\boldsymbol{\epsilon}} = C\,|\dot{\boldsymbol{\epsilon}}|\,\mathbf{n},$$

or

$$\frac{1}{\sqrt{2}}(\dot{\sigma}_2 - \dot{\sigma}_3) = C\,(\dot{\epsilon}_2^{\,2} + \dot{\epsilon}_3^{\,2})^{\frac{1}{2}} = \sqrt{2}\,C\,\dot{\epsilon}_2,$$

since $\dot{\epsilon}_3 = -\dot{\epsilon}_2$ on this face of the yield cylinder. Thus the flow rules are

$$\dot{\epsilon}_1 = 0,$$

$$C\,\dot{\epsilon}_2 = -C\,\dot{\epsilon}_3 = \tfrac{1}{2}(\dot{\sigma}_2 - \dot{\sigma}_3). \tag{2.1}$$

When the stress point is on the edge passing through A, the strain-rate vector $\dot{\boldsymbol{\epsilon}}$ lies in the plane normal to this edge, and is proportional to the rate of translation of the yield cylinder, given by the component of $\dot{\boldsymbol{\sigma}}$ in this plane, the proportionality factor again being the constant C. Thus, if $\dot{\boldsymbol{\sigma}}$ is resolved into components normal and parallel to the edge in question,

$$\dot{\boldsymbol{\sigma}} = \boldsymbol{C}\,\dot{\boldsymbol{\epsilon}} + \boldsymbol{a},$$

where

$$\boldsymbol{a} = \alpha\,(\mathbf{i} + \mathbf{j} + \mathbf{k})$$

is parallel to the edge. In terms of components:

$$\dot{\sigma}_1 = C\,\dot{\epsilon}_1 + \alpha,$$

$$\dot{\sigma}_2 = C\,\dot{\epsilon}_2 + \alpha,$$

$$\dot{\sigma}_3 = C\,\dot{\epsilon}_3 + \alpha.$$

Eliminating the parameter α yields

$$\dot{\sigma}_1 - \dot{\sigma}_3 = C\,(\dot{\epsilon}_1 - \dot{\epsilon}_3),$$

$$\dot{\sigma}_2 - \dot{\sigma}_3 = C\,(\dot{\epsilon}_2 - \dot{\epsilon}_3). \tag{2.2}$$

Plane stress and plastic incompressibility imply that

$$\dot{\sigma}_3 = 0, \quad \dot{\epsilon}_3 = -\,(\dot{\epsilon}_1 + \dot{\epsilon}_2).$$

The flow rules then reduce to

$$\dot{\sigma}_1 = 0, \quad \dot{\sigma}_2 = 2\,C\,\dot{\epsilon}_1, \tag{2.3}$$

on side AB, and

$$\dot{\sigma}_1 = C\,(2\,\dot{\epsilon}_1 + \dot{\epsilon}_2), \quad \dot{\sigma}_2 = C\,(\dot{\epsilon}_1 + 2\,\dot{\epsilon}_2) \tag{2.4}$$

on edge A. The flow rules for other plastic regimes may be obtained similarly and, in fact, in all edge regimes the flow rules are identical.

As the three dimensional yield cylinder translates in stress space, and assuming that all stress points progress regularly, the normal planes to the faces intersecting in an edge define the boundaries between the plastic regimes associated with the faces and that corresponding to the edge. The intersections of these planes with the σ_1, σ_2 plane are shown by the dotted lines in Fig. 2. These lines, however, do not furnish the regime boundaries in plane stress. Even though the stress point is confined to the σ_1, σ_2, plane, part of the displacement of the yield cylinder will be out of this plane; consequently the two dimensional yield polygon is given, at different times, by different sections of the three dimensional yield cylinder. As all such sections are geometrically similar, it is possible to visualize successive yield polygons in terms of a translation of the original one; this translation, however, is not normal to the polygon, but in the directions suggested by the solid lines in Fig. 2, which also serve to define the regime boundaries. For example, in regime AB, the displacement of the yield cylinder is given by the vector

$$\mathbf{u} = \alpha\,(\mathbf{j} - \mathbf{k}),$$

taking the original yield polygon a distance α below the σ_1, σ_2 plane. To obtain the new yield polygon in the σ_1, σ_2 plane the vector

$$\mathbf{v} = \alpha\,(\mathbf{i} + \mathbf{j} + \mathbf{k}),$$

parallel to the axis of the yield cylinder, must be added to $\mathbf{u}$; then

$$\mathbf{u} + \mathbf{v} = \alpha\,(\mathbf{i} + 2\,\mathbf{j})$$

represents the apparent displacement of the yield polygon in the σ_1, σ_2 plane. This is in the direction of the solid lines emanating upward from points A and B in Fig. 2. Consequently, the rate of displacement of the yield polygon cannot be identified with the plastic strain-rate, as in the three dimensional stress situation.

3. The Circular Plate

Now consider a thin circular plate of radius R and thickness $2h$ acted upon by a uniform transverse load p per unit area. The principal stresses are the radial and circumferential normal stresses, σ_r and σ_θ respectively. It is more convenient, however, to phrase the discussion in terms of generalized stresses and strains: the radial bending moment per unit length $M = \sigma_r h^2$, the circumferential bending moment per unit length $N = \sigma_\theta h^2$, and the corresponding curvatures κ and λ. In terms of the transverse displacement w of the middle surface of the plate,

$$\kappa = -\frac{\partial^2 w}{\partial r^2}, \qquad \lambda = -\frac{1}{r}\frac{\partial w}{\partial r}, \tag{3.1}$$

r designating a generic point of the plate. The yield condition then has the same form as a function of M and N as of σ_r and σ_θ, the co-ordinate axes in Fig. 2 merely being relabelled. The size of the yield polygon is determined by the yield moment $M_0 = \sigma_0 h^2$.

For a partially clamped plate the appropriate support condition at the edge is

$$M(R) = k\frac{\partial w}{\partial r}(R), \qquad k \geqslant 0. \tag{3.2}$$

When $k = 0$ the plate is simply supported; as $k \to \infty$ it becomes fully clamped.

As the load p slowly increases from zero, the plate remains rigid until p attains a value p_0, called the yield load, at which time the entire plate becomes plastic. Since the plate is rigid for $p < p_0$, it follows that $\partial w/\partial_r \equiv 0$ in this range of loading; consequently the plate behaves as though it were simply supported for loads up to the yield load. Thus, the yield load found by Hopkins and Prager (1953) for the simply supported plate is also valid for one partially clamped, that is, $P_0 P^2/M_0 = 6$. As the same authors found that a fully clamped plate yields when $p_0 R^2/M_0 = 11{\cdot}26$, there is a discontinuity in the yield load during the passage from partial to total clamping.

For a simply supported (or partially clamped) plate, at $p = p_0$, the edge is in regime B; the centre, where $M = N$ from symmetry, is in regime A; the rest of the plate is in regime AB. As loading proceeds, either this situation persists, or else additional zones may appear in the plate: a central zone in regime A and edge zone in regime B, as well as an intermediate zone remaining in regime AB. Under the assumption of regular progression no other plastic zones may appear.

In order to introduce dimensionless variables, let

$$m = \frac{M}{M_0}, \quad n = \frac{N}{M_0}, \quad K = \frac{c\kappa}{M_0}, \quad \Lambda = \frac{c\lambda}{M_0}, \quad W = \frac{cw}{M_0 R^2},$$

$$\rho = \frac{r}{R}, \quad P = \frac{pR^2}{M_0}, \quad P_0 = \frac{p_0 R^2}{M_0}, \quad \gamma = \frac{P}{P_0} = \frac{p}{p_0}, \quad c = \tfrac{2}{3} h^3 C. \tag{3.3}$$

The appropriate flow rules can be written down immediately from (2·3) and (2.4), that is

$$\text{Regimes } A,\ B: \quad \begin{cases} \dot{m} = 2\dot{K} + \dot{\Lambda}, \\ \dot{n} = \dot{K} + 2\dot{\Lambda}; \end{cases} \tag{3.4}$$

$$\text{Regime } AB: \quad \begin{cases} \dot{K} = 0, \\ \dot{n} = 2\dot{\Lambda}. \end{cases} \tag{3.5}$$

These incremental flow rules may be integrated subject to the initial conditions at $P = P_0$, yielding the following total stress–strain laws:

$$\text{Regime } A: \quad \begin{cases} m - 1 = 2K + \Lambda, \\ n - 1 = K + 2\Lambda; \end{cases} \tag{3.6}$$

$$\text{Regime } AB: \quad \begin{cases} K = 0, \\ n - 1 = 2\Lambda; \end{cases} \tag{3.7}$$

$$\text{Regime } B: \quad \begin{cases} m = 2K + \Lambda, \\ n - 1 = K + 2\Lambda. \end{cases} \tag{3.8}$$

The transition between regimes AB and A occurs at the point $\rho = \xi$ where

$$2m - n - 1 = 0. \tag{3.9}$$

Similarly, the transition between regimes AB and B takes place when

$$2m - n + 1 = 0 \tag{3.10}$$

at some point $\rho = \eta$. The points ξ and η depend on the load and must be determined as part of the solution. Finally the equilibrium and compatibility equations are

$$\frac{\partial}{\partial \rho}(\rho m) - n = -3\gamma\rho^2, \tag{3.11}$$

and

$$\frac{\partial}{\partial \rho}(\rho\Lambda) - K = 0, \tag{3.12}$$

both valid in $0 \leqslant \rho \leqslant 1$. To complete the formulation of the problem it is necessary to specify the boundary conditions. Symmetry at the centre of the plate requires that $m = n$ there. Further, the stresses must be continuous at the internal boundaries between adjacent zones. Finally, the support condition (3.2) at $\rho = 1$, in terms of dimensionless variables, becomes

$$m = \frac{kR}{c}\frac{\partial W}{\partial \rho} = -3\beta\Lambda, \tag{3.13}$$

where

$$3\beta = \frac{kR}{c}. \tag{3.14}$$

To express the support condition in terms of m and n only, it is necessary to solve (3.8) for Λ in terms of the stresses,

$$3\Lambda = 2n - m - 2,$$

and (3.13) then takes the form

$$(1 - \beta)\, m + 2\beta\, n = 2\beta. \tag{3.15}$$

This equation represents a straight line in the stress plane originating at B. In order to fulfil the assumption of regular progression this line must lie within the wedge-shaped region corresponding to regime B. This requires $0 \leqslant \beta \leqslant \frac{1}{3}$. Thus appropriate boundary conditions are

$$\begin{aligned} &\rho = 0: \quad m = n, \\ &\rho = \xi, \eta: \quad m, n \text{ continuous}, \\ &\rho = 1: \quad (1 - \beta)\, m + 2\beta\, n = 2\beta, \quad 0 \leqslant \beta \leqslant \tfrac{1}{3} \end{aligned} \tag{3.16}$$

The mathematical problem consists of solving equations (3.11) and (3.12) simultaneously with the appropriate flow rule (3.6), (3.7), or (3.8) in each zone, determining the constants of integration from the boundary and continuity conditions (3.16), and the zone boundaries ξ and η from the transition equations (3.9) and (3.10). Finally, the displacement W can be evaluated from the equation

$$\frac{\partial W}{\partial \rho} = -\rho\, \Lambda, \tag{3.17}$$

which was previously used as the definition of Λ. As Λ is now known, a simple quadrature gives W in each zone. Constants of integration are found from the conditions

$$\begin{aligned} &\rho = 1: \quad W = 0, \\ &\rho = \xi, \eta: \quad W \text{ continuous}. \end{aligned} \tag{3.18}$$

The symmetry condition, $\partial W/\partial \rho = 0$ at $\rho = 0$, is automatically satisfied.

The problem is susceptible to straightforward methods of solution, such as have been discussed before (Prager 1956, Boyce 1956, Perrone and Hodge 1959). Therefore only the results are given here.

Regime A, $0 \leqslant \rho \leqslant \xi$:

$$m = 1 + \tfrac{3}{16}\, \gamma\, (9\, \xi^2 - 7\, \rho^2), \tag{3.19}$$

$$n = 1 - \tfrac{3}{16}\, \gamma\, (9\, \xi^2 - 5\, \rho^2), \tag{3.20}$$

$$\begin{aligned} W = {} & \tfrac{9}{32}\, \gamma\, \xi^2\, (\xi^2 - \rho^2) - \tfrac{3}{64}\, \gamma\, (\xi^4 - \rho^4) + \tfrac{3}{8}\, \gamma\, \xi^3\, (\eta - \xi) - \\ & - \tfrac{1}{8}\, \eta^2 \ln \eta - \tfrac{3}{64}\, \gamma\, (1 - \eta^4) - \tfrac{1}{2}\, k_1 \ln \eta + \tfrac{1}{6}\, (k_2 - \tfrac{7}{8})\, (1 - \eta^2) \end{aligned} \tag{3.21}$$

Regime AB, $\xi \leqslant \rho \leqslant \eta$:

$$m = 1 - \gamma\, \rho^2 + \tfrac{1}{8}\, \frac{\gamma \xi^3}{\rho} \left(11 + 6 \ln \frac{\rho}{\xi}\right), \tag{3.22}$$

$$n = 1 + \tfrac{3}{4}\, \gamma\, \frac{\xi^3}{\rho}, \tag{3.23}$$

$$\begin{aligned} W = {} & \tfrac{3}{8}\, \gamma\, \xi^3\, (\eta - \rho) - \tfrac{1}{8}\, \eta^2 \ln \eta - \tfrac{3}{64}\, \gamma\, (1 - \eta^4) - \\ & - \tfrac{1}{2}\, k_1 \ln \eta + \tfrac{1}{6}\, (k_2 - \tfrac{7}{8})\, (1 - \eta^2). \end{aligned} \tag{3.24}$$

Regime B, $\eta \leqslant \rho \leqslant 1$:

$$m = \tfrac{3}{4} \ln \rho - \tfrac{21}{16} \gamma \rho^2 - \tfrac{1}{2} \frac{k_1}{\rho^2} + k_2, \tag{3.25}$$

$$n = \tfrac{3}{4} + \tfrac{3}{4} \ln \rho - \tfrac{15}{16} \gamma \rho^2 + \tfrac{1}{2} \frac{k_1}{\rho^2} + k_2, \tag{3.26}$$

$$W = \tfrac{1}{8} p^2 \ln \rho - \tfrac{3}{64} \gamma (1 - \rho^4) - \tfrac{1}{2} k_1 \ln \rho + \tfrac{1}{6} (k_2 - \tfrac{7}{8}) (1 - \rho^2). \tag{3.27}$$

The equations determining ξ and η as functions of γ are

$$\gamma \left(\eta^3 - \xi^3 - \tfrac{3}{4} \xi^3 \ln \frac{\eta}{\xi} \right) - \eta = 0, \tag{3.28}$$

and

$$\gamma \left(\tfrac{3}{4} \frac{\xi^3}{\eta} + \tfrac{15}{16} \eta^2 \right) + \tfrac{1}{4} (1 - 3\eta) - \tfrac{1}{2} \frac{k_1}{\eta^2} - k_2 = 0. \tag{3.29}$$

In all of the above expressions k_1 and k_2 are given by

$$k_1 = \frac{\tfrac{3}{4} \beta + \tfrac{1}{4} + \tfrac{3}{16} \gamma (7 + 3\beta) + \tfrac{3}{4} (\beta + 1) \ln \eta - \tfrac{27}{16} (\beta + 1) \gamma \eta^2}{\tfrac{3}{2} \left(\beta - \tfrac{1}{3} + \dfrac{\beta + 1}{\eta^2} \right)} \tag{3.30}$$

$$k_2 = \tfrac{3}{2} \frac{k_1}{\eta^2} + \tfrac{27}{16} \gamma \eta^2 - \tfrac{3}{4} \ln \eta - \tfrac{1}{4}. \tag{3.31}$$

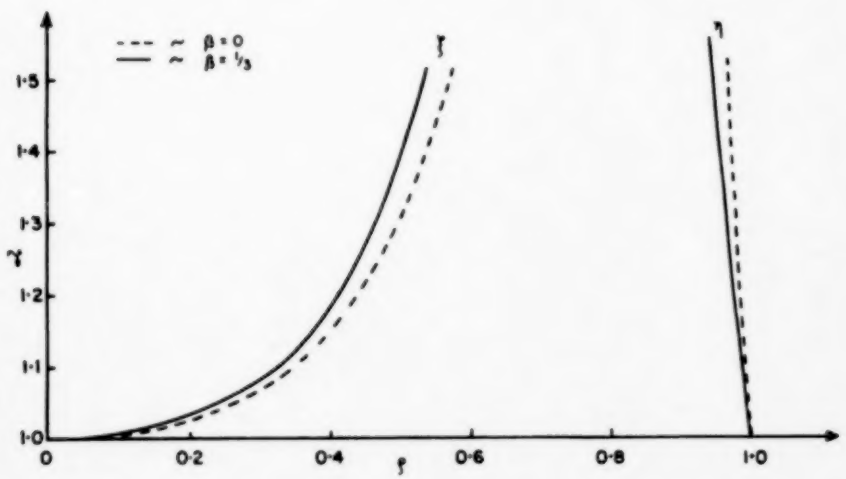

Fig. 3.

These equations have been evaluated numerically for $\beta = \frac{1}{3}$, corresponding to the maximum degree of clamping for which this procedure is valid. The zone boundaries ξ and η are plotted against the load parameter γ by means of the solid lines in Fig. 3. The plots of load versus maximum deflexion and load versus maximum stress appear as the solid lines in Figs. 4 and 5. The dotted curves in

these figures refer to the simply supported plate ($\beta = 0$), and were previously available (Perrone and Hodge 1959). Lack of a solution for the fully clamped plate makes accurate comparisons difficult, but these curves indicate that the post-yield stresses and displacements are relatively insensitive to variations in the support condition, at least in the neighbourhood of simple support.

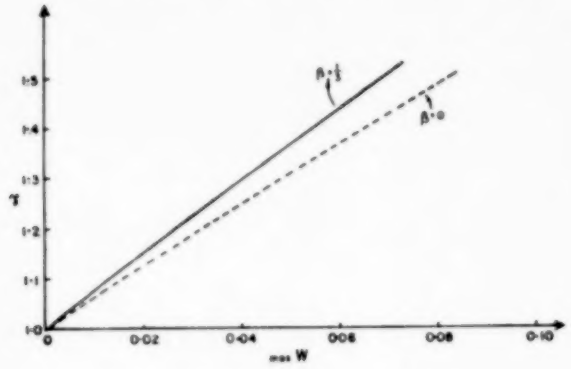

Fig. 4

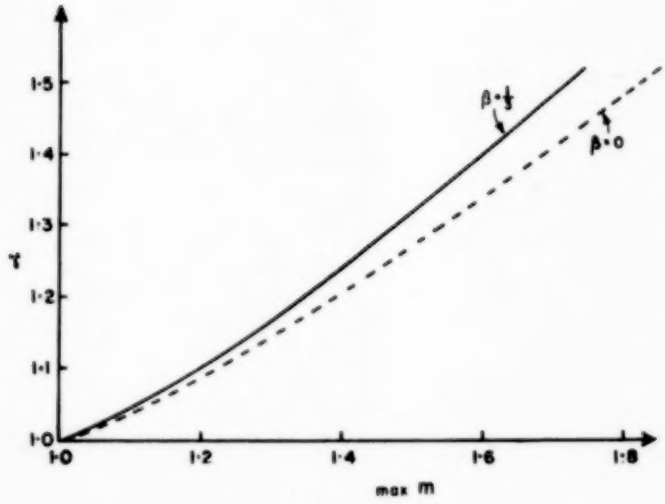

Fig. 5

4. Dependence of Solution on Parameters

The solution given by equations (3.19) to (3.31) depends explicitly on the independent variables r (or ρ) and p (or γ), and also on physical parameters such as the plate radius R, hardening coefficient c, and yield moment M_0. The radius R can be accurately measured, but c and M_0 are likely to be subject to some dispersion even among plates carefully constructed from apparently homogeneous material. It is thus of interest to ascertain the effect on the stresses and displacements when c and M_0 are perturbed about a mean value.

The dependence of M, N, and w upon c is easily seen. In fact, M and N do not depend on c at all. Moreover, if c^* is a new value of the hardening coefficient, and w^* the displacement associated with it, they must be related to the old values by

$$c^* w^* = cw \tag{4.1}$$

for any r and p.

The dependence of M, N, and w upon M_0 is more complicated, since a change in M_0 will change the yield load P_0, and hence alter the value of the load ratio γ for a given P. Let

$$M_0^* = M_0(1 + \alpha), \tag{4.2}$$

so that α represents a perturbation of the yield moment. Then the new yield load P_0^* is given by

$$p_0^* = \frac{p_0^* R^2}{M_0} = \frac{p_0^* R^2}{M_0^*} \frac{M_0^*}{M_0} = 6(1 + \alpha). \tag{4.3}$$

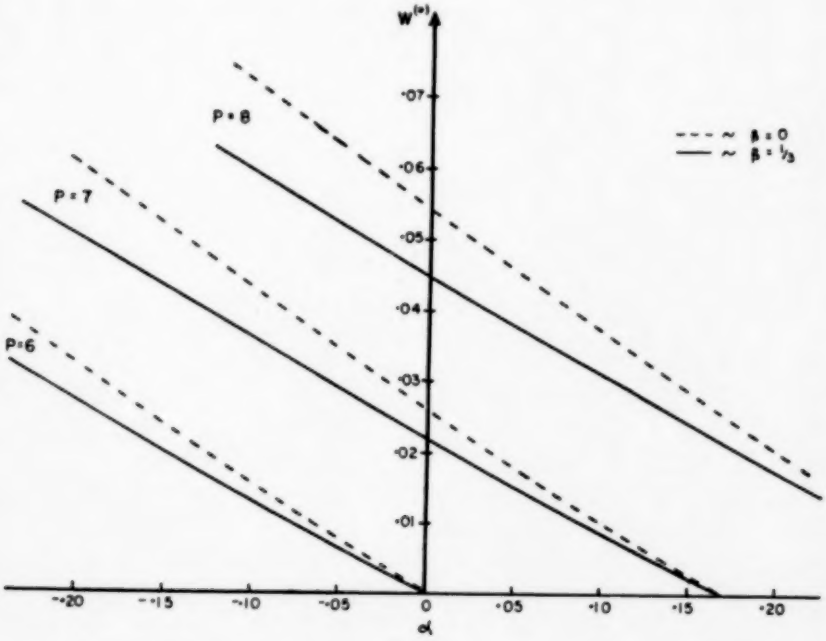

Fig. 6.

Thus $\alpha > 0$ produces a higher yield load associated with the larger yield moment. For a given post-yield load $P = pR^2/M_0$, and the corresponding load ratio γ^*, it follows that

$$\gamma^* = \frac{P}{P_0^*} = \frac{P}{P_0(1 + \alpha)} = \frac{\gamma}{1 + \alpha}. \tag{4.4}$$

Thus new zone boundaries ξ^* and η^* will be generated by (3.28) and (3.29) and the associated moments m^* and n^* and displacement W^* can be calculated from equations (3.19) to (3.27) by replacing γ, ξ, and η with γ^*, ξ^*, and η^* respec-

tively. Finally, normalization to the original yield moment requires that m^*, n^*, and W^* be multiplied by $(1 + \alpha)$;

$$m(\alpha) = (1 + \alpha)\, m^*, \tag{4.5}$$

and similarly for n and W.

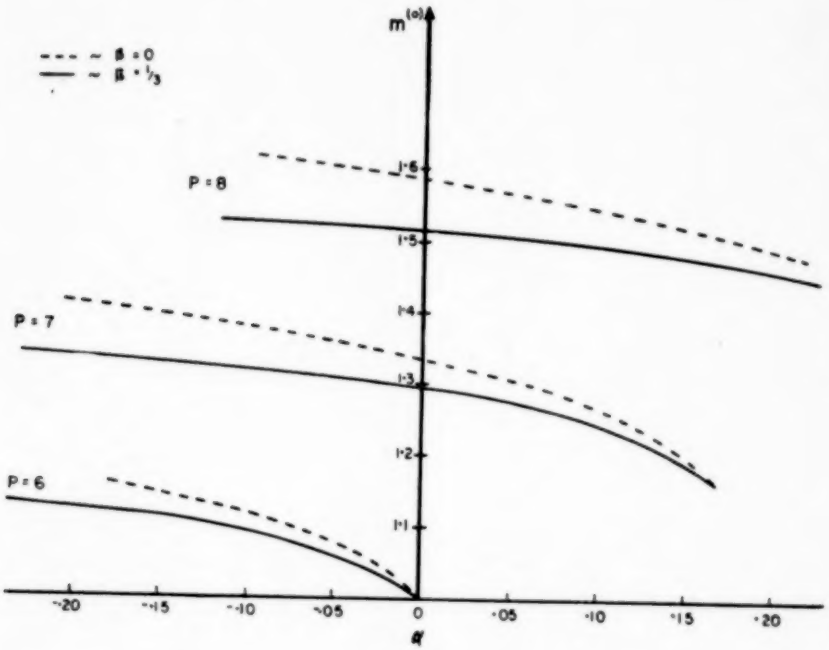

Fig. 7.

Figs. 6 and 7 show the dependence of the maximum displacement $W^{(0)}(\alpha, P)$ and maximum bending moment $m^{(0)}(\alpha, P)$ on the parameter α for several values of the load beyond yield. The superscript (0) indicates that these are actually the values of displacement and bending moment at $r = 0$. Again the solid and broken curves refer to the partially clamped ($\beta = \frac{1}{3}$) and simply supported ($\beta = 0$) plates respectively. In both cases the maximum displacement depends on α in essentially a linear manner over a wide range of α, and the slope of this linear relation is virtually independent of the load. On the other hand, the maximum stress is less strongly dependent on α except in the immediate vicinity of the yield load. This relative indifference of the maximum stress at a post-yield load to the size of the initial yield stress is more marked for the partially clamped plate than for the simply supported one.

More precisely, because of the monotone character of the dependence of $W^{(0)}$ and $m^{(0)}$ on α (Figs. 6 and 7), the probabilities that

$$W^{(0)}(\alpha_2, p) \leqslant W^{(0)}(\alpha, p) \leqslant W^{(0)}(\alpha_1, p)$$

and

$$m^{(0)}(\alpha_2, p) \leqslant m^{(0)}(\alpha, p) \leqslant m^{(0)}(a_1, p)$$

are the same as the probability that

$$\alpha_1 \leqslant \alpha \leqslant \alpha_2.$$

The latter quantity can be determined, or at least estimated, by analysing statistically the data from a large number of tension tests, for example.

Acknowledgment

The results presented in this paper were obtained in the course of research sponsored by the Air Force Office of Scientific Research of the Air Research and Development Command under Contract No. AF 18 (600)-1586.

References

Boyce, W. E. 1956 *Quart. Appl. Math.* **14**, 277.

Hodge, P. G., Jr. 1955 *Proc. Colloquium Deformation and Flow of Solids, IUTAM, Madrid*, 147-169.

1957 *J. Mech. Phys. Solids* **5**, 242.

Hopkins, H. G. and Prager, W. 1953 *J. Mech. Phys. Solids* **2**, 1.

Perrone, N. and Hodge, P. G., Jr. 1959 *J. Appl. Mech.* To be published.

Prager, W. 1955 *James Clayton Lecture, Proc. Instn. Mech. Engrs., Lond.* **169**, 41.

1956 *J. Appl. Mech.* **23**, 493.

Shield, R. T. and Ziegler, H. 1958 *Z. angew. Math. Phys.* **9a**, 260.

J. Mech. Phys. Solids, 1959, Vol. 7, pp. 126 to 134. Pergamon Press Ltd., London. Printed in Great Britain

THE SLIP THEORY OF PLASTICITY FOR CRYSTALLINE AGGREGATES*

By H. Payne
Physics Department, University of Detroit

(*Received 24th November*, 1958)

Summary

The model for predicting the plastic behaviour of a crystalline aggregate under uniaxial stress from empirical data on slip in the single crystal which has been developed by Taylor and modified by Bishop and Hill, and by Lin is presented in a mathematical form which provides for the case in which the stress is not uniaxial.

1. Introduction

A number of schemes (Cottrell 1953) have been proposed for calculating the stress–strain relation for the plastic region of a polycrystalline material, treated as macroscopically homogeneous and isotropic, from empirical data on the plastic deformation of the corresponding single crystal under simple tension. Of these, the one due to Taylor (1938a, b) appears to be the most realistic. Although he considered only simple tension (or compression) on a face-centred cubic polycrystal, for which his results on aluminium are in reasonable agreement with experiment, his model is readily applicable to an aggregate of another lattice type pursuing a linear strain path, i.e., a path along which the ratios of the strain tensor components are constant, in the plastic region. Other such strain paths have been investigated by Bishop and Hill (1951). However, since Taylor treated the specimen as perfectly rigid except for the occurrence of slip, his method applies only where the plastic strain greatly exceeds the elastic strain. It is based upon four assumptions:

Table 1. *Designation of slip systems in a face-centred cubic crystal*

Crystalline plane	(111)			(1$\bar{1}$1)			($\bar{1}$11)			($\bar{1}\bar{1}$1)		
Direction	01$\bar{1}$	101	1$\bar{1}$0	01$\bar{1}$	101	110	01$\bar{1}$	101	110	01$\bar{1}$	101	110
Slip system	a_1	a_2	a_3	b_1	b_2	b_3	c_1	c_2	c_3	d_1	d_2	d_3

(1) The plastic strain in a face-centred cubic crystal is due entirely to slip, which may occur in the four crystalline planes and in the three directions per plane as shown in Table 1. Following Taylor, the resulting twelve slip systems

*Research sponsored by the Solid State Physics Branch of the Office of Scientific Research, Air Research and Development Command, U.S. Air Force, under Contract No. AF 18 (600) 1466.

are designated according to plane by a, b, c, or d and to direction by the subscripts 1, 2, or 3.

(2) The strain hardening is uniform with respect to the twelve systems of a given crystal, i.e., the critical shear stress τ_c is the same for the twelve systems irrespective of the distribution of slip.

(3) For a given crystal undergoing increasing strain along a linear path

$$\tau_c = f(\sum_{\alpha} |\gamma^{\alpha}|), \tag{1}$$

where γ^{α} represents the shear attributed to slip in the α^{th} of the twelve systems. Accordingly, f in the example of aluminium was determined from measurements on the single crystal of the applied stress and resulting slip.

(4) Each crystal of the aggregate undergoes the macroscopic strain.

With the exception of the fourth, these assumptions are supported, at least as approximations, by the results of tests on single crystals exhibiting both single and duplex slip. The fourth assumption ensures the maintenance of the grain boundaries, but results in a violation of Newton's third law. It was employed for computational convenience and was considered by Taylor as providing an upper limit to the calculated macroscopic stress for a given macroscopic strain.

Thus, for a crystalline aggregate subjected to a given macroscopic plastic strain the strain occurring in each crystal follows immediately from the fourth assumption. For a crystal of selected orientation one determines that distribution of slip over its twelve systems which accounts for this plastic strain and from which is computed under the second and third assumptions a deviatoric stress tensor for the crystal which satisfies the yield conditions. Bishop and Hill (1951) have shown that, while this distribution is not uniquely determined, the corresponding stress is so determined by the given strain. They have developed a simple procedure for obtaining the distribution of slip as well as the stress, which is averaged over the crystals of all orientations to produce the macroscopic stress for the aggregate corresponding to the given macroscopic strain.

Lin (1957) has extended this method so that it may predict the entire stress–strain relation for an aggregate pursuing a linear strain path by removing the restriction that the specimen be considered as rigid except for slip. Then a given strain in a crystal must first be resolved into its elastic and plastic components in accordance with the yield conditions.

It is the purpose of this paper to present, in mathematical language, the extension of this model to render it capable of predicting the complete stress-strain relation for a polycrystalline material following a nonlinear strain path.

It is assumed that the strain path in a given crystal of the aggregate is known and it is desired to determine the corresponding stress path, the elastic and plastic contributions to the strain, and the distribution of slip over the twelve systems. Accordingly, the fourth assumption above is not essential to this discussion. It need only be assumed that the crystal is strained uniformly. Even this restriction could be withdrawn if instead of the whole crystal a portion thereof, over which the strain could be regarded as essentially the same, were considered.

The first three assumptions apply, with some question arising as to how equation (1) should be modified to account for the possibility that over the nonlinear strain path a reversal in the sense of the slip γ^{α} might occur, giving perhaps

$\tau_c = f(\sum_\alpha \int |d\gamma^\alpha|)$. If no such reversal occurs for a particular problem, relation (1) suffices. This will be assumed to be the case.

The use of this model in the example of a torsional stress superposed upon a tensile stress is discussed qualitatively.

2. Vector Notation

The tensors employed in the following discussion are presented in a six-vector form. For example, the deviatoric strain tensor for a given crystal is represented by

$$\boldsymbol{\epsilon} = (\epsilon_{11},\ \epsilon_{22},\ \epsilon_{33},\ \sqrt{2}\,\epsilon_{12},\ \sqrt{2}\,\epsilon_{23},\ \sqrt{2}\,\epsilon_{31}),$$

where ϵ_{ij} is the ij^{th} component of the tensor. Similarly the deviatoric stress tensor is represented by

$$\boldsymbol{\sigma} = (\sigma_{11},\ \sigma_{22},\ \sigma_{33},\ \sqrt{2}\,\sigma_{12},\ \sqrt{2}\,\sigma_{23},\ \sqrt{2}\,\sigma_{31}).$$

An advantage of this particular form of vector notation is that the scalar product of two such pseudovectors is invariant with respect to a transformation of the Cartesian co-ordinate axes with respect to which the tensors are described. For example, the differential work dW required to effect the differential strain $d\boldsymbol{\epsilon}$ is given by $dW = \boldsymbol{\sigma} \cdot d\boldsymbol{\epsilon}$.

3. Development of Theory

Let $\boldsymbol{\epsilon}$ represent the deviatoric elastic strain tensor, and $\bar{\boldsymbol{\epsilon}}$ be the plastic strain. Then

$$\boldsymbol{\epsilon} = \boldsymbol{\epsilon} + \bar{\boldsymbol{\epsilon}}. \tag{2}$$

Also,

$$\boldsymbol{\sigma} = 2\mu\,\boldsymbol{\epsilon}, \tag{3}$$

where μ is the shear modulus of elasticity.

To express the conditions upon $\boldsymbol{\epsilon}$ and $\bar{\boldsymbol{\epsilon}}$ let a set of pseudovectors

$$\mathbf{B}^\alpha = (B^\alpha_{11},\ B^\alpha_{22},\ B^\alpha_{33},\ \sqrt{2}\,B^\alpha_{12},\ \sqrt{2}\,B^\alpha_{23},\ \sqrt{2}\,B^\alpha_{31}),$$

be defined by

$$B^\alpha_{ij} = (1/\sqrt{2})\ (n^\alpha_i\, l^\alpha_j + n^\alpha_j\, l^\alpha_i),$$

where n^α_i is the i^{th} component of the three dimensional unit vector $\mathbf{n}^\alpha$ normal to the plane of the α^{th} slip system and l^α_i is the i^{th} component of the unit vector $\mathbf{l}^\alpha$ in the direction of slip in the α^{th} system. Table 2 gives the B^α_{ij} for a particular sense in each of the twelve systems of a face-centred cubic crystal expressed in terms of the co-ordinate axes and system notation of Table 1.

Since there is a choice of the sense of $\mathbf{B}^\alpha$, it is assumed that this choice has been made with reference to the problem at hand such that $(1/\sqrt{2})\,\boldsymbol{\epsilon} \cdot \mathbf{B}^\alpha$, which represents the resolved elastic shear strain in the α^{th} system, is non-negative for each value of α.

Then the yield conditions require

$$\boldsymbol{\epsilon} \cdot \mathbf{B}^\alpha \leqslant \tau_c/\sqrt{2}\,\mu.$$

An active system may be defined as one for which the equality holds. If there are m active systems in the crystal, let these be designated by a $\alpha = 1, 2, 3, \ldots, m$, giving

$$\bar{\boldsymbol{\epsilon}} \cdot \mathbf{B}^{\alpha} \begin{cases} = \tau_c/\sqrt{2}\,\mu & \text{for} \quad \alpha \leqslant m. \\ < \tau_c/\sqrt{2}\,\mu & \text{for} \quad \alpha > m. \end{cases} \tag{4}$$

TABLE 2. *The $B^{\alpha}{}_{ij}$ for the slip systems in a face-centred cubic crystal*

	$\sqrt{3}\,B^{\alpha}{}_{ij}$					
$\alpha/(ij)$	(11)	(22)	(33)	(12)	(23)	(31)
a_1	0	−1	1	$-\frac{1}{2}$	0	$\frac{1}{2}$
a_2	1	0	−1	$\frac{1}{2}$	$-\frac{1}{2}$	0
a_3	−1	1	0	0	$\frac{1}{2}$	$-\frac{1}{2}$
b_1	0	−1	1	$-\frac{1}{2}$	0	$-\frac{1}{2}$
b_2	1	0	−1	$\frac{1}{2}$	$\frac{1}{2}$	0
b_3	−1	1	0	0	$-\frac{1}{2}$	$\frac{1}{2}$
c_1	0	−1	1	$\frac{1}{2}$	0	$-\frac{1}{2}$
c_2	1	0	−1	$-\frac{1}{2}$	$-\frac{1}{2}$	0
c_3	−1	1	0	0	$\frac{1}{2}$	$\frac{1}{2}$
d_1	0	−1	1	$\frac{1}{2}$	0	$\frac{1}{2}$
d_2	1	0	−1	$-\frac{1}{2}$	$\frac{1}{2}$	0
d_3	−1	1	0	0	$-\frac{1}{2}$	$-\frac{1}{2}$

For a differential strain

$$d\boldsymbol{\epsilon} = d\bar{\boldsymbol{\epsilon}} + d\bar{\bar{\boldsymbol{\epsilon}}}, \tag{5}$$

one obtains

$$d\bar{\boldsymbol{\epsilon}} = \sum_{\alpha=1}^{m} dg_{\alpha}\,\mathbf{B}^{\alpha} \tag{6}$$

$$d\boldsymbol{\theta} = (1/\sqrt{2}) \sum_{\alpha=1}^{m} dg_{\alpha}\,\mathbf{n}^{\alpha} \times \mathbf{l}^{\alpha},$$

where $g_{\alpha} = \gamma^{\alpha}/\sqrt{2}$ and $d\boldsymbol{\theta}$ represents the angular displacement of the crystal that results from the differential slip. Relations (3) and (4) and the requirement that the slip occur in the same sense as the resolved shear stress ensure that

$$dg_{\alpha} \geqslant 0. \tag{7}$$

Also, as a consequence of relations (1), (4) and (7)

$$\mathbf{B}^{\alpha} \cdot d\boldsymbol{\epsilon} \leqslant (1/\sqrt{2}\,\mu)\,d\tau_c = (f'/\mu) \sum_{\beta=1}^{m} dg_{\beta} \quad \text{for} \quad \alpha \leqslant m, \tag{8}$$

where f' denotes the derivative of f. The empirical f indicates

$$f' > 0, \tag{9}$$

which in conjunction with relation (7) requires the quantity on the right in relation (8) to be non-negative. Where the inequality holds in relation (8) the corresponding previously active system becomes inactive, requiring $dg_{\alpha} = 0$ for that value of α. Furthermore, since $dg_{\alpha} = 0$ for $\alpha > m$, it follows that

$$dg_\alpha \left[\mathbf{B}^\alpha \cdot d\bar{\boldsymbol{\epsilon}} - (1/\sqrt{2}\,\mu)\, d\tau_c \right] = 0. \tag{10}$$

To prove that, for a given $d\boldsymbol{\epsilon}$ at the terminus of a given strain path, the values of $d\boldsymbol{\epsilon}$ and $d\bar{\boldsymbol{\epsilon}}$ satisfying relations (5), (6), (7), (8) and (10) are unique let it be supposed that $\boldsymbol{\epsilon}$ and $\bar{\boldsymbol{\epsilon}}$ are uniquely determined by these relations through integration along the strain path but that there exist $d\boldsymbol{\epsilon}^*$ and $d\bar{\boldsymbol{\epsilon}}^*$ for which

$$d\boldsymbol{\epsilon} = d\boldsymbol{\epsilon}^* + d\bar{\boldsymbol{\epsilon}}^*, \tag{5'}$$

$$d\bar{\boldsymbol{\epsilon}}^* = \sum_{\alpha=1}^{m} dg^*_\alpha \, \mathbf{B}^\alpha, \tag{6'}$$

$$dg^*_\alpha \geqslant 0, \tag{7'}$$

$$\mathbf{B}^\alpha \cdot d\boldsymbol{\epsilon}^* \leqslant (1/\sqrt{2}\,\mu)\, d\tau^*_c = (f'/\mu) \sum_{\beta=1}^{m} dg^*_\beta \quad \text{for} \quad \alpha \leqslant m, \tag{8'}$$

$$dg^*_\alpha \left[\mathbf{B}^\alpha \cdot d\boldsymbol{\epsilon}^* - (1/\sqrt{2}\,\mu)\, d\tau^*_c \right] = 0. \tag{10'}$$

Then, from equations (5) and (5′) one has

$$\begin{aligned} 0 &= \left[(d\boldsymbol{\epsilon} - d\boldsymbol{\epsilon}^*) + (d\bar{\boldsymbol{\epsilon}} - d\bar{\boldsymbol{\epsilon}}^*) \right]^2 \\ &= (d\boldsymbol{\epsilon} - d\boldsymbol{\epsilon}^*)^2 + (d\bar{\boldsymbol{\epsilon}} - d\bar{\boldsymbol{\epsilon}}^*)^2 + 2\,(d\boldsymbol{\epsilon} - d\boldsymbol{\epsilon}^*) \cdot (d\bar{\boldsymbol{\epsilon}} - d\bar{\boldsymbol{\epsilon}}^*). \end{aligned}$$

Applying relations (6), (6′), (7), (7′), (8), (8′), (10), and (10′) gives

$$0 \geqslant (d\boldsymbol{\epsilon} - d\boldsymbol{\epsilon}^*)^2 + (d\bar{\boldsymbol{\epsilon}} - d\bar{\boldsymbol{\epsilon}}^*)^2 + 2\,(f'/\mu) \left[\sum_{\alpha=1}^{m} (dg_\alpha - dg^*_\alpha) \right]^2.$$

The quantity on the right, as a consequence of relation (9), must be non-negative, requiring $d\boldsymbol{\epsilon}^* = d\boldsymbol{\epsilon}$ and $d\bar{\boldsymbol{\epsilon}}^* = d\bar{\boldsymbol{\epsilon}}$. Since $\boldsymbol{\epsilon}$ and $\bar{\boldsymbol{\epsilon}}$ are uniquely determined by the strain path while it is within the purely elastic region ($\boldsymbol{\epsilon} = \boldsymbol{\epsilon}$, $\bar{\boldsymbol{\epsilon}} = 0$), by induction it follows that $\boldsymbol{\epsilon}$ and $\bar{\boldsymbol{\epsilon}}$ are uniquely determined by the integration of $d\boldsymbol{\epsilon}$ and $d\bar{\boldsymbol{\epsilon}}$ obtained through relations (5), (6), (7), (8) and (10) along the given strain path. The stress path is then obtained from equation (3).

However, the distribution of slip need not be uniquely determined since, in general, the dg_α are not so determined by relations (6) and (7). The rank of the set of twelve $\mathbf{B}^\alpha$ is five. However, not all subsets of five are linearly independent. For example, the subset of three comprising those pertaining to the three systems of a given crystal plane is linearly dependent as is the subset of four corresponding to systems designated by symbols with the same subscript in the notation of Table 2. Thus, if r represents the rank of the set of m $\mathbf{B}^\alpha$ corresponding to m active systems, $r \leqslant m$. If $r < m$, it follows that $d\bar{\boldsymbol{\epsilon}}$ may be accounted for by more than one arrangement of differential slip among the active systems.

If, on the other hand, a stress path were first assumed, it would not in general be possible to determine uniquely the corresponding strain path on the basis of the above relations. If $d\boldsymbol{\sigma}$ at the terminus of a given stress path were specified, $d\boldsymbol{\epsilon}$ would be immediately obtained from the differential form of equation (3). Then the systems remaining active would be determined from relation (8) as the ones represented by those values of α from the set $\alpha \leqslant m$ for which $\mathbf{B}^\alpha \cdot d\boldsymbol{\epsilon}$ would assume its largest value, which would have to be non-negative. Applying the equality in relation (8) for these values of α, which may be designated as $\alpha = 1, 2, \ldots, m'$, would yield $d\tau_c$ and $\sum_{\alpha=1}^{m'} dg_\alpha$, which represents the only restriction other than relation

(7) upon the magnitudes of the slip in the m' systems. Thus, if $m' > 1$, $d\bar{\epsilon}$ would be indeterminate.

From relation (4) it may be seen that the yield surface of the crystal, as has been described by BISHOP (1953), is constructed in strain space of the planes

$$|\epsilon \cdot \mathbf{B}^\alpha| = \tau_c/\sqrt{2}\,\mu.$$

That is, each slip system α is represented by a pair of planes perpendicular to $\mathbf{B}^\alpha$ corresponding to opposite senses of slip. If the point ϵ lies on the yield surface in a single plane, that plane represents the single active system ($m = 1$). If the point

TABLE 3. *Solutions of relation* (11) *for a face-centred cubic crystal*

$\mathbf{A}_i$	*Slip systems for which* $\mathbf{B}^\alpha \cdot \mathbf{A}_i = 1$
$\sqrt{6}$ (0, 0, 0, 1, 0, 0)	$\underline{a}_1$, a_2, $\underline{b}_1$, b_2, c_1, $\underline{c}_2$, d_1, $\underline{d}_2$
$\sqrt{6}$ (0, 0, 0, 0, 1, 0)	$\underline{a}_2$, a_3, b_2, $\underline{b}_3$, $\underline{c}_2$, c_3, d_2, $\underline{d}_3$
$\sqrt{6}$ (0, 0, 0, 0, 0, 1)	a_1, $\underline{a}_3$, $\underline{b}_1$, b_3, $\underline{c}_1$, c_3, d_1, $\underline{d}_3$
$\sqrt{6}/2$ (0, 0, 0, 1, 1, 1)	$\underline{b}_1$, b_2, $\underline{c}_2$, c_3, d_1, $\underline{d}_3$
$\sqrt{6}/2$ (0, 0, 0, -1, 1, 1)	a_1, $\underline{a}_2$, $\underline{c}_1$, c_3, d_2, $\underline{d}_3$
$\sqrt{6}/2$ (0, 0, 0, 1, -1, 1)	a_2, $\underline{a}_3$, $\underline{b}_1$, b_3, d_1, $\underline{d}_2$
$\sqrt{6}/2$ (0, 0, 0, 1, 1, -1)	$\underline{a}_1$, a_3, b_2, $\underline{b}_3$, c_1, $\underline{c}_2$
$1/\sqrt{3}$ (1, 1, -2, 0, 0, 0)	$\underline{a}_1$, a_2, $\underline{b}_1$, b_2, $\underline{c}_1$, c_2, $\underline{d}_1$, d_2
$1/\sqrt{3}$ (1, -2, 1, 0, 0, 0)	a_1, $\underline{a}_3$, b_1, $\underline{b}_3$, c_1, $\underline{c}_3$, d_1, $\underline{d}_3$
$1/\sqrt{3}$ (-2, 1, 1, 0, 0, 0)	$\underline{a}_2$, a_3, $\underline{b}_2$, b_3, $\underline{c}_2$, c_3, $\underline{d}_2$, d_3
$\sqrt{3}/2$ (1, -1, 0, $\sqrt{2}$, 0, 0)	a_2, $\underline{a}_3$, b_2, $\underline{b}_3$, c_1, $\underline{c}_3$, d_1, $\underline{d}_3$
$\sqrt{3}/2$ (1, -1, 0, $-\sqrt{2}$, 0, 0)	a_1, $\underline{a}_3$, b_1, $\underline{b}_3$, c_2, $\underline{c}_3$, d_2, $\underline{d}_3$
$\sqrt{3}/2$ (-1, 0, 1, 0, 0, $\sqrt{2}$)	a_1, $\underline{a}_2$, $\underline{b}_2$, b_3, $\underline{c}_2$, c_3, d_1, $\underline{d}_2$
$\sqrt{3}/2$ (-1, 0, 1, 0, 0, $-\sqrt{2}$)	$\underline{a}_2$, a_3, b_1, $\underline{b}_2$, c_1, $\underline{c}_2$, $\underline{d}_2$, d_3
$\sqrt{3}/2$ (0, 1, -1, 0, $\sqrt{2}$, 0)	$\underline{a}_1$, a_3, $\underline{b}_1$, b_2, $\underline{c}_1$, c_3, $\underline{d}_1$, d_2
$\sqrt{3}/2$ (0, 1, -1, 0, $-\sqrt{2}$, 0)	$\underline{a}_1$, a_2, $\underline{b}_1$, b_3, $\underline{c}_1$, c_2, $\underline{d}_1$, d_3
$1/2\sqrt{3}$ (1, 1, -2, 0, $3\sqrt{2}$, $3\sqrt{2}$)	$\underline{b}_1$, b_2, $\underline{c}_1$, c_3, d_2, $\underline{d}_3$
$1/2\sqrt{3}$ (1, 1, -2, 0, $-3\sqrt{2}$, $3\sqrt{2}$)	a_2, $\underline{a}_3$, $\underline{b}_1$, b_3, $\underline{c}_1$, c_2
$1/2\sqrt{3}$ (1, 1, -2, 0, $3\sqrt{2}$, $-3\sqrt{2}$)	$\underline{a}_1$, a_3, b_2, $\underline{b}_3$, $\underline{d}_1$, d_2
$1/2\sqrt{3}$ (1, 1, -2, 0, $-3\sqrt{2}$, $-3\sqrt{2}$)	$\underline{a}_1$, a_2, c_2, $\underline{c}_3$, $\underline{d}_1$, d_3
$1/2\sqrt{3}$ (1, -2, 1, $3\sqrt{2}$, $3\sqrt{2}$, 0)	b_2, $\underline{b}_3$, c_1, $\underline{c}_2$, d_1, $\underline{d}_3$
$1/2\sqrt{3}$ (1, -2, 1, $-3\sqrt{2}$, $3\sqrt{2}$, 0)	a_1, $\underline{a}_2$, b_1, $\underline{b}_3$, d_2, $\underline{d}_3$
$1/2\sqrt{3}$ (1, -2, 1, $3\sqrt{2}$, $-3\sqrt{2}$, 0)	a_2, $\underline{a}_3$, c_1, $\underline{c}_3$, d_1, $\underline{d}_2$
$1/2\sqrt{3}$ (1, -2, 1, $-3\sqrt{2}$, $-3\sqrt{2}$, 0)	a_1, $\underline{a}_3$, b_1, $\underline{b}_2$, c_2, $\underline{c}_3$
$1/2\sqrt{3}$ (-2, 1, 1, $3\sqrt{2}$, 0, $3\sqrt{2}$)	$\underline{b}_1$, b_3, $\underline{c}_2$, c_3, d_1, $\underline{d}_2$
$1/2\sqrt{3}$ (-2, 1, 1, $-3\sqrt{2}$, 0, $3\sqrt{2}$)	a_1, $\underline{a}_2$, $\underline{b}_2$, b_3, $\underline{c}_1$, c_3
$1/2\sqrt{3}$ (-2, 1, 1, $3\sqrt{2}$, 0, $-3\sqrt{2}$)	$\underline{a}_1$, a_3, c_1, $\underline{c}_2$, $\underline{d}_2$, d_3
$1/2\sqrt{3}$ (-2, 1, 1, $-3\sqrt{2}$, 0, $-3\sqrt{2}$)	$\underline{a}_2$, a_3, b_1, $\underline{b}_2$, $\underline{d}_1$, d_3

on the yield surface occupies an edge, an intersection of two planes, there are two active systems ($m = 2$). Proceeding in this manner, the point will eventually arrive at a vertex of the yield surface, which is represented by $(\tau_c/\sqrt{2}\,\mu)\,\mathbf{A}_i$, where

$$\mathbf{A}_i \cdot \mathbf{B}^\alpha \begin{cases} = 1 & \text{for} \quad \alpha \leqslant m \quad \text{with} \quad m \geqslant 5 = r \\ < 1 & \text{for} \quad \alpha > m, \end{cases} \tag{11}$$

i.e., at the vertex at least five planes intersect, five being the rank of the set of $\mathbf{B}^\alpha$ or the number of independent components of the plastic strain tensor. In accordance with equation (3), at the vertex $\boldsymbol{\sigma} = \sqrt{2}\,\tau_c\,\mathbf{A}_i$. Table 3 presents in the co-ordinate axes and system notation of Table 1 the solutions to relation (11) in a particular sense together with the slip systems for which the equality holds. The underlining of the symbol representing a particular system denotes that the slip occurs in the opposite sense to that in which the system is defined in Table 1. The set of $\mathbf{A}_i$ of Table 3 with their negatives represents the vertices of the yield surface. This Table is equivalent to the one presented by BISHOP (1953).

If the point $\bar{\boldsymbol{\epsilon}}$ on the yield surface occupies the vertex represented by $\mathbf{A}_i$, a necessary and sufficient condition that it remain there for a differential strain $d\boldsymbol{\epsilon}$ is

$$d\bar{\boldsymbol{\epsilon}} = (d\tau_c/\sqrt{2}\,\mu)\,\mathbf{A}_i, \tag{12}$$

as may be seen from relations (8), (10) and (11) and the fact that $d\boldsymbol{\epsilon}$ (like $d\bar{\boldsymbol{\epsilon}}$) is a function of five independent variables. Then, from relations (6), (8), (11) and (12) one obtains

$$\mathbf{A}_i \cdot d\boldsymbol{\epsilon} = A^2_i\,(f'/\mu) \sum_{\alpha=1}^{m} dg_\alpha, \quad \mathbf{A}_i \cdot d\bar{\boldsymbol{\epsilon}} = \sum_{\alpha=1}^{m} dg_\alpha. \tag{13}$$

From Table 3 it is seen that A^2_i varies from 2 to 6. Since $f' < < \mu$ it is evident from these equations along with equation (12) that $d\boldsymbol{\epsilon} > > d\bar{\boldsymbol{\epsilon}}$ and to a good approximation $d\bar{\boldsymbol{\epsilon}} = d\boldsymbol{\epsilon}$.

Under these circumstances the model reduces to that of TAYLOR, who assumed that $\mu \to \infty$. Now it follows from relations (6), (7) and (11) that a necessary condition that the slip systems represented by $\alpha = 1, 2, \ldots, m$, where $m \geqslant 5 = r$, constitute the active systems is that the corresponding $\mathbf{A}_i$ determined from relation (11) satisfy

$$\mathbf{A}_i \cdot d\bar{\boldsymbol{\epsilon}} \geqslant \mathbf{A}_j \cdot d\bar{\boldsymbol{\epsilon}}, \tag{14}$$

where $\mathbf{A}_j$ is any member of the set. Furthermore, one may show that this is a sufficient condition. For $\mu \to \infty$, giving $d\boldsymbol{\epsilon} = d\bar{\boldsymbol{\epsilon}}$, relation (14) becomes

$$\mathbf{A}_i \cdot d\boldsymbol{\epsilon} \geqslant \mathbf{A}_j \cdot d\boldsymbol{\epsilon}, \tag{15}$$

from which one may deduce with the aid of Table 3 the combination of active systems for the given $d\boldsymbol{\epsilon}$. Finally, from the $\mathbf{A}_i$ so determined and the given $d\boldsymbol{\epsilon}$ one may obtain the corresponding differential stress through the equation

$$d\boldsymbol{\sigma} = 2f'\,(\mathbf{A}_i \cdot d\bar{\boldsymbol{\epsilon}})\,\mathbf{A}_i, \tag{16}$$

which follows from relations (8), (12) and (13), the differential form of equation (3), and $d\boldsymbol{\epsilon} = d\bar{\boldsymbol{\epsilon}}$. This is equivalent to the method developed by BISHOP and HILL.

If the restriction $\mu \to \infty$, which is equivalent to setting $d\tau_c = 0$, is discarded, this procedure yields a first approximation when $\bar{\boldsymbol{\epsilon}} = (\tau_c/\sqrt{2}\,\mu)\,\mathbf{A}_i$ and condition (15) is satisfied. The second approximation of $d\bar{\boldsymbol{\epsilon}}$, which vanishes in the first, results from the differential form of equation (3). Then the second approximation of $d\bar{\boldsymbol{\epsilon}}$ follows from equation (5); the second approximation of $d\boldsymbol{\sigma}$, from equation

(16). Succeeding approximations should converge rapidly to the solution. A slight modification of this process would be necessary should some higher approximation of $d\bar{\boldsymbol{\epsilon}}$ violate condition (14).

Before reaching the vertex, $\bar{\boldsymbol{\epsilon}} = (\tau_c/\sqrt{2}\,\mu)\,\mathbf{A}_i$, application of the above relations to a linear strain path becomes equivalent to LIN's model. According to it, for increasing strain the point $\bar{\boldsymbol{\epsilon}}$ moves linearly away from the point $\bar{\boldsymbol{\epsilon}} = 0$ until the yield surface is attained, i.e., until the equality in relation (4) is satisfied for at least one value of α, say for $\alpha = 1$. Then, the point $\bar{\boldsymbol{\epsilon}}$ moves over the plane defined by relation (4) for $m = 1$ — as demanded by equation (10) for $\alpha = 1$ in the first approximation, i.e., for $d\tau_c = 0$ — until it comes to an edge, which is defined by relation (4) for $m = 2$ if $\alpha = 2$ designates the second active system. Continuing in this fashion, the point $\bar{\boldsymbol{\epsilon}}$ attains the vertex.

For a nonlinear strain path, consider the example of a thin-walled cylinder of polycrystalline material which has undergone a simple tensile strain along its axis until the fully plastic region has been reached in each crystal, i.e., $\bar{\boldsymbol{\epsilon}} = (\tau_c/\sqrt{2}\,\mu)\,\mathbf{A}_i$, and then undergoes a differential torsional strain. Employing TAYLOR's fourth assumption as an approximation assigns the given tensile strain and differential shear strain of the aggregate as $\boldsymbol{\epsilon}$ and $d\boldsymbol{\epsilon}$, respectively, for a particular crystal.

Accordingly, it is readily shown that for the given crystal

$$\boldsymbol{\epsilon} \cdot d\boldsymbol{\epsilon} = 0. \tag{17}$$

Now, since $\boldsymbol{\epsilon}$ is the terminus of a linear path, on the basis of the above discussion it must be possible to write

$$\boldsymbol{\epsilon} = \sum_{\alpha=1}^{m} h_\alpha \mathbf{B}^\alpha, \tag{18}$$

where $h_\alpha \geqslant 0$. In general, as indicated by the results of TAYLOR, at least five non-vanishing h_α corresponding to independent systems are necessary. Then, the set $\mathbf{B}^\alpha \cdot d\boldsymbol{\epsilon}$ for $\alpha = 1, 2, \ldots, m$ must contain both positive and negative values as a consequence of equations (17) and (18) and the fact that all of the $\mathbf{B}^\alpha \cdot d\boldsymbol{\epsilon}$ could not vanish without the vanishing of $d\boldsymbol{\epsilon}$. This means that in the first approximation, for which $d\tau_c = 0$,

$$d\bar{\boldsymbol{\epsilon}} \neq 0, \tag{19}$$

in accordance with conditions (5) and (8).

Also, in the first approximation,

$$\mathbf{A}_i \cdot d\boldsymbol{\epsilon} \leqslant 0, \tag{20}$$

from relation (8) and the fact that one may write $\mathbf{A}_i = \sum_{\alpha=1}^{m} q_\alpha \mathbf{B}^\alpha$, where $q_\alpha \geqslant 0$ (since $d\bar{\boldsymbol{\epsilon}}' = \mathbf{A}_i\,dp$, where $dp > 0$, satisfies condition (14)). Furthermore, if the crystal axes are related to the cylindrical axis through the Eulerian angles θ, ϕ and ψ, one may show that for $\psi \to \psi + \pi$, $d\boldsymbol{\epsilon} \to -\,d\boldsymbol{\epsilon}$. Consequently, it is not possible for $\mathbf{A}_i \cdot d\boldsymbol{\epsilon}$ to be positive for all values of ψ. Considering expressions (6), (7), (13) and (19), one deduces that the inequality must hold in relation (20) for some values of ψ.

From relations (3), (20) and $\bar{\boldsymbol{\epsilon}} = (\tau_c/\sqrt{2}\,\mu)\,\mathbf{A}_i$ one obtains

$$\boldsymbol{\sigma} \cdot d\boldsymbol{\sigma} \leqslant 0.$$

Thus, the result of averaging $d\sigma$ over all values of θ, ϕ and ψ should show a compressive component as well as the torsional one. That is, in agreement with experiment, a compressive stress is necessary to prevent further elongation of the specimen while it is being strained torsionally.

A quantitative investigation of this problem is in progress at the University of Detroit.

REFERENCES

BISHOP, J F W.	1953	*Phil. Mag.* **43**, 51.
BISHOP, J. F. W. and HILL, R.	1951	*Phil. Mag.* **42**, 414 and 1298.
COTTRELL, A. H.	1953	*Dislocations and Plastic Flow in Crystals* p. 116. (Clarendon Press, Oxford).
LIN, T. H.	1957	*J. Mech. Phys. Solids* **5**, 143.
TAYLOR, G. I.	1938a	*J. Inst. Metals* **62**, 307.
	1938b	*Stephen Timoshenko Anniversary Volume* pp. 218-224 (Macmillan).

J. Mech. Phys. Solids, 1959, Vol. 7, pp. 135 to 142. Pergamon Press Ltd., London. Printed in Great Britain

STRESS–STRAIN CYCLES OF LARGE AMPLITUDE

By D. S. Dugdale
Engineering Department, University College of Swansea

(*Received 17th December*, 1958)

Summary

Strain cycles of constant amplitude were imposed on specimens of copper, steel and aluminium alloy while variations in stress amplitude were recorded. For annealed materials the stress increased with successive cycles, but for cold-worked materials it diminished, reaching steady values after definite amounts of plastic strain. These materials became conditioned in various ways by their strain history.

1. Introduction

Mechanical hysteresis in metals has frequently received attention from investigators who believed that it might lead to a better understanding of fatigue failure. For instance, Haigh (1928) measured the heat generated during a fatigue test and found that, after an irregular initial phase, the width of the hysteresis loop remained reasonably constant until fracture was imminent. Forrest (1956) demonstrated a clear correlation between strain hysteresis and notch sensitivity. However, these results leave the impression that hysteresis can vary in a complicated way and can sometimes be entirely absent without affecting the inherent fatigue strength of metals to any discernable extent.

The present work was begun with the intention of examining the effects of reversed strains in an elementary way without reference to any particular practical problem. It was thought that, if the reversed plastic strain was made large enough, a fairly simple pattern of behaviour might emerge. The specimens fractured after numbers of cycles ranging from 5 to 5,000. Such endurances are much too brief for machine parts. Nevertheless it is hoped that the results may allow the complexities of very thin hysteresis loops to be viewed in better perspective. To facilitate experimental work it was decided that the amplitude of total strain rather than any other variable should be kept constant.

2. Testing Machine and Specimens

The testing machine shown in Fig. 1 was specially constructed for the present work. Tensile or compressive loads up to 5 tons could be applied to the specimen through a heavy bar sliding vertically in bearings supported in a rigid steel frame. This bar was prevented from rotating by a key and was threaded at its lower end to engage with a nut which produced axial motion. The nut was rotated by means of a worm gear which could be operated by hand or by an electric motor. Suitable switchgear made the machine self-acting with any desired range of motion,

the speed being about 3 c/min. For measuring applied load, the test specimen was anchored to a master specimen fitted with extensometers.

Test specimens of 6 in. overall length with cylindrical ends 1·25 in. long and 0·74 in. diameter were clamped firmly into the sockets of the machine. The working portion of the specimen was 0·3 in. diameter and was parallel over a length of 0·7 in. To this portion were attached diametrically opposite Huggenburger extensometers of 0·5 in. gauge length.

3. MATERIALS

All materials were in the form of 0·75 in. diameter bar, the aluminium alloy and copper being extruded and the steel cold drawn. Aluminium alloy, containing nominally 4 per cent copper, complied with British Standard Specification L 65 and was fully age-hardened. The copper, of high-conductivity grade, was initially in a hard condition, but a batch of specimens was annealed for 1 hr at 600°C. The steel had an analysis as follows: carbon 0·16 per cent, manganese 0·59 per cent, phosphorous 0·02 per cent, sulphur 0·03 per cent, nitrogen 0·01 per cent. A batch of these specimens was annealed for 1 hr at 650°C. Mechanical properties are shown in Table 1.

TABLE 1

	0·2% *Proof stress* (*tons/in²*)	*Ultimate tensile stress* (*tons/in²*)	*Elongation* (%)	*Young's modulus* (*tons/in²*)	*Vickers hardness number*
Aluminium Alloy	31·0	34·6	13	4,700	144
Copper (hard)	21·0	22·2	20	7,600	104
Copper (soft)	2·0	14·8	62	7,600	45
Steel (hard)	34·5	40·0	18	13,400	187
Steel (soft)	13·6	26·0	48	13,400	107

4. EXPERIMENTAL METHOD

It was invariably observed that the stress-strain curve obtained during unloading was linear and of slope equal to Young's modulus E. This means that the plastic strain increment ϵ_p for one half-cycle is given simply by the width of the stress–strain loop measured along the strain axis (Fig. 2). The loop may be circumscribed by a parallelogram as shown, and the plastic strain is related to the amplitude of total strain ϵ_t and the stress amplitude σ_0 by the equation $\epsilon_p = 2(\epsilon_t - \sigma_0/E)$. For one complete cycle the plastic strain increment is $2\epsilon_p$.

The machine was operated by hand to obtain values for plotting the first few loops. Meanwhile, a limit switch for the electrical drive was set so that the strain amplitude remained at the desired value, only small adjustments being necessary from time to time. At suitable intervals the electric motor was switched off, the number of cycles was recorded and a stress–strain loop was plotted. From this the plastic strain increment and stress amplitude were measured.

An obvious way of presenting the results would be to show graphs of the measured quantities. However, a strain cycle of large amplitude will obviously have a greater

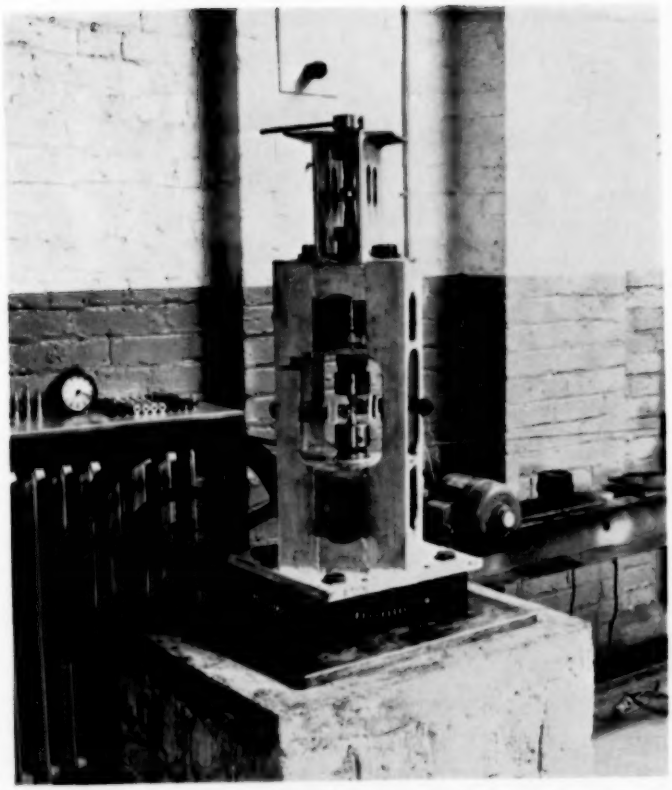

Fig. 1. Testing Machine.

effect than one of small amplitude, so that curves plotted against number of cycles would have quite different shapes. A possible alternative is to plot results against cumulative strain. In computing this, it is logical to exclude the elastic component of strain, as this is unlikely to contribute to any permanent change within the material. Cumulative plastic strain was obtained by summing products of the current width of loop and the incremental number of cycles. If the need should arise, the measured quantities can be quite easily recovered from these graphs.

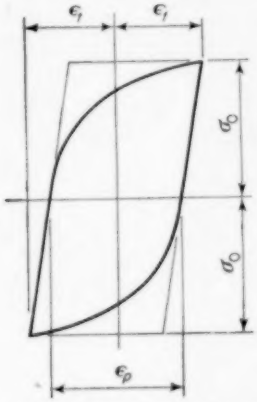

Fig. 2. Geometry of stress–strain loop.

Stress amplitude was taken as the average of tensile and compressive peak stresses. When a series of cycles was begun, the first half-cycle was necessarily irregular, so the stress amplitude for the first cycle was taken as the average peak stress for the second and third half-cycles. Tensile and compressive peak stresses were usually equal, except when the strain amplitude was suddenly reduced by a large amount. Then it was found that an inequality persisted for a while, the numerically greater stress being of the same sign as the stress during the last half-cycle of the previous series. Tests on any one specimen usually extended over two days. Careful checks failed to reveal any effects due to resting for periods up to 24 hr. However, steel and aluminium specimens gave a measurable increase in stress amplitude (about 2 per cent) when rested for ten days.

5. Discussion of Results

Results for soft copper may be considered first, as they follow a trend that might be expected from the shape of the static stress–strain curve. For the first cycle the stress amplitude was very small, but subsequent cycles produced a rapid increase (Fig. 3). Most of this increase was brought about by a plastic strain of 0·5, and no measurable increase occurred after a value of 2·0. In this respect the curves differ from the static stress–strain curve which continues to rise at a diminishing rate with increasing strain. The behaviour of a specimen subjected to a constant stress amplitude can be visualized by drawing the appropriate horizontal line on this graph. Large amplitudes of strain with high rates of heat generation would be followed by steady conditions, as described by Haigh.

The results for cold-worked copper present a marked contrast to the usual stress–strain curve (Fig. 4). A rapid fall in stress amplitude occurred, the change being almost complete after a plastic strain of 10. Tests continued to a strain of

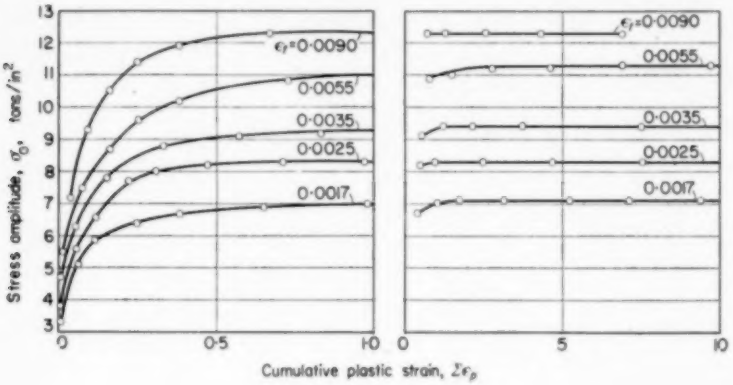

Fig. 3. Soft copper.

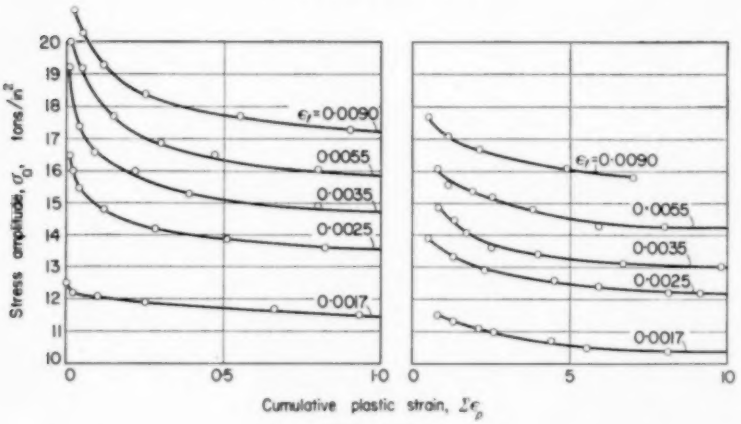

Fig. 4. Hard copper.

30 showed no further measurable change. It appears that the negative change in stress for a cold-worked material takes place more slowly than the positive change for an annealed material. A reduction in hardness of cold-worked materials during fatigue tests has been reported by POLAKOWSKI and PALCHOUDHURI (1954). When the present tests were completed, the Vickers hardness numbers for the specimens of hard copper were found to be 79 to 83 as compared with the initial value of 104.

The curves for steel (Figs. 5 and 6) bear a general resemblance to those for copper, and the same remarks are applicable. There are some differences, however. For soft steel the initial increase in stress amplitude was not so marked, and took place largely within the range of plastic strain 0–0·1. A continued increase took place over the range 1–10 for the larger values of strain amplitude (Fig. 5). For the smaller values, no such increase was observed. It was noted that large cyclic strains caused a pronounced wrinkling of the surface of soft steel specimens.

Similar tests were carried out on aluminium alloy, with the amplitude of total strain maintained constant for each specimen. It was found that no measurable change in stress amplitude occurred after the first cycle up to the point where fracture occurred. These results are not plotted in a separate graph, but are indicated by horizontal lines in Fig. 8b.

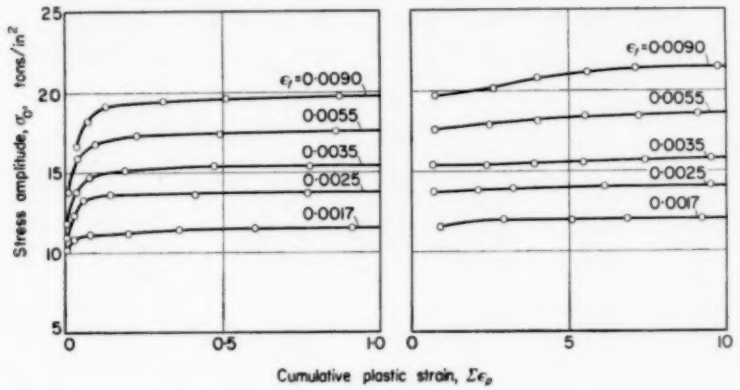

Fig. 5. Soft steel.

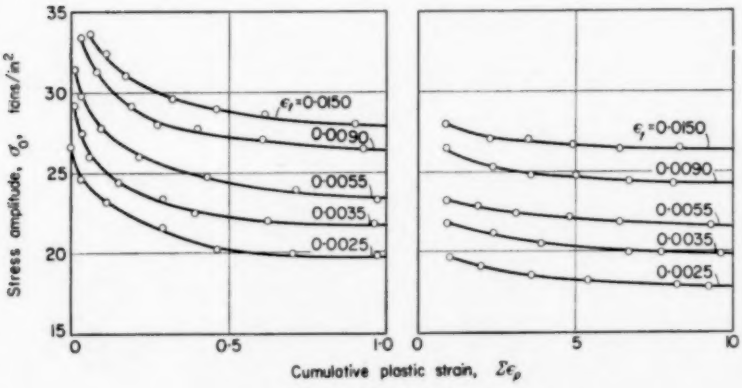

Fig. 6. Hard steel.

A qualitative discussion of the above results can be based on the idea of the dislocations in the crystalline structure becoming locked together in groups (Cottrell 1953, p. 168). During unidirectional straining it may be supposed that these groups are both formed and dispersed, but an excess number formed ensures that the stress–strain curve rises continuously. During reversed straining it is reasonable to suppose that there would be a greater tendency for groups to be dispersed, so that a balance is reached. Reversed straining of an initially cold-worked material would expose all the previously existing groups to a new additional disruptive influence resulting in rapid softening. However, it appears that some

of the groups must be very stable as the material is not quite reduced to the corresponding state for the initially annealed material.

It might be useful here to mention some previous work. When mild steel is stressed over a range lying between its elastic limits, a thin hysteresis loop is gradually developed during the first million cycles (BAIRSTOW 1911). This is probably due to dislocations breaking away for the first time from their atmospheres of solute atoms (see COTTRELL 1953, p. 134), as the effect can be nullified by a low-temperature heat treatment. Clearly this effect should not be looked for when appreciable plastic flow is enforced during the first cycle and during all subsequent cycles.

6. STRAIN HISTORY

The similar shapes of the curves in Figs. 3, 4, 5 and 6 show that changes in stress amplitude tend to take place in step with the value of plastic strain, irrespective of strain amplitude. This raises the question of whether a certain amount of strain at one amplitude is exactly equivalent to the same amount at another amplitude. If this were so, a change in strain amplitude would give an immediate transition from one curve to another in the above graphs. The curves for copper (Fig. 7) show that this simple idea is not strictly true. When a greatly increased

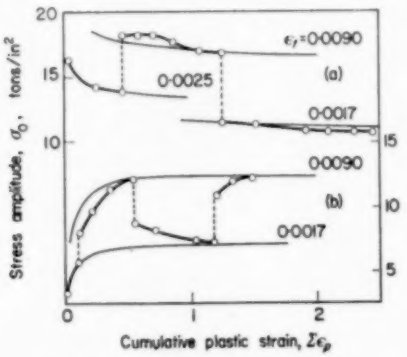

Fig. 7. Varying strain amplitude.
(a) Hard copper. (b) Soft copper.

amplitude of strain was imposed on a specimen of soft copper, the resulting curve shows that previous plastic strain was not of much account. On reducing the amplitude to its former value, it can be seen that the drop in stress amplitude was not immediate. This means that the material must become conditioned in some way to a particular range of strain and cannot adjust itself instantly to a different range. Nevertheless the curve always converges on the appropriate curve for a fixed amplitude, showing that for this material the strain history leaves no lasting effect.

Similar tests were carried out on soft steel and aluminium. These curves (Fig. 8) show that when cyclic strain was increased, the above conclusion can still be drawn. When, however, it was reduced from a large value, the stress amplitude did not fall quite to the expected level. This effect may possibly be due to strain ageing which

occurs to a disproportionate extent while cycles of large amplitude are being imposed. Ageing proceeding at a uniform rate cannot account for this difference, as the same time was taken for tests at both fixed and varying amplitudes. It is concluded that strain history can have a permanent effect on these materials.

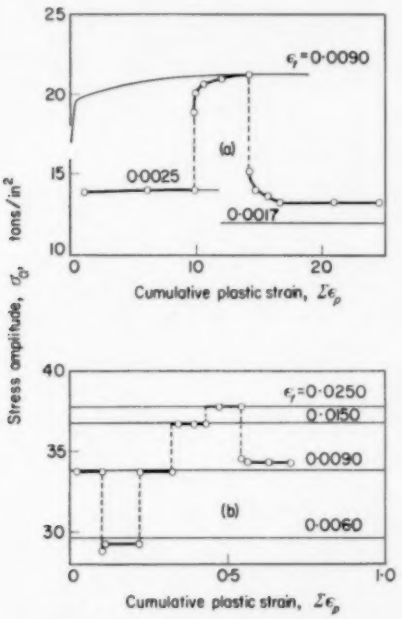

Fig. 8. Varying strain amplitude.
(a) Soft steel, (b) Aluminium alloy.

It is noticeable that the amount of plastic strain required for bringing about a readjustment of stress is large for steel and small for aluminium alloy. A suggested explanation is that the microstructure of the former may be coarse compared with that of the latter, both being assessed in terms of the range of motion of mobile crystal defects.

7. Fracture

It was not intended that the present tests should yield precise data on this topic. Fracture did not occur until a crack had formed. Cracks formed at the fillets of the specimen or at scores made by the extensometers. In copper specimens a crack spread slowly across the section, but in aluminium alloy brittle fracture occurred after the crack had grown only a short distance. In order to record the observations as briefly as possible, they are presented in the manner suggested by Low (1956), who plotted values of total strain amplitude against number of cycles N. For reverse bending tests, the points were found to lie between lines which may be represented by the equation $N = N_0/\epsilon_t^{2\cdot4}$, the values for the constant N_0 being 0·026 and 0·006. Values from the present tests were found to lie along the line of constant $N_0 = 0{\cdot}003$.

It is thought remarkable that results of the tests described here offer no support to the idea that metal suffers some kind of permanent damage throughout its volume when subjected to cyclic straining. This question is of interest in the study of fatigue failure, since material at the tip of a growing crack must undergo inelastic straining. One is led to doubt that the mechanism of growth can be merely one of progressive exhaustion of ductility and fracture.

REFERENCES

BAIRSTOW, L.	1911	*Phil. Trans. Roy. Soc.* A **210**, 35.
COTTRELL, A. H.	1953	*Dislocations and Plastic Flow in Crystals* (Clarendon Press, Oxford).
FORREST, P. G.	1956	*Inst. Mech. Engrs. International Conference on Fatigue of Metals*, 171.
HAIGH, B. P.	1928	*Trans. Faraday Soc.* **24**, 125.
LOW, A. C.	1956	*Inst. Mech. Engrs. International Conference on Fatigue of Metals*, 206.
POLAKOWSKI, N. H. and PALCHOUDHURI, A.	1954	*Proc. ASTM*, **54**, 701.

BOOK REVIEWS

Dislocations and Mechanical Properties of Crystals. Edited by J. C. Fisher, W. G. Johnstone, R. Thomson and T. Vreeland Jr. John Wiley, New York; (Chapman and Hall, London), 1957. xiv + 634 pp., 120s.

In September, 1956, an international group of forty-one scientists met at Lake Placid, New York State, to consider the mechanical aspects of dislocations in solids. Membership of the Conference was by personal invitation only and it seems that in this way the sponsors have secured a thoroughly workmanlike and coherent review of those parts of the subject where most rapid advances have recently been made. The book now published contains a record of the contributions and of the subsequent oral and written discussions. A few contributors evidently took along a 'party piece' and related work which had been or was soon to be published elsewhere, but the majority gave considered accounts of their work which are otherwise not available or are not conveniently accessible to readers of English only.

The contributions are by specialists and for specialists: the general reader may admire the many pictures which give visual evidence for the existence of dislocations, but unless he has a grounding in dislocation theory the text will be heavy going. For those actively concerned with dislocations in research or in teaching, an acquaintance with the contents of the book is essential. The book would be described as indispensable were it not for the price which puts it beyond the means of many British research students. It is warmly commended to all libraries concerned with metallurgy and solid state physics.

The first section of the book amounting to eight articles in 175 pages is concerned with direct observations of dislocations and is illustrated with a wealth of photographs and clear diagrams. The topics and authors include dislocations in transparent crystals generally (Amelinckx), in silicon (Dash), silver halides (Mitchell), aluminium (Hirsch, Horne & Whelan) and lithium fluoride (Gilman and Johnson). Many of the discoveries described in these papers have rightly had considerable publicity and it is now pleasant to be able to study at leisure the striking way in which so many dislocation concepts have been verified by visual observations. The next section, on deformation of pure single crystals, includes an account of discontinuous flow and twinning in copper single crystals at low temperatures (Blewitt, Coltman & Redman) and of surface sources and plastic flow in KCl crystals (T. Suzuki).

The middle of the book is dominated by a review article of eighty-seven pages by Seeger who deals in a masterly fashion with mechanisms of work-hardening and glide in close-packed metals. It is very readable but a trifle overwhelming as the wealth of experimental evidence and detailed explanation is revealed. There are other good things in the section on work-hardening and recovery which should not be overlooked. The most useful articles in the section on alloy crystals, impurities and yield point phenomena, will probably prove to be those on the yield strength of binary alloys (H. Suzuki) and the deformation of alloy single crystals (Garstone and Honeycombe).

There then follow contributions on dislocation damping (Lucke and Granato) and on fatigue, in theory (Mott) and in practice (Wadsworth). The remainder of the book, some 100 pages, contains thirteen contributions on dislocation theory, whiskers and thin crystals, and radiation damage. Generally, only special topics are treated but as the authors include Liebfried, Seeger, Cottrell, Fisher, Nabarro, W. T. Read, Hirsch, Friedel, Shockley, Koehler and Blewitt, it will be appreciated that there is much to stimulate discussion and further experiment.

The conference discussions which followed the presentation of the papers appear to have been well edited and they form useful indications of related work, of disagreements and of fields where more research is urgently needed. The book is a model of high-class scientific publication, but its excellence has to be paid for. It is a pity that the proceedings of a conference held in September 1956 were not published and available for review in this country until April, 1958.

T. Broom

P. M. COOKE and A. W. McCRUM: **The Calculation of Load and Torque in Hot Flat Rolling.** British Iron and Steel Research Assoc., 1958.

THIS B.I.S.R.A. publication consists of data on the plastic stress–strain properties of a wide range of steels up to an engineering strain of 0·5, at temperatures between 900°C and 1,200°C, and at strain–rates between 0 and 100/sec. Extrapolations have been made up to 300/sec but these are often so badly drawn that it would be advisable for the user to make his own extrapolations. The data are plotted as a series of curves in a form suitable for the calculation of rolling load and torque in sheet rolling, but could also be adapted for use in any other calculations for which similar mean values of the yield stress are required. The original stress–strain curves, obtained on a high speed compression testing machine, are not included but have been published elsewhere.

Data of this kind on hot steels have been almost non-existent, and are difficult and laborious to obtain. This collection will be invaluable to engineers designing hot-working plants or carrying out experimental hot-working operations on steel.

A. P. GREEN

Proceedings of the Third Midwestern Conference on Solid Mechanics : University of Michigan Press 1957. 250 pp., $5.50.

FIFTEEN papers are published here, the majority having to do with vibrations in elastic, viscoelastic, or fluid media in the contexts of theories of damping, flutter and stability. The remainder are concerned with dynamical plasticity, elastic torsion of tapered beams, and thermal phenomena. The standard of the contributions is uniformly high.

R. HILL

J. Mech. Phys. Solids, 1959, Vol. 7, pp. 145 to 156. Pergamon Press Ltd., London. Printed in Great Britain

THE TRANSVERSE FLEXURE OF UNIFORMLY LOADED AND FULLY RESTRAINED THIN ISOTROPIC PLATES WITH CURVILINEAR EDGES

By W. A. Bassali
Faculty of Science, University of Alexandria

(*Received 12th January*, 1959)

Summary

This paper deals with the application of complex variable analysis to establish exact solutions in finite terms for the complex potentials and small transverse deflexions of certain thin clamped elastic plates subject to uniform loading distributed over the entire plate. The isotropic plates considered are bounded by certain regular curvilinear polygons which include as special cases the inverse of an ellipse with respect to its centre as well as plates bounded by approximately circular arcs. Explicit formulae for the moments and shears are given at the centres of the plates and at the mid-points of their curvilinear edges. The usual assumptions relating to the classical theory of thin plates are adopted.

1. Introduction

Problems concerning the transverse bending of normally loaded thin isotropic homogeneous slabs having different shapes have been discussed by several authors when the boundary of the plate is rigidly clamped, simply supported or free. An extensive bibliography of previous work is to be found at the end of a recent paper by Deverall (1957) who considered some problems in bending of thin clamped plates by means of the method of Muskhelishvili (1949). Numerical results for the maximum deflexion of clamped and uniformly loaded curvilinear plates approximating to square, rectangular and equilateral triangular plates are given and compared with those found previously by other writers. The methods of complex function theory have been applied by Bassali and Dawoud (1956) to derive solutions for a thin circular plate subject to a general boundary condition including the usual clamped and simply supported boundaries and acted upon by various types of loading distributed over the area of an eccentric circle. In two recent papers the author (1957, 1958) obtained the solutions for a thin circular plate supported at several interior or boundary points and partially and normally loaded over the area of an eccentric circle; the general loadings considered include the uniform and linearly varying pressures and the boundary of the plate being free.

Solutions for an elliptic plate with a clamped edge and bent by a uniform or a uniformly varying pressure were given by Bryan (see Timoshenko 1940, p. 290). More generally the bending of clamped plates bounded by conics has been considered by Woinowsky-Kreiger (1954). The problem of a uniformly loaded elliptic plate with simply supported edge was investigated by Galerkin (1923) and Sen

(1929). STEVENSON (1942) has given detailed solutions for the circular, elliptic and equilateral triangular plate under uniform pressure. Uniformly loaded rectilinear polygonal plates with clamped or simply supported edges have been studied by SETH (1947, 1948). Approximate solutions based upon an energy method and upon GALERKIN's method have been given by OSSELEKDO (1955) to the problem of a thin equilateral trapezoidal plate built in at its edges and subject to uniform transverse pressure. Some experimental results for the deflexion of a plate are shown to be in very good agreement with theoretical results furnished by the energy method. Uniformly loaded trapezoidal plates simply supported at the edges have been discussed by VARVAK (1940).

Using curvilinear co-ordinates SEN (1942) has obtained the solutions appropriate to clamped and uniformly loaded thin elastic plates bounded by the cardioid, the loop of a lemniscate of Bernoulli and the inverses of an ellipse with respect to its centre or its focus. Bipolar co-ordinates have also been applied by WOINOWSKY-KREIGER (1956) to derive expressions for the deflexion and bending moments of thin clamped and uniformly loaded plates bounded by two circular arcs or having the shape of a circular segment. The half-circle under hydrostatic pressure and the eccentric ring under a symmetrical loading have also been treated. STEVENSON (1943) has given the solution for a clamped and uniformly loaded regular curvilinear polygonal plate with n sides. The plate, taken in the z-plane, can be mapped on the unit circle γ in the ζ-plane by the mapping function

$$z = c\zeta\,(1 + m\zeta^n), \tag{1.1}$$

where c, m, n are real constants, n being a positive integer and $0 \leqslant m\,(n+1) \leqslant 1$. The purpose of this paper is to determine, within the restrictions of the small deflexion theory of thin plates, the complex potentials and deflexion at any point of a thin clamped and uniformly loaded regular curvilinear polygonal plate with n sides, that can be mapped on γ by the function

$$z = c\zeta/\,(1 + m\zeta^n), \tag{1.2}$$

where $n \geqslant 2$ and $-1 \leqslant m\,(n-1) \leqslant 1$. The plate corresponding to $n = 2$ has the form of the inverse of an ellipse with respect to its centre while for $m = -2/\{n\,(n-1)\}$ it will be shown that the plate is bounded by approximately circular arcs. In a recent paper the author (1959) has presented solutions for clamped plates mapped on γ by the two foregoing functions and acted upon by concentrated forces or concentrated couples applied at arbitrary or specified points.

2. BASIC EQUATIONS

Consider a thin elastic plate of uniform thickness $2h$, made of isotropic homogeneous material and bounded by one simple closed rectifiable contour Γ, the plate being rigidly clamped along Γ and subject to normal loading distributed over the entire upper face of the plate. Let

$$D = 2hP = 2Eh^3/3\,(1 - \nu^2) \tag{2.1}$$

be the flexural rigidity of the plate, where E is Young's modulus, ν is Poisson's ratio for the material of the plate and P is a plate constant. Referred to rectangular

axes $O(x, y, Z)$ with the origin O in the mid-plane of the plate the transverse displacement w at any point $z = x + iy = re^{i\theta}$ of the mid-plane, measured positively upwards in the direction OZ, satisfies the biharmonic equation

$$\nabla^4 w = 16\partial^4 w/\partial z^2\,\partial \bar{z}^2 = -p(z, \bar{z})/D, \tag{2.2}$$

where $p(z, \bar{z})$ is the transverse load intensity at the point z and bars are used to denote conjugate complex quantities.

It is well known that the general solution of (2.2) may be expressed as

$$w = \bar{z}\Omega(z) + z\bar{\Omega}(\bar{z}) + \omega(z) + \bar{\omega}(\bar{z}) + W(z, \bar{z}), \tag{2.3}$$

where the complex potentials $\Omega(z)$ and $\omega(z)$ are analytical functions of z in the region of the z-plane which is occupied by elastic material and $W(z, \bar{z})$ is a particular integral of (2.2).

With the notation of STEVENSON (1943) the mean stress couples $\widetilde{xy}, \widetilde{yx}, \widetilde{xx}(= -\widetilde{yy})$ and the mean stresses $x\breve{Z}, y\breve{Z}$ are given by the equations

$$\left.\begin{aligned} \widetilde{xy} - \widetilde{yx} &= -4P(1+\nu)\,\partial^2 w/\partial z\,\partial\bar{z}, \\ \widetilde{xy} + \widetilde{yx} + 2i\widetilde{xx} &= -4P(1-\nu)\,\partial^2 w/\partial z^2, \\ x\breve{Z} - iy\breve{Z} &= -8P\,\partial^3 w/\partial z^2\,\partial\bar{z}. \end{aligned}\right\} \tag{2.4}$$

We now suppose that the transformation

$$z = z(\zeta), \quad \zeta = \xi + i\eta = \rho e^{i\psi}, \quad z'(\zeta) \neq 0, \quad \infty \text{ for } \rho \leqslant 1, \tag{2.5}$$

maps the finite region inside Γ conformally on the area inside the unit circle γ in the ζ-plane. Curvilinear co-ordinates (ρ, ψ) are thus introduced in the z-plane which are the maps of the polar co-ordinates in the ζ-plane as given by $\zeta = \rho e^{i\psi}$. The moments and shearing forces at any point in the plate with reference to the curvilinear co-ordinates (ρ, ψ) are given in terms of those with reference to the (x, y) co-ordinates by

$$\left.\begin{aligned} \widetilde{\rho\psi} - \widetilde{\psi\rho} &= \widetilde{xy} - \widetilde{yx}, \\ \widetilde{\rho\psi} + \widetilde{\psi\rho} + 2i\widetilde{\rho\rho} &= e^{2i\alpha}(\widetilde{xy} + \widetilde{yx} + 2i\widetilde{xx}), \\ \rho\breve{Z} - i\psi\breve{Z} &= e^{i\alpha}(x\breve{Z} - iy\breve{Z}), \end{aligned}\right\} \tag{2.6}$$

where α is the angle between the x and ρ-directions at the point. It was shown by MUSKHELISHVILI (1949, p. 182) that

$$e^{i\alpha} = \zeta z'(\zeta)/\rho|z'(\zeta)|. \tag{2.7}$$

Equations (2.3), (2.4), (2.6) and (2.7) now lead to

$$\left.\begin{aligned} \widetilde{\rho\psi} - \widetilde{\psi\rho} &= -4P(1+\nu)\left[2\,Re\,G(\zeta) + \partial^2 W/\partial z\,\partial\bar{z}\right], \\ \widetilde{\rho\psi} + \widetilde{\psi\rho} + 2i\widetilde{\rho\rho} &= -\frac{4P(1-\nu)\,\zeta^2}{\rho^2\,\bar{z}'(\bar{\zeta})}\left[\bar{z}(\bar{\zeta})\,G'(\zeta) + g'(\zeta) + z'(\zeta)\,\partial^2 W/\partial z^2\right], \\ \widetilde{\rho\breve{Z}} - i\widetilde{\psi\breve{Z}} &= -\frac{8P\zeta}{\rho\,|z'(\zeta)|}\left[G'(\zeta) + z'(\zeta)\,\partial^3 W/\partial z^2\,\partial\bar{z}\right], \end{aligned}\right\} \tag{2.8}$$

where
$$\left.\begin{aligned} &\Omega(z) = F(\zeta), \quad \omega(z) = f(\zeta), \\ &G(\zeta) = F'(\zeta)/z'(\zeta), \quad g(\zeta) = f'(\zeta)/z'(\zeta), \end{aligned}\right\} \tag{2.9}$$

and accents denote derivatives with respect to the argument stated.

3. Boundary Conditions

The conditions that the boundary Γ is horizontally clamped may be taken as

$$w = 0, \quad \partial w/\partial n = 0 \text{ along } \Gamma, \tag{3.1}$$

where $\partial/\partial n$ denotes differentiation along the outwards drawn normal. It is easily shown that these conditions are equivalent to

$$w = 0, \quad \partial w/\partial z = 0 \text{ along } \Gamma \tag{3.2}$$

or
$$w = 0, \quad \partial w/\partial \zeta = 0 \text{ along } \gamma. \tag{3.3}$$

Substituting from (2.3) and (2,5) in (3.3) we find that the conditions for a fully restrained boundary may be written in the forms

$$\bar{z}(\sigma^{-1})\, F(\sigma) + z(\sigma)\, \overline{F}(\sigma^{-1}) + f(\sigma) + \overline{f}(\sigma^{-1}) + T(\sigma, \sigma^{-1}) = 0, \tag{3.4}$$

$$z'(\sigma)\, \overline{F}(\sigma^{-1}) + \bar{z}(\sigma^{-1})\, F'(\sigma) + f'(\sigma) + \left[\partial T(\zeta, \bar{\zeta})/\partial \bar{\zeta}\right]_{\zeta=\sigma} = 0, \tag{3.5}$$

where
$$W(z, \bar{z}) = T(\zeta, \bar{\zeta}), \tag{3.6}$$

$\sigma = e^{i\phi}$ is any point on γ, and accents denote differentiation with respect to σ.

4. Mapping Function

Stevenson (1943) has investigated the deformation of the clamped and uniformly loaded epitrochoidal plate with n sides. The plate considered by him is conformally mapped on the unit circle γ by the transformation

$$z = c\zeta(1 + m\zeta^n), \tag{4.1}$$

where n is a positive integer, and c, m are real positive constants such that $0 \leqslant m(n+1) \leqslant 1$. We here consider the mapping function

$$z = c\zeta/(1 + m\zeta^n), \quad c > 0, \quad n \geqslant 2, \tag{4.2}$$

where $-1 \leqslant m(n-1) \leqslant 1$. This transformation is everywhere conformal and there will be no critical points inside γ. It is sufficient to consider either positive or negative values of m. This follows from the fact that the transformation (4.2) is equivalent to the transformation $z' = c\zeta'/(1 - m\zeta'^n)$, where $z = z'\, e^{i\pi/n}$ and $\zeta = \zeta'\, e^{i\pi/n}$. Putting the mapping function in the form (4.2) we have the advantage that while the size of the map is governed by the constant c alone, the shape of the map is determined by the other two constants m and n only. By varying m and n many shapes may be obtained. The circle $|\zeta| = 1$ corresponds in the z-plane to the contour Γ_n with the parametric representation

$$\left.\begin{aligned} x/c &= (\cos\psi + m\cos q\psi)/(1 + 2m\cos n\psi + m^2), \\ y/c &= (\sin\psi - m\sin q\psi)/(1 + 2m\cos n\psi + m^2) \end{aligned}\right\} (q = n - 1). \tag{4.3}$$

It can be easily shown that Γ_n is the inverse with respect to the circle $|z| = c$ of the closed curve C_n which has the parametric equations

$$\left.\begin{aligned} x/c &= \cos\psi + m\cos q\psi, \\ y/c &= \sin\psi - m\sin q\psi. \end{aligned}\right\} \tag{4.4}$$

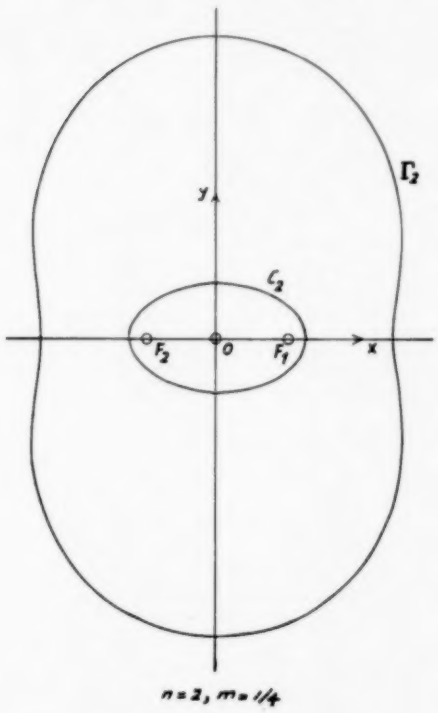

Fig. 1.

Each of C_n or Γ_n is a regular curvilinear polygon with n sides. The contour Γ_2 (Fig. 1) is the inverse of the ellipse $x^2/a^2 + y^2/b^2 = 1$ with respect to the circle $x^2 + y^2 = f^2$, where in this case

$$z = c\zeta/(1 + m\zeta^2), \quad c = 2f^2/(a + b), \quad 0 \leqslant m = (a - b)/(a + b) < 1. \tag{4.5}$$

A study of the map of the unit circle $|\zeta| \leqslant 1$ obtained with the aid of (4.5) shows that when m is numerically near unity, the resulting figure in the z-plane differs little from the figure consisting of a pair of touching circles of equal radii (MUSKHELISHVILI 1949, p. 180).

When $m = -1/(n-1)$ $(n > 2)$ the contour Γ_n is the inverse with respect to a concentric circle of a star-shaped hypocycloid with n cusps, and hence Γ_n also has n cusps which correspond to the points $\sigma_s = \exp\left[(2s+1)\,i\pi/n\right]$ $(s = 0, 1, 2, \ldots, n-1)$. From (4.2) we see that these cusps lie at the points

$$z_s = c\,(1 - 1/n)\,\exp\left[(2s + 1)\,i\pi/n\right].$$

In Figs. 2 and 3 the cases $n = 3$, $m = -1/2$ and $n = 4$, $m = -1/3$ are illustrated.

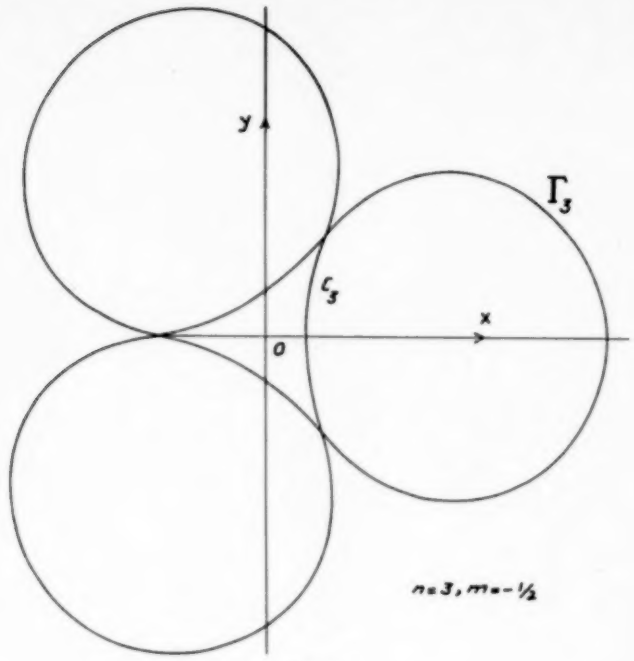

Fig. 2.

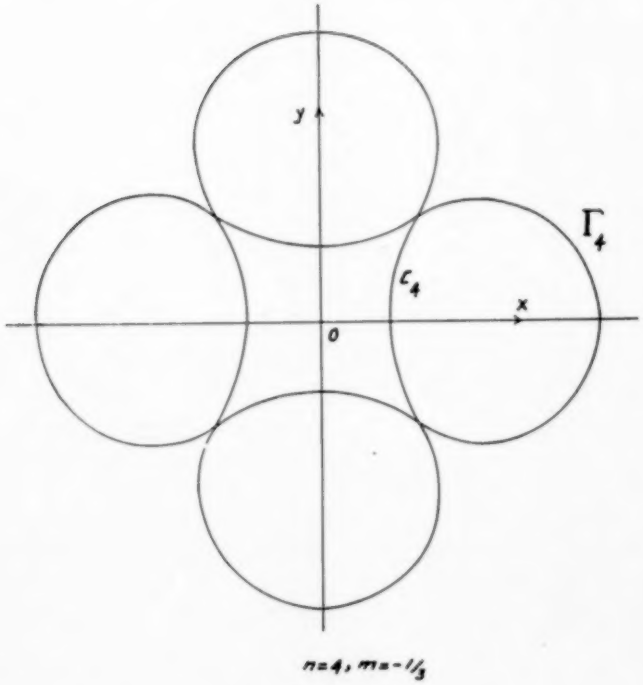

Fig. 3.

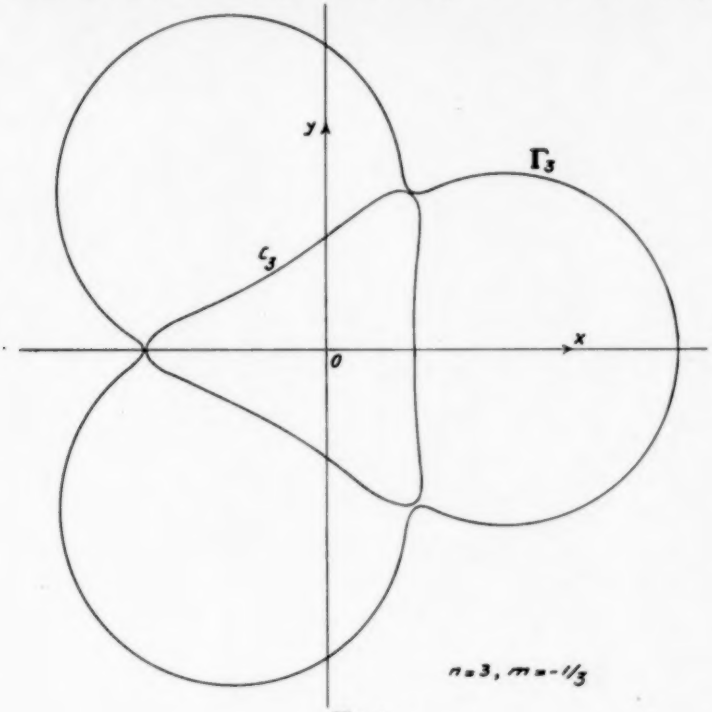

Fig. 4.

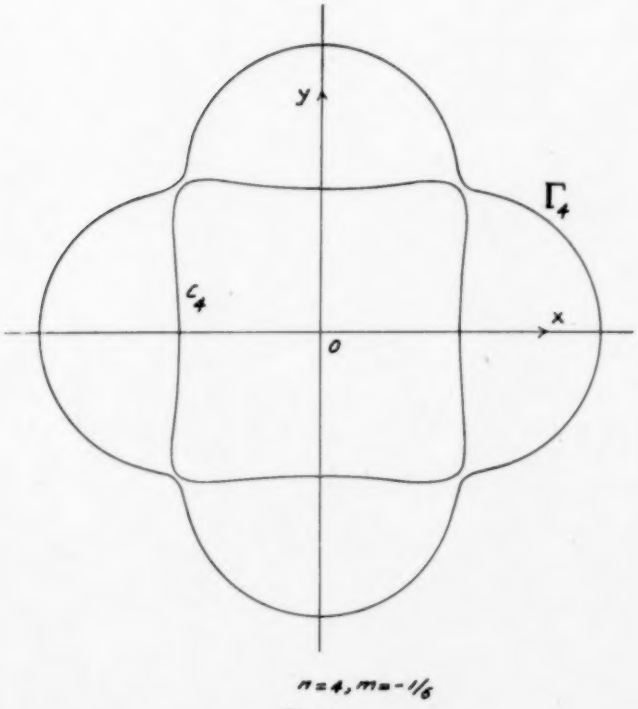

Fig. 5.

It can be shown (MUSKHELISHVILI 1949, p. 370) that the transformation

$$z = c\zeta \left[1 - \sum_{\lambda=1}^{\infty} \frac{2}{n}\left(\frac{2}{n} - 1\right)\left(\frac{2}{n} - 2\right)\cdots\left(\frac{2}{n} - \lambda + 1\right)\zeta^{-\lambda n}/\lambda\,!\,(\lambda n - 1)\right] \quad (4.6)$$

maps the infinite region outside a regular rectilinear polygon with n sides in the z-plane on the area exterior to the unit circle in the ζ-plane. Retaining only the first term of the infinite summation entering in (4.6) we get as an approximation

$$z = c\zeta\left[1 - 2\zeta^{-n}/n\,(n-1)\right]. \quad (4.7)$$

If z' is the inverse of z with respect to the circle $|z| = c$ in the z-plane and ζ' is the inverse of ζ with respect to $|\zeta| = 1$ then

$$\bar{z}z' = c^2, \quad \bar{\zeta}\zeta' = 1. \quad (4.8)$$

Introducing (4.8) in (4.7) now leads to the transformation

$$z' = c\zeta'/(1 + m\zeta'^n) \quad (4.9)$$

where

$$m = -2/n\,(n-1). \quad (4.10)$$

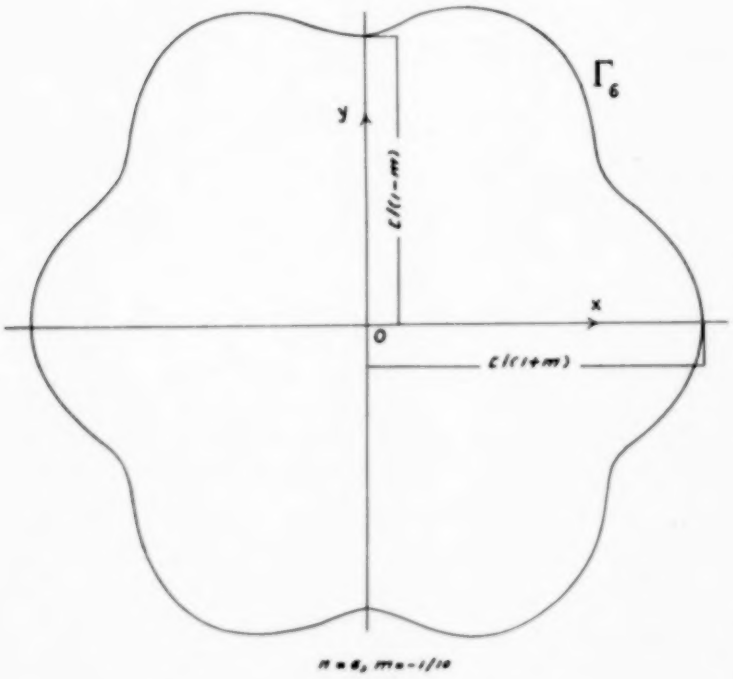

Fig. 6.

Noting the agreement between (4.9) and (4.2) we see that with the value of m given by (4.10) inserted in (4.4) and (4.3) the closed curve C_n approximates to a regular rectilinear polygon with n sides and the corresponding curve Γ_n differs slightly from the figure bounded by n approximately circular arcs each of which passes through the centre and two consecutive vertices of a regular rectilinear polygon with n sides.

The curves C_n and Γ_n corresponding to $n = 3$, $m = -1/3$ and $n = 4$, $m = -1/6$ are shown in Figs. 4 and 5 respectively. The little deviations of the sides from the rectilinear and circular forms are to be noted in the figures.

For large values of n the plate bounded by Γ_n is a grooved or fluted plate of a special type. The plate for which $n = 6$, $m = -1/10$ is drawn in Fig. 6.

5. Bending of Clamped and Uniformly Loaded Curvilinear Polygonal Plates

We now deal with the problem of clamped and uniformly loaded plates that can be mapped on γ by means of (4.2). The particular integral $W(z, \bar{z})$ corresponding to uniform loading of intensity p distributed over the entire plate may be taken as

$$W(z, \bar{z}) = -kz^2\bar{z}^2, \tag{5.1}$$

where
$$k = p/64D = p/128\,hP. \tag{5.2}$$

The complex potentials will now be sought in the forms

$$\left.\begin{aligned} \Omega &= kc^2 z\,[A_0 + A_1/(1 + m\zeta^n)], \\ \omega &= kc^4\,[B_0 + B_1/(1 + m\zeta^n) + B_2/(1 + m\zeta^n)^2], \end{aligned}\right\} \tag{5.3}$$

where A_0, A_1 ; B_0, B_1 and B_2 are real constants to be determined from the boundary conditions. Substitution from (4.2), (5.1) and (5.3) in (3.4) and (3.5) yields the two following identities

$$2A_0(1 + m^2 + m\lambda + m\lambda^{-1}) + A_1(2 + m\lambda + m\lambda^{-1}) + 2(1 + m^2 + m\lambda + m\lambda^{-1})^2 B_0$$
$$+(1+m^2+m\lambda+m\lambda^{-1})(2+m\lambda+m\lambda^{-1})B_1+(2+2m\lambda+2m\lambda^{-1}+m^2\lambda^2+m^2\lambda^{-2})B_2-1\equiv 0, \tag{5.4}$$

$$(\lambda + m)\left[2(1 + m\lambda)(1 - mq\lambda)A_0 + \{1 - (2q + 1)m\lambda\}A_1\right] + \lambda(1 + m\lambda)(1 - mq\lambda)A_1$$
$$- mn(\lambda + m)^2\{(1 + m\lambda)B_1 + 2B_2\} - 2\lambda(1 - mq\lambda) \equiv 0, \tag{5.5}$$

where
$$\lambda = \sigma^n, \quad q = n - 1. \tag{5.6}$$

Equating the coefficients of various powers of λ in (5.4) and (5.5) separately to zero we obtain the following system of equations

$$(1 + m^2)A_0 + A_1 + (1 + 4m^2 + m^4)B_0 + (1 + 2m^2)B_1 + B_2 = \tfrac{1}{2}, \tag{5.7}$$

$$2A_0 + A_1 + 4(1 + m^2)B_0 + (3 + m^2)B_1 + 2B_2 = 0, \tag{5.8}$$

$$2B_0 + B_1 + B_2 = 0\,; \tag{5.9}$$

$$2A_0 + A_1 - m^2 n(B_1 + 2B_2) = 0, \tag{5.10}$$

$$2(1 + m^2 - m^2 q)A_0 + (2 - m^2 - 2qm^2)A_1 - m^2 n\{(2 + m^2)B_1 + 4B_2\} = 2, \tag{5.11}$$

$$2(q - 1 + m^2 q)A_0 + 3qA_1 + n\{(1 + 2m^2)B_1 + 2B_2\} = 2q, \tag{5.12}$$

$$2qA_0 + qA_1 + nB_1 = 0. \tag{5.13}$$

It can be easily seen that the seven equations (5.7) to (5.13) are consistent in the five unknowns A_0, A_1 ; B_0, B_1 and B_2. The compatibility of these equations shows that the forms (5.3) are plausible expressions for the complex potentials Ω and ω. Solving the foregoing equations we find

$$\left.\begin{aligned} &A_0 = (m^4 q - 2m^2 q - 1)/K,\ A_1 = 2/(1 - m^2)\,; \\ &B_0 = (1 - m^2 q)/2K, \quad B_1 = 2m^2 q/K, \quad B_2 = -1/(1 - m^2)^2, \\ &\text{where} \qquad K = (1 - m^2)^2(1 + m^2 q). \end{aligned}\right\} \tag{5.14}$$

The complex potentials are completely determined by inserting these values in (5.3). The transverse displacement w at any point $z(\zeta)$ of the plate is now obtained by substituting from (4.2), (5.1),

(5.3) and (5.14) in (2.3). After some algebraic manipulation the following closed expression for the deflexion is arrived at:

$$\left.\begin{aligned} w &= kc^4\left[U(\rho) + 4m^3\, V(\rho)\, Re\,\zeta^n\right]/\left|1 + m\zeta^n\right|^4 K, \\ \text{where}\quad U(\rho) &= m^2 q - 1 + 2(1 - 2m^2 - m^4 q)\rho^2 - K\rho^4 \\ &\quad + m^2\rho^{2n}\left\{4(1 + m^2 q) - 2(1 + 2m^2 q - m^4 q)\rho^2 + m^2(1 - m^2 q)\rho^{2n}\right\}, \\ V(\rho) &= q(1 - \rho^2) - \rho^2(1 - \rho^{2q}),\ q = n - 1. \end{aligned}\right\} \quad (5.15)$$

Setting $m = 0$ in (5.15) we find that the expression for the deflexion reduces to

$$w = -kc^4(1 - \rho^2)^2, \quad (5.16)$$

which is the well known solution (TIMOSHENKO 1940, p. 60) for a thin clamped and uniformly loaded circular plate. Furthermore, it is easily proved that $(1 - \rho^2)^2$ is a common factor of both $U(\rho)$ and $V(\rho)$ so that

$$U(\rho) = (1 - \rho^2)^2\, U_1(\rho), \quad V(\rho) = (1 - \rho^2)^2\, V_1(\rho), \quad (5.17)$$

where $U_1(\rho)$ and $V_1(\rho)$ are two polynomials in ρ of degrees $4n - 4$ and $2n - 4$ respectively. Thus the deflexion may be written as

$$w = kc^4(1 - \rho^2)^2\left[U_1(\rho) + 4m^3\, V_1(\rho)\, Re\,\zeta^n\right]/\left|1 + m\zeta^n\right|^4 K, \quad (5.18)$$

a form which clearly shows that the two boundary conditions (3.1) are satisfied.

The deflexion w_0 at the centre of the plate is furnished by putting $\zeta = 0$ in (5.15) and we obtain

$$w_0 = -\delta_n kc^4, \quad (5.19)$$

where

$$\delta_n = (1 - m^2 q)/(1 - m^2)^2(1 + m^2 q), \quad q = n - 1, \quad (5.20)$$

and k is given by (5.2). Substituting for m from (4.10) in (5.20) we find, for regular curvilinear plates bounded by approximately circular arcs (Figs. 4 and 5),

$$\delta_n = \frac{(n-1)n^2 - 4}{(n-1)n^2 + 4} \cdot \frac{n^4(n-1)^4}{\left[n^2(n-1)^2 - 4\right]^2}. \quad (5.21)$$

In the accompanying Table we give the numerical values of this coefficient corresponding to various values of n.

TABLE 1

n	δ_n	n	δ_n	n	δ_n
3	0.805408	5	0.941819	8	0.984812
4	0.895196	6	0.965081	∞	1

6. THE SPECIAL CASE $n = 2$

Putting $n = 2$ and $q = 1$ in (5.15) and performing some reduction we obtain the following result for the deflexion at any point of the clamped and uniformly loaded plate bounded by the inverse of the ellipse $x^2/a^2 + y^2/b^2 = 1$ with respect to a concentric circle of radius f:

$$w = -\frac{k(1 - \rho^2)^2 c^4}{(1 - m^4)\left|1 + m\zeta^2\right|^4}\left[1 + \frac{2m\rho^2}{1 - m^2}(1 - 2m\cos 2\psi + m^2) - m^4\rho^4\right], \quad (6.1)$$

where, in this case, the mapping function is given by (4.5). Setting

$$m^{\frac{1}{2}}\zeta = e^{\hat{w}}, \quad \hat{w} = u + iv, \quad (6.2)$$

in (4.5) so that

$$m^{\frac{1}{2}}\rho = e^{-v}, \quad \psi = u, \quad (6.3)$$

we find that the transformation (4.5) can be replaced by

$$z = d \sec t, \tag{6.4}$$

where
$$d = c/2m^{\frac{1}{2}} = f^2/\sqrt{(a^2 - b^2)}. \tag{6.5}$$

Writing
$$m = e^{-2\beta}\ (0 < \beta \leqslant \infty), \tag{6.6}$$

so that
$$\beta = \tanh^{-1}(b/a), \tag{6.7}$$

we see that (6.3) and (6.5) lead to

$$\rho = e^{\beta - v}, \quad \psi = u, \quad c = 2d\, e^{-\beta}. \tag{6.8}$$

It is now clear that the straight line $v = \beta$ in the t-plane is mapped on the boundary γ of the unit circle in the ζ-plane and hence on the boundary Γ_2 in the z-plane. The solution (6.1) can be expressed in terms of the curvilinear co-ordinates (u, v). Substituting from (5.2), (6.2), (6.6) and (6.8) in (6.1) we get

$$w = -\frac{p_0\, d^4 \sinh^2(v - \beta)}{4D \sinh 4\beta\, (\cosh 2v + \cos 2u)^2}\left[\sinh 2(v + \beta) + \frac{\cosh 2\beta - \cos 2u}{\sinh 2\beta}\right], \tag{6.9}$$

which may be shown to be equivalent to the solution derived by Sen (1942).

7. Moments and Shears

The bending and twisting moments and shearing forces at any point $z(\zeta)$ of the clamped and uniformly loaded plate bounded by Γ_n are determined by substitution from (4.2), (5.1), (5.3) in (2.8), (2.9) and using the values of the constants given by (5.14). The boundary values of these moments and shears at the mid-points of the curvilinear edges of Γ_n are then found by putting $\zeta_s = \exp(2\pi i s/n)$ $(s = 0,1,2, \ldots, n-1)$ in the final results. After some straightforward calculations and substituting for k from (5.2), the following expressions are obtained

$$\left.\begin{aligned}
\widetilde{\rho\psi} &= \frac{pc^2}{16(1-m^2)h}\left[\frac{m^2}{1-m^2} + \frac{2}{1-mq} - \frac{1}{1+m^2q}\right],\\
\widetilde{\psi\rho} &= -\frac{pvc^2}{16(1-m^2)h}\left[\frac{m^2}{1-m^2} + \frac{2}{1-mq} - \frac{1}{1+m^2q}\right],\\
\widetilde{\rho\rho} &= 0,\\
\widetilde{\rho Z} &= \frac{pc}{8(1+m)h}\left[2 + \frac{mn\{q + 2 - 2mq + q(2q+1)m^2\}}{(1-m)(1-mq)^3}\right],\\
\widetilde{\psi Z} &= 0.
\end{aligned}\right\} \tag{7.1}$$

From (7.1) we notice that $\widetilde{\rho\rho} = 0$ and $\widetilde{\psi\rho} = -\nu\,\widetilde{\rho\psi}$. This is in agreement with the more general result obtained by Stevenson (1943) in which he shows that if n and s are unit vectors normal and tangential to any built-in boundary, then

$$\left.\begin{aligned}
&\widetilde{nn} = \widetilde{ss} = 0\\
\text{and}\quad &\widetilde{ns} = -\widetilde{sn}/\nu = -P\nabla^2 w = \frac{p}{8h} z(\sigma)\bar{z}(\sigma^{-1}) - 8PReG(\sigma).
\end{aligned}\right\} \tag{7.2}$$

The application of the latter formula leads to the expression

$$\widetilde{ns} = \frac{pc^2}{16(1-m^2)h}\left[\frac{1}{1-m^2} - \frac{1}{1+m^2q} + \frac{1-m^2q^2}{1-2mq\cos n\psi + m^2q^2}\right] \tag{7.3}$$

for the clamping couple at any point of the boundary.

At the centre $z = 0$ of the plate we have $\zeta = 0$ and we immediately get

$$\left.\begin{aligned} &\widetilde{xx} = \widetilde{yy} = \breve{x}\breve{Z} = \breve{y}\breve{Z} = 0, \\ &\widetilde{xy} = -\widetilde{yx} = \frac{pc^2(1+\nu)}{32h(1-m^2)}\left[\frac{m^2}{1-m^2} - \frac{1}{1+m^2q}\right]. \end{aligned}\right\} \tag{7.4}$$

Setting $m = 0$ in the foregoing results yields the corresponding values on the boundary and at the centre of a clamped and uniformly loaded thin circular plate. It is easily seen that the resulting expressions for the bending moments agree with those given by TIMOSHENKO (1940, equations (65) and (66)) on noting that the relations between STEVENSON's notations adopted here and those of TIMOSHENKO are

$$M_n = -2h\,\widetilde{ns}, \quad M_s = 2h\,\widetilde{sn}, \quad M_{ns} = 2h\,\widetilde{ss} = -2h\,\widetilde{nn};$$
$$Q_n = -2h\,n\breve{Z}, \quad Q_s = -2h\,s\breve{Z}.$$

REFERENCES

BASSALI, W. A.	1956	*Proc. Camb. Phil. Soc.* **52**, 734.
	1957	*Ibid.* **53**, 728.
	1958	*Ibid.* **54**, 265.
	1959	*Ibid.* **55**, 121.
BASSALI, W. A. and DAWOUD, R. H.	1956	*Proc. Camb. Phil. Soc.* **52**, 584.
DEVERALL, L. I.	1957	*J. Appl. Mech.* **24**, 295.
GALERKIN, B. G.	1923	*Z. angew. Math. Mech.* **3**, 113.
MUSKHELISHVILI, N. I.	1949	*Some Basic Problems of the Mathematical Theory of Elasticity.* (3rd Ed.) (Moscow).
OSSELEKDO, A. I.	1955	*Inz. Sb. Akad. Nauk. SSSR.* **21**, 142.
SEN, B.	1929	*J. Indian Math. Soc.* **18**, 149.
	1942	*Phil. Mag.* **33**, 294.
SETH, B. R.	1947	*Phil. Mag.* **38**, 292.
	1948	*Bull. Calcutta Math. Soc.* **40**, 36.
STEVENSON, A. C.	1942	*Phil. Mag.* **33**, 639.
	1943	*Ibid.* **34**, 105.
TIMOSHENKO, S.	1940	*Theory of Plates and Shells* (McGraw-Hill).
VARVAK, P. M.	1940	*Sb. in-ta Stroit. mekh. Akad. Nauk. USSR*, **10**.
WOINOWSKY-KREIGER, S.	1954	*J. Appl. Mech.* **21**, 296.
	1956	*Ing.-Arch.* **24**, 47.

J Mech. Phys. Solids, 1959, Vol. 7, pp. 157 to 162. Pergamon Press Ltd., London. Printed in Great Britain

ON TORSION OF THIN CYLINDRICAL SHELLS

By E. Reissner
Massachusetts Institute of Technology

(*Received* 13th *January*, 1959)

Summary

In the following we consider an application of the theory of elastic, thin, cylindrical shells to the problem of St. Venant torsion. We obtain in this way simple explicit general results for non-homogeneous shells, which include as special case Bredt's formulas for closed tubes and known results for tubes slit along a generator. We also find that the problem of St. Venant torsion requires use of a formulation of shell theory which is more accurate than Love's first approximation theory.

1. Equilibrium Equations

We designate co-ordinates in the middle surface of the cylindrical shell by z and s where z is measured along generators and s is the arc-length of the meridian curves.

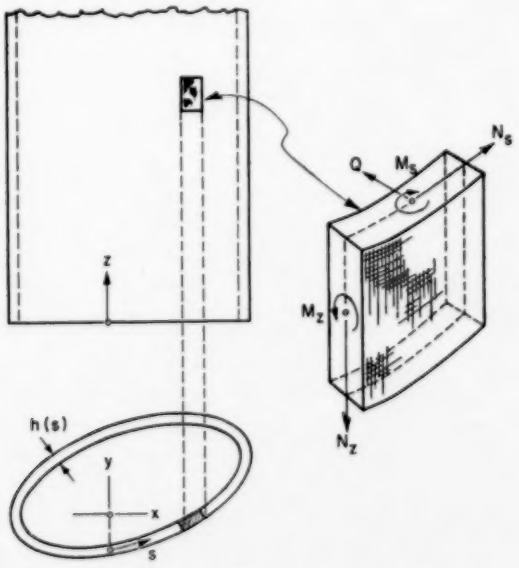

Fig. 1.

The radius of curvature of the meridian curves is designated by R. We obtain the relevant differential equations of the problem by specializing appropriate general

systems of shell equations. In the problem of St. Venant torsion we have to consider shearing stress resultants N_s and N_z, twisting couples M_s and M_z, and a transverse shear-stress resultant Q, in accordance with Fig. 1. The three resultants and two couples are all independent of the axial co-ordinate z.

Of the six equilibrium equations for elements of the shell three are identically satisfied and the remaining three reduce to

$$\frac{dN_z}{ds} = 0, \tag{1}$$

$$\frac{dM_z}{ds} - Q = 0, \tag{2}$$

$$N_s - N_z - \frac{M_z}{R} = 0. \tag{3}$$

An additional macroscopic equilibrium condition, the significance of which has been discussed elsewhere (REISSNER 1959), is

$$M_s - M_z - \frac{h^2}{24R}(N_s + N_z) = 0. \tag{4}$$

The radius of curvature R which occurs in (3) and (4) is defined by $1/R = -\mathbf{n}.(\partial^2 \mathbf{r}/\partial s^2)$ where $\mathbf{n} = (\partial \mathbf{r}/\partial z) \times (\partial \mathbf{r}/\partial s)$ and $\mathbf{r} = x(s)\,\mathbf{i} + y(s)\,\mathbf{j} + z\mathbf{k}$. We find

$$\frac{1}{R} = y' x'' - x' y'' \tag{5}$$

where from now on primes indicate differentiation with respect to s. We further have

$$y' = \sin\phi, \quad x' = \cos\phi \tag{6}$$

where ϕ is the angle between x-axis and meridian tangent. Introduction of (6) into (5) indicates that, alternatively, $1/R = -\phi'$ and then, by differentiation of (6)

$$\frac{1}{R} = \frac{x''}{y'} = -\frac{y''}{x'}. \tag{5'}$$

Equations (5') and (6) are used in an evaluation of forces and moments over the cross-section of the shell. We have

$$F_x = \oint (N_s \cos\phi - Q \sin\phi)\, ds, \tag{7}$$

$$F_y = \oint (N_s \sin\phi + Q \cos\phi)\, ds, \tag{8}$$

$$T = \oint [M_s + y(N_s \cos\phi - Q \sin\phi) - x(N_s \sin\phi + Q \cos\phi)]\, ds. \tag{9}$$

The form of the equilibrium equations (1) to (4) suggests expressing the integrands in (7) to (9) in terms of N_z and M_z. If this is done in equations (7) and (8) we find that both components of force, F_x and F_y, vanish identically, as they should. Equation (9) for the torque T becomes

$$T = \oint \left[M_z + \frac{h^2}{24R}\left(2N_z + \frac{M_z}{R}\right) - (yy' + xx')\, M_z' \right.$$
$$\left. + (yx' - xy')\left(N_z + \frac{M_z}{R}\right)\right] ds. \tag{10}$$

Upon integration by parts of the term with M_z' equation (10) may be reduced to

$$T = \oint \left[2M_z \left(1 + \tfrac{1}{12}\frac{h^2}{R^2}\right) + N_z \left(yx' - xy' + \frac{h^2}{12R}\right)\right] ds \tag{11}$$

and, in view of the fact that terms of the order h^2/R^2 but not terms of the order h/R are assumed to be negligible in comparison with unity,

$$T = \oint [2M_z + N_z (yx' - xy')]\, ds. \tag{12}$$

In equation (12) the stress resultant N_z has a constant value, by (1), while the distribution of the couple M_z is not known. We may then write (12) in the form

$$T = 2 \oint M_z\, ds - 2AN_z \tag{13}$$

where A is the area enclosed by the meridian curve of the middle surface of the shell.

We note that when M_z is neglected in (13) we obtain from it Bredt's first formula for a closed shell, whereas setting $N_z = 0$ leads to a formula which may be shown to give the correct result for a longitudinally slit tube. We will show in what follows that under certain circumstances *both* N_z and M_z must be retained for a meaningful result.

2. Torque-twist Relation

In order to express the torque T, as well as stress resultants and couples in terms of an angle of twist θ we use the principle of minimum complementary energy in conjunction with the Lagrange multiplier method. Assuming linearity and homogeneity in wall thickness direction, we take as expression for complimentary energy an appropriate formula by Trefftz, supplemented for consistency's sake by a transverse shear stress term (Reissner, op. cit.):

$$\Pi = \tfrac{1}{2} \oint \left[\frac{1}{Gh}\left(\frac{N_s + N_z}{2}\right)^2 + \frac{12}{Gh^3}\left(\frac{M_s + M_z}{2}\right)^2 + \frac{6}{5}\frac{Q^2}{G_t h}\right] ds. \tag{14}$$

In view of the fact that T is given in terms of N_z and M_z we also express Π in terms of these quantities. Taking account of the equilibrium equations (1) to (4) and consistently disregarding terms of order of h^2/R^2 in comparison with unity we obtain from (14) the equivalent expression

$$\Pi = \tfrac{1}{2} \oint \left[\frac{N_z^2}{Gh} + \frac{12\, M_z^2}{Gh^3} + \frac{2N_z M_z}{GhR} + \frac{6\,(M_z')^2}{5G_t h}\right] ds. \tag{15}$$

We now assume that the torque T is prescribed and minimize Π with this side condition by requiring satisfaction of the variational equation

$$\delta (\Pi + \theta T) = 0. \tag{16}$$

Upon carrying out all variations and eliminating derivatives of variations by integration by parts, equation (16) assumes the following form

$$\left[N_z \oint \frac{ds}{Gh} + \oint \frac{M_z\, ds}{GhR} - 2A\theta\right] \delta N_z + \oint \left[\frac{12 M_z}{Gh^3} + \frac{N_z}{GhR} - \frac{6}{5}\left(\frac{M_z'}{G_z h}\right)' + 2\theta\right] \delta M_z\, ds = 0, \tag{17}$$

with which are associated as natural transition conditions at points of discontinuity of section properties the conditions of continuous M_z and $M_z' - /G_z h$.

Equation (17) is equivalent to the differential equation

$$\frac{6}{5}\left(\frac{M_z'}{G_t h}\right)' - \frac{12\, M_z}{Gh^3} = 2\theta + \frac{N_z}{GhR} \tag{18}$$

and to the finite equation

$$N_z \oint \frac{ds}{Gh} = 2A\theta - \oint \frac{M_z\, ds}{GhR}. \tag{19}$$

While equations (18) and (19) in their present form are for shells which are homogeneous in the thickness direction, they are readily changed so as to apply to problems of sandwich shells by changing $Gh^3/12$ into suitable a factor D, Gh into a factor C, and $G_t h$ into a factor B.

In what follows we are limiting ourselves to further discussion of problems with negligible transverse shear-stress deformability. Setting $G_t = \infty$ we may take M_z from (18) in order to obtain from (19) a relation for N_z:

$$N_z \oint \left[1 - \frac{1}{12}\frac{h^2}{R^2}\right] \frac{ds}{Gh} = 2\left[A + \oint \frac{h^2\, ds}{12R}\right] \theta. \tag{20}$$

Since terms of order h^2/R^2 are assumed negligible in comparison with unity, equation (20) is effectively Bredt's relation

$$N_z = \frac{2A\theta}{\oint (ds/Gh)}. \tag{21}$$

Introduction of (21) into (18) gives an expression for M_z in terms of the angle θ:

$$M_z = -\frac{Gh^3}{6}\left[1 + \frac{A}{GhR \oint (ds/Gh)}\right] \theta \tag{22}$$

where both terms inside the brackets generally are of the same order of magnitude.

Equations (21) and (22) are introduced into equation (13) for the torque T, and by again neglecting terms of order h^2/R^2 in comparison with unity there follows as a generalization of Bredt's torque-twist relation,

$$T = -\left[\frac{4A^2}{\oint (ds/Gh)} + \oint \frac{Gh^3}{3}\, ds\right] \theta. \tag{23}$$

For a homogeneous, or nearly homogeneous, closed shell the second term in (23) is negligible and (23) reduces to Bredt's formula. The case of a shell with longitudinal slit is obtained from (23) by assuming $G = 0$ over a small circumferential distance. If this is done the first term in brackets disappears and the second term correctly represents the torsional stiffness of the slit tube.

A case where both terms in brackets in (23) must be retained is given by a closed shell composed of longitudinal sections of widely differing elastic properties. For example, for a circular cylindrical shell of constant wall thickness, with $G = G_0$ from $s = 0$ to $s = (2\pi - \alpha) R$ and $G = G_1$ from $s = (2\pi - \alpha) R$ to $s = 2\pi R$, equation (23) becomes

$$T = -\left\{\frac{4\pi^2 R^3 h}{[(2\pi - \alpha)/G_0] + [\alpha/G_1]} + \frac{h^3 R}{3}[(2\pi - \alpha) G_0 + \alpha G_1]\right\}\theta. \tag{24}$$

If we assume $\alpha \ll 2\pi$ and $G_1 \ll G_0$ we may write (24) in the form

$$T = -2\pi R^3 h G_0 \left\{\frac{1}{1 + (\alpha G_0/2\pi G_1)} + \frac{1}{3}\frac{h^2}{R^2}\right\}\theta. \tag{25}$$

The first term in brackets in (25) represents the weakening influence of the insert with rigidity G_1, and when $G_1 = 0$ the case of the slit tube is reproduced. For small, but finite, values of G_1 both terms in (25) can be of equal importance.

For the same problem of the non-homogeneous circular shell we obtain stresses τ_D and τ_B from (21) and (22) in the following form

$$\tau_D = \frac{N_z}{h} = \frac{2\pi R\theta}{[(2\pi - \alpha)/G_0] + [\alpha/G_1]}, \tag{26}$$

$$\tau_B = \pm\frac{6M_z}{h^2} = \mp\left[Gh + \frac{\pi h}{[(2\pi - \alpha)/G_0] + [\alpha/G_1]}\right]\theta. \tag{27}$$

When G_1 and G_0 are of the same order of magnitude then τ_B/τ_D is of order of magnitude h/R. For sufficiently small G_1/G_0 the ratio τ_B/τ_D can be of order of unity or larger.

We conclude this note by showing that the assumptions of Love's first approximation shell theory do not allow a solution of the problem of the non-homogeneous tube and in particular of the longitudinally slit tube. Setting

$$N_z = N_s = N, \quad M_z = M_s = M, \tag{28}$$

and disregarding the equilibrium equations (3) and (4) we obtain from the torque equation (9)

$$T = \oint[M + (yx' - xy')\,N - (yy' + xx')\,M']\,ds. \tag{29}$$

The last term in (29) is integrated by parts and account is taken of the fact that N is constant. In this way (29) becomes

$$T = 2\oint\left(1 + \frac{xy' - yx'}{R}\right)M ds - 2AN. \tag{30}$$

Use of (30) in conjunction with the energy expression (15), either in its complete form or in the suitably abbreviated form

$$\Pi = \tfrac{1}{2} \oint \left[\frac{N^2}{Gh} + \frac{12\, M^2}{Gh^3} \right] ds, \tag{31}$$

leads to an incorrect version of the torque-twist relation (23). In looking for the reason for this discrepancy it is found that while it is legitimate in the present problem to disregard the difference between M_z and M_s it is not legitimate to disregard the difference between N_z and N_s. The term M_z/R in the moment equation (3) is responsible for the difference between the correct torque expression (13) and the incorrect torque expression (30).

Acknowledgment—The work reported in this article has been supported by the Office of Naval Research of the United States Navy, under a contract with the Massachusetts Institute of Technology.

REFERENCE

REISSNER, E. 1959 *On Some Problems of Shell Theory*; *Proc. Symp. 8. Naval Structural Mechanics* (Pergamon Press).

J. Mech. Phys. Solids, 1959, Vol. 7, pp. 163 to 168. Pergamon Press Ltd., London. Printed in Great Britain

DISTRIBUTION OF INTERFACE STRESS IN PLANE STRAIN AND AXIAL SYMMETRIC COMPRESSION

G. T. VAN ROOYEN* and W. A. BACKOFEN†

(*Received 3rd February* 1959)

SUMMARY

MEASUREMENTS have been made of the stress distribution in compressing lead between roughened steel plates with sticking over the interface. The method involved use of pressure sensitive pins embedded in one plate. A general agreement was found between plane strain theory (HILL *et al.* 1951) and experiment for the condition examined of $w_0/h_0 = 12$. The plane strain solution was also found to describe the pressure distribution over most of the interface in axial symmetric compression; over a narrow region at the periphery, however, a pressure discontinuity occurred which resembled a plateau and was dependent upon geometry, becoming less apparent with d_0/h_0 increasing from 4 to 12.

1. INTRODUCTION

SOLUTIONS of various problems in plasticity have been made with slip-line field analysis for the condition of plane strain (HILL 1950). In particular, the compression of a non-hardening plastic-rigid block between rough plates has been investigated by PRANDTL (1923) and more recently by HILL *et al.* (1951), with differences in computed pressure distributions. A solution for the axial symmetric case has been made by SHIELD (1955), while an approximate treatment has been given by SIEBEL (1923) for the compression of a cylinder with low friction and the assumption of equal stresses in the radial and circumferential directions. SCHROEDER and WEBSTER (1949) have also used the analysis of SIEBEL to deal with large values of the friction coefficient. This is further discussed by BISHOP (1958).

Analytical study of the axial symmetric problem would appear to be an involved undertaking, yet it would be of much interest to know: (1) the stress distribution over the interface for both plane strain and axial symmetric compression with plastic shearing at the interface, and (2) the extent to which the plane-strain solution fits the axial symmetric case. Experiments described below were made to develop such information.

2. PROCEDURES

Chemically pure lead was used as a convenient test material approximating the theoretical non-hardening solid. Both square and cylindrical pieces were carefully machined, to minimize distortion, from rolled plate of 0·375 thickness. Square

*National Mechanical Engineering Research Institute, South Africa Council for Scientific and Industrial Research, Pretoria.

†Massachusetts Institute of Technology, Cambridge, Massachusetts.

samples were 4·5 × 4·5 in. to give an initial width/thickness ratio, w_0/h_0, of twelve. Disks were turned with various diameters to give a range of initial diameter/thickness ratio, d_0/h_0, of four to twelve. Surfaces of all specimens were abraded with 240-grit emery cloth before compression between steel plates uniformly roughened by sand blasting. Such preparation was found to give the condition of no relative displacement at the specimen-platen interface. Plane strain was produced by confining the square specimens in a channel on one plate, formed by polished and lubricated steel guides, into which the other plate fitted closely. In all cases the plates overlapped the specimen.

Normal pressure, σ, was measured with the pressure-sensitive pin technique (van Rooyen and Backofen 1957). From experience in the previous work, a solid steel pin was designed with a 1/16in. diameter, 1/4in. length, and a slightly reduced midsection around which a length of strain-gauge wire was wrapped and cemented. The pin was lapped into a cavity bored in the plate, firmly seated with lead wires running through fine holes from the back of the plate, and finally ground flush with the plate surface; it was at this point that the surface was sand blasted. Sensitivity of the pin was regularly checked by a calibration with hydrostatic pressure applied over the pin and surrounding area in the surface of the plate. In all data given below maximum uncertainty in measurement is estimated at 4 per cent.

There was much freedom in locating the pin with cylindrical specimens, but for the plane strain case, measurements were confined to a position through the guide channel at the mid-point. A number of measurements, usually from six to ten, were made at as many locations on each specimen. The procedure was to make reductions of a small, nominally constant, amount (1 – 2 per cent) for each measurement on a given specimen; an essentially constant pin load was indicated at the time of measurement. Thus, the change in specimen geometry was relatively small and a substantial amount of data could be obtained for a particular geometry with a single specimen before its size was altered too greatly.

Some measurements were also made, on cylindrical specimens, of the interface shear stress, τ, which are reported in terms of the friction coefficient, $\mu = \tau/\sigma$. A pair of pins was used in these experiments, each one inclined 30° and in opposite directions to the platen normal. Such a design can give values of τ (and μ) with rather high precision; the reason for oblique pins has been discussed (van Rooyen and Backofen 1957) and additional data obtained with the technique are forthcoming.

3. Results

The variation of normal pressure from centre to edge is given in Fig. 1 for both types of deformation, with w_0/h_0 and $d_0/h_0 = 12$ and r defining distance in each case. Several specimens were used, and measurements on each began with the pin located at its position closest to the free edge. The datum point is plotted to give the location of the measurement relative to the free edge, which is considered fixed. Accordingly, some inaccuracy is introduced because, in effect, the origin is displaced to the left as the pin is moved inwards to make the successive measurements on any one specimen. However, this geometry change is relatively slight, being a maximum of 15 – 20 per cent in w_0/h_0. Furthermore, the data from different specimens blend satisfactorily.

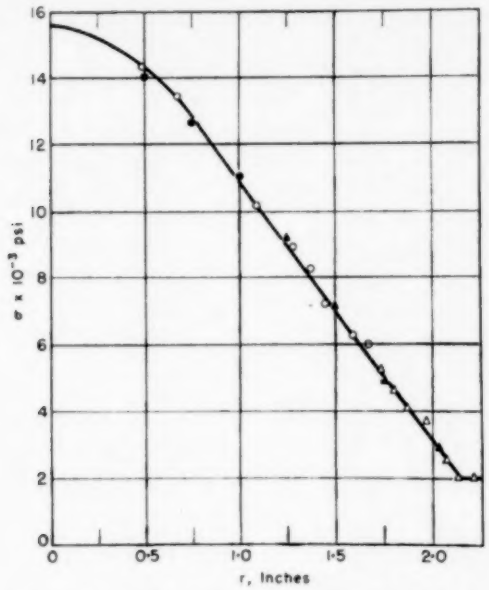

Fig. 1. Pressure distribution for axial symmetric and plane strain compression of lead with sticking at the interface. $d_0/h_0 = w_0/h_0 = 12$. ●, ▲. axial symmetric ; ○, △ : plane strain.

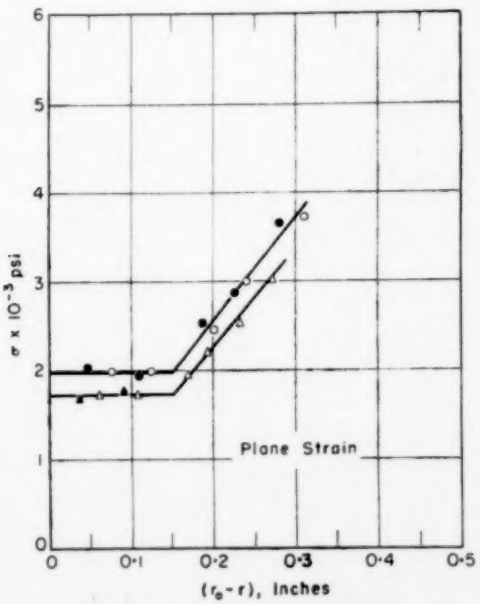

Fig. 2. Pressure distribution on lead. Two different lots of material are represented by the two curves. $w_0/h_0 = 12$.

Additional experiments were made to examine details of the pressure distribution near the edge with the results given in Figs. 2 and 3. In plane strain, the plateau extended inwards about 5/32in., or approximately $2\frac{1}{2}$ pin diameters ($\sim 0{\cdot}40h_0$).

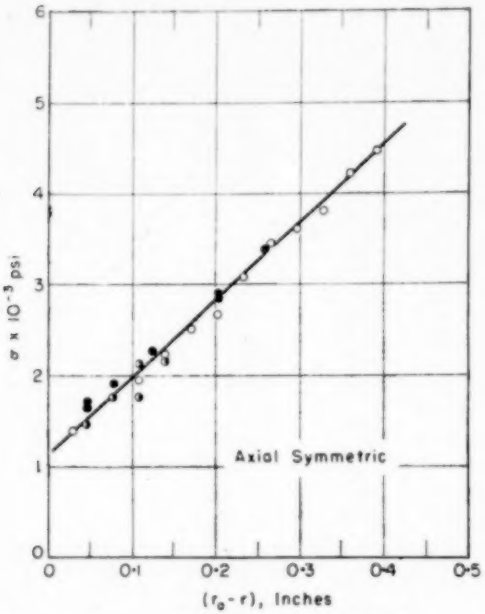

Fig. 3. Pressure distribution on lead. $d_0/h_0 = 12$.

In tests on disks the pin was located as close as possible to the edge, without overlapping, yet no clear indication of a plateau was found. Two alternatives were considered next: either a plateau is not a characteristic of the pressure distribution over a cylinder, or the existence of the plateau is influenced by the geometry of the specimen.

To survey any possible geometry effect, without the tedium of point-by-point measurements, experiments were made on disks of $d_0/h_0 = 4$, 5·34, 6·67, 8·00, 9·34, and 10·67 in which only one-half of the pin was located on the disk surface at the beginning. Upon compression, the pin, in effect, was displaced inwards and gave a continuous record of pressure variation from the free edge. Tracings of actual records are shown in Fig. 4 with the abscissa calibrated approximately in terms of movement of the pin from the free edge. A dependence on geometry is demonstrated with the slope marked A on the $d_0/h_0 = 6{\cdot}67$ record most effected. As A increases with d_0/h_0, it is reasonable to expect difficulty in detecting a pressure plateau, or discontinuity of any sort, even with pins as small in diameter as those of the present work.

As a final experiment, measurements were made of both τ and σ near the centre of a disk for $d_0/h_0 = 12$ and 6, the latter being produced by stacking two disks of $h_0 = 0{\cdot}375$ and $d_0 = 4{\cdot}50$ (Fig. 5). Values of σ and μ are located on the abscissa axis, as before, at correct distances from the free edge at the time of measurement.

However, data in Fig. 5 were obtained by locating pins first at the position closest to the disk centre and then moving outwards for subsequent measurements.

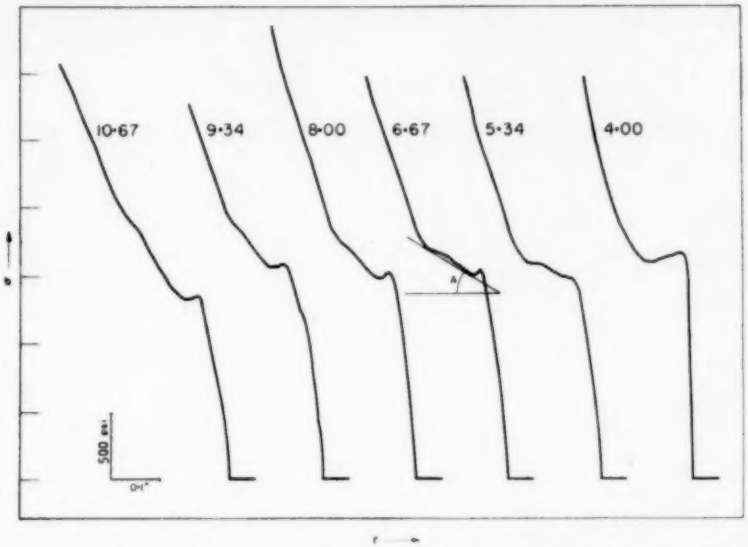

Fig. 4. Experimental records showing variation of pressure with distance from free edge, for lead disks of different d_0/h_0.

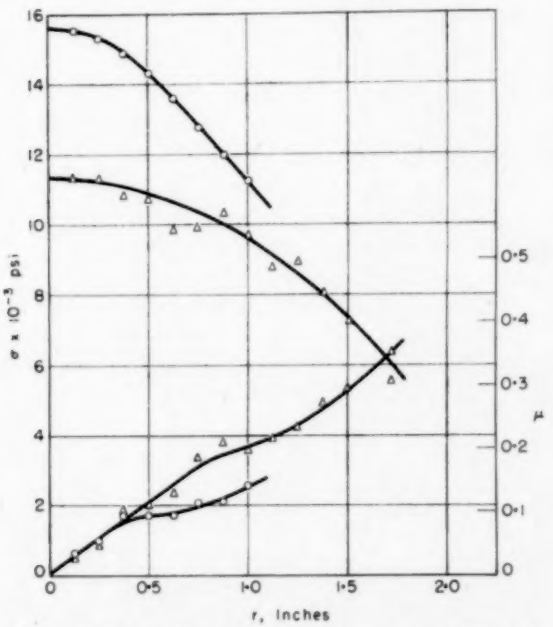

Fig. 5. Variation of pressure, σ, and friction coefficient, μ, on lead disks. △, $d_0/h_0 = 6$; ○, $d_0/h_0 = 12$.

The trend in μ is consistent with plastic shearing at the interface; if τ is the shear yield strength of lead and is more or less constant with position, then $\mu = \tau/\sigma$ must

decrease on approaching the centre with σ steadily increasing. The linear section of μ vs. r may well be associated with the development of a central non-plastic zone. The eventual joining of the curves for both d_0/h_0 near the centre also suggests such development.

4. Discussion

There is at least a general agreement between theoretical and experimental pressure distributions in plane strain. A pressure plateau exists at the edge, as predicted by Hill *et. al.* (1951) with an inclined straight line representing pressure increasing over the interface (Figs. 1 and 2). Although the theory gives a distribution oscillating slightly about the line, the amplitude is so small that its absence in the experimental results is reasonably expected ; the straight line would, therefore, be taken to represent the less exact solution of Prandtl (1923).

The outstanding disagreement is found in a pressure plateau which is too short experimentally. The calculated length is $h/\sqrt{2} = 0{\cdot}265$in. while the measurement, approximately 0·15in., is smaller by nearly a factor of two. If the plateau were placed at a higher pressure level, however, to obtain increased length, the ratio (extrapolated pressure, at $r = r_0$)/(plateau height) would be greatly reduced. To obtain a value of this ratio consistent with theory would demand a substantial decrease in the slope of the straight line distribution.

Accordingly, experimental support has not been provided for all details of the analysis. Differences between conditions of theory and experiment would seem to be important in this regard. Full sticking over the interface was assumed and reasonably expected on the basis of observations such as those in Fig. 5. Still, some departure from this condition might well have occurred at the small reductions particularly near the edge. With reference to the disk compression, it may be argued that the initial pressure drop on advancing inwards from the periphery in Fig. 4 is not a characteristic of sticking, but rather it represents a sliding-to-sticking friction transition.

From the experiments on disks, the pressure distribution over the bulk of the interface is the same as that in plane strain. This finding may be viewed as in accord with the Haar-Kármán hypothesis, considered in analysis by Shield (1955), of equality between the circumferential stress and one of the principal stresses in the meridian plane. Near the periphery of a disk, however, a pressure discontinuity exists, dependent upon geometry and becoming less marked with d_0/h_0 increasing beyond about ten.

References

Bishop, J. F. W.	1958	*J. Mech. Phys. Solids* **6**, 132.
Hill, R.	1950	*Mathematical Theory of Plasticity* (Clarendon Press, Oxford).
Hill, R., Lee, E. H. and Tupper, S. J.	1951	*J. Appl. Mech.* **18**, 46.
Prandtl, L.	1923	*Z. angew. Math Mech.* **3**, 401.
Shield, R. T.	1955	*Proc. Roy. Soc. A.* **233**, 267.
Schroeder, W. and Webster, D. A.	1949	*J. Appl. Mech.* **16**, 289.
Siebel, E.	1923	*Stahl u. Eisen*, Dusseldorf **43**, 129.
van Rooyen, G. T. and Backofen, W. A.	1956	*J. Iron and Steel Inst.* **186**, 235.

J. Mech. Phys. Solids, 1959, Vol. 7, pp. 169 to 181. Pergamon Press Ltd., London. Printed in Great Britain

THE LOAD CARRYING CAPACITIES OF CYLINDRICAL SHELLS SUBJECTED TO A RING OF FORCE

By G. Eason
King's College, Newcastle upon Tyne

(*Received 3rd February*, 1959)

Summary

Stress fields and associated velocity fields are obtained under conditions of axial symmetry, for circular cylindrical shells of rigid – plastic material satisfying the Tresca yield condition. The particular problem of a shell of any length subjected to a ring of force is considered in detail.

1. Introduction

Drucker (1953) first considered the plastic collapse of circular cylindrical shells under conditions of axial symmetry. The yield condition for rigid–plastic material obeying the Tresca yield criterion was formulated in terms of the axial bending moment and the circumferential stress-resultant, and an approximated version of this condition was used to obtain upper and lower bounds to the collapse pressure of an infinitely long shell subjected to constant applied load. Drucker also obtained some results for the exact Tresca yield condition by integrating the basic differential equations numerically. The same approximated yield condition was also used by Eason and Shield (1955), and Hodge (1954) applied a different approximated yield condition to solve other statical circular cylindrical shell problems.

In this paper the equations with the exact Tresca yield condition are integrated for a circular cylindrical shell of any length subjected to a ring of force. The value of the collapse force is found for all values of the shell length. Five possible types of deformation are found to arise, depending on the length of the shell. These five cases are similar in principle to those found by Eason and Shield (1955) in considering the same problem with an approximate yield condition. Velocity fields associated with the stress fields are also obtained, and some numerical results are presented graphically.

2. Basic Equations

The stress and moment resultants acting upon an element of a cylindrical shell under axially symmetric loading conditions are shown in Fig. 1. The axial stress resultant N_x is assumed zero, and since the circumferential bending moment M_ϕ does not enter explicitly into the equations of equilibrium, or yield condition, it may be ignored. In axially symmetric loading the equations of equilibrium are

$$\frac{dQ}{dx} = p - \frac{N}{R}, \tag{1}$$

$$\frac{dM}{dx} = Q, \tag{2}$$

where M is the axial bending moment, N the circumferential stress resultant, Q the shearing force resultant, R the radius of the shell, x the axial co-ordinate and p

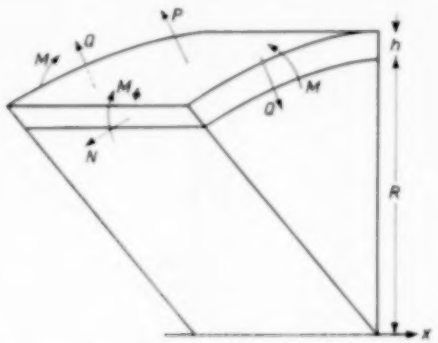

Fig. 1. Stresses on element of shell.

the applied lateral pressure, considered positive when it acts outwards. It is convenient to rewrite (1) and (2) in the dimensionless forms

$$\frac{dq}{d\xi} = \psi - n, \tag{3}$$

$$\frac{dm}{dx} = q, \tag{4}$$

so that, combining these equations,

$$\frac{d^2 m}{d\xi^2} = \psi - n, \tag{5}$$

where

$$\left.\begin{aligned} &\xi = x/(Rh)^{\frac{1}{2}}, \quad \psi = pR/\sigma_0 h, \quad q = Q(Rh)^{\frac{1}{2}}/\sigma_0 h^2, \\ &m = M/\sigma_0 h^2, \quad n = N/\sigma_0 h, \end{aligned}\right\} \tag{6}$$

h is the thickness of the shell and σ_0 the yield stress of the material of the shell.

The yield condition for cylindrical shells obeying the Tresca yield criterion was first formulated by DRUCKER (1953). The maximum permissible values of m and n are $\frac{1}{4}$ and 1 respectively. The yield curve (Fig. 2) is symmetrical about both axes. The approximations to the yield condition used by DRUCKER to obtain upper and lower bounds to the collapse pressure of an infinitely long cylindrical shell subjected to constant applied load are indicated by the broken lines. The effect of the shearing force resultant on the yield condition is neglected. In plastic régimes BC and CD

$$m = \zeta n\,(1 - n), \tag{7}$$

with $$\zeta = \begin{cases} -1 \text{ for plastic régime } BC, \\ +1 \text{ for plastic régime } CD. \end{cases} \tag{8}$$

In plastic régimes EF and FA

$$m = \zeta n\,(1 + n), \tag{9}$$

with $$\zeta = \begin{cases} -1 \text{ for plastic régime } EF, \\ +1 \text{ for plastic régime } FA. \end{cases} \tag{10}$$

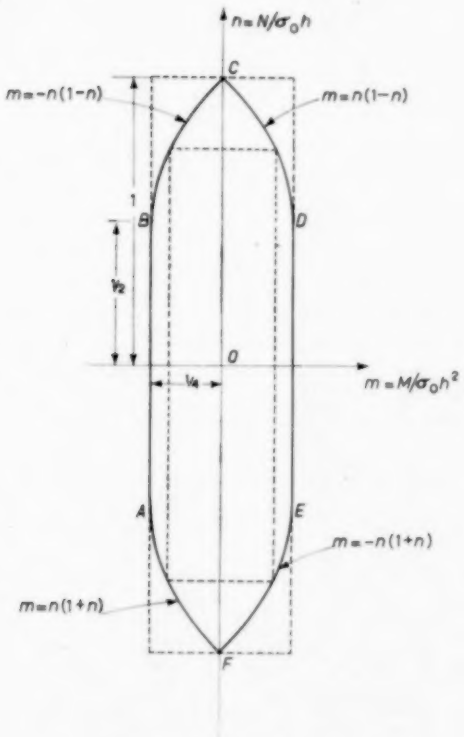

Fig. 2. Yield condition.

Let u be the radial velocity of the shell. The strain-rate vector has components $\varkappa h = h\,d^2u/dx^2$, $\epsilon = u/R$ associated with the bending moment M and the stress resultant N respectively. During deformation the strain-rate vector must be normal to the yield curve, so that in plastic régimes BC and CD

$$(2n - 1)\frac{d^2u}{d\xi^2} = \zeta u, \tag{11}$$

and $u \Big/ \dfrac{d^2u}{d\xi^2}$ lies between O and ζ. In plastic régimes EF and FA

$$(2n + 1)\frac{d^2u}{d\xi^2} = -\zeta u, \tag{12}$$

and $u \Big/ \dfrac{d^2 u}{d\xi^2}$ lies between O and ζ.

3. Integration of the Basic Equations

The integration of the basic equations given in Section 2 is carried out here for zero applied pressure, the same method may be used when the applied pressure is constant.

(i) *Plastic régimes BC and CD*

Equations (5) and (7) determine the stresses for material in plastic régimes BC and CD. Making the change of variable defined by

$$t = 2n - 1, \quad v = \frac{dt}{d\xi}, \qquad (0 \leqslant t \leqslant 1), \tag{13}$$

these equations combine to give

$$t^2 v^2 = \zeta\,(t^2 + \tfrac{2}{3} t^3 + A), \tag{14}$$

$$\frac{1}{v} = \frac{d\xi}{dt} = \frac{\pm t}{\{\zeta\,(t^2 + \tfrac{2}{3} t^3 + A)\}^{\frac{1}{2}}}, \tag{15}$$

where A is a constant of integration, and in (15) the correct sign is taken in accordance with the physical conditions of the problem under consideration. With this change of variable

$$m = \tfrac{1}{4}\,\zeta\,(1 - t^2), \qquad \frac{dm}{d\xi} = q = -\tfrac{1}{2}\,\zeta t v. \tag{16}$$

For non-zero A, (15) may be integrated in terms of elliptic integrals of the first and second kinds (Gröbner and Hofreiter 1949, p. 76) but it is generally simpler to integrate numerically.

Equation (11) gives velocity fields associated with the stress fields defined by (14) and (15) in the form

$$tv\frac{du}{d\xi} = t^2 v^2 \frac{du}{dt} = \zeta u\,(1 + t) + B, \tag{17}$$

$$\frac{d}{dt}\left(\frac{u}{tv}\right) = \frac{B}{t^2 v^3}, \tag{18}$$

where B is a constant of integration.

(ii) *Plastic régimes EF and FA*

Stress fields and associated velocity fields for material in plastic régimes EF and FA are determined by (5), (9) and (12). Making the change of variable defined by

$$t = -(2n + 1), \qquad v = \frac{dt}{d\xi}, \qquad (0 \leqslant t \leqslant 1), \tag{19}$$

these equations give

$$t^2 v^2 = \zeta\,(t^2 + \tfrac{2}{3} t^3 + C), \tag{20}$$

$$\frac{1}{v} = \frac{d\xi}{dt} = \frac{\pm t}{\{\zeta\,(t^2 + \tfrac{2}{3} t^3 + C)\}^{\frac{1}{2}}}, \tag{21}$$

$$m = -\tfrac{1}{4}\zeta(1-t^2), \qquad q = \frac{dm}{d\xi} = \tfrac{1}{2}\zeta tv, \tag{22}$$

$$tv\frac{du}{d\xi} = tv^2\frac{du}{dt} = \zeta u(1+t) + D, \tag{23}$$

$$\frac{d}{dt}\left(\frac{u}{tv}\right) = \frac{D}{t^2 v^3}, \tag{24}$$

where C and D are constants of integration, and the correct sign in (21) is determined by physical conditions.

These results will now be applied to a particular problem.

4. Ring of Force

Consider a tube of any length subjected to a ring of lateral force of magnitude P, in terms of the dimensionless forms (6). The origin of the dimensionless co-ordinate ξ is taken at the point of application of the force, and the free ends of the tube are given by $\xi = -a$, $\xi = b$ with the assumption $b \geqslant a$. The boundary conditions are $m = q = 0$ at the ends of the tube, and at the origin q has a discontinuity of amount P, so that the lateral pressure is zero everywhere except at $\xi = 0$.

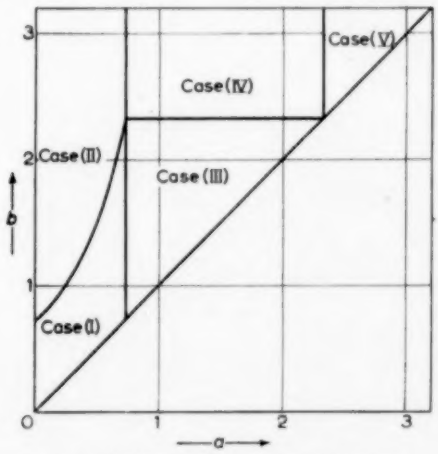

Fig. 3. Limiting values of possible cases.

Five different cases arise according to the values of a and b (Fig. 3). These cases are distinguished by the number of hinge circles (sections of the tube at which $|m| = \frac{1}{4}$) which occur during plastic deformation.

Referring to Figs. 4 – 8, we have in all cases:

sections OK, ON are in plastic régime BC;

sections KJ, NM are in plastic régime CD;

sections JI, ML are in plastic régime CD;

sections IH, LG are in plastic régime EF.

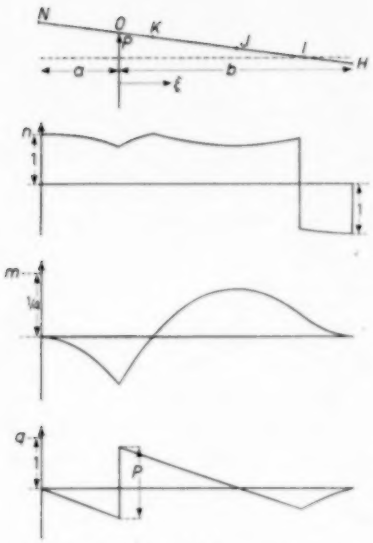

Fig. 4. Stress distribution, case (i)

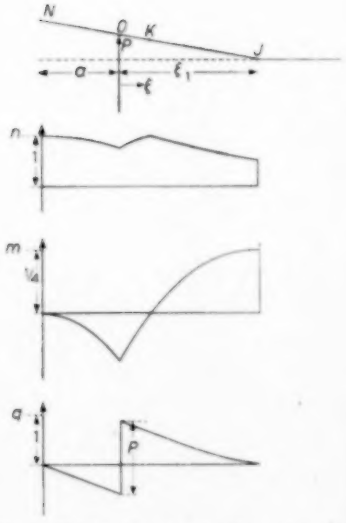

Fig. 5. Stress distribution in plastic region, case (ii).

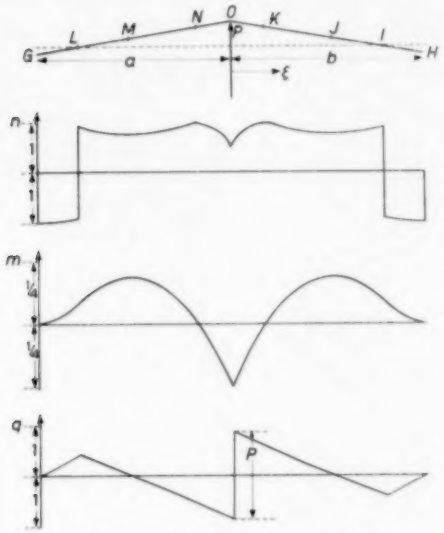

Fig. 6. Stress distribution, case (iii).

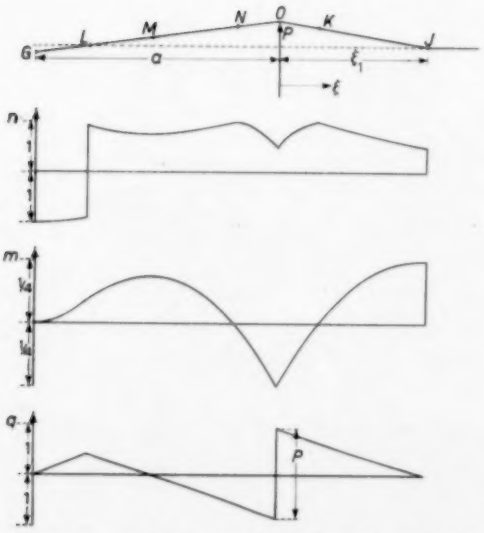

Fig. 7. Stress distribution in plastic region, case (iv)

We also have $t = s$ or 0 at 0 ; $m = 0$, $t = 1$ at K and N ; $q = 0$, $t = r_1$ or 0 at J ; $q = 0$, $t = r_2$ or 0 at M ; $u = 0$, $t = p_1$ at I ; $u = 0$, $t = p_2$ at L ; $q = 0$, $t = 1$ at G and H.

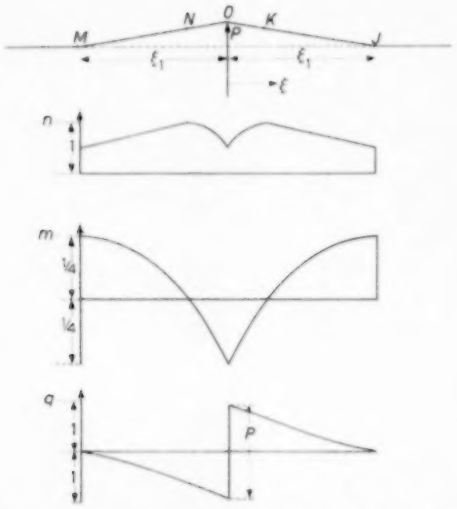

Fig. 8. Stress distribution in plastic region, case (v)

At the boundaries of the plastic régimes t and u are always continuous, q is continuous except at the origin, and $du/d\xi$ is continuous except at a hinge circle. At the points I and L, n has a discontinuity of amount $(1 + p_1)$ and $(1 + p_2)$ respectively. In Figs. 5, 7 and 8, ξ_1 denotes the distance of the yield hinge J from the origin. The stress fields shown are the result of calculations in particular cases. In (ii), (iv) and (v) extensions of the stress field into the rigid region are not given, but these may be obtained. For instance, an extension to the stress field in (ii) may be obtained by assuming that the section of the shell immediately beyond J (Fig. 5) is fully plastic the stresses being given by (27), (28) of (i), and that the remainder of the shell is unstressed.

Due to the algebraic complexity of the results for the velocity fields, these will only be presented in (ii) and (v) when they take relatively simple forms. The conditions $u = 0$, $du/d\xi = -\eta$ are taken at J ; the latter condition is taken for convenience, but it may easily be converted into one concerning the velocity at the origin. Velocity fields for (i), (iii) and (iv) may be obtained by integrating (17), (18), (23) and (24). The velocity fields indicated in Figs. 4 – 8 are intended to show the general form of the deformation and are not the result of calculation.

Before considering particular cases in detail it is convenient to make the definitions

$$I(t) = \sqrt{3}\int_0^t \frac{t\,dt}{(5 - 3t^2 - 2t^3)^{\frac{1}{2}}}$$

$$= \frac{1}{\sqrt{3}}\left\{\sqrt{5} - \frac{(5 - 3t^2 - 2t^3)^{\frac{1}{2}}}{1+t} - \int_0^t \frac{(5 - 3t^2 - 2t^3)^{\frac{1}{2}}\,dt}{(1+t)^2}\right\}, \tag{25}$$

$$J(t, r) = \sqrt{3}\int_r^t \frac{t\,dt}{(3t^2 + 2t^3 - 3r^2 - 2r^3)^{\frac{1}{2}}}$$

$$= \frac{1}{\sqrt{3}}\left\{\frac{3t^2 + 2t^3 - 3r^2 - 2r^3)^{\frac{1}{2}}}{1+t} + \int_r^t \frac{(3t^2 + 2t^3 - 3r^2 - 2r^3)^{\frac{1}{2}}\,dt}{(1+t)^2}\right\}. \tag{26}$$

(i) *No hinge circles*

In this case, shown in Fig. 4, $|m| < \frac{1}{4}$ everywhere and $u = 0$ at I.

In section HI,

$$\left.\begin{aligned} m &= \tfrac{1}{4}(1 - t^2), \qquad n = -\tfrac{1}{2}(1+t), \\ 2q &= -tv = -\frac{1}{\sqrt{3}}(5 - 3t^2 - 2t^3)^{\frac{1}{2}}, \\ \xi &= b + I(t) - I(1), \end{aligned}\right\} \tag{27}$$

In section IJ,

$$\left.\begin{aligned} m &= \tfrac{1}{4}(1 - t^2), \qquad n = \tfrac{1}{2}(1+t), \\ 2q &= -tv = -\frac{1}{\sqrt{3}}(3t^2 + 2t^3 - 3r_1^2 - 2r_1^3)^{\frac{1}{2}}, \\ \xi &= b + I(p_1) - I(1) - J(p_1, r_1) + J(t, r_1); \end{aligned}\right\} \tag{28}$$

In section JK,

$$\left.\begin{aligned} m &= \tfrac{1}{4}(1 - t^2), \qquad n = \tfrac{1}{2}(1+t), \\ 2q &= -tv = \frac{1}{\sqrt{3}}(3t^2 + 2t^3 - 3r_1^2 - 2r_1^3)^{\frac{1}{2}}, \\ \xi &= b + I(p_1) - I(1) - J(p_1, r_1) - J(t, r_1); \end{aligned}\right\} \tag{29}$$

In section KO,

$$\left.\begin{aligned} m &= -\tfrac{1}{4}(1 - t^2), \qquad n = \tfrac{1}{2}(1+t), \\ 2q &= tv = \frac{1}{\sqrt{3}}(10 - 3r_1^2 - 2r_1^3 - 3t^2 - 2t^3)^{\frac{1}{2}}, \\ \xi &= \sqrt{3}\int_s^t \frac{t\,dt}{(10 - 3r_1^2 - 2r_1^3 - 3t^2 - 2t^3)^{\frac{1}{2}}}; \end{aligned}\right\} \tag{30}$$

In section ON,

$$\left.\begin{aligned} m &= -\tfrac{1}{4}(1 - t^2), \qquad n = \tfrac{1}{2}(1+t), \\ 2q &= tv = -\frac{1}{\sqrt{3}}(5 - 3t^2 - 2t^3)^{\frac{1}{2}}, \\ \xi &= I(s) - I(t); \end{aligned}\right\} \tag{31}$$

with the further relations

$$\left.\begin{aligned} &3r_1^2 + 2r_1^3 + 5 - 6p_1^2 - 4p_1^3 = 0,\\ &2P\sqrt{3} = (5 - 3s^2 - 2s^3)^{\frac{1}{2}} + (10 - 3r_1^2 - 2r_1^3 - 3s^2 - 2s^3)^{\frac{1}{2}},\\ &a = I(1) - I(s),\\ &b = I(1) - I(p_1) + J(p_1, r_1) + J(1, r_1)\\ &\qquad + \sqrt{3}\int_s^1 \frac{t\,dt}{(10 - 3r_1^2 - 2r_1^3 - 3t^2 - 2t^3)^{\frac{1}{2}}}; \end{aligned}\right\} \tag{32}$$

connecting a, b, p_1, r_1, s, and P. Once r_1 and s are prescribed equations (32) enable a, b, p_1, and P to be calculated.

(ii) *One yield hinge at J*

In this case, shown in Fig. 5, there is one yield hinge at J where $m = \frac{1}{4}$ and $q = 0$. The conditions on the velocity field are taken as $u = 0$, $du/d\xi = -\eta$ at J.
In section JK,

$$\left.\begin{aligned} &m = \tfrac{1}{4}(1 - t^2), \qquad n = \tfrac{1}{2}(1 + t),\\ &2q = -tv = \frac{t}{\sqrt{3}}(3 + 2t)^{\frac{1}{2}},\\ &\xi = \xi_1 - \sqrt{3}\{(3 + 2t)^{\frac{1}{2}} - \sqrt{3}\},\\ &u = -\eta v = \frac{\eta t}{\sqrt{3}}(3 + 2t)^{\frac{1}{2}}; \end{aligned}\right\} \tag{33}$$

In section KO,

$$\left.\begin{aligned} &m = -\tfrac{1}{4}(1 - t^2), \qquad n = \tfrac{1}{2}(1 + t),\\ &2q = tv = \frac{1}{\sqrt{3}}(10 - 3t^2 - 2t^3)^{\frac{1}{2}},\\ &\xi = \sqrt{3}\int_s^t \frac{t\,dt}{(10 - 3t^2 - 2t^3)^{\frac{1}{2}}},\\ &u = \eta v = \frac{\eta}{\sqrt{3}}(10 - 3t^2 - 2t^3)^{\frac{1}{2}}; \end{aligned}\right\} \tag{34}$$

In section ON equations (31) hold together with

$$u = -\frac{\eta}{\sqrt{3}}(5 - 3t^2 - 2t^3)^{\frac{1}{2}} + 2P\eta(1 + s)\left\{\frac{1}{1 + t} + (5 - 3t^2 - 2t^3)^{\frac{1}{2}}\int_s^t \frac{dt}{(5 - 3t^2 - 2t^3)^{\frac{1}{2}}(1 + t)^2}\right\}. \tag{35}$$

The equations connecting a, s, P and ξ_1, are

$$\left.\begin{aligned} &2P\sqrt{3} = (10 - 3s^2 - 2s^3)^{\frac{1}{2}} + (5 - 3s^2 - 2s^3)^{\frac{1}{2}},\\ &a = I(1) - I(s),\\ &\xi_1/\sqrt{3} = \sqrt{5} - \sqrt{3} + \int_s^1 \frac{t\,dt}{(10 - 3t^2 - 2t^3)^{\frac{1}{2}}}; \end{aligned}\right\} \tag{36}$$

so that once s is prescribed the other quantities may be calculated.

(iii) *One yield hinge at* 0

In this case, shown in Fig. 6, there is one yield hinge at 0 where $m = -\frac{1}{4}$. The velocity is zero at I and L. In sections III, IJ and JK (27), (28) and (29) hold respectively and in section KO (30) holds with $s = 0$.

In section GL,

$$\left.\begin{aligned} m &= \tfrac{1}{4}(1-t^2), \qquad n = -\tfrac{1}{2}(1+t), \\ 2q &= -tw = \frac{1}{\sqrt{3}}(5-3t^2-2t^3)^{\frac{1}{2}}, \\ \xi &= -a + I(1) - I(t); \end{aligned}\right\} \tag{37}$$

In section LM,

$$\left.\begin{aligned} m &= \tfrac{1}{4}(1-t^2), \qquad n = \tfrac{1}{2}(1+t), \\ 2q &= -tw = \frac{1}{\sqrt{3}}(3t^2+2t^3-3r_2^2-2r_2^3)^{\frac{1}{2}}, \\ \xi &= -a + I(1) - I(p_2) + J(p_2, r_2) - J(t, r_2); \end{aligned}\right\} \tag{38}$$

In section MN,

$$\left.\begin{aligned} m &= \tfrac{1}{4}(1-t^2), \qquad n = \tfrac{1}{2}(1+t), \\ 2q &= -tw = -\frac{1}{\sqrt{3}}(3t^2+2t^3-3r_2^2-2r_2^3)^{\frac{1}{2}}, \\ \xi &= -a + I(1) - I(p_2) + J(p_2, r_2) + J(t, r_2); \end{aligned}\right\} \tag{39}$$

In section NO,

$$\left.\begin{aligned} m &= -\tfrac{1}{4}(1-t^2), \quad n = \tfrac{1}{2}(1+t), \\ 2q &= tw = -\frac{1}{\sqrt{3}}(10-3r_2^2-2r_2^3-3t^2-2t^3)^{\frac{1}{2}}, \\ \xi &= -\sqrt{3}\int_0^t \frac{t\,dt}{(10-3r_2^2-2r_2^3-3t^2-2t^3)^{\frac{1}{2}}}; \end{aligned}\right\} \tag{40}$$

together with the equations

$$\left.\begin{aligned} 3r_1^2 + 2r_1^3 + 5 - 6p_1^2 - 4p_1^3 &= 0, \\ 3r_2^2 + 2r_2^3 + 5 - 6p_2^2 - 4p_2^3 &= 0 \\ 2P\sqrt{3} &= (10-3r_1^2-2r_1^3)^{\frac{1}{2}} + (10-3r_2^2-2r_2^3)^{\frac{1}{2}}, \\ a &= I(1) - I(p_2) + J(p_2, r_2) + J(1, r_2) \\ &\quad + \sqrt{3}\int_0^1 \frac{t\,dt}{(10-3r_2^2-2r_2^3-3t^2-2t^3)^{\frac{1}{2}}}, \\ b &= I(1) - I(p_1) + J(p_1, r_1) + J(1, r_1) \\ &\quad + \sqrt{3}\int_0^1 \frac{t\,dt}{(10-3r_1^2-2r_1^3-3t^2-2t^3)^{\frac{1}{2}}}; \end{aligned}\right\} \tag{41}$$

connecting a, b, p_1, p_2, r_1, r_2 and P, so that once r_1 and r_2 are prescribed the remaining quantities may be calculated.

(iv) *Two yield hinges*

In this case, shown in Fig. 7, there is a yield hinge at 0 with $m = -\frac{1}{4}$ and one at J with $m = \frac{1}{4}$. In sections JK and KO of the shell (33) and (34), (with $s = 0$), hold respectively and in sections GL, LM, MN and NO of the shell (37), (38), (39) and (40) hold. The equations connecting a, p_2, r^2, P and ξ_1, are

$$
\left.\begin{aligned}
3r_2^2 + 2r_2^3 + 5 - 6p_2^2 - 4p_2^3 &= 0,\\
2P\sqrt{3} &= \sqrt{10} + (10 - 3r_2^2 - 2r_2^3)^{\frac{1}{2}},\\
\xi_1/\sqrt{3} &= \sqrt{5} - \sqrt{3} + \int_0^1 \frac{t\,dt}{(10 - 3t^2 - 2t^3)^{\frac{1}{2}}},\\
a &= I(1) - I(p_2) + J(p_2, r_2) + J(1, r_2)\\
&\quad + \sqrt{3}\int_0^1 \frac{t\,dt}{(10 - 3r_2^2 - 2r_2^3 - 3t^2 - 2t^3)^{\frac{1}{2}}};
\end{aligned}\right\} \qquad (42)
$$

so that $\xi_1 = 1{\cdot}190$, and once r_2 is prescribed a, p_2 and P may be calculated.

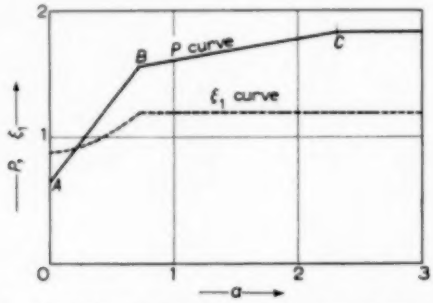

Fig. 9. Variation of P and ξ_1 with a, semi-infinite shell.

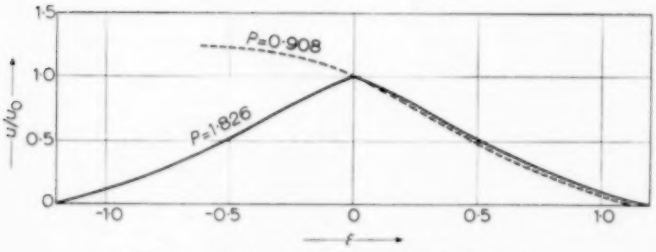

Fig. 10. Velocity fields, semi-infinite shell.

(v) *Three yield hinges*

In this case $a, b > 2{\cdot}33$ and there is symmetry about O with yield hinges at O, where $m = -\frac{1}{4}$, and at J and M, where $m = \frac{1}{4}$. Referring to Fig. 8, (33) and (34) hold in sections JK and KO respectively and the equations for P and ξ_1 are

$$
\left.\begin{aligned}
P &= \sqrt{10}/\sqrt{3} = 1{\cdot}826,\\
\xi_1/\sqrt{3} &= \sqrt{5} - \sqrt{3} + \int_0^1 \frac{t\,dt}{(10 - 3t^2 - 2t^3)^{\frac{1}{2}}},
\end{aligned}\right\} \qquad (43)
$$

so that $\xi_1 = 1{\cdot}190$.

The stress distributions shown in Figs. 4 – 8 are all the result of calculations for a typical value of P within each case considered. These stress fields have a close resemblance to those obtained by EASON and SHIELD (1955) using an approximation to the yield curve.

Due to the general nature of the problem considered, further numerical results are only given for a semi-infinite shell. Fig. 9 shows the variation of P and ξ_1 with a, the distance of P from the free end of the shell. The sections AB and BC of the P-curve are very nearly linear. In Fig. 10 the velocity fields are shown for $P = 0{\cdot}908$ (within (ii)) and $P = 1{\cdot}826$. The second of these is the same field as for an infinitely long shell and is defined by the equations of (v). In both cases the velocities are given in terms of u_0, the velocity at the origin.

Note added in proof : The yield condition (7) for régimes BC and CD may be written more conveniently

$$f = \zeta m - n(1 - n) = 0$$

where ζ is defined by (8). The strain-rate vector components are then given by

$$\frac{d^2 u}{d\xi^2} = \lambda \frac{\partial f}{\partial m} = \lambda \zeta, \qquad u = \lambda \frac{\partial f}{\partial n} = \lambda (2n - 1),$$

where λ has to be a non-negative quantity. In the second of these equations $n \geqslant \frac{1}{2}$, so that the condition for λ to be non-negative is $u \geqslant 0$. In plastic régimes EF and FA the corresponding condition is $u \leqslant 0$. These conditions are satisfied by the velocity fields given here.

Acknowledgment

The author wishes to thank Dr. R. T. Shield for helpful discussion of this problem, and Miss S. Boyd for assistance with the computation.

References

Drucker, D. C. 1953 *Proc. 1st Midw. Conf. Solid Mech.* (Urbana), p. 158 (A.S.M.E., New York).

Eason, G. and Shield, R. T. 1955 *J. Mech. Phys. Solids* **4**, 17.

Gröbner, W. and Hofreiter, N. 1949 *Integraltafel I. Unbestimmte Integrale* (Springer, Vienna).

Hodge, P. G., Jr. 1954 *J. Appl. Mech.* **21**, 336.

J. Mech. Phys. Solids, 1959, Vol. 7, pp. 182 to 192. Pergamon Press Ltd., London. Printed in Great Britain

A METHOD FOR SOLVING LINEAR THERMOELASTIC PROBLEMS

By R. J. Knops
Department of Mathematics, University of Nottingham

(*Received 7th February*, 1959)

Summary

The equations of thermoelasticity are shown to be identical in form to those obtained by subtracting the isothermal elastic equations for two arbitrary Poisson's ratios. The identity is used to formulate a relation between the two branches of elasticity which is applied to the solutions of thermoelastic problems. The procedure is illustrated by the problems of the half-space and the space bounded by two infinite planes and gives shorter solutions than hitherto.

1. Introduction

The recent revival of interest in thermoelasticity has produced solutions to several new problems but no essentially new approach to the subject. These problems are invariably regarded as independent of any corresponding isothermal ones although, from the functions entering into the solutions, it would appear likely that some relation exists. The object of this note is to supply the relation and to show that each isothermal problem is related in a definite manner to a thermoelastic one.

The method depends upon the thermoelastic equations being identical in form to the equations obtained by subtracting those of the isothermal elastic state for two arbitrary values of Poisson's ratio. From this it follows that the temperature field in the heat problem is proportional to the sum of the normal stresses in one of the isothermal solutions, and that the elastic field induced by the temperature is equal to the difference in the elastic fields of the two isothermal solutions.

Boundary conditions can easily be derived but often these are impractical and this is the main deficiency in the method. However, for problems of the half-space and space bounded by two infinite parallel planes the relation yields some important results. Many known solutions can be reproduced and some new problems solved. A sketch is given of the procedure to be adopted and a new solution presented for the thick plate with stress-free boundaries having the temperature prescribed along one of the boundaries and radiation along the other. The procedure is shorter and easier to apply than any of the existing ones as it involves only the simple operation of subtraction.

To prepare for the relation formulated in Section 4 we first briefly discuss in Sections 2 and 3 the equations of thermal and isothermal classical elasticity. The remaining sections are devoted to applications.

2. The Thermoelastic Problem

Consider an isotropic elastic solid bounded by a smooth surface S and subjected to an uneven temperature field T, which induces a stress distribution whose cartesian components are σ_{ij}. In the absence of body force and inertial effects the stresses satisfy the equilibrium equations,

$$\frac{\partial \sigma_{ij}}{\partial x_j} = 0, \tag{1}$$

referred to rectangular co-ordinates, x_i. Here and in the following the convention of summing over repeated suffixes is used.

Provided that the variation of temperature is small the stresses are related to the strains, ϵ_{ij} by means of the Duhammel-Neumann law,

$$\sigma_{ij} = \lambda \epsilon_{kk}\, \delta_{ij} + 2\mu \epsilon_{ij} - (3\lambda + 2\mu)\, \alpha T, \tag{2}$$

valid within the classical theory. Here, δ_{ij} is the Kronecker delta, α the coefficient of linear thermal expansion, and the Lamé constant λ is connected to the shear modulus μ and Poisson's ratio ν by

$$\lambda = \frac{2\mu\nu}{1 - 2\nu}.$$

The quantities λ, μ, ν, α may be functions of position but not of temperature.

The strains are derivable from a displacement u_i according to

$$\epsilon_{ij} = \tfrac{1}{2}\left(\frac{\partial u_i}{\partial x_j} + \frac{\partial u_j}{\partial x_i}\right) \tag{3}$$

and for single-valued displacements satisfy the six compatibility relations

$$e_{ikm}\, e_{jln} \frac{\partial^2 \epsilon_{kl}}{\partial x_m\, \partial x_n} = 0, \tag{4}$$

where e_{ijk} is the alternating tensor having the value 1 if i, j, k, is an even permutation of 1, 2, 3, and -1 if it is an odd permutation but is otherwise zero.

The boundary conditions are assumed homogeneous, i.e. the tractions and displacement vanish on those parts of the surface where they are defined.

The temperature field is determined from its boundary conditions and the Fourier law

$$\rho c \frac{\partial T}{\partial t} = \operatorname{div}(\kappa \operatorname{grad} T) + H \tag{5}$$

where ρ is the density of the solid, c the specific heat per unit mass, κ the thermal conductivity and t the time. H represents the amount of heat generated per unit time at a point and may be a function of both position and time. In the exact theory (5) should contain an interaction term of the type $\partial \epsilon_{kk}/\partial t$ between the temperature and strain, but for present purposes this term is neglected and only the approximate theory is used.

Along the surface it is usual to assume that radiation occurs so that

$$\frac{\partial T}{\partial n} + h(T - T_0) = 0 \qquad \text{on } S,$$

where n is the outward normal direction to S, T_0 the temperature of the surrounding medium and h the coefficient of heat transfer between this and the surface of the body. Alternatively the temperature or its normal derivative may be prescribed.

In what follows we are particularly interested in a homogeneous body with a steady-state field of temperature. Then (5) becomes

$$\kappa \nabla^2 T + H = 0 \tag{6}$$

and thus in regions free from heat sources, T is harmonic. A fundamental solution of (6) is given by

$$T = \frac{1}{4\pi R}, \qquad R^2 = (x_i - x_i')^2, \tag{7}$$

which is appropriate to a unit simple source situated at (x_i') inside an infinite solid. Another solution is

$$T = \frac{1}{4\pi} \mathbf{d}.\,\mathrm{grad}\,(R^{-1}) \tag{8}$$

and represents the field due to a unit heat-dipole at (x_i') whose axis is parallel to the positive direction of the unit vector $\mathbf{d}$, the solid again being infinite. For finite solids containing these sources regular solutions must be added which adjust the boundary conditions to their prescribed values.

The complete solution of the thermoelastic problem consists in finding the temperature field from the Fourier law (5) and then calculating the stresses, strains and displacement satisfying the elastic field equations (1) – (3) for the known temperature and given boundary conditions. Methods previously used in this solution include that of STERNBERG and MCDOWELL who employed a combination of Green's theory and the Papcovich stress functions and solved the problem of the half-space (STERNBERG and MCDOWELL 1957) and thick plate (MCDOWELL 1957) subjected to prescribed values of surface temperature. MUKI (1959) has treated the same problems subjected to axisymmetric fields by means of Hankel transforms and also considers the thick plate with radiation along the boundaries. GOODIER (1937) gave a partial solution to the problem in terms of a displacement potential which was later used by several authors in dealing with heated inclusions bonded to an otherwise cold matrix (see, for instance, ROBINSON 1951, and MINDLIN and CHENG 1950).

3. THE ISOTHERMAL PROBLEM AND THE ADDITIONAL STATE

In order to derive the state which is related to the thermoelastic one we require the field equations of classical elasticity which are now collected together. Suppose the isotropic elastic body is subjected to body force $\mathbf{X} = (X_i)$ and to surface tractions on a part S_F of the surface, with the displacement prescribed over the remainder S_u. The stresses, σ'_{ij}, strains, ϵ'_{ij}, and displacement, u'_i, satisfy the stress equilibrium equations, the linear stress-strain relations and the strain-displacement relations so that if the Lamé constant is λ' we have inside the body

$$\left.\begin{aligned} \frac{\partial \sigma'_{ij}}{\partial x_j} + X_i &= 0, \\ \sigma'_{ij} &= \lambda' \epsilon'_{kk} \delta_{ij} + 2\mu \epsilon'_{ij}, \\ \epsilon'_{ij} &= \tfrac{1}{2}\left(\frac{\partial u'_i}{\partial x_j} + \frac{\partial u'_j}{\partial x_i}\right), \end{aligned}\right\} \tag{9}$$

while $l_j \sigma_{ij}$ is given on S_F and μ'_i on S_u. When the displacement is single-valued the strains satisfy compatibility relations of the type (4).

Now let Poisson's ratio change from ν' to a new value ν, but let the shear modulus and boundary conditions remain as before. The stresses, strains and displacement are altered and their new values σ_{ij}, ϵ_{ij}, u_i satisfy a system of equations of the same form as (9).

Next define $\sigma''_{ij} = \sigma_{ij} - \sigma'_{ij}$, $\epsilon''_{ij} = \epsilon_{ij} - \epsilon_{ij}'$, $u''_i = u_i - u'_i$, and let these components form the *additional state* which thus records the change in the elastic field accompanying the change in Poisson's ratio. Equations governing this state are obtained by subtracting the corresponding equations (8) for the dashed and undashed states which for convenience will be called the *initial* and *final* states respectively. Evidently

$$\left.\begin{aligned} &\frac{\partial \sigma''_{ij}}{\partial x_j} = 0, \\ &\sigma''_{ij} = \lambda \epsilon''_{kk}\, \delta_{ij} + 2\mu \epsilon''_{ij} + \left(\frac{\lambda - \lambda'}{3\lambda' + 2\mu}\right) \sigma'_{kk}\, \delta_{ij}, \\ &\epsilon''_{ij} = \tfrac{1}{2}\left(\frac{\partial u''_i}{\partial x_j} + \frac{\partial u''_j}{\partial x_i}\right), \end{aligned}\right\} \tag{10}$$

and on remembering that the boundary conditions remained unaltered we see also that

$$l_i \sigma''_{ij} = 0 \quad \text{on} \quad S_F, \qquad u''_i = 0 \quad \text{on} \quad S_u.$$

That is, the tractions and displacements vanish on those parts of the surface where they are originally defined, and so the boundary conditions are homogeneous.

Inspection of equations (10) reveals that they are identical in form to equations (1) – (3) for the thermoelastic problem, and this fact suggests a relation between the two branches of elasticity.

4. Relation Between Isothermal and Thermal Elasticity

If in equations (10) for the additional state we put

$$\left(\frac{\lambda - \lambda'}{3\lambda' + 2\mu}\right) \sigma'_{kk} = -(3\lambda + 2\mu)\, \alpha T \tag{11}$$

we recover equations (1) – (3) for the thermoelastic state. This leads to the following relation between the two states.

An inhomogeneous isotropic elastic body of shear modulus μ and Poisson's ratio ν' is deformed by tractions prescribed over part of the surface and the displacement over the remainder; a body force may also act. The sum of the normal stresses in this deformation is denoted by σ'_{kk}. The value of Poisson's ratio now changes to ν but the boundary conditions and shear modulus remain as before. A second body of the same size and shape as the first whose moduli are μ and ν is heated to a non-uniform temperature T. No body force acts and the tractions and displacement vanish on those parts of the surface where they are defined in the first

body. Then provided that equation (11) holds between T and σ'_{kk} at every point the stresses, strains and displacement of the heated body are equal to the increments in the stresses, strains and displacement accompanying the change in Poisson's ratio of the first body.

Solutions for the additional state are therefore immediately transferable and become solutions in the thermoelastic state. Expressions for such solutions are easily derived by subtracting the initial state from the final state in any known elastic problem. These expressions are then the solution to *some* thermoelastic problem with homogeneous boundary conditions and whose temperature field is given by (11). The temperature boundary conditions must be calculated in an inverse fashion from this known field and a choice made from among the possible forms so as to obtain the most practical. Frequently, however, it must be expected that none of these boundary conditions is satisfactory since the temperature is essentially determined by σ'_{kk} which in the isothermal problem has usually no pre-assigned surface values. We cannot therefore say from the boundary conditions alone whether a particular isothermal solution is useful in solving a practical thermoelastic problem. It is this failure of not always producing realistic temperature fields that is the chief disadvantage of the method, although where successful it is enhanced by the trivial operations necessary to secure a solution. Examples illustrating the simplicity of the method are afforded by the homogeneous half-space and space bounded by two parallel planes (Sections 6 and 7). It so happens in these examples that our procedure produces general solutions from which many special problems can easily be derived with the help of an extra calculation. There is no reason to doubt that other problems can be treated by the same means.

We observe that both the relation and the above remarks following it are not in any way restricted to steady-states and apply equally well to quasi-static and inertial systems since their field equations have the same structure.

Finally we remark that the reverse process of using the relation to deduce isothermal solutions from known thermoelastic ones is more difficult to apply since it involves the calculation of the initial state from its sum of normal stresses. Particular values of Poisson's ratio ν' can be taken to simplify the calculation but even then the method cannot be expected to yield many new useful solutions since we encounter the same difficulties in determining the boundary conditions as we do in the temperature field.

5. Point Singularities

From equation (7) the singularity in the temperature field appropriate to a simple heat source is of order $O(R^{-1})$ so that from (11) the initial stresses and strains have a singularity of the same order while the displacement possesses a logarithmic singularity. Since fields of this type are uncommon in the literature of elasticity we will not consider them further.

On the other hand, the order of the singularity in the temperature field due to a heat dipole is $O(R^{-2})$ which upon using (11) again corresponds to the order of the singularity in the sum of normal stresses. A singularity of this type is well-known to be caused by a point force and thus it may be deduced that heat problems containing dipoles are associated with isothermal problems containing point forces.

For infinite media there is an exact equivalence between the magnitudes of the singularities which we now determine.

Suppose that the magnitude of the force is P and that it acts at the origin of co-ordinates in the positive z direction. From the solution given by LOVE (1952, p. 185) it easily follows for a homogeneous medium that

$$\sigma_{kk}' = \frac{1+\nu'}{1-\nu'}\frac{P}{4\pi}\frac{\partial}{\partial z}\left(\frac{1}{R}\right), \qquad R^2 = x_i^2,$$

which upon using (11) yields the steady-state temperature field

$$T = \frac{\beta}{4\pi}\frac{\partial}{\partial z}(R^{-1}), \qquad \beta = \frac{\nu-\nu'}{2\mu(1+\nu)(1-\nu')}\frac{P}{\alpha}.$$

This is appropriate to a dipole placed at the origin along the negative z direction and of magnitude β. Further, the relation of Section 4 shows the heated medium to be unloaded and with moduli μ and ν. The stresses induced by the temperature field are calculated by subtracting the isothermal stresses for the Poisson's ratio ν and ν' and in cylindrical polar co-ordinates (r, θ, z) become

$$\sigma_r = -\frac{\mu\beta}{2\pi}\left(\frac{1+\nu}{1-\nu}\right)\left(\frac{z}{R^3}+\frac{3zr^2}{R^5}\right), \qquad \sigma_\theta = -\frac{\mu\beta}{2\pi}\left(\frac{1+\nu}{1-\nu}\right)\frac{z}{R^3},$$

$$\sigma_z = \frac{\mu\beta}{2\pi}\left(\frac{1+\nu}{1-\nu}\right)\left(\frac{z}{R^3}-\frac{3z^3}{R^5}\right), \qquad \sigma_{rz} = \frac{\mu\beta}{2\pi}\left(\frac{1+\nu}{1-\nu}\right)\left(\frac{r}{R^3}-\frac{3rz^2}{R^5}\right).$$

To deduce solutions applicable for finite bodies we must superpose in the isothermal problem regular solutions which adjust the boundary conditions to their prescribed values. These conditions are generally imposed upon the tractions and displacement so that it is entirely fortuitous if the initial sum of the normal stresses assumes boundary values which after using (11) produce any practical temperature fields.

6. HALF SPACE

We now consider the problem of the homogeneous half-space and show how to deduce from the known isothermal solutions several important thermoelastic ones.

Suppose the half-space occupies the region $z \geqslant 0$ and its plane boundary is loaded by tractions $\mathbf{F}$ over finite regions, with the remainder stress-free. LOVE (1952, p. 241) has shown that the solution may be expressed in terms of the Boussinesq logarithmic potential $\mathbf{T}$ defined by

$$\mathbf{T} = \int \mathbf{F} \log(R+z)\, dS$$

where the integral is taken over the region of loading and R denotes the distance between a generic point of this and the point at which $\mathbf{T}$ is evaluated. Love also proves that the scalar components of $\mathbf{T}$ together with their derivatives are harmonic functions.

It is useful to define a second function ψ by the equation

$$\frac{\partial \psi}{\partial z} = \operatorname{div} \mathbf{T}$$

and then the sum of the normal stresses becomes

$$\sigma_{kk} = \frac{1+\nu}{\pi}\frac{\partial^2 \psi}{\partial z^2},$$

so that with the previous notation

$$\sigma''_{kk} = \frac{\nu - \nu'}{\pi}\frac{\partial^2 \psi}{\partial z^2}. \tag{12}$$

According to (11) the steady state temperature field corresponding to this problem is given by

$$T = \frac{\beta}{2\pi}\frac{\partial^2 \psi}{\partial z^2}, \qquad \beta = -\frac{(\nu - \nu')}{\alpha\mu(1+\nu)}, \tag{13}$$

and is therefore proportional to the sum of the induced normal stresses, by (12). Since **F** remains unaltered during the change in Poisson's ratio it follows that the surface of the half-space for the additional state and hence the thermoelastic one is entirely stress-free. To find the complete stress distribution in this heated problem we now determine the additional stresses by subtracting those for the final and initial state:

$$\left.\begin{aligned} \sigma_x &= \frac{\alpha\beta\mu}{\pi}(1+\nu)\frac{\partial^2 \psi}{\partial y^2}, \qquad \sigma_y = \frac{\alpha\beta\mu}{\pi}(1+\nu)\frac{\partial^2 \psi}{\partial x^2}, \\ \sigma_{xy} &= -\frac{\alpha\beta\mu}{\pi}(1+\nu)\frac{\partial^2 \psi}{\partial x\,\partial y}, \qquad \sigma_z = \sigma_{zx} = \sigma_{zy} = 0. \end{aligned}\right\} \tag{14}$$

These expressions reveal that the heated body is stressed only in planes parallel to the boundary and moreover since ψ and its derivatives are harmonic the maximum values of these stresses are attained on the boundary. These facts were first remarked on by STERNBERG and MCDOWELL (1957) and the peculiar form of the stress distribution (14) was used by STERNBERG and KOITER (1957) to suggest a general method for solving the heated half-space. This consists in first calculating the steady temperature field by some means such as Green's theorem and then obtaining the function ψ by integrating equation (13). Once this function is known the stresses can be found from (14). STERNBERG and MCDOWELL used a different approach which still requires the temperature to be calculated by Green's theorem but which, instead of (14) expresses the stresses in the form of Papcovich functions. For a point source of heat on an otherwise cold boundary the stresses are shown to reduce to the form (14) and by a surface integration it is proved that this form is retained for arbitrary temperature distributions over the boundary. The surface integration also shows that the temperature field is given by equation (13) with the restriction that ψ is derived from the logarithmic potential for *normal* distributions of **F** over regions coincident with those of the temperature distribution. LOVE has evaluated ψ and its derivatives for a variety of problems so that these known values can be used to solve thermoelastic examples. In this way STERNBERG and MCDOWELL solve the steady-state problem of the unloaded half-space whose surface is heated by a uniform or hemi-spherical temperature distribution over a circular region, or by a uniform temperature distribution over a rectangular region, with the remainder of the surface maintained at zero temperature.

Although the eventual form of STERNBERG and MCDOWELL's solution is identical to (13) and (14) their procedure is more lengthy and indirect than the one adopted here. We have no need for a separate calculation of the temperature field as it follows directly from the expression (11) and the stresses induced by the temperature follow just as automatically. It only remains in our case to interpret the boundary conditions for the temperature field which is done by recalling the properties of **T**. We notice that for tractions tangential to the surface the value of $\partial^2\psi/\partial z^2$ does not generally vanish or take uniform values on the surface so that the derived temperature field cannot be very useful. When the tractions are normal, however, this is no longer true for then if the magnitude of the tractions is $P(x, y)$ we have that $\partial^2\psi/\partial z^2$ becomes zero outside the region of loading and equal to $P(x, y)$ inside. From (13) the surface values of the temperature assume a similar pattern, becoming zero outside the load region and proportional to $P(x, y)$ inside. Our isothermal problem therefore corresponds to the heat problem of a half-space with stress-free surface subjected to a steady-state temperature field taking specified values over a finite region of the surface with the remainder held at zero temperature.

In particular, for a point-normal load of magnitude P at the origin the isothermal solution yields

$$\psi = P \log (R + z),$$

so that after using (13) the temperature becomes

$$T = \frac{\delta}{2\pi}\frac{z}{R^3}, \qquad \delta = -\beta P.$$

From the previous remarks this field corresponds to a point-source of heat on an otherwise cold surface. Alternatively it can be regarded as due to a dipole placed at the origin in the direction of the outward normal and of magnitude

$$\delta = \beta P.$$

The induced stresses are obtained from (14) and in cylindrical polar co-ordinates become

$$\sigma_r = -\frac{\mu\alpha\delta(1+\nu)}{\pi}\frac{1}{R(R+z)}, \qquad \sigma_\theta = -\frac{\mu\alpha\delta(1+\nu)}{\pi}\left(\frac{z}{R^3} - \frac{1}{R(R+z)}\right),$$

$$\sigma_z = \sigma_{zr} = 0.$$

By using other known values for ψ and its derivatives we can reproduce in a manner similar to that above all the solutions given by STERNBERG and MCDOWELL.

7. THICK PLATE

Finally we consider the problem of a thick plate loaded by normal tractions along both bounding planes and from the known elastic solutions show how to derive solutions to the problem of a thick plate heated in a specified manner. MCDOWELL (1957) has treated problems of this type when one boundary is maintained at a given temperature while the other is at zero temperature. He has shown how explicit solutions may be given in terms of infinite series if the corresponding solution is known to the problem of the half-space whose surface is maintained at the same

temperature. MUKI (1959) has presented solutions to the axisymmetric problem and includes a discussion when radiation occurs along both boundaries.

We consider here only the axisymmetric case since SNEDDON (1951, p. 468) has extensively dealt with the isothermal problem. From the general solution given by SNEDDON we derive, by the procedure already described in Section 4, the solution to a thick plate with stress-free boundaties subjected to an arbitrary regular temperature field. As an example we solve the problem when one of the boundaries of the plate is subjected to a uniform distribution of temperature over a circular region outside of which the temperature is zero, while the second boundary radiates heat into the surrounding medium. The solution is obtained in the form of infinite integrals and no numerical discussion is given.

Suppose that the plate occupies the region between $z = \pm d$ and that in the isothermal problem the boundary conditions are

$$\sigma_z = -p_1(r), \qquad \sigma_{rz} = 0 \qquad \text{on} \qquad z = +d,$$

$$\sigma_z = -p_2(r), \qquad \sigma_{rz} = 0 \qquad \text{on} \qquad z = -d,$$

where (r, θ, z) are the cylindrical polar co-ordinates. Let $\bar{p}_1$ and $\bar{p}_2$ be the Hankel transforms of zero order of p_1 and p_2 respectively, so that

$$\bar{p}_{1,2}(\xi) = \int_0^\infty r\, p_{1,2}(r) J_0(\xi r)\, dr.$$

Then in the previous notation it follows from SNEDDON's solution that

$$\sigma'_{kk} = -2(1+\nu') \int_0^\infty (A \sinh \xi z + B \cosh \xi z) J_0(\xi r)\, d\xi, \tag{15}$$

$$\left.\begin{aligned}
\sigma_{kk}'' &= \frac{\nu - \nu'}{1+\nu'}\sigma'_{kk}, \\
\sigma_r'' &= -2\frac{(\nu-\nu')}{r}\int_0^\infty (A \sinh \xi z + B \cosh \xi z) J_1(\xi r)\, d\xi, \\
\sigma_\theta'' &= -2(\nu-\nu')\int_0^\infty \Big(A \sinh \xi z \left\{ \xi J_0'(\xi r) - \frac{1}{r} J_1(\xi r) \right\} \\
&\qquad + B \cosh \xi z \left(\xi J_0(\xi r) - \frac{1}{r} J_1(\xi r) \right) \Big) d\xi, \\
\sigma_z'' &= \sigma_{r\theta}'' = \sigma_{rz}'' = 0,
\end{aligned}\right\} \tag{16}$$

with

$$A(\xi, d) = \frac{(\bar{p}_1 - \bar{p}_2)\, \xi \cosh \xi d}{(\sinh 2\xi d - 2\xi d)}, \qquad B(\xi, d) = \frac{\bar{p}_1 + \bar{p}_2)\, \xi \sinh \xi d}{(\sinh 2\xi d + 2\xi d)}.$$

These expressions represent the additional stresses for the general axisymmetric problem and are thus the stresses induced in a thick plate subjected to a temperature field (11) with σ'_{kk} given by (15) and having stress-free boundaries. These stresses exhibit the same feature as those in the half-space since they vanish in planes not parallel to the surface. This has previously been proved by MCDOWELL (1957).

Particular temperature fields can be derived by giving special values to $\bar{p}_1$ and $\bar{p}_2$ in (15), and we remark that these need not correspond to any physically significant loading but can be chosen solely to produce a desired temperature field. We do this by determining the required surface values of σ'_{kk} from (11) and the temperature boundary conditions and then take the Hankel transform of (15) along the boundaries $z = \pm d$. We then have two equations for the unknowns $A(\xi, d)$ and $B(\xi, d)$ which can be determined and used in the calculation of σ_r'', σ_θ'' and σ_{kk}' thus giving the complete solution.

Several important problems can be solved by this method which differs slightly from the direct approach used in the half-space. As illustration we consider the one whose boundary conditions are specified by

$$\frac{\partial T}{\partial z} + h(T - \tau) = 0 \qquad \text{on} \qquad z = +d, \tag{17}$$

$$T = \tau \qquad \text{on} \qquad z = -d, \tag{18}$$

where

$$\tau = \tau_0, \text{ a constant}, \quad r < a,$$

$$= 0 \qquad\qquad r > a,$$

and with

$$\sigma_z = \sigma_{rz} = 0 \qquad \text{on} \qquad z = \pm d.$$

In these conditions h represents the coefficient of heat transfer between the external medium and the plate and is a constant. We have chosen τ to have the same values on $z = \pm d$ in order to simplify the calculations, but this is not essential to the method.

From (11) the temperature field corresponding to the isothermal problem is given by

$$T = \beta\sigma'_{kk}, \qquad \beta = \frac{\nu - \nu'}{2(1 + \nu')(1 + \nu)\mu\alpha}.$$

We now take the Hankel transforms of zero order of the boundary conditions (17) with the value (15) for σ'_{kk} and obtain the equation

$$-2\beta(1 + \nu')\left[A(\xi\cosh\xi d + h\sinh\xi d) + B(\xi\sinh\xi d + h\cosh\xi d)\right] = ah\tau_0 J_1(a\xi)$$

where use has been made of the relation

$$\int_0^\infty aJ_1(a\xi)J_0(ar)\,d\xi = 1 \qquad r < a,$$

$$= 0 \qquad r > a.$$

By similarly treating the second boundary condition (18) we obtain

$$-2\beta(1 + \nu')\left[-A\sinh\xi d + B\cosh\xi d\right] = a\tau_0 J_1(a\xi).$$

The stress boundary conditions are automatically satisfied by the form of the stress-distribution.

On solving the two equations for A and B and substituting into (15) and (16) we get the final expressions for the solution of the problem. These are

$$T = a\tau_0\int_0^\infty C(\xi, d)J_1(a\xi)J_0(r\xi)\,d\xi,$$

$$\sigma_r = -2\mu\varepsilon a(1+\nu)\tau_0 \int_0^\infty C(\xi, d)\frac{J_1(a\xi)J_1(r\xi)}{r\xi}\,d\xi,$$

$$\sigma_\theta = -2\mu\varepsilon a(1+\nu)\tau_0 \int_0^\infty C(\xi, d)\left[J_1(a\xi)\,J_0(r\xi) - \frac{J_1(a\xi)J_1(r\xi)}{a\xi}\right]d\xi,$$

$$\sigma_z = \sigma_{rz} = 0,$$

where

$$C(\xi, d) = \frac{\xi\cosh\xi(d-z) + 2h\sinh\xi d\cosh\xi z}{(\xi\cosh 2\xi d + h\sinh 2\xi d)}.$$

A numerical discussion of the integrals involved in this solution might possibly be developed along lines suggested by SNEDDON (1951, p. 476.)

ACKNOWLEDGMENT

The author wishes to thank PROFESSOR R. HILL for help during the course of this investigation.

REFERENCES

GOODIER, J. N.	1937	*Phil. Mag.* **23**, 1017.
LOVE, A. E. H.	1929	*Trans. Roy. Soc.* A **228**, 377.
	1952	*Mathematical Theory of Elasticity* (Cambridge).
MCDOWELL, E. L.	1957	*Proc. 3rd Midw. Conf. Solid Mech.*, (Univ. of Michigan), p. 72.
MINDLIN, R. D. and CHENG, D. H.	1950	*J. Appl. Phys.* **21**, 931.
MUKI, R.	1959	*Progress in Solid Mechanics*, **1**, (North-Holland Pub.)
ROBINSON, K.	1951	*J. Appl. Phys.* **22**, 1045.
SNEDDON, I. N.	1951	*Fourier Transforms* (McGraw-Hill).
STERNBERG, E. and KOITER, W. T.	1957	*J. Appl. Mech.* **24**, 487.
STERNBERG, E. and MCDOWELL, E. L.	1957	*Quart. Appl. Math.* **14**, 381.

J. Mech. Phys. Solids, 1959, Vol. 7, pp. 193 to 208. Pergamon Press Ltd., London. Printed in Great Britain

ON SOME PHYSICAL PROPERTIES OF CEMENTITE*

By F. Laszlo and H. Nolle
Engineering School, University of Melbourne

(*Received* 18*th February* 1959)

Summary

Young's modulus and the shear modulus of elasticity of low carbon steel as supplied, and after case carburization to hypereuctectoid carbon content, were determined from the natural frequencies of free-free resonant longitudinal and torsional vibrations of tubular test specimens. The coefficients of thermal expansion of this steel in these states were also established. Since it was discovered that the tube used was not sufficiently quasi-isotropic, only two carbon concentrations were examined, and the individual elastic constants and coefficients of thermal expansion of random aggregates of crystals of low alloy ferrite of a certain chemical composition on the one hand, and of random aggregates of cementite crystals on the other hand, were determined from only two sets of measurements. However, different methods of checking the results suggest that their accuracy may be nevertheless fair. Finally, the thermal stresses which develop in normalized steels of carbon contents used for these experiments were computed.

1. Introduction

Earlier papers (Laszlo 1943a, 1943b, 1945) described analytical investigations regarding, among other questions, the internal stresses developing in steel consisting of ferrite and cementite, owing to change in temperature.

It was recognized that, in addition to the change in temperature, such stresses depend on the difference between the coefficients of thermal expansion of ferrite and cementite, on the elastic constants of the latter, and on the proportion and possibly also on the shape and arrangement of the particles of ferrite and cementite.

It was known that the elastic constants of ferrite and cementite were not identical (Sisco 1937, p. 383). Published experimental results did not, however, encourage attempts to derive these constants from measurements taken with plain carbon steels of different carbon content, since such specimens are always taken from different heats, and contain different amounts of manganese, silicon, phosphorus and sulphur and not only of carbon. The difference between the elastic constants being certainly small, it appeared advisable to neglect it until experimental observations were obtained with specimens having equal amounts of all elements other than carbon.

When considering identical elastic constants for ferrite and cementite, the coefficient of thermal expansion α of the mixture is exactly the proportional combination of those of the ingredients, viz:

$$\alpha = v_f \alpha_f + v_c \alpha_c \tag{1}$$

*This paper is based on part of the thesis submitted by one of the authors (H. Nolle) for the degree of Master of Engineering Science at the Engineering School of the University of Melbourne.

where α_f, α_c, v_f and $v_c = 1 - v_f$ denote the coefficients of thermal expansion and the volume fractions of ferrite and cementite, respectively, in a given steel. The measurement of α with only two different carbon contents would be sufficient. Nevertheless, experimental results with a great number of different steels (Sisco 1937, p. 375, Table 97) were evaluated (Laszlo 1943a, p, 184) leading to

$$\alpha_f = 14{\cdot}98 \times 10^{-6}, \quad \alpha_c = 12{\cdot}16 \times 10^{-6} \quad \text{and} \quad \alpha_f - \alpha_c = 2{\cdot}82 \times 10^{-6}.$$

Stresses developed in cooling by 680° were calculated (Laszlo 1943a, pp. 185 – 186) for normalized and spheroidized steel.

Variations between steels from different heats are of lesser importance as regards the coefficients of thermal expansion, but are still undesirable. Hence it was decided to determine the elastic constants and the coefficient of thermal expansion of some low carbon steel as supplied and of high carbon steels obtained from the former by case carburization. This procedure suggested the use of thin walled specimens in order to facilitate a fairly uniform case carburization. The wall thickness was sufficient, however, to permit cutting out of specimens for a dilatometer. It was also to be attempted to determine the elastic constants at smallest possible stresses.

All this could be achieved by using fairly thin walled tubular specimens and determining their longitudinal modulus of elasticity E as well as their shear modulus of elasticity

$$G = \frac{E}{2\,(1 + \mu)} \tag{2}$$

where μ denotes Poisson's ratio, from the frequencies of free-free resonant longitudinal and torsional vibrations, in the state as supplied as well as at increased carbon contents. Of course, dilatometer specimens were also to be investigated of corresponding carbon contents introduced into the same basic material. In order to eliminate experimental difficulties which can be caused by transverse vibrations, tubes of a fairly large diameter were used.

While all expectations were fulfilled otherwise, an unexpected degree of anisotropy of the tube as supplied forced a restriction of the experimental work with this basic material to a minimum.

2. Basic Material

Specimens were prepared from a 19 ft length of tubing with external diameter of 2 in. and wall thickness of 0·156 in. The choice of the length of the tubular specimens for resonant longitudinal and torsional free-free vibration was influenced by the availability of a beat-frequency oscillator of the ' fastest ' range of 6,400 – 12,800 c/s. For suspension at quarter and three-quarter length the second mode of push-pull and torsional vibration was used to obtain shortest specimens.

Since it is a further advantage to carry out in quick sequence both the longitudinal and torsional experiments without changing the range of the beat-frequency oscillator, a length of 17·5 in. was chosen for the tubular specimens, giving resonance in longitudinal vibration at some 11,530 c/s, and in torsion at some 7,200.

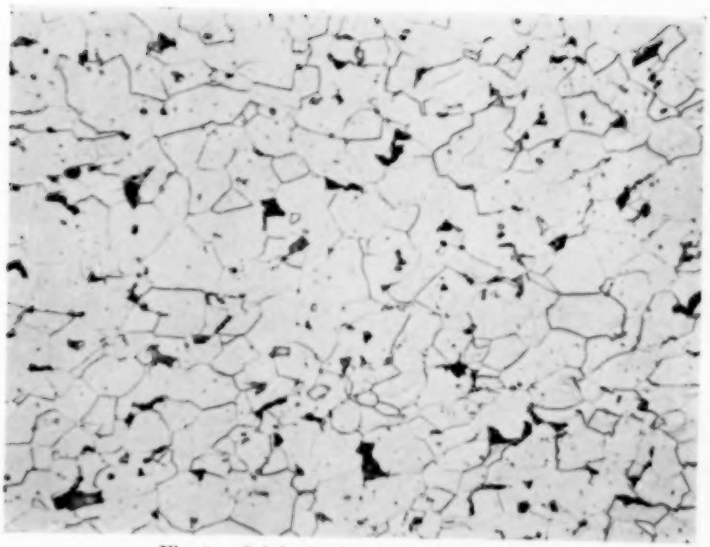

Fig. 1. Original tube, 0·085% *C* (× 200).

The chemical composition as supplied was found to be

	% C	% Mn	% P	% S	% Si
End A	0·085	0·395	0·027	0·029	0·040
End B	0·088	0·400	0·027	0·029	0·040

Fig. 1 shows the microstructure of the tube material as supplied.

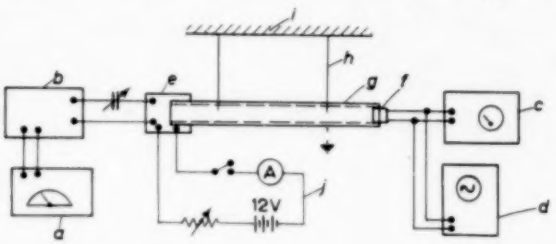

a Oscillator
b Power amplifier
c V T V.M.
d C.R.O.
e Exiter unit
f Pick-up
g Specimen
h Suspension thread
i Support stand
j Polarizing circuit

Fig. 2. Layout of apparatus.

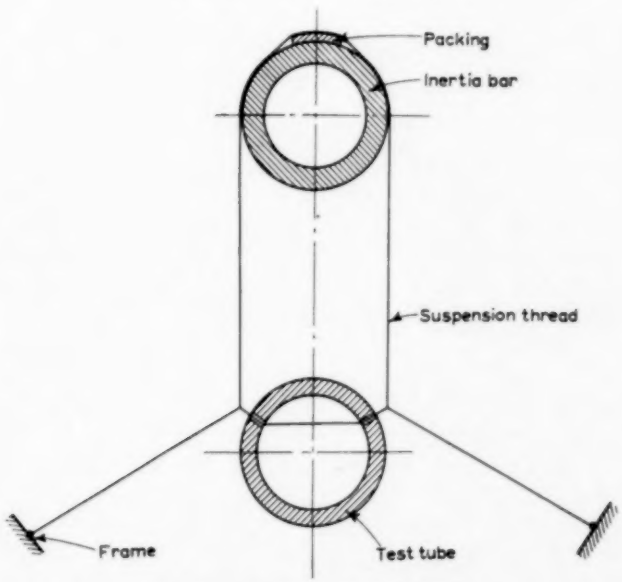

Fig. 3. Suspension of test-tube.

3. Apparatus for Dynamic Elastic Measurements

Fig. 2 shows the layout, Fig. 3 the arrangement of the suspension thread; and Fig. 4 the assembly of specimen, exciting coil and search coil. Note in Fig. 2 the indication of a variable condenser between power amplifier *b* and exciter unit *c* to bring the current as much in phase with the output voltage as desirable for a certain amplitude of resonant vibration. The tuning was of course

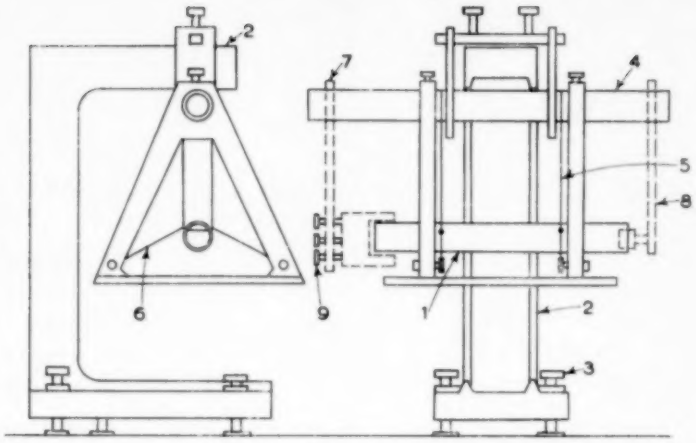

1 Specimen
2 Support stand
3 Levelling screws
4 Inertia bar
5 Suspension thread
6 Stabilizing thread
7 Exciter unit assembly
8 Pick-up unit
9 Adjusting screws

Fig. 4. Details of support stand and suspension.

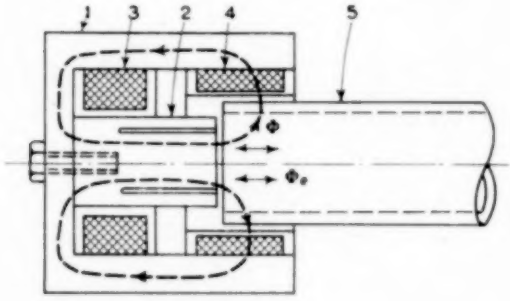

1 Mild steel pot
2 Mild steel pot piece
3 Polarizing field coil
4 A.C. coil
5 Specimen

Fig. 5. Exciter unit.

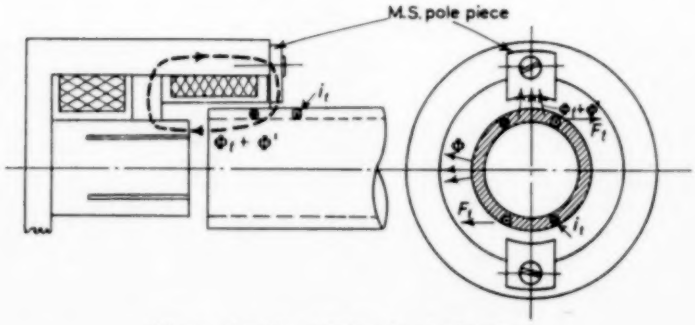

Fig. 6. Exciter unit (torsional vibration).

different for longitudinal and torsional vibration. In fact, solid condenser packages were made up for the two different modes of vibration and circuited so that the change-over was done by switching.

To eliminate possible errors, two identical set-ups were prepared, one for the various experimental specimens, and the other for an invariable reference specimen. The two set-ups were furnished with independent components such as the tuning condenser packages for longitudinal and torsional vibrations, exciter unit and search coil. Switches were installed to facilitate rapid and easy change-over.

The original exciter unit was designed for longitudinal vibration only (Fig. 5). It works on the customary principle of producing a steady flux by the d.c. – coil (3) which reacts with an alternating eddy current induced in the tube by the a.c. – coil (4).

For torsional vibration two pole pieces were added to the exciter as shown in Fig. 6. Around each of these pole pieces a short eddy current circuit i_t develops, the two of them producing an alternating couple of $T = F_f \times 2r$ which is proportional among other things to i_t. This modified exciter was still suitable for inducing longitudinal vibrations, and was subsequently used for both types of vibration.

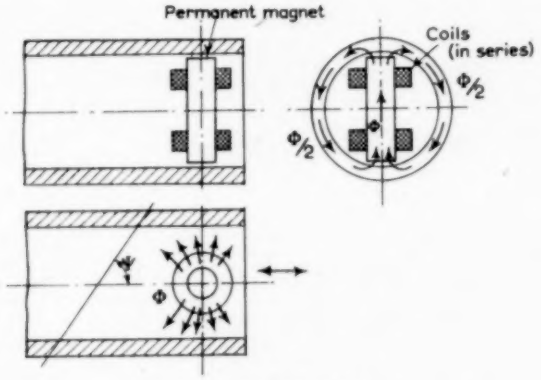

Fig. 7. Pick-up device.

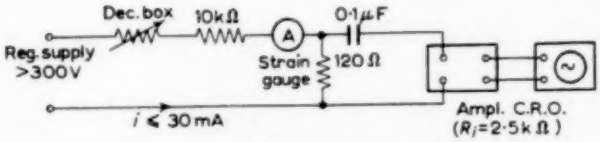

Fig. 8. Strain measuring circuit.

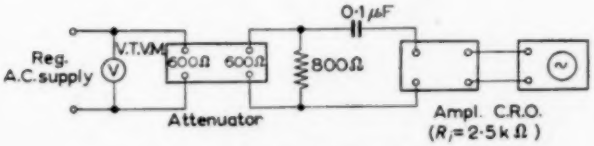

Fig. 9. Calibration circuit.

Identical units were tried for pick-up purposes at the un-excited end of the tubes, but were unsatisfactory. Pick-ups as shown in Fig. 7 proved satisfactory for both longitudinal and torsional vibrations. The pick-ups were shielded against direct induction by the tube itself, the latter being grounded by a hair-wire attached at a nodal plane.

The resonant frequency was of course obtained by tuning the oscillator to produce a peak on the vacuum tube voltmeter (*V.T.V.M.* in Fig. 2).

The oscillator was calibrated before and after measurements by using the standard frequency of 1000 c/s supplied by the P.M.G., Melbourne. The combined errors were found to be less than $\pm$ 7 cycles for longitudinal and $\pm$ 4 cycles for torsional vibrations.

To check the magnitude of the stresses accompanying the resonant vibrations applied, three electric resistance strain gauges, PR 9211-120 ohm of Phillips, were attached to the tube in the nodal plane in the longitudinal, circumferential and in the direction of a helix of 45°. The signal from the strain gauges was amplified by a two stage transistor amplifier with selective band frequency characteristics (Fig. 8) and then measured by a cathode ray oscilloscope. The amplifier was tuned to give peak attenuation near 11000 c/s or near 7500 c/s depending on whether stresses in longitudinal or torsional vibrations were examined. The amplifier was calibrated with the circuit shown in Fig 9.

Since a considerable voltage was picked up by the strain gauges while the exciter was operating a relay was used which switched off the exciter half the time during which the strain gauge was operated. It was found that in longitudinal vibration the direct stress amounted to approximately 60 lb/in^2 and in torsional vibration the shear stress to approximately 30lb/in^2.

4. Method of Evaluation of the Elastic Measurement

Since engineers generally use static elastic constants the reduction of the dynamic constants was given consideration. The latter are obtained from the measurement of the frequency f_E or f_G for longitudinal or torsional vibrations respectively as

$$E' \text{ or } G' = \frac{\gamma}{g}\left(\frac{2l f_{E \text{or} G}}{k}\right)^2 \tag{2.1}$$

where γ, g, l and k denote the specific weight, acceleration due to gravity, the length of the specimen, and the mode of vibration respectively, the latter being the second in all the experiments. Of course, E' and G' issue in gravitational units from (2.1) as required in engineering.

(i) The above values E' and G' are adiabatic while in engineering preference is generally given to the isothermal ones, viz. E'' and G''. The relation between the two kinds is given (Grueneisen 1907) as

$$E'' \text{ or } G'' = (E' \text{ or } G')\left(1 + \frac{\alpha^2 T E'}{\gamma c}\right) \tag{3}$$

where α, and T and c denote the linear coefficient of thermal expansion, the absolute temperature, and the specific heat at constant pressure respectively.

(ii) When longitudinal vibration takes place it is accompanied by a lateral one, due to the phenomenon of lateral contraction and expansion. The lateral vibration reduces the longitudinal wave velocity from the ideal value of

$$V = \sqrt{\left(\frac{Eg}{\gamma}\right)} \tag{4}$$

to

$$V_R = \sqrt{\left(\frac{Eg}{\gamma(1+\epsilon)^2}\right)} \tag{5}$$

where the approximate value of ϵ as derived by Rayleigh (1894) is taken into consideration. Rayleigh determined ϵ for a solid circular rod of radius r. His result is to be increased for a tube of bore radius ρ, by the factor $(r^2 + \rho^2)/r^2$ to

$$\epsilon = \frac{\pi^2 \mu^2 k^2 (r^2 + \rho^2)}{4l^2} \tag{6}$$

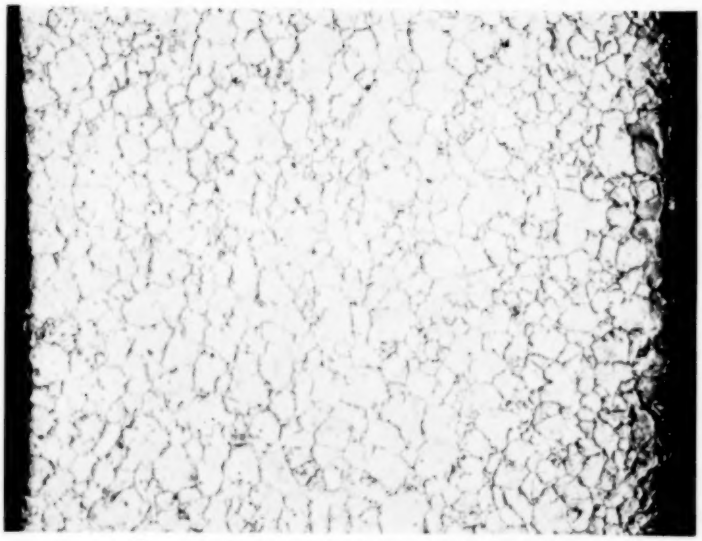

Fig. 10. Case carburized tube, 1·354 % *C* (× 25).

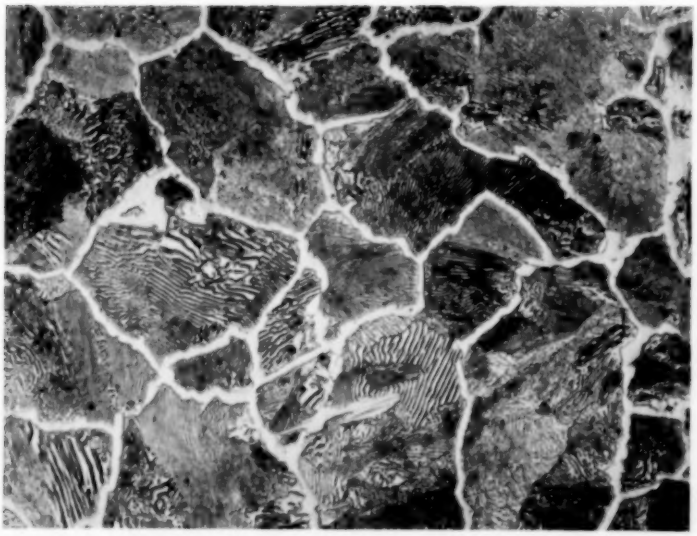

Fig. 11. Case carburized tube, 1·354 % *C* (× 200).

Hence

$$E = (1 + \epsilon)^2 E'' \approx (1 + 2\epsilon) E'' \qquad \text{and} \qquad G = G'' \tag{7}$$

since lateral inertia effects do not develop in torsional vibrations.

RAYLEIGH's method of correction is reliable only for $kr/l < 0{\cdot}55$ for solid rods, and is comparatively superfluous for $kr/l < 0{\cdot}1$ (BOYLE and SPROULE 1931). Here $k = 2$, $l = 17{\cdot}5$, $r = 1{\cdot}31$ and $kr/l = 0{\cdot}15$, a figure for which RAYLEIGH's correction is advisable and reliable.

(iii) The velocity of wave propagation is lowered by internal friction (STOKES 1845). The correction is negligible for the frequencies used here.

Similarly, the effect of the three perforations of 0·03125 in. diameter in both nodal planes for the threads of suspension (PURSEY 1952) and the magnetic effect (HONDA and TANAKA 1926), on the frequency of vibration are negligible.

5. ELASTIC CONSTANTS OF SPECIMENS

Because of the lack of quasi-isotropy of the material of the tube, exact values for random aggregates of ferrite and cementite crystals could not be obtained. Hence only one tube of approximately 20in. length, together with pieces of the tube for specimens for the determination of the coefficients of thermal expansion, was case carburized at 950°C for two periods of each 10 hr, using charcoal and some 11 per cent of $BaCO_3$. The carburizing compound was renewed after the first period. The tubular specimen was accommodated in a 6in. diameter steel pipe placed on V-supports. The 6in. diameter pipe was rotated periodically on the supports in order to obtain best uniformity of carburisation.

The tube was cut to 17·5in. length after the final furnace cooling and subsequently examined as to its natural frequencies.

Finally the carbon content, specific weight and micro structure of the case carburized tube were investigated. Drillings were taken for the carbon analysis from three points placed uniformly in a circumferential direction of the end cross-sections, of those of the nodal planes and of the centre of the specimen, i.e. from 15 positions. The average carbon content amounted to 1·354 per cent with variation within + 0·034 and − 0·062 per cent. The specific weight of the case carburized tube was found to be

$$\gamma_2 = 7{\cdot}821 \text{ g/cm}^3 = 0{\cdot}28255 \text{ lb/in}^3$$

against

$$\gamma_1 = 7{\cdot}852 \text{ g/cm}^3 = 0{\cdot}28367 \text{ lb/in}^3$$

of the tube material as supplied.

The metallographical examination of the case carburized tube showed a very uniform microstructure of pearlite grains in a network of cementite across the thickness of the tube (see Figs. 10 and 11). No trace of graphite could be found either by analysis or by the microscopic examination.

The measured frequencies of natural vibration, and the uncorrected dynamic elastic constants from (2) were as follows:

	Tube as supplied	Tube case carburized	
Longitudinal vibration	11545	11519	c/s
Torsional ,,	7230	7174	c/s
Length of Specimen	17·500	17·498	in
E'	$29{\cdot}967 \times 10^6$	$29{\cdot}707 \times 10^6$	lb/in^2
G'	$11{\cdot}752 \times 10^6$	$11{\cdot}529 \times 10^6$	lb/in^2
$\mu' = \left(\frac{E'}{2G'} - 1\right)$	0·275	0·289	

To obtain the isothermal correction according to (3), $T = 291°C$ abs., $c = 2050{\cdot}6$ in.-lb per lb per °C, $\gamma_1 = 0{\cdot}28367$, $\gamma_2 = 0{\cdot}28255$, $\alpha_1 = 11{\cdot}16 \times 10^{-6}$ and $\alpha_2 = 10{\cdot}12 = 10^{-6}$ were adapted, the values of α_1 and α_2 being taken from Sisco (1937, p. 575) for the range of temperatures of 20 – 50°C. The corrected moduli are

	Tube as supplied	Tube case carburized	
E''	$29{\cdot}911 \times 10^6$	$29{\cdot}662 \times 10^6$	lb/in^2
G''	$11{\cdot}743 \times 10^6$	$11{\cdot}516 \times 10^6$	lb/in^2

Using the above dynamic values of $\mu'_{10} = 0{\cdot}275$ and $\mu'_{20} = 0{\cdot}289$ in (6) and (7) for a first correction, calculating improved values of μ'_{11} and μ'_{21} and using these in (6) and (7), we obtain the following isothermal elastic constants:

Tube as supplied	Tube case carburized	
$E = 30{\cdot}158 \times 10^6$	$29{\cdot}933 \times 10^6$	lb/in^2
$G = 11{\cdot}743 \times 10^6$	$11{\cdot}516 \times 10^6$	lb/in^2
$\mu = 0{\cdot}2841$	$0{\cdot}2996$	

6. Elastic Constants of Ferrite and Cementite

In the absence of graphite the volume fraction of cementite is given by Laszlo (1943a, p. 184) as

$$V_c = \frac{C}{n_1 + n_2 C} \tag{8}$$

where

$$n_1 = c\frac{\gamma_c}{\gamma_f}, \qquad n_2 = \frac{\gamma_f - \gamma_c}{\gamma_f},$$

and C, c, γ_f and γ_c denote the weight fraction of carbon content, the weight fraction of carbon in cementite $= 0{\cdot}0667$, the densities of ferrite and cementite, respectively. Consider, for a first approximation, $\gamma_f' = 7{\cdot}864$ and $\gamma_c' = 7{\cdot}67$.
It is then found that

$$V_{c1}' \text{ as supplied} = 0{\cdot}01352 \text{ for } C_1 = 0{\cdot}00088^*,$$

$$V_{c2}' \text{ case carburized} = 0{\cdot}2071 \text{ for } C_2 = 0{\cdot}01354.$$

The corrected values $\gamma_f = 7{\cdot}8542$ and $\gamma_c = 7{\cdot}6940$ for this particular steel are then obtained from

$$7{\cdot}852 = 0{\cdot}98648\,\gamma_f + 0{\cdot}01352\,\gamma_c$$

$$7{\cdot}821 = 0{\cdot}7929\,\gamma_f + 0{\cdot}2071\,\gamma_c;$$

and the improved values

$$V_{c1} = 0{\cdot}01346 \text{ for } C_1 = 0{\cdot}00088,$$

$$V_{c2} = 0{\cdot}2064 \text{ for } C_2 = 0{\cdot}01354,$$

are found with (8).

Since the tube was not satisfactorily quasi-isotropic and only one case carburized sample was produced, only the simplest proportional method of de-combination can be carried out. This is the coarsest possible approximation.

*This specimen was taken from End B.

It may be suggested, for example, that cementite and ferrite crystals undergo equal direct strains in the direction of the axis of the tube in longitudinal vibration as well as equal shear strains in torsional vibration, so that from

$$30{\cdot}158 \times 10^6 = 0{\cdot}98654 \quad E^\circ_f + 0{\cdot}01346\, E^\circ,$$

$$29{\cdot}933 \times 10^6 = 0{\cdot}7936 \quad E^\circ_f + 0{\cdot}2064\, E^\circ_c,$$

$$11{\cdot}743 \times 10^6 = 0{\cdot}98654 \quad G^\circ_f + 0{\cdot}01346\, G^\circ_c,$$

$$11{\cdot}516 \times 10^6 = 0{\cdot}7936 \quad G^\circ_f + 0{\cdot}2064\, G^\circ_c,$$

the values of

$$\left.\begin{aligned} &E^\circ_f = 30{\cdot}174 \times 10^6 \text{ lb/in}^2, \quad G^\circ_f = 11{\cdot}759 \times 10^6 \text{ lb/in}^2, \quad \mu^\circ_f = 0{\cdot}283 \\ &E^\circ_c = 29{\cdot}008 \times 10^6 \text{ lb/in}^2, \quad G^\circ_c = 10{\cdot}582 = 10^6 \text{ lb/in}^2, = 0{\cdot}371 \end{aligned}\right\} \quad (9)$$

are obtained.

The above approximation does not provide for equilibrium of forces even in a statististical sense between cementite and ferrite crystals alternating in the direction of the strain. Such equilibrium would require in simplest approximation that

$$\frac{1}{30{\cdot}158 \times 10^6} = \frac{0{\cdot}98654}{E_f} + \frac{0{\cdot}01346}{E_c}$$

$$\frac{1}{29{\cdot}933 \times 10^6} = \frac{0{\cdot}7936}{E_f} + \frac{0{\cdot}2064}{E_c}$$

$$\frac{1}{11{\cdot}743 \times 10^6} = \frac{0{\cdot}98654}{G_f} + \frac{0{\cdot}01346}{G_c}$$

$$\frac{1}{11{\cdot}516 \times 10^6} = \frac{0{\cdot}7936}{G_f} + \frac{0{\cdot}2064}{G_c}$$

and that

$$\left.\begin{aligned} &E_f = 30{\cdot}174 \times 10^6 \text{ lb/in}^2, \quad G_f = 11{\cdot}759 \times 10^6 \text{ lb/in}^2, \quad \mu_f = 0{\cdot}283 \\ &E_c = 29{\cdot}042 \times 10^6 \text{ lb/in}^2, \quad G_c = 10{\cdot}668 \times 10^6 \text{ lb/in}^2, \quad \mu_c = 0{\cdot}361 \end{aligned}\right\} \quad (10)$$

The question of the de-combination of the elastic constants has been duly studied. With $\gamma_f = 7{\cdot}8542$, $\gamma_c = 7{\cdot}6940$, $c = 0{\cdot}0667$, $p = 0{\cdot}0083$, the volume fraction of cementite in pearlite was determined as 0·1267, and the volume fraction of pearlite as 0·10605 in steel of $C_1 = 0{\cdot}00088$, and 0·90820 in steel of $C_2 = 0{\cdot}01354$.

It was shown theoretically (Laszlo 1945 p. 208) that the elastic behaviour of a ' compound ' solid varies with the shape of the constituents if their moduli of shear are different. The compound sphere was compared with its inversion on that occasion for a different purpose (Laszlo 1945 p. 219). Let, now, such a comparison be used in regard to the bulk moduli of elasticity $K = E/(1 - 2\mu)$ for one and the same carbon content, and for a spread-shape of the cementite on the one hand versus compact shape of cementite on the other. This comparison is theoretically exact.

Consider a sphere of volume V_i with elastic constants E_i, μ_i, to be cohesively joined to a spherical shell of volume V_0 with elastic constants E_0, μ_0, and make $V_i + V_0 = 1$. Apply to the outer surface of the compound sphere unit radial tension per unit surface area. We derive the following expression for the tangential strain at the outer surface, equal to the reciprocal of $K = E/(1 - 2\mu)$ of the compound sphere as a whole :

$$\frac{1}{K} = \frac{1-2\mu}{E} = \left(\frac{1-\mu_0}{E_0}\right)\left(\frac{3-V_0}{2V_0}\right) - \frac{\mu_0}{E_0} - \left(\frac{1-\mu_0}{E_0}\right)\left(\frac{1-V_0}{2V_0}\right)$$
$$\left[\frac{9}{3-2V_0+\left(\frac{\mu_0}{1-\mu_0}\right)2V_0+\left(\frac{1-2\mu_i}{E_i}\right)\left(\frac{E_0}{1-\mu_0}\right)2V_0}\right]. \qquad (11)$$

If the moduli E and G of steel of certain carbon concentration have been experimentally determined, and also E_f, μ_f, E_c and μ_c in some way we could compare K in (11) with $E/(3-E/G)$, in order to assess the accuracy of the determination of E_f through to μ_c from experimental values of E's and G's.

Let pearlite eutectoid of $C_1 = 0{\cdot}0083$ be considered as a first example. E and μ as well as G and K may be approximately calculated* according to LASZLO (1943b, p. 144, equation (14)) for the volume fraction of cementite in pearlite of 0·1267, either with the figures of (9) or (10).

TABLE 1

	With the figures of (9)	With the figures of (10)
E	$30{\cdot}077 \times 10^6$	$30{\cdot}072 \times 10^6$
μ	0·295	0·294
G	$11{\cdot}611 \times 10^6$	$11{\cdot}618 \times 10^6$
K	$73{\cdot}434 \times 10^6$	$73{\cdot}008 \times 10^6$
K_{11}	$73{\cdot}598 \times 10^6$	$73{\cdot}002 \times 10^6$
$K_{r,11}$	$73{\cdot}639 \times 10^6$	$73{\cdot}034 \times 10^6$

The last two rows of Table 1 were calculated with (11) for a compound sphere consisting of 0·1267 volume fraction of cementite and 0·8733 ferrite ; cementite being the outer spherical shell of volume fraction 0·1267 for K_{11}, and ferrite being the outer shell of volume fraction 0·8733 for $K_{r,11}$. Note by comparing K_{11} with $K_{r,11}$ that the shape effect on the elastic constants in this case is very small, and that the compound sphere with cementite in the outer 'spread' position K_{11} is well comparable with the 'lamellar' results K.

The elastic constants for ferrite and cementite in (9) and (10) were obtained by fractional decombination of the experimental results. Obtain by proportional combination for pearlite from

$$0{\cdot}8733\,E^\circ_f + 0{\cdot}1267\,E^\circ_c = E^\circ_p$$
$$0{\cdot}8733\,G^\circ_f + 0{\cdot}1267\,G^\circ_c = G^\circ_p$$
$$\frac{0{\cdot}8733}{E_f} + \frac{0.1267}{E_c} = \frac{1}{E_p}$$
$$\frac{0{\cdot}8733}{G_f} + \frac{0{\cdot}1267}{G_c} = \frac{1}{G_p}$$

the values of $E^\circ_p = E_p = 30{\cdot}0126 \times 10^6$, $G^\circ_p = G_p = 11{\cdot}609 \times 10^6$; $\mu^\circ_p = \mu_p = 0{\cdot}293$ and $K^\circ_p = K_p = 72{\cdot}604$. It is recognized that this proportional combin-

*C.S.I.R.A.C. computer of the Computation Laboratory of Melbourne University.

ation leads to a volumetric modulus of elasticity for pearlite which is 0·54 per cent outside the range of the values of Table 1 for K. This, of course, was to be expected (Laszlo 1945, p. 209, equation (41)) since the shear moduli of the structural components are not equal.

The last check on the question of elastic constants was the determination of the volumetric modulus of elasticity, by using (11), of the actual specimens of $C_1 = 0{\cdot}00088$ and $C_2 = 0{\cdot}01354$, by considering compound spheres having cores of pearlite of volume fractions of $1 - V_0 = 0{\cdot}10605$ and $1 - V_0 = 0{\cdot}90820$ respectively, and outer spherical shells of $V_0 = 0{\cdot}89395$ of ferrite and of $V_0 = 0{\cdot}09180$ of cementite respectively. These calculations use for the outer spherical shell either the figures of (9) or (10), and for $(1 - 2\mu_i)/E_i$ in the denominator of the third term of the right-hand side of (11), the values of $K^{\circ}_{11} = 73{\cdot}598 \times 10^6$ and $K_{11} = 73{\cdot}002 \times 10^6$ respectively. Table 2 contains as the last rows the experimental results K_1 and K_2 calculated from $K = E/(3 - E/G)$ and the percentage error in the results of the calculations against K_1 and K_2.

Table 2

	$C_1 = 0{\cdot}00088$		$C_2 = 0{\cdot}01354$	
	Calculated with figures of (9)	*Calculated with figures of* (10)	*Calculated with figures of* (9)	*Calculated with figures of* (10)
K_{calc}	$69{\cdot}944 \times 10^6$	$69{\cdot}884 \times 10^6$	$76{\cdot}328 \times 10^6$	$75{\cdot}320 \times 10^6$
K_{exp}	$69{\cdot}837 = 10^6$		$74{\cdot}693 \times 10^6$	
Error (%)	0·153	0·067	2·19	0·84

It is to be reiterated that the proportional de-combination is by no means exact for a structure consisting of ferrite and cementite. Correct values of the elastic constants for ferrite and cementite may be obtained by making up four specimens of identical basic analysis but of four different carbon contents, the whole carbon being combined to form cementite, and solving a set of four different equations (11). Of course, a nearly quasi-isotropic material should be used.

In our case the figures of (10) should be used for finding the individual coefficients of thermal expansion of ferrite and cementite. The error in values in the (10) is possibly not in excess of 0·5 per cent.

7. Coefficients of Thermal Expansion

Specimens of 2 in. length were tested in Leitz dilatometers, using a purified argon atmosphere. The specimens were taken from the end A of the tube the original carbon content being there 0·085 per cent. The carbon content of a case carburized specimen was found to be 1·340 per cent and analytical and microscopic investigations showed that all of the carbon content was in the form of cementite.

Using (8) with $C = 0{\cdot}0667$, $\gamma_f = 7{\cdot}8542$ and $\gamma_c = 7{\cdot}694$, we obtain $V_{c3} = 0{\cdot}01301$ for $C_3 = 0{\cdot}00085$ and $V_{c4} = 0{\cdot}2042$ for $C_4 = 0{\cdot}0134$.

The average coefficients of thermal expansion were found by experiment for the range of 20 – 700°C to be

$$15{\cdot}11 \times 10^{-6} \text{ for } C_3 = 0{\cdot}00085 \text{ and } 14{\cdot}63 \times 10^{6-} \text{ for } C_4 = 0{\cdot}0134.$$

Neglecting temporarily the difference in the elastic constants of ferrite and cementite the following individual coefficients of thermal expansion are obtained (LASZLO 1943a, p. 180, equation (4)) by proportional de-combination, for ferrite and cementite:

From $15{\cdot}11 \times 10^{-6} = 0{\cdot}98699\ \alpha_{f1} + 0{\cdot}0\ 1301\ \alpha_{c1}$ and

$$14{\cdot}63 \times 10^{-6} = 0{\cdot}7958\ \alpha_{f1} + 0{\cdot}2042\ \alpha_{c1},$$

$$\alpha_{f1} = 15{\cdot}14 \times 10^{-6} \quad \text{and} \quad \alpha_{c1} = 12{\cdot}63 \times 10^{-6}.$$

Note that $(\alpha_{f1} - \alpha_{c1}) = 2{\cdot}51 \times 10^{-6}$ only, against a previous finding (LASZLO 1943a, p. 184) of $2{\cdot}82 \times 10^{-6}$.

Encouraged by the agreement between the values of K and K_{11} in Table 1, the coefficient of thermal expansion of ferrite and cementite was next calculated in the following relatively simple fashion.

Consider for the specimen of $C_3 = 0{\cdot}00085$ a compound sphere, the ferrite core of which is a volume of $V_i = 4\pi\, r_i^3/3 = 0{\cdot}08967$ cohesively joined to an intermediate shell of cementite of volume $V_c = 4\pi\,(r_m^3 - r_i^3)/3 = 0{\cdot}01301$, this cementite shell being cohesively joined to the outer shell of ferrite of volume $V_0 = 4\pi(r^3_0 - r^3_m)/3 = 0{\cdot}89732$, the three components making up a unit volume.

Take for the elastic constants of ferrite and cementite the figures of (10), and express the tangential strain ϵ_3 at the outer surface, r_0, owing to a rise in temperature by unity, in terms of the unknown coefficients of thermal expansion of ferrite α_{f2} and cementite α_{c2}. Now require that the measured thermal coefficient of this specimen of C_3 be

$$\alpha_1 = 15{\cdot}11 \times 10^{-6} = \alpha_{f2} + \epsilon_3 \tag{12}$$

where

$$\epsilon_3 = -\frac{1-\mu_f}{E_f} \cdot \frac{3r_m^3\,(\alpha_{f2} - \alpha_{c2})\,(D - B)}{2\,(r_0^3 - r_m^3)\,(AD - BC)},$$

$$A = \left(\frac{1-\mu_c}{E_c}\right)\frac{3r^3_m}{2\,(r_m^3 - r_1^3}, \quad -B = \left(\frac{1-\mu_c}{E_c}\right)\frac{(2r_i^3 + r_m^3)}{2\,(r_m^3 - r_i^3)} + \frac{\mu_c}{E_c} + \frac{1-2\mu_f}{E_f},$$

$$C = \left(\frac{1-\mu_c}{E_c}\right)\frac{(2r_m^3 + r_i^3)}{2\,(r_m^3 - r_i^3)} + \left(\frac{1-\mu_f}{E_f}\right)\frac{(2r_m^3 + r_0^3)}{2\,(r_0^3 - r_m^3)} - \frac{\mu_c}{E_c} + \frac{\mu_f}{E_f},$$

$$-D = \left(\frac{1-\mu_c}{E_c}\right)\frac{3r_i^3}{2\,(r_m^3 - r_i^3}.$$

Consider another compound sphere simulating the specimen of $C_4 = 0{\cdot}0134$, having a ferrite core of $V_i = \dfrac{4\pi\rho^3}{3} = 0{\cdot}7958$ which is cohesively joined to a spherical shell of cementite of a volume of $V_0 = \dfrac{4\pi}{3}\,(r_0^3 - \rho^3) = 0{\cdot}2042$, the joint volume being unity. Express the tangential strain ϵ_4 also of this compound sphere at the outer surface, r_0, owing to unit rise in temperature, in terms of α_{f2} and α_{c2} and require

that the measured coefficient of thermal expansion of this specimen be such that

$$\alpha_2 = 14{\cdot}63 \times 10^{-6} = \alpha_{c2} + \epsilon_4 \qquad (13)$$

where

$$\epsilon_4 = \frac{\left(\frac{1-\mu_c}{E_c}\right) \cdot \frac{3\rho^3}{2\,(r_0^3 - \rho^3)} \cdot (\alpha_{f2} - \alpha_{c2})}{\left(\frac{1-\mu_c}{E_c}\right) \cdot \frac{3\rho^3 + r_0^3}{2\,(r_0^3 - \rho^3)} + \frac{\mu_c}{E_c} + \frac{1-2\mu_f}{E_f}}.$$

Equations (12) and (13) were solved with the elastic constants of (10) and gave $\alpha_{f2} = 15{\cdot}14 \times 10^{-6}$, $\alpha_{c2} = 12{\cdot}88 \times 10^{-6}$, and $\alpha_{f2} - \alpha_{c2} = 2{\cdot}26 \times 10^{-6}$ which is still less than the result of proportional de-combination.

Since the consequential thermal stresses are of interest, the more elaborate approximation was calculated for lamellar core spheres of volume fractions 0·10268 and 0·91065 embedded cohesively into spherical shells of ferrite of a volume fraction 0·89732 and cementite of a volume fraction of 0·08935 respectively, corresponding to $C_3 = 0{\cdot}00085$ and $C_4 = 0{\cdot}0134$.

Using the figures (10) for the elastic constants of ferrite and cementite we obtain according to Laszlo (1943b, p. 139, equation (8)), with $\alpha_1 = \alpha_f$, $\alpha_2 = \alpha_c$, $t = +1$; $1/m_1 = \mu_f$; $E_1 = E_f$; $1/m_2 = \mu_c$; $E_2 = E_c$; $f_1 = \sigma_f'$; $f_2 = \sigma_c'$; $q = \sigma'$; $\alpha = \alpha_p$; $u_1 = 0{\cdot}8733$ and $u_2 = 0{\cdot}1267$, the coefficient of thermal expansion of a random aggregate of pearlite cubes in terms of the unknown α_f and α_c

as
$$\alpha_p = 0{\cdot}8573\,\alpha_f + 0{\cdot}1427\,\alpha_c$$

as well as the stresses owing to unit rise in temperature:

$$\sigma_f' = -5{\cdot}8722 \times 10^{-6}\,(\alpha_f - \alpha_c),\ \sigma_c' = 39{\cdot}154 \times 10^6\,(\alpha_f - \alpha_c)$$

and
$$\sigma' = 0{\cdot}3349 \times 10^6\,(\alpha_f - \alpha_c)$$

where σ_f', σ_c' and σ' denote a pair of equal principal stresses in ferrite lamellae, a pair of equal principal stresses in cementite lamellae, and the third principle stress of both ferrite and cementite lamellae respectively, this latter being at right angles to the plane of both lamellae.

Random aggregates of pearlite cubes of small size are formed to core spheres of volumes of 0·10243 and 0·91065, and embedded in a spherical shell of ferrite of a volume of 0·89757 and in one of cementite of a volume of 0·08935 respectively, corresponding to $C_3 = 0{\cdot}00085$ and $C_4 = 0{\cdot}0134$, making up spheres of unit volume.

When these spheres rise in temperature by unity the radial junction stress σ_{rj} between the pearlite core and the outer spherical shell amounts to $\sigma'_{rj3} = 3{\cdot}6561 \times 10^6\ (\alpha_f - \alpha_c)$ and $\sigma'_{rj4} = -2{\cdot}2954\ 10^6\ (\alpha_f - \alpha_c)$ according to Laszlo (1943a, p. 179, equation (2)), with $p = \sigma_{rj}$, $V_i = 0{\cdot}10243$ or 0·91065, $V_0 = 0{\cdot}89757$ or 0·08935, $1/m_0 = \mu_f$ or μ_c, $\alpha_0 = \alpha_f$ or α_c, $E_0 = E_f$ or E_c, for $C_3 = 0{\cdot}00085$ or $C_4 = 0{\cdot}0134$ respectively; as well as for both carbon contents $\alpha_i = \alpha_p$,

$$\frac{m_i - 2}{m_i\,E_i} = \frac{1}{73{\cdot}008 \times 10^6} \quad \text{and} \quad t = +1.$$

The tangential stress at the junction with the core is found to be $\sigma_{tj3}' = -2{\cdot}4539 \times 10^6\,(\alpha_f - \alpha_c)$ and $\sigma'_{tj4} = 36{\cdot}239 \times 10^6\ (\alpha_f - \alpha_c)$, and at the outer surface,

$$\sigma_{t03}' = -0{\cdot}6258 \times 10^6 (\alpha_f - \alpha_c) \text{ and } \sigma_{t04}' = 35{\cdot}239 \times 10^6 (\alpha_f - \alpha_c).$$

From

$$15{\cdot}11 \times 10^{-6} = \alpha_f + \frac{1 - \mu_f}{E_f} \sigma_{t03}' \quad \text{and}$$

$$14{\cdot}63 \times 10^{-6} = \alpha_c + \frac{1 - \mu_c}{E_c} \sigma_{t04}'$$

we find $\alpha_f = 15{\cdot}14 \times 10^{-6}$, $\alpha_c = 12{\cdot}89 \times 10^{-6}$ and

$$\alpha_f - \alpha_c = 2{\cdot}25 \times 10^{-6}.$$

These figures appear to be the best that can be produced. They are practically identical with the values for compound spheres without lamellar cores, viz. α_{f2} and α_{c2}.

8. THERMAL STRESSES

The stress analysis was a by-product of the de-combination of the thermal coefficients. Both dilatometer specimens were slowly cooled from the temperature of case carburization. Let it be assumed that stresses develop due to a change in temperature by -680°C, leading to the figures stated below in lb/in^2, these being also expressed as fractions of earlier calculations (LASZLO 1943a, pp. 183-185) based on $E_f = E_c = 30 \times 10^6$, $\mu_f = \mu_c = 0{\cdot}3$ and $\alpha_f - \alpha_c = 2{\cdot}82 \times 10^6$, the fractional comparisons with the earlier findings being put into brackets.

For $C_3 = 0{\cdot}00085$,

$$\sigma_{f3} = -680 (\sigma_f' + \sigma_{rj3}') = 3395 (= 0{\cdot}81 \times 4195)$$

$$\sigma_{c3} = -680 (\sigma_c' + \sigma_{rj3}') = -65590 (= -0{\cdot}84 \times 77985)$$

$$\sigma_3 = -680 (\sigma' + \sigma_{rj3}') = -6115 (= -0{\cdot}98 \times 6255)$$

$$\sigma_{eq\,f3} = \sigma_{f3} - \sigma_3 = 9510 (= 0{\cdot}91 \times 10450)$$

$$\sigma_{eq\,c3} = \sigma_3 - \sigma_{c3} = 59475 (= 0{\cdot}83 \times 71730)$$

$$\sigma_{rj3} = -680\, \sigma_{rj3}' = -5600 (= -0{\cdot}90 \times 6255)$$

$$\sigma_{tj3} = -680\, \sigma_{tj3}' = 3760 (= 0{\cdot}90 \times 4195)$$

$$\sigma_{t03} = -680\, \sigma_{t03}' = 960 (= 0{\cdot}90 = 1070)$$

$$\sigma_{eq\,j3} = \sigma_{tj3} - \sigma_{rj3} = 9360 (= 0{\cdot}90 \times 10450)$$

where the σ_{eq} stresses stand for equivalent direct stresses according, in our case, to both the maximum shear stress theorem and the shear strain energy theorem ; and using suffices f for ferrite, c for cementite, l for lamella, j for matrix of ferrite at the junction with the core, and 0 for matrix of ferrite at the outer surface.

For $C_4 = 0{\cdot}0134$,

$$\sigma_{f4} = -680 (\sigma_f' + \sigma_{rj4}') = 12515 (= 0{\cdot}86 \times 14625)$$

$$\sigma_{c4} = -680 (\sigma_c' + \sigma_{rj4}') = -56475 (= -0{\cdot}84 \times 67555)$$

$$\sigma_4 = -680 (\sigma' + \sigma_{rj4}') = 3005 (= 0{\cdot}72 \times 4175)$$

$$\sigma_{eq\,f4} = \sigma_{f4} - \sigma_4 = 9510 (= 0{\cdot}91 \times 10450)$$

$$\sigma_{eq\,c4} = \sigma_4 - \sigma_{c4} = 59475 (= 0{\cdot}83 \times 71730)$$

$$\sigma_{rj4} = -680\, \sigma_{rj4} = 3515 (= 0{\cdot}84 \times 4175)$$

$$\sigma_{tj4} = -680\, \sigma_{tj4} = -55525 (= -0{\cdot}82 \times 67555)$$

$$\sigma_{t04} = -680\, \sigma_{t04}' = -53765 (= -0{\cdot}82 \times 65465)$$

$$\sigma_{eq\,j4} = \sigma_{rj4} - \sigma_{tj4} = 59040 (= 0{\cdot}83 \times 71730)$$

where $\sigma_{eq\,j4}$ refers to the cementite outer shell at the junction with the pearlite core.

Since $2{\cdot}25 \approx 0{\cdot}80 \times 2{\cdot}82$, the difference between the coefficients of thermal expansion of ferrite and cementite was found in the above experiments to be 20 per cent less than previously. However, the thermal stresses are reduced in general by less than 20 per cent.

Note that $\sigma_{f3} \neq \sigma_{tj3}$, $\sigma_{eq\,f3} \neq \sigma_{eq\,j3}$, $\sigma_{c4} \neq \sigma_{tj4}$ and $\sigma_{eq\,c4} \neq \sigma_{eq\,j4}$, in contradistinction to the previous findings (Laszlo 1943a, pp.183-185) for the case of $E_f = E_c$ and $\mu_f = \mu_c$. Whether all these unequalities are true cannot be decided, owing to the calculation for the lamellar structure being approximate as well as because of some lack of quasi-isotropy of the material.

9. Control Experiments

A 24 in. length of the tube as supplied was furnished at both ends with circular end plates of $\frac{1}{2}$ in. thickness, fillet welded to the tube, the plates being fitted with threaded central bosses for the application of axial pull. Internal pressure could be applied to the tube through one of the bosses using oil and controlling its pressure by a gravity calibration apparatus for pressure gauges for 10 – 10000lb/in^2 which was permanently connected to the oil supply tube.

Electric resistance strain gauges were cemented to the outer surface of the 24 in. length of the tube at mid-length, 3 gauges in the longitudinal and another three in the tangential direction.

Denote by E_a and E_t the modulus of elasticity in the axial and tangential direction respectively, and by $\mu_{a/t}$ and $\mu_{t/a}$ Poisson's ratio giving strain in the tangential direction due to stress in the axial direction and vice versa respectively. The stress-strain equations for two dimensional conditions are

$$\epsilon_t = \frac{\sigma_t}{E_t} - \mu_{a/t} \cdot \frac{\sigma_a}{E_a} \qquad \text{and}$$

$$\epsilon_a = \frac{\sigma_a}{E_a} - \mu_{t/a} \cdot \frac{\sigma_t}{E_t}.$$

The stresses due to an axial tensile force P applied to the tube are

$$\sigma_a{}' = \frac{P}{\pi\,(r_0{}^2 - r_i{}^2)}, \qquad \sigma_t{}' = 0,$$

where r_0 and r_i denote the outer and inner radii of the tube respectively.

The stresses at the outer surface of the tube due to an internal pressure p are

$$\sigma_t{}'' = 2\sigma_a{}'' = \frac{2pr_i{}^2}{r_0{}^2 - r_i{}^2}.$$

The elastic constants can be calculated from the above equations and the strain gauge readings ϵ_t and ϵ_a, for different combinations of p and P.

From a fair number of experiments the following average values were obtained:

$$E_a\ 30{\cdot}285 \times 10^6\ \text{lb/in}^2, \quad E_t = 31{\cdot}505 \times 10^6 \text{lb/in}^2, \quad \mu_{t/a} = 0{\cdot}295$$

and $\mu_{a/t} = 0{\cdot}274$.

One group of experiments gave even more diverging values as

$$E_a = 30{\cdot}126 \times 10^6\ \text{lb/in}^2, \quad E_t = 31{\cdot}502 \times 10^6\ \text{lb/in}^2,$$

$$\mu_{t/a} = 0{\cdot}297 \quad \text{and} \quad \mu_{a/t} = 0{\cdot}272.$$

The accuracy of these measurements is lower than that of the dynamic experiments. The axial force P was applied by a tensile testing machine and not by dead weights as would be preferable. The electric resistance strain gauges were not specially calibrated, neither was the pressure gauge tester. However, the accuracy of the control experiments disclosed beyond any trace of doubt a significant lack of quasi-isotropy of the tube specimen. Some further experiments with tubes of fairly perfect quasi-isotropy would, of course, be of interest.

9. Concluding Remarks

Phenomena of the physics of a solid connected with internal stresses between particles of its structure mostly depend on the different individual properties of those particles. The above experiments and analyses appear to offer a promising approach to the treatment of some of these problems.

As to the physical properties of ferrite and cementite, further work is desirable with materials having a high degree of quasi-isotropy as well as varying alloying contents in both ferrite and cementite.

The mathematical analysis of ferrite and cementite is free of any deficiency if the whole cementite is spheroidized. This may also be kept in mind in future investigations.

Acknowledgments

The work was carried out in the Civil Engineering Department of the University of Melbourne and the authors would like to thank Professors J. A. L. Matheson and A. J. Francis for making facilities available. One of us (H.N.) is very grateful for the financial assistance provided by the Civil Engineering Department.

We are indebted to Dr. A. Murray (High Duty Alloys Ltd., Slough) for valuable information on the design of the equipment, to Professor F. T. M. White of the University of Queensland (Brisbane, Australia) and Mr. J. I. Nish of the Defence Standard Laboratories of Melbourne (Australia) for permission to use their dilatometers, and to Dr. F. Hirst of the Computer Laboratory of the University of Melbourne for assistance with computations.

References

Boyle, R. W. and Sproule, D. O. 1931 *Canad. J. Res.* **5**, 601.

Grueneisen, E. 1907 *Ann. d. Phys.* **22**, 842.

Honda, K., and Tanaka, T. 1926 *Sci. Rep. Sendai.* **15**, 1.

Laszlo, F. 1943a *J. Iron Steel Inst.* 173-199.

1943b *Ibid*, 207-228.

1945 *Ibid.*

Pursey, H. 1952 *Nature, Lond.* **170**, 502.

Rayleigh, Lord. 1894 *Theory of Sound* **1**.

Sisco, F. T. 1937 *The Alloys of Iron and Carbon*, **II**.

Stokes, G. G. 1845 *Trans. Camb. Phil. Soc.* **8**, 287.

J. Mech. Phys. Solids, 1959, Vol. 7, pp. 209 to 225. Pergamon Press Ltd., London. Printed in Great Britain

SOME BASIC PRINCIPLES IN THE MECHANICS OF SOLIDS WITHOUT A NATURAL TIME

By R. Hill
Department of Mathematics, University of Nottingham

(*Received 5th March*, 1959)

Summary

The solids considered are defined by tensor relations of type stress-rate component $= f$(strain-rate components) where the functions f, homogeneous of degree one in the components of strain-rate, can be non-linear and depend also on the current stress and entire strain-history. The solids are classified by their behaviour in vanishingly small closed cycles of strain. Questions of uniqueness and stability are examined in full generality.

The results are sharpened when the functions f are the derivatives of a potential function of the strain-rate components. Extremum theorems and a generalized Rayleigh principle are proved.

Various definitions of stress-rate are discussed, particularly the convected derivative of the Kirchhoff-Trefftz stress. This is used to construct constitutive equations for a very general class of solids including metals. The concept of a yield surface is critically analysed and generalized.

1. Classification of Solids without a Natural Time.

We are concerned here with the isothermal deformation of solids whose mechanical properties do not depend in any way on time (this excludes, for instance, creep, relaxation and sensitivity to rate of strain). For an element of such a material we postulate single-valued tensor relations of type

$$\text{stress-rate component} = f(\text{strain-rate components}). \tag{1}$$

No material constant with dimensions of time can enter and so the functions f have to be homogeneous of degree one in the components of strain-rate, though by no means necessarily linear forms. They may also depend explicitly on the current stress as well as the entire strain-history from some reference configuration.

The following classification and terminology is proposed. Consider an element in a given state under a given stress, and imagine it to be subjected to any cycle of deformation that finally restores its shape. Such a cycle can be visualized as a closed circuit starting and finishing at the origin in strain-space (suitable co-ordinates would be the Lagrangian components of finite strain with reference to the given configuration). Since the circuit may or may not restore the stress to its original value, certain mutually exclusive possibilities arise.

(a) The stress is recovered on all circuits in a neighbourhood of strain space surrounding the origin: the solid will be described as *resilient* in this state. If all accessible states in a certain region are resilient, there is evidently a single-valued functional dependence of stress on strain, and equations (1) are integrable as they stand.*

*Adkins (1958, p. 520) uses ' resilient ' when there is a functional relation between stress, strain and the time-derivatives of strain. The definitions agree when the deformation is quasi-static.

Consider, in particular, solids whose behaviour is describable thermodynamically in a region of strain space. If the strain and temperature are the only independent state-variables, and if the stress is derivable from a potential function of strain under the isothermal constraint, the solid will be called *elastic*.*

(b) In every sufficiently small neighbourhood there are circuits which do not restore the stress to its initial value: the solid will be called *inelastic* † in this state. There are two especially important types of inelastic solid:

(i) If there is a neighbourhood in which the stress is not recovered on any circuit the state will be called *plastic*. (This could perhaps be taken as the definition of an ideal amorphous material). Such behaviour requires that relations (1) should either be non-linear at least in that a change of sign in strain-rate does not change merely the sign of stress-rate, or should explicitly involve some dependence on strain-history and not simply the final stress. For otherwise the initial stress would be restored by a degenerate circuit consisting of an outgoing arc and a return along it.

(ii) If, in every sufficiently small neighbourhood, the stress is recovered on circuits lying to one side of a surface through the origin in strain-space and is not recovered on circuits lying on the other side, the state will be called *resilient/plastic*.‡ If the stress is derivable from a potential function on the one side, the state will be called *elastic/plastic*; this class includes, of course, metals at sufficiently high stresses attained through monotonic loading.

TRUESDELL (1953) has isolated for special study solids for which the functions f are linear in strain-rate and depend in addition only on the final stress, and has proposed the name 'hypo-elastic.' TRUESDELL's intention was to formulate a new concept of elastic behaviour (1955a, p. 88) or, more precisely, a concept of elastic behaviour expressed entirely in terms of rates (1956, p. 441). However, probably the overwhelming majority of hypo-elastic solids are inelastic, the stress being recovered only on special circuits (such as the degenerate kind mentioned earlier). And, in general, it is not even possible to regard non-integrable rate equations as approximately equivalent to incremental relations in a small enough neighbourhood,** since differences may not remain negligible when circuits are continually repeated.

2. CRITERION OF UNIQUENESS

Rate equations are associated with the following boundary-value problem. At a generic stage in a process of quasi-static distortion the internal distribution of stress, the shape of the body, the current values of material parameters, the state of anisotropy, etc., are supposed to have been determined already. The internal velocity field has then to be calculated when the rates of change of the surface loads, body forces, and geometrical constraints are prescribed (velocity and other rates here are measured in terms of some monotonically changing geometric

*In accordance with common usage. TRUESDELL (1956), however, has suggested 'hyperelastic,' taking 'elastic' in the weaker sense of 'resilient.'

†'Unresilient' would be more consistent, but 'inelastic' is already widely used – though not with the present precision.

‡The solidus notation suggests the surface of separation.

**TRUESDELL seems to countenance the possibility (1955b, p. 123 and 1956, p. 441, especially the transition between equations (6) and (7)).

parameter). We now obtain a condition sufficient to ensure a unique solution to this boundary-value problem.

For the present purpose it suffices to specify the current (initial) positions of elements by rectangular Cartesian co-ordinates x_i and the stress at any later instant by the nominal stress tensor s_{ij} associated with the corresponding convected co-ordinates (the surfaces $x_i = constant$ being regarded as embedded in the material and deforming with it). The rate of change of s_{ij}, evaluated at the initial instant, is denoted by $\dot{s}_{ij}$; that is, after an infinitesimal time δt, $\dot{s}_{ij}\,\delta t\,dS$ is the jth component (with respect to the rectangular axes) of the increase in force on the element lying in the ith co-ordinate surface and initially of area dS. Also, the rate of change of the nominal traction on an element initially having the unit normal l_i has components

$$\dot{F}_j = l_i\,\dot{s}_{ij} \tag{2}$$

with respect to the rectangular axes; $\dot{F}_j\,\delta t\,dS$ is then the increase in the jth component of the load after time δt. For continuing equilibrium under body-force rates $\dot{g}_j$ per unit initial volume,

$$\frac{\partial \dot{s}_{ij}}{\partial x_i} + \dot{g}_j = 0. \tag{3}$$

Uniqueness will be examined here when the nominal traction-rate $\dot{F}_j$ is given on a part S_F of the surface S, the velocity v_j on the remainder S_v, and body-force rates $\dot{g}_j$ in the volume V. Suppose there could be two solutions and let the prefix Δ denote the difference of any corresponding quantities. Then

$$\frac{\partial}{\partial x_i}\,\Delta\dot{s}_{ij} = 0 \text{ in } V, \qquad l_i\,\Delta\dot{s}_{ij} = 0 \text{ on } S_F, \qquad \Delta v_j = 0 \text{ on } S_v. \tag{4}$$

Hence

$$\int \Delta\dot{s}_{ij}\,\frac{\partial}{\partial x_i}\,(\Delta v_j)\,dV = \int l_i\,\Delta\dot{s}_{ij}\,\Delta v_j\,dS = 0.$$

A sufficient condition for uniqueness is therefore that

$$\int \Delta\dot{s}_{ij}\,\frac{\partial}{\partial x_i}\,(\Delta v_j)\,dV > 0 \tag{5}$$

for all pairs of continuous differentiable velocity fields taking the prescribed values on S_v.* The $\Delta\dot{s}_{ij}$'s are functions of the velocity gradients obtained via (1) and may not be in equilibrium nor such that $\Delta\dot{F}_j$ vanishes on S_F. It is important to notice that when the relations (1) are linear the integral in (5) is a single-valued functional of Δv_j (regarded as a single field), but that when they are non-linear it is multi-valued and $\Delta\dot{s}_{ij}$ is not necessarily related by (1) to the velocity gradient field $\partial\,(\Delta v_j)/\partial x_i$.

Thus, when the equations are non-linear, the sufficient condition (5) may be satisfied for some velocity distributions on S_v but not for others. More generally, we can expect a unique solution for certain conditions on S_F and S_v but not for others; from this standpoint, the test (5) is undiscriminating in that it takes no cognizance of the particular traction-rates on S_F. By contrast, when the equations are linear,

*The reverse inequality would also give a sufficient condition, but is not considered because such states are probably unstable (Section 3).

the satisfaction of (5) for particular conditions on S_v guarantees uniqueness for all as well as for any traction-rates on S_F. And, quite apart from whether (5) holds or not, it is obvious that uniqueness in no way turns on the boundary values (the parts S_F and S_v being given); for, when a solution to the homogeneous problem (4) exists, an arbitrary multiple of it can be added to one solution to generate others for any non-homogeneous problem with the same S_F and S_v.

Even for an elastic solid condition (5) is not necessary for uniqueness, and for a general solid the positive identification of bifurcation states involves actually demonstrating solutions to (4). However, we show in Section 4 (iii), that, for certain linear solids, a solution does exist in those states for which the functional in (5) is generally positive but vanishes for at least one non-zero field Δv_j. It is such bifurcations that would normally be reached first in any *actual* process of deformation, since they terminate a continuous range of states which not only satisfy (5) but are also stable (Sections 3 and 4 (i)). Thus, while not a necessary condition, (5) is, in these circumstances and in this sense, critical.

3. STABILITY

To be definite suppose that a part S_v of the surface is rigidly constrained and that *dead loads* are maintained on the part S_F and in the volume V. The body, initially at rest, is imagined to be set in motion by any kind of transitory disturbance. The initial state is said to be stable if the amplitude of the ensuing displacement is always vanishingly small when the disturbance itself is. If, on the other hand, the amplitude is finite for at least one type of disturbance, however small this is, the state is said to be unstable. The aim here is to formulate a sufficient condition for stability in this sense. We make the simplifying assumption that the same relations (1) still apply to a close approximation even though the oscillatory motion is not actually isothermal.

The work done on the body by the dead loads in any displacement depends only on the final configuration and not on the path by which it is reached. So also does the internal work of distortion when the solid is elastic, and in this event a motion started with kinetic energy T would be contained within a surface in configuration space on which the total potential energy U of the system (body and loads) is equal to T, relative to the initial state O. If, then, U is positive everywhere in a certain neighbourhood containing O the motion is bounded for all sufficiently small T and its amplitude vanishes with T; this is the familiar Kelvin-Dirichlet condition for stability. It is still sufficient when the motion induces gyroscopic forces of the kind that do no work (but the condition is then no longer generally necessary, as ZIEGLER (1956 pp. 359-361) has shown by simple counter-examples). Also, if the motion involves some dissipation of energy the condition applies *a fortiori*.

By contrast, when the internal work of distortion is path-dependent, we can not always expect a useful sufficient condition which does not give weight to *dynamically* possible paths (by analogy with examples by ZIEGLER (1956, pp. 362 – 381), in connexion with circulatory loads which do net work in closed cycles). However, we restrict attention here to a class of inelastic solids where it is still possible to prove stability under dead loading without a detailed examination of the actual motions. Consider a state in which

$$\int \dot{s}_{ij} \frac{\partial v_j}{\partial x_i} \, dV > 0 \tag{6}$$

for all continuous differentiable velocity fields which vanish on S_v and are not identically zero. It is readily shown (cf. HILL 1958, p. 245) that, to second order in δt, the internal work minus the external work is

$$U = \tfrac{1}{2} (\delta t)^2 \int \dot{s}_{ij} \frac{\partial v_j}{\partial x_i} \, dV$$

in any geometrically possible path described in an infinitesimal time δt and starting in the ' direction ' of the velocity field v_j, where $\dot{s}_{ij}$ is obtained via (1) ; to this order the calculation does not involve the ' curvature ' of the path. Put otherwise : the net energy absorbed by the system in moving along any reasonably direct path to a neighbouring configuration specified by the displacement field δu_j is given correctly to second order by the preceding formula with $\delta u_j = v_j \, \delta t$. Introduce, now, the family of similarly situated closed surfaces of constant (positive) U surrounding the position of rest in a neighbourhood of configuration space. Let the solid be such that the net energy absorbed on *every* path (however circuitous) lying *within* any given U surface and *terminating on the surface* is never less than the corresponding value of U. (It is of no concern what happens on any path not entirely contained within the surface through its terminal point.) It follows that a motion started with kinetic energy T can never cross the surface $U = T$, no matter how long the motion may continue. Since this surface becomes vanishingly small with T the initial state is stable ; the presence of gyroscopic forces or dissipative processes does not affect this conclusion. On the other hand, even in their absence, it may well be that the condition could be unnecessary for stability. At the present time nothing definite can be said about this. Nor is it known for certain what particular solids have U surfaces with the required property (some discussion of the matter for types of *rigid/plastic* and *elastic/plastic* solids has been given by HILL 1957a, pp. 3 – 4; 1958, p. 246).

Consider, now, the relation between the conditions (5) and (6). We note first that the Δv_j fields admitted in (5) are exactly those admitted in (6) since both must vanish on S_v and are otherwise arbitrary. However, (6) is a single-valued functional while (5) is multi-valued when equations (1) are non-linear and single-valued only when they are linear. Consequently the conditions are identical only when the rate equations are linear (a category which includes hypo-elastic solids and certain other inelastic solids).

Suppose, now, that the rate equations are non-linear and that the uniqueness criterion (5) is satisfied for the boundary condition $v_j = 0$ on S_v. Since $v_j \equiv 0$ is admissible in (5) the value of the functional (6) with any other field is also assumed by (5) when this and the zero field are taken together as a pair. It follows that inequality (6) holds. Thus, when the sufficient condition for uniqueness is satisfied for rigid constraints on S_v the state is stable for solids of the required type. The converse need not be true. For, even though we know a state to be stable in the sense that (6) is satisfied, nothing can be concluded directly about the functional (5) since it is multi-valued. That is, the boundary-value problem need not have a unique solution in a stable state.

Of course, a stable bifurcation of that kind could not occur under dead loading (since this would imply that the functional (6) vanishes for the actual velocity field). In fact, the loading would have to be changing in such a way that

$$\int \dot{F}_j \, v_j \, dS_F + \int \dot{g}_j \, v_j \, dV = \int \dot{s}_{ij} \frac{\partial v_j}{\partial x_i} \, dV > 0, \tag{7}$$

where v_j is any of the possible *actual* fields at the bifurcation.

4. Rate Equations with a Potential

(i) Our general conclusions can be appreciably sharpened for solids such that

$$\dot{s}_{ij} = \frac{\partial E}{\partial \, (\partial v_j / \partial x_i)} \tag{8}$$

where E is a homogeneous function of degree two in the velocity gradients, depending on the current stress and possibly also on the entire strain-history. E is assumed to have continuous first derivatives and at least sectionally-continuous second derivatives. The equations are linear when E is polynomial, non-linear otherwise. When they have a unique inverse this is expressible through the Legendre transformation as

$$\frac{\partial v_j}{\partial x_i} = \frac{\partial E_c}{\partial \dot{s}_{ij}} \qquad \text{where} \qquad E + E_c = \dot{s}_{ij} \frac{\partial v_j}{\partial x_i}, \tag{9}$$

and E_c is expressed in terms of the nominal stress-rate (which, being unsymmetric, has nine independent components).

Any solution of the boundary-value problem, unique or not, can be characterized by a variation principle, namely that

$$\int E \, (\partial v_j / \partial x_i) \, dV - \int \dot{F}_j \, v_j \, dS_F - \int \dot{g}_j \, v_j \, dV \tag{10}$$

is stationary in the class of continuous differentiable velocity fields taking the given values on S_v. For

$$\int \delta E \, dV = \int \dot{s}_{ij} \frac{\partial}{\partial x_i} (\delta v_j) \, dV = \int \dot{F}_j \, \delta v_j \, dS + \int \dot{g}_j \, \delta v_j \, dV$$

when the stress-rates satisfy (2) and (3), and so the first variation of (10) vanishes when $\delta v_j = 0$ on S_v. In particular, if a bifurcation occurs under dead loading, the non-zero mode makes $\int E \, dV$ stationary. Similarly,

$$\int \dot{F}_j \, v_j \, dS_v - \int E_c \, (\dot{s}_{ij}) \, dV \tag{11}$$

is stationary in the class of nominal stress-rate fields satisfying (2) on S_F and (3) in V. In an actual solution the values of (10) and (11) coincide. These variation principles are analogous to the wellknown ones for the potential and complementary energies in infinitesimal (non-linear) elasticity.

The uniqueness condition (5) becomes

$$\int \Delta \left(\frac{\partial \boldsymbol{E}}{\partial \left(\partial v_j / \partial x_i \right)} \right) \Delta \left(\frac{\partial v_j}{\partial x_i} \right) dV > 0 \tag{12}$$

for pairs of velocity fields taking the given values on S_v. It can be shown (HILL 1958, p. 244) that, if (12) holds, then

$$\int \left[\Delta \boldsymbol{E} - \frac{\partial \boldsymbol{E}}{\partial \left(\partial v_j / \partial x_i \right)} \Delta \left(\frac{\partial v_j}{\partial x_i} \right) \right] dV > 0 \tag{13}$$

for permissible pairs. Conversely, if this is satisfied, (12) follows immediately by adding to (13) the dual inequality obtained by interchanging members of a pair. If, now, v_j is the actual unique solution, transformation of (13) gives

$$\Delta \left[\int \boldsymbol{E} dV - \int \dot{F}_j \, v_j \, dS_F - \int \dot{g}_j \, v_j \, dV \right] > 0. \tag{14}$$

That is, when the sufficient condition (12) for uniqueness is satisfied, the expression (10) is not only stationary for the actual field but is an absolute minimum.

Equally, when (9) holds, a sufficient condition for uniqueness is

$$\int \Delta \left(\frac{\partial \boldsymbol{E}_c}{\partial \dot{s}_{ij}} \right) \Delta \dot{s}_{ij} \, dV > 0 \tag{15}$$

for any pair of nominal stress-rate fields satisfying (2) on S_F and (3) in V. In general this criterion differs from (12); when it is satisfied the expression (11) has an absolute maximum in the actual state.

In the special case when $\boldsymbol{E}$ is strictly convex everywhere in V (i.e. the integrand in (12) is always positive), so is $\boldsymbol{E}_c$; (12) and (15) are simultaneously satisfied for all boundary values and both extremum principles apply. This situation normally arises only when geometry changes can be disregarded. The idea of convexity in the present context was introduced by HILL (1956b) and shown to be the basis of a unified treatment of uniqueness and extremum principles in several distinct branches of mechanics.

The stability condition (6) reduces to

$$\int \boldsymbol{E} \, dV > 0 \tag{16}$$

for fields vanishing on S_v, by Euler's theorem for homogeneous functions.

(ii) When $\boldsymbol{E}$ is a *quadratic form*, (12) simplifies to (16). In this case the stability and uniqueness conditions coincide, in accord with what has already been shown for a general linear solid.

The technical difficulties in applying (12) when the solid is non-linear, due to the multi-valuedness of the integral, can be eased by the following 'linearizing' device, though at the expense of weakening the criterion. Let $\boldsymbol{E}'$ be such that the difference $\boldsymbol{E} - \boldsymbol{E}'$ is a convex function of velocity gradient at every point of the body; that is,

$$\Delta \left(\frac{\partial \left(\boldsymbol{E} - \boldsymbol{E}' \right)}{\partial \left(\partial v_j / \partial x_i \right)} \right) \Delta \left(\frac{\partial v_j}{\partial x_i} \right) \geqslant 0 \tag{17}$$

or an equivalent. If, in the given state, we were able to show that (12) was satisfied

for the solid E', then it would be satisfied *a fortiori* for the solid E. If, now, we can find such an E' which is quadratic, so that this solid is linear, we would merely have to prove (16) for E'. For the best result the approximating linear solid should make the volume integral of (17) as small as possible. For example, in the treatment of a class of elastic/plastic solids (HILL 1958), where in a plastic element E is equal to a certain quadratic E' in the 'loading' part of strain-rate space and to a different quadratic E'' in the 'unloading' part, such that $E'' - E'$ is positive-definite, the best choice is the linear solid E' (equation (13), *op. cit.*, is the statement of the convexity of $E - E'$).

(iii) We consider next the bifurcation states of a *linear solid* such that

$$\dot{s}_{ij} = c_{ijkl} \frac{\partial v_l}{\partial x_k}$$

where

$$c_{ijkl} = c_{klij} \tag{18}$$

and the coefficients do not involve the velocity gradients but may be functions of position. It has the quadratic potential

$$E = \tfrac{1}{2} c_{ijkl} \frac{\partial v_j}{\partial x_i} \frac{\partial v_l}{\partial x_k}.$$

In a bifurcation state the boundary-value problem definitely has more than one solution; in fact an infinity of solutions whose differences satisfy the homogeneous equations

$$\left.\begin{aligned} L(\mathbf{v}) \equiv \frac{\partial}{\partial x_i}\left(c_{ijkl}\frac{\partial v_l}{\partial x_k}\right) = 0 \qquad & \text{in } V, \\ \dot{F}_j = l_i\, c_{ijkl}\frac{\partial v_l}{\partial x_k} = 0 \qquad \text{on } S_F, \qquad & v_j = 0 \qquad \text{on } S_v. \end{aligned}\right\} \tag{19}$$

The matrix differential operator L is self-adjoint in that the reciprocal relation

$$\int [\mathbf{v}'' L(\mathbf{v}') - \mathbf{v}' L(\mathbf{v}'')]\, dV = \int (\dot{\mathbf{F}}' \mathbf{v}'' - \dot{\mathbf{F}}'' \mathbf{v}')\, dS = 0 \tag{20}$$

holds by virtue of the symmetry property (18) for any two fields $\mathbf{v}'$, $\mathbf{v}''$ satisfying the regular boundary-conditions (19), though not necessarily the differential equations.

We introduce eigenfunctions associated with a given stress state and function E, and defined by

$$L(\mathbf{v}) + \lambda \mathbf{v} = 0, \tag{21}$$

with the same boundary conditions (19). By the standard method it follows from (20) that the eigenvalues λ_r are real and that the eigenfunctions are orthogonal in that

$$\int \mathbf{v}_r \mathbf{v}_s\, dV = 0, \qquad \lambda_r \neq \lambda_s. \tag{22}$$

For convenience suppose them normalized so that

$$\int \mathbf{v}_r^2\, dV = 1, \qquad \text{all } r. \tag{23}$$

When the solid is elastic the eigenvalues are proportional to the squares of the roots of the ' frequency equation,' the body having uniform density. But when the rate equations (8) are not integrable this interpretation cannot be given, and the eigenfunctions can merely be regarded as fields possible under dead loading and body forces proportional to the velocity.

Suppose that $\mathbf{v}$ is any continuous differentiable field vanishing on S_v, and denote its ' Fourier coefficients ' with respect to a complete set of the normalized eigenfunctions by

$$a_r = \int \mathbf{v}\,\mathbf{v}_r\,dV. \tag{24}$$

Although the $\dot{\mathbf{F}}$ corresponding to $\mathbf{v}$ need not vanish on S_F the series $\Sigma a_r\,\mathbf{v}_r$ nevertheless converges to $\mathbf{v}$ not only in V but also everywhere on S. If $\boldsymbol{L}(\mathbf{v})$ exists and is integrable,

$$\int [\mathbf{v}_r\,\boldsymbol{L}(\mathbf{v}) - \mathbf{v}\boldsymbol{L}(\mathbf{v}_r)]\,dV = \int \dot{\mathbf{F}}\mathbf{v}_r\,dS_F,$$

and so, from (21) and (24),

$$\int \mathbf{v}_r\,\boldsymbol{L}(\mathbf{v})\,dV = -\lambda_r\,a_r + \int \dot{\mathbf{F}}\mathbf{v}_r\,dS_F.$$

These are the Fourier coefficients of the vector field $\boldsymbol{L}(\mathbf{v})$. Consequently, by an obvious extension of a theorem of Parseval,

$$\Sigma a_r\left(-\lambda_r\,a_r + \int \dot{\mathbf{F}}\mathbf{v}_r\,dS_F\right) = \int \mathbf{v}\,\boldsymbol{L}(\mathbf{v})\,dV.$$

Now

$$2\int E(\mathbf{v})\,dV = \int \dot{\mathbf{F}}\mathbf{v}\,dS_F - \int \mathbf{v}\,\boldsymbol{L}(\mathbf{v})\,dV$$

and so

$$\int E(\mathbf{v})\,dV = \tfrac{1}{2}\,\Sigma\,\lambda_r\,a_r^2. \tag{25}$$

In particular:

$$\int E(\mathbf{v}_r)\,dV = \tfrac{1}{2}\,\lambda_r. \tag{26}$$

Suppose that the condition (16) is satisfied,

$$\text{i.e.} \qquad \int E(\mathbf{v})\,dV > 0 \qquad \text{for all fields vanishing on } S_v. \tag{27}$$

Then, from (26), all the eigenvalues associated with this state must be positive; the converse is also clearly true.

Suppose next that we have a state in which

$$\left.\begin{aligned} &\int E(\mathbf{v})\,dV \geqslant 0 \qquad \text{for all fields } \mathbf{v} \text{ vanishing on } S_v \\ \text{and} \quad &\int E(\mathbf{w})\,dV = 0 \qquad \text{for some of these fields, } \mathbf{w}. \end{aligned}\right\} \tag{28}$$

We deduce first from (26) that no eigenvalue can be negative. It follows that the

right side of (25) can only vanish if the eigenvalues associated with all the non-vanishing Fourier coefficients of the special $\mathbf{w}$ fields are in fact zero. Thus the eigenvalue zero exists and every $\mathbf{w}$ is an associated eigenfunction, $\mathbf{v}_0$ say, satisfying (19) and representing a mode possible under dead loading. In other words (28) defines as type of bifurcation state. Moreover, by the stationary property proved in (i) above, the value zero is an analytic, as well as absolute, minimum of $\int E\,dV$. We shall see later that these results essentially constitute a far-reaching generalization of Rayleigh's principle.

Now it often happens that the rate equations (8) involve as a parameter a material constant, μ say, whose value can be thought of as assignable independently of the given distribution of stress and the region V: for example, Young's modulus for an elastic solid when the pre-strain is negligible, or the current rate of hardening for an elastic/plastic solid. By allowing μ to vary we obtain a 'linear series' of states, and to emphasize this parametric dependence we write

$$\int E_\mu(\mathbf{v})\,dV \qquad \text{and} \qquad L_\mu(\mathbf{v}).$$

Those bifurcation states that are included in this linear series are the eigenfunctions of the operator L_μ corresponding to the eigenvalues of μ. Let μ_0 denote any eigenvalue associated with a bifurcation state of the type (28). In general, because of the non-linear dependence of L_μ on μ, an expansion theorem is not available and so μ_0 cannot be explicitly characterized by an extremum property. However, in the event that μ_0 is so small that

$$c_{ijkl}(\mu) \simeq c_{ijkl}(0) + \mu\left(\frac{\partial c_{ijkl}}{\partial \mu}\right)_0 \qquad \text{for} \qquad \mu = O(\mu_0),$$

equation (28) yields approximately

$$\int E_0\,dV + \mu_0 \int \left(\frac{\partial E_\mu}{\partial \mu}\right)_0 dV \geqslant 0$$

for all admissible fields $\mathbf{v}$, with equality for at least one. To be definite, suppose that the first term is positive (as will normally happen) and write

$$R(\mathbf{v}) = -\int E_0\,dV \Big/ \int \left(\frac{\partial E_\mu}{\partial \mu}\right)_0 dV,$$

a generalized Rayleigh quotient. The condition defines two eigenvalues, one of each sign:

$$\left.\begin{aligned} &\textit{Min}\ R(\mathbf{v}) \text{ in class of positive values of } R, \\ -&\textit{Min}.\ |R(\mathbf{v})| \text{ in class of negative values of } R. \end{aligned}\right\} \tag{29}$$

For values of μ lying between these limits the condition (27) for uniqueness is met.

When the solid is elastic μ can be taken as the ratio of a (given) stress magnitude to a (varying) elastic modulus, the dimensional changes of the body being negligible for sufficiently small μ. The result (29) is then an extended form of Rayleigh's principle in the context of the classical theory of elastic stability (Southwell 1953); when R is always positive the range of stability is (formally) unbounded below, and we have the usual form of the principle. The standard proof differs

from the present one in that it proceeds by an expansion in the orthogonal μ-eigenfunctions of the operator $\boldsymbol{L}_\mu$ (or via the Green's function for $\boldsymbol{L}_0$), taking advantage of the linear dependence on μ. This, however, cannot be done when the dependence is irreducibly non-linear; for that reason the standard method must be regarded as less significant, fundamentally, than the present expansion in λ-eigenfunctions of the operator $(\boldsymbol{L}\mu + \lambda)$ for general fixed μ.

5. Definition of Stress-rate

(i) For a more detailed classification of the rate equations (1) it is desirable to define a 'stress-rate' which is unaffected by a rigid-body spin, unlike the rate of change of nominal stress which we have used so far. To begin with we take a definition (Oldroyd 1950) based on a system of curvilinear co-ordinates embedded in the body and deforming with it. The three families of co-ordinate surfaces are arbitrarily parametrized by numerical values ξ^α ($\alpha = 1, 2, 3$); each material point is thereby specified by a triad of constant ξ^α's. At each instant any tensor is represented by its components with respect to the *current* local ξ^α surfaces. The 'convected derivative' of a tensor is then defined to be the tensor formed by the time-derivatives of *these* components.

We are especially concerned here with the 'true stress' and with the Kirchhoff (or Trefftz) stress, respectively having contravariant components $\sigma^{\alpha\beta}$ and $\tau^{\alpha\beta}$, say. These are defined by decomposing the load vector on an arbitrary plane element in the two ways

$$\sigma^{\alpha\beta}\,(\nu_\alpha\,dS)\,\mathbf{g}_\beta = \tau^{\alpha\beta}\,(\nu_\alpha{}^\circ\,dS^\circ)\,\mathbf{g}_\beta \qquad (30)^*$$

where $\mathbf{g}_\beta$ are the covariant base-vectors for the convected co-ordinates in their final position, ν_α are the corresponding covariant components of the final unit normal to the element, $\nu_\alpha{}^\circ$ are the covariant components of the unit normal in some initial configuration and with respect to the co-ordinates then, and dS, dS° are the final and initial infinitesimal areas. In view of Nanson's relation

$$\rho\nu_\alpha\,dS = \rho^\circ\,\nu_\alpha{}^\circ\,dS^\circ \qquad (31)$$

where ρ°, ρ are the initial and final densities,

$$\tau^{\alpha\beta} = \frac{\rho^\circ}{\rho}\,\sigma^{\alpha\beta}. \qquad (32)$$

Thus the Kirchhoff stress is simply proportional to the true stress (equal when the material is incompressible) and in particular is a symmetric tensor.

Now the work-rate per unit *final* volume is $\sigma^{\alpha\beta}\,\epsilon_{\alpha\beta}$, where $\epsilon_{\alpha\beta}$ is the strain-rate tensor defined by

$$\epsilon_{\alpha\beta} = \tfrac{1}{2}\,(v_{\alpha,\beta} + v_{\beta,\alpha}), \qquad (33)$$

where v_α is the velocity and a comma signifies covariant differentiation in the final configuration. By (32) the work-rate per unit *initial* volume is therefore $\tau^{\alpha\beta}\,\epsilon_{\alpha\beta}$.

On differentiating (32) with respect to time, holding the initial reference configuration fixed, we obtain a relation between the convected derivatives. *When the reference configuration is taken as that at the instant under consideration* (ρ being

*That the load vector is a *linear* function of the components of the normal is of course the essence of the basic theorem of Cauchy in stress analysis.

accordingly put equal to ρ° after the differentiation),

$$\dot{\tau}^{\alpha\beta} = \dot{\sigma}^{\alpha\beta} + \sigma^{\alpha\beta}\,\epsilon_\gamma{}^\gamma. \tag{34}$$

In passing, it is worth noting also that from (30) the convected derivative of the load vector on a plane element is $\dot{\tau}^{\alpha\beta}\,\nu_\beta\,dS$ with this choice of reference state.*

Let $\gamma_{\alpha\beta}{}^\circ$ and $\gamma_{\alpha\beta}$ be the initial and final metric tensors of the convected co-ordinates so that the initial and final lengths, ds_0 and ds, of the line element $d\xi^\alpha$ are given by

$$ds_0{}^2 = \gamma_{\alpha\beta}{}^\circ\,d\xi^\alpha\,d\xi^\beta, \qquad ds^2 = \gamma_{\alpha\beta}\,d\xi^\alpha\,d\xi^\beta.$$

Introduce the strain tensor†

$$e_{\alpha\beta} = \tfrac{1}{2}\,(\gamma_{\alpha\beta} - \gamma_{\alpha\beta}{}^\circ). \tag{35}$$

It may be shown that $\dot{\gamma}_{\alpha\beta} = 2\epsilon_{\alpha\beta}$ and so‡

$$\dot{e}_{\alpha\beta} = \epsilon_{\alpha\beta}, \tag{36}$$

the reference configuration for the finite strain being *arbitrary*. This important result is by no means as simple as the notation tends to suggest.

An expression of the rate equations (1) in a form not involving spin is

$$\dot{\tau}^{\alpha\beta} = f^{\alpha\beta}\,(\epsilon_{\gamma\delta}). \tag{37}$$

Let us see what this becomes for an elastic solid whose free energy under isothermal conditions is $W\,(e_{\alpha\beta})$ per unit initial volume (depending on $\gamma_{\alpha\beta}{}^\circ$ and on the reference state which need not be unstressed). Then

$$\tau^{\alpha\beta}\,\epsilon_{\alpha\beta} = \dot{W} = \frac{\partial W}{\partial e_{\alpha\beta}}\,\dot{e}_{\alpha\beta}$$

and so, by (36),

$$\tau^{\alpha\beta} = \frac{\partial W}{\partial e_{\alpha\beta}} = \frac{\rho^\circ}{\rho}\,\sigma^{\alpha\beta}. \tag{38}$$

Hence $\tau^{\alpha\beta}$ and $e_{\alpha\beta}$ are complementary variables with respect to W, when this is symmetrized. The isothermal rate equations of an elastic solid can now be written concisely as

$$\dot{\tau}^{\alpha\beta} = \frac{\partial^2 W}{\partial e_{\alpha\beta}\,\partial e_{\gamma\delta}}\,\epsilon_{\gamma\delta}. \tag{39}$$

The coefficients depend only on the deformation $e_{\alpha\beta}$ (and not on the rotation) and hence by (38) only on the final stress. Consequently, an elastic solid is hypo-elastic in TRUESDELL'S sense (Section 1). We can show similarly that resilient solids for which $\tau^{\alpha\beta}$ depends only on the $e_{\alpha\beta}$'s are also hypo-elastic. This is a simple proof of a theorem of NOLL (1955), stated only for isotropic materials.

*TRUESDELL'S (1955, p. 124; 1953, p. 604) 'relative time flux' of stress—which he writes as $\overset{\circ}{\sigma}{}^{\alpha\beta}$—is just the right side of (34) expressed in components referred to fixed co-ordinates, although he apparently nowhere recognizes this. TRUESDELL'S (1953, p. 598) 'absolute time flux' of the load vector is also in this sense the equivalent of its convected derivative.

†It is customary to call this the Lagrange or Euler strain measure according to whether the initial or final position of the convected co-ordinates is taken as the fixed frame of reference in the field equations. Our standpoint here, however, is entirely general.

‡OLDROYD (1950, p. 533) states this from the Eulerian viewpoint; it is essentially given from the Lagrangian viewpoint by GREEN and ZERNA (1954, equation 2.6.2.) However, it seems that priority must be assigned to the COSSERATS (1896, quoted by TRUESDELL 1952, p. 153, equation (22.14)) who also stated the result in Lagrangian terms.

Consider, next, solids for which

$$\mathring{\tau}^{\alpha\beta} = \frac{\partial F}{\partial \epsilon_{\alpha\beta}} \tag{40}$$

where F is a symmetrized homogeneous function of degree two in the strain-rate components, depending possibly also on the current stress and previous strain-history. We shall see later that (40) is equivalent to (8). Linear solids such that

$$\mathring{\tau}^{\alpha\beta} = \kappa^{\alpha\beta\gamma\delta}\,\epsilon_{\gamma\delta}, \qquad \text{where} \qquad \kappa^{\alpha\beta\gamma\delta} = \kappa^{\gamma\delta\alpha\beta},$$

belong to this group, with

$$F = \tfrac{1}{2}\,\kappa^{\alpha\beta\gamma\delta}\,\epsilon_{\alpha\beta}\,\epsilon_{\gamma\delta}.$$

Elastic solids are included since the coefficients in (39) have the required symmetry.

(ii) Return now to (30) and a third way of decomposing the load vector:

$$s^{\alpha\beta}\,(\nu_\alpha{}^\circ\,dS^\circ)\,\mathfrak{g}_\beta{}^\circ \tag{41}$$

where $\mathfrak{g}_\beta{}^\circ$ are the base-vectors of the convected co-ordinates in their initial configuration. $s^{\alpha\beta}$ is called here the 'nominal stress' tensor; this is consistent with the terminology of Section 2 since the stresses defined there are just the components of $s^{\alpha\beta}$ with respect to co-ordinates which are initially Cartesian.* On carrying out the convected differentiation, after substituting

$$\mathfrak{g}_\beta = (\delta_\beta{}^\gamma + u^\gamma{}_{,\beta})\,\mathfrak{g}_\gamma{}^\circ$$

where u^γ is the total displacement and $\delta_\beta{}^\gamma$ the Kronecker delta,

$$\mathring{s}^{\alpha\beta} = \mathring{\tau}^{\alpha\beta} + \tau^{\alpha\gamma}\,v^\beta{}_{,\gamma}, \tag{42}$$

the reference state being that at the instant considered. (Note that $\mathring{s}^{\alpha\beta}$ is not symmetric and does not vanish in a rigid-body spin).

The integrand in the stability functional (6) can thus be written

$$\mathring{s}^{\alpha\beta}\,v_{\beta,\,\alpha} = \mathring{\tau}^{\alpha\beta}\,\epsilon_{\alpha\beta} + \tau^{\alpha\gamma}\,v_{\beta,\,\alpha}\,v^\beta{}_{,\gamma}. \tag{43}$$

Taken with (39) the right-hand expression becomes the generalized form of explicit expressions for elastic solids derived in alternative ways by TREFFTZ (1933), PEARSON (1956) and HILL (1957).

If, now, (40) holds it is readily verified that (8) does too:

$$\mathring{s}^{\alpha\beta} = \frac{\partial E}{\partial\,(v_{\beta,\,\alpha})} \qquad \text{where} \qquad E\,(v_{\beta,\,\alpha}) = F\,(\epsilon_{\alpha\beta}) + \tfrac{1}{2}\,\tau^{\alpha\gamma}\,v_{\beta,\,\alpha}\,v^\beta{}_{,\gamma}. \tag{44}$$

Conversely, any admissible function E of the velocity gradients must be capable of being so expressed. Since the spin terms are separated out in (44) it leads directly to a convenient form of the functional (16).

(iii) Less sophisticated than the convected derivative is the derivative of components associated with *rigid* curvilinear co-ordinates whose origin moves with the considered material element and whose spin is the vector associated with the antisymmetric tensor

$$\omega_{\alpha\beta} = \tfrac{1}{2}\,(v_{\alpha,\,\beta} - v_{\beta,\,\alpha}).$$

*The components of the Kirchhoff double-vector, defined by the decomposition $s^{ai}\,(\nu_a{}^\circ\,dS^\circ)\,\mathfrak{g}_i$ where $\mathfrak{g}_i$ are the base-vectors of any other *fixed* system, also coincide with them when the fixed and initial convected co-ordinates are identical and Cartesian.

This, of course, is the spin of the orthogonal triad of lines of particles momentarily coinciding with the principal directions of strain-rate in the element ; this triad is instantaneously rigid. It seems appropriate to speak therefore of the ' rigid-body derivative ' ; it will be denoted here by $\mathscr{D}/\mathscr{D}t$ when the rigid and deforming frames of reference momentarily coincide.* It is easily shown that

$$\frac{\mathscr{D}T^{\alpha\beta}}{\mathscr{D}t} = \dot{T}^{\alpha\beta} + T^{\gamma\beta}\,\epsilon_{\gamma}{}^{\alpha} + T^{\alpha\gamma}\,\epsilon_{\gamma}{}^{\beta} \tag{45}$$

for any second-order tensor $T^{\alpha\beta}$.

If (40) holds then

$$\frac{\mathscr{D}\tau^{\alpha\beta}}{\mathscr{D}t} = \frac{\partial G}{\partial \epsilon_{\alpha\beta}} \qquad \text{where} \qquad G = F + \tau_{\beta}{}^{\alpha}\,\epsilon_{\gamma}{}^{\beta}\,\epsilon_{\alpha}{}^{\gamma}. \tag{46}$$

But

$$\frac{\mathscr{D}\sigma^{\alpha\beta}}{\mathscr{D}t} = \frac{\mathscr{D}\tau^{\alpha\beta}}{\mathscr{D}t} - \tau^{\alpha\beta}\,\epsilon_{\gamma}{}^{\gamma}$$

is not then derivable from a potential.

Relations (34) and (45) illustrate the fact, often mentioned, that stress-rates which are defined invariantly with respect to spin differ simply by terms (component stress $\times$ component strain-rate). It follows that rate equations which are of type (1) with one such definition of stress-rate do not lose their essential character (in particular their linearity or non-linearity) when expressed in terms of another. Consequently, in a general discussion, the choice of definition is largely a matter of taste or convenience. On the other hand, when constructing rate equations to describe the behaviour of an actual particular material or in classifying different kinds of behaviour it is obviously helpful (at least at the outset) to have regard to the physical interpretation of any considered stress-rate.

6. ELASTIC/PLASTIC SOLIDS

We now attempt an explicit characterization of a class of inelastic solids varied enough to include anything known or conjectured for metals.

Consider a stress-state associated with *non-linear* rate equations having the following special character. Take the given state as the origin of reference O in strain space. For all strain-rate vectors $\boldsymbol{\epsilon}$ represented by directions from O within a certain ' cone ' C, the relation between $\dot{\boldsymbol{\tau}}$ and $\boldsymbol{\epsilon}$ is *linear* with a quadratic potential

$$\tfrac{1}{2}\,\boldsymbol{\epsilon}\boldsymbol{K}\boldsymbol{\epsilon} \qquad \text{in} \qquad C,$$

where $\boldsymbol{K}$ is a (strain-dependent) symmetric matrix with inverse $\boldsymbol{K}^{-1}$. Suppose that there is also a potential

$$\tfrac{1}{2}\,\boldsymbol{\epsilon}\boldsymbol{K}\boldsymbol{\epsilon} - \Phi(\boldsymbol{\epsilon}) \qquad \text{outside} \qquad C,$$

where Φ need not be a quadratic but is of course homogeneous of degree two with continuous first derivatives. The assumption of a potential is analytically desirable

*This was the derivative used in the definition of a group of elastic/plastic solids (HILL 1958) ; in that paper it was denoted by a dot. Certain advantages over the convected derivative have been mentioned by OLDROYD (1958, p. 296), who refers to it as the ' material derivative.' This term is differently used by TRUESDELL (1952, p. 149) in respect of rigid axes moving, but not spinning, with the element ; OLDROYD calls this the ' intrinsic derivative.'

to make available the theorems of Section 3. In order that both potentials shall give the same stress-rate for a strain-rate on C the first partial derivatives of Φ with respect to the strain-rate components must vanish simultaneously on C:

$$\frac{\partial \Phi}{\partial \dot{\epsilon}} = 0 \qquad \text{on} \qquad C. \tag{47}$$

Φ must therefore have a stationary value at every point on C, as well as vanishing there. The composite potential surface is therefore smooth and continuous on C, but may have a discontinuity in 'curvature' there (the non-linearity would consist in just this if Φ were a single quadratic). Such a composite potential can be expected in a material capable of deforming by more than one mechanism at the atomic level.

The classification proposed in Section 1 is based on closed cycles of strain in the neighbourhood of O. Consequently, nothing can be determined purely from the rate equations for the single state: the variations of the matrix K, the potential Φ, and the surface C with further deformation have also to be assigned (this variation need by no means be continuous). The unspecified non-linearity is in itself sufficient for *inelastic* behaviour outside C. Within C suppose that the behaviour is *elastic* inside a smaller cone c (K being a Hessian matrix in a strain neighbourhood of O there, as in (39)), and *inelastic* between the cones. The solid can then be said to be *elastic/inelastic*, the smaller cone c defining an element of the 'yield surface' in strain space. This concept is broader in two ways than in conventional plastic theory: (i) the surface does not necessarily coincide with the transition between analytically distinct parts of the rate equations potential, and (ii) it is not necessarily associated with specifically plastic behaviour.* The available experimental data by no means excludes these possibilities, even in regard to metals—especially when many of the crystals in an aggregate are in an elastic state (for example on the hysteresis loop of a stress-strain curve for the aggregate).

The complete yield surface currently associated with a given state O is defined as the boundary of the region in strain space where an elastic relation of type (39) holds with respect to O (and therefore with respect to any other point in the region). At each point of the surface the rate equations can be assigned in the way described for O itself. The surface will be smooth (c degenerating to a plane) except possibly at particular points. These occur, for example, on the yield surface of a single metal crystal at stresses activating more than one family of glide planes according to the SCHMID law; the cone is 'pyramidal', consisting of a number of planes. However, the rate equations themselves at a vertex are not known for any material.†

Suppose, now, that the cones coincide. Assume further, that a yield surface is associated with any neighbouring state reached directly through a strain-rate outside the initial cone. Then, in general (not always), the solid is *elastic/plastic*. Consider a regular point of the surface where C is the tangent plane. Let its equation be $\mathbf{n}\, K\, \dot{\epsilon} = 0$ where $\mathbf{n}$ is a unit vector. Since $\dot{\tau} = K\dot{\epsilon}$ on C $\mathbf{n}$ is the normal to the

*TRUESDELL (1956) defines 'hypo-elastic (or M) yield,' in special monotonic distortions of a hypo-elastic solid, according as a certain stress invariant passes through (or attains) a maximum value; the entire incremental behaviour at a generic stage is apparently a matter of indifference. TRUESDELL's 'yield' has therefore no connexion whatever with the present concept or that in the conventional plastic theory of workhardening metals.

†Whenever, in theoretical applications, the yield surface is assumed pyramidal the rate equations proposed by KOITER (1953) have often been adopted for convenience: when the hardening is non-zero they can be generated from a convex potential obtained by adjoining a number of different positive quadratics.

yield surface in $\boldsymbol{\tau}$ space (the given state being taken as reference). Choose the sense of $\mathbf{n}$ arbitrarily as outward. By (47) the potential outside must take the form

$$\Phi = \tfrac{1}{2}(\mathbf{n}\,K\boldsymbol{\epsilon})^2\,\phi\,(\boldsymbol{\epsilon})$$

where the function ϕ is finite, homogeneous of degree zero, and with first derivatives numerically less than $O\,(\mathbf{n}\,K\boldsymbol{\epsilon})^{-1}$ near C. Then

$$\left.\begin{aligned} \dot{\boldsymbol{\tau}} &= K\,(\boldsymbol{\epsilon} - \boldsymbol{\epsilon}') \\ \text{where}\quad \boldsymbol{\epsilon}'/(\mathbf{n}K\boldsymbol{\epsilon}) &= \begin{cases} \phi\mathbf{n} + \tfrac{1}{2}\,(\mathbf{n}K\boldsymbol{\epsilon})\,K^{-1}\dfrac{\partial\phi}{\partial\boldsymbol{\epsilon}} & \text{when} \quad \mathbf{n}\,K\,\boldsymbol{\epsilon} \geqslant 0 \\ 0 & \text{when} \quad \mathbf{n}K\boldsymbol{\epsilon} \leqslant 0. \end{cases} \end{aligned}\right\} \tag{48}$$

$\boldsymbol{\epsilon}'\,\delta t$ is the remaining increment of strain (correct to first order) after a degenerate cycle in which the strain-rate $\boldsymbol{\epsilon}$ is maintained for an infinitesimal time δt and the convected components of $\boldsymbol{\tau}$ are then returned directly to their original values.

Observe that $\boldsymbol{\epsilon}'$ depends on the direction of $\boldsymbol{\epsilon}$ and not only on its magnitude. If, however, ϕ is a constant for the considered state, then

$$\left.\begin{aligned} \dot{\boldsymbol{\tau}} &= K\,(\boldsymbol{\epsilon} - \boldsymbol{\epsilon}') \\ \text{where}\quad \boldsymbol{\epsilon}'/(\mathbf{n}K\boldsymbol{\epsilon}) &= \phi\mathbf{n} \quad \text{when} \quad \mathbf{n}K\boldsymbol{\epsilon} \geqslant 0, \end{aligned}\right\} \tag{49}$$

and its direction is always normal to the $\boldsymbol{\tau}$ yield surface element. This indeed, with ϕ positive, is essentially the conventional postulate of plastic theory for metals (if the distinction between $\boldsymbol{\tau}$ and $\boldsymbol{\sigma}$ yield surfaces is ignored, the stress being small compared with elastic bulk modulus). According to experiment the postulate is approximately valid for several common metals ; it has also been derived theoretically for an aggregate of crystals deforming by multi-slip under the SCHMID law (BISHOP and HILL 1951 ; HILL 1956a). It is usually considered that $\mathbf{n}$ is deviatoric ; however, it now appears that even for metals this may theoretically not be strictly correct (HAASEN and LAWSON 1958), and no such restriction is made here. It is also customary to assert that $\boldsymbol{\tau}\,\boldsymbol{\epsilon}'$ is non-negative, so that ϕ has the sign of $\mathbf{n}\,\boldsymbol{\tau}$, but a justification from thermodynamics appears to be lacking.

To invert (49) note first that

$$\mathbf{n}\dot{\boldsymbol{\tau}} = (1 - \phi\,\mathbf{n}K\mathbf{n})\,(\mathbf{n}K\boldsymbol{\epsilon}) \qquad \text{when} \qquad \mathbf{n}\,K\,\boldsymbol{\epsilon} \geqslant 0.$$

If $\phi\,\mathbf{n}K\mathbf{n} < 1$ the state is such that plastic deformation causes the stress to move outside the present yield surface, and then

$$\left.\begin{aligned} \boldsymbol{\epsilon} &= K^{-1}\,\dot{\boldsymbol{\tau}} + \begin{cases} h^{-1}\,(\mathbf{n}\dot{\boldsymbol{\tau}})\,\mathbf{n} & \text{when} \quad \mathbf{n}\dot{\boldsymbol{\tau}} \geqslant 0 \\ 0 & \text{when} \quad \mathbf{n}\dot{\boldsymbol{\tau}} \leqslant 0 \end{cases} \\ \text{where}\quad h &= (1 - \phi\,\mathbf{n}K\mathbf{n})/\phi. \end{aligned}\right\} \tag{50}$$

If $\phi\,\mathbf{n}\,K\,\mathbf{n} > 1$ plastic deformation causes the stress to move inside the present surface (the ' yield-point drop ' in annealed mild steel is perhaps an extreme example), while if $\phi\,\mathbf{n}\,K\,\mathbf{n} = 1$ the stress moves tangentially. In both cases there is no unique inverse.

GREEN (1956a, b) has proposed quite general rate equations not necessarily admitting a potential. C is assumed plane and the equations on both sides are taken

as hypo-elastic and isotropic, though distinct (because of this the solid itself is non-linear and cannot be described as hypo-elastic). It is also required that the rate of *distortional* work should vanish for strain-rates on C. This is restrictive, and excludes most metals for example; it implies, when a complete yield surface exists, that the elastic energy of distortion is constant on it (if the strain is infinitesimal this is the Mises criterion). Actually, however, in the special case treated in detail by GREEN the equations within C do not admit a potential and could not be consistent with elastic behaviour.*

REFERENCES

ADKINS, J. E.	1958	*Phil. Trans. Roy. Soc.* A**250**, 519.
BISHOP, J. F. W. and HILL, R.	1951	*Phil. Mag.* **42**, 414.
GREEN, A. E.	1956a	*Proc. Roy. Soc.* A **234**, 46.
	1956b	*J. Rat. Mech. Anal.* **5**, 725.
GREEN, A. E. and ZERNA, W.	1954	*Theoretical Elasticity* (Clarendon Press, Oxford).
HAASEN, P. and LAWSON, A. W. JR.	1957	*Z. Metallkunde*, 280.
HILL, R.	1956a	*Surveys in Mechanics* (G. I. Taylor Anniversary Volume), p. 7 (Cambridge University Press).
	1956b	*J. Mech. Phys. Solids* **5**. 66.
	1957a	*Ibid.* **6**, 1.
	1957b	*Ibid.* **5**, 229.
	1958	*Ibid.* **6**, 236.
KOITER, W. T.	1953	*Quart. Appl. Math.* **11**, 350.
NOLL, W.	1955	*J. Rat. Mech. Anal.* **4**, 3.
OLDROYD, J. G.	1950	*Proc. Roy. Soc.* A**200**, 523.
	1958	*Ibid.* **245**, 278.
PEARSON, C. E.	1956	*Quart. Appl. Math.* **14**, 133.
SOUTHWELL, R. V.	1953	*Quart. J. Mech. Appl. Math.* **6**, 257.
TREFFTZ, E.	1933	*Z. ang. Math Mech.* **12**, 160.
TRUESDELL, C.	1952	*J. Rat. Mech. Anal.* **1**, 125.
	1953	*Ibid.* **2**, 593.
	1955a	*Ibid.* **4**, 83.
	1955b	*Comm. Pure and Appl. Math.* **8**, 123.
	1956	*J. Appl. Phys.* **27**, 441.
ZEIGLER, H.	1956	*Advances in Applied Mechanics* **4**, 352 (Academic Press, N.Y.).

*GREEN's equation (5.4) (1956b) is equivalent to $\dot{\sigma} = M\epsilon$ where M is symmetric; this does not agree with (39) here unless the material is incompressible.

PAPERS TO BE PUBLISHED IN FUTURE ISSUES

P. G. Hodge Jr.: The effect of end conditions on the dynamic loading of plastic shells.

E. Reissner: On the solution of a class of problems in membrane theory of thin shells.

J. B. Walsh and A. C. Mackenzie: Elastic-plastic torsion of a circumferentially notched bar.

A. D. Cox and L. W. Morland: Dynamic plastic deformations of simply-supported square plates.

J. de Fouquet: Modifications de structure cristalline produites par fatigue entre 20° et 750°C sur un acier extra-doux au carbone et sur un acier austenitique 18/8.

W. A. Bassali: Torsion of beams whose sections are bounded by certain quartic curves.

BOOK RECEIVED

Joseph R. Dillinger: **Low Temperature Physics and Chemistry.** The University of Wisconsin Press, 1958. 676 pp. $6.00

NOTICE

TENTH INTERNATIONAL CONGRESS OF APPLIED MECHANICS

The *Tenth International Congress of Applied Mechanics* will be held in the Congress Building at Stresa (Italy) from **Wednesday, 31 August until Wednesday, 7 September, 1960.**

Apart from a number of invited general lectures the technical sessions of the Congress will be held in two sections, viz. :

Section 1 : Fluid dynamics (hydrodynamics and aerodynamics).

Section 2 : Mechanics of solids (rigid body dynamics, vibrations, elasticity, plasticity and theory of structures).

It should be noted that thermodynamics and computational methods as such are not included, although specific applications of computational methods to pertinent problems of one of the two sections mentioned above are acceptable subjects for papers to be read at the Tenth Congress.

Previous Congresses have demonstrated the desirability of an adequate period of time for the presentation and discussion of individual papers. In order to allow a period of 45 minutes for each paper (30 min. for presentation and 15 min. for discussion) a Programme Committee will make a selection from papers submitted for presentation. Abstracts of papers should be submitted in **four copies to the Secretary of the International Committee** (Prof. Mekelweg 2, Delft, Netherlands) **before 1 January, 1960.** Preferably they should not exceed two typewritten pages (doubly-spaced) and in no case should they exceed four pages. In order to facilitate the work of the Programme Committee it is recommended that abstracts be in **two** of the official Congress languages (English, French, German and Italian). Authors are urged to make their abstracts as clear as possible, since selection of papers has to be based upon them. **Decisions of the Programme Committee are final,** and it will be understood that it is impossible to enter into correspondence about them with authors of papers. They will be informed promptly of the decision on each paper.

Day-to-day organization of the Congress is effected by the Italian Organizing Committee (President : Prof. G. Colonnetti ; Secretary : Dr. F. Rolla, *Consiglio Nazionale delle Ricerche, Ufficio relazioni internazionali, Piazza delle Scienza* 7, *Roma*). **All correspondence** (apart from submission of papers) **should be addressed to the Italian Organizing Committee.** Information on accommodation, also registration forms, will be obtainable from Dr. Rolla on and after 1 September, 1959.

The Executive Committee of the
International Committee for the
Congresses of Applied Mechanics
C. B. Biezeno, President
Richard V. Southwell
W. T. Koiter, Secretary
(Prof. Mekelweg 2-Delft)

ERRATUM

BROWN, N. and ROSENBAUM, H. S. 1959 *J. Mech. Phys. Solids* **7**, 97.

TABLE 1

Test No.	*Yield pt.* (lb/in^2)	
	Specimen No. 23	
1 – shear	32·7	aver $\tau_{shear} = 30{\cdot}5$ $\frac{\tau_{tor}}{\tau_{shear}} = \frac{51{\cdot}2}{30{\cdot}5} = 1{\cdot}67 \pm {\cdot}10$
2 – shear	29·7	
3 – shear	29·3	
4 – torsion	51·2	
	After test-4 crystal 23 was untwisted about $1\frac{1}{2}$ degrees and annealed 23 hours at 165°C and furnace cooled	
5 – shear	28·2	aver $\tau_{shear} = 27{\cdot}1 \pm {\cdot}7$ $\frac{\tau_{tor}}{\text{aver } \tau_{shear}} = 1{\cdot}75 \pm {\cdot}10$
6 – shear	26·6	
7 – shear	25·8	
8 – shear	25·8	
9 – shear	27·4	
10 – torsion	47·7	
	Specimen No. 21	
1 – shear	29·4	aver $\tau_{shear} = 29{\cdot}1 \pm {\cdot}7$ $\frac{\tau_{tor}}{\text{aver. } \tau_{shear}} = \frac{48{\cdot}0}{29{\cdot}1} = 1{\cdot}66 \pm {\cdot}10$
2 – shear	28·0	
3 – shear	29·6	
4 – shear	27·9	
5 – torsion	48·0	
	Specimen No. 26	
1 – shear	53·2	aver $\tau_{shear} = 52{\cdot}6$ $\frac{\tau_{tor}}{\text{aver. } \tau_{shear}} = \frac{79{\cdot}4}{52{\cdot}6} = 1{\cdot}51$
2 – shear	51·5	
3 – shear	51·5	
4 – shear	52·8	
5 – shear	52·6	
6 – torsion	79·4	

The grand average value of $\frac{\tau_{tor}}{\tau_{shear}} = 1{\cdot}65 \pm {\cdot}09$.

J. Mech. Phys. Solids, 1959, Vol. 7, pp. 229 to 241. Pergamon Press Ltd., London. Printed in Great Britain

DYNAMIC PLASTIC DEFORMATIONS OF SIMPLY-SUPPORTED SQUARE PLATES

By A. D. Cox* and L. W. Morland†

(*Received 16th March*, 1959)

Summary

In this paper an analysis is given within the framework of thin plate theory of the problem of a simply-supported, square plate subjected to a uniformly-distributed rectangular pressure pulse. All effects due to elastic strain, work-hardening and strain-rate are neglected, although some approximate account of the two latter may be made. To simplify the analysis further, Johansen's yield criterion is adopted as an approximation to Tresca's. The most important results concern the maximum displacement and the total time of motion. Errors in these quantities from approximating Tresca's yield criterion are estimated to be about five per cent.

1. Introduction

In this paper we give a theoretical analysis of the problem of a simply-supported square plate subjected to a uniformly-distributed, rectangular pressure pulse. Exactly as in previous related work, the analysis is in the spirit of thin plate theory together with certain simplifying assumptions. All effects due to elastic-strain, work-hardening and strain-rate are neglected. Some approximate account of the two latter may be made in the usual way or on an empirical basis once the deformations and times of motion are calculated for any particular loading. To simplify the analysis further, Johansen's yield criterion is adopted as an approximation to Tresca's. This approximation is discussed later.

There is now a considerable literature on the general theory of plastic deformation in thin plates, together with its applications to the solution of specific problems. In the main these applications have been confined to plates that are circular and to statical rather than dynamical problems. It is not intended to summarize this work in detail, and in fact it will be assumed subsequently that the reader is familiar with the analytical procedures involved. Hopkins (1957) has given a theory of the small deformations of a thin uniform plate under transverse load. The plate is supposed made of non-hardening rigid–plastic material obeying the Tresca yield condition and associated flow rule. The basic assumptions are similar to those made in the conventional engineering theory of thin elastic plates, and the effects of transverse shear strain and rotatory inertia are neglected. Previously the theory had been developed mainly under the restrictive condition of circular symmetry, and in this paper the restriction was removed. The paper gives a discussion and bibliography of work on circular plates, together with some references to work

*Armament Research and Development Establishment, Fort Halstead, Kent.
†Now at Brown University, Providence, R.I. Vacation Student at A.R.D.E., 1957.

on non-circular plates. The following additional references to the latter work will be briefly noted here for completeness. Rzhanitsyn (1954) and Mansfield (1957) have derived kinematically admissible velocity fields for variously shaped plates leading to upper bounds to yield-point loads. In addition Schumann (1957) has also considered problems for plates of arbitrary shape and has derived solutions when there is concentrated loading. Haythornthwaite and Shield (1957) have determined the extent of the deformable region in the above case.

Most of the above work has been developed on the assumption that Tresca's yield criterion is obeyed, which is a reasonable approximation when the plate material is a ductile metal, say mild steel. However, in this paper, Johansen's yield criterion is adopted, primarily to simplify the mathematical analysis. The use of this particular criterion may be viewed in two different ways according to the application in mind. Firstly, Johansen's yield criterion is a reasonable approximation when the plate is made of reinforced concrete, and the analysis developed here is then obviously relevant to problems of blast loading of building panels. Secondly, there is some evidence supporting the view that Johansen's yield criterion is a reasonable approximation to Tresca's, at least under certain conditions. For example, Hopkins (1956) has shown that, for certain dynamic circular plate problems involving fairly smooth loads, this approximation involves errors of about ten per cent in the maximum displacement and time of motion. Again, Hodge and Paul (1957) have established similar results for certain dynamic problems of thin shells when the true yield criterion is approximated. In both cases the errors may be limited to about five per cent. provided the yield stresses are suitably adjusted so that the yield-point loads for the problems are the same for the true and the approximate yield criteria. The present approximation therefore seems likely to involve errors of about ten per cent. Moreover, if the yield-point load for the present problem could be obtained for Tresca's yield criterion, then this error could be further reduced.

This paper is arranged as follows. First, the governing equations are quoted from Hopkins' (1957) paper, and a discussion given both of these equations and also of the necessary alterations due to the adoption of Johansen's, rather than Tresca's, yield criterion. In Section 3 the problem is formulated and the solution, which falls into two cases depending upon the magnitude of the applied load, is given. In Section 4 the results obtained are specialized to the case of impulsive loading. In Section 5 it is shown that the results for a square plate may be generalized in a straightforward manner to solve the problem for a regular, n-sided polygonal plate, with $n > 4$. In addition a similar solution obtains when the plate is restrained by an edge bending-moment αM_0, provided that α lies between zero and a certain critical value depending upon n. In particular, on letting n become indefinitely large, known results for circular plates are recovered.

2. Governing Equations

Rectangular Cartesian coordinates x, y (Fig. 1) are taken along the diagonals of the plate $PQRS$ of side $2L$. For convenience an auxiliary coordinate $Z = (x + y)/\sqrt{2}L$ is also defined. From symmetry it is only necessary to consider one-quarter of the plate and accordingly attention will be confined to the region OPQ, where $x \geqslant 0$, $y \geqslant 0$, $Z \leqslant 1$.

The equations of motion (HOPKINS 1957) are

$$\left.\begin{aligned} Q_x &= M_{xx,x} + M_{xy,y}, \\ Q_y &= M_{xy,x} + M_{yy,y}, \end{aligned}\right\} \tag{2.1}$$

and

$$Q_{x,x} + Q_{y,y} + P = \mu v_{,t},$$

where M_{xx}, M_{yy}, $M_{xy} = M_{yx}$ are the components of the stress-moment tensor; Q_x, Q_y the components of the shear force vector; P the applied pressure; μ the mass per unit area of middle-surface; and v the transverse velocity, defined by $v = w_{,t}$ where w is the transverse deflexion. The suffix after a comma denotes partial differentiation with respect to the coordinate indicated. The sign convention for these quantities is indicated in Fig. 2.

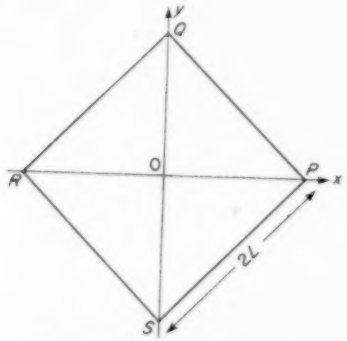

Fig. 1. Coordinate system.

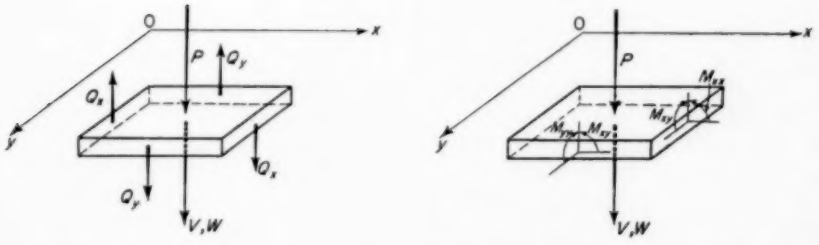

Fig. 2 (a, b). Sign conventions for the shear force and stress-moment components.

The yielding of the plate is assumed to be described by Johansen's criterion, which takes the form

$$\max.\,(|M_1|, |M_2|) = M_0, \tag{2.2}$$

where M_1, M_2, the principal stress-moments, are given by

$$M_1,\, M_2 = \tfrac{1}{2}\,(M_{xx} + M_{yy}) \pm \tfrac{1}{2}\,\{(M_{xx} - M_{yy})^2 + 4M^2_{xy}\}^{\frac{1}{2}}.$$

M_0 is the fully-plastic bending moment $\sigma_0 h^2$, σ_0 being the yield stress in tension and $2h$ the plate thickness. Fig. 3 shows this yield criterion in graphical form,

M_1 and M_2 being taken as rectangular Cartesian coordinates. The criterion is represented by the square $ABCD$; for comparison Tresca's yield criterion, represented by the hexagon $AEFCGH$, is also shown. From Fig. 3 it is apparent that using Johansen's yield criterion will in general be simpler than using Tresca's, since the former comprises only two essentially different plastic régimes, i.e. A and AD, whereas the latter comprises four, i.e. A, AH, H and HG.

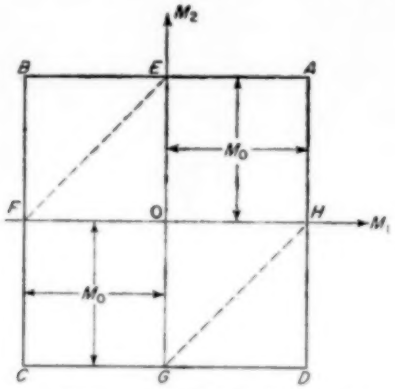

Fig. 3. Johansen's yield criterion.

Associated with the stress-moment tensor is the generalized strain-rate tensor, with components $\dot{\kappa}_{xx}$, $\dot{\kappa}_{yy}$, $\dot{\kappa}_{xy} = \dot{\kappa}_{yx}$, where

$$\dot{\kappa}_{xx} = -v_{,xx}, \qquad \dot{\kappa}_{xy} = -v_{,xy}, \qquad \dot{\kappa}_{yy} = -v_{,yy}. \tag{2.3}$$

The components of the strain-rate tensor are related to those of the stress-moment tensor firstly by the isotropy condition

$$\dot{\kappa}_{xy}/(\dot{\kappa}_{xx} - \dot{\kappa}_{yy}) = M_{xy}/(M_{xx} - M_{yy}), \tag{2.4}$$

and secondly by the flow rule. The associated flow rule states that for any stress-moment state at yield, the principal strain-rate vector $\dot{\boldsymbol{\kappa}}$, with components $\dot{\kappa}_1$, $\dot{\kappa}_2$, the principal strain-rates, is normal to the yield curve at the stress point in question (Fig. 3). Further, $\dot{\boldsymbol{\kappa}}$ must be directed along the outward-drawn normal to this curve. At the singular stress-moment points A, B, C, D it is required only that $\dot{\boldsymbol{\kappa}}$ shall lie in the angle bounded by normals to the two adjacent sides.

It is clear that the essential features of the two types of plastic régime A and AD of Johansen's criterion are the same as those of régimes A and AH of Tresca's criterion. Thus the analysis of these two régimes given by Hopkins (1957) applies to the present situation.

In the analysis that follows, it is often necessary to refer the components of the stress-moment tensor and of the shear force vector to local rectangular Cartesian coordinates n, s measured along directions respectively normal and tangential to some curve in the x, y plane. In cases where no ambiguity can arise the symbols M_{nn}, M_{ss}, M_{ns}, Q_n and Q_s will be used for these components without specific reference to the coordinate system.

Exactly as in similar problems for circular plates (see, for example, Hopkins and Prager (1954)) the solution of the present problem involves attention to

hinge lines, which are curves across which the normal velocity derivative $v_{,n}$ is discontinuous. A full discussion of the continuity conditions at hinge lines is given by HOPKINS (1957) and only the relevant results will be given here. If $[G]$ denotes the jump in G at a hinge line, then

$$[Q_n, M_{nn}, M_{ns}] = 0, \tag{2.5}$$

but Q_s and M_{ss} may be discontinuous.

The major concern of the present analysis is to determine the velocities and deflexions at any given instant, the stress-moment field itself not being of direct importance. In fact, due to limitations inherent in the assumptions of the present theory, it is not possible to determine uniquely the stress-moment field in rigid regions which occur in the solutions. The only stipulation made is that at least one stress-moment field can be obtained that does not violate the yield criterion. Further, the analysis leading to the determination of the velocity fields follows a heuristic approach, since their form is assumed *a priori*. Although this leads to a solution of the problem there is no guarantee, because no uniqueness theorems have been proved under dynamic conditions, that it is the only possible solution. However, the present fracture-line pattern agrees substantially with that frequently observed for reinforced concrete plates (see, for example, WOOD 1955, Plate 7, although the loading conditions therein are not exactly as envisaged here). Therefore, although the present solution may be only one of several possible solutions, it is thought that it is a fair representation of the situation under most practical conditions.

3. Dynamic Plastic Deformations of Simply-supported Square Plates

The problem is that of the dynamic loading of a square plate of side $2L$, simply-supported along its edges. The material is non-hardening, rigid–plastic and obeys Johansen's yield criterion and associated flow rule. The applied loading is uniformly-distributed:

$$P = \begin{cases} p = \text{const.} > 0 & 0 < t < \tau, \\ 0 & t > \tau. \end{cases} \tag{3.1}$$

Initially the plate is at rest and undeformed. The requirements of the problem lead to the following boundary conditions:

$$\left.\begin{aligned} M_{nn} = 0, \quad v = w = 0, \quad & \text{on } Z = 1, \quad t > 0, \\ v = w = 0, \quad & \text{in } 0 \leqslant Z \leqslant 1, \quad t = 0. \end{aligned}\right\} \tag{3.2}$$

Exactly as for circular plates, there are two different cases for which separate analytical treatment is required. More precisely, if p_0 is the yield-point pressure, the value of which is to be determined, it is necessary to distinguish between a 'medium' load, when $p_0 \leqslant p \leqslant 2p_0$, and a 'high' load, when $p \geqslant 2p_0$.

(i) *Medium load*: $p_0 \leqslant p \leqslant 2p_0$

Since the pressure pulse is discontinuous at $t = \tau$, it is further necessary to sub-divide the analysis into a phase I, when $0 \leqslant t < \tau$, and a phase II, when $t > \tau$. The solutions in these two phases are linked by the requirement that v and w must be continuous at $t = \tau$ although, of course, the stress-moments and the acceleration $v_{,t}$ will be discontinuous.

(a) *Phase I.* $0 \leqslant t < \tau$. $P = p$. Following the heuristic procedure discussed in Section 2, it is assumed that the velocity field has the features of that used by Mansfield (1957) to derive an upper bound to the yield-point pressure, which is an idealization of the observed fracture-line pattern. This assumes that plastic deformation only occurs along the diagonals PR, QS, where hinge lines form, the rest of the plate remaining rigid. This leads to

$$v(x, y, t) = V_1(t)(1 - Z), \tag{3.3}$$

where $V_1(t)$ is positive.

The equations of motion (2.1) show, after eliminating the shear force components Q_x, Q_y, that

$$M_{xx,xx} + 2M_{xy,xy} + M_{yy,yy} + P = \mu \dot{V}_1 (1 - Z), \tag{3.4}$$

where the dot indicates differentiation with respect to time. In addition the stress-moment components must satisfy the yield criterion

$$\text{max.}\,(|M_1|, |M_2|) \leqslant M_0, \tag{3.5}$$

and three boundary conditions. The first of these, from (3.2), is

$$M_{nn} = \tfrac{1}{2}(M_{xx} + M_{yy}) + M_{xy} = 0 \text{ on } Z = 1. \tag{3.6}$$

The other two are implicit in the assumption that OP, OQ are hinge lines since, as shown by Hopkins (1957), hinge lines must be principal stress-moment directions. Therefore the stress-moment components must satisfy $M_{nn} = \pm M_0$ on a hinge line. These two remaining conditions are

$$\left.\begin{aligned} M_{nn} = M_{xx} = M_0 \quad &\text{on} \quad x = 0 \text{ (i.e. } OQ), \\ M_{nn} = M_{yy} = M_0 \quad &\text{on} \quad y = 0 \text{ (i.e. } OP). \end{aligned}\right\} \tag{3.7}$$

Since it is assumed that the region OPQ remains rigid, the stress-moment field in this region is indeterminate. It is only necessary that at least one field can be found which satisfies the dynamical equation (3.4) and does not violate the yield condition (3.5). The simplest way of finding such a field is to assume that equality holds in equation (3.5) throughout OPQ, so that

$$\text{max.}\,(|M_1|, |M_2|) = M_0. \tag{3.8}$$

It follows, from stress-moment isotropy, that at the plate centre $M_{xx} = M_{yy} = M_0$ and $M_{xy} = 0$. Thus in the immediate vicinity of the plate centre the motion is governed by the equations relevant to (or, briefly, is governed by) plastic régime AD (see Fig. 3). Previous work on circular plates suggests that with this medium load the whole of the plate is governed by régime AD. Assuming this is to be true, it follows that the stress-moment components satisfy

$$\left.\begin{aligned} M_{xx} + M_{yy} + \{(M_{xx} - M_{yy})^2 + 4M^2_{xy}\}^{\frac{1}{2}} &= 2M_0, \\ -2M_0 \leqslant M_{xx} + M_{yy} - \{(M_{xx} - M_{yy})^2 + 4M^2_{xy}\}^{\frac{1}{2}} &\leqslant 2M_0. \end{aligned}\right\} \tag{3.9}$$

These equations, together with the equation of motion (3.4), and the boundary conditions (3.6, 7) suggest that the solution is of the form

$$\left.\begin{aligned} M_{xx} &= M_0 + x^2 f_1(Z), \\ M_{yy} &= M_0 + y^2 f_1(Z), \\ M_{xy} &= xy f_1'(Z), \end{aligned}\right\} \tag{3.10}$$

where f_1 is an arbitrary function to be determined. This immediately satisfies the condition (3.7) and, together with the analogous forms in the adjacent regions OQR, OPS, the continuity conditions (2.5). In order that (3.10) shall satisfy the conditions (3.9), $f_1(Z)$ must satisfy

$$-2M_0 \leqslant (x^2 + y^2) f_1(Z) \leqslant 0 \quad \text{for} \quad 0 \leqslant Z \leqslant 1. \tag{3.11}$$

Substitution of (3.10) into (3.4) and using (3.1) leads to a simple differential equation for $f_1(Z)$, the general solution of which is

$$f_1(Z) = (\mu \dot{V}_1 - p)/6 - \mu \dot{V}_1 Z/12 + c_1 Z^{-2} + c_2 Z^{-3},$$

where c_1 and c_2 are arbitrary constants. Since the stress-moments must be finite and single-valued at the plate centre, c_1 and c_2 must be zero and therefore

$$f_1(Z) = (\mu \dot{V}_1 - p)/6 - \mu \dot{V}_1 Z/12. \quad . \tag{3.12}$$

The condition (3.6) that the plate edge is free from applied bending-moment, now leads to a relationship between $\dot{V}_1$ and p, given by

$$\mu \dot{V}_1 = 2p - \frac{12M_0}{L^2},$$

so that since $v(x, y, 0)$ is zero, $V_1(t)$ is given by

$$\mu V_1(t) = 2\left(p - \frac{6M_0}{L^2}\right)t. \tag{3.13}$$

Since $V_1(t)$ must be non-negative, p must be greater than a certain value p_0, the yield-point pressure, where

$$p_0 = \frac{6M_0}{L^2}. \tag{3.14}$$

This result is due to PRAGER (1952) and also agrees with that obtained as an upper bound by MANSFIELD (1957).

The conditions (3.11) lead to bounds on the validity of the solution, necessary and sufficient conditions being

$$p_0 \leqslant p \leqslant 2p_0. \tag{3.15}$$

It should be noted that, if $p > 2p_0$, the conditions (3.11) are violated everywhere within a central square region, say $0 \leqslant Z \leqslant Z^*$.

Thus, subject to (3.15) the above analysis is valid. At the end of the first phase, when $t = \tau$, the velocity and deflexion are given

$$\left.\begin{aligned} \mu v(x, y, \tau) &= 2(p - p_0)(1 - Z)\tau, \\ \mu w(x, y, \tau) &= (p - p_0)(1 - Z)\tau^2. \end{aligned}\right\} \tag{3.16}$$

The deflexion at the end of the first phase is shown for the particular case $p = 1{\cdot}5p_0$ in Fig. 4.

(b) *Phase II.* $\tau < t \leqslant T$. $P = 0$. At time $t = \tau$ the load is suddenly removed, and subsequently $P = 0$. However, due to the kinetic energy the plate has acquired in phase I, the motion persists until, at time $t = T$, all this energy has been dissipated as plastic work at the hinge lines, when the motion ceases.

As is easily verified, the analysis of phase I applies, with P zero, and it is found that

$$\mu v(x, y, t) = 2(p\tau - p_0 t)(1 - Z), \tag{3.17}$$

and that the stress-moment field is given by (3.10) with $f_1(Z)$ replaced by $f_2(Z)$, where

$$f_2(Z) = -p_0(2 - Z)/6. \tag{3.18}$$

From (3.17) it is seen that $v(x, y, t)$ decreases as t increases, becoming zero when $t = T$, where

$$T = p\tau/p_0. \tag{3.19}$$

Clearly, the conditions at this instant are such that no further motion ensues. Integration of (3.17), using the condition that w must be continuous at $t = \tau$, leads to an expression for the final deflexion of the plate, viz.

$$\mu w(x, y, T) = \frac{p^2\tau^2}{p_0}\left(1 - \frac{p_0}{p}\right)(1 - Z). \tag{3.20}$$

In particular the final central deflexion is given by

$$\mu w(0, 0, T) = I(I - I_0)/p_0, \tag{3.21}$$

where $I = p\tau$ is the total impulse per unit area applied to the plate, and $I_0 = p_0\tau$ is the 'collapse' impulse. This result shows that the maximum central deflexion of a simply-supported square plate is the same, for a given impulse per unit area, as that for a simply-supported circular plate inscribed to the square, since under these circumstances the yield-point pressure is the same. The result for a circular plate is given by Hopkins and Prager (1954); for a simply-supported circular plate both Tresca's and Johansen's criteria lead to the same results.

The final deflexion of the plate given by (3.20) is shown for the particular case $p = 1{\cdot}5p_0$ in Fig. 4.

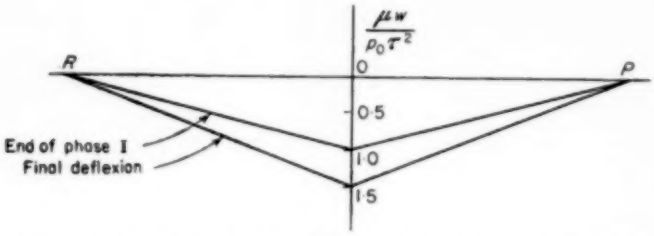

Fig. 4. Deflexions in the plane $y = 0$. 'Medium' load: $p/p_0 = 1{\cdot}5$.

(ii) *High load*: $p \geqslant 2p_0$

As was pointed out above, if the analysis for the medium load is assumed valid when $p > 2p_0$, the yield criterion is found to be violated everywhere throughout a central square region of the plate. If the relevant stress-moment points are plotted on Fig. 3 they lie on DA but above A. This fact, also a feature in the analogous problems for circular plates, suggests that with this high load a central square region $0 \leqslant Z \leqslant \theta$ is governed by plastic régime A, whereas the rest of the plate is governed by plastic régime AD.

Once again it is necessary to give separate consideration to the motion before and after $t = \tau$. In addition it is necessary to discuss the subsequent motion in two phases, depending upon whether or not the central square region, which decreases in size, still exists.

(a) *Phase I*. $0 \leqslant t < \tau$. $P = p$. It is supposed that the central square region (region I), of which only the part OTU need be considered explicitly, is governed by plastic régime A, whereas region $TPQU$ (region II) is governed by plastic régime AD (Fig. 5). It can be shown that during this phase $\theta = \text{const.}$, say θ_0, and for brevity this will be assumed.

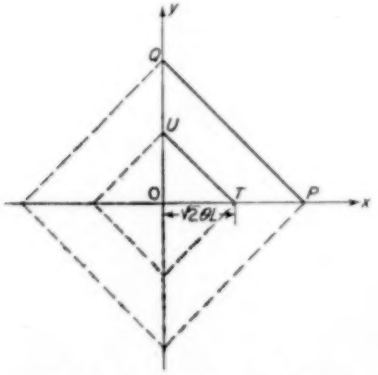

Fig. 5. Velocity field in the 'High' load case.

In region II ($\theta_0 \leqslant Z \leqslant 1$) a stress-moment field of the form (3.10) is assumed, with $f_3(Z)$ in place of $f_1(Z)$. In region I ($0 \leqslant Z \leqslant \theta_0$), since $M_1 = M_2 = M_0$, it follows that $M_{xx} = M_{yy} = M_0$, $M_{xy} = 0$.

The dynamical equation in region I shows immediately that $v(x, y, t)$ is independent of x and y, so that

$$v(x, y, t) = V_3(t), \quad 0 \leqslant Z \leqslant \theta_0. \tag{3.22}$$

In region II a velocity field is assumed of the same general linear form as for the medium load case. Since v must be continuous at $Z = \theta_0$ and vanish at $Z = 1$, it follows that

$$v(x, y, t) = V_3(t)\left(\frac{1 - Z}{1 - \theta_0}\right), \qquad \theta_0 \leqslant Z \leqslant 1. \tag{3.23}$$

As is easily verified $v_{,n}$ is discontinuous at $Z = \theta_0$ and therefore $Z = \theta_0$ must be a hinge line.

The dynamical equation in region I shows that $V_3(t)$ is given by

$$\mu V_3(t) = pt, \tag{3.24}$$

using the condition that v vanishes at $t = 0$. Then the dynamical equation in region II determines $f_3(Z)$, viz.

$$f_3(Z) = -p/6 + p(2 - Z)/12(1 - \theta_0) + c_3 Z^{-2} + c_4 Z^{-3}. \tag{3.25}$$

Now, since $Z = \theta_0$ is a hinge line, the continuity conditions (2.5) must be satisfied, leading to

$$\left.\begin{aligned} c_3 &= -p\theta_0^3/6(1 - \theta_0), \\ c_4 &= p\theta_0^4/12(1 - \theta_0). \end{aligned}\right\} \tag{3.26}$$

Further, since the edge of the plate is simply-supported, (3.6) determines θ_0 in terms of the ratio p/p_0, thus

$$(1 + \theta_0)(1 - \theta_0)^2 = 2p_0/p. \tag{3.27}$$

It is easily verified that the stress-moment fields in regions I and II do not violate the yield criterion for any finite value of $p \geqslant 2p_0$, and hence the solution derived is valid.

From equations (3.22-24), together with the initial condition (3.2), the deflexion is easily found. At the end of the phase, when $t = \tau$, the velocity and deflexion are given by

$$\left.\begin{aligned} \mu v(x, y, \tau) &= p\tau, \\ \mu w(x, y, \tau) &= \tfrac{1}{2}p\tau^2, \end{aligned}\right\} \quad 0 \leqslant Z \leqslant \theta_0.$$

$$\left.\begin{aligned} \mu v(x, y, \tau) &= p\tau(1 - \theta_0)^{-1}(1 - Z), \\ \mu w(x, y, \tau) &= \tfrac{1}{2}p\tau^2(1 - \theta_0)^{-1}(1 - Z), \end{aligned}\right\} \quad \theta_0 \leqslant Z \leqslant 1. \tag{3.28}$$

These deflexions are shown in Figs. 6 (a, b) for the two cases $p/p_0 = 128/45$, $16/3$ (or $\theta_0 = \frac{1}{4}, \frac{1}{2}$).

(b) *Phase II.* $\tau < t < T_1$. $P = 0$. At time $t = \tau$ the load is removed and subsequently $P = 0$. As with the medium load further motion takes place during which the kinetic energy is dissipated in plastic work at the hinge lines. It is easily seen that this implies that the central square region must shrink, and vanish say when $t = T_1$.

An analysis similar to that in phase I applies with $\theta(t)$ in place of θ_0, and it is straightforward to show that $\theta(t)$ satisfies

$$(1 + \theta)(1 - \theta)^2 = \frac{2p_0 t}{p\tau}. \tag{3.29}$$

Accordingly the phase ends at $t = T_1$ where

$$T_1 = \frac{p\tau}{2p_0}. \tag{3.30}$$

At the end of the phase the velocity and deflexion are given by

$$\mu v(x, y, T_1) = p\tau(1 - Z), \qquad 0 \leqslant Z \leqslant 1,$$

$$\mu w(x, y, T_1) = \begin{cases} \dfrac{p^2\tau^2}{4p_0}(1 + 2\theta_0 + 2\theta_0^2)(1 - Z), & \theta_0 \leqslant Z \leqslant 1, \\ -\tfrac{1}{2}p\tau^2 + \dfrac{p^2\tau^2}{4p_0}(2 - Z^2 - Z^3), & 0 \leqslant Z \leqslant \theta_0. \end{cases} \tag{3.31}$$

The deflexion at the end of the second phase is shown in Figs. 6 (a, b) for the two cases $p/p_0 = 128/45$, $16/3$ (or $\theta_0 = \frac{1}{4}, \frac{1}{2}$).

(c) *Phase III.* $T_1 < t \leqslant T_2$. $P = 0$. At the beginning of this phase the entire plate is governed by plastic régime AD, and this situation applies throughout the remaining motion. This situation is exactly analogous to phase II of the medium load case, and the analysis is similar. The kinetic energy now remaining is dissipated as plastic work and the whole plate comes to rest, say at time $t = T_2$, after which no further motion takes place.

The velocity is found to be

$$\mu v\,(x, y, t) = 2\,(p\tau - p_0 t)\,(1 - Z), \tag{3.32}$$

showing that T_2 is given by

$$T_2 = \frac{p\tau}{p_0}\,(= 2T_1). \tag{3.33}$$

The end of this phase completes the motion, and the final deflexion is given by

$$\mu w\,(x, y, T_2) = \begin{cases} \dfrac{p^2\tau^2}{2p_0}\,(1 + \theta_0 + \theta_0^2)\,(1 - Z), & \theta_0 \leqslant Z \leqslant 1, \\ -\frac{1}{2}\,p\tau^2 + \dfrac{p^2\tau^2}{4p_0}\,(3 - Z - Z^2 - Z^3), & 0 \leqslant Z \leqslant \theta_0. \end{cases} \tag{3.34}$$

In particular the maximum central deflexion is related to the total impulse by

$$\mu w\,(0, 0, T_2) = I\,(3I - 2I_0)/4p_0, \tag{3.35}$$

in the notation of Section 3 (i) (b).

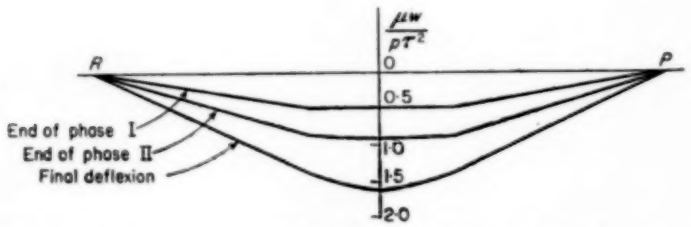

Fig. 6 (a). Deflexions in the plane $y = 0$. 'High' load: $p/p_0 = 128/45$; $\theta_0 = \frac{1}{4}$.

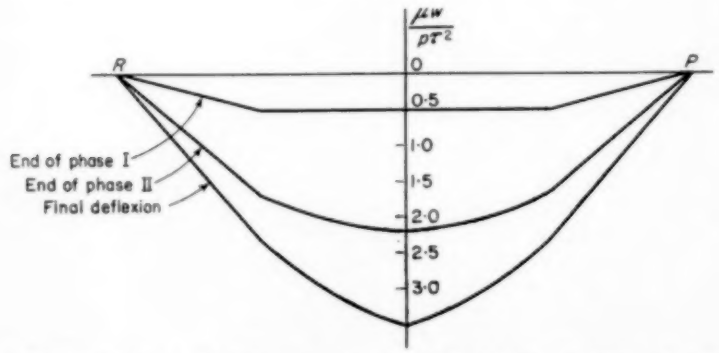

Fig. 6 (b). Deflexions in the plane $y = 0$. 'High' load: $p/p_0 = 16/3$; $\theta_0 = \frac{1}{2}$.

This result shows that the maximum central deflexion of a simply-supported square plate is the same, for a given impulse per unit area, as that for a simply-supported circular plate inscribed to the square, since under these circumstances the yield-point pressure p_0 is the same. The result

for a circular plate is given by HOPKINS and PRAGER ; for a simply-supported circular plate both Tresca's and Johansen's yield criteria lead to the same results.

The final deflexion of the plate, given by (3.34), is shown for the two cases $p/p_0 = 128/45$, $16/3$ (or $\theta_0 = \frac{1}{4}, \frac{1}{2}$) in Figs. 6 (a, b).

4. IMPULSIVE LOADING

This type of loading, often described somewhat incorrectly as blast loading, corresponds to the hypothetical situation when p becomes indefinitely large and τ indefinitely small, the product $p\tau$, however, remaining finite. The analysis now applying is simply derived from that given in Section 3 (ii). Here only the final expressions for the deflexions at the end of the two phases and the corresponding times of motion will be given.

In the circumstances now envisaged, the duration of the first phase is zero and at time $t = +0$ the entire plate, except the edges, is moving with a constant velocity, say v_0, related to $I_* = p\tau$, by

$$\mu v_0 = I_*. \tag{4.1}$$

I_* is the applied impulse per unit area of middle surface. Further, the value of θ_0 is unity.

The motion is now in two phases and the deflexions at the end of the first phase, $t = T_3$ and at the end of the motion, $t = T_4$, are given by

$$\left.\begin{aligned} \mu w(x, y, T_3) &= I_*^2 (2 - Z^2 - Z^3)/4p_0, \\ \mu w(x, y, T_4) &= I_*^2 (3 - Z - Z^2 - Z^3)/4p_0, \end{aligned}\right\} \tag{4.2}$$

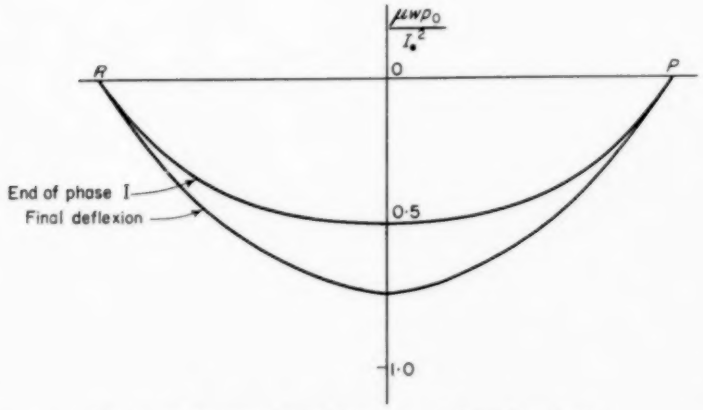

Fig. 7. Deflexions in the plane $y = 0$. Impulsive load.

T_3 and T_4 being given by

$$T_3 = \frac{I_*}{2p_0}, \qquad T_4 = \frac{I_*}{p_0} (= 2T_3). \tag{4.3}$$

The deflexions (4.2) are plotted in Fig. 7.

5. Dynamic Plastic Deformations of Regular Polygonal Plates

Finally, it will be shown that the preceding analysis for simply-supported square plates may be adopted with slight modifications to solve the same type of problem for regular, n-sided, polygonal plates with some arbitrary degree of restraint due to applied edge bending-moment. This problem is of limited physical interest. However, the problem is of some mathematical interest in that its solution includes, as limiting cases, the solutions of the square and circular plate problems.

(a) Consider firstly the case of simply-supported edges. If a stress-moment field of the form (3.10) is referred to coordinates n and s, measured along directions normal and tangential to the line OT (see Fig. 8a) which makes an angle ϕ with the x-axis, then the usual tensor transformations show immediately that

$$M_{nn} = M_0, \qquad M_{ns} = 0 \text{ for all } \phi, \tag{5.1}$$

so that the conditions are satisfied for OT to be a hinge line. Thus (Fig. 8b) the stress-moment fields derived in Section 3 are directly applicable in the sector OXY of an n-sided regular polygonal plate, the boundary condition on XY obviously being satisfied, provided that $n \geqslant 4$. As n varies, the dimensions of the polygonal plate are such that the radius of the circle inscribed to the polygon is constant and equal to L.

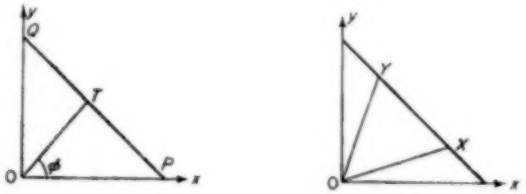

Fig. 8 (a, b). Coordinates for a polygonal plate.

Thus, it is concluded in particular that the maximum central deflexion of a simply-supported regular n-sided polygonal plate, the radius of the inscribed circle being constant and equal to L, is independent of n, being given by (3.21) for medium load and (3.35) for high load. This result holds in the limit as $n \to \infty$ and, as already discussed, (3.21) and (3.35) are identical with the results obtained by Hopkins and Prager for simply-supported circular plates.

(b) It can be seen from Section 3 that the condition that the yield criterion is nowhere violated is critical at the corners P, Q of the plate and, further, this is due to the fact that the inequality $x^2 + y^2 \leqslant 2L^2$ is only just satisfied there. As has been shown, the solution is valid for n-sided regular polygonal plates but, for $n > 4$, the inequality $x^2 + y^2 < 2L^2$ is satisfied. This suggests that a solution may be obtained when it is supposed than an edge bending-moment is applied to the plate. This supposition is correct, and if the edge bending-moment is taken as

$$M_{nn} = -\alpha M_0 \text{ on } Z = 1, \qquad 0 \leqslant \alpha \leqslant 1, \tag{5.2}$$

$\alpha = 0$ corresponding to simply-supported, and $\alpha = 1$ to built-in, edge conditions, then it is easily shown that the analysis of Section 3 can be suitably modified, provided that α satisfies

$$0 \leqslant \alpha \leqslant \cos(2\pi/n). \tag{5.3}$$

Furthermore, it is seen that the results of Section 3 are valid provided p_0 is replaced by $p_0(\alpha)$, where

$$p_0(\alpha) = \frac{6M_0(1+\alpha)}{L^2}, \tag{5.4}$$

$p_0(\alpha)$ being the yield-point pressure for a regular n-sided polygonal plate subjected to an edge bending-moment given by (5.2).

The inequality (5.3) shows that for a square plate the solution is only valid for simply-supported edge conditions, whereas for a circular plate it is valid for any degree of edge restraint lying between simple and built-in support.

6. Concluding Remarks

The foregoing analysis is mainly notable for its simplicity and this is due essentially to the nature of the boundary conditions and the yield criterion. The extension of the analysis to provide the solutions of similar problems for rectangular plates and for built-in conditions of edge support would be valuable. However, to do this, it seems clear that considerable modifications will be needed, and the exact nature of these is not yet known. In this connexion it should be noted that Mansfield (1957), in order to obtain an upper bound to the yield-point load for a problem involving a built-in square plate, had recourse to a pattern of hinge lines much more complicated than that occurring here. Further, Wood (1955) has shown that the use of the present type of stress-moment and velocity fields to find the yield-point load for a rectangular plate problem leads to unequal, albeit remarkably close, upper and lower bounds.

Acknowledgment

Crown copyright reserved. Reproduced with the permission of the Controller, H.M.S.O.

References

Haythornthwaite, R. M. and Shield, R. T. 1957 *J. Mech. Phys. Solids* **6**, 127.

Hodge, Jr., P. G. and Paul, B. 1957 *Proc. 3rd Midwestern Conf. Solid Mechanics* p. 29. (University of Michigan).

Hopkins, H. G 1956 *Proc. 9th Int. Congr. Appl. Mech.* **6**, 448. (Brussels 1957).

1957 *Proc. Roy. Soc.* A **241**, 153.

Hopkins, H. G. and Prager, W. 1954 *Z. angew. Math. Phys.* **5**, 317.

Mansfield, E. H. 1957 *Proc. Roy. Soc.* A **241**, 311.

Prager, W. 1952 *Proc. 8th Int. Congr. Appl. Mech.* **2**, 65 (Istanbul 1956).

Rzhanitsyn, A. R. 1954 *Structural Analysis taking account of Plastic Properties*, Chap. 8 (Moscow : 2nd Ed. rev.). See also translation by R. M. Haythornthwaite, Brown University, Division of Applied Mathematics, Technical Report C11-19, 1957.

Schumann, W. 1957 *Quart. Appl. Math.* **16**, 1.

Wood, R. H. 1955 *Studies in Composite Structure – II. The Interaction of Floors and Beams in Multi-storey Buildings. National Building Studies Research Paper No.* 22. (London : H.M.S.O.).

J. Mech. Phys. Solids, 1959, Vol. 7, pp. 242 to 246. Pergamon Press Ltd., London. Printed in Great Britain

ON THE SOLUTION OF A CLASS OF PROBLEMS IN MEMBRANE THEORY OF THIN SHELLS

By E. Reissner
Department of Mathematics, Massachusetts Institute of Technology

(*Received 26th March*, 1959)

Summary

It is shown that membrane stresses in shells of revolution for the class of problems for which the normal stress resultants are of the form $f(z)\cos\theta$ and the shear stress resultant is of the form $f(z)\sin\theta$ admit a particularly simple solution in terms of a stress function U which has earlier been considered. This fact is illustrated by solving the problem of flexure of a cantilever shell, and also the problem of a shell with hydrostatic lateral load. The formulas for the latter case are specialized to the form which they assume for an ellipsoidal shell, to enable comparison with an earlier solution of this problem.

1. Introduction

The following is concerned with a class of problems in membrane theory of thin shells of revolution. We assume that the equation of the shell surface is given in the form

$$r = f(z) \tag{1}$$

and we take as coordinates on the middle surface of the shell the axial coordinate z and the circumferential coordinate θ. The class of problems considered may then be characterized by the statement that meridional and circumferential stress

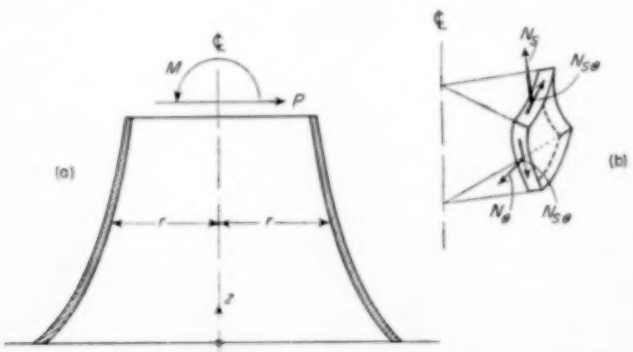

Fig. 1 (a, b). Side view and element of shell of revolution, showing orientation of stress resultants and applied loads for a cantilever shell.

resultants N_z and N_θ are proportional to $\cos\theta$. A specific problem for which the stress resultants vary in this manner is given by the problem of a cantilever shell acted upon by an end moment M and a lateral end force P (Fig. 1).

Our principal object is to show that for problems of this nature use of a stress function, which is a slight generalization of Nemenyi's stress function, and which has been described earlier (REISSNER 1947) is particularly appropriate.

2. Stress Function without Distributed Surface Loads

It has been shown (REISSNER, 1947) that in the absence of distributed surface loads it is possible to write the membrane stress resultants N_s, N_θ and $N_{s\theta}$ for a shell of revolution with middle surface equation (1) in the following form:

$$N_s = \frac{\alpha}{r^2}\frac{\partial U}{\partial \theta}, \qquad N_\theta = \frac{r''}{r\alpha}\frac{\partial U}{\partial \theta}, \qquad N_{s\theta} = -\frac{\partial}{\partial z}\left(\frac{U}{r}\right). \tag{2}$$

In these equations primes indicate differentiation with respect to z, the quantity α is $[1 + (r')^2]^{\frac{1}{2}}$ and the quantity U is a stress function which has to satisfy the following differential equation

$$\frac{\partial^2 U}{\partial z^2} - \frac{r''}{r}\left(U + \frac{\partial^2 U}{\partial \theta^2}\right) = 0. \tag{3}$$

3. Expressions for Side Force and Moment

In order to calculate section force P and section moment M expressions are needed for stress resultants N_x and N_z in x and z-directions respectively. Expressions for N_x and N_z follow from the vectorial relation

$$N_x \mathbf{i} + N_y \mathbf{j} + N_z \mathbf{k} = N_s \mathbf{t}_s + N_{s\theta}\mathbf{t}_\theta = \alpha^{-1} N_s (r'\mathbf{i}_r + \mathbf{k}) + N_{s\theta}\mathbf{i}_\theta$$
$$= \alpha^{-1} N_s [r'(\cos\theta\,\mathbf{i} + \sin\theta\,\mathbf{j}) + \mathbf{k}] + N_{s\theta}[-\sin\theta\,\mathbf{i} + \cos\theta\,\mathbf{j}]$$

in the form

$$N_x = \frac{r'}{\alpha} N_s \cos\theta - N_{s\theta}\sin\theta, \qquad N_z = \frac{1}{\alpha} N_s. \tag{4}$$

Combination of (4) and (2) gives further

$$P = \int_0^{2\pi} N_x r\, d\theta = \int_0^{2\pi}\left[\frac{r'}{r}\frac{\partial U}{\partial \theta}\cos\theta + r\frac{\partial}{\partial z}\left(\frac{U}{r}\right)\sin\theta\right] d\theta$$
$$= \int_0^{2\pi}\frac{\partial U}{\partial z}\sin\theta\, d\theta, \tag{5}$$

$$M = \int_0^{2\pi} N_z r\cos\theta\, r\, d\theta = \int_0^{2\pi}\frac{\partial U}{\partial \theta}\cos\theta\, d\theta$$
$$= \int_0^{2\pi} U\sin\theta\, d\theta. \tag{6}$$

4. Flexure of Cantilever Shell

A solution of the problem of flexure in accordance with Fig. 1 is obtained by assuming that the resultant N_z varies linearly with distance $r\cos\theta$ from the plane $\theta = \frac{1}{2}\pi$. In view of (4) and (2) we assume that the stress function U is of the form

$$U(z, \theta) = V(z)\sin\theta. \tag{7}$$

With (7) the differential equation (3) assumes the particularly simple form

$$V''(z) = 0. \tag{8}$$

From (8), (7), (6) and (5) follows that

$$U = \frac{1}{\pi}(M_0 + Pz)\sin\theta \tag{9}$$

where M_0 is the value of M for $z = 0$.

Introduction of (9) into (2) gives as expressions for stress resultants

$$N_s = \frac{1}{\pi}\cdot\frac{\alpha}{r^2}(M_0 + Pz)\cos\theta, \tag{10}$$

$$N_\theta = \frac{1}{\pi}\cdot\frac{r''}{\alpha r}(M_0 + Pz)\cos\theta, \tag{11}$$

$$N_{s\theta} = -\frac{1}{\pi}\cdot\frac{1}{r}\left[P - \frac{r'}{r}(M_0 + Pz)\right]\sin\theta. \tag{12}$$

We note that equations (10) to (12), in addition to solving the problem of flexure of a cantilever shell, also solve the problem of pure bending due to couples applied at the ends of a shell.

5. Stress Function Solution for Distributed Surface Load

A generalization of (2) to include the effect of distributed surface load intensities p_r, p_z and p_θ may be written in the form

$$N_s = \frac{\alpha}{r^2}\frac{\partial U}{\partial\theta} + N_{sa}, \qquad N_\theta = \frac{r''}{\alpha r}\frac{\partial U}{\partial\theta} + N_{\theta a}, \qquad N_{s\theta} = -\frac{\partial}{\partial z}\left(\frac{U}{r}\right), \tag{13}$$

where now U as well as N_{sa} and $N_{\theta a}$ depend on p_r, p_z and p_θ. From the conditions of axial and radial equilibrium* follows

$$N_{sa} = -\frac{\alpha}{r}\int r\alpha p_z\,\partial z, \quad N_{\theta z} = rp_r - \frac{1}{\alpha}\cdot\frac{\partial}{\partial z}\left(r'\int r\alpha p_z\,dz\right). \tag{14}$$

From the corresponding condition of circumferential equilibrium* follows

$$\frac{\partial^2 U}{\partial z^2} - \frac{r''}{r}\left(U + \frac{\partial^2 U}{\partial\theta^2}\right) = r\alpha p_\theta + \alpha\frac{\partial N_{\theta a}}{\partial\theta}. \tag{15}$$

The differential equation (15) becomes again particularly simple in the event that U may be taken in the form (7).

6. Stress Resultants due to Hydrostatic Lateral Load

We designate by hydrostatic lateral load a purely normal surface load intensity p_n such that

$$p_n = p_0\frac{r}{a}\cos\theta \tag{16}$$

*Equations (3) and (1) of Reissner (1947).

where p_0 and a are suitable constants. Axial, radial and circumferential load intensity components corresponding to (16) are, in accordance with Fig. 2,

$$p_z = -\frac{r'}{\alpha} p_n, \qquad p_r = \frac{1}{\alpha} p_n, \qquad p_\theta = 0, \tag{17}$$

and therewith

$$N_{sa} = \frac{\alpha}{r} \frac{p_0}{a} \cos\theta \int r^2 r' \, dz = \frac{p_0}{a} \frac{\alpha}{r} \frac{(r^3 - c)}{3} \cos\theta, \tag{18}$$

$$N_{\theta a} = \frac{p_0}{a} \left[\alpha r^2 + \frac{r''}{\alpha} \frac{(r^3 - c)}{3} \right] \cos\theta, \tag{19}$$

and

$$\frac{d^2 V}{dz^2} = -\frac{p_0}{a} \left[\alpha^2 r^2 + r'' \frac{(r^3 - c)}{3} \right]$$

$$= -\frac{p_0}{a} \left[r^2 + \frac{(r^3 r')' - c r''}{3} \right]. \tag{20}$$

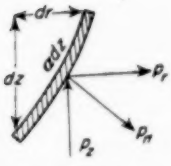

Fig. 2. Determination of p_r and p_z in terms of p_n when $p_\theta = 0$.

Equation (20) may be integrated twice in the form

$$V = -\frac{p_0}{a} \left[\int\int r^2 \, dz \, dz + \frac{r^4}{12} - \frac{cr}{3} \right] \tag{21}$$

where the remaining indefinite double integral incorporates a term of the form $k_0 + k_1 z$.

Introduction of (18), (19) and (21) into equations (13) results in the following expressions for stress resultants:

$$N_s = \frac{p_0}{a} \left[\frac{\alpha r^2}{4} - \frac{\alpha}{r^2} \int\int r^2 \, dz \, dz \right] \cos\theta, \tag{22}$$

$$N_\theta = \frac{p_0}{a} \left[\alpha r^2 + \frac{r'' r^3}{4\alpha} - \frac{r''}{\alpha r} \int\int r^2 \, dz \, dz \right] \cos\theta, \tag{23}$$

$$N_{s\theta} = \frac{p_0}{a} \left[\frac{(r^3)'}{12} + \left(\frac{1}{r} \int\int r^2 \, dz \, dz \right)' \right] \sin\theta. \tag{24}$$

The constants k_0 and k_1 which are incorporated in the indefinite double integral which appears in (22) to (24) must be evaluated by suitable boundary or regularity conditions.

7. Ellipsoidal Shell subjected to Lateral Hydrostatic Loading

As an example of application of the general formulas (22) to (24) we consider a shell which consists of the ellipsoidal head of a fluid-filled horizontal cylindrical tank. If a is the radius of the cylindrical shell and if b is the depth of the ellipsoidal head, the equation of the ellipsoidal shell may be taken as

$$\frac{r^2}{a^2} = 1 - \frac{z^2}{b^2}, \qquad 0 \leqslant z \leqslant b. \tag{25}$$

The various quantities occuring in equations (22) to (24) become

$$\iint r^2 \, dz \, dz = \tfrac{1}{2} a^2 z^2 - \tfrac{1}{12} \frac{a^2}{b^2} z^4 + k_0 + k_1 z, \tag{26}$$

$$r' = -\frac{a^2 z}{b^2 r}, \tag{27}$$

$$\alpha^2 = 1 + (r')^2 = 1 + \frac{a^4 z^2}{b^4 r^2} = \frac{a^2 \left[1 + (a^2 - b^2) z^2/b^4\right]}{r^2}, \tag{28}$$

$$r'' = -\frac{a^2}{b^2 r} + \frac{a^2 z r'}{b^2 r^2} = -\frac{a^4}{b^2 r^3}. \tag{29}$$

The constants k_0 and k_1 are determined from the condition that N_s, N_θ and $N_{s\theta}$ remain finite as r approaches zero at the apex of the shell. When $r = 0$ we have $z = b$ and the finiteness conditions reduce to the conditions that $\iint r^2 \, dz \, dz$ and its derivative are finite at $z = b$.

From equation (26) follows then

$$\tfrac{5}{12} a^2 b^2 + k_0 + k_1 b = 0, \qquad \tfrac{2}{3} a^2 b + k_1 = 0,$$

or

$$k_1 = -\tfrac{2}{3} a^2 b, \qquad k_0 = \tfrac{1}{4} a^2 b^2. \tag{30}$$

Introduction of equations (25) to (30) into equations (22) to (24) leads to formulas which are analogous to formulas which have earlier been derived by Baltrukonis (1958) by a different procedure.

Acknowledgment

The work reported in this article has been supported by the Office of Naval Research of the United States Navy, under a contract with the Massachusetts Institute of Technology.

References

Baltrukonis, J. H. 1958 *Proc. 3rd. U.S. Nat. Congr. Appl. Mech.* 247.
Reissner, E. 1947 *J. Math. Phys.* **26**, 290.

J. Mech. Phys. Solids, 1959, Vol. 7, pp. 247 to 257. Pergamon Press Ltd., London. Printed in Great Britain

ELASTIC-PLASTIC TORSION OF A CIRCUMFERENTIALLY NOTCHED BAR*

By J. B. Walsh† and A. C. Mackenzie‡
Mechanical Engineering Department, Massachusetts Institute of Technology

(*Received* 1*st April*, 1959)

Summary

The elastic-plastic torsion of a cylindrical bar with a circumferential notch is investigated. Theoretical predictions of angle of twist and notch root strain are compared with experimental values.

1. Introduction

Much effort has been expended in determining the stress and strain concentration factors due to notches in machine elements under elastic conditions. However, serious errors may arise if the results of elastic analysis are used to determine

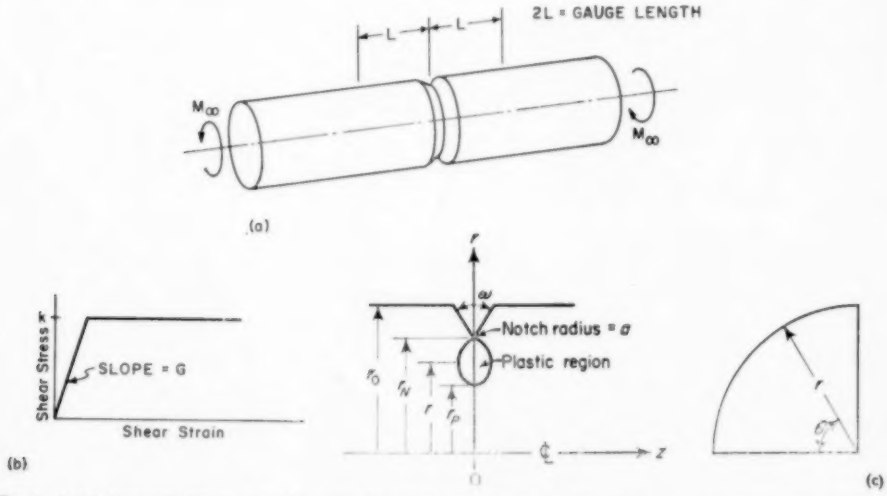

Fig. 1. (a) Schematic diagram of bar. (b) Shear stress/shear strain curve. (c) Quarter section of bar.

stresses and strains in notched elements of ductile material. In research on fracture in such materials, for example, solutions which take account of local plastic deformation are necessary. The elastic-plastic tension of a notched bar

*This research was sponsored by the United States Air Force through the Air Force Office of Scientific Research of the Air Research and Development Command under Contract No. AF 18 (600)-937, by the Massachusetts Institute of Technology Machine Method of Computation Committee under ONR Contract N5-ori-60, and by the George Westinghouse Fund of the Massachusetts Institute of Technology, Mechanical Engineering Department.

†Now at Foster-Miller Associates, Waltham, Massachusetts.
‡Now at Babcock and Wilcox, Renfrew, Scotland.

has been treated by Allen and Southwell (1949), but the strain distribution in the region of the notch has not been obtained as yet. An analytical solution to the simpler case of a notch in a semi-infinite solid subject to pure shear has been given by Hult and McClintock (1956), but their results are not directly useful for experimental study or for practical purposes. The quest for a system of more direct application but still involving a relatively simple stress–strain field led to the study of the present case of the circumferentially notched bar in torsion.

The elements of the problem under study are presented in Fig. 1 (a, b, c). The shear stress/shear strain relationship used in the analysis is that of an elastic–plastic, non-hardening continuum. Although a notch of finite root radius is depicted, attention will be centred initially on the case of the infinitely sharp notch ($a = 0$). The analysis will be discussed in three subsections, concerned with the determination of (i) a relationship between applied torque and extent of plastic region, (ii) angle of twist over a suitable gauge length, and (iii) plastic strains in the plane of the notch.

2. Applied Torque: Extent of Plastic Region

Theoretical analyses of the torsion of bars of varying diameter, as carried out by Michell (1900) for the elastic case and by Sokolovsky (1945) for the plastic non-hardening case, indicate that the assumption of only two shear stresses, $\tau_{r\theta}$ and $\tau_{z\theta}$, is adequate. Since the size and shape of the plastic region for a specified applied torque is not known *a priori*, a shape was assumed for the plastic region, following a standard procedure. A solution for the stress function in the plastic region was obtained and the value of the stress function on the plastic–plastic boundary was calculated. The boundary-value problem which then existed in the elastic region was solved using finite difference technique. A correct solution existed when the shape of the plastic region was adjusted to give equality of stresses on the elastic–plastic boundary.

A trial calculation was performed for a particular case in which the plastic zone was assumed to have the depth indicated from the complete solution but to be of zero width. Solving this problem for the stress function gave a value of torque for a given length of plastic zone which differed by less than one per cent from that used in the more complete analysis. The assumption was thus made in further calculations that the plastic region was confined to the plane $z = 0$. By carrying out the calculations for several values of torque, a graphical relation between applied torque and depth of plastic region was obtained. This relationship is presented in Fig. 2 in terms of the non-dimensional parameters M_∞/M_{fp} and r_p/r_N, M_∞ being the applied torque and M_{fp} the torque necessary for the section under the notch to become fully plastic. That is, if k is the yield stress in shear, the fully-plastic torque is given by

$$M_{fp} = \tfrac{2}{3}\pi k r_N^3 \qquad (1)$$

The relationship between the plastic zone radius ratio r_p/r_N and the torque ratio M_∞/M_{fp} is plotted in Fig. 2 for a notch-radius ratio r_N/r_0 of 0·7. Also shown in Fig. 2 are two points calculated for $r_N/r_0 = 0{\cdot}3$

In addition to the numerical results, appropriate limiting solutions are indicated in Fig. 2. These were obtained from approximate solutions for stresses when the

plastic zone radius ratio tended to zero and to unity. For the former case ($r_p/r_N \sim 0$), the equation giving the stress function in the elastic region was

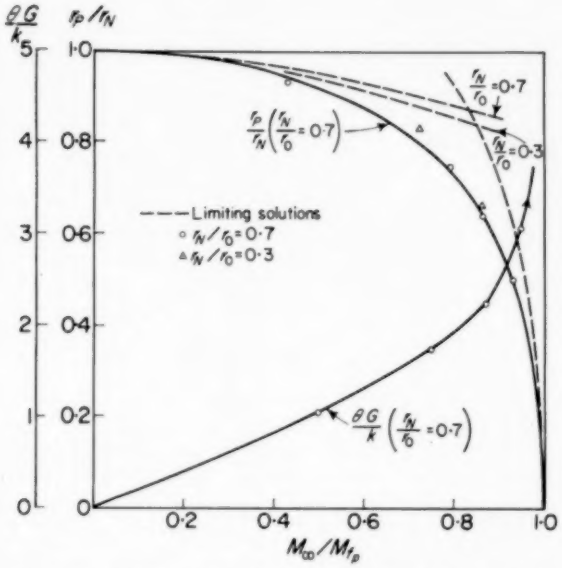

Fig. 2. Plastic zone length and angle of twist vs. torque.

solved for small values of r by WALSH (1958). The result obtained is that the plastic zone radius ratio is independent of the notch depth and is expressed by

$$\left(\frac{r_p}{r_N}\right)^3 = 4\left(1 - \frac{M_\infty}{M_{fp}}\right). \tag{2}$$

The limiting solution for small plastic regions ($r_p/r_N \sim 1$) was obtained from the elastic solutions presented by NEUBER (1937) using a method similar to that suggested by HULT (1957). The plastic zone radius ratio was found to be given by the expression

$$\left(\frac{r_p}{r_N}\right) = 1 - \frac{\left(\frac{16}{3}\right)\left(\frac{M_\infty}{M_{fp}}\right)^2\left(\frac{r_0}{r_N} - 1\right)}{1 + \frac{64}{9}\left(\frac{r_0}{r_N} - 1\right)}. \tag{3}$$

3. ANGLE OF TWIST

In determining the relation between applied torque and depth of plastic region as detailed above, stresses were obtained at stations throughout the elastic region for several values of applied torque. Strains obtained from the stresses by direct application of Hooke's law were then graphically integrated along suitable paths to give displacements and hence angles of twist. A particular case was considered for which the gauge length extended a distance of one outside radius to either side of the notch centre-line (i.e., in Fig. 1 (a), $L = r_0$). The results of this procedure

are plotted in Fig. 2, with the coordinates M_∞/M_{fp} and $\theta G/k$, where θ = angle of twist in radians over a total gauge length of $2r_0$, G = shear modulus, and k = yield stress in shear. The mathematical formulation of this problem is given in Appendix 2.

4. Plastic Strains

The solution for plastic strains was obtained by consideration of the relative displacement of characteristic surfaces in the plastic region. Although determination of strains in the plastic region has been carried out with generality by Walsh (1958), only the plastic strain component, $\gamma_{z\theta}$, (denoted γ in further reference) in the central plane of the notch ($z = 0$) is of interest here. This strain component is given by

$$\gamma = \frac{k}{G}\left(\frac{r}{r_p}\right)^2\left(\frac{r_N - r_p}{r_N - r}\right). \tag{4}$$

Equation (4) is derived in Appendix 3.

5. Extension to Notches of Finite Root Radius

The extension to notches of finite root radius involves the concept that any stress free surface (a surface bounded by a line of constant stress function) may be considered as the bounding surface of a bar. This situation is depicted in Fig. 3. The lines of constant stress function have finite curvature at $z = 0$. For small radii of curvature the lines of constant stress function in the region of the notch tip can be shown to approximate arcs of a set of concentric circles about the notchtip as centre. Any one of these constant stress function surfaces having the required radius of curvature, a, at $z = 0$ may be taken as the surface of a bar. Although the lines of constant stress function once in the plastic region remain unchanged during subsequent twisting, in the elastic region changes do occur which affect the assumed external geometry. As shown by Walsh (1958) the effect of the changes is negligible if small values of M_∞/M_{fp} are not treated. With this restriction on the ratio it follows that

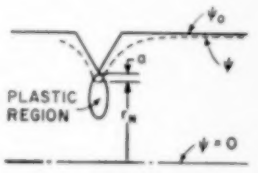

Fig. 3. Notch of finite root radius.

(a) the plastic zone radius ratio for the notch of finite root radius may be found with fractional error of the order of (a/r_N) from the $(M_\infty/M_{fp}) \times (r_p/r_N)$ relationship for the sharp notch at the same value of (r_N/r_0) and (M_∞/M_{fp});

(b) the torque-twist curve for the sharp notch may be applied to the rounded notch, incurring fractional error in twist of the order of $(a/r_N)\,(M_{fp}/M_\infty - 1)$;

(c) the expression for plastic strain given in (4) may be extended to the round notch by writing $(r_N + a)$ for r_N in (4). The plastic strain in the plane of the notch is found to be given by

$$\gamma = \frac{k}{G}\frac{(r/r_N)^2}{(r_p/r_N)^2}\cdot\frac{(1 + a/r_N - r_p/r_N)}{(1 + a/r_N - r/r_N)}. \tag{5}$$

The strain at the root of the notch, if $a \ll r_N - r_p$, is simply

$$\gamma_N = \frac{k}{G}\frac{1 - r_p/r_N}{(r_p/r_N)^2}\frac{1}{a/r_N}. \tag{6}$$

6. Experimental Study

The objects of the experimental study were (a) to obtain torque-twist curves for specimens having different notch root radii and to compare these with curves resulting from the theoretical study; and (b) to measure notch root surface strains at various values of applied torque and to compare these with theoretical strains.

The work was conducted on specimens detailed in Fig. 4, three notch root radii of 0·005 in., 0·010 in. and 0·020 in. being used. The specimens were cut from 2 in.

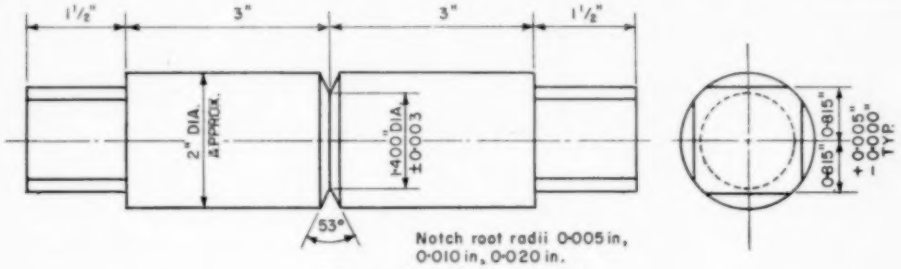

Fig. 4. Detail of specimens.

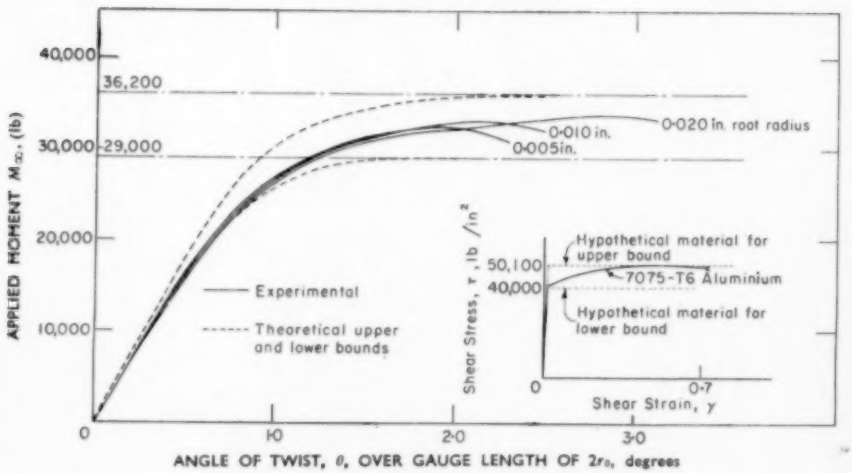

Fig. 5. Moment-twist curves.

diameter 7075-T6 aluminium alloy bars pre-stretched to slightly in excess of twice the initial yield strain to relieve residual stresses. The choice of material was made to approximate as closely as possible the ideal non-hardening material assumed in the theoretical analysis. A shear stress/shear strain curve obtained for the 7075-T6 alloy is given in the caption to Fig. 5. A method proposed by Nadai (1950) was used to obtain this curve from a torque-twist relationship for an unnotched specimen.

Electric resistance strain-gauge elements were incorporated in the torque and angle of twist measuring devices. By using a suitable recorder – in this case a two channel Sanborn (Carrier Preamplifier) – a continuous, parallel recording of torque and angle of twist was made.

Notch root strains were measured by photographing an axial mark in the notch root at various stages of the test with a camera coupled to a telescope. The slope of the mark at the central plane of the notch gave a direct measure of the local strain, γ_N.

Further details of experimental technique are given by MACKENZIE (1958).

The torque-twist curves obtained for the three specimens of different notch-root radii are given in Fig. 5. In order to plot a theoretical curve from the results of Fig. 2 a value for the yield stress k had to be assumed. The question as to the value to be used was resolved by plotting two theoretical curves, one based on the initial yield stress of 7075-T6 alloy as indicated from the shear stress/shear strain diagram and the other on the maximum shear stress. The situation is depicted in the caption to Fig. 5. The resulting theoretical curves have been designated upper and lower bounds.

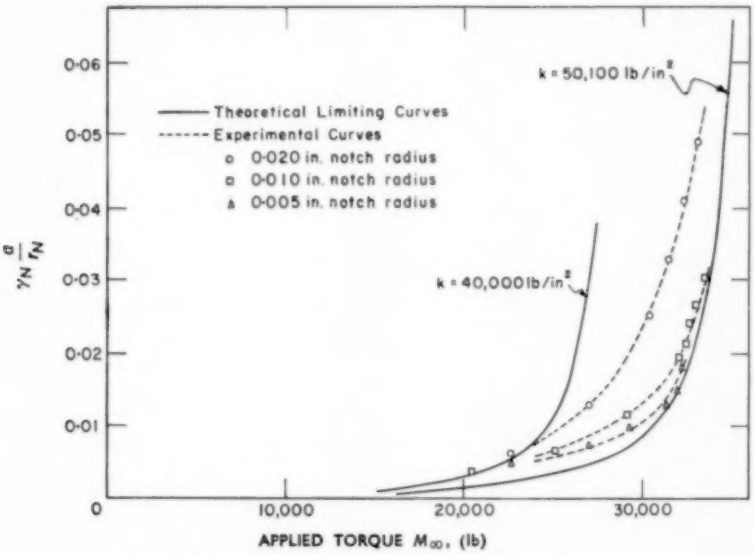

Fig. 6. Notch root strain vs. supplied torque.

Measured notch-root strains are plotted as $(\gamma_N \cdot a/r_N)$ against applied torque in Fig. 6. Theoretical curves obtained from (6) and the $M_\infty/M_{fp} \times r_p/r_N$ curve of Fig. 2 are also given. The theoretical curves are based on values of k equal to the initial yield stress of 40,000 lb/in² and the maximum yield stress of 50,100 lb/in².

7. DISCUSSION

The experimental torque-twist curves are seen from Fig. 5 to follow the lower limit theoretical curve closely in the initial stages and to tend towards the upper limit curve as the torque approaches the fully plastic torque. The departures of the experimental curves from the upper limit curve can be attributed at least in part to the effect of workhardening. In the upper limit curve the yield stress in the plastic region is taken to be the limiting shear stress. The yield stress in the

experimental bar, however, ranges between the initial yield stress and the limiting shear stress. For a given value of applied torque the depth of plastic region in the experimental bar will then exceed that predicted theoretically, and the experimental angle of twist will be correspondingly greater. It is to be noted also that the theoretical angles of twist were obtained using solutions for stress in the elastic region which were found assuming plastic regions of zero width. Thus, the angles of twist were somewhat underestimated. However, since stresses in the elastic region where the integration to find the angle of twist was carried out did not appear to be greatly affected by plastic zone width, the error introduced is not serious.

Theoretical considerations indicate that, to a first order approximation, notches of different root radii should follow the same torque-twist curve prior to fracture. The experimental curves of Fig. 5 for notches of three different root radii indicate a slight spread, however. Some of this spread can be accounted for by approximations made in the theory, but it appears that work-hardening is mainly responsible. For a given depth of plastic region, notch-root strains will be higher for sharper notches, and correspondingly higher torques will result.

Equation (6) predicts that notch-root strain data for all notch-root radii should fall on one curve when plotted as $(\gamma_N \cdot a/r_N)$ vs. M_∞. Fig. 6 indicates that work-hardening causes a spread in data. Increasing strains tend to draw the experimental curves away from the lower limit curve toward the higher, as expected.

It is of interest to consider the possibility of extending the theoretical results to bars of slightly different geometries. From the two points plotted in Fig. 2 for a bar with $r_N/r_0 = 0{\cdot}3$, it would appear that the $r_p/r_N \times M_\infty/M_{fp}$ relationship is not a strong function of r_N/r_0, at least for values of r_N/r_0 in the range 0·3 to 0·7. The effect of notch angle, ω, on the $r_p/r_N \times M_\infty/M_{fp}$ relationship, although known to be of importance for small depths of plastic region from the pure shear solution of Hult and McClintock (1956), becomes progressively less important as the fully plastic case is approached. The angle of twist results will be affected by changes in both r_N/r_0 and ω. Angles of twist may be derived for gauge lengths greater than that assumed merely by correcting for additional twist using the theory for unnotched bars in torsion. For shorter gauge lengths, however, application of such a correction will lead to progressively more serious error.

Acknowledgments

The authors wish to thank Professor F. A. McClintock for help received during the course of this investigation.

Aluminium used in the experimental programme was donated by the Kaiser Aluminium and Chemical Co. Inc.

References

Allen, D. N. de G. and Southwell, R. V. 1949 *Phil. Trans. Roy. Soc.* **242**, 379.

Hill, R. 1950 *Mathematical Theory of Plasticity*, p. 95 (Clarendon Press, Oxford).

Hult, J. A. H. 1957 *Fatigue Crack Initiation* (Sc.D. Thesis, M.I.T.).

Hult, J. A. H. and McClintock, F. A. 1956 *Proc. 9th Int. Congr. Appl. Mech.*, Brussels.

Mackenzie, A. 1958 *Crack Initiation in Circumferentially-Notched Bars in Torsion* (S.M. Thesis, M.I.T.).

Michell, J. H.	1900	*Proc. Lond. Math. Soc.* **31**, 141.
Nadai, A.	1950	*Theory of Flow and Fracture of Solids*, p. 349 (McGraw-Hill).
Neuber, H.	1958	*Kerbspannungslehre* (Springer, Berlin).
Sokolovsky, V. V.	1945	*Prik. Mat. i. Mech.* **9**, 339.
Walsh, J. B.	1958	*Notches in Plastic Torsion* (Sc.D. Thesis, M.I.T.).

Appendix I

Determination of the $M_\infty/M_{fp} - r_p/r_N$ relationship

Stresses in the plastic region were determined by Sokolovsky (1945) in terms of β, the angle between the resultant shear stress vector and the r-direction, using the method of characteristics:

$$\tau_{r\theta} = k \sin \beta, \tag{7a}$$

$$\tau_{z\theta} = k \cos \beta. \tag{7b}$$

The characteristics are defined by the equation

$$\frac{dz}{dr} = -\tan \beta. \tag{8}$$

Integration of (8) shows that the variation of β along a specific characteristic is given by

$$r^2 \sin \beta = \text{constant} = R^2. \tag{9}$$

These results of Sokolovsky are more conveniently expressed in terms of a stress function, ψ, defined as

$$\frac{\partial \psi}{\partial z} = r^2 \tau_{r\theta}, \tag{10a}$$

$$\frac{\partial \psi}{\partial r} = -r^2 \tau_{z\theta}. \tag{10b}$$

Equation (10a) can be combined with (9) and (7a) to give the variation of the stress function along a characteristic:

$$\frac{\partial \psi}{\partial z} = kR^2. \tag{11}$$

Equation (11) is now integrated to give

$$\psi = kzR^2 + f(r). \tag{12}$$

Partial differentiation of (12) with respect to r and combination with (9) and (10b) results in an expression for $f'(r)$:

$$f'(r) = -kr^2 \cos \beta = -k\sqrt{(r^4 - R^4)}. \tag{13}$$

Equation (13) is integrated and combined with (12) to give an expression for the stress function:

$$\psi = z\left(kR^2 - \int \sqrt{(r^4 - R^4)}\, dr\right). \tag{14}$$

Equation (14) is integrated with the boundary conditions that ψ has the value of ψ_0 on the surface of the bar and zero on the axis. The solution for the stress function in the plastic region is found to be

$$\frac{\psi_0 - \psi}{\psi_0} = \frac{M_{fp}}{M_\infty}\left[\sqrt{1 - \left(\frac{R}{r_N}\right)^4} - \frac{r}{r_N}\sqrt{\left(\frac{r}{r_N}\right)^4 - \left(\frac{R}{r_N}\right)^4} - \frac{R^2 z}{r_N{}^3}\right] \tag{15}$$

where

$$M_\infty = 2\pi\, \psi_0.$$

In order to evaluate ψ from (18) at any point in the plastic region and, in particular, on the elastic–plastic boundary, the value of R for the characteristic passing through that point must be be determined. Equations (8) and (9) are combined to give the equation of the characteristic in the form

$$dz = R^2 \frac{dr}{\sqrt{(r^4 - R^4)}}, \tag{16}$$

Integration of (16) using elliptic functions allows the parameter, R, to be found as a function of the coordinates r and z.

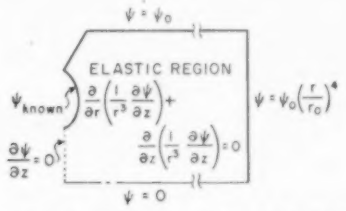

Fig. 7. Boundary-value problem in elastic region.

The stress function ψ, defined in (10), in the elastic region was found by Michell (1900) to be governed by the differential equation

$$\frac{\partial}{\partial r}\left(\frac{1}{r^3}\frac{\partial \psi}{\partial r}\right) + \frac{\partial}{\partial z}\left(\frac{1}{r^3}\frac{\partial \psi}{\partial z}\right) = 0. \tag{17}$$

A boundary-value problem in the elastic region can then be considered, as in Fig. 7, where the value of ψ on the elastic–plastic boundary is calculated from the plastic-region solution.

Appendix II

Determination of angle of twist

The determination of the angle of twist was carried out in detail by Mackenzie (1958). The essential features of the derivation are presented here for reference.

As already stated, the only non-vanishing component of displacement is that in the θ-direction, denoted by v. In order to determine the angle of twist between two points $A(-z_0, r_0)$ and $B(z_0, r_0)$ on the surface of the bar equidistant from the section of symmetry, $z = 0$, their

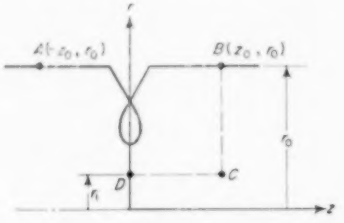

Fig. 8.

displacement must be found. The situation is shown in Fig. 8. An increment in v/r is related to differential increments in the r and z-directions by the equation

$$d\left(\frac{v}{r}\right) = \frac{\partial}{\partial r}\left(\frac{v}{r}\right) dr + \frac{\partial}{\partial z}\left(\frac{v}{r}\right) dz. \tag{18}$$

Equation (18) is combined with the definitions of strains to give

$$d\left(\frac{v}{r}\right) = \frac{\gamma_{r\theta}}{r}\,dr + \frac{\gamma_{z\theta}}{r}\,dz. \tag{19}$$

In the elastic region the strains are related to the stress by Hooke's law. Thus, (19) may thus be written as

$$d\left(\frac{v}{r}\right)_{\text{elastic}} = \frac{1}{G}\left(\frac{\tau_{r\theta}}{r}\,dr + \frac{\tau_{z\theta}}{r}\,dz\right) \tag{20}$$

or, in terms of the stress function, as

$$d\left(\frac{v}{r}\right)_{\text{elastic}} = \frac{1}{G}\left(-\frac{1}{r^3}\frac{\partial\psi}{\partial z}\,dr + \frac{1}{r^3}\frac{\partial\psi}{\partial r}\,dz\right). \tag{21}$$

The relative displacement v/r between two points A and B in Fig. 8 is found by integrating (21) along the path DCB (where D is any convenient point in the elastic region at $z = 0$) to give finally

$$\frac{v_0}{r_0} = \frac{1}{Gr_1^3}\int_0^{z_0}\left(\frac{\partial\psi}{\partial r}\right)_{r=r_1} dz - \frac{1}{G}\int_{r_1}^{r_0}\frac{1}{r^3}\left(\frac{\partial\psi}{\partial z}\right)_{z=z_0} dr. \tag{22}$$

The problem of determining v_0/r_0 then becomes one of evaluating the two integrals above. This was done graphically from the values of ψ known at various stations throughout the elastic region. The angle of twist between sections A and B is given by the quantity $2\,v_0/r_0$.

In (22), if z be taken large enough, i.e. such that the solution for the unnotched bar applies, then $\dfrac{\partial\psi}{\partial z} \sim 0$, and only the first term need be considered in evaluating v_0/r_0. This condition was found to be adequately satisfied by taking $z_0 \geqslant r_0$.

Appendix III

Strains in the plastic region at $z = 0$

Hill (1950) showed that the displacement v along a characteristic defined by (9) is given by

$$v/r = \text{constant}. \tag{23}$$

Equation (23) has the physical interpretation that surfaces formed by characteristics are not deformed during twisting. Thus, to determine the shear strain, attention is confined to the relative motion between two characteristics surfaces specified by the values R and $R + dR$. Near the plane $z = 0$, $R/r \ll 1$, and $\gamma_{z\theta}$ is the only strain component. Therefore, only the expression $\partial v/\partial z$ must be evaluated. Since the quantity v/r is constant along a characteristic one may write

$$\left[\frac{\partial}{\partial z}\left(\frac{v}{r}\right)\frac{\partial z}{\partial R}\right]_{\substack{z=0\\ r\geqslant r_p}} = \left[\frac{\partial}{\partial z}\left(\frac{v}{r}\right)\frac{\partial z}{\partial R}\right]_{\substack{z=0\\ r=r_p}}. \tag{24}$$

On carrying out the differentiation in (24), with

$$\frac{\partial v}{\partial z} = \gamma_{z\theta} \quad \text{and} \quad (\gamma_{z\theta})_{\substack{r=r_p\\ z=0}} = \frac{k}{G},$$

there results

$$(\gamma_{z\theta})_{\substack{z=0\\ r\geqslant r_p}} = \frac{k}{G}\left(\frac{r}{r_p}\right)\frac{\left(\dfrac{\partial z}{\partial R}\right)_{\substack{z=0\\ r=r_p}}}{\left(\dfrac{\partial z}{\partial R}\right)_{\substack{z=0\\ r\geqslant r_p}}}. \tag{25}$$

The quantity $\partial z/\partial R$ is evaluated near the plane $z = 0$ by integrating (16) for $R/r \ll 1$. The characteristics are found to be expressed by the equation

$$z = R^2 \left(\frac{1}{r} - \frac{1}{r_N} \right). \tag{26}$$

Equation (26) is then differentiated to give

$$\frac{\partial z}{\partial R} = 2R \left(\frac{1}{r} - \frac{1}{r_N} \right). \tag{27}$$

Substitution of (27) into (26) leads to an expression for strain in the plane of the notch:

$$\gamma_{z\theta} = \frac{k}{G} \left(\frac{r}{r_p} \right)^2 \left(\frac{r_N - r_p}{r_N - r} \right). \tag{28}$$

J. Mech. Phys. Solids, 1959, Vol. 7, pp. 258 to 263. Pergamon Press Ltd., London. Printed in Great Britain

THE EFFECT OF END CONDITIONS ON THE DYNAMIC LOADING OF PLASTIC SHELLS*

By P. G. Hodge, Jr.
Department of Mechanics, Illinois Institute of Technology

(*Received 8th April*, 1959)

Summary

A circular cylindrical shell of a rigid plastic material is uniformly loaded by a radial step pressure pulse. Explicit formulas are obtained for the maximum deformation in the shell as a function of the shell geometry and pressure magnitude. It is found that for moderately long shells the deformation is essentially independent of the support conditions at the end of the shell.

1. Introduction

The behaviour of rigid–plastic circular cylindrical shells under a load of great magnitude but small duration was first considered by Hodge (1955). Since the present paper represents an application of the theory given there, we shall refer to it frequently as Reference *A*. Specific equations and Figures in *A* will be denoted by (*A*24), Fig. *A*2, etc. The final results of the present paper will be presented in self-contained form, but no attempt will be made to duplicate the theory given in *A*. Rather, it will be assumed that the interested reader has a copy of *A* available so that specific references can be made.

A circular cylindrical shell of length $2L$, diameter $2a$, and thickness $2h$ is subjected to a step pressure pulse which acts uniformly on the entire lateral surface of the shell. The analysis is carried out in terms of dimensionless quantities defined by

$$\begin{aligned} n &= N_\phi/4kh, & m &= M_x/2kh^2, \\ P &= pa/4kh, & W &= wsa/4kht_0^2, \\ y &= x/L, & \tau &= t/t_0, \\ c &= L/\sqrt{(ah}, & \omega &= 6/c^2 = 6ah/L^2. \end{aligned} \tag{1}$$

Here N_ϕ and M_x are, respectively, the circumferential direct force and axial bending moment per unit length, p is the pressure, w the inward radial displacement, and x is measured from one end of the shell; k is the yield stress of the material in shear, s the surface density, and t_0 the duration of the pressure pulse.

The shell material is assumed to be rigid–plastic and non-hardening and to satisfy the so-called square yield condition (Fig. *A*2c). The stresses and displacements are related by the plastic potential flow law (Table *A*1).

*The results presented in this paper were obtained in the course of research conducted under USAEC Contract No. AT (11-1)-528 between the Atomic Energy Commission and the Armour Research Foundation. A more detailed study will be issued as Report No. ARF 4132-8.

The pressure pulse may be written as a function of time in the form

$$P = \begin{cases} 1 + \rho, & 0 \leqslant \tau \leqslant 1, \\ 0, & 1 \leqslant \tau. \end{cases} \tag{2}$$

We shall see in the following that different analyses are appropriate for different ranges of ρ.

It was found in *A* that the analysis was substantially different for short shells $c^2 < 6\,(\omega > 1)$ and long shells. The present analysis is concerned only with the latter case. In particular, we wish to compare the long but finite shell with the theoretical infinite one in order to determine the effect of end support conditions. Although a general description of the analysis for long shells was given in *A*, explicit results for the displacements were not obtained. In general, this cannot be done in closed form. However, as will be shown, the displacement at the centre of the shell can be simply expressed. Since it follows from the general nature of the solution that the maximum displacement occurs at the centre, we can thus obtain a meaningful measure for comparison.

2. Infinite Shell

If the shell is infinitely long it follows from symmetry that the displacement and bending moment are constant along the shell. Therefore, the equation of motion (*A*2) becomes

$$n + P - \ddot{W} = 0 \tag{3}$$

where W is constant in space. If the shell is plastic, $n = -1$; with P given by (2), the first integrals of (3) are then

$$\dot{W} = \begin{cases} \rho\tau, & 0 \leqslant \tau \leqslant 1 \\ \rho + 1 - \tau, & 1 \leqslant \tau. \end{cases} \tag{4}$$

The motion will continue only so long as $\dot{W}$ is positive, and hence the limit of validity of (4) is

$$\tau = T \equiv \rho + 1. \tag{5}$$

The displacement at any time is easily computed. In particular, the final displacement is

$$W_0 = W(T) = \tfrac{1}{2}\rho\,(\rho + 1). \tag{6}$$

The above analysis is valid for the infinite shell and also for a finite shell of any length, provided that the two ends are unsupported. It follows that the difference between (6) and the maximum displacement of a supported shell is a measure of the influence of the supports.

3. Finite Shell

It was shown in *A* that the analysis of long clamped shells was different in the three cases:

$$\text{medium loads, } \omega/3 \leqslant \rho \leqslant \omega; \tag{7a}$$

$$\text{high loads, } \omega \leqslant \rho \leqslant 1; \tag{7b}$$

$$\text{very high loads, } 1 \leqslant \rho. \tag{7c}$$

We consider the last case first.

According to Fig. *A*3e, there are four time intervals to be considered. For $0 \leqslant \tau \leqslant 1$, a central part of fixed length moves in uniformly, and the remainder of the shell deforms conically. For $1 \leqslant \tau \leqslant \frac{1}{2}(\rho + 1)$ the same pattern continues except that the central region of uniform motion is shrinking. At $\tau = \frac{1}{2}(\rho + 1)$ the ends of the shell come to rest, and the region at rest begins to grow. Thus for $\frac{1}{2}(\rho + 1) \leqslant \tau \leqslant \tau_1$, the shell is rigid for $0 \leqslant y \leqslant u$, deforms conically for $u \leqslant y \leqslant v$, and deforms uniformly for $v \leqslant y \leqslant 1$ where u and v are both increasing. The time $\tau = \tau_1$ is defined by $v = 1$. Thenceforth there is only a conically deforming part over a shrinking portion $u \leqslant y \leqslant 1$ of the shell. The shell finally comes to rest at a time $\tau = T$ before the conically moving part has disappeared.

For $0 \leqslant \tau \leqslant 1$ the solution is given by (*A*24); in the present notation

$$\begin{aligned} \dot{W} &= \rho\tau\,(y/v_0), & W &= \tfrac{1}{2}\rho\tau^2\,(y/v_0), & 0 &\leqslant y \leqslant v_0, \\ \dot{W} &= \rho\tau, & W &= \tfrac{1}{2}\rho\tau^2, & v_0 &\leqslant y \leqslant 1, \\ & & v_0 &= \sqrt{(\omega/\rho)}, & 0 &\leqslant \tau \leqslant 1. \end{aligned} \tag{8}$$

For $1 \leqslant \tau \leqslant \frac{1}{2}(\rho + 1)$, an analysis similar to that in Section *A*6 shows that

$$\begin{aligned} \dot{W} &= (\rho + 1 - \tau)\,(y/v), & 0 &\leqslant y \leqslant v, \\ \dot{W} &= \rho + 1 - \tau, & v &\leqslant y \leqslant 1, \\ v &= \sqrt{\left(\frac{\omega\tau}{\rho + 1 - \tau}\right)}, & 1 &\leqslant \tau \leqslant \tfrac{1}{2}(\rho + 1). \end{aligned} \tag{9a}$$

In particular, the displacement at the centre at $\tau = \frac{1}{2}(\rho + 1)$ is

$$W\left[(1, \tfrac{1}{2}(\rho + 1)\right] = \frac{(\rho + 1)(3\rho - 1)}{8}. \tag{9b}$$

In deriving (9) we used the continuity of velocity and displacement at $\tau = 1$ to evaluate the time-integration constants. The limiting condition $\tau = \frac{1}{2}(\rho + 1)$ on (9) derives from the associated stress field.

For $\frac{1}{2}(\rho + 1) \leqslant \tau \leqslant \tau_1$ the velocity solution is

$$\begin{aligned} \dot{W} &= 0, & 0 &\leqslant y \leqslant u, \\ \dot{W} &= \dot{A}y + \dot{B}, & u &\leqslant y \leqslant v, \\ \dot{W} &= \rho + 1 - \tau, & v &\leqslant y \leqslant 1. \end{aligned} \tag{10a}$$

We define the length of the conically deforming region by

$$z = v - u. \tag{10b}$$

The time functions $\dot{A}$ and $\dot{B}$ are given by

$$\dot{A} = (\rho + 1 - \tau)/z, \quad \dot{B} = -A\dot{u}; \tag{10c}$$

z is given as a function of time by

$$z = \left\{2\omega\left[1 - 2\left(\frac{\rho + 1 - \tau}{\rho + 1}\right)^2\right]\right\}^{\frac{1}{2}}; \tag{10d}$$

and u and v are given by

$$\begin{aligned} v &= \sqrt{(2\omega)}\left[\tfrac{1}{4}\log\left(\frac{\sqrt{2} - 1}{\sqrt{2} + 1}\right)\left(\frac{1 + z/\sqrt{(2\omega)}}{1 - z/\sqrt{(2\omega)}}\right) + \frac{1}{\sqrt{2}}\right], \\ u &= v - z. \end{aligned} \tag{10e}$$

This stage of motion will end when $v = 1$. Denoting the corresponding value of z by z_1, we obtain

$$z_1 = \sqrt{(2\omega)}\,\frac{\sqrt{2}S + C}{\sqrt{2}C + S} \tag{10f}$$

where we have defined

$$C = \cosh\sqrt{2}\left(\frac{1}{\sqrt{\omega}} - 1\right), \qquad S = \sinh\sqrt{2}\left(\frac{1}{\sqrt{\omega}} - 1\right). \tag{10g}$$

Finally, it then follows from (10d) that this solution ends at a time τ_1, defined by

$$\tau_1 = (\rho + 1)\left[1 - \frac{1}{2C + \sqrt{2}S}\right]. \tag{10h}$$

In particular, the velocity at $\tau = \tau_1$ is

$$\begin{aligned} \dot{W} &= 0, && 0 \leqslant y \leqslant u_1, \\ \dot{W} &= \frac{(\rho + 1)(y - u_1)}{2\sqrt{\omega}\,(\sqrt{2}\,S + C)}, && u_1 \leqslant y \leqslant 1\,; \end{aligned} \tag{10i}$$

the central displacement is

$$W(1, \tau_1) = \tfrac{1}{2}\rho(\rho + 1) - \frac{(\rho + 1)^2}{4(\sqrt{2}\,C + S)^2}; \tag{10j}$$

and the boundary u is at

$$u_1 = 1 - \sqrt{(2\omega)}\,\frac{\sqrt{2}S + C}{\sqrt{2}C + S}. \tag{10k}$$

Finally, we consider $\tau_1 \leqslant \tau \leqslant T$. In this case

$$\begin{aligned} \dot{W} &= 0, && 0 \leqslant y \leqslant u \\ \dot{W} &= \dot{A}y + \dot{B}, && u \leqslant y \leqslant 1, \end{aligned} \tag{11a}$$

where

$$\dot{A} = \frac{1}{\alpha}\left[1 - \frac{\omega}{(1 - u)^2}\right], \qquad \dot{B} = -\dot{A}u, \tag{11b}$$

$$u = \alpha(\tau - \tau_1) + u_1, \tag{11c}$$

and the constant α is given by

$$\alpha = \frac{\sqrt{\omega}S(3S + 2\sqrt{2}C)}{(\rho + 1)(\sqrt{2}\,S + C)}. \tag{11d}$$

The motion will stop when $\dot{A} = 0$, and hence

$$T = \tau_1 + \frac{(\rho + 1)(\sqrt{2}\,S + C)}{(3S + 2\sqrt{2}\,C)(\sqrt{2}\,C + S)}. \tag{11e}$$

The central displacement is obtained by integrating (11a) subject to the initial condition (10j) at $\tau = \tau_1$. Thus the final central displacement $W_f = W(1, \tau)$ is

$$W_f = \frac{\rho(\rho + 1)}{2} \cdot \left\{1 - \frac{1 + 1/\rho}{2S(3S + 2\sqrt{2}\,C)}\left[\frac{4(\sqrt{2}\,S + C)^2}{S(3S + 2\sqrt{2}\,C)} \log\frac{\sqrt{2}(\sqrt{2}\,S + C)}{\sqrt{2}\,C + S} - 1\right]\right\}. \tag{11f}$$

Equation (11f) may be rewritten in somewhat more convenient form by defining a new parameter

$$\beta = (3 - 2\sqrt{2})\exp\left[-2\sqrt{2}\,(\omega^{-\frac{1}{2}} - 1)\right]. \tag{11g}$$

Recalling the definitions (10g) of S and C, we obtain

$$W_f = \frac{\rho(\rho + 1)}{2}\left\{1 - \frac{2(1 + 1/\rho)\beta}{1 - 6\beta + \beta^2}\left[\frac{4(1 - \beta)^2}{1 - 6\beta + \beta^2} \log\frac{\sqrt{2}(1 - \beta)}{1 + \beta} - 1\right]\right\}. \tag{11h}$$

Next we consider values of ρ which satisfy (7b). For $0 \leqslant \tau \leqslant 1$ the results are still given by (8). However, in this case, part of the shell near the clamped ends becomes rigid immediately upon removal of the loads. Thus there is no solution corresponding to (9), and (10) must be modified to be continuous with (8) at $\tau = 1$. The resulting analysis is similar to that carried out above and leads finally to

$$W_f = \frac{\rho\,(\rho+1)}{2} - \left\{\frac{\rho^3}{2\,(C'+\sqrt{2\rho}\,S')^2 - (S'+\sqrt{2\rho}\,C')^2}\right\} \times$$

$$\times \left\{\frac{4\,(C'+\sqrt{2\rho}\,S')^2}{2\,(C'+\sqrt{2\rho}\,S')^2 - (S'+\sqrt{2\rho}\,C')^2} \cdot \log\frac{\sqrt{2}\,(C'+\sqrt{2\rho}\,S')}{S'+\sqrt{2\rho}\,C'} - 1\right\}, \tag{12}$$

where

$$C' = \cosh\sqrt{2}\left(\frac{1}{\sqrt{\omega}} - \frac{1}{\sqrt{\rho}}\right), \qquad S' = \sinh\sqrt{2}\left(\frac{1}{\sqrt{\omega}} - \frac{1}{\sqrt{\rho}}\right). \tag{13}$$

As the final case, we consider values of ρ which satisfy (7a). The stress profile history is given in Fig. 4*3*b. While the load is being applied the entire half shell deforms conically ; when the load is removed part of the shell near the ends begins to stop moving. The analysis is somewhat simpler than in the preceding cases and leads directly to

$$W_f = \tfrac{1}{8} \cdot \frac{(3\rho-\omega)^2}{1-\omega}\left[1 + \frac{\omega\log\omega}{1-\omega}\right] + \frac{(3\rho-\omega)}{4}. \tag{14}$$

4. Discussion

For the infinite or unsupported shell the maximum displacement is W_0, given by (6). As a measure of the effect of end supports we consider the quantity

$$\Delta = (W_0 - W_f)/W_0. \tag{15}$$

For very high loads, it follows from (11h) that

$$\Delta = \frac{2\,(1+1/\rho)\,\beta}{1-6\beta+\beta^2}\left[\frac{4\,(1-\beta)^2}{1-6\beta+\beta^2} \cdot \log\frac{\sqrt{2}\,(1-\beta)}{1+\beta} - 1\right]. \tag{16}$$

For values of ω less than about 0·7, β is less than 0·1, hence we can simplify (16) by keeping only second order terms in β. Thus

$$\Delta = 2\beta\,(1+1/\rho)\left[(2\log 2 - 1) + (20\log 2 - 14)\,\beta\right]$$

$$= \tfrac{1}{2}\,\beta\,(1+1/\rho)\,(1{\cdot}545 - 0{\cdot}548\,\beta).$$

Since ρ is always greater than one, the relative error is bounded by

$$\Delta \leqslant \beta\,(1{\cdot}545 - 0{\cdot}548\,\beta). \tag{17}$$

For example, if $\omega = 0{\cdot}5$, $\beta = 0{\cdot}0531$ and the relative error is less than 0·08 ; for $\omega = 0{\cdot}1$, $\beta = 0{\cdot}0004$ and $\Delta \leqslant 0{\cdot}0006$. Therefore, if $\rho > 1$, the end supports can certainly be neglected if $\omega < 0{\cdot}1$ and contribute relatively little for ω as high as 0·5. Further, the neglect of end supports will in every case lead to an overestimate of the maximum displacement.

Even for $\omega = 1$, the shortest shell being considered in the present analysis, the supported shell will deflect 75 per cent as much as the unsupported one. To analyse this case, it is advisable to expand (11f) in terms of

$$\xi = \sqrt{2}\,(\omega^{-\frac{1}{2}} - 1) \tag{18a}$$

since simple substitution of $\omega = 1$ in (11f) leads to an indeterminate form. The resulting value of Δ is

$$\Delta = \frac{1 + 1/\rho}{8}\left(1 - \frac{4\sqrt{2}}{3}\,\xi\right) \tag{18b}$$

which is less than 0·25 for all values of ξ.

Next, let us consider medium loads which satisfy (7a). In particular, we consider the two extremes $\rho = \omega$ and $\rho = \omega/3$. If $\rho = \omega$ it follows from (6), (14) and (15) that

$$\Delta = \frac{\omega^2\left[-\log\omega - (1-\omega)\right]}{(1+\omega)(1-\omega)^2}. \tag{19a}$$

This function varies monotonically from zero at $\omega = 0$ to $\frac{1}{4}$ at $\omega = 1$; for $\omega = 0{\cdot}5$ the error is 0·13; for $\omega = 0{\cdot}1$ it is 0·016. Thus, when the loads are only slightly above the static collapse loads, the effect of end supports is somewhat greater than it is for higher loads but is still relatively insignificant for $\omega < 0{\cdot}1$.

At the other extreme, $\rho = \omega/3$, the maximum displacement according to (14) is zero, whereas for the infinite shell it is not zero. Therefore $\Delta = 1$ for all values of ω; the infinite shell is certainly not a good approximation here. However, we observe that this case becomes of little importance for small ω since ρ tends to zero with ω. In most applications loads will not be so precisely known that the narrow range $\omega/3 \leqslant \rho \leqslant \omega$ is of practical importance when ω is less than 0·1.

The analysis for high loads satisfying (7b) is somewhat more involved. It can be shown that the results are substantially the same and lie between the two extreme cases considered.

Reference

Hodge, P. G., Jr. 1955 *J. Mech. Phys. Solids* **3**, 176.

J. Mech. Phys. Solids, 1959, Vol. 7, pp. 264 to 271. Pergamon Press Ltd., London. Printed in Great Britain

MODIFICATIONS DE STRUCTURE CRISTALLINE PRODUITES PAR FATIGUE ENTRE 20 et 750°C SUR UN ACIER EXTRA DOUX AU CARBONE ET SUR UN ACIER AUSTENITIQUE 18/8

Par J. DE FOUQUET
Laboratoire de Mécanique des Solides, Poitiers

(*Received 6th May*, 1959)

SOMMAIRE

L'ÉTUDE micrographique et aux rayons X d'éprouvettes de fatigue prises à différents stades de l'essai a montré l'influence considérable de la température sur le comportement cristallin du métal sollicité en torsions alternées. En deça d'une température critique, caractéristique du métal étudié, la fatigue est liée à l'apparition de glissements intragranulaires dont l'aspect et la répartition dans les grains dépendent des conditions d'essai. Au-delà de ce seuil, on observe au cours de la fatigue une polygonisation progressive du métal et dans certains cas une recristallisation continue avec un grossissement important du grain. D'où un mode de rupture par fatigue très différent selon la température d'essai.

1. INTRODUCTION

DES essais de fatigue par torsion alternée ont été effectués entre 20 et 750°C sur des éprouvettes plates d'acier extra-doux Thomas spécial (Ugiperval) et d'acier austénitique 18-8 au nickel-chrome, contenant 0·05% C en vue d'étudier l'influence de la température sur le comportement cristallin, en fatigue, de ces aciers. A ces températures il convenait d'adopter un mode d'essai tel que la déformation moyenne par cycle soit nulle, et l'amplitude totale constante évitant ainsi un effet de fluage qui aurait masqué les effets propres aux déformations alternées. Ces conditions sont réalisées dans le cas de la torsion alternée d'amplitude totale imposée, l'axe de torsion coincidant avec l'axe longitudinal de l'éprouvette. Une machine a été spécialement construite à cet effet, marchant à 75 c/s.

Des éprouvettes plates ont été utilisées, permettant un examen micrographique étendu de la surface où les déformations sont les plus grandes. Dans ce cas les contraintes en tout point de l'éprouvette se réduisent à deux contraintes de cisaillement rectangulaires et égales (τ), l'une parallèle à l'axe de torsion, l'autre perpendiculaire et situées dans un plan parallèle à la surface (Figs. 1 et 2).

En phase élastique ces contraintes augmentent linéairement à partir de l'axe où τ est nul jusqu'à la surface où $\tau = G\theta e$ [*1*], G étant le module de cisaillement, θ la torsion unitaire, e l'épaisseur de l'éprouvette.

Les enregistrements des variations du couple en torsion continue et des cycles couple-torsion décrits à faible vitesse, ont montré que dès 300° la partie linéaire

des courbes est très courte. La relation [*I*] n'est plus valable au-delà. On peut montrer que τ a alors pour expression

$$\tau = \frac{1}{le^2}\left(2C + \theta \frac{dC}{d\theta}\right),$$

relation permettant de calculer τ à partir des courbes $C(\theta)$, C désignant le couple de torsion et l la largeur de l'éprouvette.

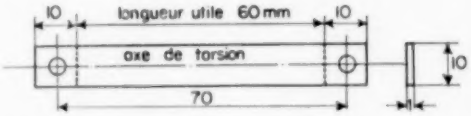

Fig. 1. Schéma de l'eprouvette utilisée dans les essais de torsion alternée.

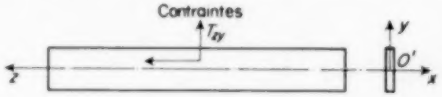

Fig. 2. Répartition des contraintes dans l'éprouvette.

Les essais ont été effectués sous argon afin d'éviter l'oxydation et les éprouvettes étaient préalablement polies électrolytiquement.

2. Aspects Micrographiques Observes apres Fatigue, en fonction de la Temperature d'Essai

(a) *Acier extra-doux*

Cet acier a subi avant essai un recuit de stabilisation à 950° sous vide, donnant un grain sensiblement uniforme de diamètre moyen 5×10^{-2} mm. Jusqu'à 400° on observe dès les premiers milliers de cycles des bandes de glissements, d'aspect différent selon la température à laquelle a été effectué l'essai. L'amplitude de la torsion alternée pour laquelle on observe les premières bandes est dans tous les cas inférieure à l'amplitude correspondant à la limite d'endurance.

A l'ambiante les glissements apparaissent à $\pm$ 0·015 rad cm^{-1} et la rupture ne se produit que pour $\theta \geqslant$ 0·02 rad cm^{-1}. Quand la température d'essai augmente cet écart tend à augmenter, en particulier entre 150 et 300° où les glissements apparaissent à $\pm$ 0·013 rad cm^{-1}, la rupture ne se produisant que pour $\theta \geqslant \pm$ 0·03.

Jusqu'à 150° environ les bandes de glissements sont ondulées et recouvrent une partie du grain d'autant plus étendue que l'amplitude de la déformation alternée est élevée (Fig. 3).

A 200° les bandes sont sensiblement rectilignes et moins denses (Fig. 4). A 300° l'écartement entre les bandes est beaucoup plus grand et devient maximum à 400° où l'on observe quelques bandes seulement sur chaque grain (Fig. 5). A ces températures, l'orientation des bandes est étroitement liée aux directions des contraintes de cisaillement maximum, les glissements s'effectuant suivant des plans parallèles à ces directions où s'en écartant d'un angle toujours inférieur à 15°.

On observe d'autre part deux ou trois directions de glissement au plus dans un même grain et les bandes de directions différentes interfèrent seulement sur une faible longueur, d'autant plus faible que la température est élevée ; de telle sorte qu'à 200° on a plutôt des bandes se croisant sans perturbation, alors qu'à l'ambiante les bandes d'un système prédominent et se raccordent par des petits bouts de l'autre, plus ou moins ondulés (glissements déviés ou ' cross-slip ').

Un polissage électrolytique effectué après essai élimine toute trace de glissement, mais une attaque au réactif de Fry révèle à nouveau les bandes les plus intenses ; lorsque l'essai a été effectué à l'ambiante, on observe des stries extrêmement serrées recouvrant l'ensemble des grains (Fig. 6) ; par contre, pour un essai effectué entre 200 et 400°, les bandes sont beaucoup plus nettes et contrastées, et partent d'un joint en s'arrêtant au milieu du grain (Fig. 7).

Quand le nombre d'alternances est assez élevé, des fissures apparaissent dans les régions de l'éprouvette où les bandes sont les plus marquées (Fig. 6). Ces fissures sont visibles au microscope optique pour un nombre d'alternances de l'ordre du dixième du nombre d'alternances à la rupture, lorsque l'amplitude de la torsion alternée n'est pas trop élevée. Il semble que les fissures atteignent très vite une longueur de l'ordre du diamètre du grain et se propagent ensuite plus difficilement d'un grain à l'autre, n'empruntant que très rarement les joints de grains.

La cassure a une forme en escalier inclinée en moyenne à 45° de l'axe longitudinal de torsion (Fig. 8).

Au-delà de 400° les glissements deviennent beaucoup moins nets et des plissements apparaissement sur les joints de grains (Fig. 9).

A 600° et principalement aux amplitudes de torsion alternée assez élevées, certains grains présentent des ondulations en surface importantes, liées à glissements intergranulaires (Fig. 10). Après polissage électrolytique et attaque au réactif de Fry, les glissements ont disparu et l'on observe une *polygonisation* très nette des grains, particulièrement marquée au voisinage des joints (Fig. 11). Une étude systématique des conditions dans lesquelles se produit cette polygonisation, a montré l'existence de seuils de déformation alternée d'autant plus faibles que la température d'essai augmente : à 450°, la polygonisation se produit pour une amplitude de $\pm$ 0·033 rad cm^{-1}, et à 600°, pour une amplitude égale ou supérieure à $\pm$ 0·01 rad cm^{-1}. Aux faibles amplitudes, les sous-joints de polygonisation restent peu marqués, même pour un nombre d'alternances élevé, et l'éprouvette peut subir plusieurs millions d'alternances sans se rompre.

L'examen de la cassure montre que la cassure n'est plus orientée suivant les directions de cisaillement maximum, mais suit les joints de grains (ou les sous-joints de polygonisation). La cassure n'est plus franche et toute une zone polygonisée de l'éprouvette est recouverte par des fissures (Fig. 12).

A 450°, température minimum pour laquelle on observe la polygonisation, certains grains présentent à la fois des glissements et une région polygonisée mais ne se superposant pas.

A 700° des migrations de joints de grains se produisent en surface au cours de l'essai. A cette température on peut observer des déplacements de joints par simple chauffage mais de tels déplacements se produisent exclusivement entre grains de grosseur différente, les plus gros absorbant les autres. Au contraire, les migrations

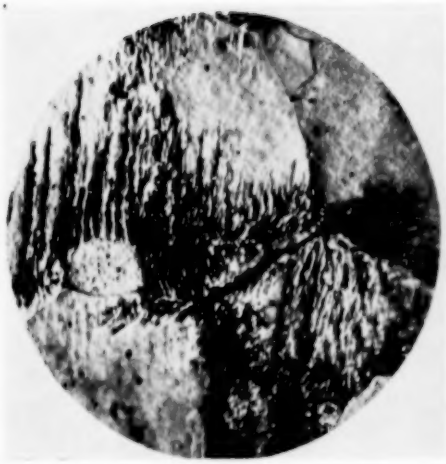

Fig. 3. Micrographie de la surface d'une éprouvette d'acier doux après $2 \cdot 10^5$ cycles à température ambiante. (× 900).

Fig. 4. Micrographie de la surface d'une éprouvette d'acier doux après $2 \cdot 10^5$ cycles à 200°C. (× 900).

Fig. 5. Micrographie de la surface d'une éprouvette d'acier doux après $2 \cdot 10^5$ cycles à 400°C. (× 900).

Fig. 6. Surface polie et attaquée d'une éprouvette d'acier doux, après essais à 20°C. (× 550).

Fig. 7. Acier doux. Surface polie et attaquée après essai à 400°C. (× 550).

Fig. 8. Acier doux, éprouvette rompue par fatigue à 20°C.

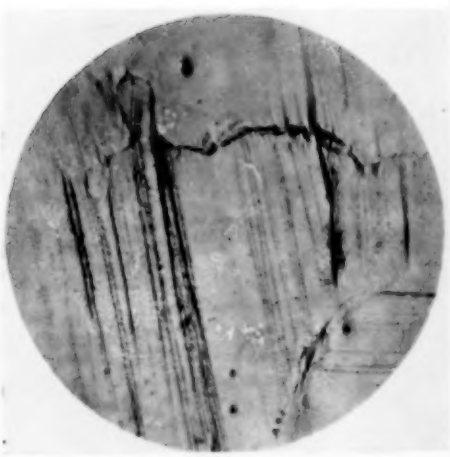

Fig. 9. Surface d'une éprouvette d'acier doux ayant subi 10^5 cycles à 500°C. Bandes de glissements plissements aux joints de grains. (× 600).

Fig. 10. Surface d'une éprouvette ayant subi un essai de fatigue à 600°C. Glissements intergranulaires et plissements marqués. (× 550).

11. Surface polie puis attaquée au réactif de Fry d'une uvette d'acier doux ayant subi un essai de fatigue à 500°C. Polygonisation. (× 550).

Fig. 12. Eprouvette d'acier doux rompue par fatigue à 500°C.

Fig. 13. Micrographie de la surface d'une éprouvette d'acier doux essayée à 700°C. Plissements et migration de joints. (× 550).

Fig. 14. Eprouvette d'acier doux rompue par fatigue à 700°C.

Fig. 15. Acier doux. Micrographie montrant le grossissement du grain après fatigue:
à gauche : coupe de la tête encastrée de l'éprouvette.
à droite : coupe au voisinage de la surface de rupture.

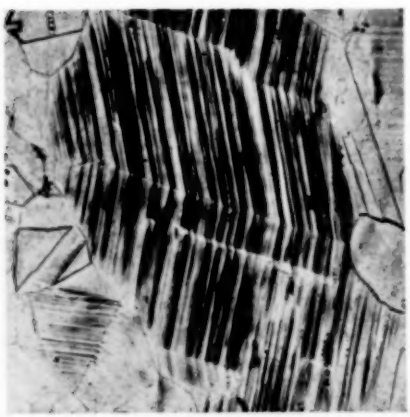

Fig. 16. Acier austénitique. Micrographie superficielle montrant les bandes de fatigue après essai à 20°C. (× 250).

Fig. 17. Acier austénitique. Micrographie après polissage et attaque d'une éprouvette essayée à 20°C. (× 500).

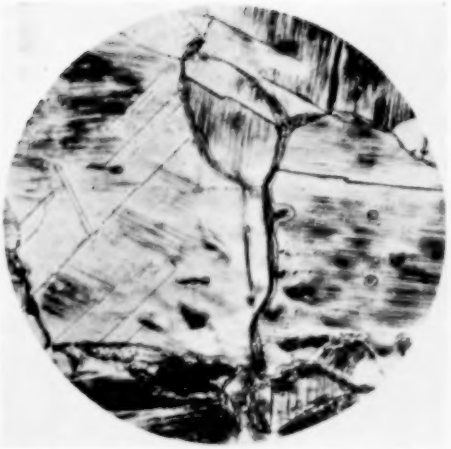

Fig. 18. Micrographie superficielle après essai à 600°C. Acier austénitique. (× 350).

Fig. 19. Acier austénitique. Aspect des glissements. Surface polie et attaquée, après essai à 600°C. (× 900).

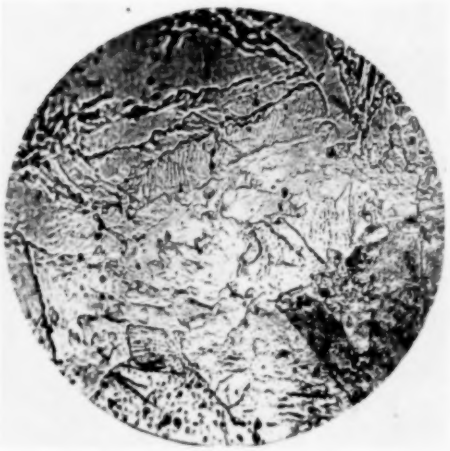

Fig. 20. Acier austénitique. Eprouvette essayée à 750°C. Polygonisation. (× 350).

observées après fatigue s'effectuent entre grains de même grosseur, l'un étant beaucoup plus perturbé que l'autre (Fig. 13).

L'aspect très granuleux de la cassure (Fig. 14) a suggéré l'examen de la section éprouvettes. On constate dans le cas d'essais effectués à 700°, au-delà d'une amplitude de torsion alternée de $\pm$ 0·005 rad cm^{-1}, un grossissement important du grain, d'autant plus rapide que l'amplitude de la déformation est grande. Fig. 15 montre deux sections de la même éprouvette, l'une faite dans la partie non fatiguée, l'autre près de la cassure ; on voit que le grossissement est maximum au voisinage de la surface où la déformation est la plus grande.

Pour un même nombre d'alternances, le grossissement est une fonction croissante de l'amplitude de torsion.

(b) *Acier austénitique*

Le comportement de l'acier austénitique est beaucoup plus simple. Jusqu'à 700° les glissements observés après fatigue sont très nets et le métal ne montre aucune tendance à polygoniser. Par rapport au fer α les glissements obtenus à l'ambiante sont beaucoup mieux définis, les bandes faisant toujours un angle faible par rapport aux directions de cisaillement maximum. Sauf aux amplitudes élevées on observe généralement une seule direction de glissements par grains (Fig. 16). Les fissures se forment dans les bandes (Fig. 17, après polissage et attaque).

Quand la température d'essai augmente les glissements deviennent de plus en plus serrés et de moins en moins marqués, contrairement à ce que l'on observait sur l'acier doux.

Au-delà de 500° l'oxydation devient difficile à éviter et l'on observe en particulier sur les joints de grains un liseré vert d'autant plus large que le taux de fatigue est élevé (Fig. 18). Cette couleur est sans doute dûe à une formation d'oxyde de chrome, accélérée dans les zones les plus distordues.

A 600° l'attaque à l'acide oxalique révèle une précipitation aux joints qui apparaissent finement ponctués. Les bandes de glissements sont elles-mêmes ponctuées (Fig. 19) mais on ne peut affirmer qu'il s'agisse de précipités identiques à ceux observés sur les joints. Aux amplitudes élevées les fissures deviennent intergranulaires à partir de 600°, et dans ce cas la précipitation aux joints est beaucoup plus faible. A 700° les fissures se produisent toujours le long des joints même aux faibles amplitudes et les glissements sont à peine visibles.

Il faut atteindre 800° pour observer des perturbations importantes de la structure cristalline après fatigue. Les glissements ne sont plus visibles ; le joints de grains et les mâcles sont complètement perturbés (Fig. 20). Le grain s'est divisé en nombreux sous-grains mais la polygonisation est beaucoup moins nette que dans le cas de l'acier doux. On ne constate aucun grossissment du grain même à 800°.

Bien que les amplitudes de torsion pour lesquelles apparaissent lesglissements soient pour l'acier austénitique, du même ordre de grandeur que pour l'acier doux, pour une même amplitude et un même nombre d'alternances les glissements sont beaucoup moins marqués. Les fissures sont visibles et la rupture a lieu pour un nombre d'alternances beaucoup plus élevé, surtout entre 400 et 700°.

3. EVOLUTION DE PROPRIETES PHYSIQUES: STRUCTURE DETERMINEE AUX RAYONS X ET DURETE

(a) *Des diagrammes de diffraction X en retour* ont été effectués après essai sur les deux types d'acier.

Pour l'acier doux on obtient après fatigue un astérisme d'autant plus prononcé que l'amplitude de torsion est élevée. A amplitude égale cet astérisme est toujours plus faible entre 200 et 350° qu'à l'ambiante. Au-delà de 400° les anneaux de

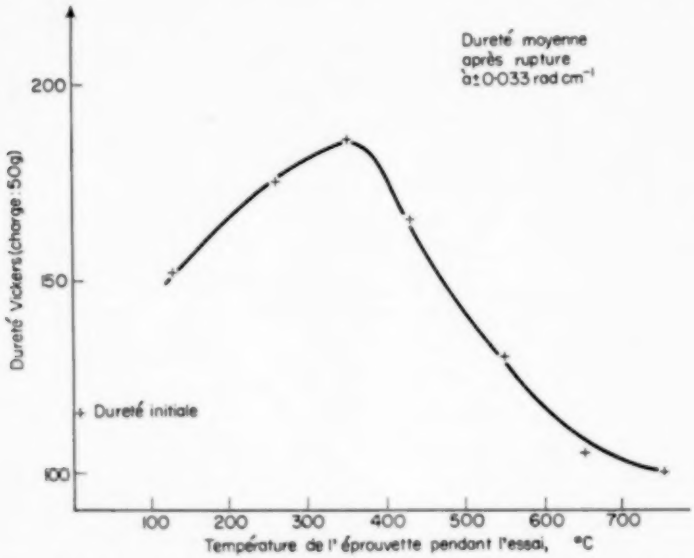

Fig. 21. Dureté de l'acier doux, mesurée après fatigue, en fontion de la température d'essai.

Debye-Scherrer, ponctués à l'état initial, deviennent à la fois continus et très finement divisés, ce qui caractérise la polygonisation, les désorientations à l'intérieur des grains pouvant atteindre 10°. A 700° les diagrammes montrent que les grains ayant grossis sont aussi polygonisés mais la polygonisation est plus parfaite qu'entre 400 et 600°.

Sur l'acier austénitique l'astérisme est toujours beaucoup plus faible, surtout aux températures peu élevées (< 400°). Entre 500 et 700° l'astérisme tend à augmenter et les diagrammes montrent un début de polygonisation sur certaines taches, qui n'apparaissait pas au microscope. Au-delà de 700° les anneaux obtenus sont comparables à ceux obtenus sur l'acier doux entre 400 et 600°, indiquant une polygonisation plus complète des grains.

(b) *L'evolution des caractéristiques mécaniques au cours de l'essai* est difficile à suivre, car il est nécessaire de tremper l'éprouvette pour obtenir un état du métal aussi voisin que possible de son état au moment ou l'on interrompt l'essai. Des mesures de microdureté ont été effectuées dans ces conditions.

Sur l'acier doux on constate jusqu'à 450° une augmentation très sensible de la dureté (Fig. 21) après fatigue. Cette augmentation de la dureté s'effectue principalement au cours des premiers milliers de cycles, la dureté se stabilisant

par la suite. On constate l'existence d'un maximum de la dureté moyenne après rupture entre 250 et 400° pour une même amplitude de torsion alternée. Par contre au-delà de 450°, la dureté diminue et à 700° la dureté après rupture est inférieure ou égale à la dureté initiale.

Pour l'acier austénitique la dureté après essai (plus forte que la dureté initiale) reste sensiblement constante jusqu'à 600°. Elle diminue ensuite très rapidement jusqu'à 800° où l'on obtient une dureté voisine de la dureté initiale.

L'augmentation de dureté en-dessous de 400° pour l'acier doux et de 600° pour l'acier austénitique croit avec l'amplitude de torsion alternée. Nous n'avons jamais constaté de rupture en fatigue sans augmentation de la dureté. La rupture se produit dans ce cas dans la région de l'éprouvette où la dureté est la plus grande. Par contre, pour les températures où la polygonisation a lieu, la rupture se produit dans les zones fortement polygonisées ou recristallisées, où la dureté est la plus faible.

4. Interpretation des Resultats

Les observations précédentes montrent principalement que pour les deux aciers étudiés il existe un intervalle de température pour lequel le mode de rupture par fatigue devient différent. Ce changement résulte d'une différence dans les modifica-

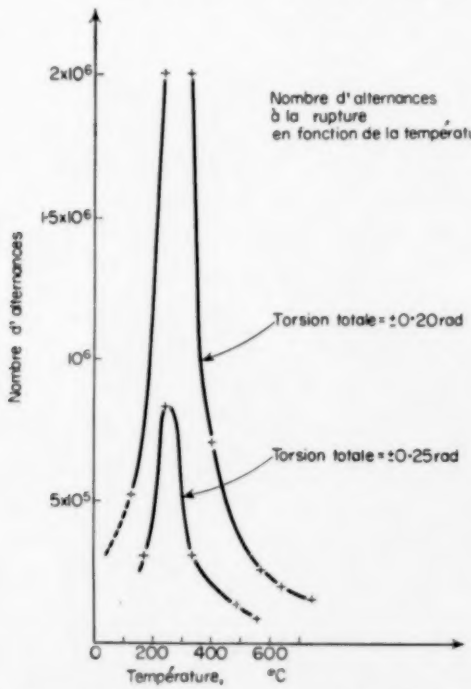

Fig. 22. Variations du nombre de cycles à la rupture en fonction de la température d'essai, pour l'acier doux.

tions de la structure cristalline sous l'effet de la température et des déformations alternées. Un de ces modes de rupture correspond à la formation de fissures

intracristallines et semble lié essentiellement au développement et à l'intensification des bandes de glissements dans les grains, cependant qu'à plus hautes températures, l'apparition de mouvements aux joints entre grains provoque une fissuration intergranulaire.

(a) Dans l'acier doux, à l'ambiante, l'astérisme observé sur les diagrammes de rayons X prouve qu'il existe après fatigue des distorsions importantes, liées semble-t-il à la formation de glissements 'ondulés' et facilement déviés. Au-dessus de 300 à 400° on voit baisser simultanément le durcissement par fatigue et le nombre de cycles à rupture pour une amplitude donnée, cependant que les possibilitiés de déviations des glissements se multiplient à nouveau (polygonisation) et que l'astérisme croit également.

Cependant, on observe entre 200 et 450° un changement d'aspect et une modification de la répartition des bandes dans les grains. Ces bandes deviennent plus contrastées, plus espacées, et sensiblement rectilignes. D'autre part, la dureté après essai est plus élevée. On constate en même temps une augmentation très sensible du nombre d'alternances à la rupture, pour une même amplitude de la torsion alternée (Fig. 22).

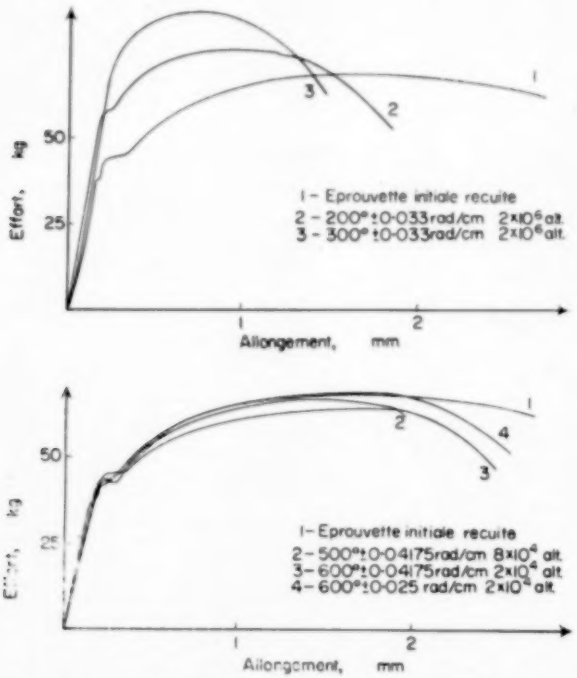

Fig. 23. Courbes de traction d'éprouvettes d'acier doux prélevées dans des éprouvettes prealablement fatiguées.

L'augmentation de la dureté, maximum lorsque le nombre de cycles à la rupture est le plus grand, tend à prouver que la formation des fissures ne résulte pas d'un écrouissage local trop important, du moins exclusivement. Cette augmentation se produit d'autre part en début d'essai. La facilité de formation de fissures semble

donc aller de pair avec celle d'apparition des distorsions et déviations de glissement. Elle est minimum entre 200 et 400°, où le métal se consoliderait au cours des premiers milliers de cycles et il est possible que des précipités de carbure se forment dans les plans de glissement. Les courbes de traction d'échantillons prélevés dans éprouvettes fatiguées à ces températures montrent en effet une diminution sensible de l'allongement per cent, une augmentation de la charge de rupture et la suppression du palier (Fig. 23).

Au-delà de 450° des phénomènes de réorganisation du réseau cristallin au cours même de la déformation modifient le mécanisme de rupture. Si la déformation par cycle est assez faible, cette réorganisation serait semble-til suffisante pour que la rupture ne puisse avoir lieu. Par contre, dès que les perturbations dues aux déformations alternées ne sont plus 'compensées' par la réorganisation, des fissures se formeraient le long des joints (et des sous-joints de polygonisation).

A 700° les migrations de joints et le grossissement du grain provoquent un effondrement des qualités mécaniques du métal. En particulier l'aire du cycle d'hystérésis mécanique croit considérablement.

(b) L'acier austénitique est caractérisé par un allongement considérable atteignant 60 pour cent. Les glissements sont toujours beaucoup plus rectilignes. En fatigue, quelle que soit la température, les glissements se répartissent uniformément dans les grains et l'astérisme reste faible même pour des amplitudes de torsion alternée assez élevées. On peut penser que les distorsions locales sont beaucoup plus faibles que pour l'acier doux, ce qui expliquerait l'augmentation considérable du nombre d'alternances à la rupture par rapport à ce dernier.

Il faut atteindre 600° pour que diminuent les amplitudes de déformation alternées admissibles, température au-delà de laquelle se produisent une précipitation aux joints de grains et des décohésions intergranulaires. La polygonisation est beaucoup moins marquée sur cet acier, et les fissures se produisent dans ce cas exclusivement aux joints de grains, les sous-joints n'intervenant pas. La migration des joints ne se produit pas sur cet acier, probablement en raison de la précipitation et de la décohésion.

Dùne façon génèrale, ces résultats montrent une grande similitude entre le comportement du métal au cours de la fatigue à chaud et son comportement en fluage, aussi bien pour l'acier doux que pour l'acier austénitique. Tamhankar *et al.* (1958) ont obtenu en effet des résultats tout-à-fait comparables au cours d'une étude de la déformation à chaud d'un fer doux et d'un acier austénitique stable au nickel-chrome.

References

Fouquet, J. de	1958a	*Thèse* (Poitiers).
	1958b	*Rev. Mét.* **55**, 1133.
	1958c	*Rev. Met.* To be published.
Jacquesson, R. et Fouquet, J. de	1957	*C.R. Acad. Sci, Paris* **224**, 2306.
Tamhankar, R., Plateau, J. et Crussard, C.	1958	*Rev. Mét.* **55**, 383.

J. Mech. Phys. Solids, 1959, Vol. 7, pp. 272 to 281. Pergamon Press Ltd., London. Printed in Great Britain

TORSION OF BEAMS WHOSE SECTIONS ARE BOUNDED BY CERTAIN QUARTIC CURVES

By W. A. Bassali
Faculty of Science, University of Alexandria

(*Received 7th May*, 1959)

Summary

Cauchy integral methods are applied to the torsion of a solid isotropic cylinder whose section is bounded by a quartic curve which is the inverse of an ellipse with respect to any point on its major or minor axis. The complex torsion function, the torsional rigidity and the shearing stresses are explicitly determined in the general case, and particular values are found to agree with those already known for Booth's lemniscate and the elliptic limacon. The distribution of shearing stress on the boundary is computed in two particular examples.

1. Introduction

Many solutions have been given to the classical Saint-Venant's torsion problem for various forms of boundary including polygons, angles, cardioids, limacons, sectors, lemniscates and others; references are to be found in standard textbooks by Love (1944), Timoshenko and Goodier (1951), Sokolnikoff (1956) and Muskhelishvili (1949). Special techniques have been developed by many investigators to treat specific problems. A complete bibliography dealing with the theory of elastic cylinders in torsion and including conventional as well as complex variable methods is contained in a recent Chinese book* (1956) which presents a resumé of almost all existing material relating to this rather special field of elasticity theory. The Schwarz-Christoffel transformation has been used by Trefftz (1921) and Seth (1934) to discuss the torsion of beams whose section is a regular rectilinear polygon of n sides. The Cauchy integral methods described by Muskhelishvili (1949, p. 561) were used by I. S. and E. S. Sokolnikoff (1938) to discuss a section bounded by two circular arcs of equal radius and intersecting at right angles. A section with the shape of Booth's lemniscate† has been considered by Muskhelishvili (1949, p. 581) and in a different but equivalent manner by Higgins (1942). Stevenson (1939), and Holl and Rock (1939) treated an elliptic-limacon† section. The corresponding problem for a hyperbolic limacon was solved by Lin and Whitehead (1951) and by Lin and Yang (1951). Recently Morris and Hawley (1958) have developed new complex variable methods to deal with the torsion and flexure of solid cylinders with cross-sections transformable to a ring-space. The particular cases of the elliptic section and a section having a circular arc as internal cut are treated.

*See the review of this book in *Appl. Mech. Reviews* 1958, 11, 110.

†Booth's lemniscate is the inverse of an ellipse with respect to its centre, while the elliptic limacon is the curve resulting from inversion of an ellipse with respect to its focus. The latter is sometimes referred to as Pascal's limacon (Muskhelishvili 1949, p. 175).

STEVENSON (1943) has considered a grooved column of a special type. The boundary curve, taken in the z-plane, can be mapped on the unit circle γ in the ζ-plane by the mapping function

$$z = c\zeta\,(1 + m\,\zeta^n), \tag{1.1}$$

where c and m are taken to be real and positive constants subject to the restriction $0 \leqslant m\,(n+1) \leqslant 1$. Sections bounded by the elliptic limacon or the cardioid are included as particular cases. Recently the author (1959a) has obtained solutions for sections bounded by regular curvilinear polygons that can be mapped on γ by the transformation

$$z = c\zeta/(1 + m\,\zeta^n), \quad c > 0, \tag{1.2}$$

where n is a positive integer and $-1 \leqslant m\,(n-1) \leqslant 1$. This mapping function has been thoroughly studied by the author (1959b) where varieties of figures corresponding to different values of m, n and having several axes of symmetry are drawn. For $n = 2$ the section has the shape of Booth's lemniscate, while for $m = -2/\{n\,(n-1)\}$ it was shown that the cross-section is bounded by n approximately circular and equal arcs. The present paper is concerned with sections bounded by quartic curves which are mapped on γ by the function

$$z = c\zeta/(1 + n\zeta + m\,\zeta^2), \quad c > 0, \tag{1.3}$$

where m, n are real and $|m| < 1$, $|n| < 2$. It will be shown in Section 3 that the bounding curve is always the inverse of an ellipse with respect to a point on its major or minor axis. For $n = 0$ we have Booth's lemniscate while if $m > 0$ and $n^2 = 4m$ the section is an elliptic limacon.

2. FUNDAMENTAL EQUATIONS

Consider the Saint-Venant torsion of a homogeneous isotropic cylinder of uniform section S bounded by a simple closed curve Γ in the z-plane ($z = x + iy = r\,e^{i\theta}$) which is chosen to coincide with the plane $Z = 0$ perpendicular to the generators of the cylinder. It is known (STEVENSON 1943) that the displacements u, v, and w and the non-vanishing stresses $\widehat{xZ}$, $\widehat{yZ}$ are given by

$$u + iv = i\tau z Z, \quad w = \tau\,\phi\,(x, y) = \tfrac{1}{2}\,\tau\,[\Omega\,(z) + \bar{\Omega}\,(\bar{z})], \tag{2.1}$$

$$\widehat{xZ} - i\widehat{yZ} = \mu\tau\,[\Omega'\,(z) - i\bar{z}], \tag{2.2}$$

where τ is the constant twist per unit length, μ is the rigidity of the material of the cylinder and $\Omega\,(z) = \phi\,(x, y) + i\,\psi\,(x, y)$ is the complex torsion function which satisfies the boundary condition

$$\Omega\,(z) - \bar{\Omega}\,(\bar{z}) = iz\bar{z} \text{ along } \Gamma; \tag{2.3}$$

bars are used to denote conjugate complex quantities and accents designate differentiation with respect to the stated argument.

Let

$$z = z\,(\zeta), \quad \zeta = \rho\,e^{i\theta} \tag{2.4}$$

be the function which maps the region S on the circle $|\zeta| \leqslant 1$. With the aid of this mapping function curvilinear coordinates (ρ, θ) are introduced into the z-plane.

The function $\Omega(z)$ can be written in terms of ζ, so that

$$\phi + i\,\psi = \Omega(z) = \omega(\zeta), \tag{2.5}$$

where $\omega(\zeta)$ is regular inside γ. It is found (Muskhelishvili 1949, p. 577) that

$$\omega(\zeta) = \frac{1}{2\pi}\int_{\gamma} \frac{z(\sigma)\,\bar{z}(\sigma^{-1})}{\sigma - \zeta}\,d\sigma + \text{constant}. \tag{2.6}$$

The twisting couple N is furnished by

$$N = \tau D,\ D = \mu\,(I + J), \tag{2.7}$$

where D is the torsional rigidity of the cylinder, I is the polar moment of inertia $\int z\bar{z}\,dS$ for the cross-section, or

$$I = -\tfrac{1}{4}\,i\int_{\gamma} z(\sigma)\,z'(\sigma)\,\bar{z}^2(\sigma^{-1})\,d\sigma, \tag{2.8}$$

and

$$J = \tfrac{1}{2}\int_{\gamma} z(\sigma)\,\bar{z}(\sigma^{-1})\,\omega'(\sigma)\,d\sigma. \tag{2.9}$$

It was shown by Morris and Hawley (1958, p. 469) that the expression $I + J$ is (of course) real.

The shearing stresses $\widehat{\rho Z}$ and $\widehat{\partial Z}$ at any point of the cross-section are given by

$$\widehat{\rho Z} - i\,\widehat{\theta Z} = \left[\zeta z'(\zeta)/\rho\left|z'(\zeta)\right|\right](\widehat{xZ} - i\,\widehat{yZ}), \tag{2.10}$$

and substituting from (2.2) in (2.10) we get the convenient formula

$$\widehat{\rho Z} - i\,\widehat{\theta Z} = \left[\mu\tau\,\zeta/\rho\left|z'(\zeta)\right|\right]\left[\omega'(\zeta) - i\bar{z}'(\zeta)\,\bar{z}(\bar{\zeta})\right]. \tag{2.11}$$

3. Mapping Function

Stevenson (1943) and the author (1959a) have solved the torsion problem for sections which are regular curvilinear polygons having n sides and n rounded vertices (which may become cusps). The boundaries of the sections, taken in the z-plane, are mapped on γ by the conformal transformations

$$z = c\zeta\,(1 + m\,\zeta^n),\ c > 0,\ 0 \leqslant m\,(n+1) \leqslant 1, \tag{3.1}$$

and

$$z = c\zeta/(1 + m\,\zeta^n),\ c > 0,\ -1 \leqslant m\,(n-1) \leqslant 1, \tag{3.2}$$

where m, n are two real constants subject to the mentioned restrictions. We here consider the section which is mapped on $|\zeta| \leqslant 1$ by

$$z = c\zeta/(1 + n\zeta + m\zeta^2),\ c > 0, \tag{3.3}$$

where n, m are taken to be real parameters, and, in order that the transformation shall be conformal at all points within the boundary Γ, $z'(\zeta)$ must not vanish or become infinite at points within Γ, and we therefore have the condition

$$-1 < m < 1. \tag{3.4}$$

If Γ' is the inverse of Γ with respect to the circle $|z| = d$ and $z' = x' + iy'$, $z = x + iy$ are the points on Γ', Γ, respectively, that correspond to $\zeta = e^{i\theta}$ on γ, then

$$z'\,\bar{z} = d^2, \tag{3.5}$$

and inserting (3.5) in (3.3) leads to

$$z' - f = d^2\,(e^{i\theta} + m\,e^{-i\theta})/c, \tag{3.6}$$

where

$$f = n\,d^2/c. \tag{3.7}$$

From (3.6) it follows immediately that Γ' is the ellipse

$$(x' - f)^2/a^2 + y'^2/b^2 = 1, \tag{3.8}$$

where

$$a = (1 + m)\,d^2/c,\ b = (1 - m)\,d^2/c. \tag{3.9}$$

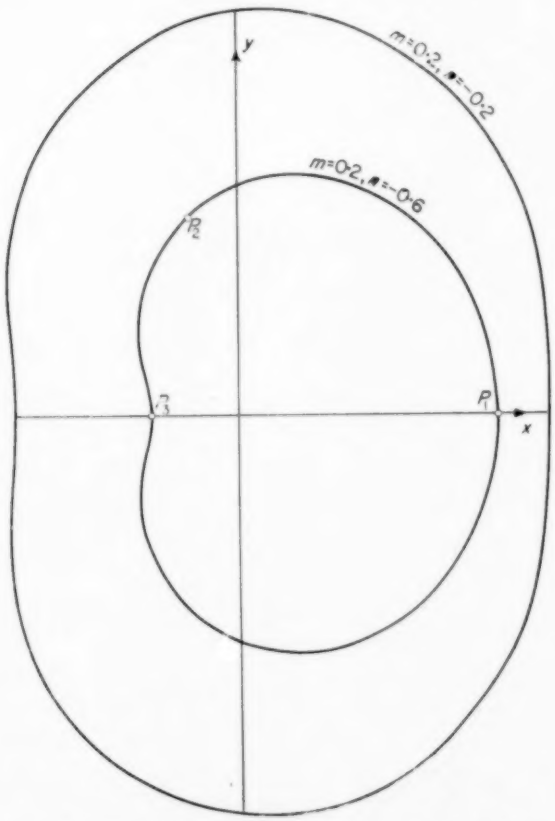

Fig. 1. Inverses of ellipse with respect to points on major axis.

The contour Γ mapped on γ by means of (3.3) may thus be identified with the inverse of the ellipse Γ' whose axes are $2a$, $2b$ with respect to a point on the first axis distant $-f$ from the centre of the ellipse, where, using (3.7) and (3.9),

$$n = 2f/(a+b), \quad m = (a-b)/(a+b), \quad c = 2d^2/(a+b), \tag{3.10}$$

d being the radius of the circle of inversion. If (3.3) is to map the area inside Γ on to the area inside γ then the centre of inversion must lie inside Γ' and the first equation of (3.10) gives the additional condition

$$-2 < n < 2. \tag{3.11}$$

It is sufficient to consider either positive or negative values of n.

The parametric equations of Γ are

$$cx/r^2 = n + (1+m)\cos\theta, \quad cy/r^2 = (1-m)\sin\theta, \tag{3.12a}$$

where

$$c^2/r^2 = 1 + n^2 + m^2 + 2n(1+m)\cos\theta + 2m\cos 2\theta. \tag{3.12b}$$

The Cartesian and polar equations of the quartic curve Γ are therefore furnished by

$$(nx^2 + ny^2 - cx)^2/(1+m)^2 + c^2y^2/(1-m)^2 = (x^2+y^2)^2, \tag{3.13}$$

and

$$(nr - c\cos\Theta)^2/(1+m)^2 + c^2\sin^2\Theta/(1-m)^2 = r^2, \tag{3.14}$$

respectively. The two curves corresponding to $m = 0{\cdot}2$, $n = -0{\cdot}2$ and $m = 0{\cdot}2$, $n = -0{\cdot}6$ are illustrated in Fig. 1. They are the inverses of the two ellipses

$$(x+1)^2/36 + y^2/16 = 1 \text{ and } (x+3)^2/36 + y^2/16 = 1,$$

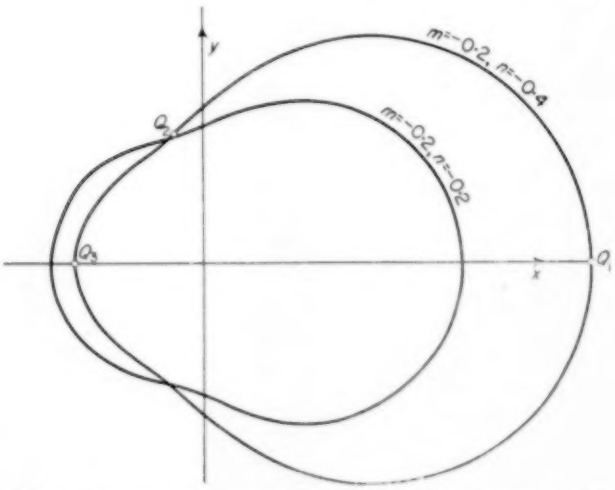

Fig. 2. Inverses of ellipse with respect to points on minor axis.

respectively, with respect to the origin. For negative values of m we have $a < b$ and the centre of inversion lies on the minor axis of the ellipse. Fig. 2 shows the two cross-sections for which $m = -0{\cdot}2$, $n = -0{\cdot}2$ and $m = -0{\cdot}2$, $n = -0{\cdot}4$. These are bounded by the inverses of the ellipses

$$(x+1)^2/16 + y^2/36 = 1 \text{ and } (x+2)^2/16 + y^2/36 = 1$$

with respect to the origin.

For $m = 0$ the contour Γ becomes Booth's lemniscate while if $m > 0\,(a > b)$ and $f = \pm\sqrt{(a^2 - b^2)}$, so that the centre of inversion coincides with one or other of the two foci of the ellipse Γ', then equations (3.10) yield

$$n = \pm 2\sqrt{m}. \tag{3.15}$$

In this case the mapping function (3.3) takes the form

$$z = c\zeta/(1 + m^{\frac{1}{2}}\zeta)^2, \tag{3.16}$$

and substituting from (3.15) in (3.14) we obtain, after simplification, the two elliptic limacons

$$r = A \pm B\cos\Theta, \tag{3.17a}$$

where

$$A = c\,(1 + m)/(1 - m)^2,\ B = 2c\,m^{\frac{1}{2}}/(1 - m)^2. \tag{3.17b}$$

4. Complex Torsion Function

Substituting from (3.3) in (2.6) we find that the torsion function which solves the problem for a section mapped on $|\zeta| \leqslant 1$ with the aid of (3.3) is furnished by

$$\omega(\zeta) = \frac{c^2}{2\pi}\int_\gamma \frac{\sigma^2\,d\sigma}{(1 + n\sigma + m\sigma^2)\,(\sigma^2 + n\,\sigma + m)\,(\sigma - \zeta)} + \text{constant}, \tag{4.1}$$

where ζ is any point inside γ. It is easily shown that, under the restrictions (3.4) and (3.11) on m and n, respectively, the integrand of (4.1), considered as a function of σ, has two simple poles ζ_1, ζ_2 that lie outside γ, where

$$\zeta_1 + \zeta_2 = -n/m, \quad \zeta_1\,\zeta_2 = 1/m, \tag{4.2}$$

and $n^2 \neq 4m$. For large values of σ the integrand in (4.1) is of the order $1/|\sigma|^3$, and we therefore have

$$\omega(\zeta) = -c^2\,i\,(R_1 + R_2) + \text{constant},$$

where R_1 and R_2 are the residues of the integrand at $\sigma = \zeta_1$ and $\sigma = \zeta_2$, respectively. Hence

$$\omega(\zeta) = -\frac{c^2\,i}{(\zeta_1 - \zeta_2)\,m}\left[\frac{\zeta_1^{\,2}}{(\zeta_1 - \zeta)\,(\zeta_1^{\,2} + n\,\zeta_1 + m)} - \frac{\zeta_2^{\,2}}{(\zeta_2 - \zeta)\,(\zeta_2^{\,2} + n\,\zeta_2 + m)}\right] + \text{constant}, \tag{4.3}$$

and, making use of (4.2), it is found that (4.3) simplifies to

$$\omega(\zeta) = \frac{c^2\,i}{(1 - m)\,k}\,\frac{1 + m + mn\zeta}{1 + n\zeta + m\zeta^2} + \text{constant}, \tag{4.4}$$

where

$$k = (1 + m)^2 - n^2. \tag{4.5}$$

In the special case of an elliptic-limacon section $n^2 = 4m$ and the integrand in (4.1) has a double pole outside γ at $\zeta_0 = \mp\, m^{-\frac{1}{2}}$. If R is the residue of the integrand at $\sigma = \zeta_0$ in this case then

$$\omega(\zeta) = -c^2 i\,R + \text{constant},$$

and it can be shown that the result agrees with (4.4) after substitution from (3.15). Taking for the constant in (4.4) the value $-c^2\,(1 + m)\,i/2\,(1 - m)\,k$, one finds for the complex torsion function:

$$\omega(\zeta) = \frac{c^2\,i}{2k}\,\frac{q - n\zeta - mq\zeta^2}{1 + n\zeta + m\zeta^2}, \tag{4.6}$$

where

$$q = (1 + m)/(1 - m) = a/b. \tag{4.7}$$

The imaginary part of (4.6) is

$$\psi = \frac{c^2}{2k}\frac{q(1-m^2\rho^4) - n^2\rho^2 + n(q-1)\rho(1-\rho^2)\cos\theta}{1+n^2\rho^2+m^2\rho^4+2n\rho(1+m\rho^2)\cos\theta+2m\rho^2\cos 2\theta}. \tag{4.8}$$

Setting $\rho = 1$ in (4.8), substituting for q from (4.7), and using (3.12b), we see that, on the boundary Γ, ψ reduces to $\frac{1}{2}zz$, as it should.

5. Torsional Rigidity

The polar moment of inertia I for the section is obtained by substitution from (3.3) in (2.8):

$$I = -\tfrac{1}{4}ic^4\int_\gamma \frac{\sigma^3(1-m\sigma^2)\,d\sigma}{(\sigma^2+n\sigma+m)^2(1+n\sigma+m\sigma^2)^3}. \tag{5.1}$$

If λ_1 and λ_2 are the two roots of the equation $\sigma^2+n\sigma+m=0$, so that

$$\lambda_1\lambda_2 = m, \quad |m|<1\,;\ \lambda_1+\lambda_2 = -n, \quad |n|<2, \tag{5.2}$$

then λ_1 and λ_2 lie inside γ and

$$I = \tfrac{1}{2}\pi c^4(P_1+P_2), \tag{5.3}$$

where P_1 and P_2 are the residues of the integrand in (5.1) at $\sigma=\lambda_1$ and $\sigma=\lambda_2$, respectively. It can be proved that

$$P_1 = \frac{3\lambda_1^2(1-m\lambda_1^2)^2}{(\lambda_1-\lambda_2)^2(1+n\lambda_1+m\lambda_1^2)^4} - \frac{2(1-m^2)\lambda_1^3}{(\lambda_1-\lambda_2)^3(1+n\lambda_1+m\lambda_1^2)^3}, \tag{5.4}$$

while P_2 is derived from (5.4) by interchanging λ_1 and λ_2. Applying (5.2) we find after considerable reduction that*

$$I = \frac{\pi c^4}{k^3}\left[\frac{3}{k}\left\{\frac{(1-n^2m+m^2+2m^3)^2+m^2(2-n^2+m+m^3)^2}{2(1-m)^4}+m(1+m)^2\right\}\right.$$
$$\left. -\frac{(1+m)(1+m^3)}{(1-m)^2}\right], \tag{5.5}$$

where k is given by (4.5).

Introducing (3.3) and the torsion function defined by (4.6) and (4.7) in (2.9) leads to the expression

$$J = -\frac{c^4 i}{(1-m)k}\int_\gamma \frac{m(1+m)\sigma^3+\frac{1}{2}n\sigma^2(1+m^2\sigma^2)}{(\sigma^2+n\sigma+m)(1+n\sigma+m\sigma^2)^3}\,d\sigma. \tag{5.6}$$

We therefore have

$$J = 2\pi c^4(Q_1+Q_2)/(1-m)k, \tag{5.7}$$

where Q_1, the residue of the integrand in (5.6) at $\sigma=\lambda_1$, is given by

$$Q_1 = \frac{\frac{1}{2}n(1+m^2\lambda_1^2)\lambda_1^2+m(1+m)\lambda_1^3}{(\lambda_1-\lambda_2)(1+n\lambda_1+m\lambda_1^2)^3}, \tag{5.8}$$

and Q_2 is deduced from Q_1 by interchanging λ_1 and λ_2. Applying (5.2) it is found after some algebraic manipulation that

$$J = -\frac{\pi c^4}{k^2}\left[\frac{2m^2}{(1-m)^4}+\frac{n^2(1+m)^2}{k^2}\right]. \tag{5.9}$$

When (5.5) and (5.9) are inserted in (2.7), it is seen that the torsional rigidity is†

$$D = \frac{\mu\pi c^4}{k^4}\left[\frac{3(1-n^2m+m^2+2m^3)^2+3m^2(2-n^2+m+m^3)^2-4m^2k^2}{2(1-m)^4}\right.$$
$$\left.+(1+m)^2\left\{3m+\frac{n^2m-(1+m)(1+m^3)}{(1-m)^2}\right\}\right]. \tag{5.10}$$

*It can be shown that the expression for I may be put in the form

$$I = \pi c^4\left[(1+m)^4(1+4m^2+m^4)+2(1+m)^3(1-6m+4m^2-6m^3+m^4)n^2+6m^2n^4\right]/2(1-m)^4k^4$$

†An equivalent and simpler expression for the torsional rigidity is

$$D = \mu\pi c^4\left[(1+m^4)(1+m^4)-4m(1+m)(1+m^3)n^2+2m^2n^4\right]/2(1-m)^4k^4.$$

Setting $n = 0$ in (5.10) and observing that

$$(1 + m^2 + 2m^3)^2 + m^2(2 + m + m^3)^2 = \tfrac{1}{2}(1 - m^2)^2(1 - m)^4 + \tfrac{1}{2}(1 + m^2)^2(1 + m)^4,$$

we find that D simplifies to

$$D = \tfrac{1}{2}\mu\pi c^4(1 + m^4)/(1 - m^2)^4 \tag{5.11}$$

which agrees with the result of MUSKHELISHVILI (1949, p. 582) for Booth's lemniscate. Substituting from (3.15) in (5.10) yields the following expression for the torsional rigidity of either of the elliptic limacons (3.17):

$$D = \tfrac{1}{2}\mu\pi c^4(1 + 8m + 16m^2 + 8m^3 + m^4)/(1 - m)^8, \tag{5.12}$$

which can be shown to be equivalent to

$$D = \tfrac{1}{16}\mu\pi(8A^4 + 8A^2B^2 + B^4), \tag{5.13}$$

on using the values of A and B given by (3.17b). The formula (5.13) was obtained by STEVENSON (1943, equation (3.4)).

As a further check on the expression (5.10) we notice that for $m = 0$ it reduces to $D = \frac{1}{2}\mu\pi c'^4$, where $c' = c/(1 - n^2)$. This result is to be expected since in this case it is easily seen that the curve Γ becomes a circle of radius c'. Putting $m = n = 0$ in (5.10) yields $D = \frac{1}{2}\mu\pi c^4$ which is the torsional rigidity for a circular cylinder of radius c.

6. Shearing Stresses

Substitution from (3.3), (4.6) and (4.7) in (2.11) leads to

$$\widehat{\rho Z} - i\widehat{\theta Z} = -\frac{\mu\tau ic}{T}\left[\frac{(\zeta + n\rho^2 + m\rho^2\bar{\zeta})^2\{n\zeta^{-1} + 2m(1 + m) + m^2 n\zeta\}}{(1 - m)\rho k} + \rho(1 - m\zeta^2)(1 + n\bar{\zeta} + m\bar{\zeta}^2)\right], \tag{6.1}$$

where k is given by (4.5) and

$$T = (1 + m^2\rho^4 - 2m\rho^2\cos 2\theta)^{\frac{1}{2}}\left[1 + n^2\rho^2 + m^2\rho^4 + 2n\rho(1 + m\rho^2)\cos\theta + 2m\rho^2\cos 2\theta\right]. \tag{6.2}$$

Putting $\zeta = \rho e^{i\theta}$ in (6.1) and separating real and imaginary parts it is found, after some straightforward computations, that the shearing stresses at any point of the cross-section are

$$\widehat{\rho Z} = \frac{2\mu\tau c(1 - \rho^2)}{(1 - m)kT}\left[n\{1 + m(3m + k)\rho^2 + m^4\rho^4\}\sin\theta + m(1 + m)(1 + m^2\rho^2)\rho\sin 2\theta + m^2 n\rho^2\sin 3\theta\right], \tag{6.3}$$

$$\widehat{\theta Z} = \frac{\mu c\tau}{T}\left[\frac{1}{(1 - m)k}\left\{2m(1 + m)(2m + n^2)\rho^3 + 2n^2\rho(1 + m^3\rho^4) + n\left(1 + 4m(1 + m)\rho^2(1 + m\rho^2) + (2m + n^2)\rho^2(1 + m^2\rho^2) + m^4\rho^6\right)\cos\theta + m(1 + m)\rho(1 + n^2\rho^2 + m^2\rho^4)\cos 2\theta + m^2 n\rho^2(1 + \rho^2)\cos 3\theta\right\} + \rho(1 - m^2\rho^4) + n\rho^2(1 - m\rho^2)\cos\theta\right]. \tag{6.4}$$

Since $\omega(\zeta)$ is regular throughout the cross-section S and $z'(\zeta)$ does not vanish at any point within S by the restriction (3.4), it follows from (2.11) that the stresses (6.3) and (6.4) are necessarily finite and physically admissible across S.

Setting $\rho = 1$ in (6.3), (6.4) and substituting for T from (6.2) we find that, on the boundary Γ of the cross-section, $\widehat{\rho Z}$ vanishes as expected while the peripheral shear stress simplifies to

$$(\widehat{\theta Z})_{\rho=1} = \frac{\mu c\tau}{(1 - m)k}\frac{(1 + m)(1 + m^2) + 2mn\cos\theta}{\sqrt{(1 + m^2 - 2m\cos 2\theta)}}. \tag{6.5}$$

From (6.5) it is seen that the maximum and minimum values of the tangential stress acting on the boundary Γ occur alternately at the three points $\theta = 0$, $\theta = \alpha$, and $\theta = \pi$, where

$$\alpha = \cos^{-1}\left[-n(1+m)/2(1+m^2)\right], \tag{6.6}$$

and the magnitudes of these values are furnished by

$$(\widehat{\theta Z})_{\rho=1,\,\theta=0} = \mu\tau c\left[(1+m)(1+m^2)+2mn\right]/(1-m)^2 k, \tag{6.7}$$

$$(\widehat{\theta Z})_{\rho=1,\,\theta=\alpha} = \mu\tau c\left[(1+m^2)^2 - n^2m\right]^{\frac{1}{2}}/(1-m)k, \tag{6.8}$$

$$(\widehat{\theta Z})_{\rho=1,\,\theta=\pi} = \mu\tau c\left[(1+m)(1+m^2)-2mn\right]/(1-m)^2 k. \tag{6.9}$$

Substituting from (3.15) in (6.7), (6.9) and using the values of A and B defined by (3.17b) it can be verified that the resulting expressions agree with those obtained by STEVENSON (1943, equations (3.7), (3.8)) for the peripheral shears of the elliptic-limacon section at the bottom of the groove and at the point where r becomes a maximum.

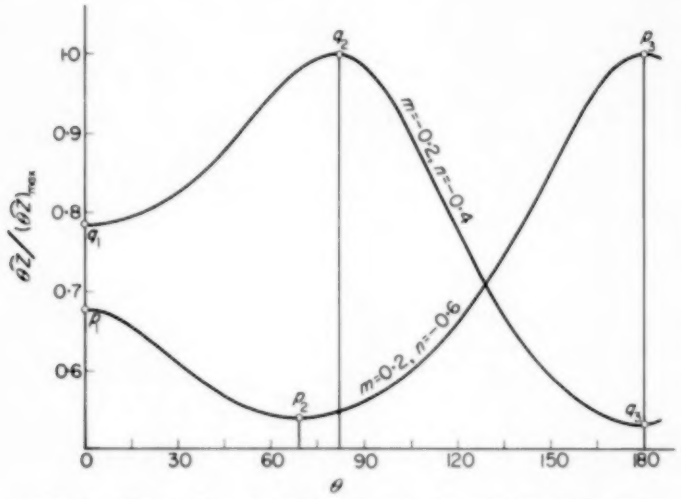

Fig. 3. Distribution of shearing stress on boundaries of sections.

Fig. 3 illustrates the variation in peripheral shear on the boundaries of the two sections in Figs. 1 and 2 which correspond to $m = 0{\cdot}2$, $n = -0{\cdot}6$ and $m = -0{\cdot}2$, $n = -0{\cdot}4$. The points at which the stresses attain their maximum and minimum values on the two boundaries are also indicated.

REFERENCES

BASSALI, W. A. 1959a *J. Math. Phys.* In press.

1959b *J. Mech. Phys. Solids* **7**, 145.

CHIEN, W. Z., HU, H. C., LIN, H. S. and YEH, C. Y. 1956 *Theory of Elastic Cylinders in Torsion* (Peking).

HIGGINS, T. J. 1942 *J. Appl. Phys.* **13**, 457.

HOLL, D. L. and ROCK, D. H. 1939 *Z. angew. Math. Mech.* **19**, 141.

LIN, T. C. and WHITEHEAD, L. G. 1951 *University of Washington, Engineering Experiment Station Series*, Bulletin 118, 108.

LIN, T. C. and YANG, H. T. 1951 *University of Washington, Engineering Experiment Station Series*, Bulletin 118, 112.

Love, A. E. H.	1944	*A Treatise on the Mathematical Theory of Elasticity*, 4th Ed. (New York).
Morris, R. M. and Hawley, F. J.	1958	*Quart. J. Mech. Appl. Math.* **11**, 462.
Muskhelishvili, N. I.	1949	*Some Basic Problems of the Mathematical Theory of Elasticity*, 3rd Ed. (Moscow).
Seth, B. R.	1934	*Proc. Camb. Phil. Soc.* **30**, 139.
Sokolnikoff, I. S.	1956	*Mathematical Theory of Elasticity*, 2nd Ed. (McGraw-Hill).
Sokolnikoff, I. S. and Sokolnikoff, E. S.	1938	*Bull. Amer. Math. Soc.* **44**, 384.
Stevenson, A. C.	1939	*Proc. Lond. Math. Soc.* **45**, 126.
	1943	*Phil. Mag.* **34**, 115.
Timoshenko, S. and Goodier, J. N.	1951	*Theory of Elasticity*, 2nd Ed. (McGraw-Hill).
Trefftz, E.	1921	*Math. Ann.* **82**, 306.

J. Mech. Phys. Solids, 1959, Vol. 7, pp. 282 to 287. Pergamon Press Ltd., London. Printed in Great Britain

AN EXPERIMENTAL STUDY OF THE V-NOTCH FATIGUE TEST

By D. S. Dugdale
Engineering Department, University College of Swansea

(*Received* 1st *July* 1959)

Summary

Rotating bending tests were carried out on sharply notched specimens of several materials. Logarithmic plotting gave S-N curves consisting of straight lines of a gradient common to all materials, suggesting a power law of crack propagation. When residual stress was introduced by pre-loading the specimens, results following a similar pattern were obtained. Correlation between results of static and fatigue tests is discussed.

1. Introduction

Alternating stress, when applied to a specimen free from geometrical notches, will eventually cause failure if the amplitude is sufficient to initiate a crack in the surface. At any stress level, part of the life is spent in initiating cracks, and the remainder in spreading one or more of these cracks across the section. The fraction of the life required for each stage may vary with material and applied stress. However, when a severe stress concentration is introduced, it may be expected that a crack will form quite early, leaving most of the life to be spent in spreading the crack. Thus it can be said that tests of this kind bring into prominence the resistance of materials to the growth of cracks.

Engineers are usually interested in obtaining a fatigue limit, which, in this context, means the minimum stress for producing extension of a crack. However, stresses near the fatigue limit cause intermittent growth of cracks, and a somewhat higher stress is required to produce continuous growth. Therefore it seemed profitable to carry out tests at stress levels rather higher than those normally considered, in an attempt to identify any features of the results that might reflect the regular growth of cracks. A phenomenological approach to testing materials is adopted. Information is simply brought together into a consistent scheme, instead of being used directly to support some pre-existing idea. For such work the rotating cantilever test is attractively simple. Over 600 specimens were tested.

2. Specimens

All specimens were made from 0·75 in. diameter bar to the dimensions shown in Fig. 1. A ball bearing for supporting the test load was attached to one end of the specimen by means of a screw, while the other end was gripped in the socket of the testing machine. The speed of testing was 1500 r.p.m. Grooves were cut

in a lathe with a cutting tool maintained sharp by careful grinding. Sectioned specimens showed that the root radius varied from 0·0001 in. for soft materials to 0·0005 in. for hard materials.

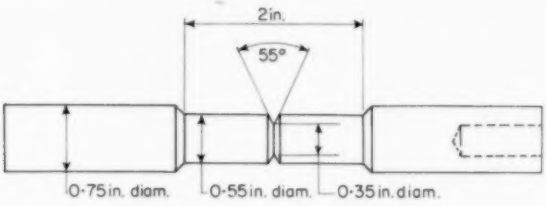

FIG. 1. Dimensions of test specimen.

Two batches of mild steel were used, both in the form of bright drawn bar. Steel *A* contained 0·17 per cent carbon and Steel *B* contained 0·10 per cent carbon, the manganese content being 0·55 per cent. Annealing was carried out at 650°C and normalizing at 850 °C. Spring steel En 43 (0·45 per cent carbon) was hardened and tempered at 600 °C. Non-ferrous materials were in the form of extruded bar. Copper of OFHC grade was used in the hard state and also after annealing at 600 °C. Half-hard bars of steel and copper were produced by stretching annealed bars by 7 per cent. Magnesium alloy conformed to specification DTD 259, and the zinc was 99·95 per cent pure. Mechanical properties are shown in Table 1, all stresses being in tons/in². Copper specimens were annealed after the grooves were cut, and specimens of normalized steel were stress-relieved at 650 °C, but no other specimens were heat treated after being machined.

3. RESULTS

Nominal bending stress was calculated from the simple formula for bending using the diameter at the root of the notch. When logarithms of stress and number

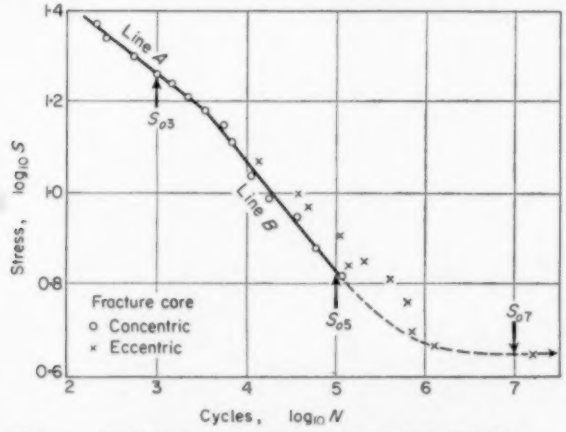

FIG. 2. Fatigue test results for Aluminium HE 10.

of cycles to fracture were plotted, it was found that results for all materials assumed a highly regular pattern. A typical curve is shown in Fig. 2. At the upper end of

the curve, the points lay on the straight line marked Line *A*, with no scatter beyond that expected from experimental inaccuracies. This segment of the curve was observed for all the materials examined, and has a negative gradient varying from 0·145 to 0·165.

Below this, the experimental points were found to be scattered over a band which increased in width as the stress was reduced. However, it was observed that the points lying on the left hand side of this band represented specimens which exhibited a concentric fracture. These points could be joined with a straight line marked Line *B*. For some materials an insufficient number of specimens was tested to establish this line with certainty, but when a satisfactory line was obtained it was found to have a negative gradient varying from 0·215 to 0·245. For most materials, this segment of the curve did not extend beyond 10^5 cycles. The lower part of the band, representing specimens that gave eccentric fractures, had a boundary indicated in Fig. 2 by a dotted line. This line became more or less horizontal at 10^7 cycles.

This pattern of behaviour suggests that the *S-N* curve can be specified in its essentials by stresses at three arbitrarily chosen numbers of cycles. These are

TABLE 1

	Static test results					*Fatigue test results*					
	0·1 *per cent. Proof stress*	1·0 *per cent. Proof stress*	*Tensile strength*	*Young's modulus E* (x 10^3)	*Vickers hardness number H*	S_{03}	S_{05}	S_{07}	S_{c7}	S_{f5}	S_{f7}
Steel A, *Hard*	32·3	38·3	40·0	13·4	195	46·0		10·0	17·4	10·4	4·0
Steel A, *Half-hard*	30·8	30·8	33·8	13·4	166	38·5		10·0			
Steel A, *Normalized*	17·6	17·6	29·5	13·4	124	33·2	13·8	7·3	11·2	9·9	5·9
Steel A, *Annealed*	14·0	14·0	26·4	13·4	107	29·6		10·0			
Steel B, *Hard*	31·0	33·5	33·6	13·4	167	40·7	13·0	9·5			
Steel B, *Annealed*	13·5	13·5	25·4	13·4	99	27·0		9·5	10·5	10·4	8·0
Spring Steel	36·7	37·9	46·4	13·4	216	47·9	17·6	12·5		9·1	2·5
Copper, Hard	20·0	21·8	22·0	7·5	102	20·7	7·5	4·5	9·6	5·4	1·9
Copper, Half-hard	9·5	10·3	17·2	7·5	70	16·0		4·4		5·5	2·2
Copper, Annealed	2·3	3·9	14·8	7·5	45	14·0		3·7	3·7		3·7
Aluminium HE 10	16·1	17·0	18·4	4·4	89	18·2	6·9	4·5	9·7	2·8	0·8
Aluminium L 65	31·7	34·3	36·3	4·7	166	28·8	10·3	8·4		2·8	0·7
Magnesium Alloy	15·8	18·4	22·2	2·9	70	13·2	4·7	3·1	6·9	1·8	0·5
Zinc	3·0	5·2	9·2	6·5	36	5·1	2·3	1·0		2·2	1·0

denoted S_{03}, S_{05} and S_{07}. They refer to the height of Line *A* at 10^3 cycles, the height of Line *B* at 10^5 cycles, and the stress corresponding to 10^7 cycles, as shown in Fig. 2. Numerical values are given in Table 1.

4. PRELOADING

Further tests were carried out on specimens preloaded in tension and compression to introduce compressive and tensile stresses respectively at the root of the notch. This method has been frequently used in the past for assessing the combined effects of a stress concentration and residual stresses (TEMPLIN 1954). It was desired that the axial load should be great enough to produce plastic deformation around the root of the notch without changing the shape of the notch appreciably. Loads

were used which were just sufficient to produce a permanent increase or decrease in the width of the notch of 0·003 in., as measured by means of dial gauges clamped to the specimen. Preliminary experiments with Aluminium L 65 showed that greater changes in width resulted in only marginal changes in the S-N curve. The exact magnitude of residual stress produced is not known, but it may be assumed that this increased with the yield stress of the material.

A typical set of curves is shown in Fig. 3. For high stresses the experimental points were found to lie on a common curve marked Line A. Specimens containing compressive residual stress gave a curve which became more or less horizontal at 10^7 cycles as shown. The stress at this point is denoted S_{c7} in Table 1. Specimens containing tensile residual stress gave points lying on a steeper curve marked Line C. It was found that this line was reasonably straight between 10^4 and 10^6 cycles, and had a gradient varying from 0·31 to 0·34 for the materials examined. The height of this line at 10^5 cycles and the stress at 10^7 cycles denoted S_{t5} and S_{t7} are given in Table 1.

5. Discussion

It is suggested that the straight lines shown in Fig. 3 imply a rate of crack propagation proportional to stress raised to some power. Stresses around the tip of a crack must increase as the crack progresses through the section. However,

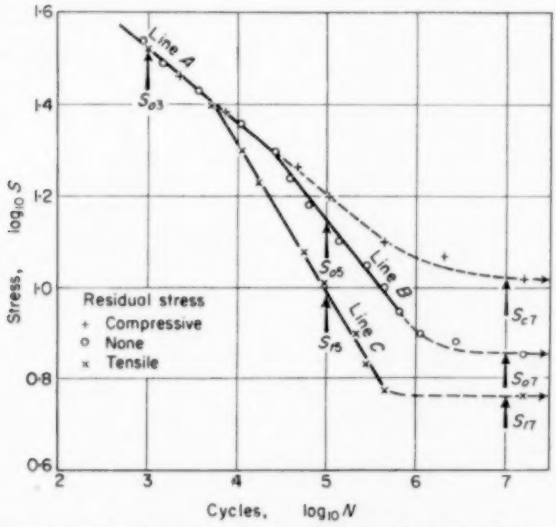

Fig. 3. Fatigue test results for Steel A (normalized), showing effect of residual stress introduced by preloading.

if it is assumed that they depend only on nominal stress and the radius of the concentric crack, they must have an average value, over prescribed radial limits, proportional to the nominal stress. If these limits are the same for all specimens, endurance must be inversely proportionate to average rate of crack growth. This argument relies on continuous growth of the crack over a fixed fraction of the section. It is known that cracks begin to grow almost immediately from the root of a very sharp notch. This was observed by Hunter and Fricke (1957) for

aluminium alloys and by SCHEVEN, SACHS and TONG (1957) for steel. The present tests showed that the statically fractured core had a diameter varying from about 70 per cent of the root diameter at high applied stresses to about 20 per cent at low stresses. It might be expected that the varying distance travelled by the fatigue crack would result in the *S-N* curves having slightly smaller gradients than they would otherwise have. The rate of growth of cracks in sheets subject to a wholly tensile cycle was measured by FROST and DUGDALE (1958) and was found to be proportional to stress raised to the power 3·0. The gradient of the curves described here for specimens containing tensile residual stress suggests a similar numerical value.

The segment of the *S-N* curve marked Line *A* in Fig. 3 has a special significance in that the specimens concerned were unaffected by residual stress. Cyclic stress must produce some change in residual stress in the region ahead of a growing crack. If this takes place at a sufficient rate and throughout a sufficient volume, it seems likely that a distribution of stress near the crack would be attained which is independent of any stresses initially present.

Line *B* in Fig. 2 extends over a range of applied stresses which may not produce continuous crack growth. It can be appreciated that if the crack was arrested at some point on its circumference, the endurance of the specimen would be increased, and the fracture would eventually exhibit an eccentric core. Many secondary factors seem to affect the stress at which the curve breaks away from this straight line and becomes horizontal. Surface stresses set up by machining may be mentioned (DUGDALE 1959).

6. CORRELATION

It can be seen that if a load applied to a specimen is great enough to cause yielding over the whole cross-section the specimen would immediately collapse. As such loads were not employed it is thought that the region of plastically deformed material around the crack was always surrounded by elastic material. Cyclic deformation ahead of the crack would therefore be governed to some extent by the elastic modulus. However, it is reasonable to suppose that the rate of growth of a crack would depend on the size of the region undergoing inelastic deformation, and this must be greater for a soft material than for a hard one. It may therefore be expected that resistance to the growth of cracks should be expressible as some combination of elastic and plastic properties. The typical heights of the *S-N* curves and the static test results shown in Table 1 were plotted together in various ways with view to finding whether there was any correlation.

At the outset it may be argued that plastic properties should predominate in deciding the height of Line *A* (Fig. 3), which is characterized by relaxation of residual stress. Inspection of the tabulated values shows that the height of this line increased with hardness. The height of Line *B* also appears to be raised by martensitic hardening in steel and precipitation hardening in aluminium alloy. However, the values for hard-drawn and normalized steel suggest that strain-hardening did not have the same effect. The height of Line *C* obtained from specimens containing residual tensile stress appeared to be little affected by changes in hardness. Of the many possible ways of correlating the tabulated results, the following relations involving Young's modulus *E* and Vickers hardness number *H* appeared to express general trends in a concise manner.

$$S_{03} = 0{\cdot}053\,(EH^2)^{\frac{1}{3}}, \quad (\pm 10\%)$$
$$S_{05} = 0{\cdot}0110\,(EH)^{\frac{1}{2}}, \quad (\pm 7\%)$$
$$S_{f5} = 0{\cdot}00068\,E, \quad (\pm 15\%).$$

Results for zinc were not taken into account, as this material gave coarse scintillating fractures unlike those of any other material. In the second of the above relations no account was taken of values for cold-worked materials.

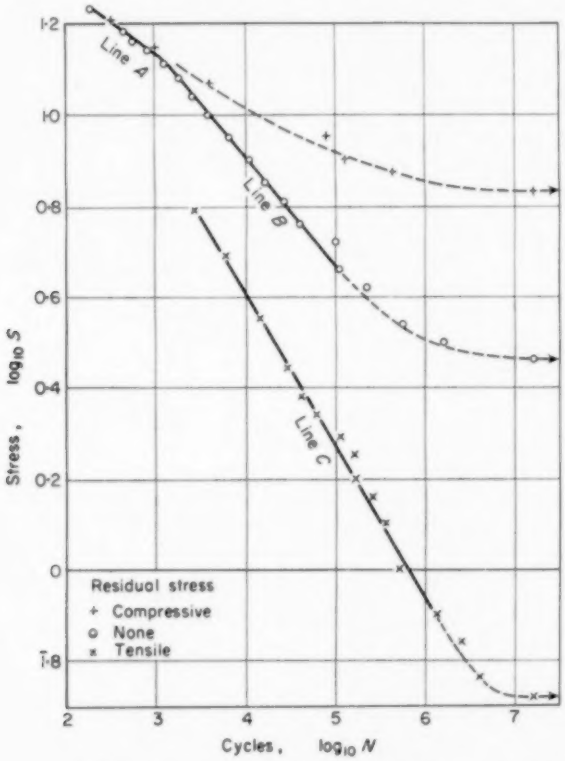

FIG. 4. Fatigue test results for Magnesium Alloy.

Referring to Figs. 3 and 4 and the tabulated values, it can be vizualized that increasing the static strength of any given base metal has the effect of raising Line *A* but not Line *C*. This makes for a greater divergence of these lines at 10^7 cycles and a greater value of the ratio S_{e7}/S_{f7} which expresses the potential effect of residual stress in the kind of specimen tested. If an indication of this effect in terms of static properties is desired, the ratio H/E is suggested.

REFERENCES

DUGDALE, D. S.	1959	*Welding J.*, New York **38**, 45-S.
FROST, N. E. and DUGDALE, D. S.	1958	*J. Mech. Phys. Solids* **6**, 92.
HUNTER, M. S. and FRICKE, W. G.	1957	*Proc. Amer. Soc. Test. Mater.* **57**, 643.
SCHEVEN, G., SACHS, G. and TONG, K.	1957	*Proc. Amer. Soc. Test. Mater.* **57**, 682.
TEMPLIN, R. L.	1954	*Proc. Amer. Soc. Test. Mater.* **54**, 641.

BOOK REVIEW

H. S. Carslaw and J. C. Jaeger: **Conduction of Heat in Solids.** (2nd Edition). Clarendon Press, Oxford, 1959. x + 510 pp. 84s.

The first edition of this work, which was a completely revised version of earlier books by Professor Carslaw, was published about twelve years' ago and it has already become a 'classic.' In nearly every modern research paper bearing on the subject, 'Carslaw and Jaeger' is to be found among the references and this can be taken as an indication of the way in which the book has fulfilled the authors' aim and of the great value it has been to its readers.

The volume under review is the second edition and, owing to Professor Carslaw's death in 1954, the task of preparing it has fallen on Professor Jaeger. In this task the author has retained the form of the first edition and has added a great many new results, bringing the number of pages from 386 to 510. Parts of the discussion, for example, those on heat generation, surface heating, melting and freezing, geophysical applications, anisotropic and moving media, and substances with variable thermal properties have been greatly expanded. In addition, two short survey chapters on integral transforms and numerical methods have been added and the great volume of modern work on the subject is reflected in the enlarged number of references to the literature. In bringing the previous volume completely up to date, Professor Jaeger has been entirely successful and there is no doubt in the reviewer's mind that 'Carslaw and Jaeger' will long remain the standard work on the subject.

The book is essentially one for the mathematical physicist but it will be of great value also to the large number of engineers who are today confronted with problems in heat transfer. The needs of the latter have been provided for by explicit solutions to a large number of problems of practical interest and by numerical results in the form of tables and graphs.

The Clarendon Press has again produced a beautiful example of mathematical printing and, in view of the size of the book and the value of its contents, the price of four guineas is not unreasonable. There is no doubt that this is a book which should be readily available to all those engaged on problems in heat conduction and both the author and his publishers have done them a great service in providing a completely modern text on the subject.

C. J. Tranter

BOOKS RECEIVED

Max Hansen and Kurt Anderko: Constitution of Binary Alloys. McGraw-Hill, 2nd Edition 1958. 1305 pp., 12 gns.

G. K. White: Experimental Techniques in Low-temperature Physics. Oxford University Press, 1959. 328 pp., 45s.

T. S. Moss: Optical Properties of Semi-conductors. Butterworth, 1959. 279 pp., 50s.

G. V. Raynor: The Physical Metallurgy of Magnesium and its Alloys. Pergamon Press, 1959. 531 pp., 75s.

END OF VOL.